IMMUNOMETABOLISM, ATHEROSCLEROSIS AND METABOLIC DISEASES

EDITED BY: Xuewei Zhu, Changcheng Zhou, Soonkyu Chung and Hanrui Zhang
PUBLISHED IN: Frontiers in Cardiovascular Medicine

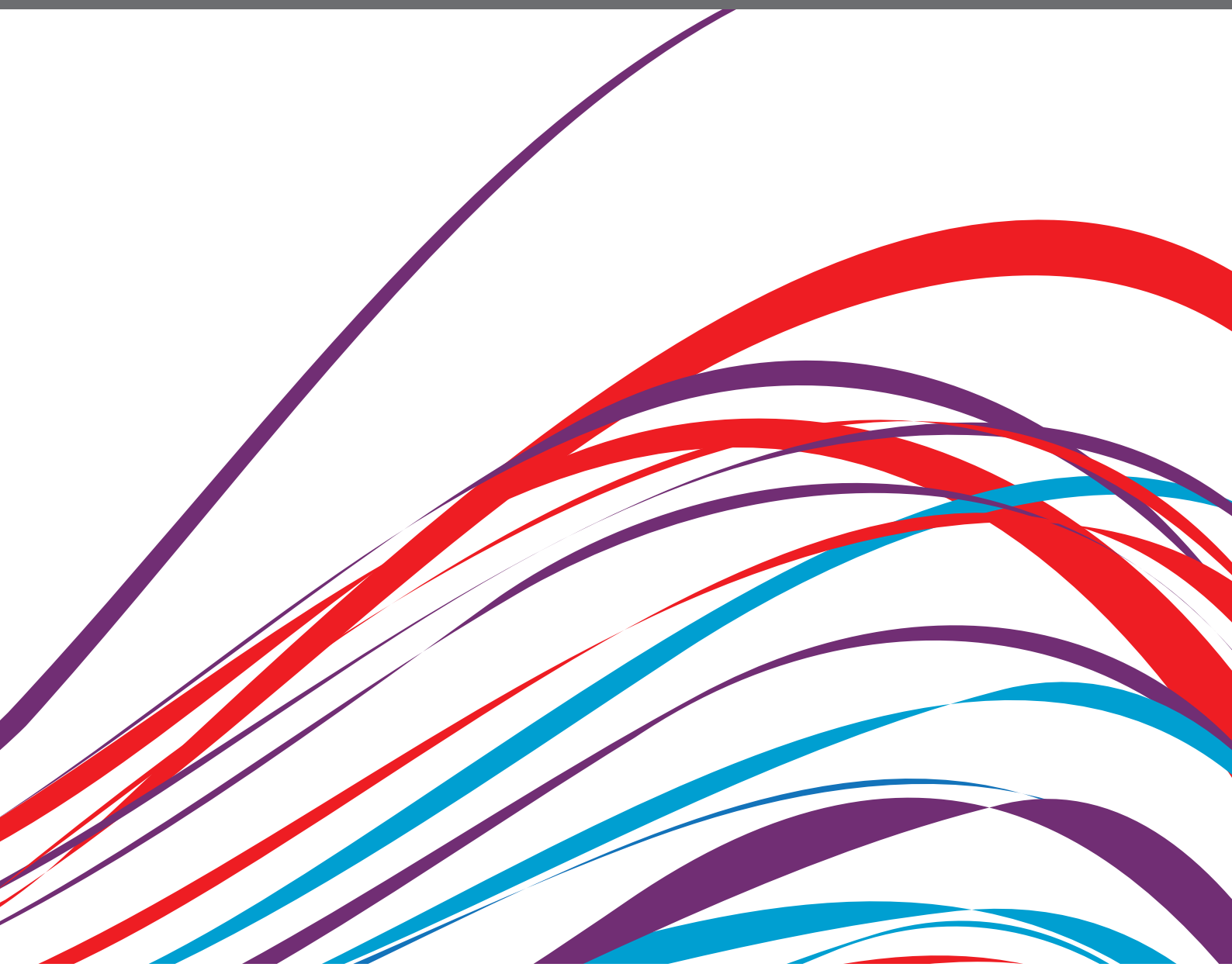

frontiers Research Topics

ISSN 1664-8714
ISBN 978-2-88974-797-9
DOI 10.3389/978-2-88974-797-9

About Frontiers

Frontiers is more than just an open-access publisher of scholarly articles: it is a pioneering approach to the world of academia, radically improving the way scholarly research is managed. The grand vision of Frontiers is a world where all people have an equal opportunity to seek, share and generate knowledge. Frontiers provides immediate and permanent online open access to all its publications, but this alone is not enough to realize our grand goals.

Frontiers Journal Series

The Frontiers Journal Series is a multi-tier and interdisciplinary set of open-access, online journals, promising a paradigm shift from the current review, selection and dissemination processes in academic publishing. All Frontiers journals are driven by researchers for researchers; therefore, they constitute a service to the scholarly community. At the same time, the Frontiers Journal Series operates on a revolutionary invention, the tiered publishing system, initially addressing specific communities of scholars, and gradually climbing up to broader public understanding, thus serving the interests of the lay society, too.

Dedication to Quality

Each Frontiers article is a landmark of the highest quality, thanks to genuinely collaborative interactions between authors and review editors, who include some of the world's best academicians. Research must be certified by peers before entering a stream of knowledge that may eventually reach the public - and shape society; therefore, Frontiers only applies the most rigorous and unbiased reviews.
Frontiers revolutionizes research publishing by freely delivering the most outstanding research, evaluated with no bias from both the academic and social point of view. By applying the most advanced information technologies, Frontiers is catapulting scholarly publishing into a new generation.

What are Frontiers Research Topics?

Frontiers Research Topics are very popular trademarks of the Frontiers Journals Series: they are collections of at least ten articles, all centered on a particular subject. With their unique mix of varied contributions from Original Research to Review Articles, Frontiers Research Topics unify the most influential researchers, the latest key findings and historical advances in a hot research area! Find out more on how to host your own Frontiers Research Topic or contribute to one as an author by contacting the Frontiers Editorial Office: frontiersin.org/about/contact

IMMUNOMETABOLISM, ATHEROSCLEROSIS AND METABOLIC DISEASES

Topic Editors:
Xuewei Zhu, Wake Forest Baptist Medical Center, United States
Changcheng Zhou, University of California, United States
Soonkyu Chung, University of Massachusetts Amherst, United States
Hanrui Zhang, Columbia University, United States

Citation: Zhu, X., Zhou, C., Chung, S., Zhang, H., eds. (2022). Immunometabolism, Atherosclerosis and Metabolic Diseases. Lausanne: Frontiers Media SA.
doi: 10.3389/978-2-88974-797-9

Table of Contents

frontiers in Cardiovascular Medicine

ORIGINAL RESEARCH
published: 15 June 2021
doi: 10.3389/fcvm.2021.685385

Change in Postprandial Level of Remnant Cholesterol After a Daily Breakfast in Chinese Patients With Hypertension

Jin Xu[1,2,3,4†], *Peiliu Qu*[1,2,3,4†], *Xiao Du*[1,2,3,4], *Qunyan Xiang*[1,2,3,4], *Liling Guo*[1,2,3,4], *Liyuan Zhu*[1,2,3,4], *Yangrong Tan*[1,2,3,4], *Yan Fu*[1,2,3,4], *Tie Wen*[5,6] *and Ling Liu*[1,2,3,4*]

[1] *Department of Cardiovascular Medicine, The Second Xiangya Hospital, Central South University, Changsha, China,* [2] *Research Institute of Blood Lipid and Atherosclerosis, Central South University, Changsha, China,* [3] *Modern Cardiovascular Disease Clinical Technology Research Center of Hunan Province, Changsha, China,* [4] *Cardiovascular Disease Research Center of Hunan Province, Changsha, China,* [5] *Department of Emergency Medicine, Second Xiangya Hospital, Central South University, Changsha, China,* [6] *Emergency Medicine and Difficult Diseases Institute, Second Xiangya Hospital, Central South University, Changsha, China*

OPEN ACCESS

Edited by:
Changcheng Zhou,
University of California, Riverside, United States

Reviewed by:
Yipeng Sui,
Baker University, United States
Xiang-An Li,
University of Kentucky, United States

****Correspondence:***
Ling Liu
feliuling@csu.edu.cn

†These authors have contributed equally to this work

Specialty section:
This article was submitted to Lipids in Cardiovascular Disease, a section of the journal Frontiers in Cardiovascular Medicine

Received: *25 March 2021*
Accepted: *11 May 2021*
Published: *15 June 2021*

Citation:
Xu J, Qu P, Du X, Xiang Q, Guo L, Zhu L, Tan Y, Fu Y, Wen T and Liu L (2021) Change in Postprandial Level of Remnant Cholesterol After a Daily Breakfast in Chinese Patients With Hypertension. Front. Cardiovasc. Med. 8:685385. doi: 10.3389/fcvm.2021.685385

Background: Hypertension (HBP) is usually accompanied by hypertriglyceridemia that represents the increased triglyceride-rich lipoproteins and cholesterol content in remnant lipoproteins [i.e., remnant cholesterol (RC)]. According to the European Atherosclerosis Society (EAS), high RC (HRC) is defined as fasting RC ≥0.8 mmol/L and/or postprandial RC ≥0.9 mmol/L. However, little is known about postprandial change in RC level after a daily meal in Chinese patients with HBP.

Methods: One hundred thirty-five subjects, including 90 hypertensive patients (HBP group) and 45 non-HBP controls (CON group), were recruited in this study. Serum levels of blood lipids, including calculated RC, were explored at 0, 2, and 4 h after a daily breakfast. Receiver operating characteristic (ROC) curve analysis was used to determine the cutoff point of postprandial HRC.

Results: Fasting TG and RC levels were significantly higher in the HBP group ($P < 0.05$), both of which increased significantly after a daily meal in the two groups ($P < 0.05$). Moreover, postprandial RC level was significantly higher in the HBP group ($P < 0.05$). ROC curve analysis showed that the optimal cutoff point for RC after a daily meal to predict HRC corresponding to fasting RC of 0.8 mmol/L was 0.91 mmol/L, which was very close to that recommended by the EAS, i.e., 0.9 mmol/L. Fasting HRC was found in 31.1% of hypertensive patients but not in the controls. According to the postprandial cutoff point, postprandial HRC was found in approximately half of hypertensive patients and ∼1-third of the controls.

Conclusion: Postprandial RC level increased significantly after a daily meal, and hypertensive patients had higher percentage of HRC at both fasting and postprandial states. More importantly, the detection of postprandial lipids could be helpful to find HRC.

Keywords: hypertension, postprandial, remnant cholesterol, cut-off point, a daily breakfast

BACKGROUND

As important atherogenic risk factors, hypertension (HBP) and hyperlipidemia usually coexist (1). Evidence showed that hypertriglyceridemia and visceral obesity predicted the prevalence of HBP in the Chinese population (2, 3). Hypertriglyceridemia represents the increased number of triglyceride-rich lipoproteins (TRLs) and their remnant lipoproteins (RLPs) in the circulation (4, 5). Compared with nascent TRLs, RLPs with smaller diameter contain more cholesterol (6). The atherosclerotic effect of RLPs is no less than that of low-density lipoprotein (LDL) (6). The content of cholesterol within RLPs is termed as remnant cholesterol (RC). Both cross-sectional study and prospective research showed that RC was associated with the development of HBP (7, 8). Moreover, elevated RC level can predict the risk of coronary heart disease, just like the increased level of LDL cholesterol (LDL-C) (9–11). Thus, it is essential to detect the RC level in hypertensive patients.

RC level can be calculated as total cholesterol (TC) minus LDL-C minus high-density lipoprotein cholesterol (HDL-C), using fasting or postprandial lipid profiles (12). Fasting RC levels in the general population should not exceed 0.8 mmol/L (13–15). Since 2016, postprandial detection of blood lipids has been recommended in the clinical practice (12). According to the European joint consensus statement from the European Atherosclerosis Society (EAS), postprandial RC level after a daily meal in the subjects with fasting RC <0.8 mmol/L should not exceed 0.9 mmol/L (12). However, the postprandial cutoff point of RC corresponding to fasting RC of 0.8 mmol/L in the Chinese population is still unclear. In this investigation, we compared the changes in blood lipids between hypertensive patients and their controls after a daily meal and further analyzed the optimal postprandial cutoff point of RC in Chinese subjects after a daily meal corresponding to fasting RC of 0.8 mmol/L.

METHODS

Study Subjects

One hundred thirty-five inpatients aged 31 to 78 years, including 90 documented HBP patients (HBP group) and 45 non-HBP controls (CON group), were recruited in this study in the Department of Cardiovascular Medicine of the Second Xiangya Hospital, Central South University. All subjects were invited to fill out a questionnaire about their medical history and use of medication before participation. Inclusion criteria for the HBP group were as follows: patients with history of systolic blood pressure values ≥140 mm Hg and/or diastolic blood pressure values ≥90 mm Hg for at least 3 days (16, 17). Inclusion criteria for the CON group were as follows: contemporaneous controls without clinical history and manifestation of HBP. Exclusion criteria were secondary HBP, diabetes, thyroid diseases, liver and kidney disease dysfunction, autoimmune disease, cancer, or other severe serious medical illnesses. This study was approved by the Ethics Committee of the Second Xiangya Hospital of Central South University, and informed consent was gained from all participants.

Specimen Collection

After at least 12 h of overnight fasting, venous blood samples were collected in all subjects before (i.e., 0 h) and at 2 h, 4 h after taking a daily breakfast according to their daily habits, such as steamed bread, rice porridge, or noodles. All subjects were required to complete the meal in 15 min. All subjects took antihypertensive drugs as usual, including angiotensin-converting enzyme inhibitor, angiotensin receptor blocker, calcium-channel blockers, diuretics, and so on. Most patients took at least two antihypertensive drugs, and blood pressure was monitored throughout the process.

Laboratory Assays

Blood samples were analyzed as described previously (11, 18). Briefly, serum levels of TC, triglyceride (TG), and HDL-C were measured by a laboratory technician who had no knowledge of this study. LDL-C level was calculated using the Friedewald formula: LDL-C = TC − (HDL-C) − (TG/2.2) when TG was <4.5 mmol/L; otherwise, it was directly measured by chemical masking method. RC and non–HDL-C levels were estimated by the following formula: RC = TC − (HDL-C) − (LDL-C), non–HDL-C = TC − (HDL-C).

Statistical Analysis

Quantitative variables were expressed as mean ± standard deviation for normal distribution and median and quartile for skew distribution unless specifically explained, and qualitative variables were expressed as numbers and percentages. Differences between the intragroup and intergroup means were analyzed by unpaired *t*-test or one-way analysis of variance. Categorical variables were compared using χ^2 test. Overweight/obesity was defined as body mass index ≥24 kg/m^2. The area under the curve (AUC) was estimated by the trapezoid method. The optimal cutoff point for postprandial RC was determined using receiver operating characteristic (ROC) curve analysis (11). All statistical analyses were performed using SPSS version 25.0, and two-tailed $P < 0.05$ was considered statistically significant.

RESULTS

Clinical Characteristics and Fasting Blood Lipids of Two Groups

There was no significant difference in age, gender, body mass index, heart rate, and the percentage of current smoking between the two groups. The HBP group had a higher percentage of overweight/obesity and diastolic and systolic blood pressures than the CON group; however, the difference did not reach statistical significance. Moreover, fasting levels of TC, TG, non–HDL-C, and RC were significantly higher in the HBP group

Abbreviations: AUC, area under the curve; CON, non-HBP controls; EAS, European atherosclerosis society; HBP, hypertension; HDL-C, high-density lipoprotein cholesterol; HRC, high remnant cholesterol; LDL, low-density lipoprotein; LDL-C, low-density lipoprotein cholesterol; non–HDL-C, non–high-density lipoprotein cholesterol; RC, remnant cholesterol; RLPs, remnant lipoproteins; ROC curve, receiver operating characteristic; TC, total cholesterol; TG, triglyceride; TRLs, triglyceride-rich lipoproteins.

TABLE 1 | Comparison of clinical characteristics and fasting blood lipids of the two groups.

	HBP ($n = 90$)	CON ($n = 45$)
Age (y)	53 (46–62)	54 (49.5–60)
Male, *n* (%)	51 (56.67)	22 (48.89)
BMI (kg/m^2)	23.63 (22.17–26.24)	23.46 (21.03–24.55)
Overweight, *n* (%)	37 (41.11)	12 (26.67)
Systolic pressure (mm Hg)	133.5 (120.75–149.25)	128 (121–136.5)
Diastolic pressure (mm Hg)	84 (73–92)	80 (74.5–88)
Heart rate (bpm)	78 (69.75–87)	77 (68–88)
Current smoking, *n* (%)	20 (22.22)	12 (26.67)
TC (mmol/L)	4.46 ± 0.92*	4.09 ± 0.66
HDL-C (mmol/L)	1.15 ± 0.29	1.20 ± 0.29
LDL-C (mmol/L)	2.56 ± 0.76	2.41 ± 0.49
TG (mmol/L)	1.48 (1.075–1.98)*	1.07 (0.78–1.29)
nonHDL-C (mmol/L)	3.31 ± 0.86*	2.89 ± 0.52
RC (mmol/L)	0.75 ± 0.37*	0.49 ± 0.16

*BMI, body mass index; bpm, beats/min; TC, total cholesterol; HDL-C, high-density lipoprotein cholesterol; LDL-C, low-density lipoprotein cholesterol; TG, triglyceride; non–HDL-C, non–high-density lipoprotein cholesterol; RC, remnant lipoprotein cholesterol; *P < 0.05 when compared with CON group.*

($P < 0.05$), whereas those of HDL-C and LDL-C were similar between the two groups (**Table 1**).

Postprandial Changes in Serum Levels of Blood Lipids in the Two Groups

After a daily breakfast, the levels of TC, HDL-C, and LDL-C significantly reduced in the two groups (**Figures 1A–C**). Postprandial non–HDL-C level significantly decreased in the HBP group ($P < 0.05$) but not in the CON group (**Figure 1D**). Postprandial levels of TG and RC increased tremendously in the two groups ($P < 0.05$, **Figures 1E,F**).

Postprandial levels of TC, TG, non–HDL-C, and RC in the HBP group were significantly higher than those in the CON group, whereas there was no significant difference in the postprandial levels of HDL-C and LDL-C between the two groups ($P < 0.05$, **Figures 1A–F**).

AUCs of TC, TG, non–HDL-C, and RC in the HBP group were significantly higher than those in the CON group ($P < 0.05$); however, AUCs of HDL-C and LDL-C were similar in the two groups (**Figure 1G**).

The Contribution of Blood Lipids to HBP

To determine the contribution of blood lipids to HBP, forward selection logistic regression analysis was performed. Among all the lipid profiles at fasting state, only the fasting RC level independently contributed to the occurrence of HBP [odds ratio (OR), 68.869; 95% confidence interval (CI), 8.533–554.560; $P < 0.001$, **Supplementary Table 1**].

For the close relationship between fasting and postprandial RC levels at 2 h ($r = 0.73$, $P < 0.001$) and 4 h ($r = 0.64$, $P < 0.001$), the contribution of postprandial RC levels to HBP was also evaluated by forward selection regression analysis. When age, sex, body mass index, smoking history, and RC level at each timepoint were included in covariates, postprandial RC level at 4 h also independently contributed to the occurrence of HBP (OR, 2.435; 95% CI, 1.044–5.675; $P = 0.039$; **Supplementary Tables 2–4**) in addition to fasting RC level.

Determination of the Postprandial Optimal Cutoff Point Corresponding to Fasting High RC

Considering that the postprandial RC level reached peak value at 4 h after a daily breakfast and the independent contribution of the RC level at 4 h to HBP, ROC analysis was performed at 4 h. The optimal cutoff point for RC at 4 h to predict high RC (HRC) in relation to fasting RC of 0.8 mmol/L was 0.9095≈0.91 mmol/L (sensitivity 82.1%, specificity 70.1%, and AUC 0.806; $P < 0.001$; **Figure 2A**), which was close to the optimal cutoff point, 0.9 mmol/L, after a daily meal recommended by the EAS expert consensus. Moreover, when RC levels at 2 and 4 h were pooled together, ROC analysis also showed 0.9095 mmol/L as the optimal cutoff point after a daily meal (sensitivity 83.9%, specificity 71.0%, and AUC 0.832; $P < 0.001$; **Figure 2B**).

Comparisons of the Percentages of Postprandial HRC Between the Two Groups

According to the optimal cutoff points of RC recommended by the EAS expert consensus (10), fasting HRC (≥0.8 mmol/L) was found in 31.1% of subjects in the HBP group; however, the percentages of postprandial HRC (≥0.9 mmol/L) significantly increased to 44.4% at 2 h and 47.8% at 4 h, respectively ($P < 0.05$). When the RC level was detected at both fasting and postprandial states at 2 or 4 h in the same subjects, the percentages of HRC significantly increased to 48.9% or 53.3% ($P < 0.05$, **Figures 3A,B**).

Although no subject in the CON group had fasting RC level ≥0.8 mmol/L, postprandial HRC (≥0.9 mmol/L) was found in 35.6% of subjects at 2 h and in 33.3% at 4 h in the CON group, respectively ($P < 0.05$, **Figures 3A,B**).

DISCUSSION

In this study, the optimal cutoff point of postprandial RC level after a daily meal corresponding to fasting RC level of 0.8 mmol/L was first determined in Chinese subjects. Interestingly, it was close to that recommended by the EAS expert consensus (12). Moreover, higher RC level and higher proportion of HRC were found in the HBP group in both fasting and postprandial states, suggesting that HBP patients could be at greater cardiovascular risk due to abnormal TRL metabolism, in addition to HBP.

RC level can be accurately detected through several expensive and complex methods, including ultracentrifugation, nuclear magnetic resonance, immune separation, and so on (19–21). However, those kinds of accurate detection are very difficult to be widely used in the primary hospitals. The formula method recommended by the EAS expert consensus gives doctors the opportunity to estimate the RC level without additional cost (12).

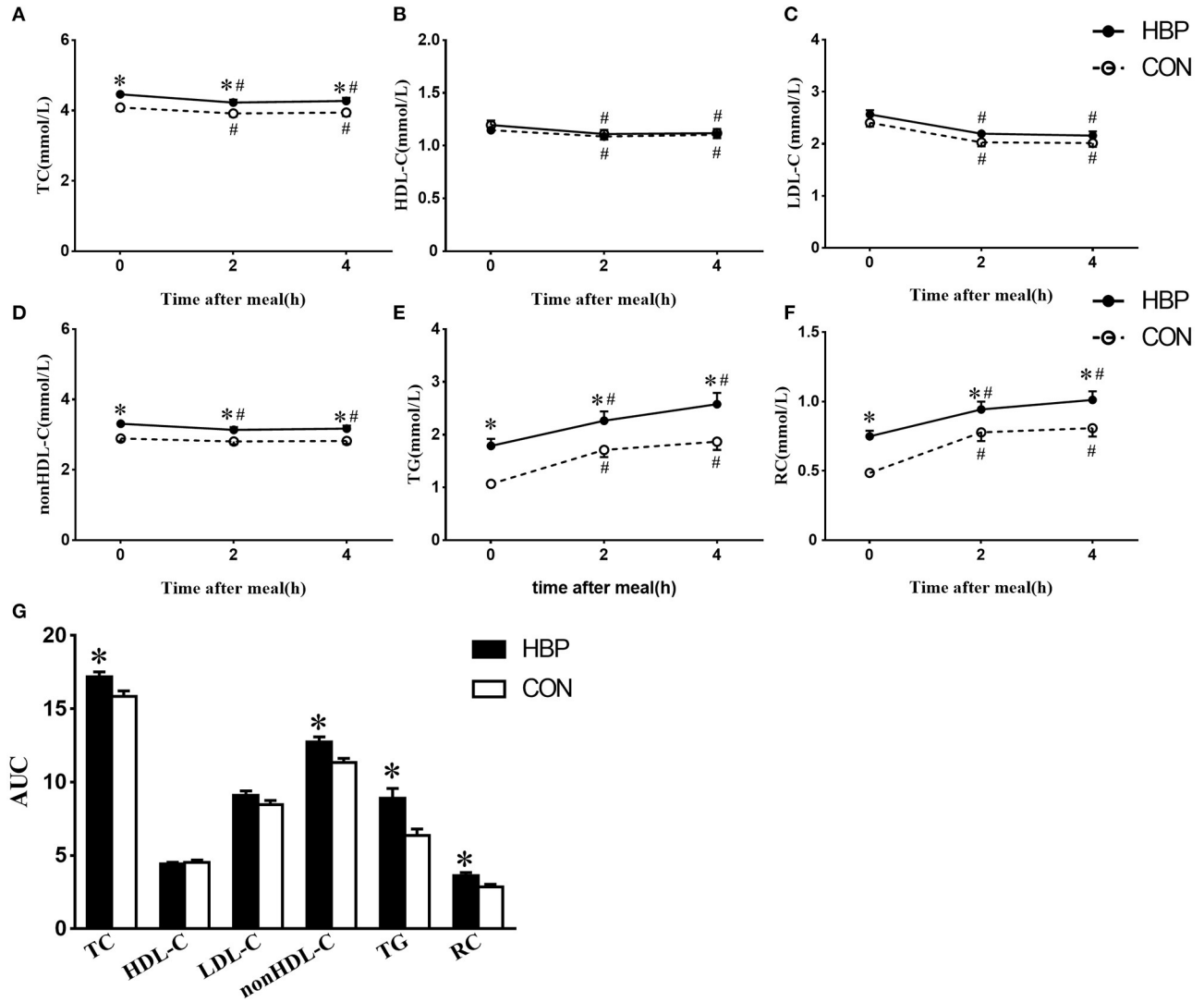

FIGURE 1 | Changes in serum levels of blood lipids after a daily meal in the two groups. **(A–F)** Postprandial changes in serum levels of TC, HDL-C, non–HDL-C, LDL-C, TG, and RC after a daily meal in the HBP group (solid line) and CON group (dotted line). The bar represents standard error of the mean. **(G)** Comparison of AUC of blood lipids after a daily meal between the two groups. $^{*}P < 0.05$ when compared with the CON group at the same time point. $^{\#}P < 0.05$ when compared with the fasting level in the same group.

Elevation of the RC level indicated the excessive overproduction of nascent TRLs and/or delayed removal of RLPs in patients with HBP. And this situation persisted in the postprandial state. Similar conditions were also found in the TG level. Those results suggested that there is a close relationship between HBP and abnormal metabolism of TRLs/RLPs.

There are several mechanisms that can explain the relationship between TRLs/RLPs and the development of HBP. First, TRLs and RLPs could directly and indirectly promote the production of aldosterone, which plays an important role in the pathogenesis of HBP (22–24). It was shown that the expression and secretion of aldosterone in adrenal cells were induced by very-low-density lipoproteins, the main ingredients of TRLs (25–27). One possible explanation is that phospholipase D mediated aldosterone synthase expression (27). Second, RLPs can cause endothelial dysfunction, which is one of the key mechanisms of HBP (28). Postprandially increased RLPs can directly impair arterial vasodilation of the separated vascular ring through inducing oxidative damage (29). In addition, clinical studies also showed the relationship between RC and HBP. It was found that high fasting RC level was associated with the development of HBP after 10 years in Japanese subjects who had normal blood pressure at baseline (8). Winkler et al. (7) also reported that TRLs were associated with HBP in preeclampsia. These findings indirectly support the potential contributions of HTG to HBP.

It is well-known that people spend most of the day at the postprandial state. Moreover, a considerable number of

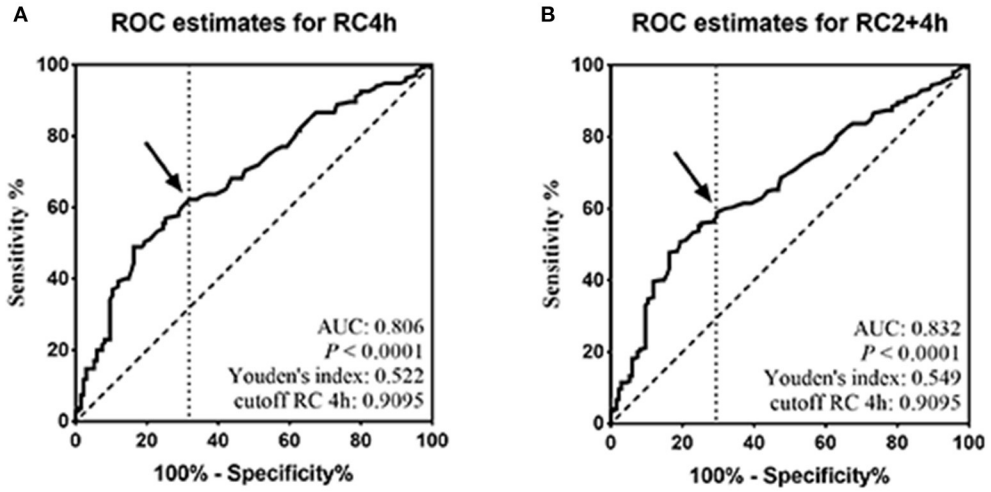

FIGURE 2 | Determination of the postprandial optimal cutoff point corresponding to fasting high RC. **(A,B)** ROC analysis and Youden index determined a cutoff point for postprandial HRC at 4 h (pRC4 h) or at both 2 and 4 h (pRC2+4 h) after a daily meal; the cutoff point was indicated by the solid arrow.

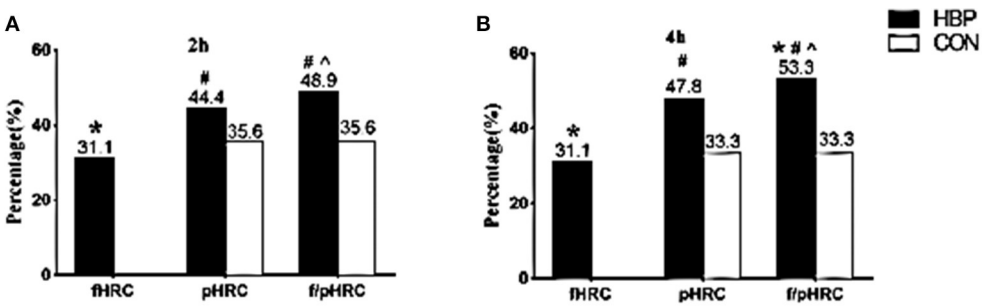

FIGURE 3 | Comparisons of the percentages of HRC between the two groups at different states. **(A,B)** Comparisons of the percentages of fasting HRC only (fasting RC ≥0.8 mmol/L, fHRC), postprandial HRC only (postprandial RC ≥0.9 mmol/L, pHRC), either fasting or postprandial HRC (fasting RC ≥0.8 mmol/L or postprandial RC ≥0.9 mmol/L, f/pHRC) at 2 or 4 h after a daily breakfast. $^{*}P < 0.05$ when compared with CON group. $^{\#}P < 0.05$ when compared with the percentage at fasting state in the HBP group. $^{\wedge}P < 0.05$ when compared with the percentage of pHRC in the HBP group.

subjects visit the medical services at the postprandial state. Thus, some patients with high TG or RC level may be missed if blood lipids were limited to detect at the fasting state. According to the EAS expert consensus and the statement from the American Heart Association, the postprandial TG level in an individual with fasting TG <1.7 mmol/L should not increase above 2.0 and 2.26 mmol/L, respectively, after consuming a daily meal (12, 15). Recently, we determined a cutoff point for postprandial TG level 2.02 mmol/L at 4 h after a daily breakfast corresponding to fasting TG level 1.7 mmol/L in Chinese subjects (30), which is close to the cutoff point for postprandial TG level 2.0 mmol/L recommended by the EAS expert consensus (12). However, as expected of the EAS expert consensus, there was no recommendation about fasting and postprandial RC levels in the United States or China.

In this study, the cutoff point of postprandial RC level corresponding to fasting RC level of 0.8 mmol/L was ∼0.91 mmol/L after a daily meal in Chinese subjects, which was quite near to that recommended by the EAS expert consensus, i.e., 0.9 mmol/L (12). It suggests that Chinese subjects may share similar cutoff points with the Europeans after a daily meal. When postprandial RC of 0.9 mmol/L was used to evaluate the percentage of postprandial HRC in each group, postprandial HRC was found in more hypertensive patients and about one-third controls. The postprandial increase in HRC in the two groups could be associated not only with their own habitual breakfasts, but also with the existence of some subjects with overweight/obesity and smoking in each group. Decreased hydrolysis of TRLs was reported in smokers and patients with obesity (31–33). If both fasting and postprandial blood lipids were detected in a certain subject, the diagnostic rate of HRC could be further improved, although it is not feasible in the real world. Certainly, the detection of postprandial RC level can find more patients with HRC and is worth carrying out in the clinical practice.

This study is associated with several limitations. First, the number of cases in this study was relatively small compared to other similar studies (34). Second, 94% of subjects had breakfasts in the hospital canteen, which could be different from their usual diets at home, although they can freely choose food according to their daily habits. Third, LDL-C and RC levels were calculated by Friedewald formula, which may cause deviation with those directly measured or calculated by other formulas (35).

In conclusion, postprandial RC level increased significantly after a daily meal, and hypertensive patients had significantly higher percentage of HRC than the controls. More importantly, the postprandial detection of blood lipids could be helpful to find HRC.

DATA AVAILABILITY STATEMENT

The raw data supporting the conclusions of this article will be made available by the authors, without undue reservation.

ETHICS STATEMENT

The studies involving human participants were reviewed and approved by Ethics Committee of the Second Xiangya Hospital of Central South University. The patients/participants provided their written informed consent to participate in this study.

AUTHOR CONTRIBUTIONS

JX, PQ, QX, LG, LZ, YT, and YF carried out the experimental work and the data collection and interpretation. PQ, XD, TW, and LL participated in the design and coordination of experimental work. JX, PQ, and LL carried out the study design, the analysis and interpretation of data, and drafted the manuscript. All authors contributed to the article and approved the submitted version.

FUNDING

This study was supported by National Natural Science Foundation of China (grant numbers 81270956, 81470577).

SUPPLEMENTARY MATERIAL

The Supplementary Material for this article can be found online at: https://www.frontiersin.org/articles/10.3389/fcvm.2021.685385/full#supplementary-material

REFERENCES

1. Sande GE, Giles TD. Hypertension and lipids: lipid factors in the hypertension syndrome. *Curr Hypertens Rep.* (2002) 4:458–63. doi: 10.1007/s11906-002-0026-1
2. Feng RN, Zhao C, Wang C, Niu YC, Li K, Guo FC, et al. BMI is strongly associated with hypertension, and waist circumference is strongly associated with type 2 diabetes and dyslipidemia, in northern Chinese adults. *J Epidemiol.* (2012) 22:317–23. doi: 10.2188/jea.JE20110120
3. Han M, Qie R, Li Q, Liu L, Huang S, Wu X, et al. Chinese visceral adiposity index, a novel indicator of visceral obesity for assessing the risk of incident hypertension in a prospective cohort study. *Br J Nutr.* (2020). doi: 10.1017/S0007114520004298. [Epub ahead of print].
4. Kolovou G, Ooi TC. Postprandial lipaemia and vascular disease. *Curr Opin Cardiol.* (2013) 28:446–51. doi: 10.1097/HCO.0b013e3283606971
5. Fernandez-Arroyo S, Hernandez-Aguilera A, de Vries MA, Burggraaf B, van der Zwan E, Pouw N, et al. Effect of Vitamin D3 on the postprandial lipid profile in obese patients: a non-targeted lipidomics study. *Nutrients.* (2019) 11:1194. doi: 10.3390/nu11051194
6. Blackburn P, Lamarche B, Couillard C, Pascot A, Bergeron N, Prud'homme D, et al. Postprandial hyperlipidemia: another correlate of the "hypertriglyceridemic waist" phenotype in men. *Atherosclerosis.* (2003) 171:327–36. doi: 10.1016/j.atherosclerosis.2003.06.001
7. Winkler K, Wetzka B, Hoffmann MM, Friedrich I, Kinner M, Baumstark MW, et al. Triglyceride-rich lipoproteins are associated with hypertension in preeclampsia. *J Clin Endocrinol Metab.* (2003) 88:1162–6. doi: 10.1210/jc.2002-021160
8. Kasahara A, Adachi H, Hirai Y, Enomoto M, Fukami A, Yoshikawa K, et al. High level of plasma remnant-like particle cholesterol may predispose to development of hypertension in normotensive subjects. *Am J Hypertens.* (2013) 26:793–8. doi: 10.1093/ajh/hpt011
9. McNamara JR, Shah PK, Nakajima K, Cupples LA, Wilson PW, Ordovas JM, et al. Remnant-like particle (RLP) cholesterol is an independent cardiovascular disease risk factor in women: results from the framingham heart study. *Atherosclerosis.* (2001) 154:229–36. doi: 10.1016/S0021-9150(00)00484-6
10. Peng J, Luo F, Ruan G, Peng R, Li X. Hypertriglyceridemia and atherosclerosis. *Lipids Health Dis.* (2017) 16:233. doi: 10.1186/s12944-017-0625-0
11. Xu J, Chen YQ, Zhao SP, Liu L. Determination of optimal cut-off points after a high-fat meal corresponding to fasting elevations of triglyceride and remnant cholesterol in Chinese subjects. *Lipids Health Dis.* (2019) 18:206. doi: 10.1186/s12944-019-1146-9
12. Nordestgaard BG, Langsted A, Mora S, Kolovou G, Baum H, Bruckert E, et al. Fasting is not routinely required for determination of a lipid profile: clinical and laboratory implications including flagging at desirable concentration cut-points-a joint consensus statement from the European atherosclerosis society and European federation of clinical chemistry and laboratory medicine. *Eur Heart J.* (2016) 37:1944–58. doi: 10.1093/eurheartj/ehw152
13. Hu DY. New guidelines and evidence for the prevention and treatment of dyslipidemia and atherosclerotic cardiovascular disease in China. *Zhonghua Xin Xue Guan Bing Za Zhi.* (2016) 44:826–7. doi: 10.3760/cma.j.issn.0253-3758.2016.10.002
14. Catapano AL, Graham I, De Backer G, Wiklund O, Chapman MJ, Drexel H, et al. 2016 ESC/EAS guidelines for the management of dyslipidaemias. *Eur Heart J.* (2016) 37:2999–3058. doi: 10.1093/eurheartj/ehw272
15. Ray KK, Kastelein JJ, Boekholdt SM, Nicholls SJ, Khaw KT, Ballantyne CM, et al. The ACC/AHA 2013 guideline on the treatment of blood cholesterol to reduce atherosclerotic cardiovascular disease risk in adults: the good the bad and the uncertain: a comparison with ESC/EAS guidelines for the management of dyslipidaemias 2011. *Eur Heart J.* (2014) 35:960–8. doi: 10.1093/eurheartj/ehu107
16. For Control CC, Society CS, Society CN, Chinese Medical Doctor Association Hypertension Committee, Chinese Stroke Association, Editorial Board of Chinese Journal of Cardiology. National guideline for hypertension management in China (2019). *Zhonghua Xin Xue Guan Bing Za Zhi.* (2020) 48:10–46. doi: 10.3760/cma.j.issn.0253-3758.2020.01.004
17. Whelton PK, Carey RM, Aronow WS, Casey DE Jr, Collins KJ, Dennison Himmelfarb C, et al. 2017 Guideline for the prevention, detection, evaluation, and management of high blood pressure in adults: a report of the American college of cardiology/American heart association task force on clinical practice guidelines. *Hypertension.* (2018) 71:e13–115. doi: 10.1161/HYP.0000000000000065

18. Xiang QY, Tian F, Lin QZ, Du X, Zhang SL, Gui YJ, et al. Comparison of remnant cholesterol levels estimated by calculated and measured LDL-C levels in Chinese patients with coronary heart disease. *Clin Chim Acta.* (2020) 500:75–80. doi: 10.1016/j.cca.2019.09.020
19. Okazaki M, Usui S, Tada N, Nakano T, Nakajima K. Relation between RLP-triglyceride to RLP-cholesterol ratio and particle size distribution in RLP-cholesterol profiles by HPLC. *Clin Chim Acta.* (2000) 296:135–49. doi: 10.1016/S0009-8981(00)00213-8
20. Leary ET, Wang T, Baker DJ, Cilla DD, Zhong J, Warnick GR, et al. Evaluation of an immunoseparation method for quantitative measurement of remnant-like particle-cholesterol in serum and plasma. *Clin Chem.* (1998) 44:2490–8. doi: 10.1093/clinchem/44.12.2490
21. Nakada Y, Kurosawa H, Tohyama J, Inoue Y, Ikewaki K. Increased remnant lipoprotein in patients with coronary artery disease–evaluation utilizing a newly developed remnant assay, remnant lipoproteins cholesterol homogenous assay (RemL-C). *J Atheroscler Thromb.* (2007) 14:56–64. doi: 10.5551/jat.14.56
22. Armitage JA, Burke SL, Prior LJ, Barzel B, Eikelis N, Lim K, et al. Rapid onset of renal sympathetic nerve activation in rabbits fed a high-fat diet. *Hypertension.* (2012) 60:163–71. doi: 10.1161/HYPERTENSIONAHA.111.190413
23. Vogt B, Bochud M, Burnier M. The association of aldosterone with obesity-related hypertension and the metabolic syndrome. *Semin Nephrol.* (2007) 27:529–37. doi: 10.1016/j.semnephrol.2007.07.009
24. Briones AM, Nguyen Dinh Cat A, Callera GE, Yogi A, Burger D, He Y, et al. Adipocytes produce aldosterone through calcineurin-dependent signaling pathways: implications in diabetes mellitus-associated obesity and vascular dysfunction. *Hypertension.* (2012) 59:1069–78. doi: 10.1161/HYPERTENSIONAHA.111.190223
25. Xing Y, Rainey WE, Apolzan JW, Francone OL, Harris RB, Bollag WB. Adrenal cell aldosterone production is stimulated by very-low-density lipoprotein (VLDL). *Endocrinology.* (2012) 153:721–31. doi: 10.1210/en.2011-1752
26. Saha S, Bornstein SR, Graessler J, Kopprasch S. Very-low-density lipoprotein mediates transcriptional regulation of aldosterone synthase in human adrenocortical cells through multiple signaling pathways. *Cell Tissue Res.* (2012) 348:71–80. doi: 10.1007/s00441-012-1346-3
27. Tsai YY, Rainey WE, Pan ZQ, Frohman MA, Choudhary V, Bollag WB. Phospholipase D activity underlies very-low-density lipoprotein (VLDL)-induced aldosterone production in adrenal glomerulosa cells. *Endocrinology.* (2014) 155:3550–60. doi: 10.1210/en.2014-1159
28. Wang L, Gill R, Pedersen TL, Higgins LJ, Newman JW, Rutledge JC. Triglyceride-rich lipoprotein lipolysis releases neutral and oxidized FFAs that induce endothelial cell inflammation. *J Lipid Res.* (2009) 50:204–13. doi: 10.1194/jlr.M700505-JLR200
29. Doi H, Kugiyama K, Ohgushi M, Sugiyama S, Matsumura T, Ohta Y, et al. Membrane active lipids in remnant lipoproteins cause impairment of endothelium-dependent vasorelaxation. *Arterioscler Thromb Vasc Biol.* (1999) 19:1918–24. doi: 10.1161/01.ATV.19.8.1918
30. Tian F, Xiang QY, Zhang MY, Chen YQ, Lin QZ, Wen T, et al. Changes in non-fasting concentrations of blood lipids after a daily Chinese breakfast in overweight subjects without fasting hypertriglyceridemia. *Clin Chim Acta.* (2019) 490:147–53. doi: 10.1016/j.cca.2019.01.004
31. Mero N, Syvanne M, Eliasson B, Smith U, Taskinen U. Postprandial elevation of ApoB-48-containing triglyceride-rich particles and retinyl esters in normolipemic males who smoke. *Arterioscler Thromb Vasc Biol.* (1997) 17:2096–102. doi: 10.1161/01.ATV.17.10.2096
32. Mero N, Van Tol A, Scheek LM, Van Gent T, Labeur C, Rosseneu M, et al. Decreased postprandial high density lipoprotein cholesterol and apolipoproteins A-I and E in normolipidemic smoking men: relations with lipid transfer proteins and LCAT activities. *J Lipid Res.* (1998) 39:1493–502. doi: 10.1016/S0022-2275(20)32531-1
33. Mekki N, Christofilis MA, Charbonnier M, Atlan-Gepner C, Defoort C, Juhel C, et al. Influence of obesity and body fat distribution on postprandial lipemia and triglyceride-rich lipoproteins in adult women. *J Clin Endocrinol Metab.* (1999) 84:184–91. doi: 10.1210/jc.84.1.184
34. Hwang YC, Ahn HY, Jeong IK, Ahn KJ, Chung HY. Optimal range of triglyceride values to estimate serum low density lipoprotein cholesterol concentration in Korean adults: the Korea national health and nutrition examination survey. (2009) *J Korean Med Sci.* (2012) 27:1530–5. doi: 10.3346/jkms.2012.27.12.1530
35. Lin QZ, Chen YQ, Guo LL, Xiang QY, Tian F, Wen T, et al. Comparison of non-fasting LDL-C levels calculated by friedewald formula with those directly measured in Chinese patients with coronary heart disease after a daily breakfast. *Clin Chim Acta.* (2019) 495:399–405. doi: 10.1016/j.cca.2019.05.010

Conflict of Interest: The authors declare that the research was conducted in the absence of any commercial or financial relationships that could be construed as a potential conflict of interest.

frontiers in Cardiovascular Medicine

ORIGINAL RESEARCH
published: 21 July 2021
doi: 10.3389/fcvm.2021.718604

Predictive Value of the Triglyceride to High-Density Lipoprotein Cholesterol Ratio for All-Cause Mortality and Cardiovascular Death in Diabetic Patients With Coronary Artery Disease Treated With Statins

Le Wang, Hongliang Cong, Jingxia Zhang, Yuecheng Hu, Ao Wei, Yingyi Zhang, Hua Yang, Libin Ren, Wei Qi and Wenyu Li*

Department of Cardiology, Tianjin Chest Hospital, Tianjin, China

OPEN ACCESS

Edited by:
Hanrui Zhang,
Columbia University, United States

Reviewed by:
Jianting Shi,
Columbia University, United States
Josep Julve,
Institut de Recerca de l'Hospital de la Santa Creu i Sant Pau, Spain

***Correspondence:**
Hongliang Cong
hongliangcong@126.com

Specialty section:
This article was submitted to Lipids in Cardiovascular Disease, a section of the journal Frontiers in Cardiovascular Medicine

Received: *01 June 2021*
Accepted: *29 June 2021*
Published: *21 July 2021*

Citation:
Wang L, Cong H, Zhang J, Hu Y, Wei A, Zhang Y, Yang H, Ren L, Qi W and Li W (2021) Predictive Value of the Triglyceride to High-Density Lipoprotein Cholesterol Ratio for All-Cause Mortality and Cardiovascular Death in Diabetic Patients With Coronary Artery Disease Treated With Statins. Front. Cardiovasc. Med. 8:718604. doi: 10.3389/fcvm.2021.718604

Background and Aims: Studies have highlighted the role of the triglyceride to high-density lipoprotein cholesterol (TG/HDL-C) ratio on subsequent cardiovascular events. However, the association of the TG/HDL-C ratio with survival outcomes in diabetic patients with coronary artery disease (CAD) treated with statins remains unknown. This study aimed to assess the predictive value of the TG/HDL-C ratio for all-cause mortality and cardiovascular death in diabetic patients with CAD treated with statins.

Methods: The data of patients with type 2 diabetes and angiographically-confirmed CAD who were undergoing statin therapy and visited Tianjin Chest Hospital between January 2016 and September 2016 were retrospectively collected. The patients were categorized based on the baseline TG/HDL-C ratio tertile. Kaplan-Meier analysis and multivariate Cox proportional hazard regression were applied to assess the role of the TG/HDL-C ratio in predicting all-cause mortality and cardiovascular death.

Results: A total of 2,080 patients were included. During the 4-year follow-up, 209 patients died, 136 of whom from cardiovascular death. The Kaplan-Meier analyses showed that an increased TG/HDL-C ratio was associated with an increased risk of all-cause mortality ($P < 0.001$) and cardiovascular death ($P < 0.001$). The multivariate cox hazard regression analysis revealed a similar effect of the TG/HDL-C ratio on the risk of all-cause mortality ($P = 0.046$) and cardiovascular death ($P = 0.009$). The role of the TG/HDL-C ratio in predicting all-cause mortality and cardiovascular death was similar among all subgroups ($P > 0.050$). For all-cause mortality, the TG/HDL-C ratio significantly improved the C-statistic from 0.799 to 0.812 ($P = 0.018$), and the net reclassification index (NRI) and integrated discrimination index (IDI) were 0.252 (95% CI: 0.112–0.392; $P < 0.001$) and 0.012 (95% CI: 0.003–0.022; $P = 0.012$), respectively. Similarly, for cardiovascular death, the TG/HDL-C ratio significantly improved the C-statistic from

0.771 to 0.804 ($P < 0.001$), and the NRI and IDI were 0.508 (95% CI: 0.335–0.680; $P < 0.001$) and 0.033 (95% CI: 0.015–0.050; $P < 0.001$).

Conclusion: TG/HDL-C ratio might be useful for predicting all-cause mortality and cardiovascular death in diabetic patients with CAD treated with statins.

Keywords: triglyceride to high-density lipoprotein cholesterol ratio, type 2 diabetes, coronary artery disease, statin, all-cause mortality, cardiovascular death

INTRODUCTION

The role of diabetes mellitus (DM) on subsequent coronary artery disease (CAD) is well-illustrated (1), and studies have demonstrated that the use of statins could reduce the risk of major cardiovascular events (MACEs) in diabetic patients (2–5). However, patients with CAD have a higher prevalence of type 2 DM, and the risk of mortality remains high even in those treated with statins. The residual risk could be attributed to abnormal lipoprotein and lipid levels (6). Therefore, it is necessary that the lipid status be re-evaluated in diabetic patients with CAD treated with statins to identify those with higher residual risk such that tailored risk reduction strategies can be developed.

Dyslipidemia is characterized by elevated triglyceride (TG) and reduced dense high-density lipoprotein cholesterol particles levels, and lower high-density lipoprotein cholesterol (HDL-C) levels in diabetic patients (7, 8). Elevated TG and lower HDL-C are associated with poor prognosis in diabetic patients (9–12), but the use TG or HDL-C alone does not reflect the risk of atherosclerosis and cardiovascular disease (CVD) (13). The TG/HDL-C ratio may reflect the actual lipid profiles, and is considered an important marker of plasma atherosclerosis (14). Moreover, studies found that the TG/HDL-C ratio was an important predictor of insulin resistance and could evaluate the degree of abnormal glucose metabolism (15–17).

Numerous studies have reported a positive relationship between the TG/HDL-C ratio and hypertension (18–20), obesity (21), metabolic syndrome (22–24), hyperuricemia (25), and non-alcoholic fatty liver disease (26, 27). Moreover, an elevated TG/HDL-C ratio plays an important role on heart rate recovery after exercise (28), increased arterial stiffness (29, 30) and increased carotid atherosclerosis (31). Studies have indicated that the TG/HDL-C ratio should be considered as an important primary prevention cardiovascular risk factor, while the strength of the predictive value differs for patients undergoing various status (32–43). Furthermore, the predictive value of the TG/HDL-C ratio for all-cause mortality and cardiovascular death in diabetic patients with CAD treated with statins is unknown. This retrospective cohort study was therefore performed to assess the potential role of the TG/HDL-C ratio in the prediction of all-cause mortality and cardiovascular death in diabetic patients with CAD who were treated with statins.

METHODS

Study Population

Patients who were admitted to Tianjin Chest Hospital between January 2016 and September 2016 were recruited in this retrospective cohort study. A total of 2,678 patients with T2DM and angiographically-confirmed CAD were included. CAD comprised stable angina pectoris (SAP) and acute coronary syndrome (ACS). ACS included unstable angina pectoris, non-ST-segment elevation myocardial infarction, and ST-segment elevation myocardial infarction (STEMI). Patients were excluded if they met any of the following criteria: (1) aged < 18.0 or > 80.0 years ($n = 72$), (2) severe valvular heart disease or congenital heart disease ($n = 34$), (3) alanine aminotransferase level $>$ 3-fold greater than the normal upper limit ($n = 15$), (4) serum creatinine level $>$ 1.5-fold greater than the normal upper limit ($n = 96$), (5) hyperthyroidism or hypothyroidism ($n = 16$), (6) incomplete clinical data ($n = 75$), and (7) not treated with statins ($n = 99$). The remaining 2,271 patients were recruited, and 2,080 patients with full clinical data after 4-year follow-up were included in the final analysis. The patients were categorized based on the tertiles of the baseline TG/HDL-C ratio, as follows: tertile 1 ($n = 693$, TG/HDL-C ratio ≤ 1.20), tertile 2 ($n = 693$, $1.20 <$ TG/HDL-C ratio ≤ 1.92), and tertile 3 ($n = 694$, TG/HDL-C ratio > 1.92). The study was approved by the Ethical Committee of Tianjin Chest Hospital (NO:2021LW-006), and the need to obtain informed consent requirement was waived as the study comprised a retrospective analysis of clinical data.

Data Collection and Definitions

Baseline demographic characteristics, clinical presentation, cardiac function, extent of lesion, treatment strategy, laboratory findings at fasting status, and medication data at discharge were collected from medical records and the data managers were blinded to the study purpose. The demographic characteristics included age; sex ratio; duration of diabetes; smoker proportion; hypertension; prior myocardial infarction (MI), percutaneous coronary intervention (PCI), coronary artery bypass graft (CABG), or stroke; and body mass index (BMI). The cardiac function included left ventricle ejection fraction (LVEF). The clinical presentation included SAP and ACS, and the extent of lesion included left main disease and multi-vessel disease (>2 vessels with $\geq 50\%$ diameter stenosis in major coronary arteries). The treatment strategies included medical therapy, PCI, and CABG. Laboratory findings included fasting plasma glucose (FPG), hemoglobin A1c (HbA1c), total cholesterol (TC), TG, low-density lipoprotein cholesterol (LDL-C), HDL-C, the TG/HDL-C ratio, serum uric acid, high-sensitivity C-reactive protein (hs-CRP), and estimated glomerular filtration rate (eGFR). The medications at discharge included aspirin, clopidogrel/ticagrelor, β-blocker, angiotensin II coenzyme inhibitor (ACEI) or angiotensin II receptor blocker (ARB), calcium channel blocker (CCB), nitrate, and insulin.

Endpoints and Follow-Up Data

The investigated endpoints included all-cause mortality and cardiovascular death. All-cause mortality was defined as death from any cause, and cardiovascular death was defined as death caused by acute MI, heart failure, cardiac arrhythmia, or stroke. The follow-up information was collected by telephone or electronic medical record review.

Statistical Analysis

Continuous variables are presented as the mean [standard deviation (SD)] and median (interquartile) based on data

TABLE 1 | Baseline characteristics of included patients.

Clinical characteristics	Tertile 1 *N* = 693	Tertile 2 *N* = 693	Tertile 3 *N* = 694	*P*-value
Age, years	66.2 ± 6.7	66.2 ± 6.9	66.1 ± 6.7	0.870
Female	293 (42.3)	302 (43.6)	318 (45.8)	0.405
Duration of diabetes	9.5 ± 7.9	9.8 ± 7.5	9.9 ± 7.7	0.636
Smoker	265 (38.2)	289 (41.7)	267 (38.5)	0.337
Hypertension	529 (76.3)	531 (76.6)	525 (75.6)	0.909
Previous MI	80 (11.5)	86 (12.4)	91 (13.1)	0.674
Previous PCI	153 (22.1)	130 (18.8)	132 (19.0)	0.228
Previous CABG	24 (3.5)	25 (3.6)	32 (4.6)	0.479
Previous stroke	157 (22.7)	143 (20.6)	134 (19.3)	0.303
BMI, kg/m^2	25.3 ± 2.9	25.5 ± 2.7	25.7 ± 2.8	0.020
LVEF	58 ± 8	58 ± 9	58 ± 9	0.193
Clinical presentation				0.353
SAP	131 (18.9)	111 (16.0)	118 (17.0)	
ACS	562 (81.1)	582 (84.0)	576 (83.0)	
Left main disease	69 (10.0)	78 (11.3)	71 (10.2)	0.707
Multi-vessel disease	561 (81.0)	563 (81.2)	570 (82.1)	0.841
Treatment strategy				0.880
MT	219 (31.6)	202 (29.1)	214 (30.8)	
PCI	399 (57.6)	410 (59.2)	406 (58.5)	
CABG	73 (10.5)	79 (11.4)	73 (10.5)	
Laboratory findings				
FPG, mmol/L	7.9 ± 2.9	8.0 ± 3.0	8.2 ± 3.3	0.077
HbA1c, %	7.4 ± 1.3	7.5 ± 1.4	7.7 ± 1.6	0.002
TC, mmol/L	4.58 ± 1.16	4.45 ± 1.07	4.31 ± 1.10	<0.001
TG, mmol/L	1.01 (0.81–1.21)	1.52 (1.28–1.79)	2.41 (1.94–3.06)	<0.001
LDL-C, mmol/L	2.96 ± 1.02	2.96 ± 0.94	2.85 ± 0.95	0.053
HDL-C, mmol/L	1.20 ± 0.29	1.01 ± 0.23	0.92 ± 0.22	<0.001
TG/HDL-C ratio	0.88 ± 0.21	1.54 ± 0.20	3.09 ± 1.62	<0.001
Uric acid, umol/L	305.4 ± 93.4	321.7 ± 92.0	331.1 ± 100.3	<0.001
hs-CRP, mg/L	1.50 (0.59–4.76)	1.83 (0.79–4.64)	2.08 (0.94–4.82)	<0.001
eGFR, mL/min	94.0 ± 24.8	92.3 ± 23.8	89.6 ± 24.6	0.003
Medications at discharge				
Aspirin	668 (96.4)	673 (97.1)	675 (97.3)	0.605
Clopidogrel/Ticagrelor	559 (80.7)	574 (82.8)	581 (83.7)	0.307
β-blocker	450 (64.9)	461 (66.5)	456 (65.7)	0.824
ACEI/ARB	404 (58.3)	381 (55.0)	407 (58.6)	0.313
CCB	174 (25.1)	199 (28.7)	203 (29.3)	0.172
Nitrate	382 (55.1)	379 (54.7)	391 (56.3)	0.814
Insulin	284 (41.0)	280 (40.4)	273 (39.3)	0.818

Data are expressed as mean ± SD, medians with interquartile ranges or percentage. MI, myocardial infarction; PCI, percutaneous coronary intervention; CABG, coronary artery bypass graft; BMI; body mass index; LVEF, left ventricle ejection fraction; SAP, stable angina pectoris; ACS, acute coronary syndrome; MT, medical therapy; FPG, fasting plasma glucose; HbA1c, Hemoglobin A1c; TC, total cholesterol; TG, triglycerides; LDL-C, low-density lipoprotein cholesterol; HDL-C, high-density lipoprotein cholesterol; hs-CRP, high-sensitivity C-reactive protein; eGFR, estimated glomerular filtration rate; ACEI, angiotensin II coenzyme inhibitor; ARB, angiotensin II receptor blocker; CCB, calcium channel blocker; SD, standard deviation.

distribution, and the differences among groups were compared using an analysis of variance or the Kruskal-Wallis test. Categorical variables are presented as frequencies and proportions, and the differences among groups were compared using the Chi-square or Fisher's exact tests. The association between the TG/HDL-C ratio and subsequent all-cause mortality and cardiovascular death were assessed using Kaplan-Meier analysis and the log-rank test. Multivariate Cox regression analysis was performed to identify the independent predictors of all-cause mortality and cardiovascular death. All the variables in **Table 1** were listed in univariate model and then were introduced into the multivariate model if the *P*-value was <0.10. The possible factors included age, duration of diabetes, hypertension, previous MI, previous PCI, previous stroke, LVEF, left main disease, multi-vessel disease, FPG, TC, LDL-C, uric acid, hs-CRP, and eGFR. Sensitivity analyses were performed for all-cause mortality and cardiovascular death by sequential adjustment of potential confounders. The C-statistics, net reclassification improvement (NRI), and integrated discrimination improvement (IDI) were applied to assess the incremental predictive value of the TG/HDL-C ratio over the established model (including age, duration of diabetes, previous PCI, LVEF, left main disease, multi-vessel disease, FPG, and eGFR). The optimal cut-off values of the TG/HDL-C ratio for predicting all-cause mortality and cardiovascular death were determined using receiver operating characteristic (ROC) curves. Subgroup analyses for all-cause mortality and cardiovascular death were conducted according to sex (male or female), smoker (yes or no), BMI (≤28 or >28 kg/m^2), duration of DM (≤10 or >10 years), ACS (yes or no), HbA1c (≤7.0 or >7.0%), LDL-C (≤1.8 or >1.8 mmol/L), insulin treatment (yes or no), and revascularization (yes or no). The differences between subgroup analyses were also compared using the interaction *t*-test. All *P*-values are two-sided, and the inspection level was 0.050. The statistical analyses in this study were performed using SPSS version 20.0 (IBM Corp, Armonk, New York) and SAS version 9.1.3 (Cary, NC, USA).

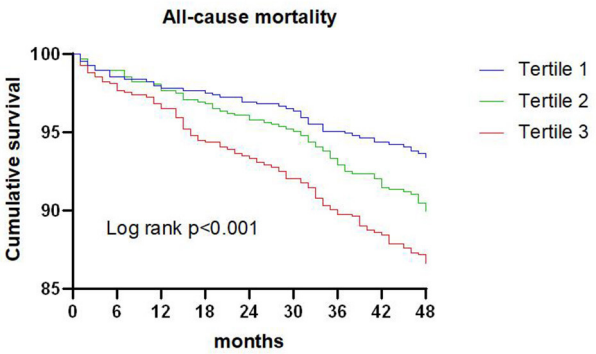

FIGURE 1 | Kaplan-Meier survival curve for all-cause mortality across triglyceride to high density lipoprotein-C ratio tertiles.

RESULTS

Baseline Characteristics

A total of 2,080 diabetic patients with CAD who were treated with statins were selected for analysis. The baseline characteristics of the patients in the three TG/HDL-C ratio categories are summarized in **Table 1**. Most variables did not significantly differ among the groups, including age; sex ratio; duration of diabetes; smoker proportion; hypertension; prior MI, PCI, CABG, or stroke; LVEF; clinical presentation; left main disease; multi-vessel disease; treatment strategy; FPG; LDL-C; aspirin; clopidogrel/ticagrelor; β-blocker; ACEI or ARB; CCB; nitrate; and insulin ($P > 0.050$). However, there were significant differences among the three groups in BMI ($P = 0.020$), HbA1c ($P = 0.002$), TC ($P < 0.001$), TG ($P < 0.001$), HDL-C ($P < 0.001$), TG/HDL-C ratio ($P < 0.001$), serum uric acid ($P < 0.001$), hs-CRP ($P < 0.001$), and eGFR ($P = 0.003$).

TG/HDL-C Ratio and All-Cause Mortality

A total of 209 patients died during the 4-year follow-up, and the proportions of all-cause mortality in tertiles 1, 2, and 3

TABLE 2 | Cox regression models in the prediction of all-cause mortality and cardiovascular death according to the triglyceride to high density lipoprotein-C ratio at baseline.

Endpoint	Events, *n*/total (%)	Crude HR (95% CI)	Crude *P*-value	Adjusted HR (95% CI)	Adjusted *P*-value
All-cause mortality			<0.001		0.046
Tertile 1	46/693 (6.6)	1.00 (reference)		1.00 (reference)	
Tertile 2	70/693 (101.)	1.54 (1.06–2.23)		1.19 (0.81–1.75)	
Tertile 3	93/694 (13.4)	2.09 (1.47–2.98)		1.52 (1.05–2.19)	
Per 1-SD		1.17 (1.10–1.24)	<0.001	1.20 (1.11–1.30)	<0.001
Cardiovascular death			<0.001		0.009
Tertile 1	27/693 (3.9)	1.00 (reference)		1.00 (reference)	
Tertile 2	43/693 (6.2)	1.65 (1.02–2.67)		1.40 (0.85–2.30)	
Tertile 3	66/694 (9.5)	2.55 (1.63–4.00)		2.01 (1.27–3.21)	
Per 1-SD		1.22 (1.16–1.29)	<0.001	1.27 (1.19–1.36)	<0.001

Adjusted variables were age, duration of diabetes, hypertension, previous MI, previous PCI, previous stroke, LVEF, left main disease, multi-vessel disease, FPG, TC, LDL, Uric acid, hs-CRP, eGFR. HR, hazard ratio; CI, confidential interval; SD, standard deviation.

were 6.6, 10.1, and 13.4%, respectively. Kaplan-Meier analysis indicated that an increased TG/HDL-C ratio was associated with an increased risk of all-cause mortality ($P < 0.001$; **Figure 1**). The Cox proportional hazard regression indicated that an increased TG/HDL-C ratio tertile was associated with an increased risk of all-cause mortality, irrespective of whether the unadjusted ($P < 0.001$) or adjusted ($P = 0.046$) was used. Moreover, per SD increment in the TG/HDL-C ratio was associated with an increased risk of all-cause mortality in both the unadjusted model (HR: 1.17; 95% CI: 1.10–1.24; $P < 0.001$) and the adjusted model (HR: 1.20; 95% CI: 1.11–1.30; $P < 0.001$) (**Table 2**). The role of the TG/HDL-C ratio in predicting the risk of all-cause mortality was robust after sequential adjustment for potential confounders (**Table 3**).

ROC analysis indicated that the optimal cutoff value of the TG/HDL-C ratio for predicting all-cause mortality was 1.77 (sensitivity: 53.1% and specificity: 62.8%), and the area under the curve (AUC) was 0.601 (95% CI: 0.561–0.640; $P < 0.001$). Adding the TG/HDL-C ratio to the model of established risk factors including age, duration of diabetes, previous PCI, LVEF, left main disease, multi-vessel disease, FBG, and eGFR improved the prediction of all-cause mortality in terms of the C-statistic (from 0.799 to 0.812; $P = 0.018$), and the NRI and IDI were 0.252 (95% CI: 0.112–0.392; $P < 0.001$) and 0.012 (95% CI: 0.003–0.022; $P = 0.012$), respectively (**Table 4**).

The results of subgroup analyses for all-cause mortality are illustrated in **Table 5**. An elevated TG/HDL-C ratio was associated with an increased risk of all-cause mortality in all subgroups, and the differences between subgroups were not significant based on sex ($P = 0.985$), smoker ($P = 0.173$), BMI ($P = 0.741$), duration of DM ($P = 0.090$), ACS ($P = 0.438$), HbA1c ($P = 0.524$), LDL-C ($P = 0.788$), insulin treatment ($P = 0.265$), and revascularization ($P = 0.780$).

TABLE 3 | Sensitivity analysis of the association of the triglyceride to high density lipoprotein-C ratio per 1 standard deviation with mortality after separate adjustment for each of the other significant variables.

	Multivariable analysis for all-cause mortality			Multivariable analysis for cardiovascular death		
Adjustment	**HR for TG/HDL-C per**			**HR for TG/HDL-C per**		
Variable	**1-SD**	**95%CI**	***P*-value**	**1-SD**	**95%CI**	***P*-value**
Age	1.20	1.13–1.28	<0.001	1.26	1.19–1.33	<0.001
Smoker	1.17	1.10–1.24	<0.001	1.23	1.16–1.30	<0.001
Duration of diabetes	1.17	1.10–1.24	<0.001	1.23	1.16–1.30	<0.001
Hypertension	1.19	1.11–1.26	<0.001	1.25	1.18–1.33	<0.001
Previous MI	1.17	1.10–1.24	<0.001	1.22	1.16–1.29	<0.001
Previous PCI	1.18	1.11–1.25	<0.001	1.24	1.17–1.32	<0.001
Previous stroke	1.17	1.10–1.24	<0.001	1.22	1.16–1.29	<0.001
LVEF	1.20	1.12–1.27	<0.001	1.26	1.19–1.34	<0.001
Left main disease	1.17	1.10–1.24	<0.001	1.23	1.16–1.30	<0.001
Multi-vessel disease	1.17	1.10–1.24	<0.001	1.22	1.16–1.29	<0.001
FPG	1.17	1.10–1.24	<0.001	1.23	1.17–1.30	<0.001
TC	1.16	1.09–1.24	<0.001	1.22	1.16–1.29	<0.001
LDL-C	1.16	1.10–1.24	<0.001	1.23	1.16–1.30	<0.001
Uric acid	1.15	1.08–1.23	<0.001	1.21	1.15–1.29	<0.001
hs-CRP	1.17	1.10–1.25	<0.001	1.23	1.17–1.30	<0.001
eGFR	1.15	1.08–1.23	<0.001	1.21	1.14–1.28	<0.001

MI, myocardial infarction; PCI, percutaneous coronary intervention; LVEF, left ventricle ejection fraction; FPG, fasting plasma glucose; HbA1c, Hemoglobin A1c; TC, total cholesterol; LDL-C, low-density lipoprotein cholesterol; hs-CRP, high-sensitivity C-reactive protein; eGFR, estimated glomerular filtration rate; TG, triglycerides; HDL-C, high-density lipoprotein cholesterol; HR, hazard ratio; CI, confidential interval; SD standard deviation.

TABLE 4 | Evaluation of predictive models for all-cause mortality and cardiovascular death.

Endpoint		**C-Statistic**	***P*-value**	**NRI (95%CI)**	***P*-value**	**IDI (95%CI)**	***P*-value**
All-cause mortality	Original model	0.799 (0.766–0.833)	Ref.		Ref.		Ref.
	Original model+ TG/HDL-C ratio	0.812 (0.780–0.844)	0.018	0.252 (0.112–0.392)	<0.001	0.012 (0.003–0.022)	0.012
Cardiovascular death	Original model	0.771 (0.728–0.814)	Ref.		Ref.		Ref.
	Original model+ TG/HDL-C ratio	0.804 (0.765–0.844)	<0.001	0.508 (0.335–0.680)	<0.001	0.033 (0.015–0.050)	<0.001

Original model included age, duration of diabetes, previous PCI, LVEF, left main disease, multi-vessel disease, FPG and eGFR. TG, triglycerides; HDL-C, high-density lipoprotein cholesterol; NRI, net reclassification improvement; IDI, integrated discrimination improvement; CI, confidential interval.

TABLE 5 | All-cause mortality and cardiovascular death in the various patient subgroups.

Variable	Subgroups	All-cause mortality				Cardiovascular death			
		≤1.77	>1.77	HR (95%CI)	*P* for interaction	≤1.57	>1.57	HR (95%CI)	*P* for interaction
All patient	Total	99/1,274	110/806	1.821 (1.388–2.389)		36/1,083	100/997	3.124 (2.135–4.573)	
Sex	Women	45/555	47/358	1.661 (1.104–2.500)	0.985	15/462	49/451	3.453 (1.936–6.156)	0.552
	Men	54/719	63/448	1.956 (1.360–2.813)		21/621	51/546	2.867 (1.725–4.766)	
Smoker	No	61/770	57/489	1.498 (1.044–2.150)	0.173	21/646	59/613	3.041 (1.848–5.003)	0.537
	Yes	38/504	53/317	2.360 (1.556–3.580)		15/437	41/384	3.262 (1.805–5.893)	
BMI (kg/m^2)	≤28	79/1,058	91/655	1.930 (1.428–2.609)	0.741	33/905	83/808	2.918 (1.949–4.367)	0.285
	>28	20/216	19/151	1.409 (0.752–2.640)		3/178	17/189	5.504 (2.613–8.783)	
Duration of DM (years)	≤10	53/773	63/491	1.933 (1.341–2.785)	0.090	17/654	62/610	4.052 (2.369–6.929)	0.442
	>10	46/501	47/315	1.697 (1.130–2.548)		19/429	38/387	2.291 (1.321–3.973)	
ACS	No	16/241	15/119	1.973 (0.975–3.990)	0.438	4/241	12/119	6.312 (2.036–9.587)	0.346
	Yes	83/1,033	95/687	1.783 (1.328–2.394)		32/842	88/878	2.726 (1.819–4.085)	
HbA1c (%)	≤7.0	41/584	46/336	2.016 (1.323–3.071)	0.524	14/499	43/421	3.803 (2.081–6.952)	0.697
	>7.0	58/690	64/470	1.682 (1.179–2.400)		22/584	57/576	2.700 (1.651–4.415)	
LDL-C (mmol/L)	≤1.8	13/149	16/118	1.608 (0.773–3.343)	0.788	8/136	11/131	3.853 (1.075–13.810)	0.345
	>1.8	86/1,125	94/688	1.854 (1.384–2.483)		51/947	89/866	3.064 (2.055–4.568)	
Insulin treatment	No	51/751	66/492	2.065 (1.433–2.976)	0.265	18/632	61/611	3.616 (2.136–6.112)	0.502
	Yes	48/523	44/314	1.566 (1.040–2.357)		18/451	39/386	2.641 (1.511–4.617)	
Revascularization	No	31/393	35/247	1.876 (1.157–3.042)	0.780	9/327	37/313	4.432 (2.139–9.183)	0.476
	Yes	68/881	75/559	1.796 (1.293–2.494)		27/726	63/684	2.673 (1.703–4.195)	

BMI, body mass index; DM, diabetes mellitus; ACS, acute coronary syndrome; HbA1c, Hemoglobin A1c; LDL-C, low-density lipoprotein cholesterol; HR, hazard ratio; CI, confidential interval.

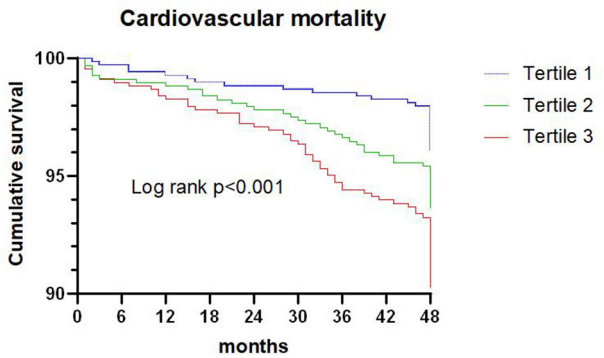

FIGURE 2 | Kaplan-Meier survival curve for cardiovascular death across triglyceride to high density lipoprotein-C ratio tertiles.

TG/HDL-C Ratio and Cardiovascular Death

A total of 136 patients died from cardiovascular death during the 4-year follow-up, and the proportion of cardiovascular death in tertiles 1, 2, and 3 were 3.9, 6.2, and 9.5%, respectively. Kaplan-Meier analysis suggested that the risk of cardiovascular death was significantly increased with an elevated TG/HDL-C ratio ($P < 0.001$; **Figure 2**).

Cox proportional hazard regression indicated that an increased TG/HDL-C ratio tertile was associated with an increased risk of cardiovascular death in both the unadjusted model ($P < 0.001$) and the adjusted model ($P = 0.009$). Furthermore, the risk of cardiovascular death was significantly increased per SD increment in the TG/HDL-C ratio in both the unadjusted model (HR: 1.22; 95% CI: 1.16–1.29; $P < 0.001$) and the adjusted model (HR: 1.27; 95% CI: 1.19–1.36; $P < 0.001$) (**Table 2**). Sensitivity analysis revealed that the association between the TG/HDL-C ratio and the risk of cardiovascular death was robust and not altered by sequential adjustment for potential confounders (**Table 3**).

ROC analysis indicated that the optimal cutoff value of the TG/HDL-C ratio for predicting cardiovascular death was 1.57 (sensitivity: 74.3% and specificity: 53.8%), with an AUC of 0.672 (95% CI: 0.625–0.718; $P < 0.001$). Adding the TG/HDL-C ratio to the established model improved the prediction of cardiovascular death in terms of the C-statistic (from 0.771 to 0.804; $P < 0.001$), and the NRI and IDI were 0.508 (95% CI: 0.335–0.680; $P < 0.001$) and 0.033 (95% CI: 0.015–0.050; $P < 0.001$), respectively (**Table 4**).

The results of the subgroup analyses for cardiovascular death based on pre-defined variables are shown in **Table 5**. An elevated TG/HDL-C ratio was associated with an increased risk of cardiovascular death in all subgroups, and sex ($P = 0.552$), smoker ($P = 0.537$), BMI ($P = 0.285$), duration of DM ($P = 0.442$), ACS ($P = 0.346$), HbA1c ($P = 0.697$), LDL-C ($P = 0.345$), insulin treatment ($P = 0.502$), and revascularization ($P = 0.476$) did not affect the role of TG/HDL-C ratio in predicting the risk of cardiovascular death.

DISCUSSION

This study systematically analyzed the predictive value of the TG/HDL-C ratio for subsequent all-cause mortality and cardiovascular death in diabetic patients with CAD who were treated with statins. An elevated TG/HDL-C ratio was associated with an increased risk of all-cause mortality and cardiovascular death. Sensitivity analyses indicated that the role of TG/HDL-C ratio in predicting subsequent all-cause mortality and cardiovascular death was robust and not altered by sequential adjusted potential confounders. Furthermore, adding the TG/HDL-C ratio to the established model resulted in a significant enhancement of the predictive value. The risk of all-cause mortality and cardiovascular death was significantly increased when the TG/HDL-C ratio was increased in all subgroups, and these associations were not affected by sex, smoker, BMI, duration of DM, ACS, HbA1c, LDL-C, insulin treatment, or revascularization. The above results indicate that the TG/HDL-C ratio is a marker of poor prognosis even in the era of statin treatment and may contribute to the early identification of high-risk diabetic patients and CAD. Furthermore, routine TG/HDL-C ratio calculation may further improve risk stratification for all-cause mortality and cardiovascular death.

LDL-C plays a key role in the development and progression of atherosclerotic CVD (ASCVD) and statins are the first-line therapy for lowering LDL-C levels to reduce ASCVD risk. However, diabetic patients with CAD remain at high cardiovascular risk even after LDL-C reduction, which indicates that there are residual cardiovascular risk factors other than LDL-C. One study found that diabetic patients treated with statins had a high prevalence of persistent atherogenic dyslipidemia (13). Elevated TG levels and lower HDL-C levels, as typical lipid features of diabetes, are considered to indicate atherogenic dyslipidemia in diabetic patients (44, 45). However, the levels of TG and HDL-C are mutually independent, and the single lipid parameter could not reflect the actual status of plasma atherogenicity and CVD risk in the absence of insulin resistance (13). Therefore, the TG/HDL-C ratio could reflect TG and HDL-C simultaneously, and is regarded as a better marker in primary and secondary prevention of CVD (34, 36, 46). A study conducted by Edwards et al. suggested that the TG/HDL-C ratio has better predictive value for mortality than that of individual lipid parameters (47). Furthermore, a high TG/HDL-C ratio may strongly predict the extent of coronary lesions (48, 49). Moreover, the TG/HDL-C ratio is significantly related to vulnerable plaque features in diabetic patients treated with statins (50). Routine lipid examinations do not reflect the actual compositional changes of lipid parameters in diabetic patients with CAD. Therefore, evaluation of the TG/HDL-C ratio may have great clinical significance with regards to risk stratification for diabetic patients with CAD who are treated with statins.

Although previous studies have demonstrated the role of the TG/HDL-C ratio in predicting adverse cardiovascular events in patients with CAD (51–55), the potential role of TG/HDL-C ratio as a prognostic marker for patients with diabetes is still debated. The Swedish National Diabetes Register found that elevated TG/HDL-C ratio could increase the risk of CVD independent of the LDL-C level in obese T2DM patients (56). Yang et al. reported that the TG/HDL-C ratio was an important predictor of MACEs in patients with diabetes and CAD (42). Contrary to these studies, several other studies did not find significant associations between the TG/HDL-C ratio and the prognosis of T2DM. Tohidi et al. demonstrated that the TG/HDL-C ratio was not an independent predictor of cardiovascular events in diabetic patients without CVD (57). The sub analysis of the Management of Elevated Cholesterol in the Primary Prevention Group of Adult Japanese (MEGA) study was not able to establish an independent association between TG/HDL ration and CVD risk in patients with DM and without history of CVD (43). The potential reasons for this discrepancy could be the variation in definition of endpoints, patient characteristics among studies.

This study is the first to focus on the role of the TG/HDL-C ratio in the prediction of prognosis in diabetic patients with CAD who were treated with statins. Compared with previous studies focusing on patients with diabetes or CAD, this large cohort study included higher risk patients with a higher prevalence of a history of CVD. This study demonstrated that an elevated TG/HDL-C ratio was associated with poor prognosis in diabetic patients with CAD treated with statins. Although higher TG/LDL-C ratio were relevant for chronic kidney disease (CKD) in patients with diabetes (58), TG/LDL-C ratio remained a significant and independent predictor of all-cause mortality and cardiovascular death after adjustment for potential confounders including renal function measures (eGFR). This finding suggested that the association between TG/HDL-C ratio and the risk of mortality might not be mediated by the presence of kidney dysfunction. These associations were persistent in sensitivity and subgroup analyses. An elevated TG/HDL-C ratio was still associated with an increased risk of mortality in patients with LDL-C levels of $\leq$1.80 mmol/L, suggesting that the ratio may explain part of the residual cardiovascular risk. The use of statins has less impact on the prognostic value of the TG/HDL-C ratio in diabetic patients with CAD. Several potential mechanisms may account for the association of the TG/HDL-C ratio with all-cause mortality and cardiovascular death in diabetic patients with CAD: (1) an elevated TG level and lower HDL-C plays an important role in endothelial dysfunction and atherosclerosis. Combined TG and HDL-C are significantly related to other atherogenic lipid phenotypes, characterized by higher levels of small dense LDL particles along with higher levels of remnant particle cholesterol and non-HDL-C, which contribute to the progression of atherosclerosis (14, 58, 59); (2) the TG/HDL-C ratio is significantly related to insulin resistance and glycemic control in diabetic patients (15, 16, 60, 61). Insulin resistance is related to the progression of atherosclerosis, vulnerability of coronary plaques, and MACEs in patients with CAD (62–64). Moreover, a hyperglycemic environment could induce the progression of macrovascular and microvascular disease in diabetic patients, including diabetic nephropathy, CAD and peripheral artery disease, which could cause excess risk of all-cause mortality and cardiovascular death (65, 66).

Additionally, the addition of the TG/HDL-C ratio in the risk prediction model for subsequent all-cause mortality and cardiovascular death was associated with a high predictive value. These results suggest that the use of TG/HDL-C ratio could refine risk stratification for all-cause mortality and cardiovascular death in diabetic patients with CAD who are treated with statins. Moreover, this study identified the optimal cutoff value of the TG/HDL-C ratio in this context, suggesting that the ratio should be maintained at <1.57 to reduce the risk of all-cause mortality and cardiovascular death. The results of this study provide new evidence to reduce all-cause mortality and cardiovascular death in diabetic patients with CAD treated with statins. Further large-scale prospective cohort studies should be performed to verify whether implementation of screening TG/HDL-C ratio will change the prognosis of diabetic patients with CAD.

However, several limitations of this study should be acknowledged. First, the current study was retrospective. The lack of information of waist circumference made it difficult to calculate the fatty liver index. Therefore, fatty liver index was not included in the analysis. Second, the follow-up information was collected by telephone or electronic medical record review. The follow-up information mainly included survival data. Baseline data after 4-year follow-up was not collected. Third, the information about glycemic control optimization and changes in medications was not collected during follow-up. The effect of changes in medications should be taken into consideration in the future, prospective study. Fourth, the complications and severity of T2DM and CAD differ, which could have affected the risk of all-cause mortality and cardiovascular death. Finally, as lipid levels vary among different ethnicities, it is not known whether these findings can be applicable to other ethnicities.

CONCLUSION

An elevated TG/HDL-C ratio was associated with an increased risk of all-cause mortality and cardiovascular death in diabetic patients with CAD who were treated with statins. Moreover, the addition of the TG/HDL-C ratio into the traditional risk model increased the predictive value for subsequent all-cause mortality and cardiovascular death. Therefore, the TG/HDL-C ratio may be a useful marker for evaluating the prognosis in diabetic patients with CAD who are treated with statins.

DATA AVAILABILITY STATEMENT

The raw data supporting the conclusions of this article will be made available by the authors, without undue reservation.

ETHICS STATEMENT

The studies involving human participants were reviewed and approved by the Ethical Committee of Tianjin Chest Hospital. The ethics committee waived the requirement of written informed consent for participation.

AUTHOR CONTRIBUTIONS

LW, HC, and JZ participated in the study design. LW, YH, AW, YZ, HY, LR, WQ, and WL participated in data collection. LW, HY, and LR performed the statistical analysis. LW drafted the article. All authors contributed to the article and approved the submitted version.

ACKNOWLEDGMENTS

We thank all of the investigators and patients who participated in this project.

REFERENCES

1. Norhammar A, Malmberg K, Diderholm E, Lagerqvist B, Lindahl B, Rydén L, et al. Diabetes mellitus: the major risk factor in unstable coronary artery disease even after consideration of the extent of coronary artery disease and benefits of revascularization. *J Am Coll Cardiol.* (2004) 43:585–91. doi: 10.1016/j.jacc.2003.08.050
2. Colhoun HM, Betteridge DJ, Durrington PN, Hitman GA, Neil HA, Livingstone SJ, et al. Primary prevention of cardiovascular disease with atorvastatin in type 2 diabetes in the collaborative atorvastatin diabetes study (CARDS): multicentre randomised placebo-controlled trial. *Lancet.* (2004) 364:685–96. doi: 10.1016/S0140-6736(04)16895-5
3. Sever PS, Poulter NR, Dahlöf B, Wedel H, Collins R, Beevers G, et al. Reduction in cardiovascular events with atorvastatin in 2,532 patients with type 2 diabetes: anglo-scandinavian cardiac outcomes trial–lipid-lowering arm (ASCOT-LLA). *Diabetes Care.* (2005) 28:1151–7. doi: 10.2337/diacare.28.5.1151
4. Knopp RH, d'Emden M, Smilde JG, Pocock SJ. Efficacy and safety of atorvastatin in the prevention of cardiovascular end points in subjects with type 2 diabetes: the atorvastatin study for prevention of coronary heart disease endpoints in non-insulin-dependent diabetes mellitus (ASPEN). *Diabetes Care.* (2006) 29:1478–85. doi: 10.2337/dc05-2415
5. Tajima N, Kurata H, Nakaya N, Mizuno K, Ohashi Y, Kushiro T, et al. Pravastatin reduces the risk for cardiovascular disease in Japanese hypercholesterolemic patients with impaired fasting glucose or diabetes: diabetes subanalysis of the management of elevated cholesterol in the primary prevention group of adult Japanese (MEGA) study. *Atherosclerosis.* (2008) 199:455–62. doi: 10.1016/j.atherosclerosis.2008.05.027
6. Rawshani A, Rawshani A, Franzén S, Sattar N, Eliasson B, Svensson AM, et al. Risk factors, mortality, and cardiovascular outcomes in patients with type 2 diabetes. *N Engl J Med.* (2018) 379:633–44. doi: 10.1056/NEJMoa1800256
7. Verges B. Pathophysiology of diabetic dyslipidaemia: where are we? *Diabetologia.* (2015) 58:886–99. doi: 10.1007/s00125-015-3525-8
8. Filippatos T, Tsimihodimos V, Pappa E, Elisaf M. Pathophysiology of diabetic dyslipidaemia. *Curr Vasc Pharmacol.* (2017) 15:566–75. doi: 10.2174/1570161115666170201105425
9. Chan WB, Tong PC, Chow CC, So WY, Ng MC, Ma RC, et al. Triglyceride predicts cardiovascular mortality and its relationship with glycaemia and obesity in Chinese type 2 diabetic patients. *Diabetes Metab Res Rev.* (2005) 21:183–8. doi: 10.1002/dmrr.497
10. Joo HJ, Cho SA, Hong SJ, Hur SH, Bae JH, Choi DJ, et al. Impact of low high-density lipoprotein-cholesterol level on 2-year clinical outcomes after acute myocardial infarction in patients with diabetes mellitus. *Lipids Health Dis.* (2016) 15:197. doi: 10.1186/s12944-016-0374-5
11. Li XL, Hong LF, Luo SH, Guo YL, Zhu CG, Sun J, et al. Impact of admission triglyceride for early outcome in diabetic patients with stable coronary artery disease. *Lipids Health Dis.* (2014) 13:73. doi: 10.1186/1476-511X-13-73

12. Ogita M, Miyauchi K, Miyazaki T, Naito R, Konishi H, Tsuboi S, et al. Low high-density lipoprotein cholesterol is a residual risk factor associated with long-term clinical outcomes in diabetic patients with stable coronary artery disease who achieve optimal control of low-density lipoprotein cholesterol. *Heart Vessels.* (2014) 29:35–41. doi: 10.1007/s00380-013-0330-5
13. Quispe R, Martin SS, Jones SR. Triglycerides to high-density lipoprotein-cholesterol ratio, glycemic control and cardiovascular risk in obese patients with type 2 diabetes. *Curr Opin Endocrinol Diabetes Obes.* (2016) 23:150–6. doi: 10.1097/MED.0000000000000241
14. Yokoyama K, Tani S, Matsuo R, Matsumoto N. Increased triglyceride/high-density lipoprotein cholesterol ratio may be associated with reduction in the low-density lipoprotein particle size: assessment of atherosclerotic cardiovascular disease risk. *Heart Vessels.* (2019) 34:227–36. doi: 10.1007/s00380-018-1247-9
15. Ren X, Chen ZA, Zheng S, Han T, Li Y, Liu W, et al. Association between triglyceride to HDL-C ratio (TG/HDL-C) and insulin resistance in Chinese patients with newly diagnosed type 2 diabetes mellitus. *PLoS ONE.* (2016) 11:e0154345. doi: 10.1371/journal.pone.0154345
16. Zhou M, Zhu L, Cui X, Feng L, Zhao X, He S, et al. The triglyceride to high-density lipoprotein cholesterol (TG/HDL-C) ratio as a predictor of insulin resistance but not of beta cell function in a Chinese population with different glucose tolerance status. *Lipids Health Dis.* (2016) 15:104. doi: 10.1186/s12944-016-0270-z
17. Uruska A, Zozulinska-Ziolkiewicz D, Niedzwiecki P, Pietrzak M, Wierusz-Wysocka B. TG/HDL-C ratio and visceral adiposity index may be useful in assessment of insulin resistance in adults with type 1 diabetes in clinical practice. *J Clin Lipidol.* (2018) 12:734–40. doi: 10.1016/j.jacl.2018.01.005
18. Liu D, Guan L, Zhao Y, Liu Y, Sun X, Li H, et al. Association of triglycerides to high-density lipoprotein-cholesterol ratio with risk of incident hypertension. *Hypertens Res.* (2020) 43:948–55. doi: 10.1038/s41440-020-0439-8
19. Yeom H, Kim HC, Lee JM, Jeon Y, Suh I. Triglyceride to high density lipoprotein cholesterol ratio among adolescents is associated with adult hypertension: the Kangwha study. *Lipids Health Dis.* (2018) 17:212. doi: 10.1186/s12944-018-0861-y
20. Tohidi M, Hatami M, Hadaegh F, Azizi F. Triglycerides and triglycerides to high-density lipoprotein cholesterol ratio are strong predictors of incident hypertension in Middle Eastern women. *J Hum Hypertens.* (2012) 26:525–32. doi: 10.1038/jhh.2011.70
21. Karelis AD, Pasternyk SM, Messier L, St-Pierre DH, Lavoie JM, Garrel D, et al. Relationship between insulin sensitivity and the triglyceride-HDL-C ratio in overweight and obese postmenopausal women: a MONET study. *Appl Physiol Nutr Metab.* (2007) 32:1089–96. doi: 10.1139/H07-095
22. Ho CI, Chen JY, Chen SY, Tsai YW, Weng YM, Tsao YC, et al. Relationship between TG/HDL-C ratio and metabolic syndrome risk factors with chronic kidney disease in healthy adult population. *Clin Nutr.* (2015) 34:874–80. doi: 10.1016/j.clnu.2014.09.007
23. Shin HG, Kim YK, Kim YH, Jung YH, Kang HC. The relationship between the triglyceride to high-density lipoprotein cholesterol ratio and metabolic syndrome. *Korean J Fam Med.* (2017) 38:352–7. doi: 10.4082/kjfm.2017.38.6.352
24. Aslan Çin NN, Yardimci H, Koç N, Uçaktürk SA, Akçil Ok M. Triglycerides/high-density lipoprotein cholesterol is a predictor similar to the triglyceride-glucose index for the diagnosis of metabolic syndrome using international diabetes federation criteria of insulin resistance in obese adolescents: a cross-sectional study. *J Pediatr Endocrinol Metab.* (2020) 33:777–84. doi: 10.1515/jpem-2019-0310
25. Liu XY, Wu QY, Chen ZH, Yan GY, Lu Y, Dai HJ, et al. Elevated triglyceride to high-density lipoprotein cholesterol (TG/HDL-C) ratio increased risk of hyperuricemia: a 4-year cohort study in China. *Endocrine.* (2020) 68:71–80. doi: 10.1007/s12020-019-02176-5
26. Wu KT, Kuo PL, Su SB, Chen YY, Yeh ML, Huang CI, et al. Nonalcoholic fatty liver disease severity is associated with the ratios of total cholesterol and triglycerides to high-density lipoprotein cholesterol. *J Clin Lipidol.* (2016) 10:420–5.e1. doi: 10.1016/j.jacl.2015.12.026
27. Fan N, Peng L, Xia Z, Zhang L, Song Z, Wang Y, et al. Triglycerides to high-density lipoprotein cholesterol ratio as a surrogate for nonalcoholic fatty liver disease: a cross-sectional study. *Lipids Health Dis.* (2019) 18:39. doi: 10.1186/s12944-019-0986-7
28. Shishehbor MH, Hoogwerf BJ, Lauer MS. Association of triglyceride-to-HDL cholesterol ratio with heart rate recovery. *Diabetes Care.* (2004) 27:936–41. doi: 10.2337/diacare.27.4.936
29. Chen C, Dai JL. Triglyceride to high-density lipoprotein cholesterol (HDL-C) ratio and arterial stiffness in Japanese population: a secondary analysis based on a cross-sectional study. *Lipids Health Dis.* (2018) 17:130. doi: 10.1186/s12944-018-0776-7
30. Chung TH, Shim JY, Kwon YJ, Lee YJ. High triglyceride to high-density lipoprotein cholesterol ratio and arterial stiffness in postmenopausal Korean women. *J Clin Hypertens.* (2019) 21:399–404. doi: 10.1111/jch.13484
31. Li X, Deng YP, Yang M, Wu YW, Sun SX, Sun JZ. Triglyceride to high-density lipoprotein cholesterol ratio and carotid intima-medial thickness in Chinese adolescents with newly diagnosed type 2 diabetes mellitus. *Pediatr Diabetes.* (2016) 17:87–92. doi: 10.1111/pedi.12250
32. Turak O, Afşar B, Ozcan F, Öksüz F, Mendi MA, Yayla Ç, et al. The role of plasma triglyceride/high-density lipoprotein cholesterol ratio to predict new cardiovascular events in essential hypertensive patients. *J Clin Hypertens.* (2016) 18:772–7. doi: 10.1111/jch.12758
33. Park JH, Lee J, Ovbiagele B. Nontraditional serum lipid variables and recurrent stroke risk. *Stroke.* (2014) 45:3269–74. doi: 10.1161/STROKEAHA.114.006827
34. Chen Z, Chen G, Qin H, Cai Z, Huang J, Chen H, et al. Higher triglyceride to high-density lipoprotein cholesterol ratio increases cardiovascular risk: 10-year prospective study in a cohort of Chinese adults. *J Diabetes Investig.* (2020) 11:475–81. doi: 10.1111/jdi.13118
35. Chang TI, Streja E, Soohoo M, Kim TW, Rhee CM, Kovesdy CP, et al. Association of serum triglyceride to HDL cholesterol ratio with all-cause and cardiovascular mortality in incident hemodialysis patients. *Clin J Am Soc Nephrol.* (2017) 12:591–602. doi: 10.2215/CJN.08730816
36. He S, Wang S, Chen X, Jiang L, Peng Y, Li L, et al. Higher ratio of triglyceride to high-density lipoprotein cholesterol may predispose to diabetes mellitus: 15-year prospective study in a general population. *Metabolism.* (2012) 61:30–6. doi: 10.1016/j.metabol.2011.05.007
37. Vega GL, Barlow CE, Grundy SM, Leonard D, DeFina LF. Triglyceride-to-high-density-lipoprotein-cholesterol ratio is an index of heart disease mortality and of incidence of type 2 diabetes mellitus in men. *J Investig Med.* (2014) 62:345–9. doi: 10.2310/JIM.0000000000000044
38. Chen Z, Hu H, Chen M, Luo X, Yao W, Liang Q, et al. Association of triglyceride to high-density lipoprotein cholesterol ratio and incident of diabetes mellitus: a secondary retrospective analysis based on a Chinese cohort study. *Lipids Health Dis.* (2020) 19:33. doi: 10.1186/s12944-020-01213-x
39. Zheng D, Li H, Ai F, Sun F, Singh M, Cao X, et al. Association between the triglyceride to high-density lipoprotein cholesterol ratio and the risk of type 2 diabetes mellitus among Chinese elderly: the Beijing longitudinal study of aging. *BMJ Open Diabetes Res Care.* (2020) 8:e000811. doi: 10.1136/bmjdrc-2019-000811
40. Cheng C, Liu Y, Sun X, Yin Z, Li H, Zhang M, et al. Dose-response association between the triglycerides: high-density lipoprotein cholesterol ratio and type 2 diabetes mellitus risk: the rural Chinese cohort study and meta-analysis. *J Diabetes.* (2019) 11:183–92. doi: 10.1111/1753-0407.12836
41. Lee MY, Hsiao PJ, Huang JC, Hsu WH, Chen SC, Chang JM, et al. Associations between triglyceride/high-density lipoprotein cholesterol ratio and micro- and macroangiopathies in type 2 diabetes mellitus. *Endocr Pract.* (2018) 24:615–21. doi: 10.4158/EP-2017-0254
42. Yang SH, Du Y, Li XL, Zhang Y, Li S, Xu RX, et al. Triglyceride to high-density lipoprotein cholesterol ratio and cardiovascular events in diabetics with coronary artery disease. *Am J Med Sci.* (2017) 354:117–24. doi: 10.1016/j.amjms.2017.03.032
43. Sone H, Nakagami T, Nishimura R, Tajima N, MEGA Study Group. Comparison of lipid parameters to predict cardiovascular events in Japanese mild-to-moderate hypercholesterolemic patients with and without type 2 diabetes: Subanalysis of the MEGA study. *Diabetes Res Clin Pract.* (2016) 113:14–22. doi: 10.1016/j.diabres.2015.12.002
44. Miller M, Cannon CP, Murphy SA, Qin J, Ray KK, Braunwald E, et al. Impact of triglyceride levels beyond low-density lipoprotein cholesterol after acute coronary syndrome in the PROVE IT-TIMI 22 trial. *J Am Coll Cardiol.* (2008) 51:724–30. doi: 10.1016/j.jacc.2007.10.038

45. Bos G, Dekker JM, Nijpels G, de Vegt F, Diamant M, Stehouwer CD, et al. A combination of high concentrations of serum triglyceride and non-high-density-lipoprotein-cholesterol is a risk factor for cardiovascular disease in subjects with abnormal glucose metabolism–The Hoorn Study. *Diabetologia.* (2003) 46:910–6. doi: 10.1007/s00125-003-1141-5
46. Matsumoto I, Misaki A, Kurozumi M, Nanba T, Takagi Y. Impact of nonfasting triglycerides/high-density lipoprotein cholesterol ratio on secondary prevention in patients treated with statins. *J Cardiol.* (2018) 71:10–5. doi: 10.1016/j.jjcc.2017.07.012
47. Edwards MK, Blaha MJ, Loprinzi PD. Atherogenic index of plasma and triglyceride/high-density lipoprotein cholesterol ratio predict mortality risk better than individual cholesterol risk factors, among an older adult population. *Mayo Clin Proc.* (2017) 92:680–1. doi: 10.1016/j.mayocp.2016.12.018
48. da Luz PL, Favarato D, Faria-Neto JR Jr, Lemos P, Chagas AC. High ratio of triglycerides to HDL-cholesterol predicts extensive coronary disease. *Clinics.* (2008) 63:427–32. doi: 10.1590/S1807-59322008000400003
49. Yunke Z, Guoping L, Zhenyue C. Triglyceride-to-HDL cholesterol ratio. Predictive value for CHD severity and new-onset heart failure. *Herz.* (2014) 39:105–10. doi: 10.1007/s00059-013-3788-0
50. Takata K, Kataoka Y, Andrews J, Puri R, Hammadah M, Duggal B, et al. Triglyceride-to-high-density lipoprotein cholesterol ratio and vulnerable plaque features with statin therapy in diabetic patients with coronary artery disease: frequency-domain optical coherence tomography analysis. *JACC Cardiovasc Imaging.* (2018) 11:1721–3. doi: 10.1016/j.jcmg.2018.02.017
51. Wan K, Zhao J, Huang H, Zhang Q, Chen X, Zeng Z, et al. The association between triglyceride/high-density lipoprotein cholesterol ratio and all-cause mortality in acute coronary syndrome after coronary revascularization. *PLoS ONE.* (2015) 10:e0123521. doi: 10.1371/journal.pone.0123521
52. Dai XY, Zheng YY, Tang JN, Yang XM, Guo QQ, Zhang JC, et al. Triglyceride to high-density lipoprotein cholesterol ratio as a predictor of long-term mortality in patients with coronary artery disease after undergoing percutaneous coronary intervention: a retrospective cohort study. *Lipids Health Dis.* (2019) 18:210. doi: 10.1186/s12944-019-1152-y
53. Sultani R, Tong DC, Peverelle M, Lee YS, Baradi A, Wilson AM. Elevated triglycerides to high-density lipoprotein cholesterol (TG/HDL-C) ratio predicts long-term mortality in high-risk patients. *Heart Lung Circ.* (2020) 29:414–21. doi: 10.1016/j.hlc.2019.03.019
54. Bittner V, Johnson BD, Zineh I, Rogers WJ, Vido D, Marroquin OC, et al. The triglyceride/high-density lipoprotein cholesterol ratio predicts all-cause mortality in women with suspected myocardial ischemia: a report from the women's ischemia syndrome evaluation (WISE). *Am Heart J.* (2009) 157:548–55. doi: 10.1016/j.ahj.2008.11.014
55. Prasad M, Sara J, Widmer RJ, Lennon R, Lerman LO, Lerman A. Triglyceride and triglyceride/ HDL (high density lipoprotein) ratio predict major adverse cardiovascular outcomes in women with non-obstructive coronary artery disease. *J Am Heart Assoc.* (2019) 8:e009442. doi: 10.1161/JAHA.118.009442
56. Eeg-Olofsson K, Gudbjörnsdottir S, Eliasson B, Zethelius B, Cederholm J; NDR. The triglycerides-to-HDL-cholesterol ratio and cardiovascular disease risk in obese patients with type 2 diabetes: an observational study from the Swedish National Diabetes Register (NDR). *Diabetes Res Clin Pract.* (2014) 106:136–44. doi: 10.1016/j.diabres.2014.07.010
57. Tohidi M, Hatami M, Hadaegh F, Safarkhani M, Harati H, Azizi F. Lipid measures for prediction of incident cardiovascular disease in diabetic and non-diabetic adults: results of the 8.6 years follow-up of a population based cohort study. *Lipids Health Dis.* (2010) 9:6. doi: 10.1186/1476-511X-9-6
58. Tsuruya K, Yoshida H, Nagata M, Kitazono T, Hirakata H, Iseki K, et al. Association of the triglycerides to high-density lipoprotein cholesterol ratio with the risk of chronic kidney disease: analysis in a large Japanese population. *Atherosclerosis.* (2014) 233:260–7. doi: 10.1016/j.atherosclerosis.2013.12.037
59. Moriyama K. The association between the triglyceride to high-density lipoprotein cholesterol ratio and low-density lipoprotein subclasses. *Intern Med.* (2020) 59:2661–9. doi: 10.2169/internalmedicine.4954-20
60. Quispe R, Manalac RJ, Faridi KF, Blaha MJ, Toth PP, Kulkarni KR, et al. Relationship of the triglyceride to high-density lipoprotein cholesterol (TG/HDL-C) ratio to the remainder of the lipid profile: the very large database of lipids-4 (VLDL-4) study. *Atherosclerosis.* (2015) 242:243–50. doi: 10.1016/j.atherosclerosis.2015.06.057
61. Zonszein J, Lombardero M, Ismail-Beigi F, Palumbo P, Foucher S, Groenewoud Y, et al. Triglyceride high-density lipoprotein ratios predict glycemia-lowering in response to insulin sensitizing drugs in type 2 diabetes: a post hoc analysis of the BARI 2D. *J Diabetes Res.* (2015) 2015:129891. doi: 10.1155/2015/129891
62. An X, Yu D, Zhang R, Zhu J, Du R, Shi Y, et al. Insulin resistance predicts progression of de novo atherosclerotic plaques in patients with coronary heart disease: a one-year follow-up study. *Cardiovasc Diabetol.* (2012) 11:71. doi: 10.1186/1475-2840-11-71
63. Nishimura M, Tokoro T, Nishida M, Hashimoto T, Kobayashi H, Yamazaki S, et al. Association of insulin resistance with de novo coronary stenosis after percutaneous coronary artery intervention in hemodialysis patients. *Nephron Clin Pract.* (2008) 109:c9–17. doi: 10.1159/000132391
64. Iguchi T, Hasegawa T, Otsuka K, Matsumoto K, Yamazaki T, Nishimura S, et al. Insulin resistance is associated with coronary plaque vulnerability: insight from optical coherence tomography analysis. *Eur Heart J Cardiovasc Imaging.* (2014) 15:284–91. doi: 10.1093/ehjci/jet158
65. Sowers JR, Stump CS. Insights into the biology of diabetic vascular disease: what's new? *Am J Hypertens.* (2004) 17:2S—6S. doi: 10.1016/j.amjhyper.2004.08.007
66. Wolf G. New insights into the pathophysiology of diabetic nephropathy: from haemodynamics to molecular pathology. *Eur J Clin Invest.* (2004) 34:785–96. doi: 10.1111/j.1365-2362.2004.01429.x

Conflict of Interest: The authors declare that the research was conducted in the absence of any commercial or financial relationships that could be construed as a potential conflict of interest.

frontiers in Cardiovascular Medicine

REVIEW
published: 24 August 2021
doi: 10.3389/fcvm.2021.738325

The Role of the VEGF Family in Coronary Heart Disease

Yan Zhou[1,2†], *Xueping Zhu*[1†], *Hanming Cui*[1], *Jingjing Shi*[1], *Guozhen Yuan*[1], *Shuai Shi*[1] *and Yuanhui Hu*[1*]

[1] *Guang'anmen Hospital, China Academy of Chinese Medical Sciences, Beijing, China,* [2] *Beijing University of Chinese Medicine, Beijing, China*

The vascular endothelial growth factor (VEGF) family, the regulator of blood and lymphatic vessels, is mostly investigated in the tumor and ophthalmic field. However, the functions it enjoys can also interfere with the development of atherosclerosis (AS) and further diseases like coronary heart disease (CHD). The source, regulating mechanisms including upregulation and downregulation, target cells/tissues, and known functions about VEGF-A, VEGF-B, VEGF-C, and VEGF-D are covered in the review. VEGF-A can regulate angiogenesis, vascular permeability, and inflammation by binding with VEGFR-1 and VEGFR-2. VEGF-B can regulate angiogenesis, redox, and apoptosis by binding with VEGFR-1. VEGF-C can regulate inflammation, lymphangiogenesis, angiogenesis, apoptosis, and fibrogenesis by binding with VEGFR-2 and VEGFR-3. VEGF-D can regulate lymphangiogenesis, angiogenesis, fibrogenesis, and apoptosis by binding with VEGFR-2 and VEGFR-3. These functions present great potential of applying the VEGF family for treating CHD. For instance, angiogenesis can compensate for hypoxia and ischemia by growing novel blood vessels. Lymphangiogenesis can degrade inflammation by providing exits for accumulated inflammatory cytokines. Anti-apoptosis can protect myocardium from impairment after myocardial infarction (MI). Fibrogenesis can promote myocardial fibrosis after MI to benefit cardiac recovery. In addition, all these factors have been confirmed to keep a link with lipid metabolism, the research about which is still in the early stage and exact mechanisms are relatively obscure. Because few reviews have been published about the summarized role of the VEGF family for treating CHD, the aim of this review article is to present an overview of the available evidence supporting it and give hints for further research.

Keywords: VEGF, lipid metabolism, angiogenesis, lymphangiogenesis, inflammation, atherosclerosis, coronary heart disease

OPEN ACCESS

Edited by:
Changcheng Zhou,
University of California, Riverside, United States

Reviewed by:
Wenxing Chen,
Nanjing University of Chinese Medicine, China
Hongmei Tan,
Sun Yat-sen University, China

***Correspondence:**
Yuanhui Hu
huiyuhui55@sohu.com

[†] These authors have contributed equally to this work

Specialty section:
This article was submitted to Atherosclerosis and Vascular Medicine, a section of the journal Frontiers in Cardiovascular Medicine

Received: *08 July 2021*
Accepted: *27 July 2021*
Published: *24 August 2021*

Citation:
Zhou Y, Zhu X, Cui H, Shi J, Yuan G, Shi S and Hu Y (2021) The Role of the VEGF Family in Coronary Heart Disease. Front. Cardiovasc. Med. 8:738325. doi: 10.3389/fcvm.2021.738325

INTRODUCTION

Coronary heart disease (CHD) is the primary disease that threatens the safety of humans and burdens countries with heavy economic load. The morbidity of CHD has transcended 10% in some Western countries. The elderly over 65 years old are more susceptible to CHD, making the median incidence rate of the high-risk group 19.34% worldwide (1). The number of CHD patients in China has reached 11 million and the morbidity is still increasing (2).

The pathological basis of CHD is atherosclerosis (AS). AS is the asymmetric local thickening of the intima of the artery. Factors like lipid metabolism disorder, vascular endothelial cell (VEC)

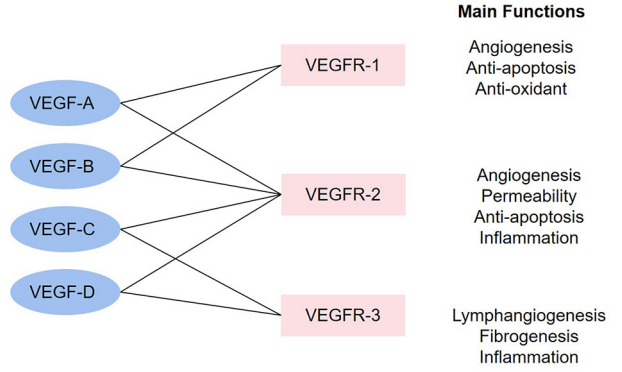

FIGURE 1 | The combinations in the VEGF family and main functions. The linkage between VEGF factors and VEGFR represents that the factors can combine with the receptors. The main functions stand for the functions after the activation of each receptor.

damage, inflammation, and immune dysfunction can promote the occurrence and development of AS, which then may lead to CHD (3). Lipid infiltration theory and inflammation theory are two classic theories about AS. The former claims that the elevated lipids such as low-density lipoprotein (LDL), very-low-density lipoprotein (VLDL), and its residues intrude into the artery wall and accumulate between smooth muscle cells (SMCs), collagen, and elastic fibers, which then cause proliferation of SMCs. Then, macrophages turn to foam cells by infiltrating lesions and devouring large amounts of lipids. AS plaques are formed eventually. Clinically, over 70% of CHD patients suffer from dyslipidemia concurrently (4). Active lipid-lowering therapy has been confirmed to reduce CHD risk and the target value of LDL-C is 1.8 mmol/L. It has been concluded that CHD risk will be reduced by 21% when LDL-C drops 1 mmol/L (5). While the inflammation theory suggests that AS is closely related to inflammatory response. Leukocyte recruitment and proinflammatory factors are mainly involved in the early steps of AS formation, including inflammation activating endothelial cells (ECs), monocytes invading lesions, and chemokines further promoting the recruitment of inflammatory cells to the endometrium, foam cells secreting inflammatory media, and macrophage apoptosis (6). Thus, inflammatory cells and immune cells form important parts of plaques, and the lift of inflammatory markers can be applied to assess the prognosis of patients with acute coronary syndrome (ACS) (7). Therefore, improving lipid metabolism and alleviating inflammatory response play a crucial role to prevent and control CHD.

The vascular endothelial growth factor (VEGF) family governs functions including promoting angiogenesis, promoting lymphopoiesis, regulating inflammation, resisting oxidative stress, and regulating lipid metabolism, which presents potential therapeutic value for CHD. The VEGF family consists of the following members: VEGF-A, VEGF-B, VEGF-C, VEGF-D, VEGF-E (virus source), VEGF-F (snake venom source), placenta growth factor (PlGF), and EG-VEGF. VEGF receptors (VEGFRs) include VEGFR-1, VEGFR-2, and VEGFR-3. VEGFR-1 and VEGFR-2 are mainly expressed on VECs, while VEGFR-3 is mostly expressed on lymphatic endothelial cells (LECs) (8). These factors perform functions *via* combining to related receptors (see **Figure 1**). Recently, a large number of studies have shown the capacity of the VEGF family to interfere with lipid metabolism, especially through the regulation of lymphatic system. This system is a one-way transport pathway from extracellular space to venous system, which participates in the absorption of lipid in the gastrointestinal tract. In particular, VEGF-C and VEGF-D, as significant regulatory factors of lymphatic system, influence lipid level from this aspect. As for inflammation, dilation and proliferation of lymphatic vessels mediated by VEGF family provide an exit for local accumulated inflammatory media, thus inhibiting inflammatory response and AS progress. The VEGF family can also prevent AS by promoting angiogenesis and regulating oxidative stress. In terms of angiogenesis, coronary artery AS can lead to ischemia and hypoxia in local myocardium. The expression of some factors in the VEGF family would be enhanced in such environment, thus promoting the proliferation and migration of ECs and forming compensatory neovascularization. Oxidative stress has been proved to be an accelerator for AS, and the balance effect of the VEGF family on oxidation–reduction may also slow down the progress of AS.

In conclusion, the multiple perspectives and targets presented by the VEGF family predict their ability to regulate the progress of AS and provide potential therapeutic strategies for treating cardiovascular diseases. Until now, no relevant review about the biological effects of the VEGF family on CHD has been published. Therefore, based on previous studies, we summarized the known mechanisms of the VEGF family on blood vessels and lymphatic vessels, as well as their influence on inflammation, apoptosis, fibrogenesis, and lipid metabolism. The study incorporates and arranges information from four main aspects, the origin of the VEGF family, up/downregulation mechanism, receptors/target cells, and functions, aiming to provide a literature review for further study to explore more effective applications of the VEGF family to CHD.

VEGF-A

VEGF-A, namely, VEGF, is one of the polypeptide proteins and the most established factor in the VEGF family. By combining with VEGFR-1 and VEGFR-2, it mediates angiogenesis, vascular permeability, and inflammation, making itself known as a vascular permeability factor (VPF) (9). Physiological angiogenesis, that is, forming blood vessels in the process of tissue revascularization, involves the cascade of multiple signals. VEGF-A, the core of the process, is crucial for angiogenesis and the functions of ECs, while pathological angiogenesis is a marker of inflammatory and ischemic diseases. A clinical study has shown that the level of VEGF-A is independently associated with microvascular occlusion (MVO) during ST segment elevation myocardial infarction (STEMI), and correlated with mid-term left ventricular ejection fraction (LVEF). Therefore, VEGF-A can

be regarded as a biomarker of MVO in STEMI patients and can be applied for prognosis stratification (10). However, the role of VEGF-A to AS is controversial; for instance, the increase of VEGF-A can both promote vascular proliferation to compensate for myocardial hypoxia and enhance vascular permeability to speed up inflammation.

Human VEGF-A, composed of eight exons separated by seven introns, presents subtypes with different length, such as VEGF165, VEGF121, and VEGF206, after the splicing of alternative VEGF mRNA. All subtypes contain the same regions, exons 1–5 and 8. Their differences in exons 6–7, namely, heparin affinity and heparin sulfate proteoglycan (HSPG) affinity regions, contribute to their different biological characteristics (11) (see **Figure 2**). Meanwhile, as a double-edged factor, it comprises isoforms that antagonize with each other, which accentuates its arcane mechanisms. Concretely, anti-angiogenic VEGFxxxb isoforms oppose to VEGFxxxa isoforms and reduce VEGFR-2 activation (12). Like VEGF165a, the most active subtype in vascular reconstruction is inhibited by VEGF165b (13).

Source of VEGF-A

VEGF-A is expressed in most systems in the human body. In the cardiovascular system, pericytes, ECs, and angioblasts are the primary expression sites. Under hypoxia and inflammatory environment, VEGF-A can also be produced by blood cells including monocytes, activated T cells, neutrophils, dendritic cells, and platelets (8). In CHD patients, VEGF-A will be secreted by myocardium due to local inflammation, mechanical stress, and cytokines, resulting in myocardial deformation, contraction, and impaired recovery (14) (see **Figure 3**). Other cells, such as terminal chondrocytes, hypertrophic chondrocytes, tumor cells, keratinocytes, and retinal pigment epithelial cells, can also produce VEGF-A under certain circumstances.

Mechanisms Regulating the Level of VEGF-A

Upregulation Mechanism of VEGF-A

It is widely held that in cardiovascular diseases, cardiomyocytes and ECs are often exposed to hypoxia and inflammation, which stimulate hypoxia-inducible factors (HIFs). HIFs can upregulate various pro-angiogenic factors *via* the HIF-1α pathway, especially VEGF to promote angiogenesis. Increased VEGF-A favors the proliferation of VECs, improves vascular permeability, and restores the integrity of endothelium and vascular function. Therefore, it compensates for ischemia and hypoxia, and protects the injured myocardium (15). In addition to the typical pathway, many recent studies have uncovered other mechanisms of upregulating VEGF-A. For example, a study published on *Nature* claimed that lack of oxygen and nutrition caused the activation of transcription coactivator PGC-1, a major regulator of mitochondrial function, and promoted angiogenesis by lifting the expression of VEGF. PGC-1 further synergistically activated orphan nuclear receptor ERR-α to control an angiogenesis pathway independent of HIFs (16). Jin found that hypoxia also induced ECs to produce TNFα, which suggested that the autocrine cycle could activate HIFs by a NF-κB dependent process, to upregulate VEGF and promote angiogenesis. This forms the TNFα/NF-κB/HIF/VEGF signaling cascade in ECs (17). Longchamp discovered that thioamino acid restriction was a trigger of angiogenesis as it enhanced the expression of VEGF and capillary density of skeletal muscle in mice through GCN2/ATF4 amino acid starvation pathway independent of hypoxia or HIF-1α. In addition, hydrogen sulfide (H2S) was observed to promote angiogenesis by inhibiting mitochondrial electron transport and oxidative phosphorylation, resulting in increased glucose uptake and ATP production in glycolysis (18). Guo found that in AS plaque, CD163+ macrophages contributed to the expression of VEGF-A through the CD163/HIF1α/VEGF-A pathway (19). Annexin A1 (AnxA1) directly led cardiac macrophages to polarize to angiogenic and repair phenotypes, and stimulated cardiac macrophages to release large amounts of VEGF-A, thus inducing angiogenesis and cardiac repair (20). By contrast, one study revealed that mild hypoxia (14% O_2) did not induce coronary angiogenesis or VEGF-A expression in hearts of developing mice (21).

In addition to environmental factors, some drugs have also been confirmed to protect myocardium by upregulating VEGF-A. For instance, hydroxysafflor yellow A in safflower improved the function of endothelial progenitor cells (EPCs) and increased VEGF-A in ECs in MI model mice *via* the HO-1/VEGF-A/SDF-1α signaling cascade, which then significantly recovered cardiac hemodynamics induced by ischemia, improved survival rate, and alleviated myocardial injury (22, 23). *Pueraria* and *Salvia miltiorrhiza* extracts promoted angiogenesis by upregulating the VEGF/VEGFR2 pathway, thus preserving myocardium of MI model rats (24). Salidroside increased the expression of HIF-1α and then the level of VEGF to inhibit necrosis and apoptosis of cardiomyocytes induced by hypoxia (25).

Downregulation Mechanism of VEGF-A

The above TNFα/NF-κB/HIF/VEGF signaling cascade in ECs has been proved to be destroyed by LDL, because it can suppress TNFR1, prevent the expression of HIFs in ECs exposed to hypoxia or TNFα, and thus decrease VEGF. Similarly, knocking out HIF-1α or HIF-2α also significantly reduced the production of VEGF induced by hypoxia, thereby inhibiting angiogenesis (17). In addition, E2F1 transcription factor inhibited the upregulation of VEGF and PIGF through p53-dependent and -independent mechanisms, respectively, thus limiting cardiac neovascularization and functional recovery after MI (26). In the rat model of myocardial reperfusion injury, overexpression of ANXA1 inhibited inflammatory factors and the infiltration and apoptosis of polymorphonuclear neutrophils (PMNs), which further downregulated STAT3 signaling pathway to hamper the expression of VEGF (27). Many studies unearthed that lipid-lowering drugs could also downregulate VEGF. For example, high-dose rosuvastatin monotherapy lowered VEGF in patients with dyslipidemia, while low-dose rosuvastatin and polyunsaturated fatty acids significantly increase VEGF (28). After undergoing percutaneous coronary intervention (PCI), VEGF level climbed up at first in MI patients, which could reflect transient ischemia and lead to neovascularization in AS plaque, while later rosuvastatin treatment reduced the previously elevated VEGF (29). Simvastatin combined with coniferin were

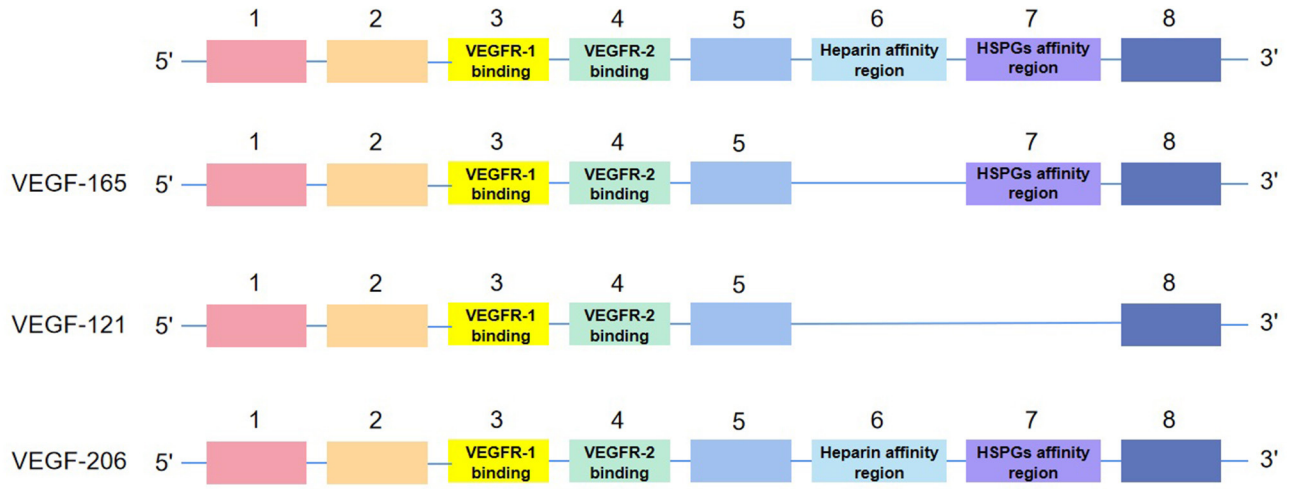

FIGURE 2 | The structure of isoforms of VEGF-A. VEGF-165, VEGF-121, and VEGF-206 are examples of the structure.

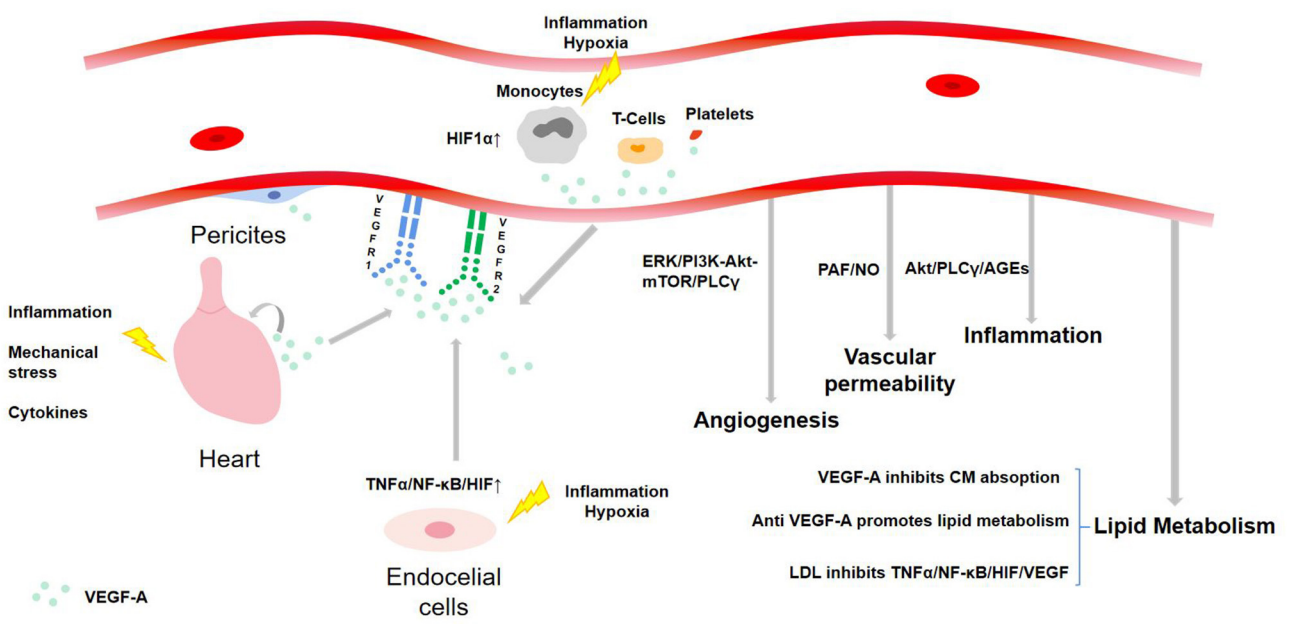

FIGURE 3 | The source and regulation mechanism of VEGF-A with functions.

claimed to inhibit the expression of VEGF and endothelin (ET) and increase the level of NO and the activity of superoxide dismutase (SOD) in ApoE –/– mice fed with a high-fat diet (HFD). The levels of serum total cholesterol, triglyceride, and LDL-C were significantly reduced, thus restraining the development of AS (30).

Receptors and Target Cells

VEGFR-1

VEGFR-1 is a member of receptor tyrosine kinase family (RTKs), with high affinity with VEGF-A but 10 times weaker kinase activity compared to VEGFR-2. It is mainly expressed in ECs and also in other cells including inflammatory cells, monocytes/macrophages, vascular smooth muscle cells (VSMCs), bone marrow-derived hematopoietic progenitor cells, and cardiac fibroblasts in myocardial infarction (MI) (31). VEGFR-1 regulates the migration of these cells and plays an important part in angiogenesis. VEGFR-1 contains three domains, intracellular domain, extracellular domain, and transmembrane domain, the latter two relating to angiogenesis (32). VEGFR-1 competes with VEGFR-2 for VEGF-A depending on high affinity, but due to its low kinase activity, it can

inhibit angiogenesis in some condition. In the embryonic stage, VEGFR-1 restrains angiogenesis by "seizing" VEGF-A, while in adulthood, it ameliorates macrophage function to adjust the development of inflammatory diseases, cancer metastasis, and AS in a creatine kinase-dependent manner. The activity of VEGFR-1 tyrosine kinase affects pathological angiogenesis and inflammation. Mice with VEGFR-1 which lacked tyrosine kinase region showed milder inflammatory response (33).

VEGFR-2

VEGFR-2, another member of RTKs, is mainly expressed in ECs of blood vessels and lymphatic vessels, and weakly spotted in neurons, tumor cells, and hematopoietic cells. The combination of VEGF-A and VEGFR-2 is key to controlling angiogenesis, vascular permeability, and inflammation. VEGFR-2, like VEGFR-1, contains three domains. When VEGF-A binds to the extracellular domain of VEGFR-2, it can lead to the autophosphorylation of tyrosine residues and energizing signaling pathways that can promote the proliferation of ECs. Unlike other RTK family members that regulate the Ras pathway, VEGFR-2 mainly activates MAPK and DNA synthesis using the phospholipase-Cγ-protein kinase-C pathway (34).

Functions of VEGF-A

Angiogenesis

VEGF-A-induced pathways are strictly regulated in space and dynamics to coordinate the proliferation, migration, and invasion of ECs into surrounding tissues, leading to the formation of lumen structures and further neovascularization. The binding of VEGF to VEGFR-2 causes receptor endocytosis and activates a variety of downstream signaling pathways, including ERK, PI3K-Akt-mTOR, and PLCγ, which promotes the proliferation and migration of VECs and vascular remodeling. The proliferation of ECs is primarily stimulated by ERK and PI3K/Akt signaling pathways. Furthermore, the activation of ERK is mainly influenced by upstream signals including PLCγ, IQGAP1, FAK, and Gab1, while PI3K is affected by Shb, IQGAP1, AXL, Gab1, and FAK (9). The migration of ECs is mainly regulated by G protein in Rho family stimulated by PI3K. The invasion of ECs occurs due to the release of matrix metalloproteinases (MMPs), which degrade the basement membrane and extracellular matrix to allow the migration of new ECs, leading to the formation of capillary sprouts. VEGF-A has been proved to induce MMP, MMP-2, MMP-9, and urokinase plasminogen, and the potential mechanism may be the activation of β-Kartin and NF-κb (35).

It has been found that multiple proteins that work on the above pathways can affect angiogenesis of VEGF-A. For example, N-myc downstream regulatory gene 1 (NDRG1) formed a complex with PLCγ1 through its phosphorylation site. PLCγ1 inhibited angiogenesis induced by VEGF-A, which indicated that NDRG1 plays an important role in VEGF-A-induced angiogenesis through PLCγ1 signal transduction (36). In breast cancer patients, downregulation of angiotensin-converting enzyme 2 (ACE2) checked the expression of VEGF-A and deactivated the phosphorylation of VEGFR2, MEK1/2, and ERK1/2 in human umbilical vessel endothelial cells (HUVECs), thereby inhibiting angiogenesis through the VEGF-A/VEGFR-2/ERK pathway (37). The activation of mineralocorticoid receptor (MR) inhibited VEGF-induced gene expression, resulting in the disorder of angiogenesis-related gene network in ECs, which destroyed the ability of VEGF to induce angiogenesis (38). Increased vascular permeability also promoted vascular growth by promoting the rapid growth of extracellular proteases required for angiogenesis. In addition, leukocyte extravasation helped early angiogenesis by enhancing the local production of cytokines/chemokines and release of proteases (9). However, a recent study has shown that VEGF-A also induced vascular degeneration, which was regulated by phosphatidylinositol metabolic cycle controlled by CDP diacylglycerol synthase-2 (CDS2). ECs with mutant CDS2 suppressed vascular degeneration through reverse migration and apoptosis after being stimulated by VEGF-A (39).

At present, studies about VEGF (VEGF-A) and CHD mainly focus on angiogenesis of VEGF. Zhao found that the extracts of Radix Puerariae and Radix Salviae Miltiorrhizae could induce salient angiogenesis in HUVECs by regulating the VEGF/VEGFR-2 signaling pathway. Meanwhile, the infarct size of the treatment group was smaller than that of the model group, with significantly increased expression of related proteins. It was then suggested that the extracts may protect myocardial cells after MI by promoting angiogenesis *via* the VEGF/VEGFR-2 pathway (24). Li found that Shexiang Xintongning could promote angiogenesis by activating VEGF/VEGFR2 and ERK1/2 pathways to protect HUVECs from oxidative stress, reduce infarct size, and prevent AS plaque rupture-induced worsening CHD (40). Xu found that Shenzhu Guanxin granules could upregulate the expression of PECAM-1/CD31 and VEGF in a dose-dependent manner to improve cardiac hemodynamic function and reduce MI area (41). Zhang claimed that Shexiang Baoxin Pill could significantly enhance the expression of VEGF so as to promote angiogenesis, improve microvascular count, and reduce the size of MI (42). Besides, hampering the activity of VEGF-A and angiogenesis can also work in clinical practices. For example, cryptotanshinone, the active component of *S. miltiorrhiza*, has been found to check VEGF-induced VEGFR2 phosphorylation and its downstream Src/FAK and ERK1/2 signaling pathways, including p-ERK1/2, p-p90RSK, py416-Src, and pY576/577-FAK proteins, which are responsible for EC migration, proliferation, and survival. This component effectively inhibited VEGF-induced angiogenesis, highlighting the therapeutic potential for treating angiogenesis-related diseases (43). The development of abdominal aortic aneurysm (AAA) is characterized by VEGF-induced angiogenesis through cyclooxygenase-2 (COX-2), while quercetin can inhibit COX-2 and reduce HIF-1α/VEGF signaling-related angiogenesis, thereby inhibiting aneurysm growth (44). A kind of marine fungus extract, asperchalasine A, can inhibit angiogenesis by downregulating VEGF, p-p38, ERK, p-VEGFR-2, and p-Akt signaling pathways (45). Mesenchymal stem cell processed by atorvastatin can activate the Akt/eNOS pathway, increase VEGF level, and promote vascular proliferation (46). In addition to pharmacological studies, the level of VEGF in CHD patients can be significantly raised after physiological ischemia training,

indicating that such training in an appropriate period may ameliorate blood pressure and cardiac structure by increasing the secretion of VEGF (47).

Vascular Permeability

High vascular permeability caused by twisted EC cell–cell junction is associated with no reflow phenomenon after reopening occluding vessels in CHD patients, which also accounts for the main cause of death in these patients (48). Angiogenesis and vascular permeability are essential for normal tissue homeostasis. Chronic high permeability can lead to destructive tissue edema, like edema in CHD patients due to permeability imbalance. The VEGF-A/VEGFR-2 pathway is that by which VEGF-A regulates vascular permeability. The synthesis of endogenous endothelial platelet activating factor (PAF) and nitric oxide (NO) contributes to vascular permeability mediated by VEGF-165 (49). Inhibiting vascular permeability regulated by VEGFA/VEGFR2 was found to reduce edema in MI model mice without affecting the vascular density associated with survival rate after MI (50).

The two mechanisms of vascular permeability are the formation of transcellular pores and transient opening of paracellular junction. Firstly, transcellular pores such as vesicle-vacuole organelles (VVOs) are assembled by lipid microstructural domains and cross the vein endothelium. VEGFR-2 is located in the cave membrane and forms a complex with caveolin-1 (Cav-1) through its C-terminal tail. Secondly, permeability induced by VEGF-A depends on the transient opening of adhesion junction and tight junction. Vascular endothelial cadherin (VE-cadherin) is a kind of adhesion protein that controls vascular permeability. Adhesion is a cell–cell interaction, mainly created by the intermolecular binding of VE-cadherin. VEGF-A causes the short opening of endothelial cell–cell connections and dissolve the adhesion junction and tight junction. VEGF-A can dissolve the VE-cadherin complex by activating Src and Yes protein, which both then phosphorylate VE-cadherin and β-Kartin to improve vascular permeability. The third mechanism for the dissociation of VE-cadherin from the junction involves vessel endothelium-phosphotyrosine phosphatase (VE-PTP), which has been confirmed to be related to VEGFR-2 and VE-cadherin. The exact mechanism has not been elucidated, and one possibility is that the interaction between VE-PTP and angiopoietin receptor Tie2 affects angiopoietin 1 and 2. The decrease of tyrosine phosphatase activity may be conducive to the increase of tyrosine phosphorylation of VE-cadherin, thus accelerating the opening of the connection. Shb deficiency may cause abnormal signal conduction of G protein in Rho family and then reduce vascular permeability induced by VEGF-A and dissociate VE-cadherin at the adhesion junction. Vascular permeability induced by VEGF165 requires VEGFR-2 and NRP1, including NRP1 cytoplasmic domain (NCD). In the VEGF165 binding receptor complex, NCD promotes the activation of ABL kinase, while ABL kinase then activates the SRC family kinase (SFK) recruited by VEGFR-2. In the mice model of choroidal neovascularization, the loss of NCD reduced the leakage of blood vessels without affecting neovascularization. The result demonstrated that the targeted regulation of NRP1 or NCD could reduce edema induced by VEGF165 without changing the growth of blood vessels, which was made a potential strategy for the treatment of neovascular diseases (51). Akt, the downstream protein of the VEGF signaling pathway, can activate eNOS and produce NO to expand blood vessels and enhance vascular permeability. The active Akt can also promote vascular permeability independently from the VEGF pathway, which involves the activation of mTOR and phosphorylation of eNOS. The VEGF-dependent activation of eNOS can be achieved by the direct binding of eNOS with Ca2+/calmodulin (CAM) or by phosphorylation of Akt and AMP-activated protein kinase, CaM-dependent kinase II, and PKA (52). In addition, VEGFR-3 can inhibit the expression of VEGFR-2 and the activity of VEGF/VEGFR2 pathway in VECs, so as to prevent excessive vascular permeability. It was found that long-term exposure to VEGF-A inhibited the release of Ca2+ mediated by agonists and the further activation of the IKCa channel. The depressed channel promoted vasodilation through endothelial-dependent hyperpolarization (EDH) of the resistance artery in mice. VEGF-A downstream of MEK signaling weakened the above vasodilation response of ECs, indicating that VEGF-A played a new role in the resistance artery and provided a novel aspect of treating cardiovascular disease with VEGF-A (53).

In drug research, melatonin was observed to inhibit VEGF-induced monolayer permeability of HUVECs, which was related to the phosphorylation of VE-cadherin. Blocking PI3K/AKT and MEK/ERK pathways could inhibit the permeability of HUVECs, implying that AKT (Ser473) phosphorylation might be a key event in the change of monolayer permeability (54). Rosiglitazone activated PI3K-AKT or protein kinase C (PKC) β to promote the migration of ECs and induce vascular permeability. In addition, rosiglitazone might promote angiogenesis and vascular leakage by increasing the expression of VEGF and suppressing the expression of tight junction proteins (JAM-A and ZO-1), while inhibiting AKT reached the opposite (55). Excessive vascular permeability occurs during inflammation. Anti-VE-cadherin monoclonal antibodies (mAbs) activated cell adhesion and inhibited the increase of monolayer permeability of ECs induced by thrombin receptor activating peptide-6 (TRAP-6). Among mAbs, 8A12c and 3A5a could decrease vascular permeability, while the inhibitory mAb 2E11d could enhance vascular permeability. Activated mAbs could also depress vascular permeability induced by VEGF or TNF-α (56).

Inflammation

Inflammation, often accompanied by neovascularization, is a crucial feature of inducing pathological angiogenesis. Therefore, higher vascular permeability is often viewed together with the recruitment of inflammatory cells. VEGF can promote the recruitment of inflammatory cells, which are mostly composed of neutrophils and macrophages and, to a lesser extent, of T cells and B cells (57). In addition, VEGF-A-induced PLCγ activation can increase Ca^{2+}, which will activate the transcription factor NFAT through calcineurin. This way can not only energize angiogenesis but also induce inflammation gene expression pattern similar to IL-1β. Activating NF-κB downstream of AKT

can also cause inflammatory type response, leading to changes in gene expression profile. Advanced glycation end products (AGEs) can activate RAGE-NF-κB pathway in human synovial cells to induce the expression of cyclooxygenase-2 (COX-2) and VEGF, and then promote the production of prostaglandin-E2 (PGE2), VEGF, IL-6, and MMP-13 to exacerbate inflammation (58). Therefore, depressing VEGF may play an anti-inflammatory role and the value of VEGF can reflect the level of local inflammatory response (59). When treated by lipopolysaccharide (LPS), a kind of inflammatory mimic, human microvascular endothelial cells (HMEC-1) were found to secrete VEGF and prostaglandin (bFGF). However, further use of ibuprofen only reduced bFGF, but further enhanced the level of VEGF (60). In the MI mouse model, resveratrol (RSV)-loaded scaffolds increased the expression of cTnT, Cx-43, Trx-1, and VEGF; decreased inflammatory cell infiltration; and improved vascular network formation after MI (61). Therefore, higher VEGF level does not ensure increased inflammatory response and worse prognosis because complex regulatory mechanisms will form a comprehensive impact.

The Relation Between VEGF-A and Lipid Metabolism

VEGF-A has been shown to induce the accumulation of triglycerides in large lipoprotein granules, including VLDL, chylomicrons (CM), and residues. A VEGF-A transfer study found that VEGF-A decreased the activity of plasma lipoprotein lipase (LPL), and each model group showed the change of promoting AS in lipid spectrum (62). VEGF-A can also regulate lipid metabolism in intestinal lymphatic vessels through the VEGF-A/Nrp1/VEGFR-1 pathway (63). The mechanism lies in that the deletion of Nrp1 and VEGFR1 can inhibit CM entering chylous duct, promote the combination of VEGF-A and VEGFR-2, enhance the biological activity of VEGF-A, and then inhibit CM absorption (64). Anti-VEGF therapy can also affect serum lipids. The most common clinical treatment related to VEGF is antiangiogenic therapy applied in human tumors. In addition to increasing glycolysis and lactate production, bevacizumab, an anti-VEGF neutralizing antibody, can upregulate lipid metabolism pathways, resulting in spectacular changes in tumor lipid mass spectrometry, including increased triglyceride levels and decreased lipid chain saturation (65).

At the same time, the value of blood lipid can also regulate the level of VEGF-A and affect its biological activity. HFD has been proved to increase serum VEGF level (66). There is a self-regulating TNFα/NF-κB/HIF/VEGF signaling network in ECs that can mediate and regulate angiogenesis in a hypoxic environment, while elevated LDL can hamper angiogenesis by destroying this network, which may lead to decompensation of CHD patients (17). Adipocyte-conditioned medium from human adipocytes enhanced the expression of VEGFR-1 and VEGFR-2, and the secretion of VEGF by VSMCs. The increased VEGF then stimulated the proliferation of VSMCs. Therefore, VEGF may associate the inflammation of adipose tissue with the increased proliferation of VSMCs (67).

VEGF-B

VEGF-B discovered in 1995 is a homolog of VEGF, with which it shares high sequence homology, but it can only function by binding with VEGFR-1. There are two subtypes of VEGF-B, VEGF-B167 and VEGF-B186. As the main subtype, VEGF-B167, accounting for over 80% of the total number of VEGF-B, is expressed in most tissues. It can bind to cell surface or extracellular matrix (ECM) elements and easily interact with neuropeptide-1 (NP-1). VEGF-B186 exists in free state and will interact with NP-1 only when it undergoes proteolysis. VEGF-B conduces to the development of cardiovascular system and the formation of embryonic myocardium, but pertinent research about the effect and mechanism of VEGF-B is more limited than that of VEGF-A (68, 69).

Source of VEGF-B

VEGF-B is mainly expressed in myocardium, coronary artery smooth muscle cells, ECs, and pancreas, as well as in lung, kidney, gallbladder, and fat (70, 71).

Mechanisms Regulating the Level of VEGF-B

Upregulation Mechanism of VEGF-B

Vagal neurotransmitter acetylcholine upregulated the expression of VEGF-A and VEGF-B through the m/nACh-R/PI3K/Akt/Sp1 pathway in ECs. VEGF-B induced VSMC proliferation and EC migration, and finally promoted angiogenesis/arteriogenesis to repair MI heart under the synergistic effect with VEGF-A (70). RSV pretreatment increased the expression of VEGF-B, p-eNOS, and p-AMPK and the production of NO in rats treated with subcutaneous injection of isoproterenol (ISO) (72).

Downregulation Mechanism of VEGF-B

Some antitumor drugs can introduce cardiotoxicity by downregulating the expression of VEGF-B in cardiomyocytes. For example, doxorubicin (DOX) is a broad antineoplastic drug, which can suppress the expression of VEGF-B, while RSV significantly attenuated DOX-induced cardiotoxicity by lifting VEGF-B (73).

Receptors and Target Cells

VEGF-B functions on assorted kinds of cells and tissues in humans by binding to VEGFR-1. Not only can it promote the survival of VECs, but it also contributes to the survival of pericytes, smooth muscle cells (SMCs), and vascular stem cells/progenitor cells. *In vivo*, VEGF-B has been proved to inhibit choroidal and retinal neovascularization by regulating the expression of multiple vascular pro-survival genes (74).

Functions of VEGF-B

Angiogenesis

VEGF-B bears a weak angiogenesis capacity, but still plays a significant role in vascular growth and survival. VEGF-B is saliently expressed in tissues with high metabolic activity like heart. Studies have shown that overexpression of VEGF-B in myocardium could promote neovascularization directly from

the ventricle, maintain the connection with coronary vessels in subendocardial myocardium, accelerate the proliferation of subendocardial myocardial endothelium, and rescue the structure and function of myocardial tissue after MI (75). VEGF-B in cardiomyocytes can increase VEGF signal through VEGFR-2, activate Erk1/2, and promote vascular growth. VEGF-B can upregulate Akt and mTORC1 pathway, downregulate AMPK pathway, and reorganize the metabolic process of myocardium, which is conducive to glucose oxidation and macromolecular biosynthesis. Therefore, VEGF-B can be applied to increase the coronary vascular system in patients with ischemic heart disease and reprogram myocardial metabolism to improve cardiac function. However, the expression of VEGF-B decreases in CHD patients (76). A number of studies have revealed that adenovirus (AD) VEGF-B186 gene transfer caused significant angiogenesis in myocardium, increasing myocardial perfusion without increasing coronary steal effect. Some mechanisms may be related to G protein signaling. AdVEGF-B186 also enjoys tissue specificity and high efficiency on ischemic myocardium. It can also inhibit myocardial apoptosis and regulate myocardial metabolism, becoming a potential drug for the treatment of myocardial ischemia (77, 78).

Antioxidation

Oxidative stress can cause damage to VECs and increase the risk of CHD. It has been found that VEGF-B can lift many key antioxidant genes by binding with VEGFR-1, including Gpx1, one of the downstream effectors, in order to exert antioxidant effect (79). RSV is a natural antitoxin in polyphenol plant. Pretreatment with RSV significantly reduced the production of superoxide and malondialdehyde (MDA) in ISO-treated rats and increased superoxide dismutase (SOD) to play an antioxidant role. Besides, RSV prevented the adverse changes of infarct size and apoptosis in ISO-treated rats. Therefore, RSV may protect myocardium after MI through the VEGF-B/AMPK/eNOS/NO signaling pathway (72).

Anti-apoptosis

VEGF-B has a strong anti-apoptotic effect on both myocardial cells cultured *in vitro* and myocardial cells after MI. It has been found that VEGF-B could induce specific gene expression profiles of compensatory hypertrophy by activating VEGFR-1. Concretely, VEGF-B activated αMHC; inhibited βMHC and bone αactin; increased SERCA2a, RYR, PGC1α, and cardiac natriuretic peptide transcripts; and ultimately prevented the loss of myocardial mass and maintained myocardial contractility (80).

The Relation Between VEGF-B and Lipid Metabolism

VEGF-B enjoys effective lipid-lowering function. By binding with VEGFR-1 and NP-1, VEGF-B transcriptionally regulates vascular fatty acid transporters and specifically controls the uptake of fatty acids by ECs, which promotes the uptake and transcytosis of fatty acids from blood flow to lower tissues including heart and skeletal muscle, so as to reduce the circulating lipid. Moreover, the lipid uptake of ECs is closely related to the lipid utilization of mitochondria (81). The lipid regulation function of VEGF-B was elucidated by a research in which ceramide enhanced and triglyceride decreased in the heart of VEGF-B transgenic mice (82). VEGF-B also induced the expression of carnitine palmitoyltransferase-1 (CPT-1), and phosphorylated ACC and AMPK in the muscle and liver of mice fed with HFD to lower lipid (83). For type 2 diabetes mellitus (T2DM) patients, increased lipid handling and lipid toxicity may lead to dysfunction of islet β cells. Systemic inhibition of VEGF-B signal in T2DM patients prevented lipid accumulation, improved insulin sensitivity and glucose tolerance, and reduced the content of islet triglyceride. Mice, which owned islets β cells selectively had VEGF-B cleared, expressed higher islet genes. However, glucose homeostasis and islet lipid uptake were not affected by the clearance of VEGF-B (84). Another study also showed that inhibition of VEGF-B signal reconstructed membrane cholesterol level and restored glucose uptake, while enhancement of VEGF-B signal weakened LDL receptor (LDLR)-mediated cholesterol uptake, resulting in lower plasma membrane cholesterol load (85).

VEGF-C

VEGF-C, the central factor of lymphangiogenesis, promotes lymphangiogenesis by binding with VEGFR-3 on the surface of LECs and regulates the physiological and pathological proliferation of lymphatic vessels. Compared to VEGFR-3, VEGF-C has less affinity with VEGFR-2, while binding with which can also promote angiogenesis. In addition to the effect on lymphatic and blood vessels, VEGF-C is closely associated with dyslipidemia and AS (86). A prospective study found that low levels of VEGF-C could independently predict all-cause mortality in patients with suspected or confirmed coronary artery disease (CAD) (87), while high levels of VEGF-C could degrade inflammation after MI, which was beneficial to the repair of injured myocardium (88).

Source of VEGF-C

VEGF-C is highly expressed in embryonic tissues, such as syncytiotrophoblasts, cells in maternal decidua and endothelium of large placental vessels (89). In adults, VEGF-C is expressed in many parts including heart, lung, brain, kidney, intestine, and lymph nodes (90, 91).

Mechanisms Regulating the Level of VEGF-C

Upregulation Mechanism of VEGF-C

Studies about the upregulation mechanism of VEGF-C in the cardiovascular field are relatively scarce. High salt (HS) diet could upregulate the TonEBP/VEGF-C signaling pathway, leading macrophage to infiltrate and accelerate the process of left ventricular remodeling in hypertension (92). Hyperglycemia could also induce the VEGF-C expression through LPA1/3, PLC, Akt, ROS, and LEDGF-dependent pathways (93).

Most relevant studies focus on tumors. For example, the oncoprotein PLCE1 of esophageal squamous cell carcinoma (ESCC) was observed to promote the growth and proliferation of tumor blood vessels by upregulating VEGF-C (94).

Lysophosphatidic acid (LPA) also enhanced VEGF-C by stimulating LPA (1/3), COX-2, NF-κB, and EGFR trans activation-dependent mechanisms. Lymph markers were then increased, indicating these factors to be potential targets for controlling tumor metastasis (95). Higher VEGF-C stimulated by LPS promoted cell movement and lymphangiogenesis through TLR4-NF-κB/JNK signaling and then pushed the migration and invasion of colorectal cancer (CRC) (96). Noteworthily, oxLDL, as a risk factor of cardiovascular disease, was found to activate LOX-1-mediated NF-κB signaling pathway, lifted VEGF-C expression, and then promoted lymphatic metastasis of gastric cancer (97). In addition, there are related research in the field of cerebrovascular disease and skin disease. Theta pulse stimulation (CTBS) increased the expression of VEGF-C in cerebral meninges and promoted lymphangiogenesis (98). MiR-27b enhanced the expression of VEGF-C to promote the proliferation, migration, and angiogenesis of human microvascular endothelial cells (HMEC-1), thus conducing to angiogenesis and skin repair in scalded rats (99).

Downregulation Mechanism of VEGF-C

Because promoting lymphangiogenesis and angiogenesis can benefit the development of tumor, some studies have selected suppressing VEGF-C as a treatment to inhibit tumor growth, such as the highly specific RNA interference (RNAi) method (100). Through downregulating VEGF-C, miR-182-5p inhibited ERK and Akt signaling pathways to regulate angiogenesis and lymphangiogenesis, and partially regulate the tumorigenesis of colon cancer (101). Some drugs also present their direct suppressing effect on VEGF-C, like kolaviron in treating lymphatic filariasis (102) and norcantharidin in inhibiting lymphangiogenesis (103).

Receptors and Target Cells

VEGFR-2 and VEGFR-3 are the receptors of VEGF-C, and by binding with VEGFR-3 can VEGF-C have a major biological effect. VEGFR-3 is expressed in lymphatic endothelium and high endothelial venules, which affects the differentiation, proliferation, migration, and survival of LECs. It is also expressed in other cells, such as osteoblasts, macrophages, and neural progenitor cells. VEGFR-3 helps to shape the lymphatic network during embryonic development and promote the formation of novel lymphatic vessels in adulthood. Inflammation or tumor may promote the expression of VEGF-C and VEGFR-3, and stimulate high endothelial venules to reform lymphatic vessels (104–106).

Functions of VEGF-C

Inflammation and Lymphangiogenesis

The VEGF-C/VEGFR-3 signaling axis is of great importance to regulate the lymphatic system. Blocking the axis can interfere with lymphangiodilation and aggravate inflammation in a variety of disease models, including inflammatory bowel disease (IBD), rheumatoid arthritis, and skin inflammation. On the contrary, the targeted increase of VEGF-C can improve lymphangiodilation and reduce inflammation in such diseases (107). Many studies have proved that the cardiac lymphatic system can affect the regeneration potential of myocardium, making lymphangiogenesis a therapeutic target to accelerate the repair of injured heart (108, 109). After acute MI, VEGF-C stimulation conduce to the proliferation of cardiac lymphatic vessels, and transport immune cells to mediastinal lymph nodes (MLNs) through lymphatic vessel endothelial hyaluronic acid receptor-1 (LYVE-1), thus promoting the clearance of acute inflammatory response and cardiac repair (110). In addition, pre-treating lymphatic contractility with VEGF-C may prevent AS. As a study showed, early treatment with VEGF-C improved lymphatic molecule transport in LDLR –/– mice by lifting VEGFR-3 and FOXC2, and then limited plaque formation and macrophage accumulation (111). Some studies also illuminate that the inhibition or enhancement of VEGF-C can benefit hypertrophic cardiomyopathy. LCZ696, a new combination of angiotensin and enkephalinase inhibitor, could reduce the protein expression levels of VEGF-C, VEGFR3, and LYVE-1 in heart tissue of mice and improve the transport load of lymphatic vessels to macrophages, thus inhibiting the remodeling of lymphatic system in a hypertrophic cardiomyopathy model (112). However, a recent study also showed that the activation of the VEGF-C/VEGFR-3 axis prevented hypertrophic heart to heart failure (HF) and highlighted the selective stimulation of cardiac lymphangiogenesis as a potential treatment for hypertrophic cardiomyopathy (113). HS diet can also affect the level of VEGF-C. It was found that HS diet upregulated the TonEBP/VEGF-C signaling pathway, leading to severe macrophage infiltration and accelerating the process of left ventricular remodeling during hypertension (92). By contrast, overexpression of VEGF-C in HS mice promoted cardiac lymphangiogenesis, reduced myocardial fibrosis and macrophage infiltration, and preserved left ventricular function (114). In addition to the VEGF-C/VEGFR-3 pathway, the VEGFC/FLT4/PROX1 signal transduction axis could also promote the migration, proliferation, and differentiation of LECs, with hemopoietic expression homeobox (HHEX) as its upstream regulator (115).

Angiogenesis

VEGF-C regulates angiogenesis when binding with VEGFR-2. There is a link between angiogenesis and lymphangiogenesis; that is, angiogenesis will be significantly weakened when the lymphatic network is growing continually. Therefore, angiogenesis controlled by VEGF-C preferentially occurs far away from sites where lymphangiogenesis is happening. VEGF-C presents angiogenesis capacity through hydrolyzing and activating proteins in ECs. Intramyocardial injection of VEGF-C can induce the establishment of collateral circulation in ischemic myocardium (116). In addition, the angiogenic effect of VEGF-C is manifested in its influence on the development of coronary artery (CA). During the embryonic stage, VEGF-C plays a key role in the correct location and growth of CA stem on the aorta. In this process, VEGF-C is required to stimulate the vascular growth around the outflow tract and the absence of VEGF-C will lead to severe hypoplastic peripheral vessels in the heart, and delayed development and abnormal position of CA stem (117). Some specific forms of

VEGF-C, like VEGF-C156S, lack angiogenesis function and only retain lymphangiogenesis function. In all, VEGF-C enjoys better lymphangiogenesis function than angiogenesis and improves lymphatic reflux disorder. Although it shows certain dilation effect on blood vessels, no evidence of angiogenesis or increased vascular permeability has ever been observed (118).

Anti-apoptosis

In the myocardial ischemia/reperfusion (I/R) injury model, myocardium pretreated with VEGF-C showed a lower MI area and a lower value of CK-MB, MDA, troponin, and apoptotic protein Bax. The mechanism lies in that VEGF-C activates Akt signaling pathway by binding to VEGFR-2 and blocks Bax expression and mitochondrial membrane translocation, thus inhibiting cardiomyocyte apoptosis and exerting cardioprotective effect after I/R injury (119).

Fibrogenesis

VEGF-C/VEGFR-3 significantly increased in a MI mice study. In addition to its regulatory effects on lymphatic vessels and inflammation, it directly promoted the proliferation, migration, and collagen synthesis of cardiac fibroblasts by activating TGF-β1 and ERK signaling pathways, and ultimately promoted myocardial fibrosis after MI (120).

The Relation Between VEGF-C and Lipid Metabolism

The lymphatic system transports lipids from food that is absorbed by intestinal cells and packaged as CM into blood. The VEGF-C/VEGFR-3 pathway is involved in the lipid transport of intestinal lymphatic vessels, and dysfunction of the transport can lead to dyslipidemia. VEGF-C-deficient mice showed defected lipid absorption and increased excretion of fecal with dietary cholesterol and fatty acids. These mice also resisted obesity and improved glucose metabolism when fed with HFD. The mechanism may be related to intestinal lymphatic atrophy caused by VEGF-C deficiency (121). Another study observed that the inactivation of VEGFR-3 resulted in the retention of triglycerides (TGs) in the intestinal epithelial cells of the small intestine, reduced the postprandial level of plasma TGs, and increased the excretion of free fatty acids (FFA) and TGS into feces (122). Furthermore, systemic blockade of VEGFR-3 was demonstrated to reduce the infiltration of macrophages in adipose tissue and lipid accumulation in liver, and improve insulin sensitivity, revealing the unexpected effect of blocking VEGF-C and VEGF-D on the treatment of metabolic syndrome, which constituted a new therapeutic strategy for the prevention of obesity related insulin resistance (123). On the contrary, overexpression of VEGF-C transfer gene induced weight gain and insulin resistance in mice, and promoted the progress of metabolic syndrome (124).

Meanwhile, lipids can also influence the capacity of lymphatic vessels. Concretely, long-term HFD may cause adipose tissue expansion and the dysfunction of lymphatic system, especially collecting lymphatic vessels, further promoting the accumulation of adipose tissue (125).

VEGF-D

VEGF-D, like VEGF-C, is a secretory glycoprotein. They share structural homology with each other and both promote lymphangiogenesis and angiogenesis by binding with VEGFR-2 and VEGFR-3. They emphasize on different functions, however, with VEGF-C being an essential factor for lymphangiogenesis, while VEGF-D compensates for the loss of VEGF-C during lymphangiogenesis and behaves more subtly. Besides, VEGF-D presents higher angiogenic potential than VEGF-C. A prospective study concluded that high levels of VEGF-D independently predicted all-cause mortality in patients with suspected or confirmed CAD (126). The increased VEGF-D was also associated with atrial fibrillation (AF) and ischemic stroke. The relationship between VEGF-D and ischemic stroke was more obvious in subjects diagnosed with AF (127).

Source of VEGF-D

VEGF-D is highly expressed in the lung in the embryonic stage (128), while in adulthood, it is highly expressed in the heart, lung, and small intestine, but is expressed less in skeletal muscle, pancreas, and colon (129).

Mechanisms Regulating the Level of VEGF-D

Upregulation Mechanism of VEGF-D

Inflammation can induce lymphangiogenesis. Studies have proved that inflammation can energize NF-κB to lift Prox1 and VEGFR-3. Then, the response of LECs to VEGF-C and VEGF-D is enhanced, which further promotes lymphangiogenesis (130). In a mice study, proinflammatory cytokine onterleukin-1β (IL-1β) activated NF-κB and then enhanced the production of VEGF-A, VEGF-C, and VEGF-D, ultimately inducing lymphangiogenesis in cornea (131). Higher VEGF-D levels can also result from a variety of tumor cells. For example, STAT3 in gastric cancer cells was found to promote lymphangiogenesis and lymph node metastasis by upregulating the expression of VEGF-D (132). Also, IL-7 could promote lymphatic proliferation and lymphatic spread in breast cancer cells by upregulating VEGF-D (133).

Downregulation Mechanism of VEGF-D

In terms of cardiovascular disease, the elevated level of VEGF-D in HF patients can be regulated to normal after heart transplantation (HT), which reflects the reversal of pulmonary congestion and the recovery of pulmonary artery compliance (PAC) and pulmonary vascular resistance (PVR) after HT (134). IL-1β is an increased proinflammatory cytokine in heart after MI. The factor is involved in downregulating VEGF-D in cardiac microvascular endothelial cells (CMECs) through ERK1/2, JNK, and PKCα/β, which then affects angiogenesis (135). Related studies about lung have shown that LPS induced lung injury suppressed the expression of VEGF-D, as well as VEGF-A, -B, -C, and VEGFR-1,−2,−3 (136). In addition, transforming growth factor-β1 (TGF-β1) abated VEGF-D expression in a dose- and time-dependent manner in human lung fibroblasts (137). In the field of cancer, sophocarpine was viewed to cut down the

expression of VEGF-A, -C, and -D in CRC cells by decreasing N-cadherin, MMP-9, phosphorylated ERK, and phosphorylated MEK (138).

Receptors and Target Cells

VEGF-D mediates angiogenesis and lymphangiogenesis by binding to VEGFR-2 and VEGFR-3 on ECs. VEGFR-2 is the core receptor of angiogenesis, and VEGFR-3 is essential for lymphangiogenesis. However, VEGFR-3 can also participate in angiogenesis by promoting the transformation of ECs from tip cell to stalk cell phenotype at the fusion point of vascular bud. Blocking VEGFR-3 can inhibit angiogenesis. Meanwhile, VEGFR-2 can also induce lymphatic vessel enlargement to regulate lymphangiogenesis. VEGF-D can also signal through the VEGFR-2/VEGFR-3 heterodimer, which can further boost the expansion of tumor collecting lymphatic vessels (139).

Functions of VEGF-D

Lymphangiogenesis

Lymphangiogenesis is the cardinal biological effect of VEGF-D. In patients with aortic stenosis, the number of lymphatic vessels and the expression of VEGF-D, VEGFR-3, and VEGFR-2 in aortic valves were increased, indicating that lymphangiogenesis was induced in the progression of aortic stenosis (140). In a mice study, chronic overexpression of VEGF-D induced growth of novel lymphatic vessels in white adipose tissue and lymphangiodilation in brown adipose tissue, which benefited lipid metabolism and alleviated chronic inflammation. VEGF-D in white adipose tissue also increased macrophage infiltration and tissue fibrosis (141).

Angiogenesis

The mature form of human VEGF-D is an effective angiogenesis factor as it can increase the expression of VEGF-A, stanniocalcin-1 (STC1), and neuropilin (NRP)-2 to promote angiogenesis (142). Angiogenesis is the core of cardiac repair after MI. Cardiac angiotensin-converting enzyme (ACE)2 produces angiotensin (Ang)1–7, which in turn stimulates the expression of VEGF-D and MMP-9 in the heart to promote angiogenesis, thus conducing to heart recovery and improving ventricular function (143). As for treatment, the biological bypass of angiogenesis induced by VEGF-D gene therapy (GT) is a new concept for treating cardiac ischemia. Serotype 5 adenovirus is used to transfer VEGF-D cDNA to ischemic myocardium (144). A phase I/II a clinical trial showed that adenovirus VEGF-D ΔNΔC gene increased myocardial perfusion in the damaged area of myocardial perfusion reserve (145). Adenovirus-mediated VEGF-D gene transfer also presented excellent angiogenesis in rabbit skeletal muscle (146). In addition, VEGF-D-related angiogenesis is correlated to tumor progression. Cathepsin L (CTSL) could induce angiogenesis by regulating the CDP/Cux/VEGF-D pathway (147).

Fibrogenesis

VEGF-D can promote cardiac fibrosis, which regulates cardiac repair and remodeling. VEGF-D and VEGFR-3 were significantly upregulated in hearts of MI patients, especially in myofibroblasts at MI sites. A study proved that VEGF-D could stimulate the synthesis of MMP-2/-9 and tissue inhibitor of MMP (TIMP)-1/-2, and activate ERK phosphorylation, thus significantly increasing the proliferation and migration of cardiac fibroblasts. Last, the synthesis of type I collagen was significantly upregulated in a dose- and time-dependent manner, which promoted cardiac fibrosis (148).

Anti-apoptosis

VEGF-D may inhibit AS progression by its antioxidant virtue. Exogenous stimulation (such as hypochlorite) on ECs can be regulated by VEGF-D through mTOR kinase signal transduction to induce antioxidant response and maintain redox balance (149).

The Relation Between VEGF-D and Lipid Metabolism

VEGF-D is an important regulator of lipid metabolism. Downregulation of VEGF-D/VEGFR3 signaling can decrease the genes that regulate the production of TGs and cholesterol, as well as the peroxisome β-oxidative pathway. In a LDLR –/– ApoB 100/100 mice study, knockout of VEGF-D gene could significantly increase plasma TGs and cholesterol and delay clearance of residual particles of large CMs that could not easily penetrate VECs. The mechanism was that inhibiting VEGF-D signal would reduce the expression of SCD1 (one of the main CMs residual receptors in LDLR deficiency) in the liver (150). In contrast, overexpression of VEGF-D in adipose tissue induced lymphangiogenesis in adipose tissue of mice, enhanced glucose clearance, and reduced insulin level and liver triglyceride, thereby resisting obesity-related immune accumulation and improving metabolic response (151).

CONCLUSIONS

The VEGF family shows its extraordinary potential in the treatment of CHD by regulating angiogenesis, lymphangiogenesis, inflammation, apoptosis, redox, fibrogenesis, and lipid metabolism. Previous studies mostly focus on tumor and ophthalmic diseases, while studies about applying VEGF treating cardiovascular disease are relatively scarce. The following insights into the VEGF-related direction of treating CHD may be illuminating in the obscure field. The VEGF family interferes with humans in a complicated way because these factors present duality in their functions and the outcomes in target tissues can also be opposite with the stimulation of an identical factor. Concretely, a certain degree of angiogenesis conduces to cardiac recovery from hypoxia, while an excessive amount of it may push AS plaques to an unstable state. Different isoforms of VEGF-A can vary in quantities in disparate environments and thus display an overall angiogenetic or anti-angiogenetic function. Researchers can analyze the dynamics of the isoforms in CHD patients and locate the favorable realm by incorporating their health condition. Then, the realm may be set for a treatment target for CHD and a predictor for prognosis. Regarding lymphangiogenesis, the VEGF family is closely tied to the lymphatic system, which further regulates inflammation,

redox, lipid metabolism, and so on, while clinical studies rarely extract lymph from patients to test its component, let alone the different composition between CHD and healthy people. Their level in lymph may not be comparable to that in serum. In addition to lymph, the lymphatic system in the intestinal tract makes another attraction due to its intimate association with lipid metabolism. The imaging of the intestinal lymphatic system may be a possible way for predicting VEGF level, lipid level, and CHD progression. Therefore, by summarizing and assorting functions and mechanisms of the VEGF family, we hope that this study can provide help for researchers who start from the VEGF family to find therapeutic targets for CHD.

AUTHOR CONTRIBUTIONS

YZ chose the title, assorted information, and drafted the manuscript. XZ drafted the manuscript. HC offered advice about the structure. JS, GY, and SS assorted information. YH governed the whole process and offered advice. All authors contributed to the article and approved the submitted version.

REFERENCES

1. Zhu KF, Wang YM, Zhu JZ, Zhou QY, Wang NF. National prevalence of coronary heart disease and its relationship with human development index: a systematic review. *Eur J Prev Cardiol.* (2016) 23:530–43. doi: 10.1177/2047487315587402
2. Hu SS, Gao RL, Liu LS, Zhu ML, Wang W, Wang YJ, et al. The abstract of 2018 report of Chinese cardiovascular disease. *Chin Circ Mag.* (2019) 34:209–20.
3. Hansson GK. Inflammation, atherosclerosis, and coronary artery disease. *N Engl J Med.* (2005) 352:1685–95. doi: 10.1056/NEJMra043430
4. Genest JJ, Martin-Munley SS, McNamara JR, Ordovas JM, Jenner J, Myers RH, et al. Familial lipoprotein disorders in patients with premature coronary artery disease. *Circulation.* (1992) 85:2025–33. doi: 10.1161/01.CIR.85.6.2025
5. Sabatine MS, Wiviott SD, Im K, Murphy SA, Giugliano RP. Efficacy and safety of further lowering of low-density lipoprotein cholesterol in patients starting with very low levels: a meta-analysis. *Jama Cardiol.* (2018) 3:823–8. doi: 10.1001/jamacardio.2018.2258
6. Geovanini GR, Libby P. Atherosclerosis and inflammation: overview and updates. *Clin Sci.* (2018) 132:1243–52. doi: 10.1042/CS20180306
7. Li H, Sun K, Zhao R, Hu J, Hao Z, Wang F, et al. Inflammatory biomarkers of coronary heart disease. *Front Biosci.* (2018) 10:185–96. doi: 10.2741/s508
8. Melincovici CS, Bosca AB, Susman S, Marginean M, Mihu C, Istrate M, et al. Vascular endothelial growth factor (VEGF) - key factor in normal and pathological angiogenesis. *Rom J Morphol Embryol.* (2018) 59:455–67.
9. Claesson-Welsh L, Welsh M. VEGFA and tumour angiogenesis. *J Intern Med.* (2013) 273:114–27. doi: 10.1111/joim.12019
10. Garcia R, Bouleti C, Sirol M, Logeart D, Monnot C, Ardidie-Robouant C, et al. VEGF-A plasma levels are associated with microvascular obstruction in patients with ST-segment elevation myocardial infarction. *Int J Cardiol.* (2019) 291:19–24. doi: 10.1016/j.ijcard.2019.02.067
11. Itatani Y, Kawada K, Yamamoto T, Sakai Y. Resistance to anti-angiogenic therapy in cancer-alterations to anti-VEGF pathway. *Int J Mol Sci.* (2018) 19:1232. doi: 10.3390/ijms19041232
12. Ganta VC, Choi M, Kutateladze A, Annex BH. VEGF165b modulates endothelial VEGFR1-STAT3 signaling pathway and angiogenesis in human and experimental peripheral arterial disease. *Circ Res.* (2017) 120:282–95. doi: 10.1161/CIRCRESAHA.116.309516
13. Arcondeguy T, Lacazette E, Millevoi S, Prats H, Touriol C. VEGF-A mRNA processing, stability and translation: a paradigm for intricate regulation of gene expression at the post-transcriptional level. *Nucleic Acids Res.* (2013) 41:7997–8010. doi: 10.1093/nar/gkt539
14. Braile M, Marcella S, Cristinziano L, Galdiero MR, Modestino L, Ferrara AL, et al. VEGF-A in cardiomyocytes and heart diseases. *Int J Mol Sci.* (2020) 21:5294. doi: 10.3390/ijms21155294
15. Ferrara N. Vascular endothelial growth factor: basic science and clinical progress. *Endocr Rev.* (2004) 25:581–611. doi: 10.1210/er.2003-0027
16. Arany Z, Foo SY, Ma Y, Ruas JL, Bommi-Reddy A, Girnun G, et al. HIF-independent regulation of VEGF and angiogenesis by the transcriptional coactivator PGC-1alpha. *Nature.* (2008) 451:1008–12. doi: 10.1038/nature06613
17. Jin F, Zheng X, Yang Y, Yao G, Ye L, Doeppner TR, et al. Impairment of hypoxia-induced angiogenesis by LDL involves a HIF-centered signaling network linking inflammatory TNFalpha and angiogenic VEGF. *Aging (Albany NY).* (2019) 11:328–49. doi: 10.18632/aging.101726
18. Longchamp A, Mirabella T, Arduini A, MacArthur MR, Das A, Trevino-Villarreal JH, et al. Amino acid restriction triggers angiogenesis via GCN2/ATF4 regulation of VEGF and H2S production. *Cell.* (2018) 173:117–29. doi: 10.1016/j.cell.2018.03.001
19. Guo L, Akahori H, Harari E, Smith SL, Polavarapu R, Karmali V, et al. CD163+ macrophages promote angiogenesis and vascular permeability accompanied by inflammation in atherosclerosis. *J Clin Invest.* (2018) 128:1106–24. doi: 10.1172/JCI93025
20. Ferraro B, Leoni G, Hinkel R, Ormanns S, Paulin N, Ortega-Gomez A, et al. Pro-angiogenic macrophage phenotype to promote myocardial repair. *J Am Coll Cardiol.* (2019) 73:2990–3002. doi: 10.1016/j.jacc.2019.03.503
21. Cai LX, Alkassis FF, Kasahara H. Defective coronary vessel organization and reduction of VEGF-A in mouse embryonic hearts with gestational mild hypoxia. *Dev Dyn.* (2020) 249:636–45. doi: 10.1002/dvdy.149
22. Wei G, Yin Y, Duan J, Guo C, Zhu Y, Wang Y, et al. Hydroxysafflor yellow A promotes neovascularization and cardiac function recovery through HO-1/VEGF-A/SDF-1alpha cascade. *Biomed Pharmacother.* (2017) 88:409–20. doi: 10.1016/j.biopha.2017.01.074
23. Zou J, Wang N, Liu M, Bai Y, Wang H, Liu K, et al. Nucleolin mediated pro-angiogenic role of Hydroxysafflor Yellow A in ischaemic cardiac dysfunction: Post-transcriptional regulation of VEGF-A and MMP-9. *J Cell Mol Med.* (2018) 22:2692–705. doi: 10.1111/jcmm.13552
24. Zhai S, Zhang XF, Lu F, Chen WG, He X, Zhang CF, et al. Chinese medicine GeGen-DanShen extract protects from myocardial ischemic injury through promoting angiogenesis via up-regulation of VEGF/VEGFR2 signaling pathway. *J Ethnopharmacol.* (2021) 267:113475. doi: 10.1016/j.jep.2020.113475
25. Zhang J, Liu A, Hou R, Zhang J, Jia X, Jiang W, et al. Salidroside protects cardiomyocyte against hypoxia-induced death: a HIF-1alpha-activated and VEGF-mediated pathway. *Eur J Pharmacol.* (2009) 607:6–14. doi: 10.1016/j.ejphar.2009.01.046
26. Wu M, Zhou J, Cheng M, Boriboun C, Biyashev D, Wang H, et al. E2F1 suppresses cardiac neovascularization by down-regulating VEGF and PlGF expression. *Cardiovasc Res.* (2014) 104:412–22. doi: 10.1093/cvr/cvu222
27. Zhao C, Zhang B, Jiang J, Wang Y, Wu Y. Up-regulation of ANXA1 suppresses polymorphonuclear neutrophil infiltration and myeloperoxidase activity by activating STAT3 signaling pathway in rat models of myocardial ischemia-reperfusion injury. *Cell Signal.* (2019) 62:109325. doi: 10.1016/j.cellsig.2019.05.010
28. Chantzichristos VG, Agouridis AP, Moutzouri E, Stellos K, Elisaf MS, Tselepis AD. Plasma VEGF and IL-8 Levels in Patients with Mixed Dyslipidaemia. Effect of Rosuvastatin Monotherapy or its Combination at a Lower Dose with Omega-3 Fatty Acids: A Pilot Study. *Curr Vasc Pharmacol.* (2016) 14:474–80. doi: 10.2174/1570161114666160404125341
29. Semenova AE, Sergienko IV, Masenko VP, Ezhov MV, Gabrusenko SA, Kuharchuk VV, et al. The influence of rosuvastatin therapy and percutaneous coronary intervention on angiogenic growth factors in coronary artery disease patients. *Acta Cardiol.* (2009) 64:405–9. doi: 10.2143/AC.64.3.2038029
30. Sang H, Yuan N, Yao S, Li F, Wang J, Fang Y, et al. Inhibitory effect of the combination therapy of simvastatin and pinocembrin

on atherosclerosis in ApoE-deficient mice. *Lipids Health Dis.* (2012) 11:166. doi: 10.1186/1476-511X-11-166
31. Shibuya M. Vascular endothelial growth factor receptor-1 (VEGFR-1/Flt-1): a dual regulator for angiogenesis. *Angiogenesis.* (2006) 9:225–30. doi: 10.1007/s10456-006-9055-8
32. Koch S, Claesson-Welsh L. Signal transduction by vascular endothelial growth factor receptors. *Cold Spring Harb Perspect Med.* (2012) 2:a6502. doi: 10.1101/cshperspect.a006502
33. Shibuya M. Differential roles of vascular endothelial growth factor receptor-1 and receptor-2 in angiogenesis. *J Biochem Mol Biol.* (2006) 39:469–78. doi: 10.5483/BMBRep.2006.39.5.469
34. Long YM, Yang XZ, Yang QQ, Clermont AC, Yin YG, Liu GL. et al. PM25 induces vascular permeability increase through activating MAPK/ERK signaling pathway and ROS generation. *J Hazard Mater.* (2020) 386:121659. doi: 10.1016/j.jhazmat.2019.121659
35. Jiang BH, Liu LZ. PI3K/PTEN signaling in angiogenesis and tumorigenesis. *Adv Cancer Res.* (2009) 102:19–65. doi: 10.1016/S0065-230X(09)02002-8
36. Watari K, Shibata T, Fujita H, Shinoda A, Murakami Y, Abe H, et al. NDRG1 activates VEGF-A-induced angiogenesis through PLCgamma1/ERK signaling in mouse vascular endothelial cells. *Commun Biol.* (2020) 3:107. doi: 10.1038/s42003-020-0829-0
37. Zhang Q, Lu S, Li T, Yu L, Zhang Y, Zeng H, et al. ACE2 inhibits breast cancer angiogenesis via suppressing the VEGFa/VEGFR2/ERK pathway. *J Exp Clin Cancer Res.* (2019) 38:173. doi: 10.1186/s13046-019-1156-5
38. Lother A, Deng L, Huck M, Furst D, Kowalski J, Esser JS, et al. Endothelial cell mineralocorticoid receptors oppose VEGF-induced gene expression and angiogenesis. *J Endocrinol.* (2019) 240:15–26. doi: 10.1530/JOE-18-0494
39. Zhao W, Cao L, Ying H, Zhang W, Li D, Zhu X, et al. Endothelial CDS2 deficiency causes VEGFA-mediated vascular regression and tumor inhibition. *Cell Res.* (2019) 29:895–910. doi: 10.1038/s41422-019-0229-5
40. Li J, Cao GY, Zhang XF, Meng ZQ, Gan L, Li JX, et al. Chinese medicine She-Xiang-Xin-Tong-Ning, containing moschus, corydalis and ginseng, protects from myocardial ischemia injury via angiogenesis. *Am J Chin Med.* (2020) 48:107–26. doi: 10.1142/S0192415X20500068
41. Xu DP, Zou DZ, Qiu HL, Wu HL. Traditional chinese medicine ShenZhuGuanXin granules mitigate cardiac dysfunction and promote myocardium angiogenesis in myocardial infarction rats by upregulating PECAM-1/CD31 and VEGF expression. *Evid Based Complement Alternat Med.* (2017) 2017:5261729. doi: 10.1155/2017/5261729
42. Zhang KJ, Zhu JZ, Bao XY, Zheng Q, Zheng GQ, Wang Y. Shexiang baoxin pills for coronary heart disease in animal models: preclinical evidence and promoting angiogenesis mechanism. *Front Pharmacol.* (2017) 8:404. doi: 10.3389/fphar.2017.00404
43. Xu X, Wu L, Zhou X, Zhou N, Zhuang Q, Yang J, et al. Cryptotanshinone inhibits VEGF-induced angiogenesis by targeting the VEGFR2 signaling pathway. *Microvasc Res.* (2017) 111:25–31. doi: 10.1016/j.mvr.2016.12.011
44. Wang L, Wu H, Xiong L, Liu X, Yang N, Luo L, et al. Quercetin downregulates cyclooxygenase-2 expression and HIF-1alpha/VEGF signaling-related angiogenesis in a mouse model of abdominal aortic aneurysm. *Biomed Res Int.* (2020) 2020:9485398. doi: 10.1155/2020/9485398
45. Park JY, Ji YS, Zhu H, Zhang Y, Park DH, Kim YJ, et al. Anti-angiogenic effect of asperchalasine a via attenuation of VEGF signaling. *Biomolecules.* (2019) 9:358. doi: 10.3390/biom9080358
46. Yu M, Liu W, Li J, Lu J, Lu H, Jia W, et al. Exosomes derived from atorvastatin-pretreated MSC accelerate diabetic wound repair by enhancing angiogenesis via AKT/eNOS pathway. *Stem Cell Res Ther.* (2020) 11:350. doi: 10.1186/s13287-020-01824-2
47. Chen W, Ni J, Qiao Z, Wu Y, Lu L, Zheng J, et al. Comparison of the clinical outcomes of two physiological ischemic training methods in patients with coronary heart disease. *Open Med.* (2019) 14:224–33. doi: 10.1515/med-2019-0016
48. Li Y, Yao Y, Li J, Chen Q, Zhang L, Wang QK. Losartan protects against myocardial ischemia and reperfusion injury via vascular integrity preservation. *FASEB J.* (2019) 33:8555–64. doi: 10.1096/fj.201900060R
49. Brkovic A, Sirois MG. Vascular permeability induced by VEGF family members *in vivo*: role of endogenous PAF and NO synthesis. *J Cell Biochem.* (2007) 100:727–37. doi: 10.1002/jcb.21124
50. Li X, Redfors B, Sainz-Jaspeado M, Shi S, Martinsson P, Padhan N, et al. Suppressed vascular leakage and myocardial edema improve outcome from myocardial infarction. *Front Physiol.* (2020) 11:763. doi: 10.3389/fphys.2020.00763
51. Fantin A, Lampropoulou A, Senatore V, Brash JT, Prahst C, Lange CA, et al. VEGF165-induced vascular permeability requires NRP1 for ABL-mediated SRC family kinase activation. *J Exp Med.* (2017) 214:1049–64. doi: 10.1084/jem.20160311
52. Zhang S, Hu X, Guo S, Shi L, He Q, Zhang P, et al. Myricetin ameliorated ischemia/reperfusion-induced brain endothelial permeability by improvement of eNOS uncoupling and activation eNOS/NO. *J Pharmacol Sci.* (2019) 140:62–72. doi: 10.1016/j.jphs.2019.04.009
53. Ye X, Beckett T, Bagher P, Garland CJ, Dora KA, VEGF-A. inhibits agonist-mediated Ca(2+) responses and activation of IKCa channels in mouse resistance artery endothelial cells. *J Physiol.* (2018) 596:3553–66. doi: 10.1113/JP275793
54. Yang L, Zhang Y, Ma Y, Du J, Gu L, Zheng L, et al. Effect of melatonin on EGF- and VEGF-induced monolayer permeability of HUVECs. *Am J Physiol Heart Circ Physiol.* (2019) 316:H1178–91. doi: 10.1152/ajpheart.00542.2018
55. Ku YH, Cho BJ, Kim MJ, Lim S, Park YJ, Jang HC, et al. Rosiglitazone increases endothelial cell migration and vascular permeability through Akt phosphorylation. *BMC Pharmacol Toxicol.* (2017) 18:62. doi: 10.1186/s40360-017-0169-y
56. Park KS, Schecterson L, Gumbiner BM. Enhanced endothelial barrier function by monoclonal antibody activation of vascular endothelial cadherin. *Am J Physiol Heart Circ Physiol.* (2021) 320:H1403–10. doi: 10.1152/ajpheart.00002.2021
57. Sinnathamby T, Yun J, Clavet-Lanthier ME, Cheong C, Sirois MG. VEGF and angiopoietins promote inflammatory cell recruitment and mature blood vessel formation in murine sponge/Matrigel model. *J Cell Biochem.* (2015) 116:45–57. doi: 10.1002/jcb.24941
58. Chen YJ, Chan DC, Chiang CK, Wang CC, Yang TH, Lan KC, et al. Advanced glycation end-products induced VEGF production and inflammatory responses in human synoviocytes via RAGE-NF-kappaB pathway activation. *J Orthop Res.* (2016) 34:791–800. doi: 10.1002/jor.23083
59. Lucarini G, Zizzi A, Rubini C, Ciolino F, Aspriello SD. VEGF Microvessel Density, and CD44 as Inflammation Markers in Peri-implant Healthy Mucosa, Peri-implant Mucositis, and Peri-implantitis: Impact of Age, Smoking, PPD, and Obesity. *Inflammation.* (2019) 42:682–9. doi: 10.1007/s10753-018-0926-0
60. Wiktorowska-Owczarek A, Namiecinska M, Owczarek J. The effect of ibuprofen on bFGF, VEGF secretion and cell proliferation in the presence of LPS in HMEC-1 cells. *Acta Pol Pharm.* (2015) 72:889–94.
61. Campbell JD, Lakshmanan R, Selvaraju V, Accorsi D, McFadden DW, Maulik N, et al. Engineered resveratrol-loaded fibrous scaffolds promotes functional cardiac repair and regeneration through Thioredoxin-1 mediated VEGF pathway. *Int J Pharm.* (2021) 597:120236. doi: 10.1016/j.ijpharm.2021.120236
62. Heinonen SE, Kivela AM, Huusko J, Dijkstra MH, Gurzeler E, Makinen PI, et al. The effects of VEGF-A on atherosclerosis, lipoprotein profile, and lipoprotein lipase in hyperlipidaemic mouse models. *Cardiovasc Res.* (2013) 99:716–23. doi: 10.1093/cvr/cvt148
63. Hokkanen K, Tirronen A, Yla-Herttuala S. Intestinal lymphatic vessels and their role in chylomicron absorption and lipid homeostasis. *Curr Opin Lipidol.* (2019) 30:370–6. doi: 10.1097/MOL.0000000000000626
64. Zhang F, Zarkada G, Han J, Li J, Dubrac A, Ola R, et al. Lacteal junction zippering protects against diet-induced obesity. *Science.* (2018) 361:599–603. doi: 10.1126/science.aap9331
65. Curtarello M, Tognon M, Venturoli C, Silic-Benussi M, Grassi A, Verza M, et al. Rewiring of lipid metabolism and storage in ovarian cancer cells after anti-VEGF therapy. *Cells-Basel.* (2019) 8:1601. doi: 10.3390/cells8121601
66. Schuler R, Seebeck N, Osterhoff MA, Witte V, Floel A, Busjahn A, et al. VEGF and GLUT1 are highly heritable, inversely correlated and affected by dietary fat intake: consequences for cognitive function in humans. *Mol Metab.* (2018) 11:129–36. doi: 10.1016/j.molmet.2018.02.004
67. Schlich R, Willems M, Greulich S, Ruppe F, Knoefel WT, Ouwens DM, et al. VEGF in the crosstalk between human adipocytes and smooth muscle

cells: depot-specific release from visceral and perivascular adipose tissue. *Mediators Inflamm.* (2013) 2013:982458. doi: 10.1155/2013/982458
68. Li X, Aase K, Li H, von Euler G, Eriksson U. Isoform-specific expression of VEGF-B in normal tissues and tumors. *Growth Factors.* (2001) 19:49–59. doi: 10.3109/08977190109001075
69. Takahashi H, Shibuya M. The vascular endothelial growth factor (VEGF)/VEGF receptor system and its role under physiological and pathological conditions. *Clin Sci.* (2005) 109:227–41. doi: 10.1042/CS20040370
70. Lv YX, Zhong S, Tang H, Luo B, Chen SJ, Chen L, et al. VEGF-A and VEGF-B coordinate the arteriogenesis to repair the infarcted heart with vagus nerve stimulation. *Cell Physiol Biochem.* (2018) 48:433–49. doi: 10.1159/000491775
71. Hagberg CE, Mehlem A, Falkevall A, Muhl L, Fam BC, Ortsater H, et al. Targeting VEGF-B as a novel treatment for insulin resistance and type 2 diabetes. *Nature.* (2012) 490:426–30. doi: 10.1038/nature11464
72. Feng L, Ren J, Li Y, Yang G, Kang L, Zhang S, et al. Resveratrol protects against isoproterenol induced myocardial infarction in rats through VEGF-B/AMPK/eNOS/NO signalling pathway. *Free Radic Res.* (2019) 53:82–93. doi: 10.1080/10715762.2018.1554901
73. Tian W, Yang L, Liu Y, He J, Yang L, Zhang Q, et al. Resveratrol attenuates doxorubicin-induced cardiotoxicity in rats by up-regulation of vascular endothelial growth factor B. *J Nutr Biochem.* (2020) 79:108132. doi: 10.1016/j.jnutbio.2019.01.018
74. Zhang F, Tang Z, Hou X, Lennartsson J, Li Y, Koch AW, et al. VEGF-B is dispensable for blood vessel growth but critical for their survival, and VEGF-B targeting inhibits pathological angiogenesis. *Proc Natl Acad Sci U S A.* (2009) 106:6152–7. doi: 10.1073/pnas.0813061106
75. Rasanen M, Sultan I, Paech J, Hemanthakumar KA, Yu W, He L, et al. VEGF-B promotes endocardium-derived coronary vessel development and cardiac regeneration. *Circulation.* (2021) 143:65–77. doi: 10.1161/CIRCULATIONAHA.120.050635
76. Kivela R, Bry M, Robciuc MR, Rasanen M, Taavitsainen M, Silvola JM, et al. VEGF-B-induced vascular growth leads to metabolic reprogramming and ischemia resistance in the heart. *Embo Mol Med.* (2014) 6:307–21. doi: 10.1002/emmm.201303147
77. Nurro J, Halonen PJ, Kuivanen A, Tarkia M, Saraste A, Honkonen K, et al. AdVEGF-B186 and AdVEGF-DDeltaNDeltaC induce angiogenesis and increase perfusion in porcine myocardium. *Heart.* (2016) 102:1716–20. doi: 10.1136/heartjnl-2016-309373
78. Lahteenvuo JE, Lahteenvuo MT, Kivela A, Rosenlew C, Falkevall A, Klar J, et al. Vascular endothelial growth factor-B induces myocardium-specific angiogenesis and arteriogenesis via vascular endothelial growth factor receptor-1- and neuropilin receptor-1-dependent mechanisms. *Circulation.* (2009) 119:845–56. doi: 10.1161/CIRCULATIONAHA.108.816454
79. Arjunan P, Lin X, Tang Z, Du Y, Kumar A, Liu L, et al. VEGF-B is a potent antioxidant. *Proc Natl Acad Sci U S A.* (2018) 115:10351–6. doi: 10.1073/pnas.1801379115
80. Zentilin L, Puligadda U, Lionetti V, Zacchigna S, Collesi C, Pattarini L, et al. Cardiomyocyte VEGFR-1 activation by VEGF-B induces compensatory hypertrophy and preserves cardiac function after myocardial infarction. *FASEB J.* (2010) 24:1467–78. doi: 10.1096/fj.09-143180
81. Hagberg CE, Falkevall A, Wang X, Larsson E, Huusko J, Nilsson I, et al. Vascular endothelial growth factor B controls endothelial fatty acid uptake. *Nature.* (2010) 464:917–21. doi: 10.1038/nature08945
82. Karpanen T, Bry M, Ollila HM, Seppanen-Laakso T, Liimatta E, Leskinen H, et al. Overexpression of vascular endothelial growth factor-B in mouse heart alters cardiac lipid metabolism and induces myocardial hypertrophy. *Circ Res.* (2008) 103:1018–26. doi: 10.1161/CIRCRESAHA.108.178459
83. Hu L, Shan Z, Wang F, Gao X, Tong Y. Vascular endothelial growth factor B exerts lipid-lowering effect by activating AMPK via VEGFR1. *Life Sci.* (2021) 276:119401. doi: 10.1016/j.lfs.2021.119401
84. Ning FC, Jensen N, Mi J, Lindstrom W, Balan M, Muhl L, et al. VEGF-B ablation in pancreatic beta-cells upregulates insulin expression without affecting glucose homeostasis or islet lipid uptake. *Sci Rep.* (2020) 10:923. doi: 10.1038/s41598-020-57599-2
85. Moessinger C, Nilsson I, Muhl L, Zeitelhofer M, Heller SB, Skogsberg J, et al. VEGF-B signaling impairs endothelial glucose transcytosis by decreasing membrane cholesterol content. *EMBO Rep.* (2020) 21:e49343. doi: 10.15252/embr.201949343
86. Wada H, Ura S, Kitaoka S, Satoh-Asahara N, Horie T, Ono K, et al. Distinct characteristics of circulating vascular endothelial growth factor-a and C levels in human subjects. *PLoS ONE.* (2011) 6:e29351. doi: 10.1371/journal.pone.0029351
87. Wada H, Suzuki M, Matsuda M, Ajiro Y, Shinozaki T, Sakagami S, et al. VEGF-C and mortality in patients with suspected or known coronary artery disease. *J Am Heart Assoc.* (2018) 7:e10355. doi: 10.1161/JAHA.118.010355
88. Houssari M, Dumesnil A, Tardif V, Kivela R, Pizzinat N, Boukhalfa I, et al. Lymphatic and immune cell cross-talk regulates cardiac recovery after experimental myocardial infarction. *Arterioscler Thromb Vasc Biol.* (2020) 40:1722–37. doi: 10.1161/ATVBAHA.120.314370
89. Dunk C, Ahmed A. Expression of VEGF-C and activation of its receptors VEGFR-2 and VEGFR-3 in trophoblast. *Histol Histopathol.* (2001) 16:359–75. doi: 10.14670/HH-16.359
90. Detoraki A, Staiano RI, Granata F, Giannattasio G, Prevete N, de Paulis A, et al. Vascular endothelial growth factors synthesized by human lung mast cells exert angiogenic effects. *J Allergy Clin Immunol.* (2009) 123:1142-9. doi: 10.1016/j.jaci.2009.01.044
91. Suh SH, Choe K, Hong SP, Jeong SH, Makinen T, Kim KS, et al. Gut microbiota regulates lacteal integrity by inducing VEGF-C in intestinal villus macrophages. *Embo Rep.* (2019) 20:e46927. doi: 10.15252/embr.201846927
92. Yang GH, Zhou X, Ji WJ, Liu JX, Sun J, Dong Y, et al. VEGF-C-mediated cardiac lymphangiogenesis in high salt intake accelerated progression of left ventricular remodeling in spontaneously hypertensive rats. *Clin Exp Hypertens.* (2017) 39:740–7. doi: 10.1080/10641963.2017.1324478
93. Huang YL, Lin YC, Lin CC, Chen WM, Chen B, Lee H. High glucose induces VEGF-C expression via the LPA1/3-Akt-ROS-LEDGF signaling axis in human prostate cancer PC-3 cells. *Cell Physiol Biochem.* (2018) 50:597–611. doi: 10.1159/000494177
94. Chen Y, Wang D, Peng H, Chen X, Han X, Yu J, et al. Epigenetically upregulated oncoprotein PLCE1 drives esophageal carcinoma angiogenesis and proliferation via activating the PI-PLCepsilon-NF-kappaB signaling pathway and VEGF-C/ Bcl-2 expression. *Mol Cancer.* (2019) 18:1. doi: 10.1186/s12943-018-0930-x
95. Lin CI, Chen CN, Huang MT, Lee SJ, Lin CH, Chang CC, et al. Lysophosphatidic acid upregulates vascular endothelial growth factor-C and tube formation in human endothelial cells through LPA(1/3), COX-2, and NF-kappaB activation- and EGFR transactivation-dependent mechanisms. *Cell Signal.* (2008) 20:1804–14. doi: 10.1016/j.cellsig.2008.06.008
96. Zhu G, Huang Q, Huang Y, Zheng W, Hua J, Yang S, et al. Lipopolysaccharide increases the release of VEGF-C that enhances cell motility and promotes lymphangiogenesis and lymphatic metastasis through the TLR4- NF-kappaB/JNK pathways in colorectal cancer. *Oncotarget.* (2016) 7:73711–24. doi: 10.18632/oncotarget.12449
97. Ma C, Xie J, Luo C, Yin H, Li R, Wang X, et al. OxLDL promotes lymphangiogenesis and lymphatic metastasis in gastric cancer by upregulating VEGFC expression and secretion. *Int J Oncol.* (2019) 54:572–84. doi: 10.3892/ijo.2018.4648
98. Li MN, Jing YH, Wu C, Li X, Liang FY Li G, et al. Continuous theta burst stimulation dilates meningeal lymphatic vessels by up-regulating VEGF-C in meninges. *Neurosci Lett.* (2020) 735:135197. doi: 10.1016/j.neulet.2020.135197
99. Liu J, Sun F, Wang X, Bi Q. miR-27b promotes angiogenesis and skin repair in scalded rats through regulating VEGF-C expression. *Lasers Med Sci.* (2020) 35:1577–88. doi: 10.1007/s10103-020-02991-7
100. Sun P, Gao J, Liu YL, Wei LW, Wu LP, Liu ZY, et al. interference (RNAi)-mediated vascular endothelial growth factor-C (VEGF-C) reduction interferes with lymphangiogenesis and enhances epirubicin sensitivity of breast cancer cells. *Mol Cell Biochem.* (2008) 308:161–8. doi: 10.1007/s11010-007-9624-1
101. Yan S, Wang H, Chen X, Liang C, Shang W, Wang L, et al. MiR-182-5p inhibits colon cancer tumorigenesis, angiogenesis, and lymphangiogenesis by directly downregulating VEGF-C. *Cancer Lett.* (2020) 488:18–26. doi: 10.1016/j.canlet.2020.04.021
102. Muhammad A, Funmilola A, Aimola IA, Ndams IS, Inuwa MH, Nok AJ. Kolaviron shows anti-proliferative effect and down regulation of

vascular endothelial growth factor-C and toll like receptor-2 in Wuchereria bancrofti infected blood lymphocytes. *J Infect Public Health.* (2017) 10:661–6. doi: 10.1016/j.jiph.2017.05.006

103. Yuan X, Chen Y, Li X, Zhang G, Jin D, Zhao H, et al. Norcantharidin inhibits lymphangiogenesis by downregulating the expression of VEGF-C and VEGF-D in human dermal lymphatic endothelial cells *in vitro*. *Pharmacology.* (2015) 95:1–9. doi: 10.1159/000362418
104. Murakami J, Ishii M, Suehiro F, Ishihata K, Nakamura N, Nishimura M. Vascular endothelial growth factor-C induces osteogenic differentiation of human mesenchymal stem cells through the ERK and RUNX2 pathway. *Biochem Biophys Res Commun.* (2017) 484:710–8. doi: 10.1016/j.bbrc.2017.02.001
105. Wagner M, Steinskog ES, Wiig H. Blockade of lymphangiogenesis shapes tumor-promoting adipose tissue inflammation. *Am J Pathol.* (2019) 189:2102–14. doi: 10.1016/j.ajpath.2019.06.010
106. Choi JS, Shin YJ, Lee JY, Yun H, Cha JH, Choi JY, et al. Expression of vascular endothelial growth factor receptor-3 mRNA in the rat developing forebrain and retina. *J Comp Neurol.* (2010) 518:1064–81. doi: 10.1002/cne.22263
107. Schwager S, Detmar M. Inflammation and lymphatic function. *Front Immunol.* (2019) 10:308. doi: 10.3389/fimmu.2019.00308
108. Klotz L, Norman S, Vieira JM, Masters M, Rohling M, Dube KN, et al. Cardiac lymphatics are heterogeneous in origin and respond to injury. *Nature.* (2015) 522:62–7. doi: 10.1038/nature14483
109. Harrison MR, Feng X, Mo G, Aguayo A, Villafuerte J, Yoshida T, et al. Late developing cardiac lymphatic vasculature supports adult zebrafish heart function and regeneration. *Elife.* (2019) 8:e42762. doi: 10.7554/eLife.42762
110. Vieira JM, Norman S, Villa DCC, Cahill TJ, Barnette DN, Gunadasa-Rohling M, et al. The cardiac lymphatic system stimulates resolution of inflammation following myocardial infarction. *J Clin Invest.* (2018) 128:3402–12. doi: 10.1172/JCI97192
111. Milasan A, Smaani A, Martel C. Early rescue of lymphatic function limits atherosclerosis progression in Ldlr(-/-) mice. *Atherosclerosis.* (2019) 283:106–19. doi: 10.1016/j.atherosclerosis.2019.01.031
112. Ge Q, Zhao L, Liu C, Ren X, Yu YH, Pan C, et al. LCZ696, an angiotensin receptor-neprilysin inhibitor, improves cardiac hypertrophy and fibrosis and cardiac lymphatic remodeling in transverse aortic constriction model mice. *Biomed Res Int.* (2020) 2020:7256862. doi: 10.1155/2020/7256862
113. Lin QY, Zhang YL, Bai J, Liu JQ Li HH. VEGF-C/VEGFR-3 axis protects against pressure-overload induced cardiac dysfunction through regulation of lymphangiogenesis. *Clin Transl Med.* (2021) 11:e374. doi: 10.1002/ctm2.374
114. Yang GH, Zhou X, Ji WJ, Zeng S, Dong Y, Tian L, et al. Overexpression of VEGF-C attenuates chronic high salt intake-induced left ventricular maladaptive remodeling in spontaneously hypertensive rats. *Am J Physiol Heart Circ Physiol.* (2014) 306:H598–609. doi: 10.1152/ajpheart.00585.2013
115. Gauvrit S, Villasenor A, Strilic B, Kitchen P, Collins MM, Marin-Juez R, et al. HHEX is a transcriptional regulator of the VEGFC/FLT4/PROX1 signaling axis during vascular development. *Nat Commun.* (2018) 9:2704. doi: 10.1038/s41467-018-05039-1
116. Patila T, Ikonen T, Rutanen J, Ahonen A, Lommi J, Lappalainen K, et al. Vascular endothelial growth factor C-induced collateral formation in a model of myocardial ischemia. *J Heart Lung Transplant.* (2006) 25:206–13. doi: 10.1016/j.healun.2005.08.013
117. Chen HI, Poduri A, Numi H, Kivela R, Saharinen P, McKay AS, et al. VEGF-C and aortic cardiomyocytes guide coronary artery stem development. *J Clin Invest.* (2014) 124:4899–914. doi: 10.1172/JCI77483
118. Visuri MT, Honkonen KM, Hartiala P, Tervala TV, Halonen PJ, Junkkari H, et al. VEGF-C and VEGF-C156S in the pro-lymphangiogenic growth factor therapy of lymphedema: a large animal study. *Angiogenesis.* (2015) 18:313–26. doi: 10.1007/s10456-015-9469-2
119. Chen XG, Lv YX, Zhao D, Zhang L, Zheng F, Yang JY, et al. Vascular endothelial growth factor-C protects heart from ischemia/reperfusion injury by inhibiting cardiomyocyte apoptosis. *Mol Cell Biochem.* (2016) 413:9–23. doi: 10.1007/s11010-015-2622-9
120. Zhao T, Zhao W, Meng W, Liu C, Chen Y, Sun Y. Vascular endothelial growth factor-C: its unrevealed role in fibrogenesis. *Am J Physiol Heart Circ Physiol.* (2014) 306:H789–96. doi: 10.1152/ajpheart.00559.2013
121. Nurmi H, Saharinen P, Zarkada G, Zheng W, Robciuc MR, Alitalo K, et al. is required for intestinal lymphatic vessel maintenance and lipid absorption. *Embo Mol Med.* (2015) 7:1418–25. doi: 10.15252/emmm.201505731
122. Shew T, Wolins NE, Cifarelli V. VEGFR-3 signaling regulates triglyceride retention and absorption in the intestine. *Front Physiol.* (2018) 9:1783. doi: 10.3389/fphys.2018.01783
123. Karaman S, Hollmen M, Robciuc MR, Alitalo A, Nurmi H, Morf B, et al. Blockade of VEGF-C and VEGF-D modulates adipose tissue inflammation and improves metabolic parameters under high-fat diet. *Mol Metab.* (2015) 4:93–105. doi: 10.1016/j.molmet.2014.11.006
124. Karaman S, Hollmen M, Yoon SY, Alkan HF, Alitalo K, Wolfrum C, et al. Transgenic overexpression of VEGF-C induces weight gain and insulin resistance in mice. *Sci Rep.* (2016) 6:31566. doi: 10.1038/srep31566
125. Blum KS, Karaman S, Proulx ST, Ochsenbein AM, Luciani P, Leroux JC, et al. Chronic high-fat diet impairs collecting lymphatic vessel function in mice. *PLoS ONE.* (2014) 9:e94713. doi: 10.1371/journal.pone.0094713
126. Wada H, Suzuki M, Matsuda M, Ajiro Y, Shinozaki T, Sakagami S, et al. Distinct characteristics of VEGF-D and VEGF-C to predict mortality in patients with suspected or known coronary artery disease. *J Am Heart Assoc.* (2020) 9:e15761. doi: 10.1161/JAHA.119.015761
127. Berntsson J, Smith JG, Johnson L, Soderholm M, Borne Y, Melander O, et al. Increased vascular endothelial growth factor D is associated with atrial fibrillation and ischaemic stroke. *Heart.* (2019) 105:553–8. doi: 10.1136/heartjnl-2018-313684
128. Farnebo F, Piehl F, Lagercrantz J. Restricted expression pattern of vegf-d in the adult and fetal mouse: high expression in the embryonic lung. *Biochem Biophys Res Commun.* (1999) 257:891–4. doi: 10.1006/bbrc.1999.0562
129. Hoeben A, Landuyt B, Highley MS, Wildiers H, Van Oosterom AT, De Bruijn EA. Vascular endothelial growth factor and angiogenesis. *Pharmacol Rev.* (2004) 56:549–80. doi: 10.1124/pr.56.4.3
130. Flister MJ, Wilber A, Hall KL, Iwata C, Miyazono K, Nisato RE, et al. Inflammation induces lymphangiogenesis through up-regulation of VEGFR-3 mediated by NF-kappaB and Prox1. *Blood.* (2010) 115:418–29. doi: 10.1182/blood-2008-12-196840
131. Watari K, Nakao S, Fotovati A, Basaki Y, Hosoi F, Bereczky B, et al. Role of macrophages in inflammatory lymphangiogenesis: enhanced production of vascular endothelial growth factor C and D through NF-kappaB activation. *Biochem Biophys Res Commun.* (2008) 377:826–31. doi: 10.1016/j.bbrc.2008.10.077
132. Deng J, Cui J, Jiang N, Zhang R, Zhang L, Hao X, et al. STAT3 regulation the expression of VEGF-D in HGC-27 gastric cancer cell. *Am J Transl Res.* (2014) 6:756–67.
133. Al-Rawi MA, Watkins G, Mansel RE, Jiang WG. Interleukin 7 upregulates vascular endothelial growth factor D in breast cancer cells and induces lymphangiogenesis *in vivo*. *Br J Surg.* (2005) 92:305–10. doi: 10.1002/bjs.4832
134. Ahmed S, Ahmed A, Saleby J, Bouzina H, Lundgren J, Radegran G. Elevated plasma tyrosine kinases VEGF-D and HER4 in heart failure patients decrease after heart transplantation in association with improved haemodynamics. *Heart Vessels.* (2020) 35:786–99. doi: 10.1007/s00380-019-01548-1
135. Mountain DJ, Singh M, Singh K. Downregulation of VEGF-D expression by interleukin-1beta in cardiac microvascular endothelial cells is mediated by MAPKs and PKCalpha/beta1. *J Cell Physiol.* (2008) 215:337–43. doi: 10.1002/jcp.21315
136. Ito Y, Betsuyaku T, Nagai K, Nasuhara Y, Nishimura M. Expression of pulmonary VEGF family declines with age and is further down-regulated in lipopolysaccharide (LPS)-induced lung injury. *Exp Gerontol.* (2005) 40:315–23. doi: 10.1016/j.exger.2005.01.009
137. Cui Y, Osorio JC, Risquez C, Wang H, Shi Y, Gochuico BR, et al. Transforming growth factor-beta1 downregulates vascular endothelial growth factor-D expression in human lung fibroblasts via the Jun NH2-terminal kinase signaling pathway. *Mol Med.* (2014) 20:120–34. doi: 10.2119/molmed.2013.00123
138. Wang Q, Wang T, Zhu L, He N, Duan C, Deng W, et al. Sophocarpine Inhibits Tumorgenesis of Colorectal Cancer via Downregulation of MEK/ERK/VEGF Pathway. *Biol Pharm Bull.* (2019) 42:1830–8. doi: 10.1248/bpb.b19-00353
139. Stacker SA, Achen MG. Emerging roles for VEGF-D in human disease. *Biomolecules.* (2018) 8:1. doi: 10.3390/biom8010001

140. Syvaranta S, Helske S, Lappalainen J, Kupari M, Kovanen PT. Lymphangiogenesis in aortic valve stenosis–novel regulatory roles for valvular myofibroblasts and mast cells. *Atherosclerosis.* (2012) 221:366–74. doi: 10.1016/j.atherosclerosis.2011.12.034
141. Lammoglia GM, Van Zandt CE, Galvan DX, Orozco JL, Dellinger MT, Rutkowski JM. Hyperplasia, de novo lymphangiogenesis, and lymphatic regression in mice with tissue-specific, inducible overexpression of murine VEGF-D. *Am J Physiol Heart Circ Physiol.* (2016) 311:H384–94. doi: 10.1152/ajpheart.00208.2016
142. Jauhiainen S, Hakkinen SK, Toivanen PI, Heinonen SE, Jyrkkanen HK, Kansanen E, et al. Vascular endothelial growth factor (VEGF)-D stimulates VEGF-A, stanniocalcin-1, and neuropilin-2 and has potent angiogenic effects. *Arterioscler Thromb Vasc Biol.* (2011) 31:1617–24. doi: 10.1161/ATVBAHA.111.225961
143. Zhao W, Zhao T, Chen Y, Sun Y. Angiotensin 1-7 promotes cardiac angiogenesis following infarction. *Curr Vasc Pharmacol.* (2015) 13:37–42. doi: 10.2174/1570161113119990006
144. Leikas AJ, Laham-Karam N, Agtereek E, Peltonen HM, Selander T, Korpisalo P, et al. Efficacy and safety of clinical-grade human vascular endothelial growth factor-D(DeltaNDeltaC) gene therapy containing residual replication-competent adenoviruses. *Hum Gene Ther.* (2021) 32:761–70. doi: 10.1089/hum.2020.299
145. Hartikainen J, Hassinen I, Hedman A, Kivela A, Saraste A, Knuuti J, et al. Adenoviral intramyocardial VEGF-DDeltaNDeltaC gene transfer increases myocardial perfusion reserve in refractory angina patients: a phase I/IIa study with 1-year follow-up. *Eur Heart J.* (2017) 38:2547–55. doi: 10.1093/eurheartj/ehx352
146. Roy H, Bhardwaj S, Babu M, Lahteenvuo JE, Yla-Herttuala S. VEGF-DdeltaNdeltaC mediated angiogenesis in skeletal muscles of diabetic WHHL rabbits. *Eur J Clin Invest.* (2010) 40:422–32. doi: 10.1111/j.1365-2362.2010.02285.x
147. Pan T, Jin Z, Yu Z, Wu X, Chang X, Fan Z, et al. Cathepsin L promotes angiogenesis by regulating the CDP/Cux/VEGF-D pathway in human gastric cancer. *Gastric Cancer.* (2020) 23:974–87. doi: 10.1007/s10120-020-01080-6
148. Zhao T, Zhao W, Meng W, Liu C, Chen Y, Bhattacharya SK, et al. Vascular endothelial growth factor-D mediates fibrogenic response in myofibroblasts. *Mol Cell Biochem.* (2016) 413:127–35. doi: 10.1007/s11010-015-2646-1
149. Papiewska-Pajak I, Balcerczyk A, Stec-Martyna E, Koziolkiewicz W, Boncela J. Vascular endothelial growth factor-D modulates oxidant-antioxidant balance of human vascular endothelial cells. *J Cell Mol Med.* (2017) 21:1139–49. doi: 10.1111/jcmm.13045
150. Tirronen A, Vuorio T, Kettunen S, Hokkanen K, Ramms B, Niskanen H, et al. Deletion of lymphangiogenic and angiogenic growth factor vegf-d leads to severe hyperlipidemia and delayed clearance of chylomicron remnants. *Arterioscler Thromb Vasc Biol.* (2018) 38:2327–37. doi: 10.1161/ATVBAHA.118.311549
151. Chakraborty A, Barajas S, Lammoglia GM, Reyna AJ, Morley TS, Johnson JA, et al. Vascular endothelial growth factor-D (VEGF-D) overexpression and lymphatic expansion in murine adipose tissue improves metabolism in obesity. *Am J Pathol.* (2019) 189:924–39. doi: 10.1016/j.ajpath.2018.12.008

Conflict of Interest: The authors declare that the research was conducted in the absence of any commercial or financial relationships that could be construed as a potential conflict of interest.

Publisher's Note: All claims expressed in this article are solely those of the authors and do not necessarily represent those of their affiliated organizations, or those of the publisher, the editors and the reviewers. Any product that may be evaluated in this article, or claim that may be made by its manufacturer, is not guaranteed or endorsed by the publisher.

frontiers in Cardiovascular Medicine

REVIEW
published: 07 September 2021
doi: 10.3389/fcvm.2021.742382

Non-alcoholic Steatohepatitis Pathogenesis, Diagnosis, and Treatment

*Bo Zhu, Siu-Lung Chan, Jack Li, Kathryn Li, Hao Wu, Kui Cui and Hong Chen**

Department of Surgery, Vascular Biology Program, Harvard Medical School, Boston Children's Hospital, Boston, MA, United States

There has been a rise in the prevalence of non-alcohol fatty liver disease (NAFLD) due to the popularity of western diets and sedentary lifestyles. One quarter of NAFLD patients is diagnosed with non-alcoholic steatohepatitis (NASH), with histological evidence not only of fat accumulation in hepatocytes but also of liver cell injury and death due to long-term inflammation. Severe NASH patients have increased risks of cirrhosis and liver cancer. In this review, we discuss the pathogenesis and current methods of diagnosis for NASH, and current status of drug development for this life-threatening liver disease.

Keywords: non-alcohol fatty liver disease, non-alcoholic steatohepatitis, pathogenesis, diagnosis, treatment

OPEN ACCESS

Edited by:
Changcheng Zhou, University of California, Riverside, United States

Reviewed by:
Jun Yu, Temple University, United States
Yanqiao Zhang, Northeast Ohio Medical University, United States

****Correspondence:***
Hong Chen
hong.chen@harvard.childrens.edu

Specialty section:
This article was submitted to Lipids in Cardiovascular Disease, a section of the journal Frontiers in Cardiovascular Medicine

Received: *16 July 2021*
Accepted: *13 August 2021*
Published: *07 September 2021*

Citation:
Zhu B, Chan S-L, Li J, Li K, Wu H, Cui K and Chen H (2021) Non-alcoholic Steatohepatitis Pathogenesis, Diagnosis, and Treatment. Front. Cardiovasc. Med. 8:742382. doi: 10.3389/fcvm.2021.742382

INTRODUCTION

There has been an increased interest in non-alcoholic fatty liver disease (NAFLD), and its advanced stage, non-alcoholic steatohepatitis (NASH) because of their increasing impact on global health (1). In the United States, the number of NAFLD cases is rapidly expanding, and is expected to reach 100.9 million patients in 2030 (∼1/3 of the population) (2). During the past three decades, the number of patients with NAFLD has increased from 20 to 32% of the United States population (3). Recently, there is an increasing tendency for young people to be diagnosed with NAFLD due to being overweight or obese (4). As an increased proportion (∼25% of NAFLD cases) of NAFLD will lead to NASH, there will be increased number of NASH patients with cirrhosis, leading to elevated liver transplantation for end-stage cirrhosis (5). Worse still, the risk of hepatocellular carcinoma (HCC) increases significantly for NAFLD or NASH patients who have cirrhosis (6–8).

NASH is strongly associated with overweight or obesity and metabolic syndromes (9, 10). Recent studies have shown that more than 80% of patients with NASH are overweight or obese (11, 12). NASH is highly associated with type 2 diabetes mellitus (13–15). NAFLD is the general term that comprises hepatic steatosis and steatohepatitis. Unlike isolated hepatic steatosis, NASH is strongly associated with fibrosis found in liver biopsy (5). The level of fibrosis varies among different NASH patients and advanced fibrosis progresses into liver cirrhosis and the eventual scarring (16). Currently, fibrosis-induced liver cell death and further functional failure is a major cause of liver transplantation (17). In addition to liver functional failure, cirrhosis and HCC, associated non-liver adverse outcomes are primarily related to increased cardiovascular diseases (18–21) and type 2 diabetes mellitus (22). Recently, studies have suggested that NAFLD should be defined as a disease of global metabolic dysfunction (23), and not just limited to the liver. The metabolic dysfunctions in fat tissue and muscle, and microbiota variation in the gut contribute to fatty liver disease progression. Therefore, to more accurately describe NAFLD, scientists suggest renaming it as "metabolic associated fatty liver disease" or MAFLD (24).

At present, steady progress in clarifying the pathogenesis of NASH has been made, leading to the identification of therapeutic targets for drug development. However, there is currently no FDA-approved drug that can cure NASH. In addition, the lack of precise predictive biomarkers limits early diagnosis of NASH. Liver biopsy remains the gold standard for diagnosis of NASH. This review focuses on discussing the risks for NASH pathogenesis, current development of biomarkers, and therapeutic target identification for drug development.

PATHOGENESIS OF NAFL/NASH

The "two-hit" theory for the development of NASH was first proposed more than two decades ago (25). The theory assumed that the setting in of steatosis is the first hit, and that a second hit from other factors is required for the development of NASH (26), such as oxidative stress. However, this theory is now considered outdated. Multiple-hit pathogenesis was proposed, suggesting that many different factors have been considered to contribute to NASH progression, such as inherited and environmental factors (27, 28). Diet-induced obesity is the most common inducer of NASH development, because the severe accumulation of fat in liver leads to dysfunction of lipid metabolism. At present, the accumulation of hepatic free cholesterol and free fatty acid is considered the primary source of stress to the liver (29–31). Particularly, hepatic free cholesterol is a major lipotoxic molecule critical for NASH progression (32). Its metabolites trigger hepatocellular stress (for example, oxidative stress) and induce hepatocyte injury and death, leading to fibrosis and further cirrhosis (**Figure 1A**).

Fibrosis in the liver and hepatocyte injury and death are the key features that distinguish NASH from isolated steatosis (5, 33). It is, however, debatable whether hepatocyte injury causes liver inflammation or if hepatocyte injury is the consequence of liver inflammation. Both hepatocyte injury and liver inflammation are relevant to the pathogenesis of NASH because injured hepatocytes release factors that promote inflammation, resulting in a downward spiral as inflammation further triggers hepatocyte injury (34, 35). This is because inflammation in the liver is caused by released proinflammatory chemokines and cytokines (such as TNF-α, IL-6, and CCL2), which further damage the injured hepatocytes (36). In the liver, Kupffer cells, a kind of resident macrophage, are localized in the lumen of the liver sinusoids and play a central role in liver inflammation (37). The initiation of liver injury stems from the activation of Kupffer cells resulting in cytokine and chemokine production (38). Kupffer cells can be divided into classically activated M1 Kupffer cells (proinflammatory M1) and alternatively activated M2 Kupffer cells (wound-healing M2) (39). The activation of pro-inflammatory M1 Kupffer cells is the critical step that contributes to the pathogenesis of fibrogenesis during NASH progression. In contrast, the polarization and activation of anti-inflammatory M2 Kupffer cells play a protective role against fibrogenesis in NASH (40). Importantly, M2 Kupffer cells promote the apoptosis of M1 Kupffer cells, which is protective against NAFL/NASH (41). Under high fat diet treatment, mice with a high M2:M1 Kupffer cell ratio are resistant to developing liver lesions, while mice with a high M1:M2 Kupffer cell ratio are more likely to develop liver lesions (42).

In addition to resident Kupffer cells in liver, monocyte-derived macrophages play an important role in the pathogenesis of NAFL/NASH (40). The infiltrating monocyte-derived macrophages can be divided into two major subtypes, Ly-6C^{hi} macrophages and Ly-6C^{lo} macrophages (43), both of which affect hepatic stellate cells (HSCs), though in differing ways. HSCs have been identified as the major extracellular matrix protein (ECM) producing cells in injured liver (44) that play the central role in the formation of hepatic fibrosis (45). HSCs have two different states, quiescent and activated states, and the transdifferentiation from the quiescent into the activated state is the major cause of fibrosis (44). The proinflammatory Ly-6C^{hi} macrophages activate HSCs by secreting IL-1β and CCL2 that enhance the fibrotic process (46), while the pro-restorative Ly-6C^{lo} macrophages promote apoptosis of HSCs and accelerate extracellular matrix degradation by upregulation of matrix metalloproteinase 9 (MMP9), MMP12 and MMP13 (47). The pro-restorative Ly-6C^{lo} macrophages express chemokine (C-X3-C motif) receptor 1 (CX3CR1), and because its ligand1 (CX3CL1) is mainly expressed in HSCs, CX3CL1-CX3CR1 interaction negatively regulates inflammatory properties in macrophages within the liver (48). Chemokine CCL2 production, working through CCR2, is a major cause of monocyte-derived macrophage (inflammatory Ly-6C^{hi} macrophages) recruitment induced by Toll-like receptor 4 (TLR4) signaling (49). The infiltration of monocytes from blood that rapidly differentiate into pro-inflammatory macrophages in the liver contributes to NAFL/NASH progression (46). Extensive studies have reported that genetic deficiency or pharmacological inhibition of CCR2 decreased monocyte recruitment to the liver and ameliorated NASH in mice (50–52). In addition to chemokine CCL2, cytokines like TNF-α and IL-1β released from macrophages are important drivers of steatosis, inflammation, and fibrosis in NAFL/NASH (40).

A number of risk factors promote the pathogenesis of NASH, including inherited and environmental factors (**Figure 1B**). Dietary factors are one of the most important environmental factors that lead to NASH.

Genetic and Epigenetic Factors

Genome-wide association studies (GWAS) suggest that polymorphisms in patatin-like phospholipase domain-containing 3 (PNPLA3) and transmembrane 6 superfamily, member 2 (TM6SF2) promote the development of NASH (53). Particularly, PNPLA3 polymorphisms (I148M) are strongly associated with hepatic steatosis caused by accumulation of PNPLA3 on hepatic lipid droplets (54–56). TM6SF2 polymorphism reduces very-low density lipoprotein (VLDL) secretion that is associated with NASH and fibrosis (57, 58). The polymorphism of several other genes, including glucokinase regulator (GCKR), membrane bound O-acyltransferase domain-containing 7 (MBOAT7) and hydroxysteroid 17β-dehydrogenase (HSD17B13), are closely associated with susceptibility to NAFL and progression of NASH (53).

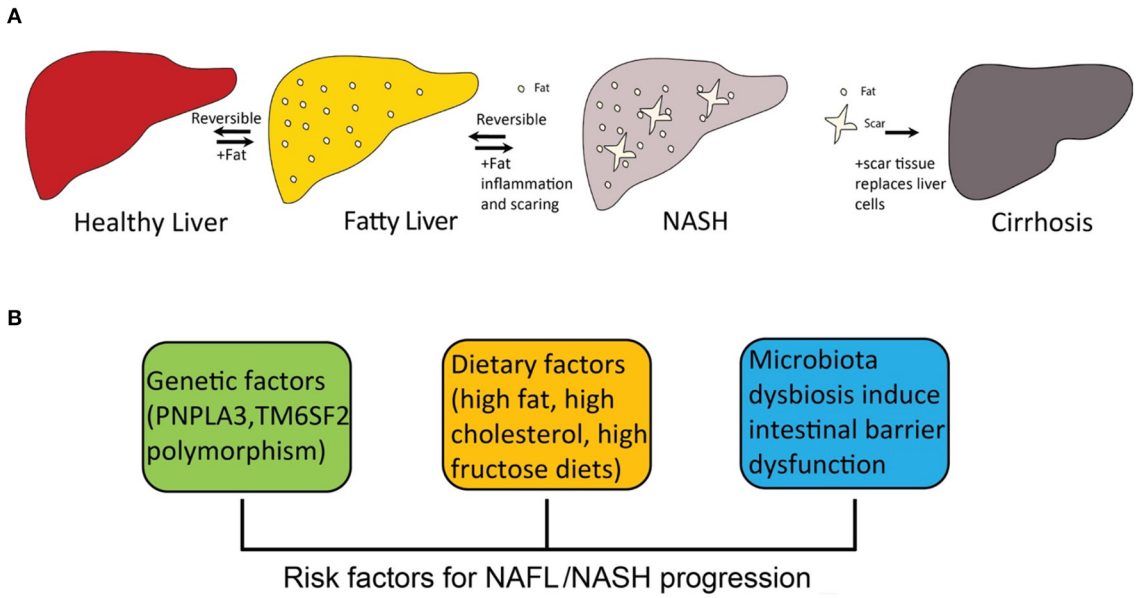

FIGURE 1 | The progression of fatty liver disease and risk factors for NAFL/NASH progression. **(A)** the spectrum of fatty liver disease; **(B)** risk factors for NAFL/NASH progression.

Epigenetic mechanisms are special genetic regulations without any change in gene sequence in the genome but with different modifications, such as DNA methylation, histone modification, and non-coding RNAs (59). By analysis of liver samples from NAFLD patients, the heavy methylation of NAFLD associated genes, such as PNPLA3 (60) and PPARG (61), increases the severity of NAFLD. Recently studies have indicated that non-coding RNAs could regulate NAFLD progression, including miR-122 and miR-125b, which show significantly decreased expression in NAFLD patients (62, 63). Moreover, hepatic-specific deletion of miR-21 prevents steatosis, and thus may be a potential therapeutic target for NAFLD (64). In addition, changes in hepatic lncRNA expression patterns are associated with NAFLD. For example, a strong increase in hepatic lncRNA un.372 is detected in NAFLD patients (65), while hepatic lncRNA lnc18q22.2 is reported to correlate with the severity of NASH (66). A list of microRNAs and long non-coding RNAs that are involved in NAFL/NASH progression are summarized in **Table 1**. Furthermore, studies in rodents have demonstrated the existence of epigenetic factors that regulate fibrogenic liver cell development to cirrhosis (124). A similar phenomenon is observed in NASH patients. Therefore, epigenetic mechanisms may be related to susceptibility for NASH.

Dietary Factors

Consumption of a high-calorie diet with high fat and high sugar (western diet) results in weight gain and is the initial event for the development of fatty liver (125–127). Particular types of lipids and carbohydrates play important roles in the progression of NASH. For dietary lipids, polyunsaturated fatty acids (PUFAs) induce inflammation and fibrosis formation in NASH (128). For dietary carbohydrates, over-consumption of carbohydrates extensively promotes the development of NAFLD (129), especially fructose, a highly lipogenic sugar and a common component in almost all major sweet foods (130, 131). Extensive experimental studies support the association between the increasing rates of obesity and the progression of NAFLD (132–134). Obese individuals who have an excessive body mass index (BMI) and visceral obesity are at a high risk for developing NAFLD (135). Studies have reported that more than 95% people that had severe obesity have NAFLD (136). Type 2 diabetes mellitus (T2DM) patients have higher risks for NAFLD due to insulin resistance, and T2DM and NAFLD can be developed simultaneously (137). In addition, people who have dyslipidemia and hypertension are also at high risk for NAFLD (138).

Microbiota Dysbiosis

The relationship between intestinal microbiota and NAFL/NASH has been proposed for decades. Intestinal microbiota is altered in genetically obese mice that have metabolic syndrome and fatty liver (139). Studies indicate that microbiota dysbiosis is associated with inflammatory signaling, which promotes hepatic steatosis and NASH (140, 141). Recently, extensive studies on the gut-liver axis have suggested that intestinal microbiota influenced host susceptibility to obesity, hepatic steatosis, and NASH (142–144). The homeostasis of intestinal microbiota is essential to maintaining proper function of the intestinal barrier, and recent studies have shown that intestinal microbiota dysbiosis triggers intestinal inflammation and further impairs the intestinal barrier. Microbial products released can reach the liver and induce hepatic inflammation and further lead to NAFL/NASH (145). This intestinal barrier is hepatoprotective, and microbiota-driven gut-vascular barrier disruption is a prerequisite for NASH

TABLE 1 | microRNAs and long non-coding RNAs that are involved in NAFLD pathogenesis.

miRNAs	Expression in NAFL/NASH	References	lncRNAs	Expression in NAFL/NASH	References
miR-15b	Upregulated	(67)	ApoA4-AS	Upregulated	(68)
miR-16	Upregulated	(69)	APTR	Upregulated	(70)
miR-19	Upregulated	(71)	FLRL2	Downregulated	(72)
miR-21	Upregulated	(73)	Gm15622	Upregulated	(74)
miR-22	Upregulated	(75)	HOTAIR	Upregulated	(76)
miR-26a	Downregulated	(77)	HULC	Upregulated	(78)
miR-27a/b	Upregulated	(79)	lncARSR	Upregulated	(80)
miR-29a	Downregulated	(81)	AK012226	Upregulated	(82)
miR-30c	Downregulated	(83)	lnc-HC	Downregulated	(84)
miR-33a/b	Upregulated	(85)	lncHR1	Downregulated	(86)
miR-34a	Upregulated	(87)	lnc-H19	Upregulated	(88)
miR-99a	Downregulated	(89)	lnc-JAM2-6	rs2829145 A/G	(90)
miR-122	Upregulated	(62)	lncLSTR	Downregulated	(91)
miR-125b	Upregulated	(63)	lncRNA Blnc1	Upregulated	(92)
miR-130a	Downregulated	(93)	lncSHGL	Downregulated	(94)
miR-135a	Downregulated	(95)	lnc18q22.2	Upregulated	(66)
miR-146a	Downregulated	(96)	LFAR1	Upregulated	(97)
miR-155	Downregulated	(98)	MALAT1	Upregulated	(99)
miR-181b	Upregulated	(100)	MEG3	Downregulated	(101)
miR-190b	Upregulated	(102)	Mirt2	Downregulated	(103)
miR-192	Upregulated	(104)	MRAK052686	Downregulated	(105)
miR-194	Upregulated	(106)	NEAT1	Upregulated	(107)
miR-197	downregulated	(89)	NONMMUG027912	downregulated	(108)
miR-199a	Upregulated	(109)	NONMMUT010685	Downregulated	(110)
miR-200a/b	Upregulated	(111)	NONMMUT050689	Downregulated	(110)
miR-205	Upregulated	(112)	NR002155.1	Downregulated	(113)
miR-221/222	Upregulated	(114)	PVT1	Upregulated	(115)
miR-223	Upregulated	(116)	RP11-128N14.5	Upregulated	(117)
miR-335	Upregulated	(118)	Runx1	Upregulated	(119)
miR-375	upregulated	(120)	SRA	upregulated	(121)
miR-378	Upregulated	(122)	TGFB2-OT1	Upregulated	(117)
miR-451a	Downregulated	(123)	uc.372	Upregulated	(65)

development (146). This barrier disruption is caused by diet-induced dysbiosis (147). Patients with NAFL and NASH usually show dysbiosis in the gut microbiota (148). Overall, patients with NAFL and NASH have lower microbiota diversity than healthy people and have different microbiota species abundance patterns (149). For example, patients with NASH have an increased abundance of *Escherichia,* where patients with advanced fibrotic NASH or cirrhosis have dramatically increased proportions of *Bacteroides* and *Ruminococcus* (150).

DIAGNOSIS OF NAFL/NASH

At present, liver biopsy remains the gold standard for diagnosis of (151), since invasive liver biopsy for assessing different fibrosis stages is the most accurate method for NASH diagnosis (**Figure 2A**) (152). However, liver biopsy is painful for patients, and has sampling error limitations (153). Therefore, new developments in non-invasive biomarkers for early diagnosis and treatment of NAFL and NASH are urgently needed. Current progression on developing non-invasive biomarkers is mainly based on the detection of hepatic steatosis (154). There are several indices and scores for the evaluation of hepatic steatosis. Testing of blood biomarkers, determining the fatty liver index (FLI) and determining the hepatic steatosis index (HSI) are the most popular methods to evaluate the risks of NAFLD (155). Fatty liver index, BMI, and serum level of triglycerides also have moderate accuracy for fatty liver diagnosis (156). Hepatic steatosis index can be evaluated by the ratio between serum aspartate aminotransferase (AST) and alanine aminotransferase (ALT) and has moderate accuracy for the detection of fatty liver (156). The limitation of both FLI and HSI is insensitive to mild steatosis since they are designed to target indirectly on blood fat rather than liver fat.

A more sensitive and accurate method is to measure liver fat directly. The development of imaging biomarkers has

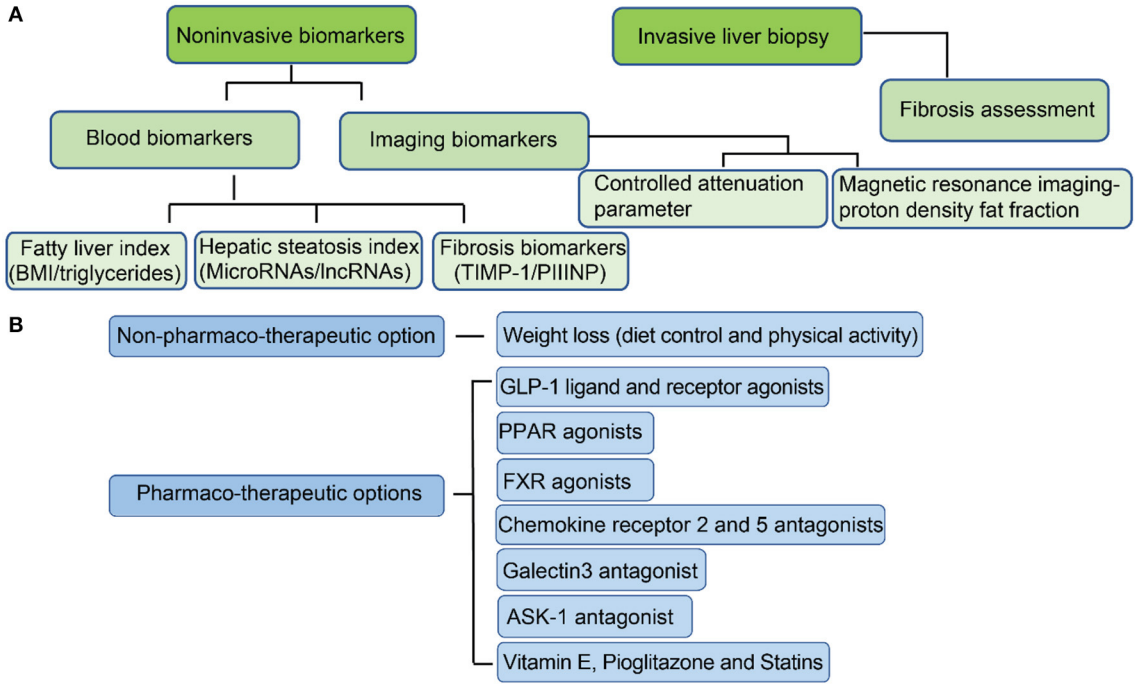

FIGURE 2 | Current approaches for the diagnosis of NAFL/NASH and options for treatment. **(A)** Methods for NAFL/NASH diagnosis; **(B)** Options for NAFL/NASH treatment.

dramatically improved the progress of NAFLD diagnosis (157). Ultrasonography is the most common method for detection of hepatic steatosis and can accurately identify moderate to severe steatosis (158). However, it is less sensitive when detecting steatosis in NASH patients who have advanced fibrosis (159). Computed tomography (CT), although sensitive in detecting moderate and severe steatosis with mild histological fibrosis (159), has not been shown to have improved sensitivity in mild steatosis (160). Both controlled attenuation parameter (CAP) and magnetic resonance imaging-proton density fat fraction (MRI-PDFF) can address sensitivity issues in mild steatosis (161, 162). Controlled attenuation parameter is a method for grading steatosis that measures the degree of ultrasound attenuation by hepatic fat using a process based on simultaneous transient elastography, which is more sensitive and accurate than previous imaging markers (163). MRI-PDFF maps can be generated within seconds and detection of hepatic fat is more accurate than CAP for detecting all grades of steatosis in patients with NAFLD (164). Magnetic resonance imaging (MRI) approaches 100% sensitivity in the detection of hepatic steatosis, even at low steatosis levels (165). At present, MRI is the best method for detecting hepatic steatosis accurately and efficiently due to its high sensitivity.

The current progress on non-invasive biomarkers development for fibrosis diagnosis has advanced. Several potential non-invasive biomarkers have been reported for NASH diagnosis. Studies indicate that serum hyaluronic acid (HA) is a non-invasive marker of liver fibrosis (166), and serum YKL-40 can also be a marker of liver fibrosis in patients with NAFLD (167). In addition, the expression of tissue inhibitor of matrix metalloproteinase 1 (TIMP-1) is increased in human and rat models of liver fibrosis (168), and its degree of expression correlates with the extent of fibrosis in human liver (169). Although functional studies indicate TIMP-1 promotes hepatic fibrogenesis, TIMP-1 deficiency does not prevent carbon tetrachloride (CCl4)-induced hepatic fibrogenesis (170). Terminal peptide of procollagen III (PIIINP) is released during the synthesis and deposition of type III collagen (171). At present, PIIINP has been validated to be effective in the detection of fibrosis, and is particularly effective in the detection of severe fibrosis (172). PIIINP is elevated in patients with advanced fibrosis (172). Therefore, serum PIIINP is potentially a good non-invasive marker of liver fibrosis.

TREATMENT OF NAFL/NASH

Most NASH patients are obese. The first and simplest management against NAFLD or NASH is to make lifestyle modifications (173). Through sustained weight loss (such as through a calorie-restricted diet) and increased physical activity (exercise), hepatic steatosis caused by western-style diet and sedentary lifestyle can be reduced significantly (174). A modest weight loss of about 3% may reduce hepatic steatosis, however, up to 10% or more is required for the resolution of NAFLD and the regression of fibrosis in NASH (175). Thus, resolution of steatosis in NAFLD and even fibrosis reversal in NASH can be achieved after significant weight loss through lifestyle modifications. Therefore, as a non-pharmaco-therapeutic option, transitioning from a high-calorie diet and a sedentary lifestyle

into a restricted calorie diet with increased physical activity is the healthiest treatment for NAFL and early stage of NASH.

In addition to lifestyle modifications, there are several therapeutic targets that are under clinical trials (**Figure 2B**). The most promising pharmaco-therapeutic candidates will be discussed.

Vitamin E, Pioglitazone, and Statins

Oxidative stress plays an essential role in the development from isolated steatosis to NASH (176). Anti-oxidation treats NAFL/NASH by removing excessive reactive oxygen species (ROS) (177). Extensive studies have indicated that vitamin E reduced steatosis and ameliorated fibrosis (178–180). However, for NASH patients with diabetes, vitamin E alone does not significantly improve histological outcomes (181). Considering NAFL/NASH is a metabolic syndrome, and thus is usually accompanied by other metabolic diseases, such as diabetes and CVD, drugs for the treatment of diabetes and CVD are used for treating NAFL/NASH, particularly pioglitazone and statins (182, 183). Pioglitazone is used for treatment of type 2 diabetes mellitus, and has been reported to significantly reduce fibrosis in NASH patients (184). The safety and efficacy of low-dose pioglitazone (NCT04501406) has been tested (185). In addition, statins, a class of drugs used for reducing cardiovascular disease risk, has been tested on NAFL/NASH patients who then displayed substantial improvement on steatosis and fibrosis (186, 187). While piloglitazone and statins have already been in the market for a while for treating other conditions, they also represent new potential therapies for NAFL/NASH.

GLP-1 Ligand and Receptor Agonists

Glucagon-like peptide 1 (GLP-1) is essential for glucose homeostasis (188). GLP-1 and its receptor agonists (GLP-1 RAs) can treat type 2 diabetes mellitus (189), which is closely associated with NAFLD (13). Evidence supports that GLP-1 secretion is impaired in patients with NAFL and NASH (190), indicating that GLP-1 agonists may be potential treatment candidates for NAFLD. GLP-1 agonists and GLP-1 RAs, including liraglutide (NCT01237119), exenatide (NCT00650546) and semaglutide (NCT02970942), have been tested for improving liver histology in NASH patients (191–193), and are currently under phase II clinical trials for NASH.

PPAR Agonists

Peroxisome proliferator-activator receptors (PPARs) are a group of nuclear receptors that play a critical role in intracellular lipid metabolism (194). Extensive studies indicate the dual PPAR alpha and delta agonist, elafibranor, is effective against NASH (195). Taking elafibranor at a dose of 120 mg/day has been shown to cause significant regression of fibrosis in NASH patients. In addition, other metabolic parameters, such as liver enzymes, are also greatly improved by elafibranor. Elafibranor is now under phase III clinical trials (NCT02704403).

FXR Agonists

Farnesoid X receptor (FXR) is a master regulator of hepatic triglyceride and glucose homeostasis (196). Obeticholic acid (OCA), a FXR agonist, has been recently studied and shown to improve histology and fibrosis scores (197). OCA is highly promising for NASH treatment and is under phase III clinical trials (NCT02548351). In addition to OCA, other FXR agonists are also under clinical trials for treating NASH. Another FXR agonist, MET-409, significantly reduces liver fat after 12 weeks of treatment in NASH patients (198). MET-409 is under phase II clinical trials for NASH (NCT04702490). EDP-305, a potent FXR agonist, reduces liver fat and is a potent inhibitor of fibrosis (199). EDP-305 is under phase II clinical trials for NASH (NCT03421413).

CCR2/5 Antagonists

NASH is a disease with inflammation and fibrosis. Chemokine receptor 2/5 (CCR2 and CCR5) are commonly increased in the liver from NASH patients. Cenicriviroc (CVC), a C-C motif chemokine receptor 2/5 (CCR2/5) antagonist, was developed to target inflammation (200). In NASH patients, liver fibrosis is caused by the accumulation of extracellular matrix proteins, mainly composed of collagen (201). CCR5 antagonist can inhibit collagen production by HSCs by impairing the migration, activation, and proliferation of HSCs (202). CVC has been shown to have antifibrotic function and has significantly improved fibrosis in NASH patients after 1 year of treatment (203). CVC is currently under phase III clinical evaluation for NASH (NCT03028740).

Galectin-3 Antagonist

Galectin-3 protein expression is essential for the development of hepatic fibrosis, which is significantly increased in NASH liver (204). In mice models, GR-MD-02, a galectin-3 inhibitor, markedly ameliorates liver fibrosis through inhibition of collagen deposition (205). GR-MD-02 has been shown to be safe and efficient for patients with NASH cirrhosis with portal hypertension (165). The safety and efficacy of GR-MD-02 for the treatment of liver fibrosis is under phase II clinical trials (NCT02462967) (206).

ASK-1 Antagonist

To improve inflammation and fibrosis in NASH, many therapeutic targets have been tested. The inhibitors of apoptosis signal-regulating kinase 1 (ASK1), a serine/threonine kinase, have been shown to significantly improve fibrosis in NASH animal models (207). Selonsertib (aka GS-4997), a selective inhibitor of ASK1, can reduce hepatic steatosis and fibrosis in NASH animal models fed with high fat and sugar. In phase II clinical trials, patients treated with selonsertib showed huge improvements in fibrosis through reduction of hepatic collagen content (208). However, a recent study has indicated that selonsertib neither leads to fibrosis regression nor reduces NASH progression (209). At present, selonsertib is undergoing phase III clinical evaluation and being studied for its efficacy on NASH (NCT03053050).

Gut and Microbiome Related Therapies

Studies between microbiome and NAFL/NASH are relatively nascent, but the consensus is that dysbiosis leads to increased

intestinal permeability, which may increase NAFL/NASH progression (210). Thus, disturbed gut-liver barrier integrity is essential in the pathogenesis of both NAFL and NASH since the release of bacterial products from the gut into blood circulation may cause a massive inflammatory response from the liver (211). Orlistat, an FDA-approved lipase inhibitor for treating obesity, reduces absorption of dietary fat (212) and may have beneficial effects on body weight through modification of the composition of gut microbiota (213), however, the efficacy of orlistat on NASH has not been clearly demonstrated. Other drugs targeting the microbiome include solithromycin. Solithromycin is an antibiotic in clinical trials for the treatment of bacterial infection. Studies in a mouse model of NASH have displayed that solithromycin had beneficial effects by reducing hepatocyte ballooning and inflammation (214). Solithromycin is currently in a phase II trial (NCT02510599) for NASH. All six patients with NASH it was tested on showed reduction in NASH parameters after 90 days of treatment (215). Notably, solithromycin may not impair the gut microenvironment since its mechanism of action against NASH may not be related to its antibacterial activity, as it is not active against gut Gram-negative bacteria (214).

Although many potential candidates for the treatment of NASH are under phase II and III clinical trials as discussed above, no drug has yet been approved by the FDA. In addition to the discovery of novel promising targets for clinical testing, existing drugs like piloglitazone and statins used for the treatment of diabetes and CVD diseases can also be viable therapeutic options for NAFL/NASH. Furthermore, antioxidant vitamin E can be a beneficial supplement for NAFL/NASH patients.

FUTURE PERSPECTIVES

Considering NAFLD is closely associated with metabolic dysfunction, metabolic dysfunction-associated fatty liver disease (MAFLD) may better describe the disease than NAFLD (216). The lack of appropriate NASH animal models is the bottleneck for NASH investigation. Although a methionine-choline-deficient (MCD) diet is a widely used model for NASH study, the body weight loss and increased insulin sensitivity of this model are not features of NASH (217). Recently, high fat, high fructose, high cholesterol diets and use of chemical inducers (such as carbon tetrachloride, CCl4) have been extensively applied as NASH models, though the feeding or induction cycle is very long (218). Despite its long-term feeding cycle, this animal model may become more popular in the future since it can accurately mimic the features of NASH.

Non-invasive diagnosis approaches can primarily detect hepatic steatosis sensitively but struggle to detect fibrosis, meaning the diagnosis of NASH still requires invasive liver biopsy. Development of non-invasive methods that can sensitively and accurately diagnose NASH is currently ongoing and such methods may be available in the future. At present, because of the absence of any existing FDA-approved medication for the treatment of NASH, an effective clinical pharmacotherapy is urgently needed for advanced NASH. For mild NASH, the most healthy and effective treatment is through management of diet and lifestyle. NASH fibrosis regression can occur with 10% weight loss, but such weight loss is difficult to achieve. In addition, NASH is commonly associated with diabetes, meaning drugs that target diabetes may have potential for treating NASH. In addition, the development of drug targets on gut microbiota may be a novel direction in the coming decades, because accumulating evidence shows microbiota dysbiosis is one of the critical causes of NASH through the gut-liver axis. Alternatively, the development of pharmacological interventions targeting the polarization of M2 Kupffer cells during the early stages of NASH may become an attractive strategy for reducing inflammation and hepatocyte injury. Similarly, in monocyte-derived macrophages, it is attractive to develop pharmacological interventions that target the polarization of pro-restorative Ly-6C^{lo} macrophages to treat NASH.

CONCLUSION

Great developments in NASH pathogenesis, diagnosis and treatment have been achieved in the past decades. This review discusses factors that may induce NASH, non-invasive methods for NASH diagnosis, and potential pharmaco-therapeutic options to resolve NASH. Dietary factors are a major cause for NAFLD that may further develop into NASH, particularly for people under long-term high fat and high sugar consumption who are obese or overweight. Body weight loss is beneficial for early-stage NASH. Accurate and sensitive non-invasive diagnosis methods for NASH are needed to replace invasive liver biopsy. Although no FDA-approved drug is available for NASH, many clinical pharmacotherapies are under phase II or phase III clinical trials. Moving forward, more potential NASH targets will likely be identified, offering more opportunities to discover effective and specific drugs to treat and resolve NASH.

AUTHOR CONTRIBUTIONS

BZ, S-LC, and HC wrote the manuscript. JL and KL edited the manuscript. HW and KC critically read the manuscript. All authors contributed to the article and approved the submitted version.

FUNDING

This work was supported in part by NIH Grants Nos. R01HL093242, R01HL137229, R01HL133216, and R01HL156362 to HC.

REFERENCES

1. Younossi Z, Anstee QM, Marietti M, Hardy T, Henry L, Eslam M, et al. Global burden of NAFLD and NASH: trends, predictions, risk factors and prevention. *Nat Rev Gastroenterol Hepatol.* (2018) 15:11–20. doi: 10.1038/nrgastro.2017.109
2. Estes C, Razavi H, Loomba R, Younossi Z, Sanyal AJ. Modeling the epidemic of nonalcoholic fatty liver disease demonstrates an exponential increase in burden of disease. *Hepatology.* (2018) 67:123–33. doi: 10.1002/hep.29466
3. Loomba R, Friedman SL, Shulman GI. Mechanisms and disease consequences of nonalcoholic fatty liver disease. *Cell.* (2021) 184:2537–64. doi: 10.1016/j.cell.2021.04.015
4. Scapaticci S, D'Adamo E, Mohn A, Chiarelli F, Giannini C. Non-alcoholic fatty liver disease in obese youth with insulin resistance and type 2 diabetes. *Front Endocrinol.* (2021) 12:639548. doi: 10.3389/fendo.2021.639548
5. Diehl AM, Day C. Cause pathogenesis, and treatment of nonalcoholic steatohepatitis. *N Engl J Med.* (2017) 377:2063–72. doi: 10.1056/NEJMra1503519
6. Ascha MS, Hanouneh IA, Lopez R, Tamimi TA, Feldstein AF, Zein NN. The incidence and risk factors of hepatocellular carcinoma in patients with nonalcoholic steatohepatitis. *Hepatology.* (2010) 51:1972–8. doi: 10.1002/hep.23527
7. Starley BQ, Calcagno CJ, Harrison SA. Nonalcoholic fatty liver disease and hepatocellular carcinoma: a weighty connection. *Hepatology.* (2010) 51:1820–32. doi: 10.1002/hep.23594
8. Kogiso T, Tokushige K. The current view of nonalcoholic fatty liver disease-related hepatocellular Carcinoma. *Cancers.* (2021) 13:516. doi: 10.3390/cancers13030516
9. Godoy-Matos AF, Silva Junior WS, Valerio CM. NAFLD as a continuum: from obesity to metabolic syndrome and diabetes. *Diabetol Metab Syndr.* (2020) 12:60. doi: 10.1186/s13098-020-00570-y
10. Sarwar R, Pierce N, Koppe S. Obesity and nonalcoholic fatty liver disease: current perspectives. *Diabetes Metab Syndr Obes.* (2018) 11:533–42. doi: 10.2147/DMSO.S146339
11. Milic S, Lulic D, Stimac D. Non-alcoholic fatty liver disease and obesity: biochemical, metabolic and clinical presentations. *World J Gastroenterol.* (2014) 20:9330–7. doi: 10.3748/wjg.v20.i28.9330
12. Younossi ZM. The epidemiology of nonalcoholic steatohepatitis. *Clin Liver Dis.* (2018) 11:92–4. doi: 10.1002/cld.710
13. Gastaldelli A, Cusi K. From NASH to diabetes and from diabetes to NASH: mechanisms and treatment options. *JHEP Rep.* (2019) 1:312–28. doi: 10.1016/j.jhepr.2019.07.002
14. Amiri Dash Atan N, Koushki M, Motedayen M, Dousti M, Sayehmiri F, Vafaee R, et al. Type 2 diabetes mellitus and non-alcoholic fatty liver disease: a systematic review and meta-analysis. *Gastroenterol Hepatol Bed Bench.* (2017) 10:S1–7.
15. Dharmalingam M, Yamasandhi PG. Nonalcoholic fatty liver disease and type 2 diabetes mellitus. *Indian J Endocrinol Metab.* (2018) 22:421–8. doi: 10.4103/ijem.IJEM_585_17
16. Bataller R, Brenner DA. Liver fibrosis. *J Clin Invest.* (2005) 115:209–18. doi: 10.1172/JCI24282
17. Pais R, Barritt A, St Calmus Y, Scatton O, Runge T, Lebray P, et al. NAFLD and liver transplantation: Current burden and expected challenges. *J Hepatol.* (2016) 65:1245–57. doi: 10.1016/j.jhep.2016.07.033
18. Francque SM, van der Graaff D, Kwanten WJ. Non-alcoholic fatty liver disease and cardiovascular risk: Pathophysiological mechanisms and implications. *J Hepatol.* (2016) 65:425–43. doi: 10.1016/j.jhep.2016.04.005
19. Patil R, Sood GK. Non-alcoholic fatty liver disease and cardiovascular risk. *World J Gastrointest Pathophysiol.* (2017) 8:51–8. doi: 10.4291/wjgp.v8.i2.51
20. Kasper P, Martin A, Lang S, Kutting F, Goeser T, Demir M, et al. NAFLD and cardiovascular diseases: a clinical review. *Clin Res Cardiol.* (2021) 110:921–37. doi: 10.1007/s00392-020-01709-7
21. Ismaiel A, Dumitrascu DL. Genetic predisposition in metabolic-dysfunction-associated fatty liver disease and cardiovascular outcomes-Systematic review. *Eur J Clin Invest.* (2020) 50:e13331. doi: 10.1111/eci.13331
22. Younossi ZM, Golabi P, de Avila L, Paik JM, Srishord M, Fukui N, et al. The global epidemiology of NAFLD and NASH in patients with type 2 diabetes: A systematic review and meta-analysis. *J Hepatol.* (2019) 71:793–801. doi: 10.1016/j.jhep.2019.06.021
23. Fouad Y, Waked I, Bollipo S, Gomaa A, Ajlouni Y, Attia D. What's in a name? Renaming 'NAFLD' to 'MAFLD'. *Liver Int.* (2020) 40:1254–61. doi: 10.1111/liv.14478
24. Eslam M, Sanyal AJ, George J. International consensus, MAFLD: A consensus-driven proposed nomenclature for metabolic associated fatty liver disease. *Gastroenterology.* (2020) 158:1999–2014.e1. doi: 10.1053/j.gastro.2019.11.312
25. Day CP, James OF. Steatohepatitis: a tale of two "hits"? *Gastroenterology.* (1998) 114:842–5. doi: 10.1016/S0016-5085(98)70599-2
26. Friedman SL, Neuschwander-Tetri BA, Rinella M, Sanyal AJ. Mechanisms of NAFLD development and therapeutic strategies. *Nat Med.* (2018) 24:908–22. doi: 10.1038/s41591-018-0104-9
27. Buzzetti E, Pinzani M, Tsochatzis EA. The multiple-hit pathogenesis of non-alcoholic fatty liver disease (NAFLD). *Metabolism.* (2016) 65:1038–48. doi: 10.1016/j.metabol.2015.12.012
28. Peng C, Stewart AG, Woodman OL, Ritchie RH, Qin CX. Non-alcoholic steatohepatitis: a review of its mechanism, models and medical treatments. *Front Pharmacol.* (2020) 11:603926. doi: 10.3389/fphar.2020.603926
29. Neuschwander-Tetri BA. Hepatic lipotoxicity and the pathogenesis of nonalcoholic steatohepatitis: the central role of nontriglyceride fatty acid metabolites. *Hepatology.* (2010) 52:774–88. doi: 10.1002/hep.23719
30. Arguello G, Balboa E, Arrese M, Zanlungo S. Recent insights on the role of cholesterol in non-alcoholic fatty liver disease. *Biochim Biophys Acta.* (2015) 1852:1765–78. doi: 10.1016/j.bbadis.2015.05.015
31. Ho CM, Ho SL, Jeng YM, Lai YS, Chen YH, Lu SC, et al. Accumulation of free cholesterol and oxidized low-density lipoprotein is associated with portal inflammation and fibrosis in nonalcoholic fatty liver disease. *J Inflamm (Lond).* (2019) 16:7. doi: 10.1186/s12950-019-0211-5
32. Ioannou GN. The role of cholesterol in the pathogenesis of NASH. *Trends Endocrinol Metab.* (2016) 27:84–95. doi: 10.1016/j.tem.2015.11.008
33. Parthasarathy G, Revelo X, Malhi H. Pathogenesis of nonalcoholic steatohepatitis: an overview. *Hepatol Commun.* (2020) 4:478–92. doi: 10.1002/hep4.1479
34. Ibrahim SH, Hirsova P, Gores GJ. Non-alcoholic steatohepatitis pathogenesis: sublethal hepatocyte injury as a driver of liver inflammation. *Gut.* (2018) 67:963–72. doi: 10.1136/gutjnl-2017-315691
35. Liu W, Baker RD, Bhatia T, Zhu L, Baker SS. Pathogenesis of nonalcoholic steatohepatitis. *Cell Mol Life Sci.* (2016) 73:1969–87. doi: 10.1007/s00018-016-2161-x
36. Koyama Y, Brenner DA. Liver inflammation and fibrosis. *J Clin Invest.* (2017) 127:55–64. doi: 10.1172/JCI88881
37. Bouwens L, Baekeland M, De Zanger R, Wisse E. Quantitation, tissue distribution and proliferation kinetics of Kupffer cells in normal rat liver. *Hepatology.* (1986) 6:718–22. doi: 10.1002/hep.1840060430
38. Kolios G, Valatas V, Kouroumalis E. Role of Kupffer cells in the pathogenesis of liver disease. *World J Gastroenterol.* (2006) 12:7413–20. doi: 10.3748/wjg.v12.i46.7413
39. Mosser DM, Edwards JP. Exploring the full spectrum of macrophage activation. *Nat Rev Immunol.* (2008) 8:958–69. doi: 10.1038/nri2448
40. Kazankov K, Jorgensen SMD, Thomsen KL, Moller HJ, Vilstrup H, George J, et al. The role of macrophages in nonalcoholic fatty liver disease and nonalcoholic steatohepatitis. *Nat Rev Gastroenterol Hepatol.* (2019) 16:145–59. doi: 10.1038/s41575-018-0082-x
41. Wan J, Benkdane M, Teixeira-Clerc F, Bonnafous S, Louvet A, Lafdil F, et al. M2 Kupffer cells promote M1 Kupffer cell apoptosis: a protective mechanism against alcoholic and nonalcoholic fatty liver disease. *Hepatology.* (2014) 59:130–42. doi: 10.1002/hep.26607
42. Smith K. Liver disease: Kupffer cells regulate the progression of ALD and NAFLD. *Nat Rev Gastroenterol Hepatol.* (2013) 10:503. doi: 10.1038/nrgastro.2013.140
43. Li H, Zhou Y, Wang H, Zhang M, Qiu P, Zhang M, et al. Crosstalk between liver macrophages and surrounding cells in nonalcoholic steatohepatitis. *Front Immunol.* (2020) 11:1169. doi: 10.3389/fimmu.2020.01169
44. Lee UE, Friedman SL. Mechanisms of hepatic fibrogenesis. *Best Pract Res Clin Gastroenterol.* (2011) 25:195–206. doi: 10.1016/j.bpg.2011.02.005

45. Zhang CY, Yuan WG, He P, Lei JH, Wang CX. Liver fibrosis and hepatic stellate cells: Etiology, pathological hallmarks and therapeutic targets. *World J Gastroenterol.* (2016) 22:10512–22. doi: 10.3748/wjg.v22.i48.10512
46. Cha JY, Kim DH, Chun KH. The role of hepatic macrophages in nonalcoholic fatty liver disease and nonalcoholic steatohepatitis. *Lab Anim Res.* (2018) 34:133–9. doi: 10.5625/lar.2018.34.4.133
47. Ramachandran P, Pellicoro A, Vernon MA, Boulter L, Aucott RL, Ali A, et al. Differential Ly-6C expression identifies the recruited macrophage phenotype, which orchestrates the regression of murine liver fibrosis. *Proc Natl Acad Sci USA.* (2012) 109:E3186–95. doi: 10.1073/pnas.1119964109
48. Seki E, Schwabe RF. Hepatic inflammation and fibrosis: functional links and key pathways. *Hepatology.* (2015) 61:1066–79. doi: 10.1002/hep.27332
49. Miura K, Yang L, van Rooijen N, Ohnishi H, Seki E. Hepatic recruitment of macrophages promotes nonalcoholic steatohepatitis through CCR2. *Am J Physiol Gastrointest Liver Physiol.* (2012) 302:G1310–21. doi: 10.1152/ajpgi.00365.2011
50. Yang SJ, IglayReger HB, Kadouh HC, Bodary PF. Inhibition of the chemokine (C-C motif) ligand 2/chemokine (C-C motif) receptor 2 pathway attenuates hyperglycaemia and inflammation in a mouse model of hepatic steatosis and lipoatrophy. *Diabetologia.* (2009) 52:972–81. doi: 10.1007/s00125-009-1309-8
51. Weisberg SP, Hunter D, Huber R, Lemieux J, Slaymaker S, Vaddi K, et al. CCR2 modulates inflammatory and metabolic effects of high-fat feeding. *J Clin Invest.* (2006) 116:115–24. doi: 10.1172/JCI24335
52. Baeck C, Wehr A, Karlmark KR, Heymann F, Vucur M, Gassler N, et al. Pharmacological inhibition of the chemokine CCL2 (MCP-1) diminishes liver macrophage infiltration and steatohepatitis in chronic hepatic injury. *Gut.* (2012) 61:416–26. doi: 10.1136/gutjnl-2011-300304
53. Eslam M, George J. Genetic contributions to NAFLD: leveraging shared genetics to uncover systems biology. *Nat Rev Gastroenterol Hepatol.* (2020) 17:40–52. doi: 10.1038/s41575-019-0212-0
54. Smagris E, BasuRay S, Li J, Huang Y, Lai KM, Gromada J, et al. Pnpla3I148M knockin mice accumulate PNPLA3 on lipid droplets and develop hepatic steatosis. *Hepatology.* (2015) 61:108–18. doi: 10.1002/hep.27242
55. BasuRay S, Wang Y, Smagris E, Cohen JC, Hobbs HH. Accumulation of PNPLA3 on lipid droplets is the basis of associated hepatic steatosis. *Proc Natl Acad Sci USA.* (2019) 116:9521–6. doi: 10.1073/pnas.1901974116
56. Dong XC. PNPLA3-A potential therapeutic target for personalized treatment of chronic liver disease. *Front Med.* (2019) 6:304. doi: 10.3389/fmed.2019.00304
57. Liu YL, Reeves HL, Burt AD, Tiniakos D, McPherson S, Leathart JB, et al. TM6SF2 rs58542926 influences hepatic fibrosis progression in patients with non-alcoholic fatty liver disease. *Nat Commun.* (2014) 5:4309. doi: 10.1038/ncomms5309
58. Jiang ZG, Tapper EB, Kim M, Connelly MA, Krawczyk SA, Yee EU, et al. Genetic determinants of circulating lipoproteins in nonalcoholic fatty liver disease. *J Clin Gastroenterol.* (2018) 52:444–51. doi: 10.1097/MCG.0000000000000816
59. Gibney ER, Nolan CM. Epigenetics and gene expression. *Heredity (Edinb).* (2010) 105:4–13. doi: 10.1038/hdy.2010.54
60. Kitamoto T, Kitamoto A, Ogawa Y, Honda Y, Imajo K, Saito S, et al. Targeted-bisulfite sequence analysis of the methylation of CpG islands in genes encoding PNPLA3, SAMM50, and PARVB of patients with non-alcoholic fatty liver disease. *J Hepatol.* (2015) 63:494–502. doi: 10.1016/j.jhep.2015.02.049
61. Hardy T, Zeybel M, Day CP, Dipper C, Masson S, McPherson S, et al. Plasma DNA methylation: a potential biomarker for stratification of liver fibrosis in non-alcoholic fatty liver disease. *Gut.* (2017) 66:1321–8. doi: 10.1136/gutjnl-2016-311526
62. Cheung O, Puri P, Eicken C, Contos MJ, Mirshahi F, Maher JW, et al. Nonalcoholic steatohepatitis is associated with altered hepatic MicroRNA expression. *Hepatology.* (2008) 48:1810–20. doi: 10.1002/hep.22569
63. Zhang ZC, Liu Y, Xiao LL, Li SF, Jiang JH, Zhao Y, et al. Upregulation of miR-125b by estrogen protects against non-alcoholic fatty liver in female mice. *J Hepatol.* (2015) 63:1466–75. doi: 10.1016/j.jhep.2015.07.037
64. Calo N, Ramadori P, Sobolewski C, Romero Y, Maeder C, Fournier M, et al. Stress-activated miR-21/miR-21* in hepatocytes promotes lipid and glucose metabolic disorders associated with high-fat diet consumption. *Gut.* (2016) 65:1871–81. doi: 10.1136/gutjnl-2015-310822
65. Guo J, Fang W, Sun L, Lu Y, Dou L, Huang X, et al. Ultraconserved element uc.372 drives hepatic lipid accumulation by suppressing miR-195/miR4668 maturation. *Nat Commun.* (2018) 9:612. doi: 10.1038/s41467-018-03072-8
66. Atanasovska B, Rensen SS, van der Sijde MR, Marsman G, Kumar V, Jonkers I, et al. A liver-specific long noncoding RNA with a role in cell viability is elevated in human nonalcoholic steatohepatitis. *Hepatology.* (2017) 66:794–808. doi: 10.1002/hep.29034
67. Zhang Y, Cheng X, Lu Z, Wang J, Chen H, Fan W, et al. Upregulation of miR-15b in NAFLD models and in the serum of patients with fatty liver disease. *Diabetes Res Clin Pract.* (2013) 99:327–34. doi: 10.1016/j.diabres.2012.11.025
68. Qin W, Li X, Xie L, Li S, Liu J, Jia L, et al. A long non-coding RNA, APOA4-AS, regulates APOA4 expression depending on HuR in mice. *Nucleic Acids Res.* (2016) 44:6423–33. doi: 10.1093/nar/gkw341
69. Cermelli S, Ruggieri A, Marrero JA, Ioannou GN, Beretta L. Circulating microRNAs in patients with chronic hepatitis C and non-alcoholic fatty liver disease. *PLoS ONE.* (2011) 6:e23937. doi: 10.1371/journal.pone.0023937
70. Yu F, Zheng J, Mao Y, Dong P, Li G, Lu Z, et al. Long non-coding RNA APTR promotes the activation of hepatic stellate cells and the progression of liver fibrosis. *Biochem Biophys Res Commun.* (2015) 463:679–85. doi: 10.1016/j.bbrc.2015.05.124
71. Gerhard GS, DiStefano JK. Micro RNAs in the development of non-alcoholic fatty liver disease. *World J Hepatol.* (2015) 7:226–34. doi: 10.4254/wjh.v7.i2.226
72. Chen Y, Chen X, Gao J, Xu C, Xu P, Li Y, et al. Long noncoding RNA FLRL2 alleviated nonalcoholic fatty liver disease through Arntl-Sirt1 pathway. *FASEB J.* (2019) 33:11411–9. doi: 10.1096/fj.201900643RRR
73. Zhang T, Yang Z, Kusumanchi P, Han S, Liangpunsakul S. Critical role of microRNA-21 in the pathogenesis of liver diseases. *Front Med.* (2020) 7:7. doi: 10.3389/fmed.2020.00007
74. Ma M, Duan R, Shen L, Liu M, Ji Y, Zhou H, et al. The lncRNA Gm15622 stimulates SREBP-1c expression and hepatic lipid accumulation by sponging the miR-742-3p in mice. *J Lipid Res.* (2020) 61:1052–64. doi: 10.1194/jlr.RA120000664
75. Hu Y, Liu HX, Jena PK, Sheng L, Ali MR, Wan YY. miR-22 inhibition reduces hepatic steatosis via FGF21 and FGFR1 induction. *JHEP Rep.* (2020) 2:100093. doi: 10.1016/j.jhepr.2020.100093
76. Yu F, Chen B, Dong P, Zheng J. HOTAIR epigenetically modulates PTEN expression via MicroRNA-29b: a novel mechanism in regulation of liver fibrosis. *Mol Ther.* (2017) 25:205–17. doi: 10.1016/j.ymthe.2016.10.015
77. Ali O, Darwish HA, Eldeib KM, Abdel Azim SA. miR-26a potentially contributes to the regulation of fatty acid and sterol metabolism *in vitro* human HepG2 cell model of nonalcoholic fatty liver disease. *Oxid Med Cell Longev.* (2018) 2018:8515343. doi: 10.1155/2018/8515343
78. Shen X, Guo H, Xu J, Wang J. Inhibition of lncRNA HULC improves hepatic fibrosis and hepatocyte apoptosis by inhibiting the MAPK signaling pathway in rats with nonalcoholic fatty liver disease. *J Cell Physiol.* (2019) 234:18169–79. doi: 10.1002/jcp.28450
79. Zhang M, Sun W, Zhou M, Tang Y. MicroRNA-27a regulates hepatic lipid metabolism and alleviates NAFLD via repressing FAS and SCD1. *Sci Rep.* (2017) 7:14493. doi: 10.1038/s41598-017-15141-x
80. Zhang M, Chi X, Qu N, Wang C. Long noncoding RNA lncARSR promotes hepatic lipogenesis via Akt/SREBP-1c pathway and contributes to the pathogenesis of nonalcoholic steatohepatitis. *Biochem Biophys Res Commun.* (2018) 499:66–70. doi: 10.1016/j.bbrc.2018.03.127
81. Jampoka K, Muangpaisarn P, Khongnomnan K, Treeprasertsuk S, Tangkijvanich P, Payungporn S. Serum miR-29a and miR-122 as potential biomarkers for non-alcoholic fatty liver disease (NAFLD). *Microrna.* (2018) 7:215–22. doi: 10.2174/2211536607666180531093302
82. Chen X, Xu Y, Zhao D, Chen T, Gu C, Yu G, et al. LncRNA-AK012226 is involved in fat accumulation in db/db mice fatty liver and non-alcoholic fatty liver disease cell model. *Front Pharmacol.* (2018) 9:888. doi: 10.3389/fphar.2018.00888
83. Fan J, Li H, Nie X, Yin Z, Zhao Y, Chen C, et al. MiR-30c-5p ameliorates hepatic steatosis in leptin receptor-deficient (db/db)

mice via down-regulating FASN. *Oncotarget.* (2017) 8:13450–63. doi: 10.18632/oncotarget.14561
84. Lan X, Wu L, Wu N, Chen Q, Li Y, Du X, et al. Long noncoding RNA lnc-HC regulates PPARgamma-mediated hepatic lipid metabolism through miR-130b-3p. *Mol Ther Nucleic Acids.* (2019) 18:954–65. doi: 10.1016/j.omtn.2019.10.018
85. Auguet T, Aragones G, Berlanga A, Guiu-Jurado E, Marti A, Martinez S, et al. miR33a/miR33b* and miR122 as possible contributors to hepatic lipid metabolism in obese women with nonalcoholic fatty liver disease. *Int J Mol Sci.* (2016) 17:1620. doi: 10.3390/ijms17101620
86. Li D, Cheng M, Niu Y, Chi X, Liu X, Fan J, et al. Identification of a novel human long non-coding RNA that regulates hepatic lipid metabolism by inhibiting SREBP-1c. *Int J Biol Sci.* (2017) 13:349–57. doi: 10.7150/ijbs.16635
87. Ding J, Li M, Wan X, Jin X, Chen S, Yu C, et al. Effect of miR-34a in regulating steatosis by targeting PPARalpha expression in nonalcoholic fatty liver disease. *Sci Rep.* (2015) 5:13729. doi: 10.1038/srep13729
88. Yang Z, Zhang T, Han S, Kusumanchi P, Huda N, Jiang Y, et al. Long noncoding RNA H19 - a new player in the pathogenesis of liver diseases. *Transl Res.* (2021) 230:139–50. doi: 10.1016/j.trsl.2020.11.010
89. Celikbilek M, Baskol M, Taheri S, Deniz K, Dogan S, Zararsiz G, et al. Circulating microRNAs in patients with non-alcoholic fatty liver disease. *World J Hepatol.* (2014) 6:613–20. doi: 10.4254/wjh.v6.i8.613
90. Sookoian S, Rohr C, Salatino A, Dopazo H, Fernandez Gianotti T, Castano GO, et al. Genetic variation in long noncoding RNAs and the risk of nonalcoholic fatty liver disease. *Oncotarget.* (2017) 8:22917–26. doi: 10.18632/oncotarget.15286
91. Li P, Ruan X, Yang L, Kiesewetter K, Zhao Y, Luo H, et al. A liver-enriched long non-coding RNA, lncLSTR, regulates systemic lipid metabolism in mice. *Cell Metab.* (2015) 21:455–67. doi: 10.1016/j.cmet.2015.02.004
92. Zhao XY, Xiong X, Liu T, Mi L, Peng X, Rui C, et al. Long noncoding RNA licensing of obesity-linked hepatic lipogenesis and NAFLD pathogenesis. *Nat Commun.* (2018) 9:2986. doi: 10.1038/s41467-018-05383-2
93. Wang Y, Du J, Niu X, Fu N, Wang R, Zhang Y, et al. MiR-130a-3p attenuates activation and induces apoptosis of hepatic stellate cells in nonalcoholic fibrosing steatohepatitis by directly targeting TGFBR1 and TGFBR2. *Cell Death Dis.* (2017) 8:e2792. doi: 10.1038/cddis.2017.10
94. Wang J, Yang W, Chen Z, Chen J, Meng Y, Feng B, et al. Long noncoding RNA lncSHGL recruits hnRNPA1 to suppress hepatic gluconeogenesis and lipogenesis. *Diabetes.* (2018) 67:581–93. doi: 10.2337/db17-0799
95. Jiang H, Qian Y, Shen Z, Liu Y, He Y, Gao R, et al. Circulating microRNA135a3p in serum extracellular vesicles as a potential biological marker of nonalcoholic fatty liver disease. *Mol Med Rep.* (2021) 24:12137. doi: 10.3892/mmr.2021.12137
96. Du J, Niu X, Wang Y, Kong L, Wang R, Zhang Y, et al. MiR-146a-5p suppresses activation and proliferation of hepatic stellate cells in nonalcoholic fibrosing steatohepatitis through directly targeting Wnt1 and Wnt5a. *Sci Rep.* (2015) 5:16163. doi: 10.1038/srep16163
97. Zhang K, Han X, Zhang Z, Zheng L, Hu Z, Yao Q, et al. The liver-enriched lnc-LFAR1 promotes liver fibrosis by activating TGFbeta and Notch pathways. *Nat Commun.* (2017) 8:144. doi: 10.1038/s41467-017-00204-4
98. Miller AM, Gilchrist DS, Nijjar J, Araldi E, Ramirez CM, Lavery CA, et al. MiR-155 has a protective role in the development of non-alcoholic hepatosteatosis in mice. *PLoS ONE.* (2013) 8:e72324. doi: 10.1371/journal.pone.0072324
99. Leti F, Legendre C, Still CD, Chu X, Petrick A, Gerhard GS, et al. Altered expression of MALAT1 lncRNA in nonalcoholic steatohepatitis fibrosis regulates CXCL5 in hepatic stellate cells. *Transl Res.* (2017) 190:25–39.e21. doi: 10.1016/j.trsl.2017.09.001
100. Wang Y, Zhu K, Yu W, Wang H, Liu L, Wu Q, et al. MiR-181b regulates steatosis in nonalcoholic fatty liver disease via targeting SIRT1. *Biochem Biophys Res Commun.* (2017) 493:227–32. doi: 10.1016/j.bbrc.2017.09.042
101. Huang P, Huang FZ, Liu HZ, Zhang TY, Yang MS, Sun CZ. LncRNA MEG3 functions as a ceRNA in regulating hepatic lipogenesis by competitively binding to miR-21 with LRP6. *Metabolism.* (2019) 94:1–8. doi: 10.1016/j.metabol.2019.01.018
102. Xu M, Zheng XM, Jiang F, Qiu WQ. MicroRNA-190b regulates lipid metabolism and insulin sensitivity by targeting IGF-1 and ADAMTS9 in non-alcoholic fatty liver disease. *J Cell Biochem.* (2018) 119:5864–74. doi: 10.1002/jcb.26776
103. Zhang B, Li H, Li D, Sun H, Li M, Hu H. Long noncoding RNA Mirt2 upregulates USP10 expression to suppress hepatic steatosis by sponging miR-34a-5p. *Gene.* (2019) 700:139–48. doi: 10.1016/j.gene.2019.02.096
104. Liu XL, Cao HX, Wang BC, Xin FZ, Zhang RN, Zhou D, et al. miR-192-5p regulates lipid synthesis in non-alcoholic fatty liver disease through SCD-1. *World J Gastroenterol.* (2017) 23:8140–51. doi: 10.3748/wjg.v23.i46.8140
105. Yuan X, Wang J, Tang X, Li Y, Xia P, Gao X. Berberine ameliorates nonalcoholic fatty liver disease by a global modulation of hepatic mRNA and lncRNA expression profiles. *J Transl Med.* (2015) 13:24. doi: 10.1186/s12967-015-0383-6
106. Nie H, Song C, Wang D, Cui S, Ren T, Cao Z, et al. MicroRNA-194 inhibition improves dietary-induced non-alcoholic fatty liver disease in mice through targeting on FXR. *Biochim Biophys Acta Mol Basis Dis.* (2017) 1863:3087–94. doi: 10.1016/j.bbadis.2017.09.020
107. Wang X. Down-regulation of lncRNA-NEAT1 alleviated the non-alcoholic fatty liver disease via mTOR/S6K1 signaling pathway. *J Cell Biochem.* (2018) 119:1567–74. doi: 10.1002/jcb.26317
108. Chen Q, Xiong C, Jia K, Jin J, Li Z, Huang Y, et al. Hepatic transcriptome analysis from HFD-fed mice defines a long noncoding RNA regulating cellular cholesterol levels. *J Lipid Res.* (2019) 60:341–52. doi: 10.1194/jlr.M086215
109. Li Y, Luan Y, Li J, Song H, Li Y, Qi H, et al. Exosomal miR-199a-5p promotes hepatic lipid accumulation by modulating MST1 expression and fatty acid metabolism. *Hepatol Int.* (2020) 14:1057–74. doi: 10.1007/s12072-020-10096-0
110. Ma TT, Huang C, Ni Y, Yang Y, Li J. ATP citrate lyase and LncRNA NONMMUT010685 play crucial role in nonalcoholic fatty liver disease based on analysis of microarray data. *Cell Physiol Biochem.* (2018) 51:871–85. doi: 10.1159/000495384
111. Feng YY, Xu XQ, Ji CB, Shi CM, Guo XR, Fu JF. Aberrant hepatic microRNA expression in nonalcoholic fatty liver disease. *Cell Physiol Biochem.* (2014) 34:1983–97. doi: 10.1159/000366394
112. Hu Y, Ye H, Shi LX. MicroRNA-205 ameliorates lipid accumulation in non-alcoholic fatty liver disease through targeting NEU1. *Eur Rev Med Pharmacol Sci.* (2019) 23:10072–82. doi: 10.26355/eurrev_201911_19575
113. Gong Z, Tang J, Xiang T, Lin J, Deng C, Peng Y, et al. Genomewide identification of long noncoding RNAs in CCl4induced liver fibrosis via RNA sequencing. *Mol Med Rep.* (2018) 18:299–307. doi: 10.3892/mmr.2018.8986
114. Jiang X, Jiang L, Shan A, Su Y, Cheng Y, Song D, et al. Targeting hepatic miR-221/222 for therapeutic intervention of nonalcoholic steatohepatitis in mice. *EBioMedicine.* (2018) 37:307–21. doi: 10.1016/j.ebiom.2018.09.051
115. Zheng J, Yu F, Dong P, Wu L, Zhang Y, Hu Y, et al. Long non-coding RNA PVT1 activates hepatic stellate cells through competitively binding microRNA-152. *Oncotarget.* (2016) 7:62886–97. doi: 10.18632/oncotarget.11709
116. He Y, Hwang S, Cai Y, Kim SJ, Xu M, Yang D, et al. MicroRNA-223 ameliorates nonalcoholic steatohepatitis and cancer by targeting multiple inflammatory and oncogenic genes in hepatocytes. *Hepatology.* (2019) 70:1150–67. doi: 10.1002/hep.30645
117. Di Mauro S, Scamporrino A, Petta S, Urbano F, Filippello A, Ragusa M, et al. Serum coding and non-coding RNAs as biomarkers of NAFLD and fibrosis severity. *Liver Int.* (2019) 39:1742–54. doi: 10.1111/liv.14167
118. Chen C, Wu CQ, Zhang ZQ, Yao DK, Zhu L. Loss of expression of miR-335 is implicated in hepatic stellate cell migration and activation. *Exp Cell Res.* (2011) 317:1714–25. doi: 10.1016/j.yexcr.2011.05.001
119. Kaur S, Rawal P, Siddiqui H, Rohilla S, Sharma S, Tripathi DM, et al. Increased expression of RUNX1 in liver correlates with NASH activity score in patients with non-alcoholic steatohepatitis (NASH). *Cells.* (2019) 8:1277. doi: 10.3390/cells8101277
120. Lei L, Zhou C, Yang X, Li L. Down-regulation of microRNA-375 regulates adipokines and inhibits inflammatory cytokines by targeting AdipoR2 in non-alcoholic fatty liver disease. *Clin Exp Pharmacol Physiol.* (2018) 45:819–31. doi: 10.1111/1440-1681.12940

121. Chen G, Yu D, Nian X, Liu J, Koenig RJ, Xu B, et al. LncRNA SRA promotes hepatic steatosis through repressing the expression of adipose triglyceride lipase (ATGL). *Sci Rep*. (2016) 6:35531. doi: 10.1038/srep 35531
122. Zhang T, Hu J, Wang X, Zhao X, Li Z, Niu J, et al. MicroRNA-378 promotes hepatic inflammation and fibrosis via modulation of the NF-kappaB-TNFalpha pathway. *J Hepatol*. (2019) 70:87–96. doi: 10.1016/j.jhep.2018.08.026
123. Zeng N, Huang R, Li N, Jiang H, Li R, Wang F, et al. MiR-451a attenuates free fatty acids-mediated hepatocyte steatosis by targeting the thyroid hormone responsive spot 14 gene. *Mol Cell Endocrinol*. (2018) 474:260–71. doi: 10.1016/j.mce.2018.03.016
124. Moran-Salvador E, Mann J. Epigenetics and liver fibrosis. *Cell Mol Gastroenterol Hepatol*. (2017) 4:125–34. doi: 10.1016/j.jcmgh.2017.04.007
125. Ishimoto T, Lanaspa MA, Rivard CJ, Roncal-Jimenez CA, Orlicky DJ, Cicerchi C, et al. High-fat and high-sucrose (western) diet induces steatohepatitis that is dependent on fructokinase. *Hepatology*. (2013) 58:1632–43. doi: 10.1002/hep.26594
126. Lytle KA, Jump DB. Is western diet-induced nonalcoholic steatohepatitis in Ldlr-/- mice reversible? *PLoS ONE*. (2016) 11:e0146942. doi: 10.1371/journal.pone.0146942
127. Zhang H, Leveille M, Courty E, Gunes A, B NN, Estall JL. Differences in metabolic and liver pathobiology induced by two dietary mouse models of nonalcoholic fatty liver disease. *Am J Physiol Endocrinol Metab*. (2020) 319:E863–76. doi: 10.1152/ajpendo.00321.2020
128. Schuster S, Cabrera D, Arrese M, Feldstein AE. Triggering and resolution of inflammation in NASH. *Nat Rev Gastroenterol Hepatol*. (2018) 15:349–64. doi: 10.1038/s41575-018-0009-6
129. Neuschwander-Tetri BA. Carbohydrate intake and nonalcoholic fatty liver disease. *Curr Opin Clin Nutr Metab Care*. (2013) 16:446–52. doi: 10.1097/MCO.0b013e328361c4d1
130. Jensen T, Abdelmalek MF, Sullivan S, Nadeau KJ, Green M, Roncal C, et al. Fructose and sugar: A major mediator of non-alcoholic fatty liver disease. *J Hepatol*. (2018) 68:1063–75. doi: 10.1016/j.jhep.2018.01.019
131. DiStefano JK, Shaibi GQ. The relationship between excessive dietary fructose consumption and paediatric fatty liver disease. *Pediatr Obes*. (2021) 16:e12759. doi: 10.1111/ijpo.12759
132. Asgharpour A, Cazanave SC, Pacana T, Seneshaw M, Vincent R, Banini BA, et al. A diet-induced animal model of non-alcoholic fatty liver disease and hepatocellular cancer. *J Hepatol*. (2016) 65:579–88. doi: 10.1016/j.jhep.2016.05.005
133. Clapper JR, Hendricks MD, Gu G, Wittmer C, Dolman CS, Herich J, et al. Diet-induced mouse model of fatty liver disease and nonalcoholic steatohepatitis reflecting clinical disease progression and methods of assessment. *Am J Physiol Gastrointest Liver Physiol*. (2013) 305:G483–95. doi: 10.1152/ajpgi.00079.2013
134. Kim Y, Chang Y, Cho YK, Ahn J, Shin H, Ryu S. Obesity and weight gain are associated with progression of fibrosis in patients with nonalcoholic fatty liver disease. *Clin Gastroenterol Hepatol*. (2019) 17:543–50.e2. doi: 10.1016/j.cgh.2018.07.006
135. Polyzos SA, Kountouras J, Mantzoros CS. Obesity and nonalcoholic fatty liver disease: From pathophysiology to therapeutics. *Metabolism*. (2019) 92:82–97. doi: 10.1016/j.metabol.2018.11.014
136. Chalasani N, Younossi Z, Lavine JE, Charlton M, Cusi K, Rinella M, et al. The diagnosis and management of nonalcoholic fatty liver disease: Practice guidance from the American association for the study of liver diseases. *Hepatology*. (2018) 67:328–57. doi: 10.1002/hep.29367
137. Targher G, Corey KE, Byrne CD, Roden M. The complex link between NAFLD and type 2 diabetes mellitus - mechanisms and treatments. *Nat Rev Gastroenterol Hepatol*. (2021) 18:599–612. doi: 10.1038/s41575-021-00448-y
138. Katsiki N, Mikhailidis DP, Mantzoros CS. Non-alcoholic fatty liver disease and dyslipidemia: An update. *Metabolism*. (2016) 65:1109–23. doi: 10.1016/j.metabol.2016.05.003
139. Arslan N. Obesity, fatty liver disease and intestinal microbiota. *World J Gastroenterol*. (2014) 20:16452–63. doi: 10.3748/wjg.v20.i44.16452
140. Leung C, Rivera L, Furness JB, Angus PW. The role of the gut microbiota in NAFLD. *Nat Rev Gastroenterol Hepatol*. (2016) 13:412–25. doi: 10.1038/nrgastro.2016.85
141. Bashiardes S, Shapiro H, Rozin S, Shibolet O, Elinav E. Non-alcoholic fatty liver and the gut microbiota. *Mol Metab*. (2016) 5:782–94. doi: 10.1016/j.molmet.2016.06.003
142. Gerard P. Gut microbiota and obesity. *Cell Mol Life Sci*. (2016) 73:147–62. doi: 10.1007/s00018-015-2061-5
143. Boursier J, Diehl AM. Implication of gut microbiota in nonalcoholic fatty liver disease. *PLoS Pathog*. (2015) 11:e1004559. doi: 10.1371/journal.ppat.1004559
144. Aron-Wisnewsky J, Warmbrunn MV, Nieuwdorp M, Clement K. Nonalcoholic fatty liver disease: modulating gut microbiota to improve severity? *Gastroenterology*. (2020) 158:1881–98. doi: 10.1053/j.gastro.2020.01.049
145. Brandl K, Schnabl B. Intestinal microbiota and nonalcoholic steatohepatitis. *Curr Opin Gastroenterol*. (2017) 33:128–33. doi: 10.1097/MOG.0000000000000349
146. Mouries J, Brescia P, Silvestri A, Spadoni I, Sorribas M, Wiest R, et al. Microbiota-driven gut vascular barrier disruption is a prerequisite for non-alcoholic steatohepatitis development. *J Hepatol*. (2019) 71:1216–28. doi: 10.1016/j.jhep.2019.08.005
147. Brown K, DeCoffe D, Molcan E, Gibson DL. Diet-induced dysbiosis of the intestinal microbiota and the effects on immunity and disease. *Nutrients*. (2012) 4:1095–119. doi: 10.3390/nu4081095
148. Boursier J, Mueller O, Barret M, Machado M, Fizanne L, Araujo-Perez F, et al. The severity of nonalcoholic fatty liver disease is associated with gut dysbiosis and shift in the metabolic function of the gut microbiota. *Hepatology*. (2016) 63:764–75. doi: 10.1002/hep.28356
149. Shen F, Zheng RD, Sun XQ, Ding WJ, Wang XY, Fan JG. Gut microbiota dysbiosis in patients with non-alcoholic fatty liver disease. *Hepatobiliary Pancreat Dis Int*. (2017) 16:375–81. doi: 10.1016/S1499-3872(17)60019-5
150. Zhu L, Baker SS, Gill C, Liu W, Alkhouri R, Baker RD, et al. Characterization of gut microbiomes in nonalcoholic steatohepatitis (NASH) patients: a connection between endogenous alcohol and NASH. *Hepatology*. (2013) 57:601–9. doi: 10.1002/hep.26093
151. Nalbantoglu IL, Brunt EM. Role of liver biopsy in nonalcoholic fatty liver disease. *World J Gastroenterol*. (2014) 20:9026–37. doi: 10.3748/wjg.v20.i27.9026
152. Sebastiani G, Alberti A. Non invasive fibrosis biomarkers reduce but not substitute the need for liver biopsy. *World J Gastroenterol*. (2006) 12:3682–94. doi: 10.3748/wjg.v12.i23.3682
153. Sumida Y, Nakajima A, Itoh Y. Limitations of liver biopsy and non-invasive diagnostic tests for the diagnosis of nonalcoholic fatty liver disease/nonalcoholic steatohepatitis. *World J Gastroenterol*. (2014) 20:475–85. doi: 10.3748/wjg.v20.i2.475
154. Stern C, Castera L. Non-invasive diagnosis of hepatic steatosis. *Hepatol Int*. (2017) 11:70–8. doi: 10.1007/s12072-016-9772-z
155. Sviklane L, Olmane E, Dzerve Z, Kupcs K, Pirags V, Sokolovska J. Fatty liver index and hepatic steatosis index for prediction of non-alcoholic fatty liver disease in type 1 diabetes. *J Gastroenterol Hepatol*. (2018) 33:270–6. doi: 10.1111/jgh.13814
156. Wong VW, Adams LA, de Ledinghen V, Wong GL, Sookoian S. Noninvasive biomarkers in NAFLD and NASH - current progress and future promise. *Nat Rev Gastroenterol Hepatol*. (2018) 15:461–78. doi: 10.1038/s41575-018-0014-9
157. Loomba R. Role of imaging-based biomarkers in NAFLD: Recent advances in clinical application and future research directions. *J Hepatol*. (2018) 68:296–304. doi: 10.1016/j.jhep.2017.11.028
158. Hernaez R, Lazo M, Bonekamp S, Kamel I, Brancati FL, Guallar E, et al. Diagnostic accuracy and reliability of ultrasonography for the detection of fatty liver: a meta-analysis. *Hepatology*. (2011) 54:1082–90. doi: 10.1002/hep.24452
159. Tobari M, Hashimoto E, Yatsuji S, Torii N, Shiratori K. Imaging of nonalcoholic steatohepatitis: advantages and pitfalls of ultrasonography and computed tomography. *Intern Med*. (2009) 48:739–46. doi: 10.2169/internalmedicine.48.1869
160. Cam I, Koc U, Genez S, Gunes A. Computed tomography measurements of hepatic steatosis in cholelitihiasis and cholecystectomy cases using unenhanced images. *J Med Imaging Radiat Sci*. (2020) 51:137–44. doi: 10.1016/j.jmir.2019.12.003

161. Desai NK, Harney S, Raza R, Al-Ibraheemi A, Shillingford N, Mitchell PD, et al. Comparison of controlled attenuation parameter and liver biopsy to assess hepatic steatosis in pediatric patients. *J Pediatr.* (2016) 173:160–4.e1. doi: 10.1016/j.jpeds.2016.03.021
162. Middleton MS, Heba ER, Hooker CA, Bashir MR, Fowler KJ, Sandrasegaran K, et al. Agreement between magnetic resonance imaging proton density fat fraction measurements and pathologist-assigned steatosis grades of liver biopsies from adults with nonalcoholic steatohepatitis. *Gastroenterology.* (2017) 153:753–61. doi: 10.1053/j.gastro.2017.06.005
163. Shi KQ, Tang JZ, Zhu XL, Ying L, Li DW, Gao J, et al. Controlled attenuation parameter for the detection of steatosis severity in chronic liver disease: a meta-analysis of diagnostic accuracy. *J Gastroenterol Hepatol.* (2014) 29:1149–58. doi: 10.1111/jgh.12519
164. Caussy C, Alquiraish MH, Nguyen P, Hernandez C, Cepin S, Fortney LE, et al. Optimal threshold of controlled attenuation parameter with MRI-PDFF as the gold standard for the detection of hepatic steatosis. *Hepatology.* (2018) 67:1348–59. doi: 10.1002/hep.29639
165. Bannas P, Kramer H, Hernando D, Agni R, Cunningham AM, Mandal R, et al. Quantitative magnetic resonance imaging of hepatic steatosis: validation in *ex vivo* human livers. *Hepatology.* (2015) 62:1444–55. doi: 10.1002/hep.28012
166. Resino S, Bellon JM, Asensio C, Micheloud D, Miralles P, Vargas A, et al. Can serum hyaluronic acid replace simple non-invasive indexes to predict liver fibrosis in HIV/Hepatitis C coinfected patients? *BMC Infect Dis.* (2010) 10:244. doi: 10.1186/1471-2334-10-244
167. Kumagai E, Mano Y, Yoshio S, Shoji H, Sugiyama M, Korenaga M, et al. Serum YKL-40 as a marker of liver fibrosis in patients with non-alcoholic fatty liver disease. *Sci Rep.* (2016) 6:35282. doi: 10.1038/srep35282
168. Yoshiji H, Kuriyama S, Miyamoto Y, Thorgeirsson UP, Gomez DE, Kawata M, et al. Tissue inhibitor of metalloproteinases-1 promotes liver fibrosis development in a transgenic mouse model. *Hepatology.* (2000) 32:1248–54. doi: 10.1053/jhep.2000.20521
169. Benyon RC, Iredale JP, Goddard S, Winwood PJ, Arthur MJ. Expression of tissue inhibitor of metalloproteinases 1 and 2 is increased in fibrotic human liver. *Gastroenterology.* (1996) 110:821–31. doi: 10.1053/gast.1996.v110.pm8608892
170. Thiele ND, Wirth JW, Steins D, Koop AC, Ittrich H, Lohse AW, et al. TIMP-1 is upregulated, but not essential in hepatic fibrogenesis and carcinogenesis in mice. *Sci Rep.* (2017) 7:714. doi: 10.1038/s41598-017-00671-1
171. Gudowska M, Gruszewska E, Panasiuk A, Cylwik B, Swiderska M, Flisiak R, et al. High serum N-terminal propeptide of procollagen type III concentration is associated with liver diseases. *Prz Gastroenterol.* (2017) 12:203–7. doi: 10.5114/pg.2017.70474
172. Tanwar S, Trembling PM, Guha IN, Parkes J, Kaye P, Burt AD, et al. Validation of terminal peptide of procollagen III for the detection and assessment of nonalcoholic steatohepatitis in patients with nonalcoholic fatty liver disease. *Hepatology.* (2013) 57:103–11. doi: 10.1002/hep.26030
173. Hallsworth K, Adams LA. Lifestyle modification in NAFLD/NASH: Facts and figures. *JHEP Rep.* (2019) 1:468–79. doi: 10.1016/j.jhepr.2019.10.008
174. Oseini AM, Sanyal AJ. Therapies in non-alcoholic steatohepatitis (NASH). *Liver Int.* (2017) 37:97–103. doi: 10.1111/liv.13302
175. Vilar-Gomez E, Martinez-Perez Y, Calzadilla-Bertot L, Torres-Gonzalez A, Gra-Oramas B, Gonzalez-Fabian L, et al. Weight loss through lifestyle modification significantly reduces features of nonalcoholic steatohepatitis. *Gastroenterology.* (2015) 149:367–78.e5. doi: 10.1053/j.gastro.2015.04.005
176. Pacana T, Sanyal AJ. Vitamin E and nonalcoholic fatty liver disease. *Curr Opin Clin Nutr Metab Care.* (2012) 15:641–8. doi: 10.1097/MCO.0b013e328357f747
177. Chen Z, Tian R, She Z, Cai J, Li H. Role of oxidative stress in the pathogenesis of nonalcoholic fatty liver disease. *Free Radic Biol Med.* (2020) 152:116–41. doi: 10.1016/j.freeradbiomed.2020.02.025
178. Phung N, Pera N, Farrell G, Leclercq I, Hou JY, George J. Pro-oxidant-mediated hepatic fibrosis and effects of antioxidant intervention in murine dietary steatohepatitis. *Int J Mol Med.* (2009) 24:171–80. doi: 10.3892/ijmm_00000220
179. Vilar-Gomez E, Vuppalanchi R, Gawrieh S, Ghabril M, Saxena R, Cummings OW, et al. Vitamin E improves transplant-free survival and hepatic decompensation among patients with nonalcoholic steatohepatitis and advanced fibrosis. *Hepatology.* (2020) 71:495–509. doi: 10.1002/hep.30368
180. Sanyal AJ, Chalasani N, Kowdley KV, McCullough A, Diehl AM, Bass NM, et al. Pioglitazone, vitamin E, or placebo for nonalcoholic steatohepatitis. *N Engl J Med.* (2010) 362:1675–85. doi: 10.1056/NEJMoa0907929
181. Bril F, Biernacki DM, Kalavalapalli S, Lomonaco R, Subbarayan SK, Lai J, et al. Role of vitamin e for nonalcoholic steatohepatitis in patients with type 2 diabetes: a randomized controlled trial. *Diabetes Care.* (2019) 42:1481–8. doi: 10.2337/dc19-0167
182. Lian J, Fu J. Pioglitazone for NAFLD patients with prediabetes or type 2 diabetes mellitus: a meta-analysis. *Front Endocrinol (Lausanne).* (2021) 12:615409. doi: 10.3389/fendo.2021.615409
183. Lee JI, Lee HW, Lee KS, Lee HS, Park JY. Effects of statin use on the development and progression of nonalcoholic fatty liver disease: a nationwide nested case-control study. *Am J Gastroenterol.* (2021) 116:116–24. doi: 10.14309/ajg.0000000000000845
184. Cusi K. Pioglitazone for the treatment of NASH in patients with prediabetes or type 2 diabetes mellitus. *Gut.* (2018) 67:1371. doi: 10.1136/gutjnl-2017-313958
185. Majima T, Komatsu Y, Doi K, Shigemoto M, Takagi C, Fukao A, et al. Safety and efficacy of low-dose pioglitazone (7.5 mg/day) vs. standard-dose pioglitazone (15 mg/day) in Japanese women with type 2 diabetes mellitus. *Endocr J.* (2006) 53:325–30. doi: 10.1507/endocrj.K05-067
186. Athyros VG, Boutari C, Stavropoulos K, Anagnostis P, Imprialos KP, Doumas M, et al. Statins: An under-appreciated asset for the prevention and the treatment of NAFLD or NASH and the related cardiovascular risk. *Curr Vasc Pharmacol.* (2018) 16:246–53. doi: 10.2174/1570161115666170621082910
187. Doumas M, Imprialos K, Dimakopoulou A, Stavropoulos K, Binas A, Athyros VG. The role of statins in the management of nonalcoholic fatty liver disease. *Curr Pharm Des.* (2018) 24:4587–92. doi: 10.2174/1381612825666190117114305
188. Nadkarni P, Chepurny OG, Holz GG. Regulation of glucose homeostasis by GLP-1. *Prog Mol Biol Transl Sci.* (2014) 121:23–65. doi: 10.1016/B978-0-12-800101-1.00002-8
189. Meier JJ. GLP-1 receptor agonists for individualized treatment of type 2 diabetes mellitus. *Nat Rev Endocrinol.* (2012) 8:728–42. doi: 10.1038/nrendo.2012.140
190. Bernsmeier C, Meyer-Gerspach AC, Blaser LS, Jeker L, Steinert RE, Heim MH, et al. Glucose-induced glucagon-like Peptide 1 secretion is deficient in patients with non-alcoholic fatty liver disease. *PLoS ONE.* (2014) 9:e87488. doi: 10.1371/journal.pone.0087488
191. Lv X, Dong Y, Hu L, Lu F, Zhou C, Qin S. Glucagon-like peptide-1 receptor agonists (GLP-1 RAs) for the management of nonalcoholic fatty liver disease (NAFLD): A systematic review. *Endocrinol Diabetes Metab.* (2020) 3:e00163. doi: 10.1002/edm2.163
192. Ghazanfar H, Kandhi SD, Nawaz I, Javed N, Abraham MC, Farag M, et al. Role of glucagon-like peptide-1 receptor agonists in the management of non-alcoholic steatohepatitis: a clinical review article. *Cureus.* (2021) 13:e15141. doi: 10.7759/cureus.15141
193. Seghieri M, Christensen AS, Andersen A, Solini A, Knop FK, Vilsboll T. Future perspectives on GLP-1 receptor agonists and GLP-1/glucagon receptor co-agonists in the treatment of NAFLD. *Front Endocrinol.* (2018) 9:649. doi: 10.3389/fendo.2018.00649
194. Chinetti G, Fruchart JC, Staels B. Peroxisome proliferator-activated receptors (PPARs): nuclear receptors at the crossroads between lipid metabolism and inflammation. *Inflamm Res.* (2000) 49:497–505. doi: 10.1007/s000110050622
195. Ratziu V, Harrison SA, Francque S, Bedossa P, Lehert P, Serfaty L, et al. Elafibranor, an agonist of the peroxisome proliferator-activated receptor-alpha and -delta, induces resolution of nonalcoholic steatohepatitis without fibrosis worsening. *Gastroenterology.* (2016) 150:1147–59.e5. doi: 10.1053/j.gastro.2016.01.038
196. Jiao Y, Lu Y, Li XY. Farnesoid X receptor: a master regulator of hepatic triglyceride and glucose homeostasis. *Acta Pharmacol Sin.* (2015) 36:44–50. doi: 10.1038/aps.2014.116
197. Abenavoli L, Falalyeyeva T, Boccuto L, Tsyryuk O, Kobyliak N. Obeticholic acid: a new era in the treatment of nonalcoholic fatty liver disease. *Pharmaceuticals (Basel).* (2018) 11:40104. doi: 10.3390/ph11040104

198. Harrison SA, Bashir MR, Lee KJ, Shim-Lopez J, Lee J, Wagner B, et al. A structurally optimized FXR agonist, MET409, reduced liver fat content over 12 weeks in patients with non-alcoholic steatohepatitis. *J Hepatol.* (2021) 75:25–33. doi: 10.1016/j.jhep.2021.01.047
199. An P, Wei G, Huang P, Li W, Qi X, Lin Y, et al. A novel non-bile acid FXR agonist EDP-305 potently suppresses liver injury and fibrosis without worsening of ductular reaction. *Liver Int.* (2020) 40:1655–69. doi: 10.1111/liv.14490
200. Krenkel O, Puengel T, Govaere O, Abdallah AT, Mossanen JC, Kohlhepp M, et al. Therapeutic inhibition of inflammatory monocyte recruitment reduces steatohepatitis and liver fibrosis. *Hepatology.* (2018) 67:1270–83. doi: 10.1002/hep.29544
201. Smith-Cortinez N, Fagundes RR, Gomez V, Kong D, de Waart DR, Heegsma J, et al. Collagen release by human hepatic stellate cells requires vitamin C and is efficiently blocked by hydroxylase inhibition. *FASEB J.* (2021) 35:e21219. doi: 10.1096/fj.202001564RR
202. Marra F, Tacke F. Roles for chemokines in liver disease. *Gastroenterology.* (2014) 147:577–94.e1. doi: 10.1053/j.gastro.2014.06.043
203. Friedman SL, Ratziu V, Harrison SA, Abdelmalek MF, Aithal GP, Caballeria J, et al. A randomized, placebo-controlled trial of cenicriviroc for treatment of nonalcoholic steatohepatitis with fibrosis. *Hepatology.* (2018) 67:1754–67. doi: 10.1002/hep.29477
204. Henderson NC, Mackinnon AC, Farnworth SL, Poirier F, Russo FP, Iredale JP, et al. Galectin-3 regulates myofibroblast activation and hepatic fibrosis. *Proc Natl Acad Sci USA.* (2006) 103:5060–5. doi: 10.1073/pnas.0511167103
205. Traber PG, Zomer E. Therapy of experimental NASH and fibrosis with galectin inhibitors. *PLoS ONE.* (2013) 8:e83481. doi: 10.1371/journal.pone.0083481
206. Chalasani N, Abdelmalek MF, Garcia-Tsao G, Vuppalanchi R, Alkhouri N, Rinella M, et al. Belapectin study, effects of belapectin, an inhibitor of galectin-3, in patients with nonalcoholic steatohepatitis with cirrhosis and portal hypertension. *Gastroenterology.* (2020) 158:1334–45.e5. doi: 10.1053/j.gastro.2019.11.296
207. Schuster-Gaul S, Geisler LJ, McGeough MD, Johnson CD, Zagorska A, Li L, et al. ASK1 inhibition reduces cell death and hepatic fibrosis in an Nlrp3 mutant liver injury model. *JCI Insight.* (2020) 5:123294. doi: 10.1172/jci.insight.123294
208. Loomba R, Lawitz E, Mantry PS, Jayakumar S, Caldwell SH, Arnold H, et al. The ASK1 inhibitor selonsertib in patients with nonalcoholic steatohepatitis: A randomized, phase 2 trial. *Hepatology.* (2018) 67:549–59. doi: 10.1002/hep.29514
209. Harrison SA, Wong VW, Okanoue T, Bzowej N, Vuppalanchi R, Younes Z, et al. Selonsertib for patients with bridging fibrosis or compensated cirrhosis due to NASH: Results from randomized phase III STELLAR trials. *J Hepatol.* (2020) 73:26–39. doi: 10.1016/j.jhep.2020.02.027
210. Saltzman ET, Palacios T, Thomsen M, Vitetta L. Intestinal microbiome shifts, dysbiosis, inflammation, and non-alcoholic fatty liver disease. *Front Microbiol.* (2018) 9:61. doi: 10.3389/fmicb.2018.00061
211. Tripathi A, Debelius J, Brenner DA, Karin M, Loomba R, Schnabl B, et al. The gut-liver axis and the intersection with the microbiome. *Nat Rev Gastroenterol Hepatol.* (2018) 15:397–411. doi: 10.1038/s41575-018-0011-z
212. Heck AM, Yanovski JA, Calis KA. Orlistat, a new lipase inhibitor for the management of obesity. *Pharmacotherapy.* (2000) 20:270–9. doi: 10.1592/phco.20.4.270.34882
213. Ke J, An Y, Cao B, Lang J, Wu N, Zhao D. Orlistat-induced gut microbiota modification in obese mice. *Evid Based Complement Alternat Med.* (2020) 2020:9818349. doi: 10.1155/2020/9818349
214. Rotman Y, Sanyal AJ. Current and upcoming pharmacotherapy for non-alcoholic fatty liver disease. *Gut.* (2017) 66:180–90. doi: 10.1136/gutjnl-2016-312431
215. Sumida Y, Yoneda M. Current and future pharmacological therapies for NAFLD/NASH. *J Gastroenterol.* (2018) 53:362–76. doi: 10.1007/s00535-017-1415-1
216. Polyzos SA, Kang ES, Tsochatzis EA, Kechagias S, Ekstedt M, Xanthakos S, et al. Commentary: Nonalcoholic or metabolic dysfunction-associated fatty liver disease? The epidemic of the 21st century in search of the most appropriate name. *Metabolism.* (2020) 113:154413. doi: 10.1016/j.metabol.2020.154413
217. Rinella ME, Green RM. The methionine-choline deficient dietary model of steatohepatitis does not exhibit insulin resistance. *J Hepatol.* (2004) 40:47–51. doi: 10.1016/j.jhep.2003.09.020
218. Tsuchida T, Lee YA, Fujiwara N, Ybanez M, Allen B, Martins S, et al. A simple diet- and chemical-induced murine NASH model with rapid progression of steatohepatitis, fibrosis and liver cancer. *J Hepatol.* (2018) 69:385–95. doi: 10.1016/j.jhep.2018.03.011

Conflict of Interest: The authors declare that the research was conducted in the absence of any commercial or financial relationships that could be construed as a potential conflict of interest.

frontiers in Cardiovascular Medicine

ORIGINAL RESEARCH
published: 29 September 2021
doi: 10.3389/fcvm.2021.745810

Deficiency of Myeloid Pfkfb3 Protects Mice From Lung Edema and Cardiac Dysfunction in LPS-Induced Endotoxemia

*Jiean Xu[1,2], Lina Wang[2], Qiuhua Yang[2], Qian Ma[2], Yaqi Zhou[2], Yongfeng Cai[2], Xiaoxiao Mao[2], Qingen Da[3], Tammy Lu[4], Yunchao Su[5], Zsolt Bagi[6], Rudolf Lucas[2], Zhiping Liu[7], Mei Hong[1], Kunfu Ouyang[1,3] and Yuqing Huo[2]**

[1] State Key Laboratory of Chemical Oncogenomics, Key Laboratory of Chemical Genomics, School of Chemical Biology and Biotechnology, Peking University Shenzhen Graduate School, Shenzhen, China, [2] Department of Cellular Biology and Anatomy, Vascular Biology Center, Medical College of Georgia, Augusta University, Augusta, GA, United States, [3] Department of Cardiovascular Surgery, Peking University Shenzhen Hospital, Shenzhen, China, [4] Oxford College, Emory University, Oxford, GA, United States, [5] Department of Pharmacology & Toxicology, Medical College of Georgia, Augusta University, Augusta, GA, United States, [6] Department of Physiology, Medical College of Georgia, Augusta University, Augusta, GA, United States, [7] College of Pharmacy, Jinan University, Guangzhou, China

Sepsis, a pathology resulting from excessive inflammatory response that leads to multiple organ failure, is a major cause of mortality in intensive care units. Macrophages play an important role in the pathophysiology of sepsis. Accumulating evidence has suggested an upregulated rate of aerobic glycolysis as a key common feature of activated proinflammatory macrophages. Here, we identified a crucial role of myeloid 6-phosphofructo-2-kinase/fructose-2,6-bisphosphatase 3 (Pfkfb3), a glycolytic activator in lipopolysaccharide (LPS)-induced endotoxemia in mice. Pfkfb3 expression is substantially increased in bone marrow derived macrophages (BMDMs) treated with LPS *in vitro* and in lung macrophages of mice challenged with LPS *in vivo*. Myeloid-specific knockout of *Pfkfb3* in mice protects against LPS-induced lung edema, cardiac dysfunction and hypotension, which were associated with decreased expression of interleukin 1 beta (Il1b), interleukin 6 (Il6) and nitric oxide synthase 2 (Nos2), as well as reduced infiltration of neutrophils and macrophages in lung tissue. Pfkfb3 ablation in cultured macrophages attenuated LPS-induced glycolytic flux, resulting in a decrease in proinflammatory gene expression. Mechanistically, Pfkfb3 ablation or inhibition with a Pfkfb3 inhibitor AZ26 suppresses LPS-induced proinflammatory gene expression via the NF-κB signaling pathway. In summary, our study reveals the critical role of Pfkfb3 in LPS-induced sepsis *via* reprogramming macrophage metabolism and regulating proinflammatory gene expression. Therefore, PFKFB3 is a potential target for the prevention and treatment of inflammatory diseases such as sepsis.

Keywords: inflammation, glycolysis, PFKFB3, macrophage, endotoxemia

OPEN ACCESS

Edited by:
Xuewei Zhu,
Wake Forest Baptist Medical Center, United States

Reviewed by:
Charles E. McCall,
Wake Forest Baptist Medical Center, United States
Julia K. Bohannon,
Vanderbilt University Medical Center, United States

***Correspondence:**
Yuqing Huo
yhuo@augusta.edu

Specialty section:
This article was submitted to Atherosclerosis and Vascular Medicine, a section of the journal Frontiers in Cardiovascular Medicine

Received: *22 July 2021*
Accepted: *06 September 2021*
Published: *29 September 2021*

Citation:
Xu J, Wang L, Yang Q, Ma Q, Zhou Y, Cai Y, Mao X, Da Q, Lu T, Su Y, Bagi Z, Lucas R, Liu Z, Hong M, Ouyang K and Huo Y (2021) Deficiency of Myeloid Pfkfb3 Protects Mice From Lung Edema and Cardiac Dysfunction in LPS-Induced Endotoxemia. Front. Cardiovasc. Med. 8:745810. doi: 10.3389/fcvm.2021.745810

INTRODUCTION

Sepsis is characterized as a life-threatening organ dysfunction caused by a dysregulated host response to an infectious organism (1), including the new virus SARS-CoV-2 responsible for the COVID-19 ongoing pandemic in humans (2). Infectious organisms stimulate the release of inflammatory cytokines such as interleukin 1 beta (IL1B) and interleukin 6 (IL6), and inducible nitric oxide synthase 2 (NOS2) (3). High levels of these inflammatory cytokines and overproduction of nitric oxide (NO) generated by NOS2 cause severe hypotension and multiple organ dysfunction, eventually leading to death. Although great advances have been made in antibiotics and supportive care, sepsis still remains a major cause of morbidity and mortality in the intensive care units (4). Therefore, there is an urgent need to increase our understanding of the mechanisms involved in the pathogenesis of sepsis for development of new therapeutic targets (5).

Compared to the previous definition of sepsis in 1991 (Sepsis 1.0) and 2001 (Sepsis 2.0), "lactate > 2 mmol/L" was added in the latest definition of sepsis shock in 2016 (Sepsis 3.0) (6), highlighting that glucose metabolism disorders are an important pathogenesis of sepsis. Macrophages, important cells of the innate immune system, play an essential role in the hyper-inflammation stage in sepsis (7). Previous evidence suggests that macrophages display different functional phenotypes depending on their metabolic profiles (8, 9). Pathogen-stimulated macrophages shift their metabolic profiles from oxidative phosphorylation to aerobic glycolysis, coupled with increased secretion of lactate and proinflammatory cytokines, and ultimately supporting the hyper-inflammatory state during sepsis. Data from genome-wide gene expression profiles show that *Pfkfb3* (6-phosphofructo-2-kinase/fructose-2,6-bisphosphatase 3) is the most upregulated gene among the glycolytic genes in LPS-stimulated macrophages (10), indicating a potential role of PFKFB3 in LPS-induced sepsis. PFKFB3 is a bifunctional enzyme that catalyzes the synthesis and hydrolysis of fructose-2,6-bisphosphate (F-2,6-BP). F-2,6-BP acts as the most effective allosteric activator of 6-phosphofructo-1-kinase (PFK1), the second rate-limiting enzyme in glycolysis (11, 12). A previous study demonstrated that zinc fingers and homeoboxes (Zhx) 2 accelerates sepsis by promoting macrophage glycolysis *via* Pfkfb3 (13). However, it remains unclear whether decreased macrophage glycolysis *via* Pfkfb3 inactivation can suppress macrophage inflammation and protect mice from LPS-induced sepsis.

In the current study, we identified a causative role of macrophage Pfkfb3-dependent glycolysis in LPS-induced sepsis through regulation of macrophage inflammation. Myeloid-specific *Pfkfb3* deletion protected mice against LPS-induced lung edema, cardiac dysfunction and inflammation. Mechanistically, Pfkfb3 inactivation in macrophages suppresses LPS-induced inflammation *via* inhibiting the NF-κB signaling pathway. Our findings here expand our understanding of glycolytic regulation of sepsis and indicate PFKFB3 as an attractive potential therapeutic target for the prevention and treatment of sepsis.

MATERIALS AND METHODS

Animals

Mice were used in accordance with the protocol approved by the Institutional Animal Care and Use Committee of Augusta University. The floxed *Pfkfb3* (*Pfkfb3*$^{flox/flox}$) mice were generated by Xenogen Biosciences Corporation (Cranbury, NJ, USA) (14). Myeloid-specific *Pfkfb3* knockout was achieved by cross-breeding *Pfkfb3*$^{flox/flox}$ mice with *Lysm*-Cre mice (stock no. 004781, The Jackson Laboratory, Bar Harbor, ME, USA) to generate *Pfkfb3*$^{flox/flox}$; *Lysm*-Cre (*Pfkfb3*$^{\Delta M\phi}$) mice. All mice were on a C57BL/6J background.

LPS-Induced Sepsis Model

For LPS-induced sepsis, age (8- to 12-week-old)- and sex-matched *Pfkfb3*$^{\Delta M\phi}$ and *Pfkfb3*^{WT} mice were administered with LPS (L2630, Sigma-Aldrich, St. Louis, MO, USA) at 12.5 mg/kg body weight by intraperitoneal injection. The mice had normal access to food and water and were monitored twice a day over the course of 10 days. The rectal temperature of mice was measured with a model BAT-12 digital thermocouple thermometer (Physitemp Instruments, Clifton, NJ, USA) before and 6 h, 24 h after LPS injection.

Blood Pressure Measurements

Mouse blood pressure (BP) was measured at the same time of day using a noninvasive tail-cuff blood pressure measurement system (Coda 6, Kent Scientific, Torrington, CT, USA). In brief, mice were trained for BP measurement conditions on a daily basis for 1 week. After training, mouse BP was measured twice before the injection of LPS and at indicated times following LPS injection. For BP measurements, we placed conscious mice in tail-cuff restrainers over a warmed surface. Twenty consecutive BP measurements were taken, and the last fifteen readings per mouse were averaged and used for analysis.

Ultrasound Imaging

Echocardiograms were performed in isoflurane-anesthetized mice using the Vevo 2100 high-frequency ultrasound imaging platform (FUJIFILM VisualSonics, Toronto, Ontario, Canada) at baseline and 6 h after LPS injection. After sedation, mice were laid on the heating platform (37 °C) to maintain normothermia and continuously delivered a gas inhalation of two percent isoflurane. The prewarmed ultrasonic gel (4238, Chattanooga, Vista, CA, USA) was added to the mouse's chest after removal of hair with depilatory cream. Two-dimensional echocardiography was performed with a 40 MHz ultrasound probe (MS-400). The percentage of left ventricular (LV) ejection fraction and fractional shortening, LV stroke volume and cardiac output were obtained from the parasternal short axis view using M-mode.

Pulmonary Permeability Assessment

Lung wet-to-dry weight ratio was used as an index of pulmonary edema formation that served as a gauge for measuring pulmonary permeability. The lung was weighed immediately after its excision (wet weight), and then placed into an oven at 60 °C for 48 h, and reweighed as dry weight. The ratio of the lung weight before and after drying was calculated.

Pulmonary permeability was also evaluated with Evans Blue dye. Briefly, LPS (1 mg/kg body weight) or saline was intratracheally injected to mice via a 20-gauge catheter. In order to assess vascular leak, Evans blue (30 mg/kg body weight, E2129, Sigma-Aldrich, St. Louis, MO, USA), was injected to mice via the tail vein 2 h before mice were sacrificed. The lungs were perfused with PBS, then dried with tissue papers, and left lung were imaged.

BMDM Culture and Treatments

After euthanization of mice, femurs and tibias were isolated and transected. Bone marrow cells were flushed from the femurs and tibias. The cell suspension was pipetted repeatedly to obtain a single-cell suspension, which was then filtered with a 70 μm cell strainer and centrifuged at 500 g for 8 min. The acquired cells were plated at a density of 2×10^6/mL and cultured in RPMI 1640 medium (SH30027.01, Cytiva, Marlborough, MA, USA) supplemented with 10% FBS (F4135, Sigma-Aldrich, St. Louis, MO, USA), 20% L929-conditioned medium, and 1×Antibiotic-Antimycotic (15240062, Thermo Scientific, Grand Island, NY, USA) in a humidified incubator with 5% CO_2 at 37°C for 6 days to induce macrophage differentiation. In some experiments, cells were incubated with 100 ng/mL LPS (L3137, Sigma-Aldrich, St. Louis, MO, USA) or 10 μm AZ26 (HY-101971, MedChemExpress, Monmouth Junction, NJ, USA) at various time points as indicated.

Measurement of Cytokines by ELISA

Serum samples were collected using a standard protocol following intraperitoneal injection with PBS (control) or LPS (12.5 mg/kg body weight) into *Pfkfb3*^{WT} and *Pfkfb3*$^{\Delta M\phi}$ mice for 6 h. Cell culture supernatants were collected from *Pfkfb3*^{WT} and *Pfkfb3*$^{\Delta M\phi}$ BMDMs treated with LPS for 16 h (100 ng/mL). Cell culture supernatants and sera were measured for mouse Il1b and Il6 with ELISA kits (Il1b, MLB00C; Il6, M6000B, R&D Systems, Minneapolis, MN, USA). All assays were carried out following the instructions provided by the manufacturer.

Analysis of Nitric Oxide (NO) Release

NO release was measured using a Sievers NOA 280i chemiluminescence analyzer (Analytix, Sunderland, UK) as previously described (15). Briefly, 20 μl of supernatant or 100 μL of serum was injected into a nitrogen-purge vessel containing a 1% solution of sodium iodide in glacial acetic acid. The output was recorded using a Labchart program (ADInstruments, Colorado Springs, CO, USA) and the area under the curve was converted to picomole NO using a calibration curve constructed after the analysis of a series of sodium nitrite standards ranging from 2.5 to 100 pmol.

Real Time Cell Metabolism Assay

Real-time changes in extracellular acidification rate (ECAR) of BMDMs were analyzed with an XF24 Extracellular Flux Analyzer as described previously (16). Briefly, BMDMs were seeded at 2×10^5 per well onto Seahorse XF24 culture microplates (100777-004, Seahorse Bioscience, North Billerica, MA, USA) and incubated in a humidified incubator with 5% CO_2 at 37°C overnight. The next day, after 100 ng/mL LPS treatment for 6 h, the medium was changed to a XF base Medium (102353-100, Seahorse Bioscience, North Billerica, MA, USA) supplemented with 2 mM glutamine, pH adjusted to 7.4 with 0.1 M NaOH, and then the plate was incubated for 45 min in a non-CO_2 incubator at 37°C. The ECAR assay was performed on the XF24 extracellular flux analyzer (Seahorse Bioscience, North Billerica, MA, USA), and the ECAR values were normalized using protein concentration. Inhibitors and activators were used in these tests at the following concentrations: glucose (10 mM), oligomycin (2 μM) and 2-DG (50 mM).

Real-Time Quantitative PCR (RT-qPCR) Analysis

Total RNA of cells and tissues were extracted using TRIzol reagent (15596018, Invitrogen, Grand Island, NY, USA) according to the manufacturer's instructions, and RT-qPCR was done as described previously (17). Briefly, one microgram of total RNA was used to synthesize first stranded cDNA with the iScript^{TM} cDNA synthesis kit (1708891, Bio-Rad, Hercules, CA, USA). RT-qPCR was performed on a QuantStudio^{TM} 3 Real-Time PCR System (Applied Biosystems, Grand Island, NY, USA) using iTaq^{TM} Universal SYBR Green Supermix (1725122, Bio-Rad, Hercules, CA, USA) with the respective gene-specific primers listed in **Supplementary Table 1**. Quantification of relative gene expression was calculated with the $2^{-\Delta\Delta Ct}$ method using *18S* rRNA as the internal control, and data were expressed as fold change relative to control groups.

Western-Blot

Western blot was performed as previously described (18). Cells and tissues were homogenized in RIPA buffer (R0278, Sigma-Aldrich, St. Louis, MO, USA) supplemented with 1% protease inhibitor cocktail (05892970001, Sigma-Aldrich, St. Louis, MO, USA) and 1% phosphatase inhibitor (4906845001, Sigma-Aldrich, St. Louis, MO, USA). After measuring protein concentration using BCA Protein Assay Kit (23225, Thermo Scientific, Grand Island, NY, USA), equal amounts of denatured proteins were loaded and separated onto a 7.5–10% SDS-PAGE gel, and transferred on nitrocellulose membranes (10600015, Cytiva, Marlborough, MA, USA). Membranes were blocked with 5% non-fat milk, then incubated with specific antibodies. The antibodies used were as follows: rabbit Pfkfb3 (1:1000, ab181861, Abcam, Cambridge, MA, USA), rabbit Nos2 (1:1000, sc-650, Santa Cruz, Dallas, TX, USA), rabbit p-Erk (1:1000, 4370S, Cell Signaling Technology, Danvers, MA, USA), rabbit Erk (1:1000, 4695S, Cell Signaling Technology, Danvers, MA, USA), rabbit p-Jnk (1:1000, 4668S, Cell Signaling Technology, Danvers, MA, USA), rabbit Jnk (1:1000, 9252S, Cell Signaling Technology, Danvers, MA, USA), rabbit p-p38 (1:1000, 9215S, Cell Signaling Technology, Danvers, MA, USA), rabbit p38 (1:1000, 9212S, Cell Signaling Technology, Danvers, MA, USA), rabbit p-p65 (1:1000, 3033S, Cell Signaling Technology, Danvers, MA, USA), rabbit p65 (1:1000, 8242S, Cell Signaling Technology, Danvers, MA, USA), and mouse Actb (1:1000, sc-47778, Santa Cruz, Dallas, TX, USA). Images were taken with the ChemiDoc Imaging System

(Bio-Rad, Hercules, CA, USA), and band densities were identified using ImageJ (National Institutes of Health, Bethesda, MD, USA).

Histological Analysis

Murine lungs were flushed with PBS and 4% PFA, fixed and embedded in paraffin according to a standard protocol. Five micrometer paraffin-embedded sections were cut and stained with hematoxylin and eosin (H&E) routinely, the lung injury score was assessed based on the method as reported previously (19). Immunohistochemical staining was performed as described previously (20), briefly, lung sections were first deparaffinized and rehydrated, endogenous peroxidase activity was destroyed with H_2O_2 (3 mL 30% H_2O_2 in 200 mL methanol) for 30 min at room temperature. After antigen retrieval with Antigen Unmasking Solution (H-3301, Vector Laboratories, Burlingame, CA, USA) at 98°C for 10 min, sections were blocked with avidin solution with 10% normal rabbit serum for 1 h at room temperature, and incubated in biotin blocking solution with primary antibodies against Mac2 (3 μg/mL, CL8942F, Cedarlane, Burlington, NC, USA), or Ly6G (3 μg/mL, 551459, BD biosciences, San Jose, CA, USA) at 4°C overnight. Sections were then incubated with a biotinylated rabbit anti-rat IgG secondary antibody (1:200, BA-4001-0.5, Vector Laboratories, Burlingame, CA, USA) for 1 h at room temperature, followed by incubation with ABC solution (PK-6100, Vector Laboratories, Burlingame, CA, USA) for 30 min at room temperature. Peroxidase substrate 3, 3′-diaminobenzidine (3468, Dako, Santa Clara, CA, USA) was used to detect the antibodies according to the manufacturer's instructions. The sections were counterstained with hematoxylin for 30 sec, then dehydrated and mounted with xylene-based mounting medium (8312-4, Thermo Scientific, Grand Island, NY, USA). Quantification of Mac2 and Ly6G staining was performed using the ImageJ (National Institutes of Health, Bethesda, MD, USA).

For immunofluorescence staining of lung sections, 5 μm paraffin-embedded sections were deparaffinized and rehydrated. After antigen retrieval with Antigen Unmasking Solution (H-3301, Vector Laboratories, Burlingame, CA, USA) at 98°C for 10 min, sections were blocked and incubated at 4°C overnight with primary antibodies against Pfkfb3 (1:100, ab181861, Abcam, Cambridge, MA, USA) and Adgre1 (1:100, ab6640, Abcam, Cambridge, MA, USA). For immunofluorescence staining of BMDMs, cells seeded on culture slides (354108, Corning, Glendale, AZ, USA) were fixed in 4% PFA for 20 min, permeabilized with 0.5% Triton X-100 for 20 min, and then blocked and incubated at 4°C overnight with primary antibodies against Pfkfb3 (1:100, ab181861, Abcam, Cambridge, MA, USA) and Adgre1 (1:100, MCA497R, Bio-Rad, Hercules, CA, USA). Sections and slices were incubated at room temperature for 1 h with Alexa Fluor 594-labeled goat anti-rabbit IgG (8 μg/mL, A11012, Molecular Probes, Grand Island, NY, USA) and Alexa Fluor 488-labeled goat anti-rat IgG (8 μg/mL, A11006, Molecular Probes, Grand Island, NY, USA), stained with 4′,6-diamidino-2-phenylindole (1 μg/mL, D1306, Invitrogen, Grand Island, NY, USA) for 5 min, and immersed in mounting medium (H-1000, Vector Laboratories, Burlingame, CA, USA). Images were acquired with a confocal microscope (Zeiss 780 Upright Confocal, Carl Zeiss, Oberkochen, Germany), and analyzed using ImageJ (National Institutes of Health, Bethesda, MD, USA).

Statistical Analysis

Statistical analyses were performed with GraphPad Prism 9 software (GraphPad, La Jolla, CA, USA). Categorical data are shown as percentages, and Mantel-Cox test was used to compare differences between the two groups (survival curves). Continuous variables are presented as the means ± SEM, two-tailed unpaired Student's *t*-test was used to compare the difference between two groups, and one-way analysis of variance (ANOVA) followed by Bonferroni's *post-hoc* test was performed for comparison among more than two groups when appropriate. Differences were considered statistically significant at $P < 0.05$ ($^{*}P < 0.05$, $^{**}P < 0.01$ and $^{***}P < 0.001$).

RESULTS

The Expression of Pfkfb3 Is Upregulated in LPS-Stimulated Macrophages

Increased glycolytic flux has been shown in LPS-stimulated macrophages. We first analyzed the expression of glycolytic molecules in BMDMs treated with LPS for 4 h using genome mRNA expression profiling data (GSE125036) from the GEO database. As shown in **Figure 1A**, the expression of *Slc2a1*, *Hk1*, *Pfkfb3* and *Pfkp* was upregulated more than 2-fold in LPS-stimulated macrophages compared to untreated macrophages, and *Pfkfb3* is the highest expressed gene among the upregulated glycolytic genes. To further confirm the upregulation of *Pfkfb3* in LPS-stimulated macrophages, we first analyzed the mRNA levels of Pfkfb3 in LPS-stimulated BMDMs using real-time PCR, and found that LPS increased *Pfkfb3* mRNA expression in a time-dependent manner (**Figure 1B**). Consistently, the protein levels of Pfkfb3 were also significantly upregulated in BMDMs 2 h after LPS stimulation (**Figure 1C**). Moreover, increased Pfkfb3 expression in macrophages was also observed in lung from LPS-challenged mice compared with that from control mice (**Figure 1D**). Together, these findings suggested that inflammatory stimulator LPS reprograms the expression of Pfkfb3 in macrophages, and this may be a critical link in severe inflammatory responses in septic mice.

Myeloid-Specific *Pfkfb3* Deficiency Protects Mice From LPS-Induced Cardiac Dysfunction

To determine the contribution of Pfkfb3-mediated glycolysis in macrophages to LPS-induced sepsis, we generated myeloid-specific *Pfkfb3* deficient mice ($Pfkfb3^{\Delta M\phi}$) and control mice ($Pfkfb3^{WT}$) by intercrossing $Pfkfb3^{flox/flox}$ mice with *Lysm*-Cre mice (**Figures 2A,B**). The protein level of Pfkfb3 was obvious decreased in main organs (including lung and liver) and bone marrow from $Pfkfb3^{\Delta M\phi}$ mice compared with those from $Pfkfb3^{WT}$ mice (**Figure 2C**), indicating that Pfkfb3 is highly expressed in myeloid cells. The mRNA and protein analysis showed that Pfkfb3 expression was barely detectable in BMDMs cultured with bone marrow from $Pfkfb3^{\Delta M\phi}$ mice compared

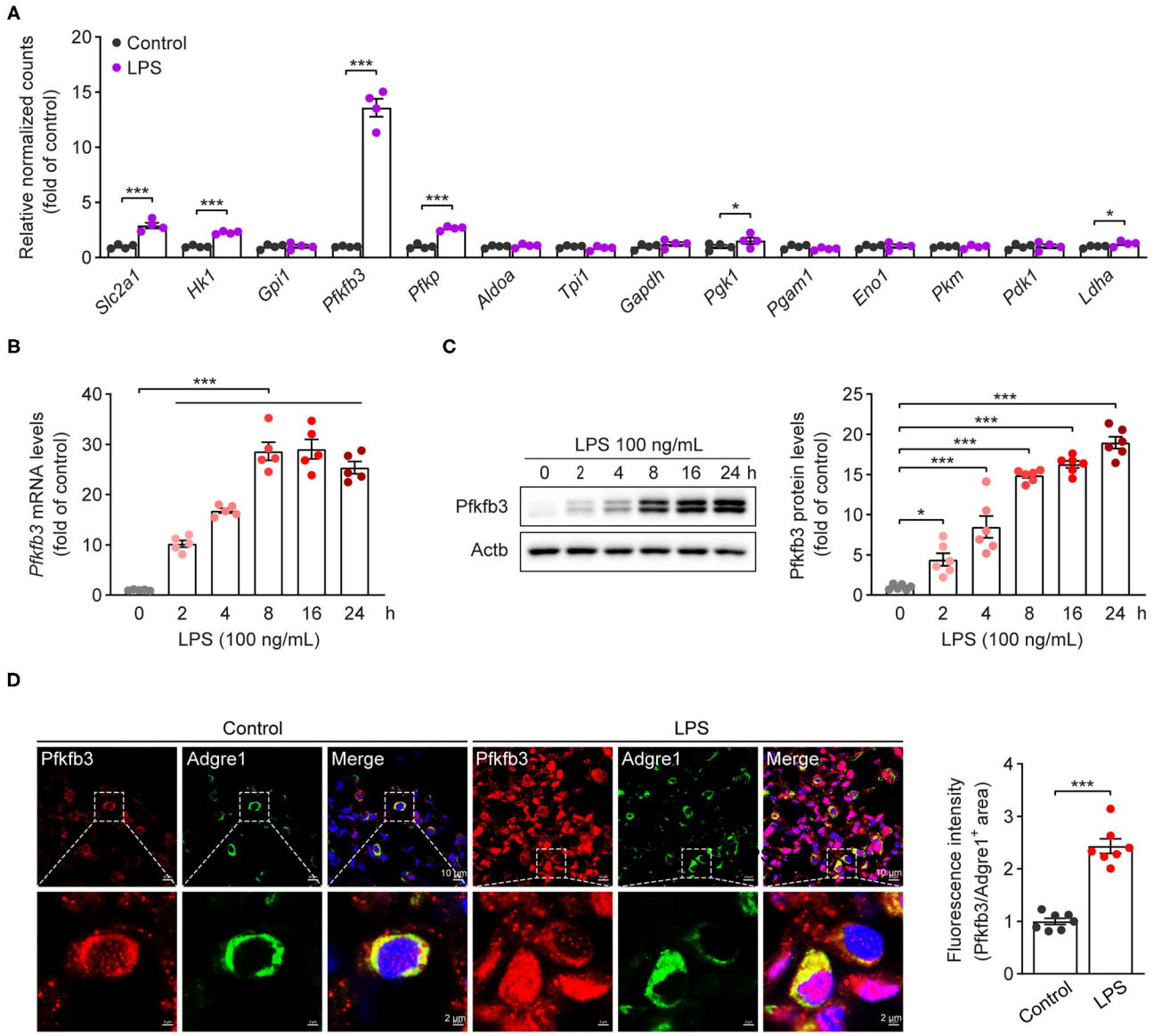

FIGURE 1 | Pfkfb3 expression is upregulated in macrophages treated with LPS. **(A)** The expression of glycolytic genes in BMDMs treated with LPS (100 ng/mL) for 4 h, the data are genome mRNA expression profiling data (GSE125036) from the GEO database ($n = 4$). **(B)** qPCR analysis of *Pfkfb3* expression in BMDMs treated with LPS (100 ng/mL) for the indicated times ($n = 5$). **(C)** Representative Western blot results of Pfkfb3 and Actb in BMDMs treated with LPS (100 ng/mL) for the indicated times (left) and relative ratio of Pfkfb3/Actb (right) were quantitated by densitometric analysis of the corresponding Western blots ($n = 6$). **(D)** Representative images (left) of triple immunofluorescence for Pfkfb3 (red), Adgre1 (green) and nuclei (DAPI, blue), and quantification (right) of Pfkfb3 expression in the pulmonary macrophages of control or LPS-treated mice ($n = 7$). All data are represented as mean ± SEM, and $^{***}P < 0.001$ for indicated comparisons. Unpaired two-tailed Student's *t* test for **(A,D)** and one-way ANOVA with Bonferroni's *post-hoc* test for **(B,C)**.

with those cultured with bone marrow of *Pfkfb3*^{WT} mice (**Figures 2D–F**), confirming effective deletion of Pfkfb3 in the myeloid cells of *Pfkfb3*$^{\Delta M\phi}$ mice.

To examine the role of myeloid Pfkfb3 in LPS-induced cardiac dysfunction (one of the features of multi-organ dysfunction in sepsis), *Pfkfb3*^{WT} and *Pfkfb3*$^{\Delta M\phi}$ mice were intraperitoneally administered with LPS, and cardiac assessment was used to record the cardiac parameters using M-mode echocardiography. As shown in **Figures 3A–E**, compared with the control mice, *Pfkfb3*^{WT} mice exhibited cardiac dysfunction 6 h after LPS challenge, as evidenced by decrease in ejection fraction, fractional shortening, left ventricle stroke volume and cardiac output. However, myeloid-specific *Pfkfb3* deficiency significantly prevented the decrease in cardiac function of *Pfkfb3*^{WT} mice observed after LPS injection (**Figures 3A–E**). Moreover, *Pfkfb3*$^{\Delta M\phi}$ mice exhibited significantly increased blood pressure compared to *Pfkfb3*^{WT} mice at 12 h after LPS injection, as indicated by increasing systolic blood pressure, diastolic blood

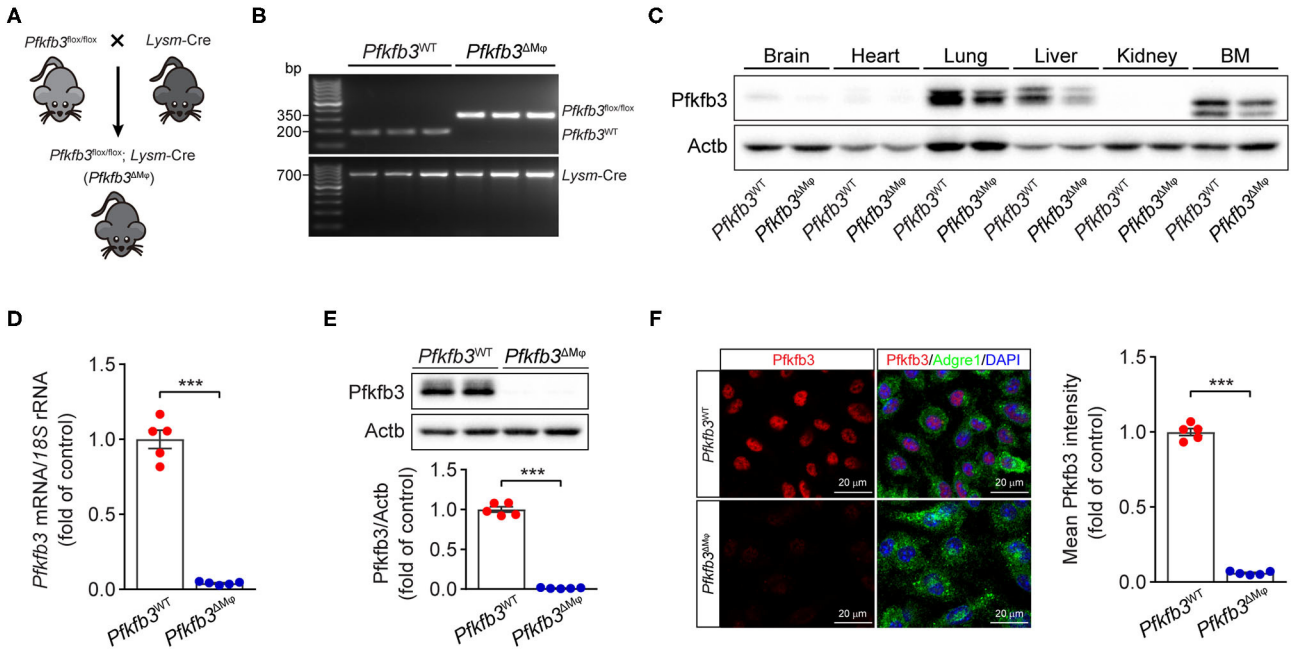

FIGURE 2 | Generation and characterization of myeloid-specific *Pfkfb3*-deficient mice. **(A)** Diagram of the generation of myeloid-specific *Pfkfb3*-deficient mice (*Pfkfb3*$^{\Delta M\phi}$) by crossing *Pfkfb3*$^{flox/flox}$ mice with *Lysm*-Cre mice. **(B)** Representative genotyping PCR results of *Pfkfb3*^{WT} mice and *Pfkfb3*$^{\Delta M\phi}$ mice. **(C)** Representative Western blot results of Pfkfb3 and Actb in bone marrow (BM) and main organs of *Pfkfb3*^{WT} and *Pfkfb3*$^{\Delta M\phi}$ mice. **(D)** qPCR analysis of *Pfkfb3* expression in BMDMs of *Pfkfb3*^{WT} mice and *Pfkfb3*$^{\Delta M\phi}$ mice ($n = 5$). **(E)** Representative Western blot results of Pfkfb3 and Actb in BMDMs of *Pfkfb3*^{WT} mice and *Pfkfb3*$^{\Delta M\phi}$ mice (top) and relative ratio of Pfkfb3/Actb (bottom) were quantitated by densitometric analysis of the corresponding Western blots ($n = 5$). **(F)** Representative images (left) of triple immunofluorescence for Pfkfb3 (red), Adgre1 (green) and nuclei (DAPI, blue), and quantification (right) of Pfkfb3 expression in BMDMs of *Pfkfb3*^{WT} mice and *Pfkfb3*$^{\Delta M\phi}$ mice ($n = 5$). All data are represented as mean ± SEM, $^{***}P < 0.001$ for *Pfkfb3*^{WT} vs. *Pfkfb3*$^{\Delta M\phi}$ (unpaired two-tailed Student's *t* test).

pressure and mean blood pressure (**Figures 3F–H**). Together, these findings suggest that myeloid Pfkfb3 is a critical mediator in LPS-induced cardiac dysfunction *in vivo*.

Myeloid-Specific *Pfkfb3* Deficiency Protects Mice From LPS-Induced Acute Lung Injury

To investigate the effect of myeloid-specific *Pfkfb3* deficiency on LPS-induced acute lung injury, we first determined the histological alterations of lungs from LPS-challenged *Pfkfb3*$^{\Delta M\phi}$ and *Pfkfb3*^{WT} mice by hematoxylin and eosin (H&E) staining. The H&E staining results indicated a lower degree of recruitment of inflammatory cells into the lungs of *Pfkfb3*$^{\Delta M\phi}$ mice compared to those of *Pfkfb3*^{WT} mice (**Figure 4A**). To further examine the protective effect of myeloid-specific *Pfkfb3* deficiency on lung injury, the pulmonary permeability was assessed *in vivo*. The lung wet-to-dry ratio, which was used as an index to evaluate lung edema, was decreased in the lungs of *Pfkfb3*$^{\Delta M\phi}$ mice compared with those of *Pfkfb3*^{WT} mice after LPS injection (**Figure 4B**). Next, we injected Evans Blue in *Pfkfb3*$^{\Delta M\phi}$ and *Pfkfb3*^{WT} mice with or without LPS treatment. As shown in **Figure 4C**, Evans Blue leakage majorly decreased in the lungs of *Pfkfb3*$^{\Delta M\phi}$ mice compared to those of *Pfkfb3*^{WT} mice after LPS injection. In addition, *Pfkfb3*$^{\Delta M\phi}$ mice exhibited higher body temperature after LPS challenge compared to *Pfkfb3*^{WT} mice (**Figure 4D**). Moreover, we observed a marked improvement in mortality: 67% *Pfkfb3*$^{\Delta M\phi}$ mice survived after 96 h of the LPS-challenge whereas none of *Pfkfb3*^{WT} mice survived in the control group (**Figure 4E**). Collectively, these observations suggest that myeloid-specific *Pfkfb3* deficiency protects mice against LPS-induced lethality and tissue injury.

Myeloid-Specific *Pfkfb3* Deficiency Attenuates LPS-Induced Inflammatory Responses in Mice

Recruitment of myeloid cells into the lung represents a key feature of LPS-induced tissue injury. We first exposed *Pfkfb3*$^{\Delta M\phi}$ and *Pfkfb3*^{WT} mice to 12.5 mg/kg LPS for 6 h and then detected the infiltration of neutrophils and macrophages in the lung tissue with immunostaining. The results showed that the infiltration of Ly6G positive cells and Mac2 positive cells was significantly decreased in the lungs of *Pfkfb3*$^{\Delta M\phi}$ mice compared to those of *Pfkfb3*^{WT} mice (**Figures 5A,B**). Given that the recruitment of myeloid cells is mainly dependent on the excessive expression of proinflammatory mediators, including interleukin 1b (Il1b), interleukin 6 (Il6) and inducible nitric oxide synthase 2 (Nos2), we next analyzed the effect of myeloid-specific *Pfkfb3* deficiency on the expression of proinflammatory genes in lungs using real-time PCR. The mRNA levels of *Il1b*,

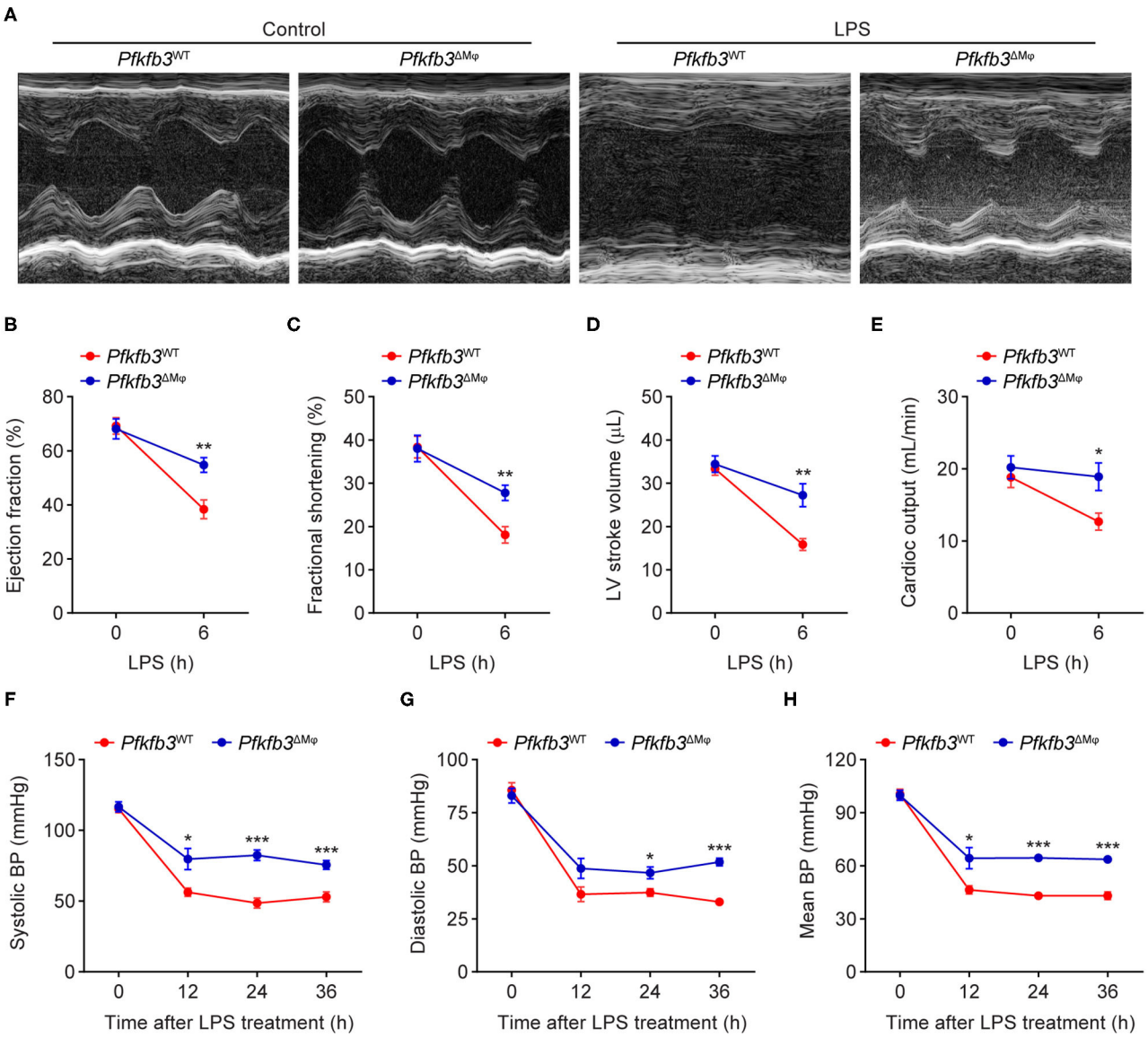

FIGURE 3 | Myeloid-specific *Pfkfb3* deficiency protects mice from LPS-induced cardiac dysfunction. **(A)** Representative M-mode echocardiograms of *Pfkfb3*^{WT} mice and *Pfkfb3*$^{\Delta M\phi}$ mice 6 h after LPS injection. **(B-E)** Quantification of ejection fraction **(B)**, fractional shortening **(C)**, left ventricle stroke volume **(D)**, and cardiac output **(E)** of *Pfkfb3*^{WT} mice and *Pfkfb3*$^{\Delta M\phi}$ mice 6 h after LPS injection ($n = 5$). **(F–H)** Systolic blood pressure **(F)**, diastolic blood pressure **(G)**, and mean blood pressure **(H)** of *Pfkfb3*^{WT} mice and *Pfkfb3*$^{\Delta M\phi}$ mice before and after LPS injection ($n = 8$). All data are represented as mean ± SEM, $^{*}P < 0.05$, $^{**}P < 0.01$ and $^{***}P < 0.001$ for *Pfkfb3*^{WT} vs. *Pfkfb3*$^{\Delta M\phi}$ (unpaired two-tailed Student's *t* test).

Il6 and *Nos2* were significantly increased in the lungs of LPS-challenged *Pfkfb3*^{WT} mice compared to those of control mice, whereas these mRNA levels were decreased in the lungs of LPS-challenged *Pfkfb3*$^{\Delta M\phi}$ mice compared to LPS-challenged *Pfkfb3*^{WT} mice (**Figures 5C–E**). Consistently, the serum levels of Il1b, Il6 and NO were significantly increased in LPS-challenged *Pfkfb3*^{WT} mice compared to control mice, whereas the serum levels of Il1b, Il6 and NO were decreased in LPS-challenged *Pfkfb3*$^{\Delta M\phi}$ mice compared to LPS-challenged *Pfkfb3*^{WT} mice (**Figures 5F–H**). Thus, these data suggest that myeloid-specific *Pfkfb3* deficiency protects mice from LPS-induced excessive inflammatory responses *in vivo*.

Enhance Glycolysis in Macrophages Supports Their Proinflammatory Activity Upon LPS Stimulation

Having observed that myeloid Pfkfb3 deficiency reduced LPS-induced inflammation *in vivo*, we further investigated whether Pfkfb3 regulates the expression of proinflammatory cytokines

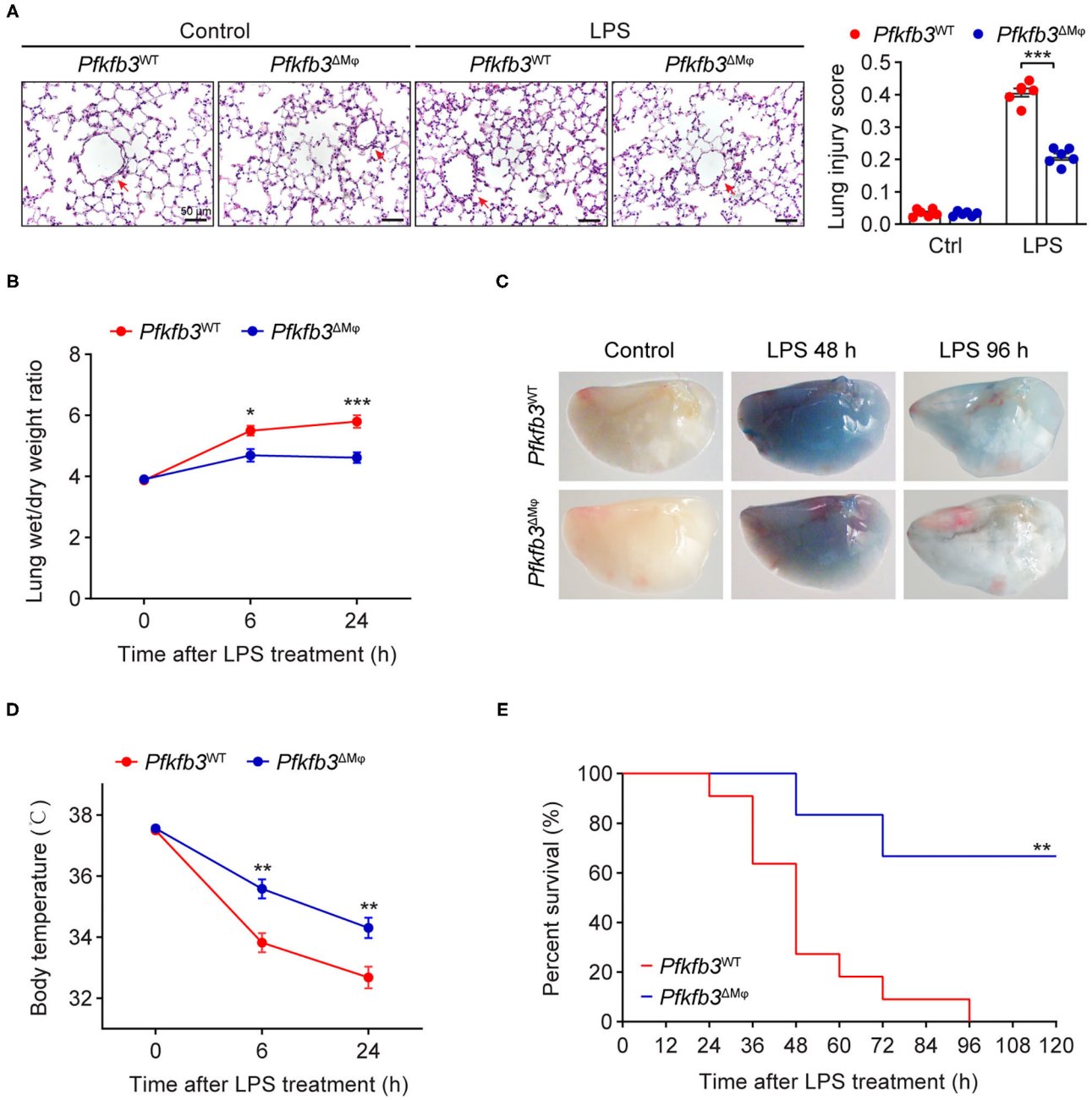

FIGURE 4 | Myeloid-specific *Pfkfb3* deficiency protects mice from LPS-induced acute lung injury. **(A)** Representative images of hematoxylin and eosin staining (left) and lung injury score analysis (right) of lung sections from *Pfkfb3*^{WT} mice and *Pfkfb3*$^{\Delta M\phi}$ mice 6 h after LPS injection ($n = 6$). **(B)** The wet/dry weight ratio of lung tissue of *Pfkfb3*^{WT} mice and *Pfkfb3*$^{\Delta M\phi}$ mice after LPS injection ($n = 6$-8). **(C)** Representative images of Evans Blue staining of lung tissue of *Pfkfb3*^{WT} mice and *Pfkfb3*$^{\Delta M\phi}$ mice after LPS injection. **(D)** Changes of body temperature of *Pfkfb3*^{WT} mice and *Pfkfb3*$^{\Delta M\phi}$ mice after LPS injection ($n = 9$). **(E)** Survival curve of *Pfkfb3*^{WT} mice and *Pfkfb3*$^{\Delta M\phi}$ mice following LPS injection ($n = 6$–11). All data are represented as mean ± SEM, $^*P < 0.05$, $^{**}P < 0.01$ and $^{***}P < 0.001$ for indicated comparisons. Unpaired two-tailed Student's *t* test for **(B,D)** and Mantel-Cox test for **(E)**.

and *Nos2* in macrophages *in vitro*. We first analyzed the glycolytic flux in BMDMs cultured with bone marrow from *Pfkfb3*$^{\Delta M\phi}$ mice or corresponding wild-type *Pfkfb3*^{WT} mice using the Seahorse Extracellular Flux analyzer. As shown in **Figures 6A–C**, *Pfkfb3*$^{\Delta M\phi}$ BMDMs displayed significantly reduced glycolysis and glycolysis capacity in response to LPS compared to *Pfkfb3*^{WT} BMDMs. Importantly, *Pfkfb3*$^{\Delta M\phi}$ BMDMs displayed reduced mRNA levels of *Il1b*, *Il6* and *Nos2* in response to LPS compared with *Pfkfb3*^{WT} BMDMs (**Figures 6D–F**). Consistent with mRNA levels, *Pfkfb3*$^{\Delta M\phi}$ BMDMs displayed significantly

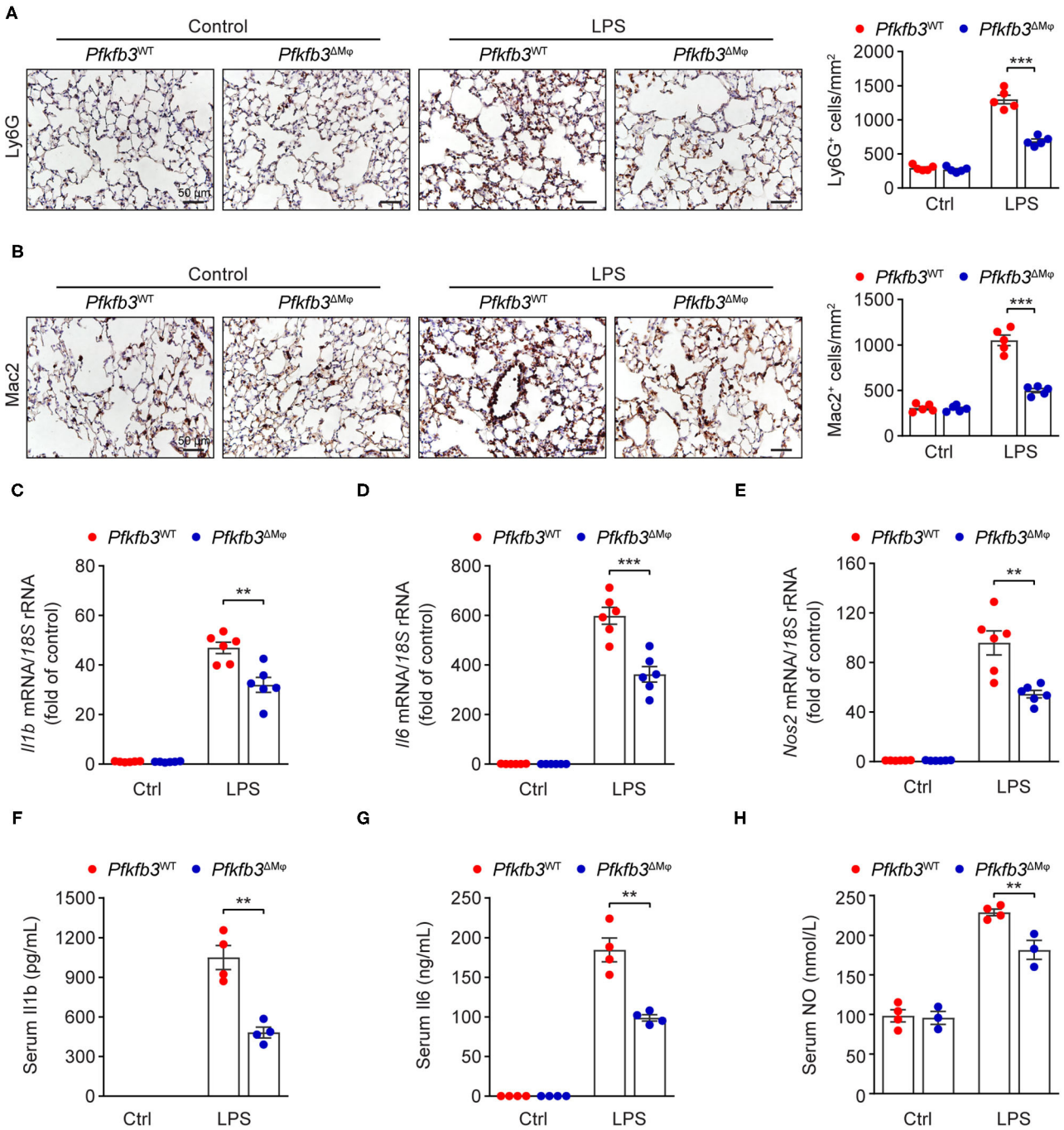

FIGURE 5 | Myeloid-specific *Pfkfb3* deficiency attenuates LPS-induced inflammatory responses. **(A)** Representative images (left) and quantification (right) for immunohistochemical staining of the neutrophil marker Ly6G in lung sections of *Pfkfb3*^{WT} mice and *Pfkfb3*$^{\Delta M\phi}$ mice 6 h after LPS injection ($n = 5$). **(B)** Representative images (left) and quantification (right) for immunohistochemical staining of the macrophage marker Mac2 in lung sections of *Pfkfb3*^{WT} mice and *Pfkfb3*$^{\Delta M\phi}$ mice 6 h after LPS injection ($n = 5$). **(C–E)** qPCR analysis of the mRNA levels of *Il1b* **(C)**, *Il6* **(D)** and *Nos2* **(E)** in the lung of *Pfkfb3*^{WT} mice and *Pfkfb3*$^{\Delta M\phi}$ mice 6 h after LPS injection ($n = 6$). **(F,G)** ELISA analysis of Il1b **(F)** and Il6 **(G)** in serum of *Pfkfb3*^{WT} mice and *Pfkfb3*$^{\Delta M\phi}$ mice 6 h after LPS injection ($n = 4$). **(H)** NO levels in serum of *Pfkfb3*^{WT} mice and *Pfkfb3*$^{\Delta M\phi}$ mice 6 h after LPS injection ($n = 3$–4). All data are represented as mean ± SEM, $^{**}P < 0.01$ and $^{***}P < 0.001$ for *Pfkfb3*^{WT} vs. *Pfkfb3*$^{\Delta M\phi}$ (unpaired two-tailed Student's *t* test).

reduced protein levels of Nos2 in response to LPS compared with *Pfkfb3*^{WT} BMDMs (**Figures 6G–I**). Moreover, the secretion of Il1b, Il6 and NO was significantly decreased in *Pfkfb3*$^{\Delta M\phi}$ BMDMs compared to that in *Pfkfb3*^{WT} BMDMs (**Figures 6J–L**). Thus, these data suggest that inhibition of glycolysis with *Pfkfb3* deletion in macrophages reduces LPS-induced expression of proinflammatory cytokines and Nos2 *in vitro*.

Pfkfb3 Inactivation in Macrophages Suppresses LPS-Induced Inflammation *via* the NF-κB Signaling Pathway

We next investigated the molecular mechanisms by which LPS-induced signal transduction is regulated by Pfkfb3 in macrophages. The activation of nuclear factor-κB (NF-κB) and mitogen-activated protein kinase (MAPK) by LPS is the key signaling pathways for the induced expression of proinflammatory genes in macrophages. We analyzed the phosphorylation of Erk, Jnk, p38 and p65 in LPS-stimulated *Pfkfb3*$^{\Delta M\phi}$ and *Pfkfb3*^{WT} BMDMs by Western blot. As shown in **Figures 7A–E**, the protein levels of p-Erk, p-Jnk, p-p38 and p-p65 were markedly increased in *Pfkfb3*^{WT} BMDMs stimulated with LPS. However, of the above observed signaling molecule changes, only the upregulation of p-p65 by LPS was suppressed in *Pfkfb3*$^{\Delta M\phi}$ BMDMs treated with LPS. Moreover, similar to *Pfkfb3* knockout, AZ26, which is an inhibitor that abolishes the enzyme activation of Pfkfb3 (21), could antagonize the upregulation of proinflammatory cytokine *Il1b* and *Il6* expression in LPS-treated wild type BMDMs (**Figures 7F,G**). Furthermore, the phosphorylation of p65 was also antagonized by AZ26 in LPS-treated BMDMs (**Figure 7H**). These data suggest that the NF-κB signaling pathway is involved in the downregulation of proinflammatory mediators in macrophages by Pfkfb3 inactivation.

DISCUSSION

In the present study, we demonstrated the effect of myeloid Pfkfb3 in LPS-induced sepsis in mice. Deletion of myeloid *Pfkfb3* reduces LPS-induced sepsis and inflammatory responses by decreasing lung infiltration of macrophages and neutrophils and improving lung edema, cardiac dysfunction and hypotension. This improved phenotype is associated with the decrease in the expression of Nos2 and inflammatory cytokines in macrophages via decreased NF-κB signaling with deficiency/inhibition of Pfkfb3.

Enhanced glycolytic flux has been recognized as a metabolic signature of activated macrophages (8, 9, 22). Increased glycolysis enables macrophages to rapidly generate ATP and biosynthetic intermediates to support proinflammatory cytokine production (23–25). Extensive studies have reported the effect of glycolytic molecules in regulation of macrophage activation (26–29). PFKFB3, an isoform of 6-phosphofructo-2-kinase/fructose-2,6-bisphosphatase (PFK-2), regulates intracellular levels of the glycolytic intermediate fructose-2,6-bisphosphate (F-2,6-BP), which allosterically activates the second rate-limiting enzyme 6-phosphofructo-1-kinase (PFK-1), leading to increase glycolytic flux (30). However, the effect of myeloid Pfkfb3 on modulation of LPS-induced sepsis has not been studied yet. RNA-Seq data reveals that macrophage *Pfkfb3* was the most significantly upregulated glycolytic gene in response to LPS treatment (10). In addition, *PFKFB3* was also upregulated in myeloid blood cells from critically ill COVID-19 patients (31). It has been reported that *Pfkfb3* is a hypoxia-inducible gene that is stimulated through HIF interaction with the consensus HRE site in its promoter region (32). Therefore, increased Pfkfb3 expression in macrophages may be attributed to an enhanced HIF pathway upon proinflammatory stimuli. Recent study has shown that p65 binds to the PFKFB3 promoter in response to treatment with proinflammatory cytokine in endothelial cells (33), thus, upregulation of Pfkfb3 in macrophages may also be due to activated NF-κB signaling under LPS stimuli.

Myeloid Pfkfb3 knockout-decreased macrophage inflammatory response protects mice from LPS-induced sepsis. It has been well accepted that inhibited macrophage glycolysis protects mice from LPS-induced sepsis (13, 26). For example, inactivation of hexokinase 1 (HK1), the first rate-limiting enzyme of the glycolytic pathway, suppressed macrophage proinflammatory responses and LPS-induced sepsis in mice (26, 27). This has been associated with reduced Il1b production in macrophages and reduced serum levels of Tnfa and nitric oxide (NO). Moreover, knockout of myeloid pyruvate kinase M2 (Pkm2), the final rate-limiting enzyme in glycolysis, also reduced septic death in mice (29). In the current study, LPS-induced septic death and organ dysfunction including pulmonary edema and cardiac dysfunction were decreased in *Pfkfb3*$^{\Delta M\phi}$ mice. Decreased serum levels of NO and proinflammatory cytokines, and reduced infiltration of macrophages in lung tissue also occurred in LPS-treated *Pfkfb3*$^{\Delta M\phi}$ mice. A further *in vitro* study demonstrated increased glycolytic flux induced by LPS was significantly dampened in *Pfkfb3*$^{\Delta M\phi}$ BMDMs, indicating LPS-induced Pfkfb3 expression is a critical step in the induction of glycolysis in activated macrophages. LPS-induced upregulation of Nos2 and proinflammatory cytokine Il1b and Il6 was also decreased in *Pfkfb3*$^{\Delta M\phi}$ BMDMs. Therefore, our findings on decreased septic death in LPS-treated *Pfkfb3*$^{\Delta M\phi}$ mice, at least in part, are associated with reduced macrophage activation through decreased the expression of Nos2 and inflammatory cytokines such as Il1b and Il6 (34–37).

Pfkfb3 deficiency/inhibition reduces macrophage proinflammatory responses through the NF-κB signaling pathway. Genetic and pharmacological inhibition of macrophage Pfkfb3 decreased LPS-induced proinflammatory gene expression. This is due to decreased NF-κB activity which is evidenced by the decreased level of p65 phosphorylation (38). The decreased level of p65 phosphorylation in this study is in line with previous studies in which the decreased level of p65 phosphorylation without affecting MAPK signaling pathway in human monocytes upon proinflammatory stimuli (39, 40). This observation is also in agreement with several recent studies in which *PFKFB3* knockdown in endothelial cells decreases proinflammatory stimuli-induced proinflammatory responses through downregulation of p65 phosphorylation (41–43). The underlying mechanisms by which Pfkfb3 deficiency directly

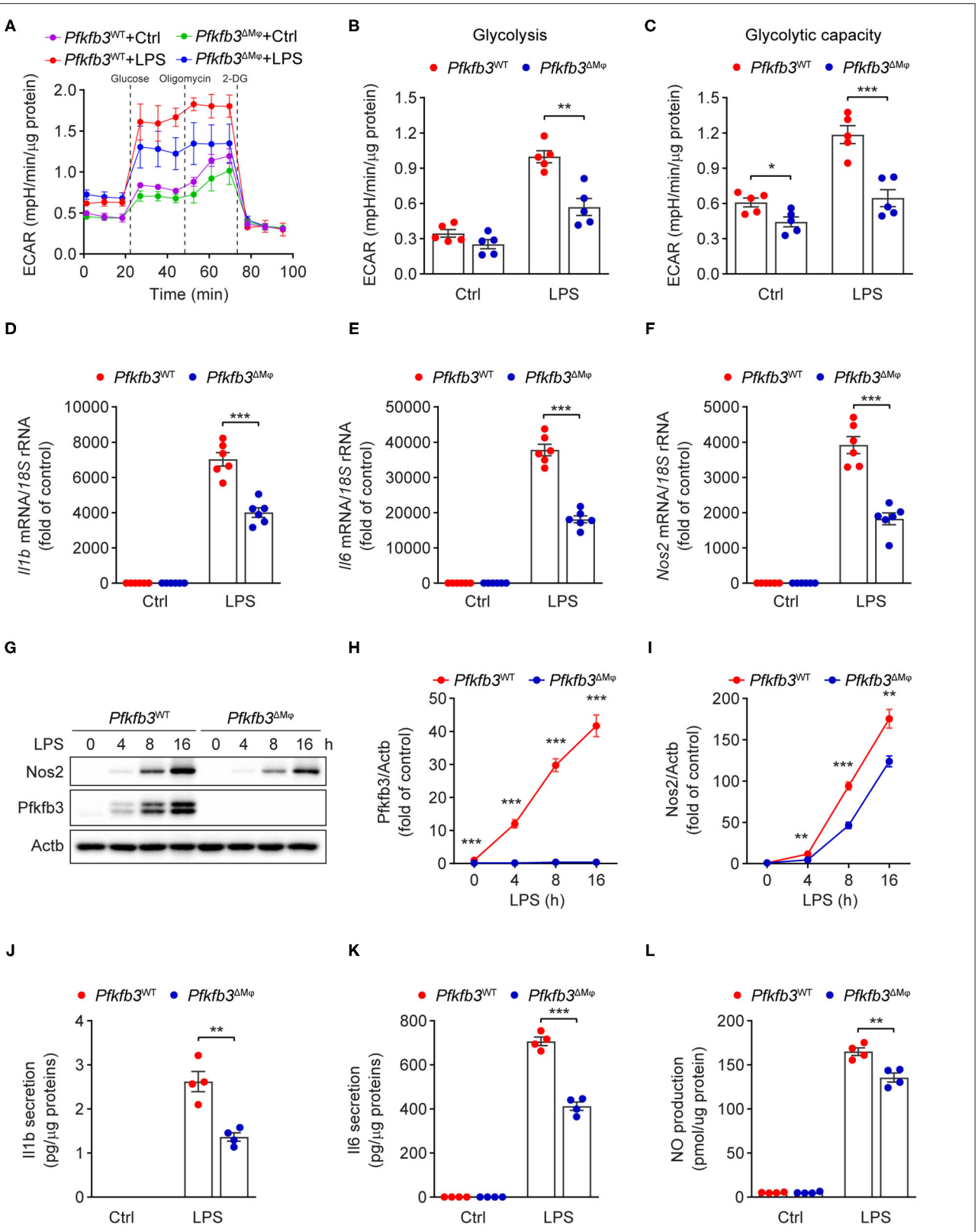

FIGURE 6 | Enhance glycolysis in macrophages supports their proinflammatory activity upon LPS stimulation. **(A)** ECAR profile shows glycolytic function in *Pfkfb3*^{WT} and *Pfkfb3*$^{\Delta M\phi}$ BMDMs treated with LPS (100 ng/mL) for 6 h ($n = 5$). **(B,C)** Quantification of glycolysis [**(B)**, ECAR after glucose addition and subtracted by the average of basal values] and glycolytic capacity [**(C)**, ECAR after oligomycin addition and subtracted by the average of basal values] from **(A)** ($n = 5$). **(D–F)** qPCR

(Continued)

FIGURE 6 | analysis of the mRNA levels of *Il1b* **(D)**, *Il6* **(E)** and *Nos2* **(F)** in *Pfkfb3*^{WT} and *Pfkfb3*$^{\Delta M\phi}$ BMDMs treated with LPS (100 ng/mL) for 4 h ($n = 6$). **(G–I)** Representative Western blot results of Nos2, Pfkfb3 and Actb in *Pfkfb3*^{WT} and *Pfkfb3*$^{\Delta M\phi}$ BMDMs treated with LPS (100 ng/mL) for the indicated times **(G)** and relative ratio of Pfkfb3/Actb **(H)** and Nos2/Actb **(I)** were quantitated by densitometric analysis of the corresponding Western blots ($n = 4$). **(J,K)** ELISA analysis of Il1b **(J)** and Il6 **(K)** secretion in the supernatants of *Pfkfb3*^{WT} and *Pfkfb3*$^{\Delta M\phi}$ BMDMs treated with LPS (100 ng/mL) for 16 h ($n = 4$). **(L)** Quantification of NO secretion in the supernatants of *Pfkfb3*^{WT} and *Pfkfb3*$^{\Delta M\phi}$ BMDMs treated with LPS (100 ng/mL) for 16 h ($n = 4$). All data are represented as mean ± SEM, $^{**}P < 0.01$ and $^{***}P < 0.001$ for *Pfkfb3*^{WT} vs. *Pfkfb3*$^{\Delta M\phi}$ (unpaired two-tailed Student's *t* test).

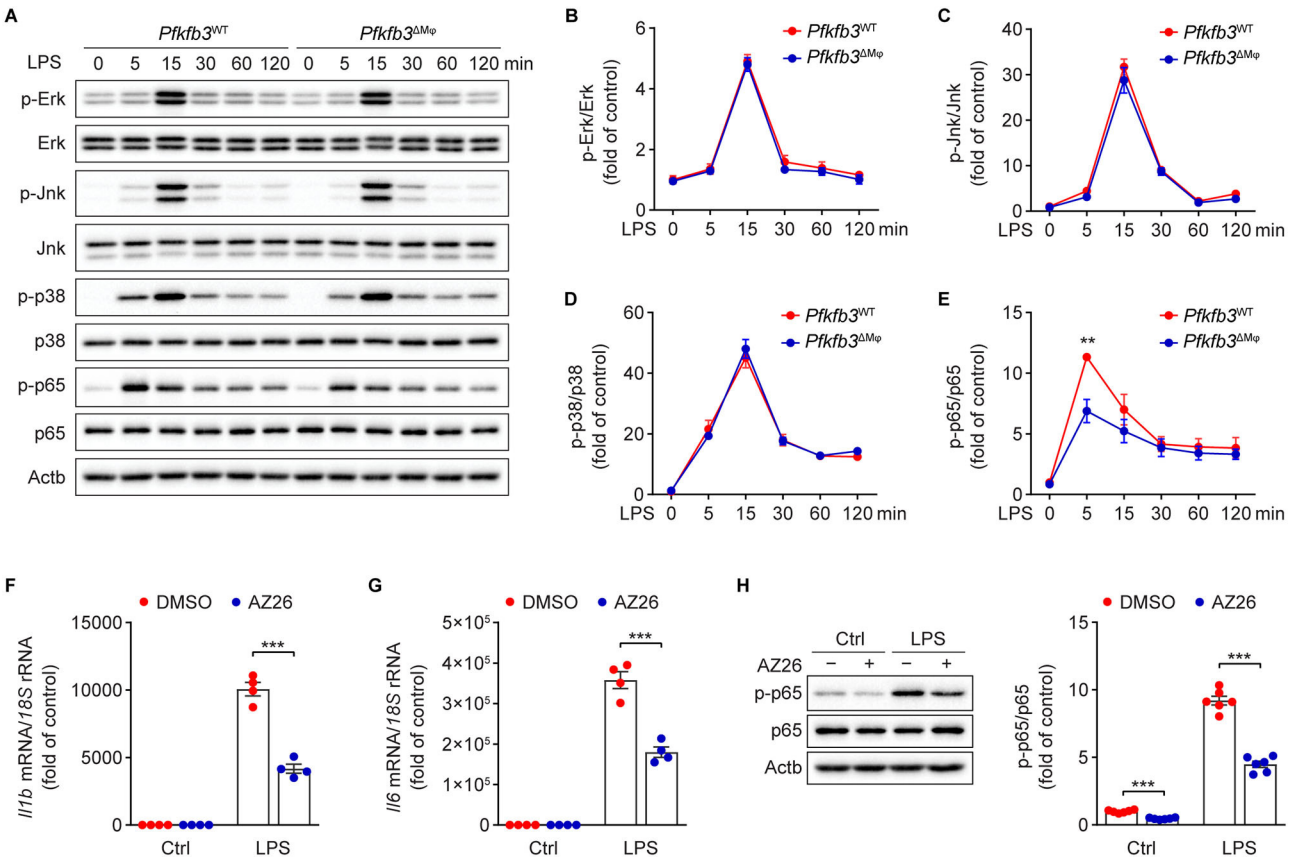

FIGURE 7 | Pfkfb3 inactivation in macrophages suppresses LPS-induced inflammation via the NF-κB signaling pathway. **(A–E)** Representative Western blot results **(A)** of phosphorylated and total level of Erk, Jnk, p38 and p65 in *Pfkfb3*^{WT} and *Pfkfb3*$^{\Delta M\phi}$ BMDMs treated with LPS (100 ng/mL) at the indicated time points, and relative ratio of p-Erk/Erk **(B)**, p-Jnk/Jnk **(C)**, p-p38/p38 **(D)** and p-p65/p65 **(E)** were quantitated by densitometric analysis of the corresponding Western blots ($n = 4$). **(F,G)** qPCR analysis of the mRNA levels of *Il1b* **(F)** and *Il6* **(G)** in BMDMs treated with LPS (100 ng/mL) for 4 h, with or without AZ26 (10 μM) pretreatment for 30 min ($n = 4$). **(H)** Representative Western blot results (left) of p-p65, p65 and Actb in BMDMs treated with LPS (100 ng/mL) for 5 min, with or without AZ26 (10 μM) pretreatment for 30 min, and relative ratio of p-p65/p65 (right) was quantitated by densitometric analysis of the corresponding Western blots ($n = 4$). All data are represented as mean ± SEM, $^{**}P < 0.01$ and $^{***}P < 0.001$ for indicated comparisons (unpaired two-tailed Student's *t* test).

controls the inactivation of NF-κB signaling may include the following possibilities. First, most of the downstream signaling processes consume ATP during activating NF-κB signaling in response to LPS. For example, LPS-induced NF-κB activation is dependent on the ATP-dependent proteolysis of pIκBα (44). Given the fact that LPS-stimulated macrophages predominantly use glycolysis to generate ATP (45), it is likely that decreased glycolytic ATP production in *Pfkfb3* knockout macrophages reduces ATP-dependent NF-κB activation after LPS stimulation. Second, LPS-driven glycolytic ATP production facilitates an increase in mitochondrial membrane potential that is required for the generation of reactive oxygen species (ROS) (46). The decreased glycolytic flux upon LPS stimulation in *Pfkfb3*-deficient macrophages may result in reduced mitochondrial ROS production, which decreases activation of the redox-sensitive NF-κB (47). Finally, a recent study shows that lactate, a byproduct of glycolysis, enhances NF-κB activity and the expression of IL1B and IL6 in macrophages (48). The data from us has shown that *Pfkfb3* knockout reduced glycolytic flux upon LPS stimulation in BMDMs, which may also be responsible for downregulated NF-κB activation in *Pfkfb3*$^{\Delta M\phi}$ BMDMs.

Other possible mechanisms, such as the epigenetic effects of myeloid *Pfkfb3* deficiency, may also contribute to the alleviated

macrophage activation and systemic inflammatory responses in LPS-treated *Pfkfb3*$^{\Delta M\phi}$ mice. Our recent study has shown that the deletion of *Pfkfb3* in macrophages reduces proinflammatory gene induction through downregulated hyperglycolysis-mediated histone acetylation (28). Therefore, it is very likely that decreased hyperglycolysis-mediated histone acetylation in *Pfkfb3*-deficient macrophages upon LPS stimulation contributes to the decreased proinflammatory gene expression in septic mice observed in the current study (49, 50).

In summary, our findings demonstrate that inactivation of macrophage Pfkfb3 can reduce LPS-induced organ dysfunction and death *via* decreased macrophage glycolysis and proinflammatory gene induction. A recent study has shown that inhibition of PFKFB3 hampers the progression of atherosclerosis and promotes plaque stability mainly through decreased glycolysis in monocytes and macrophages (51). Although further study is required to identify the role of PFKFB3 in other types of cells in the regulation of inflammatory diseases, it is very likely that regulation of macrophage PFKFB3 is a potential therapeutic strategy for the treatment of inflammatory diseases such as sepsis and atherosclerosis.

LIMITATION

This study had some limitations. First, in addition to reduced lactate production, *Pfkfb3* deficiency in activated macrophages may change glycolysis-linked pathways such as pentose phosphate, glycogenesis, hexosamine, *de novo* serine synthesis and tricarboxylic acid cycle. Each of the above flux pathways is an important regulator in inflammatory response. Assessing these pathways by glucose flux with ^{13}C-glucose tracer in activated *Pfkfb3*^{WT} and *Pfkfb3*$^{\Delta M\phi}$ BMDMs will be needed in future study. Second, as macrophages are critical in the host response to infection, thereby, it remains unclear whether blocking of macrophage glycolysis and cytokine production by deletion of *Pfkfb3* would impair the role of macrophages in bacterial clearance and resolution of infection-mediated sepsis. An infection-induced sepsis model is required in future study. Third, murine system *in vitro* and *in vivo* is solely used in this study. A difference in glucose metabolism between human and murine system has been reported (52, 53). Thus, the role of PFKFB3 in inflammatory and metabolic response in human macrophages need to be determined in future study.

DATA AVAILABILITY STATEMENT

The raw data supporting the conclusions of this article will be made available by the authors, without undue reservation.

ETHICS STATEMENT

The animal study was reviewed and approved by the Institutional Animal Care and Use Committee of Augusta University.

AUTHOR CONTRIBUTIONS

JX, LW, QY, YS, ZB, RL, ZL, MH, KO, and YH designed the research. JX, LW, QY, QM, YZ, YC, XM, and QD performed experiments. JX, LW, QY, and YH analyzed data. JX, TL, ZL, MH, KO, and YH wrote and revised the manuscript. YS, ZB, RL, ZL, MH, KO, and YH provided the reagents or materials and participated in experimental design. YH had primary responsibility for the final content. All authors read and approved the final manuscript.

FUNDING

This work was supported in part or in whole by grants from National Science Foundation of China Grants 82100506, 81870324, and 82070461; China Postdoctoral Science Foundation 2020M680003 and 2020M670051; Guangdong Basic and Applied Basic Research Foundation 2020A1515010010 and 2019A1515110111; Shenzhen Science and Technology Innovation Committee Grants JCYJ20190808155605447, JCYJ20170810163238384, JCYJ20190808155801648, JCYJ201704121-50405310, and GXWD20201231165807007-20200818123312001. Shenzhen-Hong Kong Institute of Brain Science-Shenzhen Fundamental Research Institutions 2019SHIBS0004; American Heart Association Grant 19TPA34910043. National Institutes of Health Grants R01HL134934, R01EY030500, R01HL142097, and R01HL138410. VA Merit Review Grant BX002035.

SUPPLEMENTARY MATERIAL

The Supplementary Material for this article can be found online at: https://www.frontiersin.org/articles/10.3389/fcvm.2021.745810/full#supplementary-material

REFERENCES

1. Cecconi M, Evans L, Levy M, Rhodes A. Sepsis and septic shock. *Lancet.* (2018) 392:75–87. doi: 10.1016/S0140-6736(18)30696-2
2. Wu Z, McGoogan JM. Characteristics of and important lessons from the Coronavirus Disease 2019 (COVID-19) outbreak in China: summary of a report of 72314 cases from the Chinese Center for Disease Control and Prevention. *JAMA.* (2020) 323:1239–42. doi: 10.1001/jama.2020.2648
3. Schulte W, Bernhagen J, Bucala R. Cytokines in sepsis: potent immunoregulators and potential therapeutic targets–an updated view. *Mediators Inflamm.* (2013) 2013:165974. doi: 10.1155/2013/165974
4. Rudd KE, Johnson SC, Agesa KM, Shackelford KA, Tsoi D, Kievlan DR, et al. Global, regional, and national sepsis incidence and mortality, 1990-2017: analysis for the Global Burden of Disease Study. *Lancet.* (2020) 395:200–11. doi: 10.1016/S0140-6736(19)32989-7
5. Reinhart K, Daniels R, Kissoon N, Machado FR, Schachter RD, Finfer S. Recognizing sepsis as a global health priority - a WHO resolution. *N Engl J Med.* (2017) 377:414–7. doi: 10.1056/NEJMp1707170
6. Singer M, Deutschman CS, Seymour CW, Shankar-Hari M, Annane D, Bauer M, et al. The third international consensus definitions for sepsis and septic shock (Sepsis-3). *JAMA.* (2016) 315:801–10. doi: 10.1001/jama.2016.0287
7. Cavaillon JM, Adib-Conquy M. Monocytes/macrophages and sepsis. *Crit Care Med.* (2005) 33:S506–9. doi: 10.1097/01.ccm.0000185502.21012.37

8. Pearce EL, Pearce EJ. Metabolic pathways in immune cell activation and quiescence. *Immunity.* (2013) 38:633–43. doi: 10.1016/j.immuni.2013.04.005
9. Kelly B, O'Neill LA. Metabolic reprogramming in macrophages and dendritic cells in innate immunity. *Cell Res.* (2015) 25:771–84. doi: 10.1038/cr.2015.68
10. Rodriguez AE, Ducker GS, Billingham LK, Martinez CA, Mainolfi N, Suri V, et al. Serine metabolism supports macrophage IL-1β production. *Cell Metab.* (2019) 29:1003–11. doi: 10.1016/j.cmet.2019.01.014
11. Chesney J, Mitchell R, Benigni F, Bacher M, Spiegel L, Al-Abed Y, et al. An inducible gene product for 6-phosphofructo-2-kinase with an AU-rich instability element: role in tumor cell glycolysis and the Warburg effect. *Proc Natl Acad Sci USA.* (1999) 96:3047–52. doi: 10.1073/pnas.96.6.3047
12. Okar DA, Manzano A, Navarro-Sabate A, Riera L, Bartrons R, Lange AJ. PFK-2/FBPase-2: maker and breaker of the essential biofactor fructose-2,6-bisphosphate. *Trends Biochem Sci.* (2001) 26:30–5. doi: 10.1016/s0968-0004(00)01699-6
13. Wang Z, Kong L, Tan S, Zhang Y, Song X, Wang T, et al. Zhx2 accelerates sepsis by promoting macrophage glycolysis via Pfkfb3. *J Immunol.* (2020) 204:2232–41. doi: 10.4049/jimmunol.1901246
14. Xu Y, An X, Guo X, Habtetsion TG, Wang Y, Xu X, et al. Endothelial PFKFB3 plays a critical role in angiogenesis. *Arterioscler Thromb Vasc Biol.* (2014) 34:1231–9. doi: 10.1161/ATVBAHA.113.303041
15. Xu J, Yang Q, Zhang X, Liu Z, Cao Y, Wang L, et al. Endothelial adenosine kinase deficiency ameliorates diet-induced insulin resistance. *J Endocrinol.* (2019) 242:159–72. doi: 10.1530/JOE-19-0126
16. Tan Z, Xie N, Banerjee S, Cui H, Fu M, Thannickal VJ, et al. The monocarboxylate transporter 4 is required for glycolytic reprogramming and inflammatory response in macrophages. *J Biol Chem.* (2015) 290:46–55. doi: 10.1074/jbc.M114.603589
17. Xu Y, Wang Y, Yan S, Zhou Y, Yang Q, Pan Y, et al. Intracellular adenosine regulates epigenetic programming in endothelial cells to promote angiogenesis. *EMBO Mol Med.* (2017) 9:1263–78. doi: 10.15252/emmm.201607066
18. Liu Z, Yan S, Wang J, Xu Y, Wang Y, Zhang S, et al. Endothelial adenosine A2a receptor-mediated glycolysis is essential for pathological retinal angiogenesis. *Nat Commun.* (2017) 8:584. doi: 10.1038/s41467-017-00551-2
19. Matute-Bello G, Downey G, Moore BB, Groshong SD, Matthay MA, Slutsky AS, et al. An official American Thoracic Society workshop report: features and measurements of experimental acute lung injury in animals. *Am J Respir Cell Mol Biol.* (2011) 44:725–38. doi: 10.1165/rcmb.2009-0210ST
20. Yang Q, Xu J, Ma Q, Liu Z, Sudhahar V, Cao Y, et al. PRKAA1/AMPKα1-driven glycolysis in endothelial cells exposed to disturbed flow protects against atherosclerosis. *Nat Commun.* (2018) 9:4667. doi: 10.1038/s41467-018-07132-x
21. Boyd S, Brookfield JL, Critchlow SE, Cumming IA, Curtis NJ, Debreczeni J, et al. Structure-based design of potent and selective inhibitors of the metabolic kinase PFKFB3. *J Med Chem.* (2015) 58:3611–25. doi: 10.1021/acs.jmedchem.5b00352
22. Koo SJ, Garg NJ. Metabolic programming of macrophage functions and pathogens control. *Redox Biol.* (2019) 24:101198. doi: 10.1016/j.redox.2019.101198
23. Viola A, Munari F, Sanchez-Rodriguez R, Scolaro T, Castegna A. The metabolic signature of macrophage responses. *Front Immunol.* (2019) 10:1462. doi: 10.3389/fimmu.2019.01462
24. Yu W, Wang Z, Zhang K, Chi Z, Xu T, Jiang D, et al. One-carbon metabolism supports S-adenosylmethionine and histone methylation to drive inflammatory macrophages. *Mol Cell.* (2019) 75:1147–60. doi: 10.1016/j.molcel.2019.06.039
25. Wang L, Zhang X, Cao Y, Ma Q, Mao X, Xu J, et al. Mice with a specific deficiency of Pfkfb3 in myeloid cells are protected from hypoxia-induced pulmonary hypertension. *Br J Pharmacol.* (2021) 178:1055–72. doi: 10.1111/bph.15339
26. Liu L, Lu Y, Martinez J, Bi Y, Lian G, Wang T, et al. Proinflammatory signal suppresses proliferation and shifts macrophage metabolism from Myc-dependent to HIF1α-dependent. *Proc Natl Acad Sci USA.* (2016) 113:1564–9. doi: 10.1073/pnas.1518000113
27. Moon J, Hisata S, Park M, DeNicola GM, Ryter SW, Nakahira K, et al. mTORC1-induced HK1-dependent glycolysis regulates NLRP3 inflammasome activation. *Cell Rep.* (2015) 12:102–15. doi: 10.1016/j.celrep.2015.05.046
28. Liu Z, Xu J, Ma Q, Zhang X, Yang Q, Wang L, et al. Glycolysis links reciprocal activation of myeloid cells and endothelial cells in the retinal angiogenic niche. *Sci Transl Med.* (2020) 12:eaay1371. doi: 10.1126/scitranslmed.aay1371
29. Xie M, Yu Y, Kang R, Zhu S, Yang L, Zeng L, et al. PKM2-dependent glycolysis promotes NLRP3 and AIM2 inflammasome activation. *Nat Commun.* (2016) 7:13280. doi: 10.1038/ncomms13280
30. Cao Y, Zhang X, Wang L, Yang Q, Ma Q, Xu J, et al. PFKFB3-mediated endothelial glycolysis promotes pulmonary hypertension. *Proc Natl Acad Sci USA.* (2019) 116:13394–403. doi: 10.1073/pnas.1821401116
31. Taniguchi-Ponciano K, Vadillo E, Mayani H, Gonzalez-Bonilla CR, Torres J, Majluf A, et al. Increased expression of hypoxia-induced factor 1α mRNA and its related genes in myeloid blood cells from critically ill COVID-19 patients. *Ann Med.* (2021) 53:197–207. doi: 10.1080/07853890.2020.1858234
32. Obach M, Navarro-Sabaté À, Caro J, Kong X, Duran J, Gómez M, et al. 6-Phosphofructo-2-kinase (pfkfb3) gene promoter contains hypoxia-inducible factor-1 binding sites necessary for transactivation in response to hypoxia. *J Biol Chem.* (2004) 279:53562–70. doi: 10.1074/jbc.M406096200
33. Xiao W, Oldham WM, Priolo C, Pandey AK, Loscalzo J. Immunometabolic endothelial phenotypes: integrating inflammation and glucose metabolism. *Circ Res.* (2021) 129:9–29. doi: 10.1161/CIRCRESAHA.120.318805
34. Baron RM, Carvajal IM, Liu X, Okabe RO, Fredenburgh LE, Macias AA, et al. Reduction of nitric oxide synthase 2 expression by distamycin A improves survival from endotoxemia. *J Immunol.* (2004) 173:4147–53. doi: 10.4049/jimmunol.173.6.4147
35. Farley KS, Wang LF, Razavi HM, Law C, Rohan M, McCormack DG, et al. Effects of macrophage inducible nitric oxide synthase in murine septic lung injury. *Am J Physiol Lung Cell Mol Physiol.* (2006) 290:L1164–72. doi: 10.1152/ajplung.00248.2005
36. Li P, Allen H, Banerjee S, Seshadri T. Characterization of mice deficient in interleukin-1 beta converting enzyme. *J Cell Biochem.* (1997) 64:27–32. doi: 10.1002/(sici)1097-4644(199701)64:1<27::aid-jcb5>3.0.co;2-1.
37. Wang Q, Fang CH, Hasselgren PO. Intestinal permeability is reduced and IL-10 levels are increased in septic IL-6 knockout mice. *Am J Physiol Regul Integr Comp Physiol.* (2001) 281:R1013–23. doi: 10.1152/ajpregu.2001.281.3.R1013
38. Liu SF, Malik AB. NF-kappa B activation as a pathological mechanism of septic shock and inflammation. *Am J Physiol Lung Cell Mol Physiol.* (2006) 290:L622–45. doi: 10.1152/ajplung.00477.2005
39. Peng Z, Jiang Z, Guo H, Zhou M, Huang Y, Ning W, et al. Glycolytic activation of monocytes regulates the accumulation and function of neutrophils in human hepatocellular carcinoma. *J Hepatol.* (2020) 73:906–17. doi: 10.1016/j.jhep.2020.05.004
40. Chen D, Ning W, Jiang Z, Peng Z, Zhu L, Zhuang S, et al. Glycolytic activation of peritumoral monocytes fosters immune privilege via the PFKFB3-PD-L1 axis in human hepatocellular carcinoma. *J Hepatol.* (2019) 71:333–43. doi: 10.1016/j.jhep.2019.04.007
41. Zhang R, Li R, Liu Y, Li L, Tang Y. The glycolytic enzyme PFKFB3 controls TNF-α-induced endothelial proinflammatory responses. *Inflammation.* (2019) 42:146–55. doi: 10.1007/s10753-018-0880-x
42. Wang L, Cao Y, Gorshkov B, Zhou Y, Yang Q, Xu J, et al. Ablation of endothelial Pfkfb3 protects mice from acute lung injury in LPS-induced endotoxemia. *Pharmacol Res.* (2019) 146:104292. doi: 10.1016/j.phrs.2019.104292
43. Yang Q, Xu J, Ma Q, Liu Z, Zhou Y, Cai Y, et al. Disruption of endothelial Pfkfb3 ameliorates diet-induced murine insulin resistance. *J Endocrinol.* (2021) 250:93–104. doi: 10.1530/JOE-20-0524
44. Alkalay I, Yaron A, Hatzubai A, Orian A, Ciechanover A, Ben-Neriah Y. Stimulation-dependent I kappa B alpha phosphorylation marks the NF-kappa B inhibitor for degradation via the ubiquitin-proteasome pathway. *Proc Natl Acad Sci USA.* (1995) 92:10599–603. doi: 10.1073/pnas.92.23.10599
45. Van den Bossche J, Baardman J, de Winther MP. Metabolic characterization of polarized M1 and M2 bone marrow-derived macrophages using real-time extracellular flux analysis. *J Vis Exp.* (2015) 53424. doi: 10.3791/53424
46. Mills EL, Kelly B, Logan A, Costa ASH, Varma M, Bryant CE, et al. Succinate dehydrogenase supports metabolic repurposing of mitochondria to drive inflammatory macrophages. *Cell.* (2016) 167:457–70. doi: 10.1016/j.cell.2016.08.064

47. Takada Y, Mukhopadhyay A, Kundu GC, Mahabeleshwar GH, Singh S, Aggarwal BB. Hydrogen peroxide activates NF-kappa B through tyrosine phosphorylation of I kappa B alpha and serine phosphorylation of p65: evidence for the involvement of I kappa B alpha kinase and Syk protein-tyrosine kinase. *J Biol Chem.* (2003) 278:24233–41. doi: 10.1074/jbc.M212389200
48. Samuvel DJ, Sundararaj KP, Nareika A, Lopes-Virella MF, Huang Y. Lactate boosts TLR4 signaling and NF-kappaB pathway-mediated gene transcription in macrophages via monocarboxylate transporters and MD-2 up-regulation. *J Immunol.* (2009) 182:2476–84. doi: 10.4049/jimmunol.0802059
49. Lauterbach MA, Hanke JE, Serefidou M, Mangan M, Kolbe CC, Hess T, et al. Toll-like receptor signaling rewires macrophage metabolism and promotes histone acetylation via ATP-citrate lyase. *Immunity.* (2019) 51:997–1011. doi: 10.1016/j.immuni.2019.11.009
50. Dong Z, Li R, Xu L, Xin K, Xu Y, Shi H, et al. Histone hyperacetylation mediates enhanced IL-1β production in LPS/IFN-γ-stimulated macrophages. *Immunology.* (2020) 160:183–97. doi: 10.1111/imm.13183
51. Poels K, Schnitzler JG, Waissi F, Levels JHM, Stroes ESG, Daemen MJAP, et al. Inhibition of PFKFB3 hampers the progression of atherosclerosis and promotes plaque stability. *Front Cell Dev Biol.* (2020) 8:581641. doi: 10.3389/fcell.2020.581641
52. Vijayan V, Pradhan P, Braud L, Fuchs HR, Gueler F, Motterlini R, et al. Human and murine macrophages exhibit differential metabolic responses to lipopolysaccharide - A divergent role for glycolysis. *Redox Biol.* (2019) 22:101147. doi: 10.1016/j.redox.2019.101147
53. Zhu X, Meyers A, Long D, Ingram B, Liu T, Yoza BK, et al. Frontline Science: Monocytes sequentially rewire metabolism and bioenergetics during an acute inflammatory response. *J Leukoc Biol.* (2019) 105:215–28. doi: 10.1002/JLB.3HI0918-373R

Conflict of Interest: The authors declare that the research was conducted in the absence of any commercial or financial relationships that could be construed as a potential conflict of interest.

Publisher's Note: All claims expressed in this article are solely those of the authors and do not necessarily represent those of their affiliated organizations, or those of the publisher, the editors and the reviewers. Any product that may be evaluated in this article, or claim that may be made by its manufacturer, is not guaranteed or endorsed by the publisher.

frontiers in Cardiovascular Medicine

ORIGINAL RESEARCH
published: 05 October 2021
doi: 10.3389/fcvm.2021.716916

Endothelial Function and Arterial Stiffness Should Be Measured to Comprehensively Assess Obstructive Sleep Apnea in Clinical Practice

Jinmei Luo[1†], Xiaona Wang[1†], Zijian Guo[2], Yi Xiao[1], Wenhao Cao[1], Li Zhang[2], Linfan Su[1], Junwei Guo[1] and Rong Huang[1]*

[1] Department of Pulmonary and Critical Care Medicine, Peking Union Medical College Hospital, Chinese Academy of Medical Sciences, Peking Union Medical College, Beijing, China, [2] Department of Clinical Laboratory, Peking Union Medical College Hospital, Chinese Academy of Medical Sciences, Peking Union Medical College, Beijing, China

OPEN ACCESS

Edited by:
Changcheng Zhou,
University of California, Riverside,
United States

Reviewed by:
Mehmet Ozaydin,
Akdeniz Sifa Hastanesi, Turkey
Mosharraf Sarker,
Teesside University, United Kingdom

***Correspondence:**
Yi Xiao
xiaoyipumch@sina.com

[†] These authors have contributed equally to this work and share first authorship

Specialty section:
This article was submitted to Atherosclerosis and Vascular Medicine, a section of the journal Frontiers in Cardiovascular Medicine

Received: 29 May 2021
Accepted: 06 September 2021
Published: 05 October 2021

Citation:
Luo J, Wang X, Guo Z, Xiao Y, Cao W, Zhang L, Su L, Guo J and Huang R (2021) Endothelial Function and Arterial Stiffness Should Be Measured to Comprehensively Assess Obstructive Sleep Apnea in Clinical Practice. Front. Cardiovasc. Med. 8:716916. doi: 10.3389/fcvm.2021.716916

Objective: An effective clinical tool to assess endothelial function and arterial stiffness in patients with obstructive sleep apnea (OSA) is lacking. This study evaluated the clinical significance of subclinical markers for OSA management in males without serious complications.

Patients/Methods: Males without serious complications were consecutively recruited. Clinical data, biomarker tests, reactive hyperemia index (RHI), and augmentation index at 75 beats/min (AIx75) measured by peripheral arterial tonometry were collected. An apnea hypopnea index (AHI) cutoff of ≥15 events/h divided the patients into two groups.

Results: Of the 75 subjects, 42 had an AHI ≥15 events/h. Patients with an AHI ≥15 events/h had higher high-sensitivity C-reactive protein, tumor necrosis factor-alpha (TNF-α), vascular endothelial growth factor, and AIx75 values than the control group but no statistical difference in RHI was observed. After controlling for confounders, TNF-α was negatively correlated with the average oxygen saturation ($r = -0.258$, $P = 0.043$). RHI was correlated with the rapid eye movement (REM) stage percentage ($r = 0.306$, $P = 0.016$) but not with AHI ($P > 0.05$). AIx75 was positively correlated with the arousal index ($r = 0.289$, $P = 0.023$) but not with AHI ($r = 0.248$, $P = 0.052$).

Conclusions: In males with OSA without severe complications, TNF-α and AIx75 are independently related to OSA. The role of RHI in OSA management requires further elucidation. These markers combined can comprehensively evaluate OSA patients to provide more evidence for the primary prevention of coronary heart disease and treatment response assessment.

Keywords: obstructive sleep apnea, vascular endothelial function, arterial stiffness, reactive hyperemia index, augmentation index

INTRODUCTION

Obstructive sleep apnea (OSA) is the most common sleep breathing disorder. A literature-based analysis in 2019 indicated that ∼936 million patients had OSA in China, which was the country with the largest affected population (1). Recurrent apnea and hypopnea induced by OSA lead to intermittent hypoxia and fragmented sleep and affect people's quality of life and health. OSA is associated with many diseases including hypertension, cardiovascular disease, arrhythmia, heart failure, stroke, etc. (2–5). Even mild OSA without comorbidities may lead to vascular endothelial dysfunction and elevated arterial stiffness (6–8), which characterizes the early stage of arterial atherosclerosis and can predict cardiovascular events in the future (9–13). These subclinical abnormalities may provide additional evidence for the primary prevention of coronary heart disease and treatment response assessment.

An effective clinical tool to assess endothelial function and arterial stiffness in patients with obstructive sleep apnea (OSA) is lacking. Endothelial function can be measured by carotid intima media thickness (CIMT), flow-mediated dilation (FMD), and peripheral arterial tonometry (PAT) (14). Previous studies commonly used CIMT and FMD to measure vascular endothelial function (15, 16). However, increasing studies have applied the PAT technique to measure digital microvascular damage. The role of PAT in evaluating endothelial function in patients with OSA remains controversial (7, 17, 18). A lower reactive hyperemia index (RHI) derived from PAT indicates vascular endothelial dysfunction (9, 11). PAT is simple to perform in clinical practice and has a good reproducibility. A meta-analysis reported that FMD and PAT have similar prognostic values in predicting future cardiovascular events (19). Recent studies have shown that RHI was associated with the severity of OSA while others studies had negative results. Arterial stiffness also plays an important role in OSA evaluation and is considered a marker of atherosclerosis (20). A meta-analysis including 15 randomized controlled trials with 1,090 patients showed that continuous positive airway pressure (CPAP) can improve the augmentation index (AIx), which is a marker of arterial stiffness (21).

OSA is a heterogeneous disorder. It is unknown whether different subtypes of OSA have different vascular functions and stiffness. Gender can also influence endothelial function (22). Although some studies have applied PAT to explore the association between endothelial function and OSA, few studies have been performed in Chinese patients with OSA without severe comorbidities. Thus, we aimed to measure endothelial function and arterial stiffness using the PAT technique in Chinese males to assess the early vascular damage caused by OSA in patients without severe complications in clinical practice to provide more evidence for the primary prevention of coronary heart disease and treatment response assessment.

METHODS

Participants

Participants with suspected sleep breathing disorders, hypertension, or healthy volunteers who agreed to undergo a polysomnography (PSG) in the sleep disordered breathing clinic at Peking Union Medicine College Hospital were consecutively and prospectively recruited from August 30th, 2019 to December 31st, 2019. Participants were excluded for any of the following reasons: younger than 25 years old or older than 60 years old; previously received treatment for sleep apnea with positive airway pressure therapy; self-reported chronic diseases including uncontrolled hypertension, liver diseases, kidney diseases, lung diseases, perivascular diseases, coronary atherosclerosis diseases, heart diseases, diabetes, thromboembolism diseases, tumor, nerve system diseases, and mental diseases; and acute infections in the past 2 weeks. All participants gave written informed consent, and this study was approved by local ethical review boards and was performed in accordance with the Declaration of Helsinki. Institutional review board approval was obtained from the ethics commission of Peking Union Medical College Hospital, Chinese Academy of Medical Sciences, China (protocol number JS-2013).

Study Protocol

All the patients avoided vigorous exercises, smoking, alcohol, tea, coffee, and the night shift during the prior 24 h and were requested not to take naps or to take hypnotics or stimulants during the daytime before PSG. The patients' information including name, age, weight, height, and blood pressure before and after monitoring were recorded. Medical histories were taken by physicians at the sleep center. Comorbidities were self-reported. Hypertension was diagnosed when the patients had either a systolic blood pressure of $\geq$140 mmHg or a diastolic blood pressure of $\geq$90 mmHg at two different times or the current use of antihypertensive medications. Current smoking status was defined as patients who had been smoking in the past year.

Polysomnography

Overnight PSG was performed using the standard PSG device Remlogic N7000 (USA, Medicare) in the sleep disordered breathing laboratory the same night. Electroencephalogram, electrooculograms, chin electromyogram, nasal detected by airflow pressure transducer, respiratory effort, electrocardiography, and position were recorded. All the sleep scoring and respiratory events were analyzed manually by a technician and checked by experienced sleep physicians. Manually sleep scoring and respiratory events were analyzed according to the AASM Manual 2.3 for the Scoring of Sleep and Associated Events in 2016 (23). Sleep scoring was performed for stages N1, N2, N3, rapid eye movement (REM), and wake. The apnea hypopnea index (AHI) was defined as the total number of apnea and hypopnea events each hour. The oxygen desaturation index (ODI) was defined as the frequency of instances when the blood oxygen levels decreased (desaturation) by 3% or more. The lowest pulse arterial oxygen saturation ($LSpO_2$) was defined as the lowest pulse oxygen saturation during sleep. T90 (the percentage of SpO_2 lower than 90%) was defined as the percentage of time that the oxygen saturation was lower than 90% during the monitoring time. The arousal index (AI) was defined as average number of arousals per hour of total sleep

time. According to the American Academy of Sleep Medicine practice guidelines (24), we used an AHI of ≥15 events/h as a cutoff to divide the patients into two groups: the AHI <15 events/h group and the AHI ≥15 events/h group. OSA severity was defined as follows: mild OSA, 15 events/h > AHI ≥5 events/h; moderate OSA, 30 events/h > AHI ≥15 events/h; and severe OSA, AHI ≥30 events/h; the control group was defined as AHI <5 events/h.

Digital Vascular Measurements

We used an automated device (EndoPAT2000; Itamar Medical, Caesarea, Israel) to measure the endothelial function and arterial stiffness the morning after the PSG. The participants were asked to lie on their backs for at least 30 min after blood was drawn, and the cuffs were placed on one arm 2 cm above the cubital fossa. PAT probes were placed on each index or middle finger. The baseline pulse amplitude was recorded for 5 min. Arterial flow was weakened until the pulse signal disappeared on one side for 5 min by inflating the cuffs to at least 200 mmHg (or 60 mmHg above the systolic pressure). After 5 min, the cuffs were deflated to induce reactive hyperemia, and the PAT signals were recorded for another 5 min. The contralateral fingers were used to control for systemic changes. The PAT ratio was the ratio of the post-deflate pulse amplitude 90–120 s after cuff release to the baseline mean pulse amplitude. This result was divided by the corresponding ratio from the control finger. Finally, the RHI was calculated automatically by computer software. A higher RHI value indicates better endothelial function (19). Simultaneously, EndoPAT could automatically calculate arterial stiffness, which was expressed as the augmentation index (AIx), based on radial pulse waves. Since heart rate may affect arterial stiffness, arterial stiffness was expressed by AIx75, which was corrected at a heart rate of 75 beats per minute (25).

Biological Measurements

Fasting vein blood samples were collected in the morning following the PSG. Whole blood cell analysis, liver function, renal function, plasma glucose, uric acid, glycated hemoglobin (HbA1C), and serum lipid levels were directly measured in accredited laboratories using standard techniques within an hour. We obtained plasma and serum samples after centrifugation within half an hour at 3,000 g at 4°C for 15 min; these samples were then stored at −20°C for <1 week and transferred to −80°C until the assay was performed within half a year. Serum tumor necrosis factor-alpha (TNF-α) levels were measured using the IMMULITE 1000 Automatic Chemiluminescence Immunoassay (Siemens Medical, USA). Serum vascular cell adhesion molecule (VCAM), endothelin-1 (ET-1), and plasma vascular endothelial growth factor (VEGF) were measured using the Human Svcam-1/CD106 Quantikine ELISA Kit (RD, USA), the Endothelin-1 Quantikine ELISA kit (RD, USA), and the Human VEGF Quantikine ELISA Kit (RD, USA), respectively, according to the instruction books.

Statistical Analysis

All data were analyzed using SPSS 22.0 and GraphPad Prism8 (GraphPad Software Inc., La Jolla, USA). The normality of the variables was tested with the Kolmogorov–Smirnov test. An unpaired, two-tailed *t*-test and a Chi-square analysis were used for comparisons between groups. The non-parametric Mann–Whitney *U*-test was used when the data were not normally distributed. The results were expressed as the mean ± standard deviations or as the median with the interquartile range. Pearson's or Spearman's methods were used to analyze the correlation between the laboratory data and PSG results. A partial correlation analysis was used to control for confounding factors and analyze the relationship between PSG and laboratory data. An ANOVA was used for multi-group comparisons, and the Kruskal–Wallis test was used for non-parametric multi-group comparisons. The confounding factors (biomarkers, vascular endothelial function, and arterial stiffness) were analyzed by a multiple linear regression. $P < 0.05$ was considered statistically significant.

RESULTS

A total of 502 patients underwent sleep respiratory monitoring in the sleep centers from August 30th, 2019 to December 31st, 2019. After excluding patients who did not meet the inclusion criteria or refused to join the research, or in whom more than 20% of polysomnography signals were lost, 75 subjects were enrolled in this study (**Figure 1**). The average patient age was 39.21 ± 8.34 years, and the average body mass index (BMI) was 26.68 ± 3.22 kg/m^2. There were 26 (34.7%) hypertensive patients and 19 (25.3%) current smokers. The average sleep time was 452.87 ± 37.27 min and the average sleep efficiency was 91.95 ± 7.15%. The average AHI was 28.20 ± 26.59 events/h. The average SpO_2 was 96.33 ± 2.11%. Using an AHI of ≥15 events/h as the cutoff, there were 33 participants with an AHI of <15 events/h and 42 participants with an AHI of ≥15 events/h.

The high-sensitivity C-reactive protein (hsCRP) levels ranged from 0.17 to 25.83 mg/L, but only two (2.7%) cases had hsCRP levels higher than the normal range. The average TNF-α level was 8.20 ± 3.63 pg/ml, and ET-1 levels ranged from 0.089 to 2.41 pg/ml. VCAM levels ranged from 346.48 to 1168.02 ng/ml, VEGF levels ranged from 3.91 to 217.91 pg/ml, the RHI ranged from 1.12 to 3.13, and the AIx75 ranged from −38 to 42%.

The Relationship Between OSA Severity, Endothelial Function, and Arterial Stiffness

Table 1 presents the demographic, clinical, and laboratory data of the participants. Patients with an AHI of ≥15 events/h had higher hsCRP, VEGF, and AIx75 values than the control group did; however, no significant differences in TNF-α, ET-1, VCAM, or RHI values were observed between the two groups ($P > 0.05$). **Table 2** shows that VEGF and AIx75 values were significantly and gradually elevated whereas there was no statistical association of TNF-α, ET-1, VCAM, or RHI with OSA severity. *Post-hoc* comparisons (**Figure 2**) revealed that severe patients had higher TNF-α, VEGF, and AIx75 values than those of the control group, higher VEGF levels than those of the moderate patients, and higher AIx75 values than those of the mild patients. Moderate

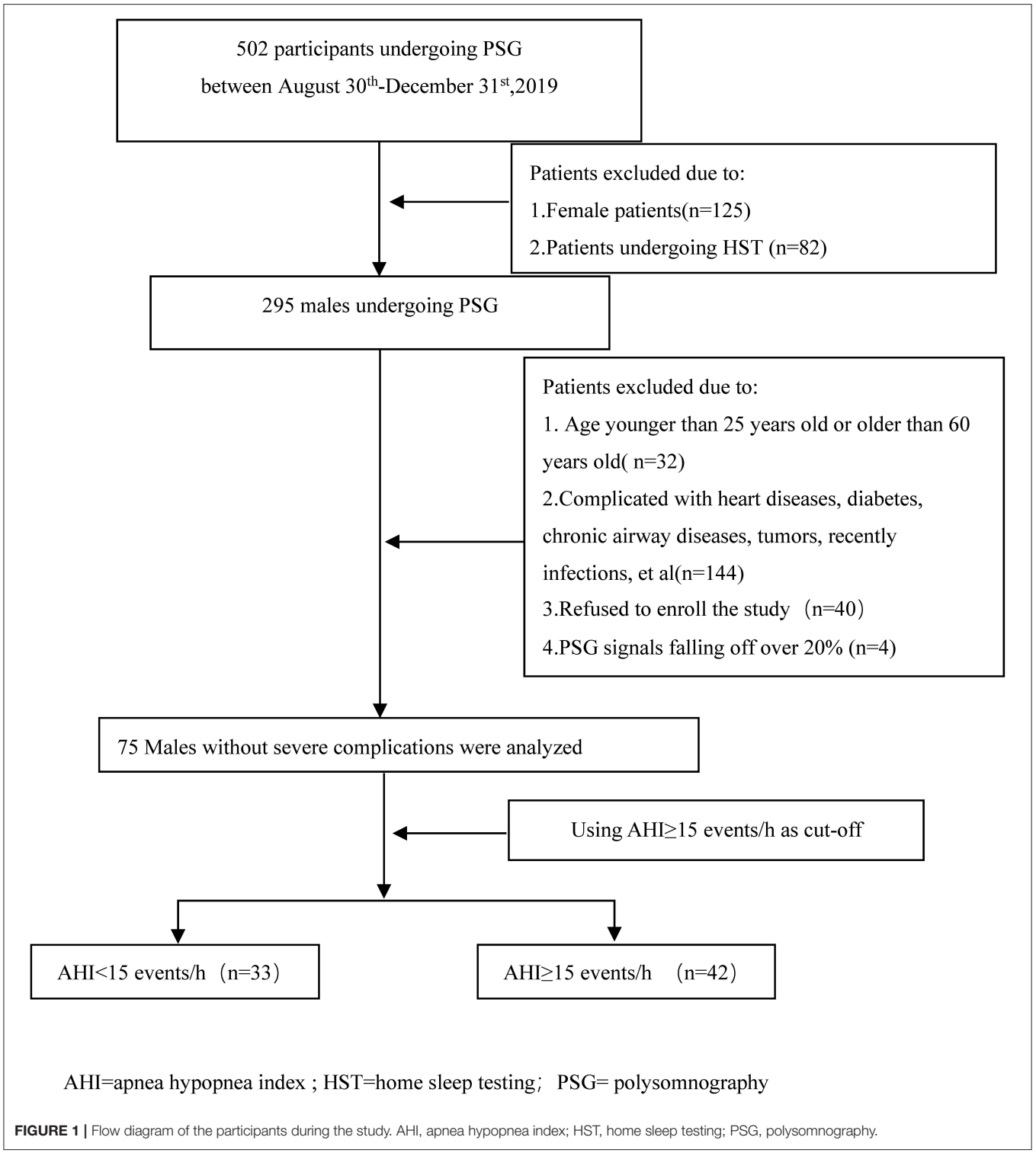

FIGURE 1 | Flow diagram of the participants during the study. AHI, apnea hypopnea index; HST, home sleep testing; PSG, polysomnography.

OSA patients had higher ET-1 and AIx75 values than those of the control group. No significant differences in VCAM or RHI were found between the different OSA severity groups in the *post-hoc* tests.

Relative Associations Between OSA, Endothelial Function, and Arterial Stiffness

We further explored the relative associations between endothelial function, arterial stiffness, and OSA using a bivariate analysis.

TABLE 1 | Clinical data and laboratory data of participants.

	All	AHI <15 events/h	AHI ≥15 events/h	*P*-value
n	75	33	42	
Age (years)	39.21 ± 8.34	38.61 ± 7.67	39.69 ± 8.90	0.58
BMI (kg/m^2)	26.68 ± 3.22	25.60 ± 3.00	27.53 ± 3.17	<0.01
Hypertension (*n*)	26	5	21	<0.01
Current smokers (*n*)	19	5	14	0.072
Rhinitis (*n*)	26	12	14	0.71
Stage N1 (%/TST)	7.72 ± 5.16	7.49 ± 4.56	7.90 ± 5.63	0.73
Stage N2 (%/TST)	41.46 ± 11.2	38.76 ± 10.37	43.58 ± 11.50	0.06
Stage N3 (%/TST)	25.31 ± 12.45	26.98 ± 10.23	24 ± 13.92	0.31
Stage REM (%/TST)	17.20 ± 6.11	17.91 ± 6.70	16.64 ± 5.62	0.38
Stage Wake (%/TST)	8.05 ± 7.15	8.57 ± 6.67	7.64 ± 7.57	0.58
AI (events/h)	8.4 (5, 14.6)	6.3 (4.15, 9.2)	12.35 (6.48, 21.65)	<0.01
AHI (events/h)	16.6 (5.90, 51.30)	3.4 (0.8, 8.3)	48 (25.58, 64.83)	<0.01
ODI (events/h)	15.50 (1.80, 47.30)	1.5 (0.65, 4.95)	41.3 (20.95, 61.65)	<0.01
Mean SpO_2 (%)	96.33 ± 2.11	97.3 ± 1.36	95.57 ± 2.30	<0.01
$LSpO_2$ (%)	85.59 ± 7.90	91.55 ± 3.73	80.90 ± 7.10	<0.01
T90 (%)	0.1 (0, 1.10)	0 (0, 0)	0.8 (0.275, 2.33)	<0.01
HB (g/L)	155.83 ± 11.26	155.15 ± 10.93	156.36 ± 11.62	0.65
ALT (U/L)	32 (20, 54)	28 (19, 40.5)	39 (25.5, 56)	0.02
Cr (μ mol/L)	76.93 ± 9.60	79.30 ± 8.97	75.07 ± 9.78	0.058
GLU (mmol/L)	4.9 (4.7, 5.3)	4.8 (4.5, 5.1)	5.1 (4.8, 5.5)	<0.01
HBA1C (%)	5.4 (5.1, 5.6)	5.2 (5.05, 5.5)	5.5 (5.3, 5.6)	<0.01
TG (mmol/L)	1.46 (1.04, 2.39)	1.14 (0.91, 1.89)	1.72 (1.36, 3.33)	<0.01
TC (mmol/L)	4.81 ± 0.77	4.73 ± 0.78	4.87 ± 0.76	0.41
LDLC (mmol/L)	3.11 ± 0.72	3.12 ± 0.68	3.10 ± 0.76	0.88
HDL (mmol/L)	1.10 ± 0.26	1.17 ± 0.24	1.05 ± 0.26	0.03
UA (μmol/L)	405.80 ± 82.98	395.85 ± 71.94	413.62 ± 90.81	0.36
hsCRP (mg/L)	1.17 (0.69, 2.01)	0.8 (0.5, 1.33)	1.64 (0.85, 2.44)	<0.01
TNF-α (pg/ml)	7.2 (6, 8.8)	6.6 (5.8, 8)	7.9 (6.08, 9.23)	0.07
ET-1 (pg/ml)	0.36 (0.26, 0.63)	0.36 (0.21, 0.54)	0.36 (0.26, 0.68)	0.46
VCAM (ng/ml)	530.36 (461.35, 617.61)	520.51 (451.62, 619.35)	532.48 (477.84, 610.27)	0.51
VEGF (pg/ml)	25.47 (19.88, 34.26)	22.28 (17.09, 29.86)	28.27 (21.28, 35.45)	0.03
AIx75 (%)	−4 (−14, 8)	−12 (−18.5, 0)	−1 (−8, 17.25)	<0.01
RHI	1.84 ± 0.48	1.78 ± 0.48	1.89 ± 0.48	0.32

Data presented as mean ± SD or the median with interquartile range. AI, arousal index; AHI, apnea hypopnea index; ALT, alanine transaminase; AIx75, augmentation Index@75 beats/minute; BMI, body mass index; Cr, Creatinine; ET-1, endothelin-1; GLU, glucose; HB, hemoglobin; HbA1C, hemoglobin A1C; HDL, high density lipoprotein; hsCRP, high sensitivity C reactive protein; LDLC, low density lipoprotein; ODI, oxygen desaturation index; $LSpO_2$, lowest pulse arterial oxygen saturation; REM, rapid eye movement; RHI, reactive hyperaemia index; SpO_2, oxygen saturation; T90, percentage of sleep time with oxygen saturation <90%; TC, total cholesterol; TG, triglyceride; TST, total sleep time; TNF-α, tumor necrosis factor alpha; UA, uric acid; VCAM, vascular cell adhesion molecule; VEGF, vascular endothelial growth factor.

TNF-α was positively associated with BMI ($r = 0.356$, $P < 0.05$), ODI ($r = 0.277$, $P < 0.05$), and T90 ($r = 0.306$, $P < 0.05$) and negatively correlated with the mean SpO_2 ($r = -0.389$, $P < 0.05$) and $LSpO_2$ ($r = -0.320$, $P < 0.05$). ET-1 was negatively correlated with the percentage in stage N1 ($r = -0.251$, $P < 0.05$). VEGF was positively correlated with BMI ($r = 0.250$, $P < 0.05$), the percentage in stage N3 ($r = 0.237$, $P < 0.05$), AHI ($r = 0.349$, $P < 0.05$), ODI ($r = 0.348$, $P < 0.05$), and T90 ($r = 0.265$, $P < 0.05$) and was negatively correlated with the percentage in the wake stage ($r = -0.254$, $P < 0.05$), the mean SpO_2 ($r = -0.259$, $P < 0.05$), and $LSpO_2$ ($r = -0.268$, $P < 0.05$). RHI was only positively correlated with the percentage in the REM stage ($r = 0.31$, $P = 0.007$). AIx75 was positively correlated with age ($r = 0.559$, $P < 0.0001$), AHI ($r = 0.367$, $P = 0.001$), ODI ($r = 0.298$, $P = 0.009$), AI ($r = 0.307$, $P = 0.007$), and T90 ($r = 0.288$, $P = 0.012$) and was negatively correlated with $LSpO_2$ ($r = 0.305$, $P = 0.008$).

After controlling for age, BMI, rhinitis, hypertension, smoking, glucose level, HbA1C, hemoglobin (Hb), creatinine (Cr), total cholesterol (TC), triglycerides (TG), low-density lipoprotein (LDLC), and high-density lipoprotein (HDL), we found that TNF-α was negatively associated with the mean SpO_2 ($r = -0.258$, $P = 0.043$; **Figure 3**). No significant correlations between hsCRP, VEGF, ET-1, VCAM, and the parameters of

TABLE 2 | The clinical data and laboratory data in different severity obstructive sleep apnea.

	Normal	Mild OSA	Moderate OSA	Severe OSA	*P*-value
N	18	15	13	29	
Age (years old)	38.28 ± 8.58	39.00 ± 6.70	41.62 ± 10.24	38.83 ± 8.28	0.72
BMI (kg/m^2)	24.89 ± 2.97	24.46 ± 2.89	26.46 ± 1.84	28.01 ± 3.54	0.01
Hypertension (*n*)	3	2	3	18	<0.01
Current smoker (*n*)	3	2	2	12	0.09
AHI (events/h)	0.85 (0.6, 1.8)	8.3 (6.6, 11.5)	19.8 (16.20, 24.75)	57.7 (46.4, 69.8)	<0.01
AI (events/h)	5.25 (3.3, 8.2)	7 (4.7, 9.9)	7.8 (5.5, 11.45)	16 (7.4, 27.5)	<0.01
Mean SpO_2 (%)	97.428 ± 1.43	97.15 ± 1.31	96.10 ± 2.01	95.33 ± 2.41	<0.01
$LSpO_2$ (%)	93.00 ± 3.12	89.8 (± 3.75)	84.54 ± 5.83	79.28 ± 7.11	<0.01
T90 (%)	0 (0, 0)	0 (0, 0.10)	0.30 (0.05, 0.80)	1.4 (0.35, 3.4)	<0.01
TNF-α (pg/ml)	6.51 (5.85, 7.63)	6.7 (5.5, 8.4)	6.8 (5.65, 16.35)	8.1 (6.4, 9.2)	0.20
VEGF (pg/ml)	20.68 (18.88, 27.87)	23.08 (13.49, 34.26)	20.68 (17.89, 31.06)	30.263 (26.27, 43.44)	<0.01
ET-1 (pg/ml)	0.33 (0.20, 0.46)	0.43 (0.22, 0.63)	0.46 (0.31, 1.3)	0.34 (0.26, 0.60)	0.14
VCAM (ng/ml)	543.42 (472.05, 622.52)	507.30 (437.69, 587.33)	522.15 (450.93, 649.52)	533.30 (486.65, 600.91)	0.72
AIx75 (%)	−15 (−18.25, −1.75)	−11 (−22, 2)	−1 (−8.5, 20)	−1 (−8, 17.5)	<0.01
RHI	1.78 ± 0.46	1.77 ± 0.51	1.98 ± 0.58	1.85 ± 0.44	0.64

Data presented as mean ± SD or the median with interquartile range. AI, arousal index; AHI, apnea hypopnea index; AIx75, augmentation Index@75 beats/minute; BMI, body mass index; ET-1, endothelin-1; GLU, glucose; HbA1C, hemoglobin A1C; $LSpO_2$, lowest pulse arterial oxygen saturation; RHI, reactive hyperaemia index; SpO_2, oxygen saturation; T90, percentage of sleep time with oxygen saturation <90%; TNF-α, tumor necrosis factor alpha; VCAM, vascular cell adhesion molecule; VEGF, vascular endothelial growth factor.

PSG were observed. RHI was also positively correlated with the percentage in the REM stage ($r = 0.306$, $P = 0.016$) but was not correlated with other parameters of PSG or clinical characteristics of OSA. AIx75 remained positively correlated with the AI ($r = 0.289$, $P = 0.023$), but the correlation between AIx75 and AHI was not statistically significant ($r = 0.248$, $P = 0.052$; **Figure 3**).

We used a multiple step regression to analyze the relationships between TNF-α, RHI, and AIx75 and age, BMI, AHI, AI, PSG parameters (mean SpO_2, $LSpO_2$, T90, percentages in stages N1, N2, N3, REM, and wake), and cardiovascular risk factors (smoking, hypertension, blood glucose, HbA1C, TC, TG, HDL, and LDLC). The results showed that TNF-α was positively correlated with the percentage in stage N1 ($B = 0.166$, $P = 0.025$) and was negatively correlated with the mean SpO_2, HDL, and TG ($B = -0.398$, $P = 0.034$; $B = -5.263$, $P = 0.002$; $B = -0.657$, $P = 0.013$, respectively). TNF-α was not significantly correlated with age, BMI, hypertension, smoking, AHI, blood glucose, or HbA1c. RHI was positively correlated with hypertension and the percentage in the REM stage ($B = 0.275$, $P = 0.013$; $B = 0.026$, $P = 0.003$, respectively) but was not significantly correlated with age, BMI, smoking, AHI, SpO_2, $LSpO_2$, T90, blood glucose, or HbA1c. AIx75 was positively correlated with age, AI, and TC ($B = 1.201$, $P < 0.001$; $B = 0.547$, $P = 0.001$; $B = 6.036$, $P = 0.004$, respectively) but was not significantly correlated with BMI, smoking, AHI, SpO_2, $LSpO_2$, T90, blood glucose, HbA1C, TG, LDLC, or HDL.

DISCUSSION

Our study comprehensively assessed systemic inflammatory biomarkers and vascular endothelial function in Chinese middle-aged men with moderate and severe OSA without severe complications. We found that these patients had only low levels of systemic inflammatory biomarkers and vascular endothelial biomarkers, which were mainly manifested by elevated hsCRP, TNF-α, and VEGF levels. After controlling for the confounding factors, TNF-α was negatively correlated with the average SpO_2 but was not correlated with AHI. RHI was still positively correlated with the REM ratio but was not with the average SpO_2, $LSpO_2$, or AHI values. There was a correlation between AIx75 and AI, but the correlation between AIx75 and AHI was not statistically significant. The multiple stepwise regression analysis showed that TNF-α was positively correlated with the percentage in stage N1 and was negatively correlated with the average SpO_2, HDL, and TG values. RHI was positively correlated with hypertension and the percentage in the REM stage whereas AIx75 was positively correlated with age, AI, and TC.

Although many studies on systemic inflammatory biomarkers and the vascular endothelial function of OSA have been reported, most such studies did not exclude patients with related cardiovascular diseases and diabetes or only assessed a single marker, which fails to effectively compare the value of various markers to evaluate OSA patients. Although we did not find a direct association between the AHI and RHI detected by PAT testing, we found that some clinical significance could be determined from measuring hsCRP, TNF-α, VEGF, arterial stiffness, and vascular endothelial function in patients with moderate and severe OSA. Additionally, the results noted that inflammatory indicators are not only associated with hypoxia induced by OSA but also with sleep structural disorders, which confirmed that hypoxia and sleep fragmentation were two mechanisms by which OSA leads to abnormal vascular endothelial function and changes in arterial stiffness.

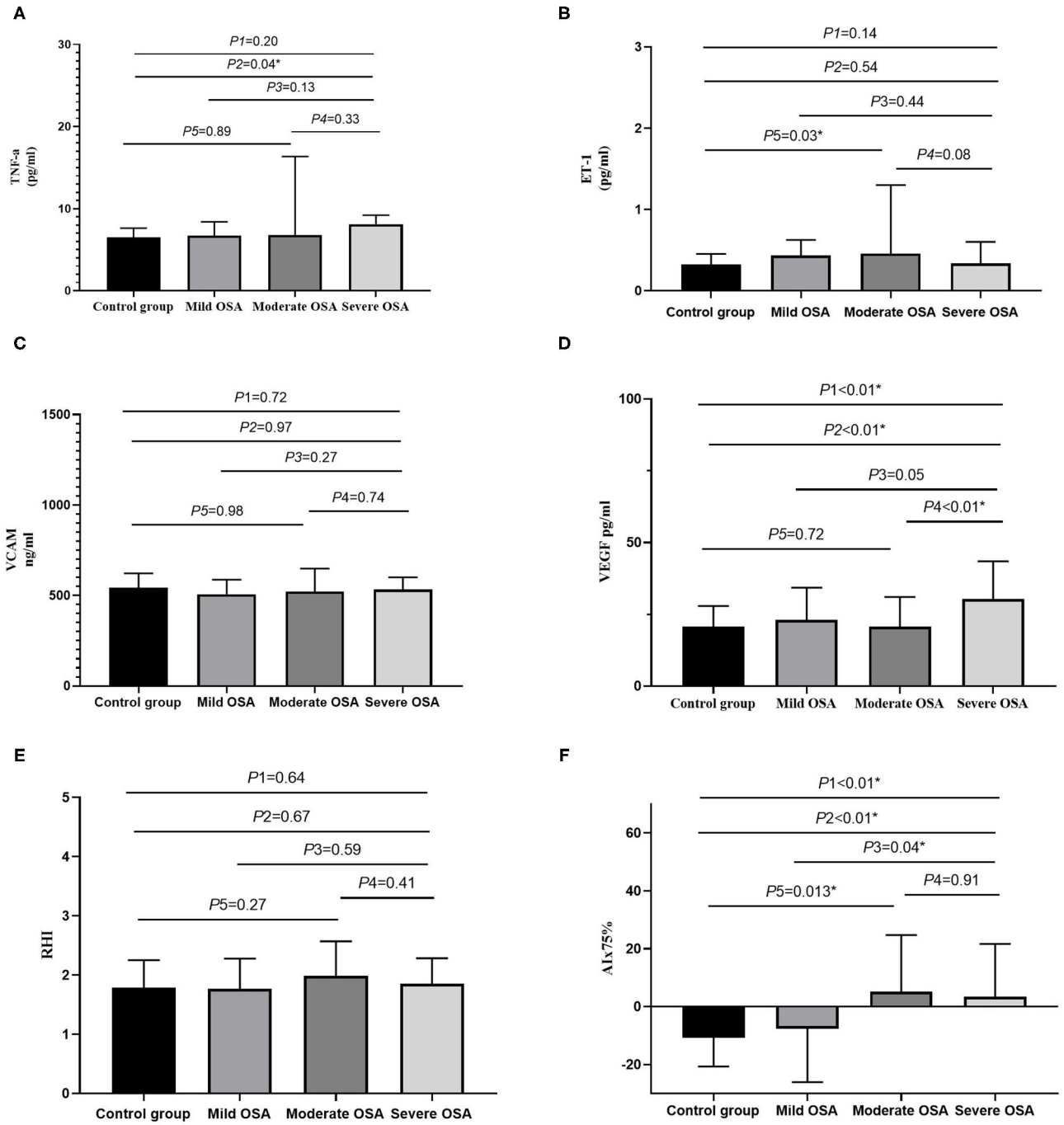

FIGURE 2 | The bar diagrams showing markers in patients with OSA. **(A)** The relationship between TNF-α and OSA severity. **(B)** The relationship between ET-1 and OSA severity. **(C)** The relationship between VCAM and OSA severity. **(D)** The relationship between VEGF and OSA severity. **(E)** The relationship between RHI and OSA severity. **(F)** The relationship between AIx75 and OSA severity. AI, arousal index; AHI, apnea hypopnea index; AIx75, augmentation Index@75 beats/minute; BMI, body mass index; ET-1, endothelin-1; GLU, glucose; HbA1C, hemoglobin A1C; $LSpO_2$, lowest pulse arterial oxygen saturation; RHI, reactive hyperaemia index; SpO_2, oxygen saturation; T90, percentage of sleep time with oxygen saturation <90%; TNF-α, tumor necrosis factor alpha; VCAM, vascular cell adhesion molecule; VEGF, vascular endothelial growth factor; *P*1, four groups comparison; *P*2, severe OSA vs. control group; *P*3, severe OSA vs. mild OSA; *P*4, severe OSA vs. moderate OSA; *P*5, moderate OSA vs. control group; $^*P < 0.05$.

Currently, there are limited studies measuring endothelial function using the PAT technique in OSA patients. However, our research did not identify an association between RHI and OSA severity. In fact, the role of RHI originating from PAT in OSA patients remains uncertain. Our results were similar with those of some previous studies. Most of these studies were performed

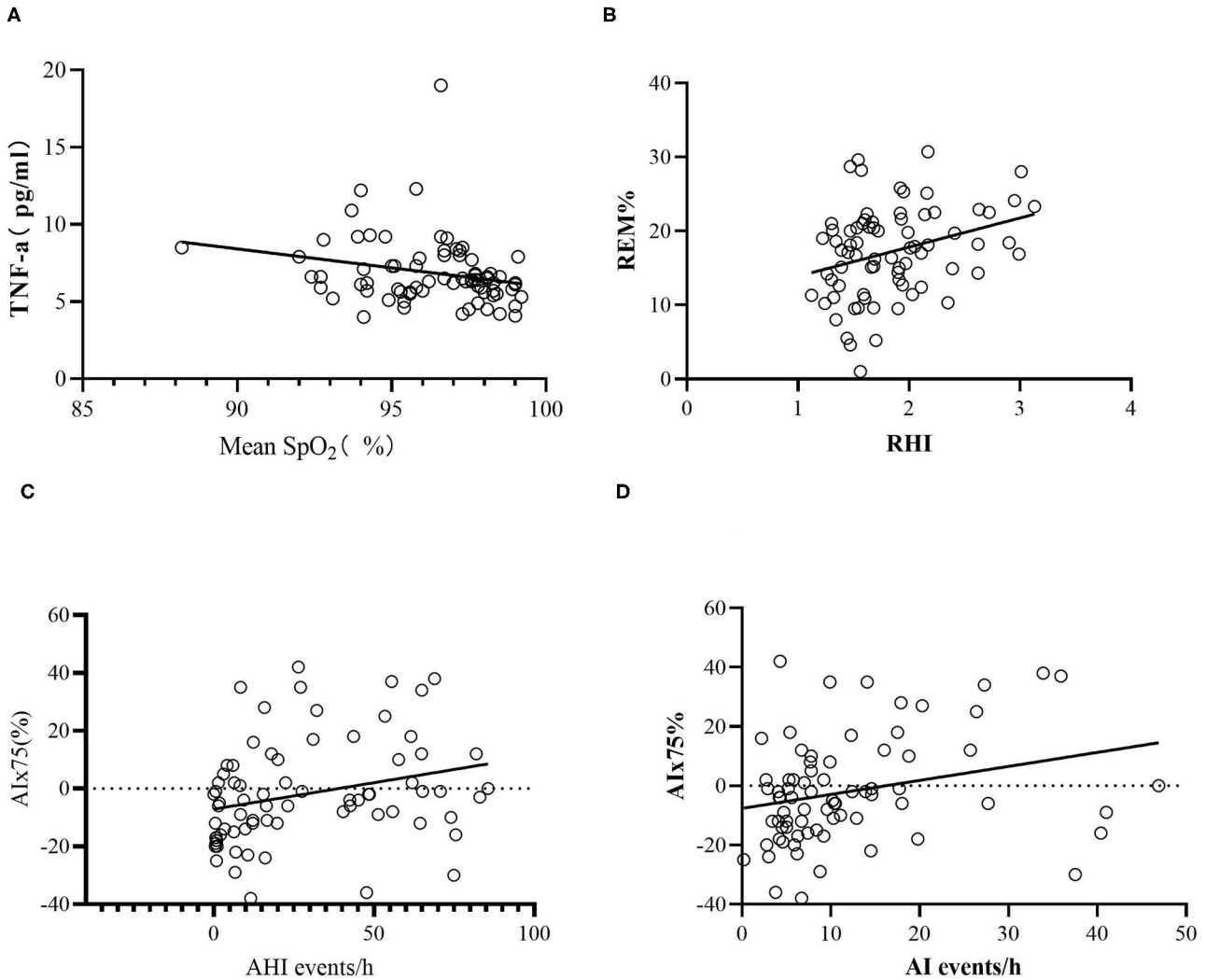

FIGURE 3 | Scatter plots of laboratory data. **(A)** The relative associations between TNF-α and mean SpO_2. **(B)** The relative associations between REM% and RHI. **(C)** The relative associations between AIx75 and AHI. **(D)** The relative associations between AIx75 and AI. AHI, apnea hypopnea index; AI, arousal index; AIx75, augmentation Index@75 beats/minute; SpO_2, oxygen saturation; TNF-α, tumor necrosis factor alpha; REM%, the percentage of stage rapid eye movement in total sleep time; RHI, reactive hyperaemia index.

in OSA patients with complications including obesity, diabetes, and ischemic stroke (18, 26, 27). However, other studies had distinct results. For example, they noted that RHI was not only associated with OSA severity but also with the level of hypoxia and sleep fragmentation (7, 8, 17, 28). Farooqui et al. compared RHI, FMD, and CIMT in 20 cases with OSA and 20 control cases without any complications and found that patients with moderate and severe OSA had lower FMD and RHI and a greater CIMT, but these variables were not correlated with OSA severity (8). Zhang et al. found that the RHI of children with OSA was significantly lower than that of simple snore patients and was independently correlated with age, BMI, and the respiratory AI using a stepwise regression (28). A systematic review of 12 studies that applied PAT and sleep breathing monitoring in 730 cases without cardiocerebrovascular diseases showed that endothelial function was related to severe OSA. In the subgroup analysis of patients with hypertension, obesity, and diabetes, the correlations between endothelial function and severe OSA were not significant (7).

Additionally, the roles of PAT and FMD in evaluating the endothelial function of OSA were inconsistent. Previous studies were mainly performed using FMD. FMD was used to assess the changes in the dilation of the diameter resulting from reactive hyperemia using B type ultrasound whereas PAT was performed to detect the volume variation of the digital vascular bed using the PAT technique. The principle of both methods involves measuring the change of blood vessel volume caused by nitric oxide (NO) released by the blood vessels after pressure (29). However, FMD measures vessels in the brachial artery and PAT measures the blood vessels at the end of the finger, which

represent the lesions of the capillaries. Also, recent studies found that lower-limb FMC responses were blunted when endothelial-derived hyperpolarizing factors or prostaglandin production was inhibited which may explain the different results of FMD and PAT (30). FMD repeatability is relatively low and requires skilled operators to perform. Conversely, PAT is performed automatically by a machine and thus has high repeatability and little correlation with the operator. The Framingham Heart Study also found no correlation between PAT-RHI and FMD, suggesting that vascular endothelial injury in different parts may provide different information for predicting cardiovascular disease, but injuries in all parts can predict cardiovascular disease (31, 32). Studies have shown that when the RHI is 1.35, the sensitivity and specificity of detecting endothelial dysfunction in the coronary arteries are 80% and 85%, respectively (13). PAT has been shown to predict cardiovascular disease in very few prospective studies. PAT was tested in a group of 270 patients and was found to be an independent predictor of cardiovascular events after 7 years of follow-up (11). The RHI was also found to be an independent predictor of cardiovascular events and to improve the predictive value of the Framingham risk score in a 2.8-year follow-up study of 528 patients with a high risk of cardiovascular disease (33). Currently, few relevant studies have reported on the ability of PAT to predict cardiovascular disease in patients with OSA.

Our research revealed that RHI was correlated with the ratio of time in the REM stage even after controlling for confounding factors including age, BMI, smoking, and metabolic factors. The association between PAT and the ratio of time in the REM stage has not been reported until now. Previous studies have reported that REM sleep was linked to vascular endothelial dysfunction. The study by Cooper et al. in 100 non-shift adults, of whom 52% had OSA, found that a decrease in FMD was associated with an increase in the Pittsburgh sleep quality index, prolonged REM sleep latent time, and a reduced REM sleep ratio (34). Furthermore, a multicenter population-based cross-sectional study also found that REM sleep deprivation was associated with greater risk of cardiovascular mortality in middle-aged and older adults (35). However, the reason for the association between vascular endothelial dysfunction and REM deprivation was unclear. REM sleep has been demonstrated to play an important role in studying, memory, and daytime function (36). The NO in the brain contributed to REM sleep (37) while FMD and PAT measure vascular function through NO-mediated vascular dilation. An animal study showed that REM sleep deprivation could induce endothelial dysfunction and hypertension through the endothelial NO synthase pathway (38). Some animal studies also showed that REM sleep deprivation could create oxidative stress and reactive oxygen species which may contribute to endothelial dysfunction (39, 40).

Our research also indicates that RHI was positively related to hypertension. Hypertension is a risk factor for many cardiovascular diseases. In theory, hypertensive patients would have a lower RHI. The study of Framingham cohorts with 1,957 subjects found that RHI was negatively correlated with hypertension in age- and sex-adjusted models but not related with hypertension in stepwise multivariable linear regression models (12). A study of a Brazilian cohort in 2014 showed that systolic pressure was positively associated with RHI and that patients using hypotensive drugs had a lower RHI (10). Another study in chronic kidney disease patients reported a positive association between systolic pressure and RHI, which was similar with our results (41). Consequently, the association between RHI and hypertension is uncertain. We speculated that the repeatability of RHI was poor in hypertensive patients because sympathetic activity changes induced increased heart rate variation (42).

Many studies have suggested that arterial stiffness is an early marker of atherosclerosis. At present, most studies on the relationship between OSA and arterial stiffness are mainly based on pulse wave velocity analysis. Founded on the theory of arterial reflected waves, increasing attention has been paid to the reflected wave enhancement index based on pulse wave shape analysis. Increased AIx has been shown to predict future cardiovascular events (43), and the radial AIx can be used as an alternative to the marker of primary prevention of atherosclerosis (44). A meta-analysis showed that the vascular AIx of moderate and severe OSA increased significantly compared with that of the control group (16), and CPAP can improve the AIx of OSA (21).

Our study found that after controlling for confounding factors, AIx75 was still associated with the AI of OSA sleep fragmentation, suggesting that OSA sleep fragmentation is one of the reasons for atherosclerosis independent of age, BMI, hypertension, and other factors. The partial correlation between AIx75 and AHI did not reach statistical significance, which may be related to the small sample size. At present, there are insufficient studies on the application of the peripheral vascular tension technique to measure arterial stiffness in OSA patients. A study assessed arterial stiffness in 37 patients with ischemic stroke using PAT technology and found that even after controlling for sex, BMI, hypertension, and diabetes, AIx was correlated with the AI and mean oxygen saturation (26). Theorell-Haglow et al. measured radial artery stiffness in OSA patients using the flat tension method and found that OSA severity was related to the radial artery stiffness AIx75 (45). The results of this study are consistent with those above-mentioned previous studies. The PAT technique is simple to conduct, highly repeatable, and can be used routinely to assess the arterial stiffness of OSA patients, which is beneficial for detecting early changes of atherosclerosis in OSA patients.

Our study has some limitations. Firstly, we only performed this study in males, so the results cannot be generalized to all patients with OSA. However, males comprise the majority of OSA patients, so these results can still help a large proportion of patients. Secondly, the PAT value is influenced by many factors including the effects of environment, stress, diet, age, BMI, exercise, smoking, and disease. To detect the evaluation role of PAT in OSA patients, we only included OSA males without severe complications. All of the patients were advised to avoid rigorous exercises within 24 h, smoking, tea, and coffee. PAT values were measured at least half an hour before or after blood drawing. However, changes in the sleep environment and stress due to blood puncture may inevitably have affected the

results of the vascular endothelial function. Additionally, the small sample size of this study may have affected the results. In the future, it is necessary to further expand the sample size and observe the changes of treatment response to verify our results.

CONCLUSION

In conclusion, our assessments including systemic inflammatory indicators, endothelial function, and arterial stiffness showed that moderate and severe OSA patients without severe complications only had low levels of inflammation and vascular endothelial injury markers, which were mainly manifested by hsCRP, TNF-α, and VEGF, among which TNF-α was independently associated with OSA. AIx75, the arterial stiffness marker measured by PAT, is closely related to OSA. The relationship between RHI and OSA requires further investigation. Endothelial function and arterial stiffness should be measured to comprehensively assess the early vascular damages by OSA without severe complications in clinical practice to provide more evidence for the primary prevention of coronary heart disease and treatment response assessment.

DATA AVAILABILITY STATEMENT

The original contributions presented in the study are included in the article/supplementary material, further inquiries can be directed to the corresponding author/s.

ETHICS STATEMENT

The studies involving human participants were reviewed and approved by the Ethics Commission of Peking Union Medical College Hospital, Chinese Academy of Medical Sciences, China (protocol number JS-2013). The patients/participants provided their written informed consent to participate in this study.

AUTHOR CONTRIBUTIONS

JL designed the study, collected and analyzed the data, and drafted the manuscript. XW collected and analyzed the data. YX supervised the study and reviewed and edited the manuscript. ZG and LZ performed the biological measurements experiments. WC, LS, JG, and RH collected the clinical and polysomnography data. All authors contributed to the article and approved the submitted version.

FUNDING

This work was supported by National Natural Science Foundation of China (81570085) and the National Key Research and Development Projects of China (No. 2018YFC1315103).

ACKNOWLEDGMENTS

The authors would like to thank Hairong Zhang, Shuning Li, and Wei Wu for their help in collecting data.

REFERENCES

1. Benjafield AV, Ayas NT, Eastwood PR, Heinzer R, Ip MSM, Morrell MJ, et al. Estimation of the global prevalence and burden of obstructive sleep apnoea: a literature-based analysis. *Lancet Respir Med.* (2019) 7:687–98. doi: 10.1016/S2213-2600(19)30198-5
2. Redline S, Yenokyan G, Gottlieb DJ, Shahar E, O'Connor GT, Resnick HE, et al. Obstructive sleep apnea-hypopnea and incident stroke: the sleep heart health study. *Am J Respir Crit Care Med.* (2010) 182:269–77. doi: 10.1164/rccm.200911-1746OC
3. Young T, Finn L, Peppard PE, Szklo-Coxe M, Austin D, Nieto FJ, et al. Sleep disordered breathing and mortality: eighteen-year follow-up of the Wisconsin sleep cohort. *Sleep.* (2008) 31:1071–78.
4. Marshall NS, Wong KK, Liu PY, Cullen SRJ, Knuiman MW, Grunstein RR. Sleep apnea as an independent risk factor for all-cause mortality: the Busselton Health Study. *Sleep.* (2008) 31:1079–85.
5. Javaheri S, Barbe F, Campos-Rodriguez F, Dempsey JA, Khayat R, Javaheri S, et al. Sleep apnea: types, mechanisms, and clinical cardiovascular consequences. *J Am Coll Cardiol.* (2017) 69:841–58. doi: 10.1016/j.jacc.2016.11.069
6. Devito F, Zito A, Dragonieri S, Carratù P, Quaranta VN, Vitale F, et al. Evaluation of endothelial function and cardiovascular risk in non-obese patients with slight degree of obstructive sleep apnea syndrome. *Monaldi Arch Chest Dis.* (2017) 87:822. doi: 10.4081/monaldi.2017.822
7. Bironneau V, Tamisier R, Trzepizur W, Andriantsitohaina R, Berger M, Goupil F, et al. Sleep apnoea and endothelial dysfunction: an individual patient data meta-analysis. *Sleep Med Rev.* (2020) 52:101309. doi: 10.1016/j.smrv.2020.101309
8. Farooqui FA, Sharma SK, Kumar A, Soneja M, Mani K, Radhakrishnan R, et al. Endothelial function and carotid intima media thickness in obstructive sleep apnea without comorbidity. *Sleep Breath.* (2017) 21:69–76. doi: 10.1007/s11325-016-1371-7
9. Higashi Y. Assessment of endothelial function. History, methodological aspects, and clinical perspectives. *Int Heart J.* (2015) 56:125–34. doi: 10.1536/ihj.14-385
10. Brant LC, Hamburg NM, Barreto SM, Benjamin EJ, Ribeiro ALP. Relations of digital vascular function, cardiovascular risk factors, and arterial stiffness: the Brazilian Longitudinal Study of Adult Health (ELSA-Brasil) cohort study. *J Am Heart Assoc.* (2014) 3:e001279. doi: 10.1161/JAHA.114.001279
11. Rubinshtein R, Kuvin JT, Soffler M, Lennon RJ, Lavi S, Nelso RE, et al. Assessment of endothelial function by non-invasive peripheral arterial tonometry predicts late cardiovascular adverse events. *Eur Heart J.* (2010) 31:1142–48. doi: 10.1093/eurheartj/ehq010
12. Hamburg NM, Keyes MJ, Larson MG, Vasan RS, Schnabel R, Pryde MM, et al. Cross-sectional relations of digital vascular function to cardiovascular risk factors in the Framingham Heart Study. *Circulation.* (2008) 117:2467–74. doi: 10.1161/CIRCULATIONAHA.107.748574
13. Bonetti PO, Pumper GM, Higano ST, Holmes DR Jr., Kuvin JT, Lerman A. Noninvasive identification of patients with early coronary atherosclerosis by assessment of digital reactive hyperemia. *J Am Coll Cardiol.* (2004) 44:2137–41. doi: 10.1016/j.jacc.2004.08.062
14. Flammer AJ, Anderson T, Celermajer DS, Creager MA, Deanfield J, Ganz P, et al. The assessment of endothelial function: from research into clinical practice. *Circulation.* (2012) 126:753–67. doi: 10.1161/CIRCULATIONAHA.112.093245
15. Bakker JP, Baltzis D, Tecilazich F, Chan RH, Manning WJ, Neilan TG, et al. The effect of continuous positive airway pressure on vascular function and cardiac structure in diabetes and sleep apnea. A randomized controlled trial. *Ann Am Thorac Soc.* (2020) 17:474–83. doi: 10.1513/AnnalsATS.201905-378OC
16. Wang J, Yu W, Gao M, Zhang F, Gu C, Yu Y, et al. Impact of obstructive sleep apnea syndrome on endothelial function, arterial stiffening, and serum

inflammatory markers: an updated meta-analysis and metaregression of 18 studies. *J Am Heart Assoc.* (2015) 4:e002454. doi: 10.1161/JAHA.115.002454
17. Shpilsky D, Erqou S, Patel SR, Kip KE, Ajala O, Aiyer A, et al. Association of obstructive sleep apnea with microvascular endothelial dysfunction and subclinical coronary artery disease in a community-based population. *Vasc Med.* (2018) 23:331–39. doi: 10.1177/1358863X18755003
18. Bironneau V, Goupil F, Ducluzeau PH, Vaillant ML, Abraham P, Henni S, et al. Association between obstructive sleep apnea severity and endothelial dysfunction in patients with type 2 diabetes. *Cardiovasc Diabetol.* (2017) 16:39. doi: 10.1186/s12933-017-0521-y
19. Matsuzawa Y, Kwon TG, Lennon RJ, Lerman LO, Lerman A. Prognostic value of flow-mediated vasodilation in brachial artery and fingertip artery for cardiovascular events: a systematic review and meta-analysis. *J Am Heart Assoc.* (2015) 4:e002270. doi: 10.1161/JAHA.115.002270
20. Vlachopoulos C, Xaplanteris P, Aboyans V, Brodmann M, Cífková R, Cosentino F, et al. The role of vascular biomarkers for primary and secondary prevention. A position paper from the European Society of Cardiology Working Group on peripheral circulation: endorsed by the Association for Research into Arterial Structure and Physiology (artery) Society. *Atherosclerosis.* (2015) 241:507–32. doi: 10.1016/j.atherosclerosis.2015.05.007
21. Ning Y, Zhang TS, Wen WW, Li K, Yang Y-X, Qin Y-W, et al. Effects of continuous positive airway pressure on cardiovascular biomarkers in patients with obstructive sleep apnea: a meta-analysis of randomized controlled trials. *Sleep Breath.* (2019) 23:77–86. doi: 10.1007/s11325-018-1662-2
22. Kallianos A, Panoutsopoulos A, Mermigkis C, Kostopoulos K, Papamichail C, Kokkonouzis I, et al. Sex differences of continuous positive airway pressure treatment on flow-mediated dilation in patients with obstructive sleep apnea syndrome. *Clin Interv Aging.* (2015) 10:1361–66. doi: 10.2147/CIA.S84199
23. Berry RB, Brooks R, Gamaldo CE, Harding SM, Lloyd RM, Marcus CL, et al. *The AASM Manual for the Scoring of Sleep and Associated Events Rules, Terminology and Technical Specifications. 2.3 Version*. Darien, IL: American Academy of Sleep Medicine (2016).
24. American Academy of Sleep Medicine. *International Classification of Sleep Disorders*. 3rd ed. Darien. IL: American Academy of Sleep Medicine (2014).
25. Yang WI, Park S, Youn JC, Son NH, Lee S-H, Kang S-M, et al. Augmentation index association with reactive hyperemia as assessed by peripheral arterial tonometry in hypertension. *Am J Hypertens.* (2011) 24:1234–38. doi: 10.1038/ajh.2011.132
26. Cereda CW, Tamisier R, Manconi M, Andreotti J, Frangi J, Pifferini V, et al. Endothelial dysfunction and arterial stiffness in ischemic stroke: the role of sleep-disordered breathing. *Stroke.* (2013) 44:1175–78. doi: 10.1161/STROKEAHA.111.000112
27. Araújo Lda S, Fernandes JF, Klein MRST, Sanjuliani AF. Obstructive sleep apnea is independently associated with inflammation and insulin resistance, but not with blood pressure, plasma catecholamines, and endothelial function in obese subjects. *Nutrition.* (2015) 31:1351–57. doi: 10.1016/j.nut.2015.05.017
28. Zhang F, Wu Y, Feng G, Ni X, Xu Z, Gozal D. Polysomnographic correlates of endothelial function in children with obstructive sleep apnea. *Sleep Med.* (2018) 52:45–50. doi: 10.1016/j.sleep.2018.07.023
29. Nohria A, Gerhard-Herman M, Creager MA, Hurley S, Mitra D, Ganz P. Role of nitric oxide in the regulation of digital pulse volume amplitude in humans. *J Appl Physiol.* (2006) 101:545–48. doi: 10.1152/japplphysiol.01285.2005
30. Petterson JL, O'Brien MW, Johns JA, Chiasson J, Kimmerly DS. Influence of prostaglandins and endothelial-derived hyperpolarizing factors on brachial and popliteal endothelial-dependent function in young adults. *J Appl Physiol.* (2021) 130:17–25.doi: 10.1152/japplphysiol.00698.2020
31. Hamburg NM, Palmisano J, Larson MG, Sullivan LM, Lehman BT, Vasan RS, et al. Relation of brachial and digital measures of vascular function in the community: the Framingham heart study. *Hypertension.* (2011) 57:390–96. doi: 10.1161/HYPERTENSIONAHA.110.160812
32. Bruno RM, Gori T, Ghiadoni L. Endothelial function testing and cardiovascular disease: focus on peripheral arterial tonometry. *Vasc Health Risk Manag.* (2014) 10:577–84. doi: 10.2147/VHRM.S44471
33. Matsuzawa Y, Sugiyama S, Sumida H, Sugamura K, Nozaki T, Ohba K, et al. Peripheral endothelial function and cardiovascular events in high-risk patients. *J Am Heart Assoc.* (2013) 2:e000426. doi: 10.1161/JAHA.113.000426
34. Cooper DC, Ziegler MG, Milic MS, Ancoli-Israel S, Mills PJ, Loredo JS, et al. Endothelial function and sleep: associations of flow-mediated dilation with perceived sleep quality and rapid eye movement (REM) sleep. *J Sleep Res.* (2014) 23:84–93. doi: 10.1111/jsr.12083
35. Leary EB, Watson KT, Ancoli-Israel S, Redline S, Yaffe K, Ravelo LA, et al. Association of rapid eye movement sleep with mortality in middle-aged and older adults. *JAMA Neurol.* (2020) 77:1241–51. doi: 10.1001/jamaneurol.2020.2108
36. Dang-Vu TT, Schabus M, Desseilles M, Sterpenich V, Bonjean M, Maquet P. Functional neuroimaging insights into the physiology of human sleep. *Sleep.* (2010) 33:1589–603. doi: 10.1093/sleep/33.12.1589
37. Cespuglio R, Amrouni D, Meiller A, Buguet A, Gautier-Sauvigné S. Nitric oxide in the regulation of the sleep-wake states. *Sleep Med Rev.* (2012) 16:265–79. doi: 10.1016/j.smrv.2012.01.006
38. Jiang J, Gan Z, Li Y, Zhao W, Li H, Zheng J-P, et al. REM sleep deprivation induces endothelial dysfunction and hypertension in middle-aged rats: roles of the eNOS/NO/cGMP pathway and supplementation with L-arginine. *PLoS ONE.* (2017) 12:e0182746. doi: 10.1371/journal.pone.0182746
39. Pandey A, Kar SK. Rapid Eye Movement sleep deprivation of rat generates ROS in the hepatocytes and makes them more susceptible to oxidative stress. *Sleep Sci.* (2018) 11:245–53. doi: 10.5935/1984-0063.20180039
40. Li CJ, Li JJ, Jiang Y, Mu Y-W, Lu D-X, Xiao Z-Y, et al. Decreased cpg15 augments oxidative stress in sleep deprived mouse brain. *Biochem Biophys Res Commun.* (2020) 522:749–56. doi: 10.1016/j.bbrc.2019.11.132
41. Wang L, Huang X, He W, Liu W, Yang J. Digital microvascular reactivity does not decline with impaired renal function in chronic kidney disease. *BMC Nephrol.* (2019) 20:288. doi: 10.1186/s12882-019-1484-x
42. Weisrock F, Fritschka M, Beckmann S, Litmeier S, Wagner J, Tahirovic E, et al. Reliability of peripheral arterial tonometry in patients with heart failure, diabetic nephropathy and arterial hypertension. *Vasc Med.* (2017) 22:292–300. doi: 10.1177/1358863X17706752
43. Vlachopoulos C, Aznaouridis K, O'Rourke MF, Safar ME, Baou K, Stefanadis C. Prediction of cardiovascular events and all-cause mortality with central haemodynamics: a systematic review and meta-analysis. *Eur Heart J.* (2010) 31:1865–71. doi: 10.1093/eurheartj/ehq024
44. Rosenbaum D, Giral P, Chapman J, Rached FH, Kahn JF, Bruckert E, et al. Radial augmentation index is a surrogate marker of atherosclerotic burden in a primary prevention cohort. *Atherosclerosis.* (2013) 231:436–41. doi: 10.1016/j.atherosclerosis.2013.10.004
45. Theorell-Haglöw J, Hoyos CM, Phillips CL, Yee BJ, Melehan KL, Liu PY, et al. Associations between obstructive sleep apnea and measures of arterial stiffness. *J Clin Sleep Med.* (2019) 15:201–6. doi: 10.5664/jcsm.7616

Conflict of Interest: The authors declare that the research was conducted in the absence of any commercial or financial relationships that could be construed as a potential conflict of interest.

Publisher's Note: All claims expressed in this article are solely those of the authors and do not necessarily represent those of their affiliated organizations, or those of the publisher, the editors and the reviewers. Any product that may be evaluated in this article, or claim that may be made by its manufacturer, is not guaranteed or endorsed by the publisher.

frontiers in Cardiovascular Medicine

ORIGINAL RESEARCH
published: 02 November 2021
doi: 10.3389/fcvm.2021.757926

Omentin-1 Modulates Macrophage Function *via* Integrin Receptors αvβ3 and αvβ5 and Reverses Plaque Vulnerability in Animal Models of Atherosclerosis

*Xuze Lin[1,2,3,4], Yan Sun[1], Shiwei Yang[1,5], Mengyue Yu[2,3,4], Liu Pan[1], Jie Yang[2,3,4], Jiaqi Yang[1,5], Qiaoyu Shao[1], Jinxing Liu[1], Yan Liu[1], Yujie Zhou[1,5] and Zhijian Wang[1,5]**

[1] Department of Cardiology, Beijing Anzhen Hospital, Capital Medical University, Beijing, China, [2] State Key Laboratory of Cardiovascular Disease, Department of Cardiology, National Center for Cardiovascular Diseases, Fuwai Hospital, Chinese Academy of Medical Science and Peking Union Medical College, Beijing, China, [3] Peking Union Medical College, Beijing, China, [4] Chinese Academy of Medical Science, Beijing, China, [5] Beijing Institute of Heart Lung and Blood Vessel Disease, Beijing, China

OPEN ACCESS

Edited by:
Soonkyu Chung,
University of Massachusetts Amherst, United States

Reviewed by:
Annalisa Chiavaroli,
University of Studies G. d'Annunzio Chieti and Pescara, Italy
Regis Moreau,
University of Nebraska–Lincoln, United States

***Correspondence:**
Zhijian Wang
zjwang1975@hotmail.com

Specialty section:
This article was submitted to Atherosclerosis and Vascular Medicine, a section of the journal Frontiers in Cardiovascular Medicine

Received: 13 August 2021
Accepted: 05 October 2021
Published: 02 November 2021

Citation:
Lin X, Sun Y, Yang S, Yu M, Pan L, Yang J, Yang J, Shao Q, Liu J, Liu Y, Zhou Y and Wang Z (2021) Omentin-1 Modulates Macrophage Function via Integrin Receptors αvβ3 and αvβ5 and Reverses Plaque Vulnerability in Animal Models of Atherosclerosis. Front. Cardiovasc. Med. 8:757926. doi: 10.3389/fcvm.2021.757926

Backgrounds: Omentin-1 is a novel cytokine that is primarily released by the epicardial adipose tissue. Molecular structure analysis revealed that it contained a fibrinogen-like domain. Clinical studies have demonstrated that the expression of omentin-1 is tightly associated with the development of cardiovascular diseases, but the receptor by which omentin-1 modulates macrophage function has not been identified yet.

Objective: This study sought to investigate the effect of omentin-1 on already-established atherosclerosis (AS) lesions in both ApoE−/− and $Ldlr^{-/-}$ mice and further, study its underlying mechanisms.

Methods and Results: We investigated the effect of omentin-1 on the plaque phenotype by implanting a minipump in ApoE−/− and $Ldlr^{-/-}$ mice. *In vivo* studies showed that the infusion of omentin-1 increased the collagen content and mitigated the formation of the necrotic core in both animal models. Immunohistochemistry and immunofluorescence analysis revealed that omentin-1 suppressed inflammatory cytokines expression, macrophage infiltration, and apoptosis within the plaque. An immunoprecipitation experiment and confocal microscopy analysis confirmed the binding of omentin-1 to the integrin receptors αvβ3 and αvβ5. The cell studies demonstrated that omentin-1 suppressed the apoptosis and inflammatory cytokines expression induced by the oxidized low-density lipoprotein in the macrophage. In addition, omentin-1 promoted the phosphorylation of the integrin-relevant signaling pathway as well as the Akt and AMPK in the macrophage. The addition of the inhibitor of the integrin receptor or interfering with the expression of the integrin subunit αv (ITGAV) both significantly abrogated the bioeffects induced by omentin-1. A flow cytometry analysis indicated that the antibodies against αvβ3 and αvβ5 had a competitive effect on the omentin-1 binding to the cell membrane.

Conclusions: The administration of adipokine omentin-1 can inhibit the necrotic cores formation and pro-inflammatory cytokines expression within the AS lesion. The mechanisms may include the suppression of apoptosis and pro-inflammatory cytokines expression in the macrophage by binding to the integrin receptors αvβ3 and αvβ5.

Keywords: plaque vulnerability, adipokine, integrin, atherosclerosis, macrophage

INTRODUCTION

Coronary artery atherosclerosis (AS), which is characterized by the formation of an atherosclerotic lesion in the lumen epicardial arteries, frequently induces the stenosis of nourishing vessels of the myocardium and eventually gives rise to the myocardial ischemia (1). Myocardial infarction is majorly caused by acute coronary syndrome (ACS), and plaque vulnerability is considered to play an important role in the induction of ACS. Many studies have demonstrated that macrophage infiltration, coupled with its apoptosis and inflammatory cytokine secretion, contributes to plaque instability and finally leads to plaque rupture (2, 3). Therefore, the macrophage is now believed to be a potential therapeutic target in treating advanced AS plaque (4).

Several *in vivo* and *in vitro* studies revealed that the adipose tissue abundantly secretes bioactive molecules, which are termed adipokines, and impacts the metabolism profile of adjacent and remote organs by the paracrine and endocrine pathways (5). Omentin-1, which is an adipokine mainly expressed by the visceral and epicardial adipose tissue (EAT), is composed of 313 amino acids and is considered to be a hydrophilic protein. Gaborit et al. reported that the expression level of omentin-1 in the EAT is 12-fold higher than that in subcutaneous fats, and, surprisingly, our previous research indicated that the omentin-1 expression is much lower in the EAT adjacent to the coronary stenotic segments (6, 7).

Previous biochemical studies have demonstrated that omentin-1 can produce favorable effects on the cardiovascular system by promoting vasodilation in isolated vessels and inhibiting the growth and migration of vascular smooth muscle cells (VSMCs) (8, 9). The study by Mizuho et al. provided evidence that omentin-1 generated beneficial effects on macrophages mainly by activating the phosphatidylinositol 3-kinase (PI3K)/protein kinase B (Akt) signaling pathway (10). Besides, omentin-1 also suppressed the expression of the intercellular cell adhesion molecule-1 (ICAM-1) and vascular cell adhesion molecule-1 (VCAM-1) in the human umbilical vein endothelial cells (HUVECs), which contributed to the reduction in the adhesion of monocytes to HUVECs (11). However, the cellular receptor by which omentin-1 exerts its conducive function has not been elucidated yet.

Integrin family receptors, which are a cluster of transmembrane receptors consisting of 18 α and 8 β subunits, serve an important role in the cellular crosstalk with its microenvironment. They frequently recognize and bind to extracellular matrix (ECM) components, including fibronectin, vitronectin, osteopontin, and fibrinogen. Integrin αvβ3 and αvβ5, which are heterodimers composed of αvβ3 and β5 subunits, have been reported to be associated with the development of AS (12, 13). Though the receptor of omentin-1 has not been fully identified yet, we noticed that omentin-1 has been reported to have a fibrinogen-like domain, which might be the integrin-binding motif on it (14). Encouraged by these profound discoveries, we decided to explore whether adipokine omentin-1 can directly bind to the integrin αvβ3 or αvβ5 in macrophage-derived foam cells and whether it can affect the phenotype of established plaques *in vivo* by regulating foam cell functions.

In this research, we used apolipoprotein E-deficient ($ApoE^{-/-}$) mice and low-density lipoprotein receptor-deficient ($Ldlr^{-/-}$) mice with an ALZET minipump implantation to investigate the therapeutic effect of omentin-1 on the already-established AS plaques. In cell studies, we applied RAW264.7 and THP1 cell lines to construct the macrophage cell model *in vitro*. Oil red O staining and immunofluorescent technology were used to confirm the lipid ingestion and phagocytosis activity of cells. To assess the role played by integrin αvβ3 and αvβ5 in transducing the signal of omentin-1, we used cilengitide to inhibit the integrin receptors and applied gene interfering technology *in vitro* to knock down the integrin subunit αv (ITGAV) expression.

METHODS

A detailed description of the methods is included in the **Supplementary Material** and Research resources.

Animal Model

The animal experiments were performed in accordance with the Institutional Animal Care and Use of Laboratory Animals and were approved by the Capital Medical University Animal Care and Use Committee. Additionally, all of the animal experiments performed conformed with the European community guiding principles in the care and use of animals (2010/63/UE). A total of 58 male ApoE−/− mice (C57BL/6 background) at the age of 8 weeks were purchased from Beijing Vital River Laboratory Animal Technology and a total of 40 male Ldlr−/− mice (C57BL/6 background) at the age of 10 weeks were purchased

Abbreviations: ACS, acute coronary syndrome; Akt, protein kinase B; AMPK, adenosine 5'-monophosphate-activated protein kinase; ApoE−/− mice, apolipoprotein E-deficient mice; AS, atherosclerosis; EAT, epicardial adipose tissue; ERK, extracellular-regulated protein kinase; FAK, focal adhesion kinase; HDL, high-density lipoprotein; ITGAV, integrin subunit αv; LDL, low-density lipoprotein; Ldlr−/− mice, low density lipoprotein receptor-deficient mice; NS, normal saline; ox-LDL, oxidized low-density lipoprotein; p38 MAPK, p38 mitogen-activated protein kinase; PI3K, phosphatidylinositol 3-kinase; Rac1, ras-related C3 botulinum toxin substrate 1; siRNA, small interfering RNA; TCFA, thin-cap fibroatheroma.

from Guangzhou Cyagen Biosciences Inc. The ApoE−/− mice were fed on a western diet for 12 weeks and the Ldlr−/− mice were fed on a western diet for 8 weeks to build up the AS lesion. The groups without minipump implantation were euthanized under deep anesthesia [induced by intraperitoneal injection with an overdose of pentobarbital sodium (200 mg/kg)] to get their aortas and blood samples. The rest of the mice were randomly divided into three groups: (i) controls (infused with normal saline), (ii) low dose omentin-1-treated group (infused with omentin-1 at the rate of 1 μg/kg/h *via* ALZET minipump), (iii) high dose omentin-1-treated group (infused with omentin-1 in the rate of 5 μg/kg/h *via* the ALZET minipump). ALZET minipumps (ALZET Model 2004; Cupertino, California, United States) were used to achieve the continuous infusion of the flag-tagged omentin-1 (Abcam, ab157030, UK) solution into the mouse jugular vein. For implanting the minipumps, anesthesia was induced to the mice by inhaling 2% isoflurane and maintained by inhaling 1.5% isoflurane. Once anesthetized, the mice were instrumented with a polyurethane catheter (ALZET, Cat No: 0007700; Cupertino, California, United States) implanted in the right jugular vein. The catheter was attached to an ALZET minipump, which was implanted subcutaneously. All of the remaining mice were fed on a western diet after the implantation of the minipumps. After 3 weeks of infusion, their blood pressure and body weight were measured before receiving euthanasia under deep anesthesia (the method was described as above). The blood and whole aorta sample of every mouse were obtained. The fasting plasma glucose, triglyceride, total cholesterol, low-density lipoprotein (LDL) cholesterol, and high-density (HDL) cholesterol were measured using enzymatic methods. The omentin-1 concentration of the plasma was measured by enzyme-linked immunoassay (ELISA) analysis (Biovendor, RD191100200R, Czech Republic).

Mouse Aortic Root Atherosclerotic Lesion Assessment

Eight micrometers (8 mm) cryosections were taken from the entire region of the valve leaflet and every 10th section (80 μm) was subjected to Oil red O staining and hematoxylin counterstaining. Images were captured under an identical microscope. All of the sections were coded and analyzed blind. Three sections from different levels of the aortic root in each mouse were obtained and subjected to hematoxylin and eosin (HE) staining (Solarbio Life Science, G1262, Beijing, China) and Masson's trichrome staining (Solarbio Life Science, G1340, Beijing, China).

The macrophage content of the plaque was expressed as the proportion of CD68+ cells. To determine the expression of the pro-inflammatory cytokines within the atherosclerotic lesion, immunohistochemistry analysis, and western blot were performed by using antibodies against TNF-α (Abcam, ab9739, UK), and IL-1β (Abcam, ab9722, UK). The mouse IgG isotype (R&D, MAB002, USA) was used as a negative control. To detect the colocalization of the exogenous omentin-1 to the plaque integrin αvβ3 and αvβ5, immunofluorescence co-localization analysis was performed by applying antibodies against flag tag (Abcam, ab205606, UK), integrin αvβ3 (Santa Cruz, sc-7312), integrin αvβ5 (Santa Cruz, sc-13588) and F4/80 (Abcam, ab16911, UK).

The cell apoptosis in the plaque was detected by using an *in situ* cell death detection kit (Roche, 11684795910, Switzerland), and the cells undergoing apoptosis were quantified by counting the TUNEL+ cells.

About 6 μm of aortic root tissue was taken from the subjects for western blot analysis. The adherent tissue of the vessel was removed carefully before adding a lysis buffer. The protein concentration of each sample was quantified and equilibrated before undergoing western blotting.

TABLE 1 | List of nucleotide sequence of small interfering RNA.

Names	Forward sequence	Reverse sequence
NC (negative control)	UUCUCCGAACGUGUCACGUTT	ACGUGACACGUUCGGAGAATT
ITGAV siRNA	GACCCGUUGUCACUGUAAATT	UUUACAGUGACAACGGGUCTT

TABLE 2 | List of primer sequence used for RT-qPCR.

Gene	Forward sequence (5′ to 3′)	Reverse sequence (5′ to 3′)
ITGAV	GTGTGAGGAACTGGTCGCCTAT	CCGTTCTCTGGTCCAACCGATA
GAPDH	CATCACTGCCACCCAGAAGACTG	ATGCCAGTGAGCTTCCCGTTCAG

Cell Culture and Functional Assays

The RAW264.7 and THP1 cell lines were purchased from Cyagen Bioscience (Guangzhou, China). The culture condition was described in the **Supplementary Materials**. Functional assays including apoptosis, foam cell formation, and small interfering RNA (siRNA) transfection were performed as described in the **Supplementary Materials**. The nucleotide sequence of siRNAs and primers is shown in **Tables 1**, **2**. To investigate the interaction between omentin-1 and the integrin receptors αvβ3 and αvβ5, we performed co-immunoprecipitation (IP) and confocal microscopy analysis as described in the **Supplementary Material**. To examine whether the neutralizing antibody against αvβ3 or αvβ5 had a competitive effect on the binding of omentin-1 to integrin receptors, we performed a flow cytometry assay, which is described in the **Supplementary Materials**.

Statistical Analysis

The results were presented as mean ± SEM for the continuous data and as frequencies for the categorical data. An unpaired two-tailed Student *t*-test was used for comparison between two groups. A one-way ANOVA followed by a Bonferroni multiple comparisons post-test was performed to assess the significance of deviation when three or more groups were involved. The χ^2 test was used to compare the categorical data. All data were analyzed by GraphPad Prism 7 (GraphPad Software Inc., San Diego, California, United States) and SPSS 26 (IBM,

Armonk, New York, United States). $P < 0.05$ were considered as statistically significant. The *P*-values are given in the figures. The representative images were selected as those that show values close to the means of the results obtained from all the analyzed samples.

RESULTS

Assessment of Omentin-1 Retention in Atherosclerotic Lesion

After being treated by flag-tagged omentin-1 for another 3 weeks, the omentin-1 concentration in the plasma of the mice was measured by ELISA analysis, and the retention of omentin-1 in their aortic root lesion was examined by immunofluorescence analysis. The result of the ELISA showed that the intravenous infusion of exogenous omentin-1 significantly elevated the plasma omentin-1 level in the ApoE−/− mice and Ldlr−/− mice (**Tables 3**, **4**). The ApoE−/− and Ldlr−/− mice treated by a high dose omentin-1 (5 μg/kg/h) exhibited elevated omentin-1 retention in their plaque area when compared with the counterparts treated with low dose omentin-1 (1 μg/kg/h) or normal saline (NS) (**Supplementary Figures 1A,B, 2A,B**). Moreover, the biomedical analysis of the blood samples indicated that the serum level of omentin-1 was positively associated with the rate of omentin-1 infusion, while the other risk factors of AS remained unaffected (**Tables 3**, **4**). These results illustrated that the intravenous infusion of omentin-1 solution can successfully bring omentin-1 to the blood and AS plaque of animals.

Omentin-1 Infusion Modulates Plaque Phenotype in ApoE−/− and Ldlr−/− Mice

After being given by NS or omentin-1 solution for 3 weeks, the aortic root lesion of the ApoE−/− and Ldlr−/− mice were stained with an HE stain reagent and Masson's trichrome stain reagent (**Figure 1A** and **Supplementary Figure 4A**). The HE staining and Masson's trichrome staining of the aortic root section from the ApoE−/− and Ldlr−/− mice indicated that a high dose of omentin-1 solution (5 μg/kg/h) treatment significantly suppressed the necrotic core formation and elevated the collagen content in the AS lesion when compared with the counterpart that was treated with NS (**Figures 1B,C** and **Supplementary Figures 4B,C**). The low dose of omentin-1 treatment (1 μg/kg/h) helped to ameliorate the necrotic formation in the ApoE−/− mice but not in the Ldlr−/− mice (**Figures 1B,C** and **Supplementary Figures 4B,C**). However, the 3-week treatment of omentin-1 did not reverse the AS plaque size in both ApoE−/− and Ldlr−/− mice (**Figure 1D** and **Supplementary Figure 4D**). In both $ApoE^{-/-}$ and $Ldlr^{-/-}$ mice, the high dose of omentin-1 (5 μg/kg/h) helped to reduce the lipid content in the AS plaque (**Figures 1E,F** and **Supplementary Figures 4E,F**).

TABLE 3 | Characteristics of $ApoE^{-/-}$ mouse.

	Before surgery	NS infusion	Omentin-1 (1 μg/kg/h)	Omentin-1 (5 μg/kg/h)
Male (%)	100	100	100	100
Age (weeks)	20	23	23	23
Body weight (g)	29.1 ± 0.7	30 ± 0.64	29.4 ± 0.65	30.4 ± 0.8
Systolic BP (mmHg)	102.4 ± 1.4	103.7 ± 1.3	103 ± 1.7	104.1 ± 1.5
Diastolic BP (mmHg)	78.3 ± 1.8	81 ± 1.9	78.1 ± 2.1	79.2 ± 2.2
Glucose (mg/dl)	192.1 ± 8.7	207.1 ± 5.2	199.7 ± 4.8	196.2 ± 5.2
Triglyceride (mg/dl)	66.7 ± 2.1	65.4 ± 2.0	64.3 ± 1.8	64.0 ± 2.0
Total cholesterol (mg/dl)	1713 ± 41.2	1723 ± 38.0	1655 ± 32.3	1594 ± 44.7
LDL-C (mg/dl)	274 ± 8.5	251.7 ± 8.5	248.4 ± 9.0	238.7 ± 9.9
HDL-C (mg/dl)	36.9 ± 0.7	36.5 ± 0.6	36.6 ± 0.6	36.4 ± 0.7
Human omentin-1 (ng/ml)	1.19 ± 0.03	1.2 ± 0.05	59.82 ± 4.3*,†	433 ± 19.1**,‡,¶
n	10	16	16	16

*Baseline characteristics of $ApoE^{-/-}$ mouse was recorded. And the blood samples of them were collected and subjected to biochemical analysis. Before surgery represents the group without ALZET minipump implantation. NS infusion represents the group infused with normal sodium solution (vehicle). Omentin-1 represents the group infused with omentin-1-containing solution [*P < 0.05, **P < 0.0001 vs. the group without ALZET minipump implantation (Before surgery); $^{\dagger}P < 0.05$, $^{\ddagger}P < 0.0001$ vs. the group infused with normal sodium solution (NS infusion); ¶P < 0.0001 vs. the group infused with low concentration of omentin-1 solution (omentin-1 1 μg/kg/h)].*

TABLE 4 | Characteristics of $Ldlr^{-/-}$ mouse.

	Before Surgery	NS infusion	Omentin-1 (1 μg/kg/h)	Omentin-1 (5 μg/kg/h)
Male (%)	100	100	100	100
Age (weeks)	18	21	21	21
Body weight (g)	30.6 ± 0.8	30.6 ± 0.7	30.3 ± 0.7	29.4 ± 0.6
Systolic BP (mmHg)	104.9 ± 2.1	103 ± 2.0	106.2 ± 2.5	105.9 ± 3.0
Diastolic BP (mmHg)	77.9 ± 1.1	79.6 ± 1.3	79.3 ± 1.3	77.7 ± 1.3
Glucose (mmol/L)	227.9 ± 7.0	219.7 ± 6.7	216.9 ± 6.2	216.7 ± 6.3
Triglyceride (mmol/L)	325.4 ± 11.6	338.7 ± 12.0	323.0 ± 10.7	322.0 ± 11.2
Total cholesterol (mmol/L)	1772 ± 46.0	1756 ± 54.6	1714 ± 49.6	1687 ± 52.9
LDL-C(mmol/L)	396.5 ± 17.4	412.1 ± 18.5	432 ± 19.2	427.8 ± 23.9
HDL-C(mmol/L)	125.2 ± 3.0	126 ± 3.0	122.9 ± 4.0	122.4 ± 2.6
Human omentin-1 (ng/ml)	2.19 ± 0.22	2.38 ± 0.28	43.17 ± 2.88*,†	385 ± 15.90**,‡,¶
n	10	10	10	10

*Baseline characteristics of $Ldlr^{-/-}$ mouse was recorded. And the blood samples of them were collected and subjected to biochemical analysis. Before surgery represents the group without ALZET minipump implantation. NS infusion represents the group infused with normal sodium solution (vehicle). Omentin-1 represents the group infused with omentin-1-containing solution [*P < 0.05, **P < 0.0001 vs. the group without ALZET minipump implantation (Before surgery); $^{\dagger}P < 0.05$, $^{\ddagger}P < 0.0001$ vs. the group infused with normal sodium solution (NS infusion); ¶P < 0.0001 vs. the group infused with low concentration of omentin-1 solution (omentin-1 1 μg/kg/h)].*

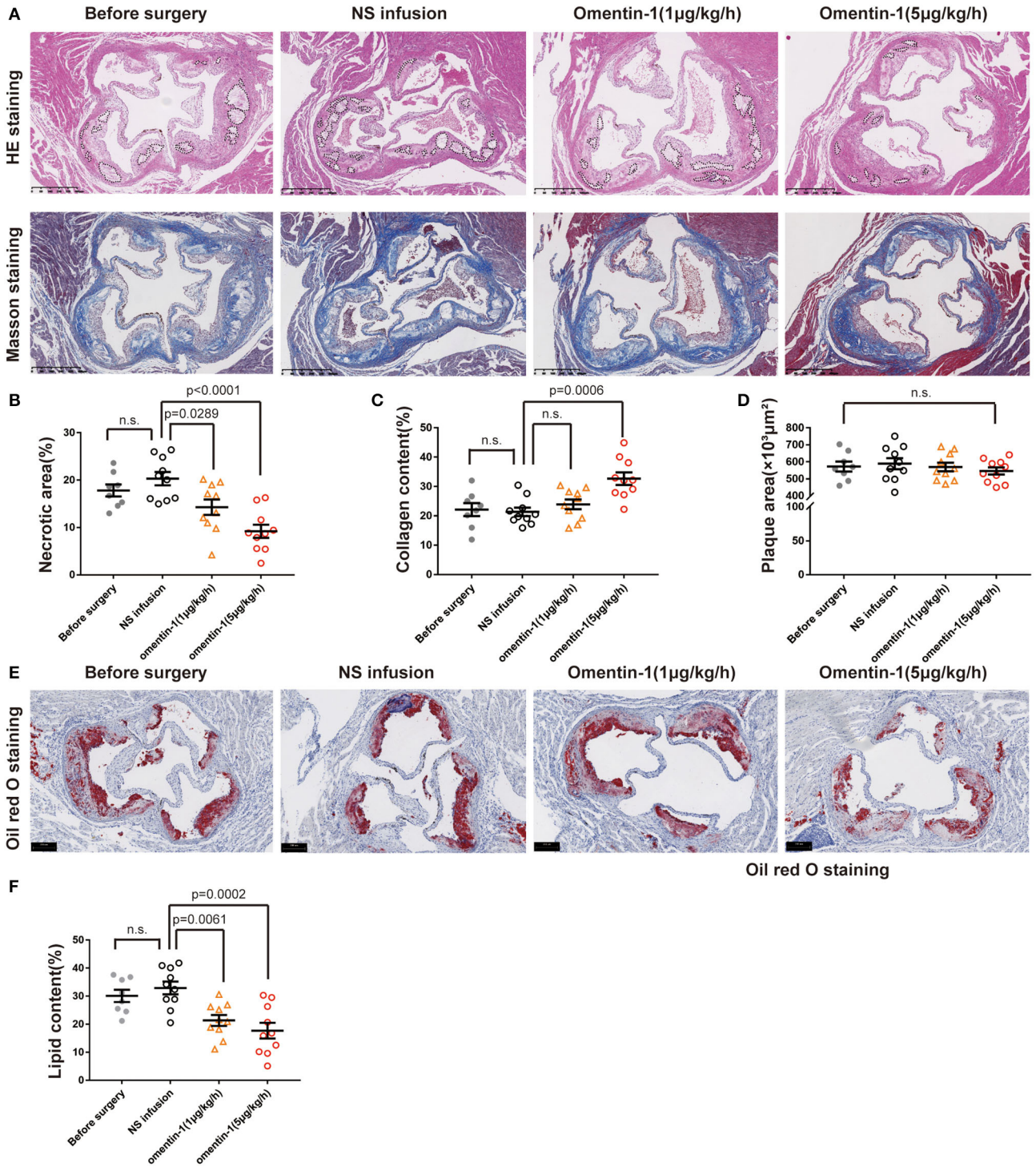

FIGURE 1 | Infusion of omentin-1 enhanced plaque stability in ApoE$^{-/-}$ mice. **(A)** Representative images of aortic root lesion sections of ApoE$^{-/-}$ mice stained by hematoxylin and Masson's trichrome. **(B)** Graph shows the formation of necrotic cores. The formation of necrotic cores (pointed out by dot line) was assessed by calculating the proportion of necrosis area in the plaque ($n_1 = 8$, $n_{2,3,4} = 10$). **(C)** Graph shows the collagen content of atherosclerosis (AS) plaque. Collagen content was expressed in the proportion of collagen fiber (blue) in the plaque area ($n_1 = 8$, $n_{2,3,4} = 10$). **(D)** Graph shows the size of the AS lesion in each group. No significant difference was found between the experimental groups and control groups ($n_1 = 8$, $n_{2,3,4} = 10$). **(E)** Representative images of the aortic root sections of mice stained by oil red O. **(F)** Graph show the lipid content (red) in the plaque area. The lipid content was expressed in the proportion of oil red positive area in plaque area ($n_1 = 8$, $n_{2,3,4} = 10$). All data in this figure were presented as mean ± SEM [n.s., non-significant; n_1, the number of subjects in Before Surgery group; n_2, the number of subjects in normal saline (NS) infusion group; n_3, the number of subjects in group infused with omentin-1 (1 μg/kg/h); n_4, the number of subjects in group infused with omentin-1 (5 μg/kg/h)].

Omentin-1 Infusion Reduces Inflammatory Cytokines Expression, Macrophage Apoptosis, and Infiltration in the AS Plaque of ApoE−/− and Ldlr−/− Mice

The recruitment of macrophages to the AS lesion is frequently accompanied by the secretion of inflammatory cytokines, which subsequently promoted cell death and increased plaque vulnerability. The mouse IgG isotype was used as a negative control in the immunohistochemical analysis (**Supplementary Figure 1C**). Here, we examined the inflammatory cytokine expression profile and macrophage infiltration in the ApoE−/− and Ldlr−/− mice (**Figure 2A** and **Supplementary Figure 5A**). Statistical analysis revealed that adding omentin-1 to the blood of the mouse significantly alleviated the expression of TNF-α (**Figure 2B** and **Supplementary Figure 5B**) and IL-1β (**Figure 2C** and **Supplementary Figure 5C**) in the AS lesion. The western blot also indicated that the omentin-1 treatment reduced the TNF-α and IL-1β in the aortic root tissue of the mice (**Figure 2D** and **Supplementary Figure 5D**).

The result of the TUNEL staining indicated that either a high or low dose of omentin-1 can reduce the cell apoptosis within the AS plaque in both ApoE−/− and Ldlr−/− mice (**Figures 2E,F** and **Supplementary Figures 5E,F**). The antibody against the mouse macrophage marker CD68 was used to investigate the macrophage infiltration in the plaque. Compared with the NS-treated group and the group treated with low dose omentin-1, the macrophage content of the AS lesion is much lower in the high dose omentin-1-treated group in both ApoE−/− and Ldlr−/− mice (**Supplementary Figures 2G, 3, 6A,D**).

The Interaction of Omentin-1 With Integrin αvβ3 and αvβ5

To validate the interaction of omentin-1 to the integrin receptor αvβ3 and αvβ5 *in vivo* and *in vitro*, we performed co-immunoprecipitation and immunofluorescence colocalization experiments. The recombinant omentin-1 proteins that have been labeled with his tag or flag tag were, respectively, used to verify their conjugation to integrin αvβ3 and αvβ5. The results of co-immunoprecipitation showed that omentin-1 can bind to the integrin αvβ3 as well as αvβ5, and the adding of artificial peptide tags had no effects on its binding ability (**Figures 3A,B**).

Furthermore, we applied confocal microscopy to confirm the spatial colocalization of omentin-1 and integrin receptors. The mouse macrophage cell line RAW264.7 was incubated with mild oxidized LDL (ox-LDL) to transform it into a macrophage-derived foam cell. The results of the immunofluorescence staining demonstrated that the cell model of the macrophage-derived foam cell can abundantly express integrin αvβ3 and αvβ5. Besides, after being added to the cell culture solution, the exogenous omentin-1 (labeled by flag tag) exhibited significant colocalization with integrin αvβ3 and αvβ5 on the cell surface in comparison with the IgG isotype (**Figures 3C,D** and **Supplementary Figure 6C**).

To further validate that the intravenous infusion of the omentin-1-containing solution can lead to the binding of exogenous omentin-1 (labeled by flag tag) to the macrophage integrin receptors in the plaque area of the plaque, we used antibodies against the F4/80, αvβ3, αvβ5, and flag tag to confirm the spatial expression profile of these proteins in the $ApoE^{-/-}$ mouse model. Immunofluorescence confocal microscopy indicated that the mouse macrophage marker F4/80 colocalized with αvβ3 and αvβ5 in the AS lesion (**Figures 4A,B**), which suggested that the macrophage infiltrating in the plaque can express these two integrin receptors. Moreover, it has also been shown that the exogenous omentin-1 (labeled by flag tag) colocalized with integrin αvβ3 and αvβ5 in the AS lesion (**Figures 4C,D**), which strongly supported what we had discovered in the co-IP analysis. In addition, we found that exogenous omentin-1 (labeled by flag tag) significantly colocalized with the macrophage marker F4/80 in the plaque site (**Figure 4E**), which demonstrated that the intravenous infusion of the omentin-1-containing solution can successfully bring omentin-1 to the macrophages that infiltrated the AS lesion. Three biological replicates were made in this analysis (**Supplementary Figures 7, 8**). The mice infused with NS were used as the control group (**Supplementary Figure 9**).

Moreover, we used the neutralizing antibodies against αvβ3 or αvβ5 to investigate the competitive effect between integrin ligands and omentin-1 (flag tag labeled) in live cells. The result of flow cytometry indicated that the pre-treatment of neutralizing antibodies impaired the binding of omentin-1 to the cell membrane in the THP-1 cells (**Figure 5A**).

Omentin-1 Regulates Apoptosis, Lipid Loading, and Inflammatory Cytokines Expression in Macrophages by Interacting With Integrin Receptors

Our preliminary experiment confirmed that mild ox-LDL could only induce lipid loading instead of apoptosis in macrophages, while high ox-LDL was able to induce inflammation and apoptosis resembling pathological conditions. Therefore, we utilized high ox-LDL to trigger cell apoptosis and stimulate the inflammatory secretion and used mild ox-LDL to induce lipid loading in the macrophages. The integrin subunit αv (ITGAV) siRNA was used to knock down the expression of αv integrin in the RAW264.7 cell line, and the transfection efficiency was examined by RT-qPCR analysis and western blot analysis (**Supplementary Figure 14A**).

The RAW264.7-derived macrophages were pretreated by omentin-1 for 1.5 h, and subsequently co-incubated with high ox-LDL to induce apoptosis. TUNEL analysis was used to verify the apoptotic rate induced by the high ox-LDL in different groups. The results showed that omentin-1 protected the macrophages from high ox-LDL induced apoptosis, and the blockade of integrin receptor αvβ3 and αvβ5 or knockdown the expression of

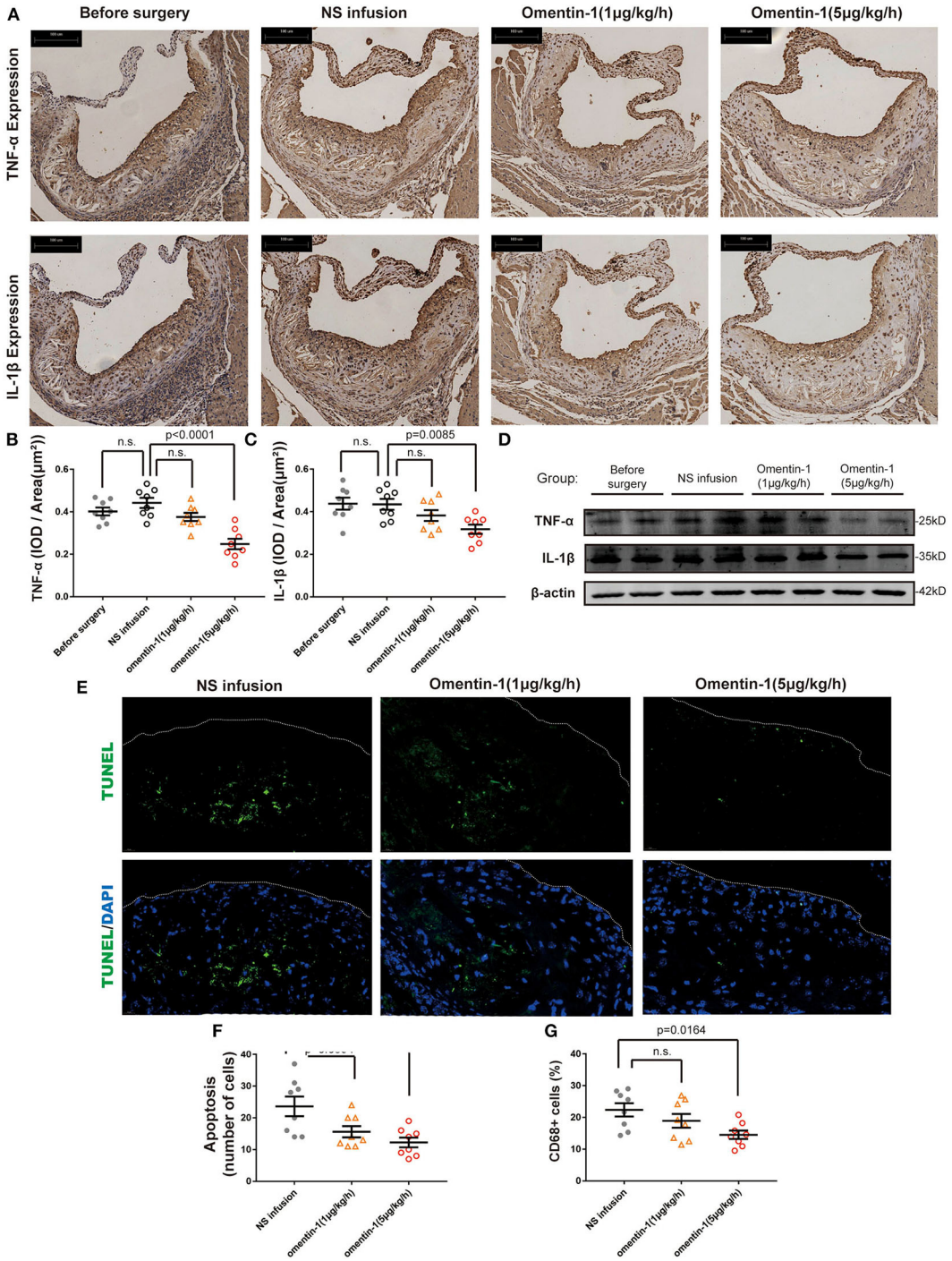

FIGURE 2 | Omentin-1 infusion reduces inflammatory cytokines expression and cell death in atherosclerotic plaque of ApoE$^{-/-}$ mouse. **(A)** Representative micrographs of the aortic root sections of ApoE$^{-/-}$ mice stained by the antibodies against IL-1β or TNF-α. **(B,C)** Graph shows the intensity of inflammatory cytokines expression ($n_{1,2,3,4} = 8$). The results of immunohistochemistry analysis were expressed in the integral optical density (IOD) of positive staining area vs. plaque area [(IOD, sum)/(Plaque area, μm^2)]. **(D)** Aortic root samples were collected from animal models and the expression of TNF-α and IL-1β were quantified by western blot analysis. **(E)** Representative images of the aortic root sections of the mouse were stained by DAPI (Abcam, ab104109, displayed in blue) and the apoptotic cell was detected by TUNEL staining (green). The plaque area was marked by a dot line. **(F)** The graph shows the cells undergoing apoptosis in the AS lesion. The intensity of apoptosis was quantified by counting the apoptotic cells (TUNEL+ cells) in each sample ($n_{1,2,3,4} = 8$). **(G)** The macrophage infiltration in each sample was quantified by calculating the proportion of CD68 positive area (CD68+ area/ total plaque area, $n_{1,2,3,4} = 8$). All the data in this figure were presented as mean ± SEM [n.s., non-significant; n_1, the number of subjects in before surgery group; n_2, the number of subjects in NS infusion group; n_3, the number of subjects in group infused with omentin-1 (1 μg/kg/h); n_4, the number of subjects in group infused with omentin-1 (5 μg/kg/h)].

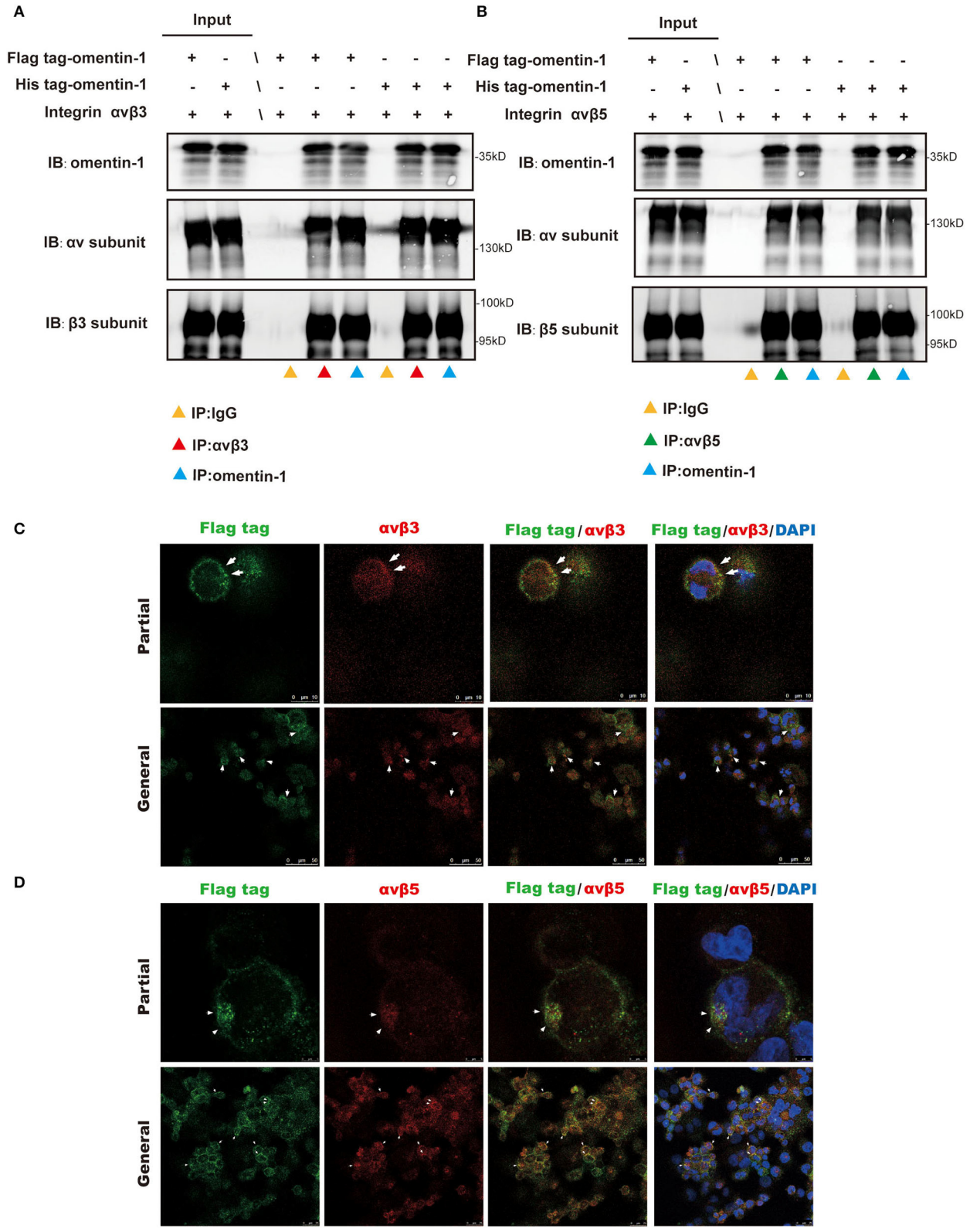

FIGURE 3 | Co-Immunoprecipitation (IP) analysis showed the molecular interaction of omentin-1 (labeled by his tag and flag tag) and integrin αvβ3 and αvβ5. *In vitro* confocal microscopy demonstrated the spatial co-localization of omentin-1 (labeled by flag tag) and integrin receptors on the surface of THP1-derived macrophages. **(A,B)** The results of the co-IP analysis of omentin-1 and integrin receptors, αvβ3 and αvβ5. **(C,D)** *In vitro* confocal microscopy of exogeneous omentin-1 and integrin receptors. The area where exhibited the co-localization of exogenous omentin-1 (green) and integrin receptors (red) was pointed out by white arrows.

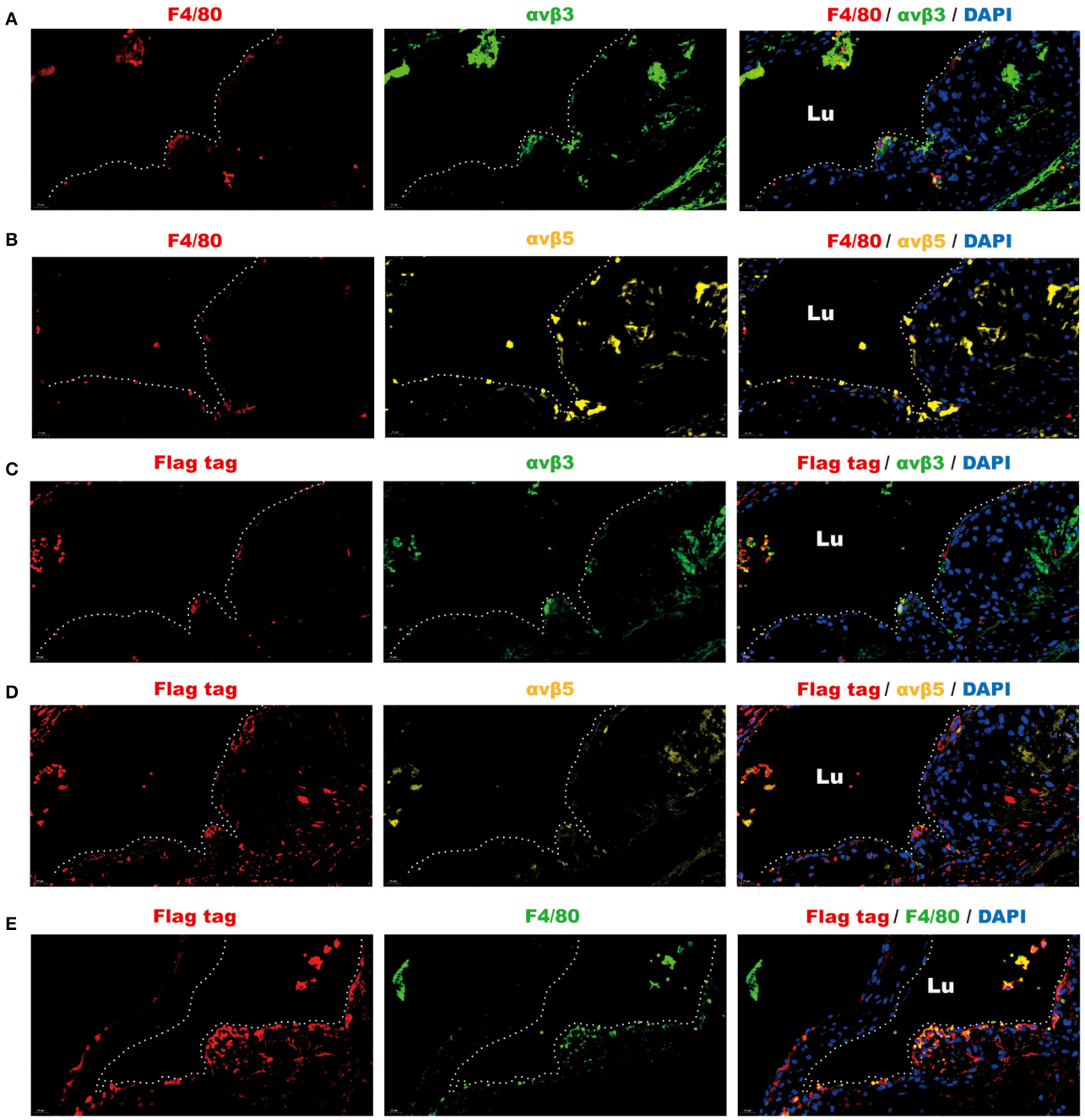

FIGURE 4 | Fluorescence analysis demonstrated the spatial co-localization of infiltrated macrophages, exogenous omentin-1 (labeled by flag tag), and integrin receptors in the atherosclerotic plaque of ApoE$^{-/-}$ mice. The aortic root sections were stained by primary antibodies against F4/80 (macrophage marker), αvβ3, αvβ5, and flag tag (the marker of exogenous omentin-1). Fluorescence secondary antibodies against protein from mice, rabbits, and rats were used to mark the localization of the primary antibodies. Three biological replicates were made in this analysis. **(A)** The macrophage (F4/80) was dyed red and αvβ3 was dyed green. The plaque area was marked by a dotted line. **(B)** The macrophage (F4/80) was dyed red and αvβ5 was dyed yellow. The plaque area was marked by a dotted line. **(C)** Flag-tagged exogenous omentin-1 (flag tag) was dyed red and αvβ3 was dyed green. The plaque area was marked by a dotted line. **(D)** Flag-tagged exogenous omentin-1 (flag tag) was dyed red and αvβ5 was dyed yellow. The plaque area was marked by a dotted line. **(E)** Flag-tagged exogenous omentin-1 (flag tag) was dyed red and macrophage (F4/80) was dyed green. The plaque area was marked by a dotted line (Lu = the lumen of the aorta).

ITGAV remarkably reversed the anti-apoptosis effect of omentin-1 (**Figures 5B,C** and **Supplementary Figures 10, 11**).

The RAW264.7-derived macrophages were treated with omentin-1 and mild ox-LDL to induce lipid loading within the cytoplasm. An oil red O stain kit was used to detect the lipid content of the macrophages. The results showed that omentin-1 remarkably reduced lipid loading in the macrophages. The effect of omentin-1 on combating lipid loading was inhibited upon the

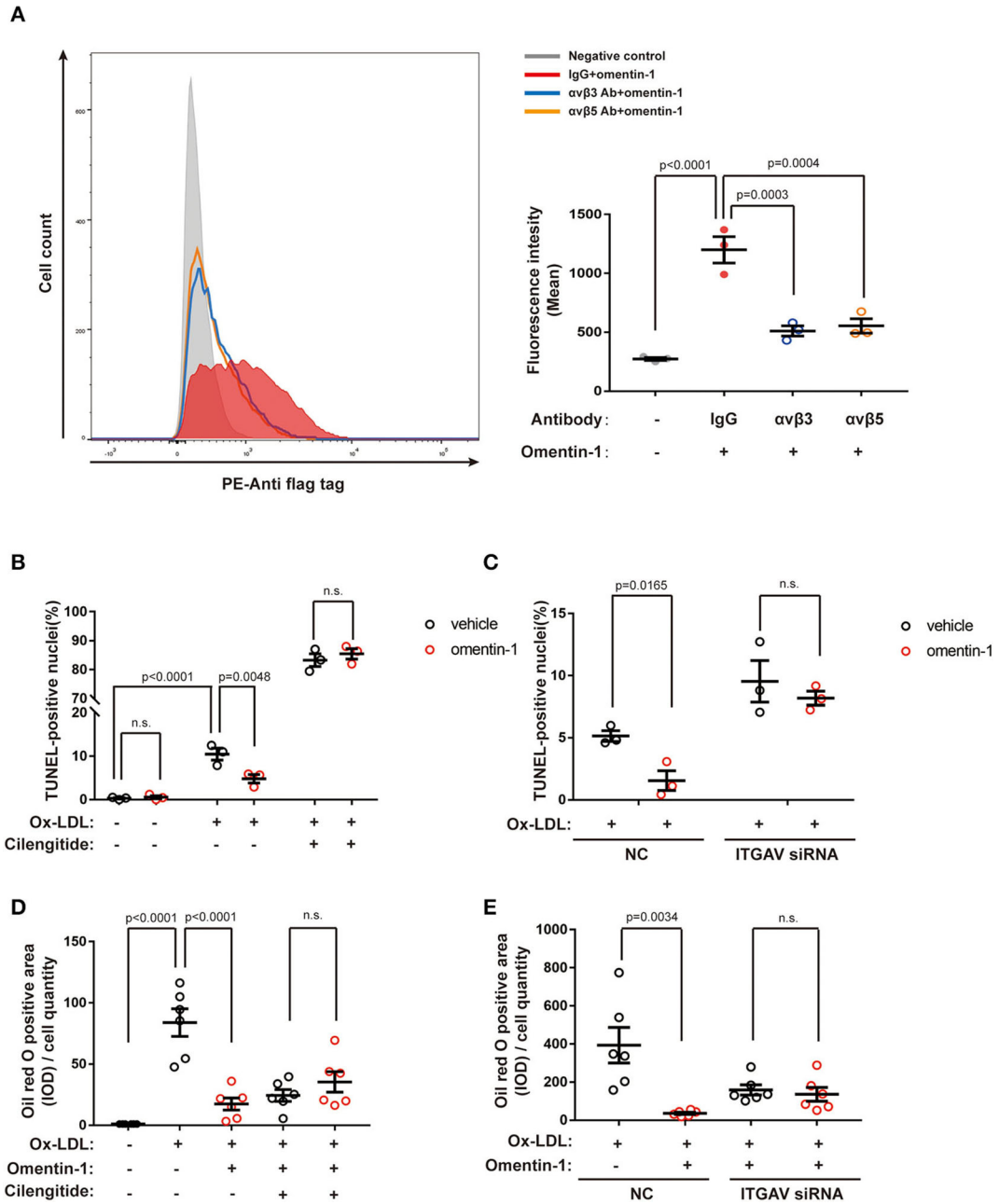

FIGURE 5 | Neutralizing the antibody against the integrin receptor reduced omentin-1 binding to the cell membrane. Omentin-1 attenuated the apoptosis and lipid burden induced by ox-low-density lipoprotein (LDL) in macrophages. **(A)** THP1 cells were induced by 100 ng/ml PMA for 48 h to transform into a macrophage phenotype. After being pretreated by the IgG isotype or neutralizing antibodies against human integrin αvβ3 or αvβ5, the cells were then incubated with Flag-tagged omentin-1. The retention of omentin-1 on the cell membrane was detected by the antibody against the flag tag (PE-labeled). The mean intensity of PE fluorescence was quantified and used to express the magnitude of omentin-1 retention ($n = 3$). **(B)** The RAW264.7-derived macrophages were pretreated by omentin-1 (800 ng/ml) for 1.5 h, and then they were co-incubated with high ox-LDL (50 μg/ml) for 24 h. Apoptosis of macrophages was probed by an *in situ* cell death detection kit (TUNEL), and the apoptotic rate was presented as the percentage of TUNEL-positive nuclei ($n = 3$). **(C)** The RAW264.7-derived macrophages were transfected by ITGAV siRNA to knock down the expression of ITGAV. Then they were incubated with omentin-1 and high ox-LDL to induce apoptosis. The apoptotic rate was assessed as described above ($n = 3$). **(D)** The RAW264.7-derived macrophages were pretreated by omentin-1 (900 ng/ml) for 1.5 h, and then they were co-incubated with mild ox-LDL (50 μg/ml) for 24 h. The lipid content of the cells was detected by an oil red o stain kit. The integral optical density (IOD) of the oil red o positive area vs. cell counts was calculated to represent the lipid retention in cells ($n = 6$). **(E)** The RAW264.7-derived macrophages were transfected by ITGAV siRNA to knock down the expression of ITGAV. Then they were incubated with omentin-1 and mild ox-LDL to induce apoptosis. The lipid retention of cells was assessed as described above ($n = 6$). All data in this figure were presented as mean ± SEM (n.s., non-significant).

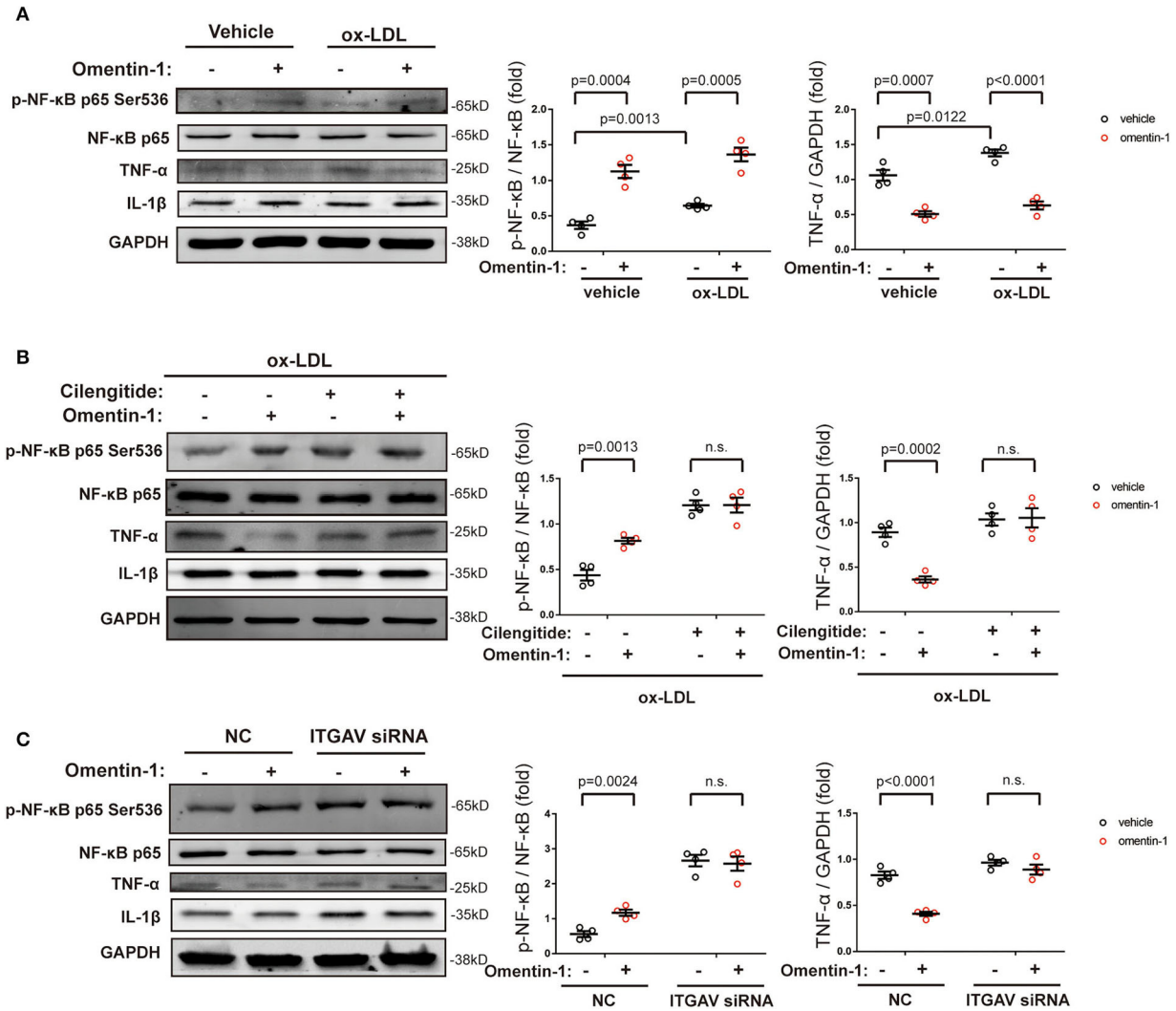

FIGURE 6 | The effects of omentin-1 on inflammatory cytokines expression in the macrophage. **(A)** The RAW264.7-derived macrophages were pretreated by omentin-1 (700 ng/ml) for 1 h. After that, the vehicle (sterilized water) and high ox-LDL (50 μg/ml) were added to the medium and co-incubated with cells for 6 h. The cells were harvested for immunoblotting analysis. The greyscale of each blot was quantified and normalized ($n = 4$). **(B)** The RAW264.7-derived macrophages were pretreated by cilengitide (2.5 μM) for 1 h and co-incubated with or without omentin-1 (700 ng/ml) for another 1 h. After that, they were all stimulated by high ox-LDL (50 μg/ml) for 6 h. The cells were harvested for immunoblotting analysis. The greyscale of each blot was quantified and normalized ($n = 4$). **(C)** The RAW264.7-derived macrophages were transfected by ITGAV siRNA for 6 h. Then the medium was replaced by RPMI 1640 [containing 5% fasting blood sugar (FBS)] and the cells were incubated for 15 h. After that, omentin-1 (700 ng/ml) was added to the medium and co-incubated with cells for 1 h. All of the cells were then treated by high ox-LDL for 6 h. The cells were harvested and subjected to immunoblotting analysis. The greyscale of each blot was quantified and normalized ($n = 4$). All data in this figure were presented as mean ± SEM (n.s., non-significant).

ligation of αvβ3 and αvβ5. The knockdown of the αv integrin suppressed the action of omentin-1 on reducing lipid loading (**Figures 5D,E** and **Supplementary Figures 12, 13**).

The immunoblotting analysis showed that the high ox-LDL had a significant influence on the NF-κB phosphorylation and TNF-α expression. Upon omentin-1 stimulation, the phosphorylation of NF-κB was enhanced while the TNF-α expression was suppressed (**Figure 6A**). Upon the inhibition of αvβ3 and αvβ5 by the cilengitide or knockdown of ITGAV by siRNA, the influence exerted by omentin-1 remarkably diminished (**Figures 6B,C**). The expression of IL-1β was not significantly impacted under the experimental condition.

Omentin-1 Activates the Downstream Signaling Pathway by Stimulating Integrin Receptors

To validate that the integrin αvβ3 and αvβ5 are functional receptors of omentin-1, we also examined the phosphorylation status of the downstream signaling pathway of the integrin

receptor. Immunoblotting analysis indicated that omentin-1 significantly promoted the activation of focal adhesion kinase (FAK) and extracellular-regulated protein kinase (ERK). On the contrary, omentin-1 reduced the phosphorylation of p38 mitogen-activated protein kinase (p38 MAPK). The ligation of integrins by cilengitide and the knockdown of ITGAV both reversed the phosphorylation of the signaling pathway induced by omentin-1 (**Figure 7**).

Ras-related C3 botulinum toxin substrate 1 (Rac1) is a member of the Rho GTPase family, which is frequently activated by integrin signals. We also examined the activity of Rac1 by assessing its membrane translocation. The membrane protein and cytosol protein were extracted, respectively, and the Rac1 expression was measured by immunoblotting analysis. The results showed that omentin-1 promoted the translocation of Rac1 from the cytoplasm to the membrane, and this process could be inhibited by cilengitide (**Supplementary Figure 14B**).

Several previous studies have demonstrated that omentin-1 induces its biological effects *via* adenosine 5′monophosphate-activated protein kinase (AMPK) and the Akt pathway. In this study, we also investigated the effect of omentin-1 on AMPK and Akt phosphorylation in the RAW264.7 macrophage model. The results of the immunoblotting showed that omentin-1 promoted the phosphorylation of both AMPK and Akt. Both the use of cilengitide and the knockdown of ITGAV mitigated the effect of omentin-1 on AMPK and Akt phosphorylation (**Figure 8**).

DISCUSSION

Previous pathological studies of AS lesions from patients with ACS indicated that plaque rupture, which was the sign of vulnerable plaque, was linked to the formation of thin-cap fibroatheroma (TCFA) (15, 16). The increase of plaque collagen content, coupled with the reduction of necrotic cores and macrophage infiltration, was proved to be associated with the reduction of TCFA (17, 18). In this research, we investigated the effects induced by omentin-1 on the AS plaque vulnerability. In both $ApoE^{-/-}$ and $Ldlr^{-/-}$ mice with already-established AS lesions, the systemic delivery of human omentin-1 significantly increased the collagen content and fibrous cap thickness, mitigated the formation of the necrotic core, and suppressed the expression of inflammatory cytokines within the plaque. Furthermore, omentin-1 modulated the macrophage viability and inflammation status by interacting with the integrin receptor αvβ3 and αvβ5 *in vitro*. These data suggest that omentin-1 acts as an anti-inflammatory adipokine that can enhance the stability of the AS plaque by modulating the macrophage function *via* the integrin receptor αvβ3 and αvβ5.

Recent studies indicated that adipose tissue not only functions as an energy storage organ but is also involved in endocrine regulation (19). Adipokines extensively participate in various physiological processes (20). Du et al. demonstrated that omentin-1 expression is lower in the EAT adjacent to the coronary stenotic segments than the non-stenotic segments (7). Watanabe et al. and Hiramatsu-Ito et al. revealed that omentin-1 had counteractive effects on atherogenesis (10, 21). But whether omentin-1 can regulate the stability of already-established plaque remain to be studied. In addition, Yoshiyuki et al. revealed that omentin-1 can protect the myocardium from ischemia-reperfusion injury by activating Akt and AMPK, but the receptor of omentin-1 has not been identified yet (22).

To investigate the therapeutic value of omentin-1, we decided to inject an omentin-1 solution into the jugular vein of a mouse with an already-established AS plaque. We found that after 3 weeks of treatment with omentin-1, the AS plaque exhibited reduced necrotic cores formation and macrophage infiltration, while the collagen content increased significantly. The changes in these three indices were linked to the elevation of plaque stability. Moreover, after the treatment with omentin-1, the expression of TNF-α and IL-1β were significantly suppressed in the AS plaque of the mice. Taken together, all these findings from the animal experiments suggested that omentin-1 treatment can attenuate the vulnerability of already-established plaque, and has a potential applicable value under clinical conditions.

Integrin receptors are expressed in almost all cell types, and they play an important role in cellular crosstalk with its microenvironment. As a transmembrane receptor, integrin serves to integrate the ECM with the internal actomyosin cytoskeleton and alter the cell adhesion and transduce viability signals concomitantly. Integrin αvβ3, which was used to be a marker of tissue repairing and angiogenesis, is now considered to be a promising biomarker of vulnerable plaque (23). The ligation of αvβ3 was proved to be an effective way of attenuating coronary artery atherosclerosis *in vivo* (24). Hoshiga et al. demonstrated that the expression of αvβ3 is higher in AS vessels compared with non-AS vessels. These findings suggest that integrin receptors may have an underlying association with the development of AS. Moreover, in their study, they also found that the expression of αvβ3 is prominent in the adventitia, in contrast to a much lower expression level of it in percutaneous similar-sized microvessels (25). Integrin αvβ3 and omentin-1 shared similar expression profiles in humans: they are primarily expressed by visceral vessels (or adipose tissue) instead of subcutaneous vessels (or adipose tissue). Tsuji et al. discovered that omentin-1 (intelectin-1) contained a fibrinogen-like domain, this discovery suggested that omentin-1 was a potential ligand of integrin (26). All these findings inspired us to further investigate the relationship between omentin-1, integrin receptors, and atherosclerosis.

Macrophages are considered to be closely associated with the progression and vulnerability of the AS plaque. In our study, we discovered that omentin-1 exhibited abundant co-localization with macrophage in the plaque site. Confocal analysis performed *in vivo* and *in vitro* indicated that omentin-1 significantly co-localized with the integrin receptor αvβ3 and αvβ5. Using co-IP analysis, we confirmed the molecular interaction between omentin-1 and integrin receptor, αvβ3 and αvβ5. Through immunoblotting analysis, we discovered that omentin-1 enhanced the phosphorylation FAK, ERK, Akt, and AMPK, while it reduced the phosphorylation of p38 MAPK. Previous studies attributed most of the biological effects of omentin-1 to the activation of Akt and AMPK (27). The study conducted by Yoshiyuki et al. found that the pretreatment

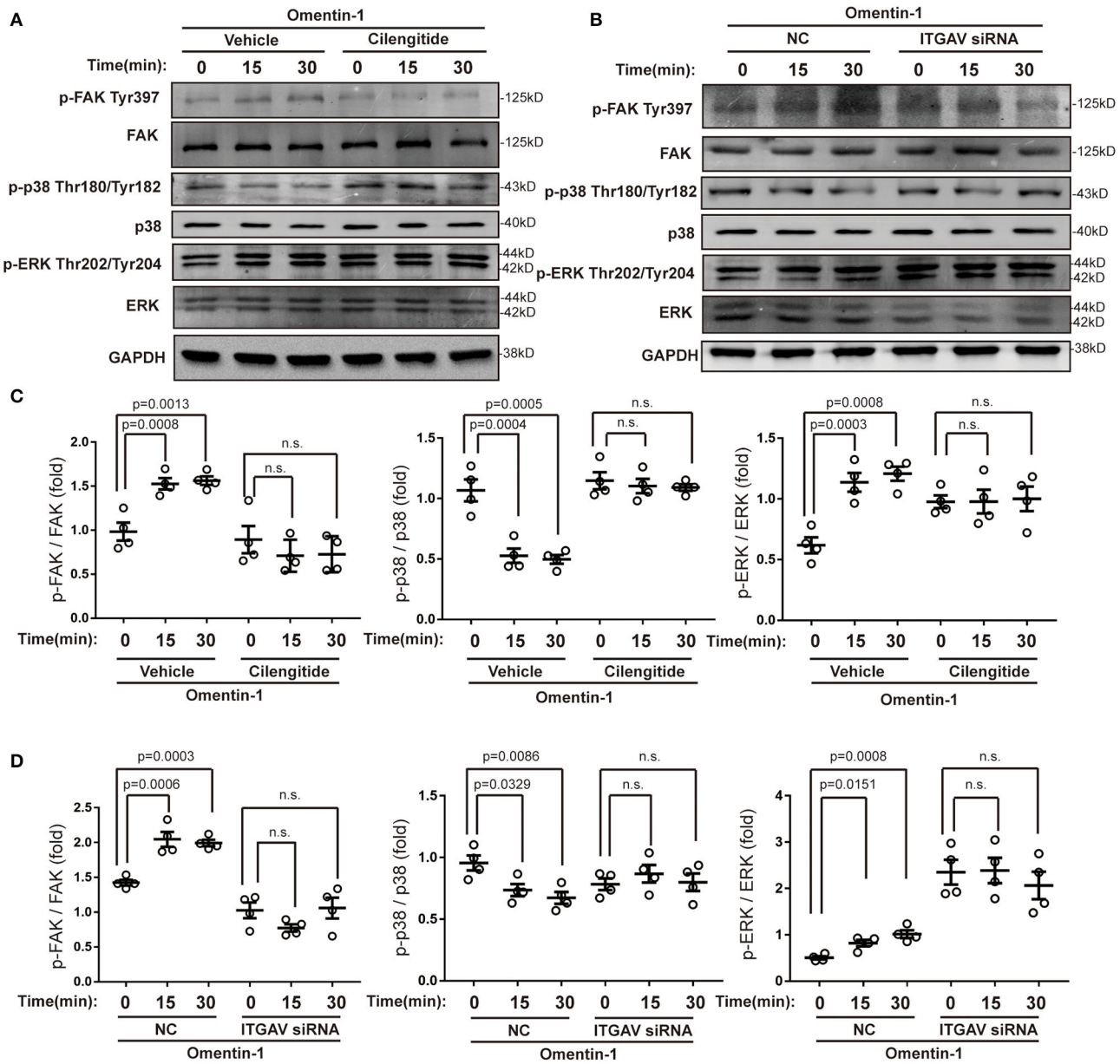

FIGURE 7 | Omentin-1 triggered signals of integrin receptor in macrophages. **(A)** The RAW264.7-derived macrophages were pretreated by vehicle or cilengitide (2.5 μM) for 1 h and were subsequently stimulated by omentin-1 (600 ng/ml) for 0, 15, and 30 min. After that, they were harvested for immunoblotting analysis. **(B)** The RAW264.7-derived macrophages were transfected by negative control (NC) small-interfering RNA (siRNA) or ITGAV siRNA. Then they were stimulated by omentin-1 (600 ng/ml) for 0, 15, and 45 min. After that, they were harvested for immunoblotting analysis. **(C)** The graphs showed that omentin-1 significantly promoted the phosphorylation of focal adhesion kinase (FAK) at Tyr397 and p38 mitogen-activated protein kinase (p38 MAPK) at Thr180/Tyr182, while it suppressed the phosphorylation of the extracellular-regulated protein kinase (ERK) at Thr202/Tyr204 concomitantly. The adding of cilengitide abrogated the influence induced by omentin-1 in the RAW264.7-derived macrophage ($n = 4$). **(D)** The graphs showed that omentin-1 significantly promoted the phosphorylation of FAK at Tyr397, p38 MAPK at Thr180/Tyr182, and suppressed the phosphorylation of ERK at Thr202/Tyr204 in the RAW264.7-derived macrophage transfected by NC siRNA. After being transfected by ITGAV siRNA, the influence induced by omentin-1 was abrogated ($n = 4$). All the data in this figure were presented as mean ± SEM (n.s., non-significant).

with αvβ3 antibody suppressed the omentin-1-induced increase in the Akt phosphorylation, whereas it did not affect the omentin-induced AMPK activation (22). In our research, we discovered that omentin-1 can bind to both αvβ3 and αvβ5, and the pretreatment with cilengitide or knockdown of ITGAV can mitigate the effect of omentin-1 on AMPK and Akt phosphorylation. Our findings are consistent with previous studies that demonstrated that while the phosphorylation of Akt can be induced *via* αvβ3, the phosphorylation of AMPK can be induced by the activation of αvβ5 (28). Protein Rac1,

which is a member of the Rho GTPase family, is frequently stimulated by integrin signals (29). The translocation of Rac1 from the cytoplasm to the membrane is required for the initiation of the activity of Rac1 (30). In our study, we observed the significant membrane translocation of Rac1 upon omentin-1 stimulation, which further proved that integrin receptors serve as the functional receptor of omentin-1. After the adding of cilengitide (potent blocker of αvβ3 and αvβ5) or knocking-down the expression of ITGAV (the common subunit of αvβ3 and αvβ5), the signals transduced by omentin-1 were significantly inhibited. This finding demonstrated that αvβ3 and αvβ5 played an indispensable role in transducing the signals of omentin-1. Additionally, through the flow cytometry analysis, we discovered that the binding of omentin-1 to the cell membrane can be reduced by the antibodies against αvβ3 or αvβ5 which further demonstrated that the biological effect induced by omentin-1 could be regulated by other integrin ligands.

The engulfment of ox-LDL tends to activate macrophages, which subsequently induces the secretion of inflammatory cytokines, cell apoptosis, and eventually contributes to the

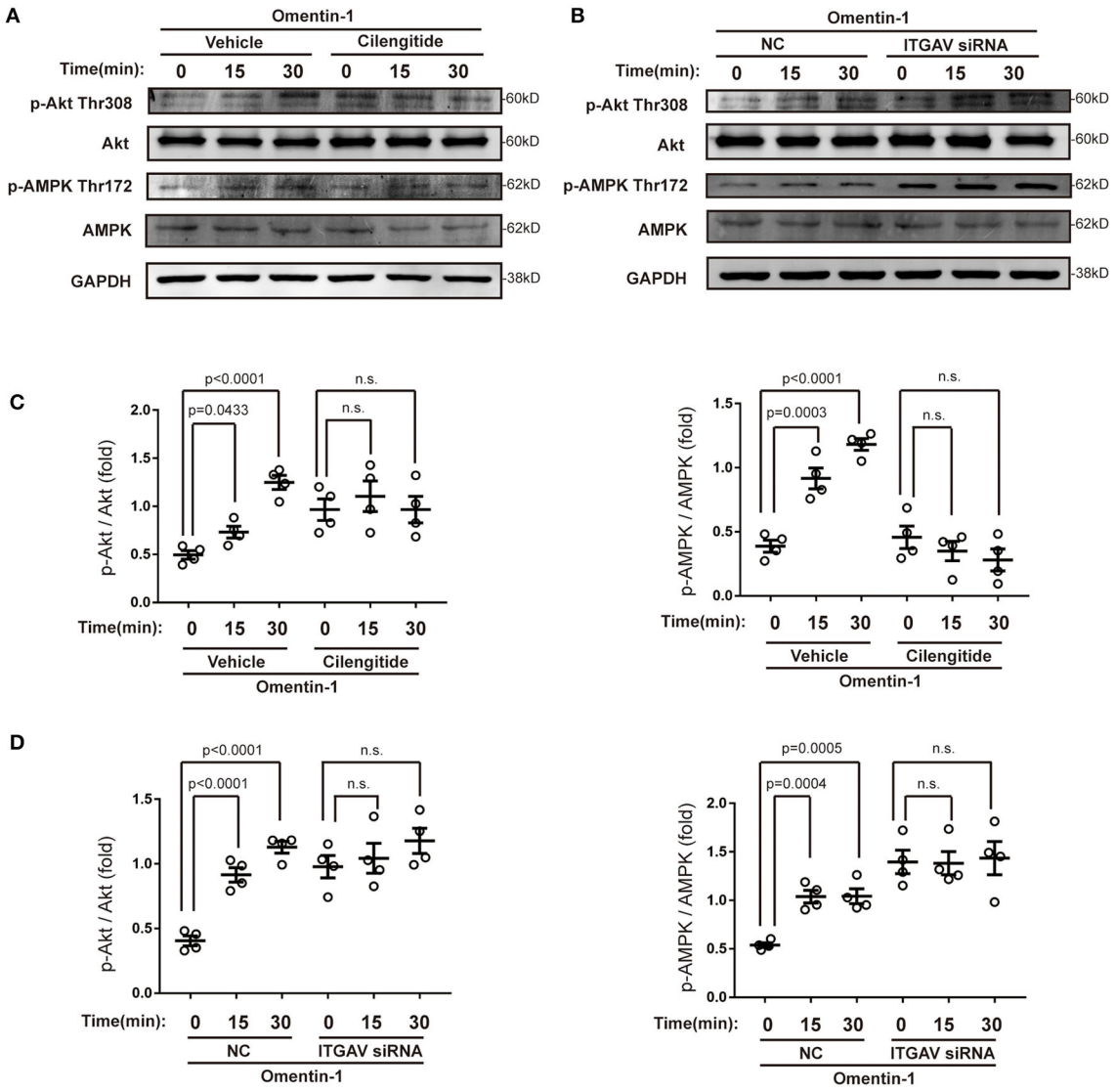

FIGURE 8 | Omentin-1 promoted the phosphorylation of Akt and AMPK *via* integrin receptor. **(A)** The RAW264.7-derived macrophages were pretreated by vehicle or cilengitide (2.5 μM) for 1 h and were subsequently stimulated by omentin-1 (600 ng/ml) for 0, 15, and 30 min. After that, they were harvested for immunoblotting analysis. **(B)** The RAW264.7-derived macrophages were transfected by NC siRNA or ITGAV siRNA. Then they were stimulated by omentin-1 (600 ng/ml) for 0, 15, and 45 min. After that, they were harvested for immunoblotting analysis. **(C)** Graphs showed that omentin-1 significantly promoted the phosphorylation of Akt at Thr308 and AMPK at Thr172. The adding of cilengitide abrogated the influence induced by omentin-1 in the RAW264.7-derived macrophage ($n = 4$). **(D)** Graphs showed that omentin-1 significantly promoted phosphorylation of Akt at Thr308 and AMPK at Thr172 in the RAW264.7-derived macrophage transfected by NC siRNA. After being transfected by ITGAV siRNA, the influence induced by omentin-1 was abrogated ($n = 4$). All the data in this figure were presented as mean ± SEM (n.s., non-significant).

formation of vulnerable AS plaques (31). In this study, we testified that omentin-1 reduced cell apoptosis and lipid loading mainly by interacting with αvβ3 and αvβ5. Animal studies indicated that the intravenous infusion of omentin-1 remarkably reduced the expression of TNF-α and IL-1β in the AS plaque. Cell experiments revealed that omentin-1 treatment only significantly attenuated the TNF-α expression induced by high ox-LDL, whereas the expression of IL-1β was not impacted. The explanation for these rather contradictory results may be that the activation of integrin receptors inhibited the cell apoptosis and necrotic core formation in the AS lesion, and the reduction in cell debris, in turn, alleviated the inflammatory response in the plaque (4). Moreover, we also discovered that omentin-1, which has long been considered an anti-inflammation adipokine, had a stimulatory effect on NF-κB p65 phosphorylation. Although the phosphorylation of NF-κB p65 on ser536 was considered to promote the transcription of inflammatory cytokines, our study indicated that the phosphorylation of NF-κB did not impact the anti-inflammation function of omentin-1. However, our research also indicated that omentin-1 inhibited the phosphorylation of p38 MAPK, which was a positive regulator of TNF-α (32). The inhibition of p38 MAPK phosphorylation, which was induced by omentin-1, may be a plausible explanation for this result.

Our data revealed that omentin-1 produced favorable effects on plaque stability by interacting with αvβ3 and αvβ5 integrins in macrophage. Extracellular matrix proteins, such as fibronectin, vitronectin, and fibrinogen, bind to integrin receptors and elicit downstream signals (outside-in signaling). Several studies have reported that the activation of integrin receptors was associated with the increase of the resistance to cell apoptosis (33). The ligand-bound integrins regulate the actin network through additional adaptor proteins, leading to integrin clustering and the activation of FAK and the Src family kinase. Upon the assistance of FAK, Src phosphorylates downstream substrates, including ERK and PI3K/Akt pathways. These pathways subsequently produce pro-survival effects by promoting the phosphorylation of cytoplasmic targets (34).

Our findings provided a key explanation for previous studies focused on omentin-1. Yin et al. reported that omentin-1 exerted beneficial effects on mesenchymal stem cells by inhibiting apoptosis, promoting proliferation, and increasing the secretion of angiogenic cytokines (35). These functions are consistent with the bioeffects induced by integrin receptors (36). Besides, Antonov AS et al. reported that the ligation of the integrin receptors also prevented the transformation of blood monocyte and macrophage into foam cell phenotype by the down-regulation of CD36 and scavenge receptor-A, which supported the results found by Hiramatsu-Ito et al. (21, 37).

Integrins are widely implicated in cell adhesion, proliferation, phagocytosis, and vascular formation. Several studies have explored that integrins played a vital role in atherosclerosis and the metabolic process (38, 39). The bioinformatic analysis of the EAT of coronary artery disease (CAD) patients revealed that the focal adhesion pathway, which was mainly a downstream signal of integrin receptors, may act a significant role in coronary AS pathogenesis (40). Because omentin-1 has exhibited a unique protective effect on the cardiovascular system, a detailed analysis of the omentin-1 structure and its biological active motif is needed to be done in the future. Furthermore, our research also suggests that the integrin receptor αvβ3 and αvβ5, as the receptor of omentin-1, are a potential target in treating cardiovascular diseases.

DATA AVAILABILITY STATEMENT

The raw data supporting the conclusions of this article will be made available by the authors, without undue reservation.

ETHICS STATEMENT

The animal study was reviewed and approved by Capital Medical University Animal Care and Use Committee.

AUTHOR CONTRIBUTIONS

XL is the first author of this study. XL, YS, and ZW conceived the experiments and conducted the experiments. XL drafted the manuscript. SY, MY, LP, JieY, JiaY, QS, JL, YL, and YZ helped to analyze and interpret the data. All authors read and approved the final manuscript.

FUNDING

This study was supported by a grant from the National Natural Science Foundation of China (81670391).

SUPPLEMENTARY MATERIAL

The Supplementary Material for this article can be found online at: https://www.frontiersin.org/articles/10.3389/fcvm.2021.757926/full#supplementary-material

REFERENCES

1. Weber C, Noels H. Atherosclerosis: current pathogenesis and therapeutic options. *Nat Med.* (2011) 17:1410–22. doi: 10.1038/nm.2538
2. Xu H, Jiang J, Chen W, Li W, Chen Z. Vascular macrophages in atherosclerosis. *J Immunol Res.* (2019) 2019:4354786. doi: 10.1155/2019/4354786
3. Moore KJ, Koplev S, Fisher EA, Tabas I, Bjorkegren JLM, Doran AC, et al. Macrophage trafficking, inflammatory resolution, and genomics in atherosclerosis: JACC Macrophage in CVD Series (Part 2). *J Am Coll Cardiol.* (2018) 72:2181–97. doi: 10.1016/j.jacc.2018.08.2147
4. Bäck M, Yurdagul A, Tabas I, Öörni K, Kovanen PT. Inflammation and its resolution in atherosclerosis: mediators and therapeutic opportunities. *Nat Rev Cardiol.* (2019) 16:389–406. doi: 10.1038/s41569-019-0169-2
5. Fuster JJ, Ouchi N, Gokce N, Walsh K. Obesity-induced changes in adipose tissue microenvironment and their impact on cardiovascular disease. *Circ Res.* (2016) 118:1786–807. doi: 10.1161/CIRCRESAHA.115.306885

6. Gaborit B, Venteclef N, Ancel P, Pelloux V, Gariboldi V, Leprince P, et al. Human epicardial adipose tissue has a specific transcriptomic signature depending on its anatomical peri-atrial, peri-ventricular, or peri-coronary location. *Cardiovasc Res.* (2015) 108:62–73. doi: 10.1093/cvr/cvv208
7. Du Y, Ji Q, Cai L, Huang F, Lai Y, Liu Y, et al. Association between omentin-1 expression in human epicardial adipose tissue and coronary atherosclerosis. *Cardiovasc Diabetol.* (2016) 15:90. doi: 10.1186/s12933-016-0406-5
8. Yamawaki H, Tsubaki N, Mukohda M, Okada M, Hara Y. Omentin, a novel adipokine, induces vasodilation in rat isolated blood vessels. *Biochem Biophys Res Commun.* (2010) 393:668–72. doi: 10.1016/j.bbrc.2010.02.053
9. Uemura Y, Shibata R, Kanemura N, Ohashi K, Kambara T, Hiramatsu-Ito M, et al. Adipose-derived protein omentin prevents neointimal formation after arterial injury. *FASEB J.* (2015) 29:141–51. doi: 10.1096/fj.14-258129
10. Watanabe K, Watanabe R, Konii H, Shirai R, Sato K, Matsuyama TA, et al. Counteractive effects of omentin-1 against atherogenesis. *Cardiovas Res.* (2016) 110:118–28. doi: 10.1093/cvr/cvw016
11. Zhong X, Li X, Liu F, Tan H, Shang D. Omentin inhibits TNF-α-induced expression of adhesion molecules in endothelial cells via ERK/NF-κB pathway. *Biochem Biophys Res Commun.* (2012) 425:401–6. doi: 10.1016/j.bbrc.2012.07.110
12. Beer AJ, Pelisek J, Heider P, Saraste A, Reeps C, Metz S, et al. PET/CT imaging of integrin alphavbeta3 expression in human carotid atherosclerosis. *JACC Cardiovasc Imaging.* (2014) 7:178–87. doi: 10.1016/j.jcmg.2013.12.003
13. Mousa SA. alphav Vitronectin receptors in vascular-mediated disorders. *Med Res Rev.* (2003) 23:190–9. doi: 10.1002/med.10031
14. Wesener DA, Wangkanont K, McBride R, Song X, Kraft MB, Hodges HL, et al. Recognition of microbial glycans by human intelectin-1. *Nat Struct Mol Biol.* (2015) 22:603–10. doi: 10.1038/nsmb.3053
15. Burke AP, Farb A, Malcom GT, Liang YH, Smialek J, Virmani R. Coronary risk factors and plaque morphology in men with coronary disease who died suddenly. *N Engl J Med.* (1997) 336:1276–82. doi: 10.1056/NEJM199705013361802
16. Virmani R, Kolodgie FD, Burke AP, Farb A, Schwartz SM. Lessons from sudden coronary death: a comprehensive morphological classification scheme for atherosclerotic lesions. *Arterioscler Thromb Vasc Biol.* (2000) 20:1262–75. doi: 10.1161/01.ATV.20.5.1262
17. Bentzon JF, Otsuka F, Virmani R, Falk E. Mechanisms of plaque formation and rupture. *Circ Res.* (2014) 114:1852–66. doi: 10.1161/CIRCRESAHA.114.302721
18. Marcu L, Jo JA, Fang Q, Papaioannou T, Reil T, Qiao JH, et al. Detection of rupture-prone atherosclerotic plaques by time-resolved laser-induced fluorescence spectroscopy. *Atherosclerosis.* (2009) 204:156–64. doi: 10.1016/j.atherosclerosis.2008.08.035
19. Oikonomou EK, Antoniades C. The role of adipose tissue in cardiovascular health and disease. *Nat Rev Cardiol.* (2019) 16:83–99. doi: 10.1038/s41569-018-0097-6
20. Cao H. Adipocytokines in obesity and metabolic disease. *J Endocrinol.* (2014) 220:T47–59. doi: 10.1530/JOE-13-0339
21. Hiramatsu-Ito M, Shibata R, Ohashi K, Uemura Y, Kanemura N, Kambara T, et al. Omentin attenuates atherosclerotic lesion formation in apolipoprotein E-deficient mice. *Cardiovasc Res.* (2016) 110:107–17. doi: 10.1093/cvr/cvv282
22. Kataoka Y, Shibata R, Ohashi K, Kambara T, Enomoto T, Uemura Y, et al. Omentin prevents myocardial ischemic injury through AMP-activated protein kinase- and Akt-dependent mechanisms. *J Am Coll Cardiol.* (2014) 63:2722–33. doi: 10.1016/j.jacc.2014.03.032
23. Jiang L, Zhu H, Li Y, Wu X, Wang H, Cheng Z. Detecting vulnerable atherosclerotic plaques by (68)Ga-labeled divalent cystine knot peptide. *Mol Pharmaceutics.* (2019) 16:1350–7. doi: 10.1021/acs.molpharmaceut.8b01291
24. Jenkins WS, Vesey AT, Vickers A, Neale A, Moles C, Connell M, et al. *In vivo* alpha-V beta-3 integrin expression in human aortic atherosclerosis. *Heart.* (2019) 105:1868–75. doi: 10.1136/heartjnl-2019-315103
25. Hoshiga M, Alpers CE, Smith LL, Giachelli CM, Schwartz SM. Alpha-v beta-3 integrin expression in normal and atherosclerotic artery. *Circ Res.* (1995) 77:1129–35. doi: 10.1161/01.RES.77.6.1129
26. Tsuji S, Uehori J, Matsumoto M, Suzuki Y, Matsuhisa A, Toyoshima K, et al. Human intelectin is a novel soluble lectin that recognizes galactofuranose in carbohydrate chains of bacterial cell wall. *J Biol Chem.* (2001) 276:23456–63. doi: 10.1074/jbc.M103162200
27. Watanabe T, Watanabe-Kominato K, Takahashi Y, Kojima M, Watanabe R. Adipose tissue-derived omentin-1 function and regulation. *Compr Physiol.* (2017) 7:765–81. doi: 10.1002/cphy.c160043
28. Bi J, Zhang J, Ren Y, Du Z, Li T, Wang T, et al. Irisin reverses intestinal epithelial barrier dysfunction during intestinal injury via binding to the integrin αVβ5 receptor. *J Cell Mol Med.* (2020) 24:996–1009. doi: 10.1111/jcmm.14811
29. Rose DM, Alon R, Ginsberg MH. Integrin modulation and signaling in leukocyte adhesion and migration. *Immunol Rev.* (2007) 218:126–34. doi: 10.1111/j.1600-065X.2007.00536.x
30. Abdrabou A, Wang Z. Post-translational modification and subcellular distribution of Rac1: an update. *Cells.* (2018) 7:20263. doi: 10.3390/cells7120263
31. Kavurma MM, Rayner KJ, Karunakaran D. The walking dead: macrophage inflammation and death in atherosclerosis. *Curr Opin Lipidol.* (2017) 28:91–8. doi: 10.1097/MOL.0000000000000394
32. Sabio G, Davis RJ. TNF and MAP kinase signalling pathways. *Seminars Immunol.* (2014) 26:237–45. doi: 10.1016/j.smim.2014.02.009
33. Cooper J, Giancotti FG. Integrin signaling in cancer: mechanotransduction, stemness, epithelial plasticity, and therapeutic resistance. *Cancer Cell.* (2019) 35:347–67. doi: 10.1016/j.ccell.2019.01.007
34. Giancotti FG, Ruoslahti E. Integrin signaling. *Science.* (1999) 285:1028–32. doi: 10.1126/science.285.5430.1028
35. Yin L, Huang D, Liu X, Wang Y, Liu J, Liu F, et al. Omentin-1 effects on mesenchymal stem cells: proliferation, apoptosis, and angiogenesis *in vitro*. *Stem Cell Res Therapy.* (2017) 8:224. doi: 10.1186/s13287-017-0676-1
36. Desgrosellier JS, Cheresh DA. Integrins in cancer: biological implications and therapeutic opportunities. *Nat Rev Cancer.* (2010) 10:9–22. doi: 10.1038/nrc2748
37. Antonov AS, Kolodgie FD, Munn DH, Gerrity RG. Regulation of macrophage foam cell formation by αVβ3 integrin. *Am J Pathol.* (2004) 165:247–58. doi: 10.1016/S0002-9440(10)63293-2
38. Finney AC, Stokes KY, Pattillo CB, Orr AW. Integrin signaling in atherosclerosis. *Cell Mol Life Sci.* (2017) 74:2263–82. doi: 10.1007/s00018-017-2490-4
39. Williams AS, Kang L, Wasserman DH. The extracellular matrix and insulin resistance. *Trends Endocrinol Metab.* (2015) 26:357–66. doi: 10.1016/j.tem.2015.05.006
40. Wang W, Liu Q, Wang Y, Piao H, Li B, Zhu Z, et al. Integration of gene expression profile data of human epicardial adipose tissue from coronary artery disease to verification of hub genes and pathways. *BioMed Res Int.* (2019) 2019:8567306. doi: 10.1155/2019/8567306

Conflict of Interest: The authors declare that the research was conducted in the absence of any commercial or financial relationships that could be construed as a potential conflict of interest.

Publisher's Note: All claims expressed in this article are solely those of the authors and do not necessarily represent those of their affiliated organizations, or those of the publisher, the editors and the reviewers. Any product that may be evaluated in this article, or claim that may be made by its manufacturer, is not guaranteed or endorsed by the publisher.

frontiers in Cardiovascular Medicine

ORIGINAL RESEARCH
published: 11 November 2021
doi: 10.3389/fcvm.2021.764024

Loss of Hepatic Surf4 Depletes Lipid Droplets in the Adrenal Cortex but Does Not Impair Adrenal Hormone Production

Xiaole Chang[1†], Yongfang Zhao[1†], Shucun Qin[1], Hao Wang[1], Bingxiang Wang[1], Lei Zhai[1], Boyan Liu[1], Hong-mei Gu[2] and Da-wei Zhang[2*]*

[1] Institute of Atherosclerosis, College of Basic Medical Sciences, Shandong First Medical University, Shandong Academy of Medical Sciences, Tai'an, China, [2] Department of Pediatrics and Group on the Molecular and Cell Biology of Lipids, Faculty of Medicine and Dentistry, University of Alberta, Edmonton, AB, Canada

OPEN ACCESS

Edited by:
Changcheng Zhou, University of California, Riverside, United States

Reviewed by:
Chieko Mineo, University of Texas Southwestern Medical Center, United States
Mary G. Sorci-Thomas, Medical College of Wisconsin, United States

***Correspondence:**
Shucun Qin
scqin@sdfmu.edu.cn
Da-wei Zhang
dzhang@ualberta.ca

[†]These authors have contributed equally to this work

Specialty section:
This article was submitted to Lipids in Cardiovascular Disease, a section of the journal Frontiers in Cardiovascular Medicine

Received: *24 August 2021*
Accepted: *20 October 2021*
Published: *11 November 2021*

Citation:
Chang X, Zhao Y, Qin S, Wang H, Wang B, Zhai L, Liu B, Gu H-m and Zhang D-w (2021) Loss of Hepatic Surf4 Depletes Lipid Droplets in the Adrenal Cortex but Does Not Impair Adrenal Hormone Production. Front. Cardiovasc. Med. 8:764024. doi: 10.3389/fcvm.2021.764024

The adrenal gland produces steroid hormones to play essential roles in regulating various physiological processes. Our previous studies showed that knockout of hepatic Surf4 (Surf4^{LKO}) markedly reduced fasting plasma total cholesterol levels in adult mice, including low-density lipoprotein and high-density lipoprotein cholesterol. Here, we found that plasma cholesterol levels were also dramatically reduced in 4-week-old young mice and non-fasted adult mice. Circulating lipoprotein cholesterol is an important source of the substrate for the production of adrenal steroid hormones. Therefore, we investigated whether adrenal steroid hormone production was affected in Surf4^{LKO} mice. We observed that lacking hepatic Surf4 essentially eliminated lipid droplets and significantly reduced cholesterol levels in the adrenal gland; however, plasma levels of aldosterone and corticosterone were comparable in Surf4^{LKO} and the control mice under basal and stress conditions. Further analysis revealed that mRNA levels of genes encoding enzymes important for hormone synthesis were not altered, whereas the expression of scavenger receptor class B type I (SR-BI), low-density lipoprotein receptor (LDLR) and 3-hydroxy-3-methyl-glutaryl-CoA reductase was significantly increased in the adrenal gland of Surf4^{LKO} mice, indicating increased *de novo* cholesterol biosynthesis and enhanced LDLR and SR-BI-mediated lipoprotein cholesterol uptake. We also observed that the nuclear form of SREBP2 was increased in the adrenal gland of *Surf4*^{LKO} mice. Taken together, these findings indicate that the very low levels of circulating lipoprotein cholesterol in Surf4^{LKO} mice cause a significant reduction in adrenal cholesterol levels but do not significantly affect adrenal steroid hormone production. Reduced adrenal cholesterol levels activate SREBP2 and thus increase the expression of genes involved in cholesterol biosynthesis, which increases *de novo* cholesterol synthesis to compensate for the loss of circulating lipoprotein-derived cholesterol in the adrenal gland of Surf4^{LKO} mice.

Keywords: proprotein convertase subtilisin/kexin 9, LDL–cholesterol, cholesterol, triglyceride, atherosclerosis, LDL receptor (LDLR)

INTRODUCTION

The adrenal cortex uses cholesterol as the substrate to produce steroid hormones, thus playing an indispensable role in regulating metabolism, water and salt balance and blood pressure, the immune system, stress response, and sexual development. Under a normal physiological condition, ∼80% of cholesterol used in adrenal cortex hormone synthesis is derived from circulating lipoproteins, such as scavenger receptor class B, type I (SR-BI)-mediated selective uptake of cholesteryl ester from high-density lipoprotein (HDL) and low-density lipoprotein receptor (LDLR)-mediated endocytosis of LDL (1). The remaining cholesterol is contributed by *de novo* biosynthesis from acetate via the mevalonate pathway (2, 3), in which 3-hydroxy-3-methylglutaryl coenzyme A reductase (HMGCR) is the rate-limiting enzyme (4, 5). Cholesterol is stored as cholesteryl ester (CE) in lipid droplets in the adrenal cortex (2, 6, 7), which can be converted to free cholesterol by lipase-mediated lipolysis as needed for steroidogenesis (8–10). Free cholesterol from lipolysis of CE in lipid droplets, *de novo* biosynthesis, and plasma membrane can be rapidly transported to mitochondria by steroidogenic acute regulatory protein (StAR) (6, 8, 11, 12), where steroid hormones are synthesized from cholesterol by different mitochondrial P450 enzymes and then immediately released to circulation. Adrenal insufficiency characterized by low blood levels of cortisol and aldosterone can lead to a series of systemic clinical symptoms, including hypotension, anorexia, fatigue, syncope, hyponatremia, sexual dysfunction, mental disorders, etc. (3).

Surfeit 4 (Surf4) is a cargo receptor resided on the endoplasmic reticulum (ER) membrane, where it facilitates the transport of secretory proteins from the ER to the Golgi apparatus. Surf4 also mediates the retrograde transport of STING from the Golgi apparatus to the ER (13–19). We and others have found that Surf4 mediates secretion of very low-density lipoprotein (VLDL) (15, 19). Circulating VLDL is catabolized and eventually converted to LDL, which is then cleared from circulation mainly through hepatic LDLR (20). Knockout of LDLR ($Ldlr^{-/-}$) in mice increases plasma cholesterol levels and risk for the development of atherosclerosis. Mutations in LDLR cause familial hypercholesterolemia (FH) in humans, which is characterized by elevated plasma LDL cholesterol levels and increased risk for cardiovascular disease. Current lipid-lowering drugs, such as statins and PCSK9 inhibitors, reduce plasma cholesterol levels mainly through increasing LDLR levels and thus LDL clearance. Therefore, they cannot effectively reduce plasma LDL cholesterol levels in FH patients.

Knockout of Surf4 in mouse liver ($Surf4^{LKO}$) and knockdown of Surf4 in $Ldlr^{-/-}$ mice significantly reduce VLDL secretion, leading to a drastic reduction in plasma cholesterol levels (15). However, we did not observe significant hepatic lipid accumulation or notable liver damage in $Surf4^{LKO}$ mice or Surf4 knockdown $Ldlr^{-/-}$ mice, indicating that hepatic Surf4 inhibition is a promising therapeutic target for lowering plasma lipids through suppressing LDL production. However, circulating lipoprotein-derived cholesterol, especially HDL cholesterol, is an important substrate for the production of adrenal cortex steroid hormones (1, 12, 21–24). Therefore, we investigated whether hepatic Surf4 silencing affected the production of adrenal cortex hormones. We found that lipid droplets and cholesterol levels were significantly reduced in the adrenal gland of $Surf4^{LKO}$ mice compared to the control $Surf4^{Flox}$ mice. However, plasma levels of adrenal cortex hormones, including corticosterone, aldosterone, and dehydroepiandrosterone (DHEA), and adrenocorticotropin (ACTH) were comparable in $Surf4^{LKO}$ and $Surf4^{Flox}$ mice. The expression of HMGCR, LDLR and SR-BI was markedly increased in the adrenal gland of $Surf4^{LKO}$ mice. Therefore, knockout of hepatic Surf4 did not affect the production of adrenal cortex hormones despite a significant reduction in plasma and adrenal cholesterol levels.

MATERIALS AND METHODS

Materials

H&E staining kit and saturated oil red O staining solution were purchased from Beijing Soleibao Technology Co., Ltd. (Beijing, China). Mouse corticosterone, aldosterone, DHEA, and ACTH ELISA kits were from Shanghai Enzyme Link Biotechnology Co., Ltd. (Shanghai, China). Total cholesterol kit was purchased from Qiyi Biotechnology Co., Ltd. (Shanghai, China). Anti-LDLR, HMGCR, SR-BI, and SREBP-2 antibodies were from Abcam. Anti-β-actin and ACAT1 antibodies were from Beijing Boaosen Biotechnology Co., Ltd. (Beijing, China) and Proteintech, respectively. Horseradish enzyme-labeled goat anti-rabbit or mouse IgG was purchased from Beijing Zhongshan Jinqiao Biotechnology Co., Ltd. (Beijing, China). RNAprep Pure Tissue Kit, EasyQuick RT MasterMix, and Top Green qPCR SuperMix were purchased from Tiangen Biochemical Technology Co., Ltd. (Beijing, China), Kangwei Century Biotechnology Co., Ltd. (Beijing, China), and Beijing Quanshijin Biotechnology Co., Ltd. (Beijing, China), respectively.

Animal

$Sur4^{Flox}$ and $Surf4^{LKO}$ mice in C57BL/6 background were generated as described (15) and were maintained in the animal facility at Shandong First Medical University (Taian, China). Three to five mice were housed per cage with free access to H_2O in a climate-controlled facility with a 12-h light/dark cycle. After weaning, mice were fed *ad libitum* a chow diet containing 20% protein, 5% fat, and 48.7% carbohydrates (Keao Xieli, Beijing, China). All animal procedures were approved by Shandong First Medical University's Animal Care and Use Committee.

Histochemistry

The experiments were performed as described (15, 25). Briefly, for H&E staining, tissues were fixed, embedded in paraffin, cut into 8 μm, and mounted on slides. After, the sections were deparaffinized, rehydrated, and then stained with hematoxylin and eosin sequentially. For Oil Red-O staining, fresh tissue samples were embedded in Optimal Cutting Temperature compound, cut into 10 μm, and then mounted on slides. After, the sections were fixed in formalin, stained with Oil Red-O and then hematoxylin. All slices were imaged on a microscope (Nikon, Tokyo, Japan). Relative stained areas were quantified

TABLE 1 | Sequences of the primers.

Name	Primer sequence	Product (bp)
StAR	Forward: 5′-TTGGGCATACTCAACAACCAG-3′	195
	Reverse: 5′-GACATTTGGGTTCCACTCTCC-3′	
Cyp11a1	Forward: 5′-GGTGTAGCTCAGGACTTCATCAAA-3′	109
	Reverse: 5′-ACTCAAAGGAAAAGCGGAATAGG-3′	
Cyp21a2	Forward: 5′-CTCCGGCTATGACATCCCTA-3′	151
	Reverse: 5′-ACAGCCAAAGGATGGTGTTC-3′	
Cyp11b1	Forward: 5′-GTATCGAGAGCTGGCAGAGG-3′	140
	Reverse: 5′-GGGTTGATGTCGTGTCAGTG-3′	
Cyp11b2	Forward: 5′-CTGAACGCTATATGCCTCAGC-3′	160
	Reverse: 5′-AGTGTCTCCACCTGGAAGGTT-3′	
Ldlr	Forward: 5′-ACCCGCCAAGATCAAGAAAG-3′	148
	Reverse: 5′-GCTGGAGATAGAGTGGAGTTTG-3′	
Hmgcr	Forward: 5′-GCCCTCAGTTCAAATTCACAG-3′	96
	Reverse: 5′-TTCCACAAGAGCGTCAAGAG-3′	
Scarb1	Forward: 5′-CCCTATTCCATTGACTCTGAGC-3′	121
	Reverse: 5′-CACATAAGAGGATTCGAGAGCG-3′	
Hmgcs1	Forward: 5′-GCGTCTTTGCTTGTGTCTAATC-3′	125
	Reverse: 5′-GAGAACACTCCAACCCTCTTC-3′	
Mvk	Forward: 5′-GGAGCAACTGGAGAAGCTAAA-3′	100
	Reverse: 5′-TGCCAGGTACAGGTAGAGAA-3′	
Fdps	Forward: 5′-TCGGGTGAAAGCACTGTATG-3′	100
	Reverse: 5′-GCACTGCTCTATGAGACTCTTG-3′	
Fdft1	Forward: 5′-CTCACCTGAAAGCCCAGAAA-3′	96
	Reverse: 5′-CCTGCTTTCCTTACCCTCATC-3′	
Gapdh	Forward: 5′-AACTTTGGCATTGTGGAAGG-3′	132
	Reverse: 5′-GGATGCAGGGATGATGTTCT-3′	

with ImageJ software (National Institute of Health) using color segmentation and threshold analysis.

ELISA

Blood samples were collected from fasted or non-fasted mice. Plasma levels of adrenal hormones and ACTH were measured with their specific ELISA kits according to the manufacturer's instruction. The optical density was measured using a SpectraMax i3x Microplate Reader (Filter: 450 nm).

Quantitative Real-Time PCR

Total RNAs were extracted from mouse tissues using RNAprep Pure Tissue Kit according to the manufacturer's protocols. Complementary DNA (cDNA) was synthesized using EasyQuick RT MasterMix from Kangwei Century Company (China). qRT-PCR was carried out using Top Green qPCR SuperMix. $2^{-\Delta\Delta ct}$ was used to analyze relative gene expression. *Gapdh* was the control. The primers were designed and synthesized by Shanghai Shenggong Biological Engineering Co., Ltd. and listed in **Table 1**.

Immunoblotting

Tissue samples were collected from euthanized mice and homogenized in RIPA buffer (50 mM Tris, pH 7.4, 150 mM NaCl, 1% TritonX-100, 1% sodium deoxycholate, 0.1% SDS, sodium orthovanadate, sodium fluoride, EDTA, leupeptin, and PMSF) as described (15). The supernatant was harvested as tissue homogenate after centrifugation. Protein concentrations were determined by the BCA protein assay. Equal amounts of total lysate proteins were applied to SDS-PAGE and then transferred to PVDF membranes (Millipore) by electroblotting. Immunoblotting was performed using specific antibodies as indicated. Antibody binding was detected by HRP-conjugated goat anti-mouse or rabbit IgG antibody, followed with Pierce™ ECL Western Blotting Substrate. The image was acquired and analyzed on a Tanon 5200 automatic chemiluminescence image analysis system. The densitometry was quantified in Image-Pro Plus.

Plasma and Tissue Lipids

Blood samples were collected into EDTA-coated tubes from mice and then centrifuged at 3000 x g for 10 min. Plasma from each mouse was subjected to analysis of triglyceride (TG), total cholesterol (TC), and HDL-C using their specific kits according to the manufacturer's instructions (Applygen, Beijing, China).

Adrenal lipids were extracted using the methyl-tert-butyl ether (MTBE) method as described (15). Briefly, tissues (3–5 mg) were homogenized in 280 μl of cold methanol containing an internal standard of cholesteryl ester (CE) 17:0. In total, 50 μl of homogenates were stored to analyze protein content using a commercial BCA protein assay kit (Solarbio Co., Beijing, China). MTBE (1 ml) was added to the remaining volume of homogenates; the samples were vortexed, rotated for 1 h at room temperature, and then mixed with 325 μl H_2O. After, the samples were centrifuged at 10,000 ×g for 10 min at 4°C. The upper hydrophobic fraction was collected and dried under nitrogen gas. The samples were dissolved in methanol. Total cholesterol and free cholesterol were measured using an enzymatic kit from Biosino Biotechnology (Beijing, China) and Applygen (Beijing, China), respectively.

Dried lipid extracts were also reconstituted in 200 μl of acetonitrile:2-propanol (1:1, v/v) and then subjected to liquid chromatography tandem mass spectrometry (LC-MS/MS) analysis as described (15). Briefly, LC-MS/MS was performed using a Shimadzu LC-20 AD binary pump system coupled to a SIL-20AC autoinjector and interfaced with an ABI 4000 QTrap mass spectrometer (Sciex, Framingham, MA, USA). Chromatographic separations were carried out on a Waters Symmetry C18 column with a Waters C18 guard column. The mobile phase comprised (A) 10 mM ammonium formate in acetonitrile: water: formic acid (83:17:0.1, v/v/v) and (B) 10 mM ammonium formate in acetonitrile: 2-propanol: formic acid (50:50:0.1, v/v/v). Isocratic elution was performed with 95% B for 16 min. Relative quantification of lipids in samples was carried out based on the intensity of each species divided by the intensity of the internal standards and protein concentrations.

Statistical Analysis

All statistical analyses were carried out by GraphPad Prism version 9.0 (GraphPad Software). The significant differences between groups were determined via a Student's *t*-test or a Mann Whitney test. All data met normal distribution criteria and variance between groups that was analyzed by F-test

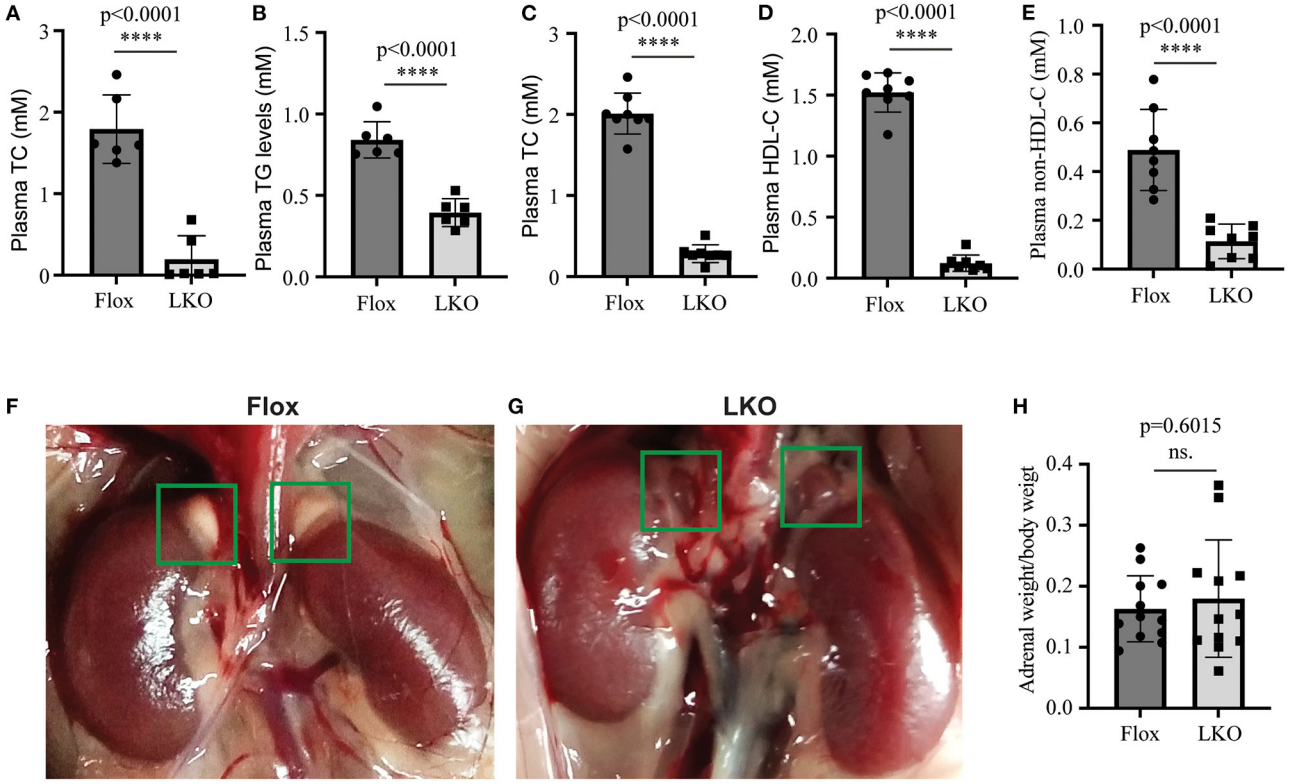

FIGURE 1 | The effect of hepatic knockout of Surf4 on plasma lipids and the adrenal gland. **(A–E)** Plasma lipid levels. Blood samples were collected from 4-week-old mice **(A,B)** fasted for 10 h or 14-week-old mice fasted for 10 h and refed for 4 h **(C–E)**. Plasma levels of total cholesterol (TC), triglycerides (TG), and HDL cholesterol (HDL-C) were measured using their specific enzymatic kits ($n \geq 6$). Non-HDL-C was calculated by subtracting HDL-C from TC. **(F,G)** Representative images of the adrenal glands of *Surf4*^{Flox} **(F)** and *Surf4*^{LKO} mice **(G)** (green frame). Similar results were observed in other mice. **(H)** Ratio of the adrenal weight to the body weight of the same mouse. Values of all data were mean ± S.D. The significance was defined as $^{****}p < 0.0001$ and $P > 0.05$, no significance (ns.).

showed no significant difference ($P > 0.05$). Values of all data, unless otherwise indicated, were depicted as mean ± S.D. All experiments, unless indicated, were repeated at least three times. The significance was defined as $^{*}p < 0.05$, $^{**}p < 0.01$, $^{***}p < 0.001$, and $^{****}p < 0.0001$.

RESULTS

Effect of Hepatic Surf4 Silencing on Cholesterol Levels in the Adrenal Gland

We have reported that knockout of hepatic Surf4 impairs VLDL secretion and markedly reduces fasting plasma cholesterol and TG levels in adult mice (15). Here, we found that fasting plasma total cholesterol and TG levels were also dramatically reduced in 4-week-old young *Surf4*^{LKO} mice (**Figures 1A,B**). Furthermore, similar to the results of the study on fasting plasma cholesterol levels (15), non-fasting plasma levels of total cholesterol, HDL cholesterol and non-HDL cholesterol were all markedly reduced in *Surf4*^{LKO} mice (**Figures 1C–E**). Therefore, the lack of hepatic Surf4 drastically reduced plasma cholesterol levels in young mice and fasted or non-fasted adult mice. Considering that circulating lipoprotein cholesterol is an important substrate for adrenal steroid hormone biosynthesis, we assessed whether the adrenal gland was affected in *Surf4*^{LKO} mice. As shown in **Figures 1F,G**, the adrenal glands in *Surf4*^{Flox} and *Surf4*^{LKO} mice were similar in size and shape. The ratio of adrenal weight to body weight was also comparable in the two genotypes (**Figure 1H**). However, their colors were different, white and red in *Surf4*^{Flox} and *Surf4*^{LKO} mice, respectively.

Next, we used H&E and Oil Red O staining to analyze the histology of the adrenal gland. As shown in **Figure 2A**, the adrenal cortex of *Surf4*^{Flox} mice displayed many vacuoles, which were essentially absent in the adrenal cortex of *Surf4*^{LKO} mice. Oil Red O staining revealed that the adrenal cortex of *Surf4*^{Flox} mice contained many lipid droplets stained red (**Figure 2B**). Conversely, in the adrenal gland of *Surf4*^{LKO} mice, the staining appeared as small puncta and was markedly reduced (**Figures 2B,C**), and the levels of total cholesterol and cholesteryl ester (CE) were also significantly reduced (**Figures 2D,E**). However, adrenal free cholesterol levels were not significantly affected by hepatic knockout of Surf4 (**Figure 2F**). A detailed analysis of adrenal lipids using LC-MS/MS revealed that the levels of CE18:1, CE20:4, and CE22:6, but not CE 16:1, CE18:0, CE18:2, CE18:3, CE20:3, or CE20:5 were significantly reduced in the adrenal gland of *Surf4*^{LKO} mice (**Table 2**). Therefore, lacking hepatic Surf4 significantly reduced cholesteryl ester levels and

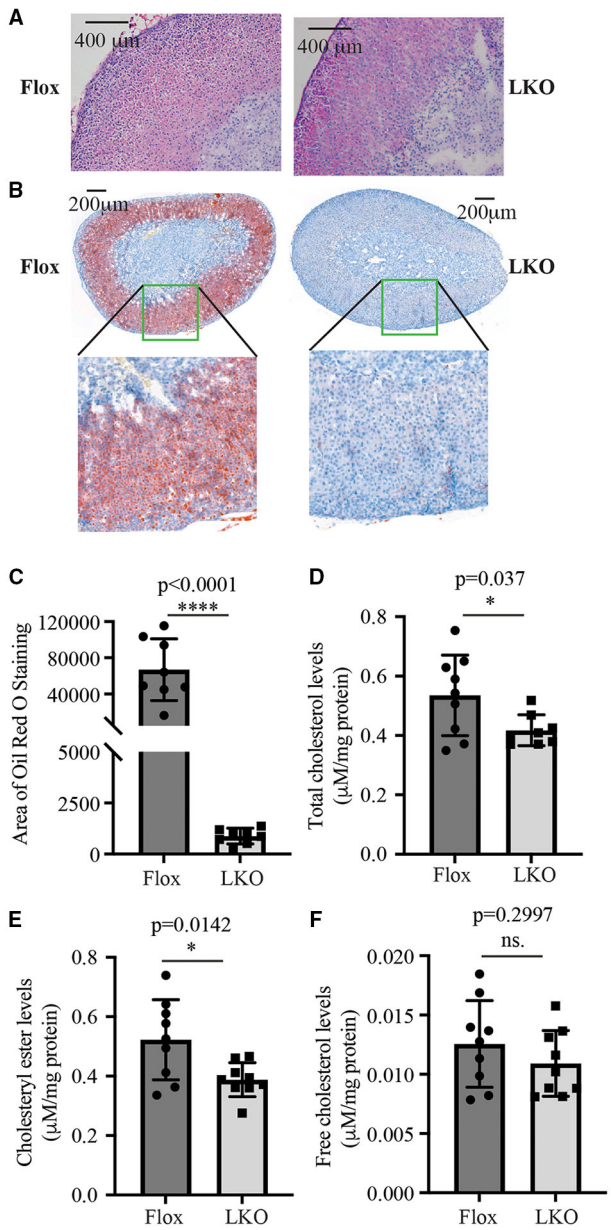

FIGURE 2 | Impact of lacking hepatic Surf4 on the adrenal gland. **(A)** H&E staining of adrenal sections. **(B,C)** Oil Red O of adrenal sections. Representative figures were shown. Similar results were obtained in other mice. The images of Oil Red O staining were quantified using ImageJ **(C)** (8 mice per group). Data were analyzed by a Student's *t*-test ($p < 0.0001$) and a Mann Whitney test ($p = 0.0002$). **(D–F)** Adrenal total cholesterol **(D)**, cholesteryl ester **(E)**, and free cholesterol **(F)** levels. Lipids were extracted from mouse adrenal glands using the MTBE method and then subjected to total cholesterol and free cholesterol measurement using their specific enzymatic kit. Cholesteryl ester levels were calculated by subtracting free cholesterol from total cholesterol. Values of all data were mean ± S.D. The significance was defined as $^{*}p < 0.05$ and $^{****}p < 0.0001$, $p > 0.05$, no significance (ns.).

virtually depleted lipid droplets in the adrenal gland, which could explain the color change observed in the adrenal gland of *Surf4*^{LKO} mice.

TABLE 2 | Adrenal cholesteryl ester levels.

CE	Flox	LKO	*P*-value
CE16:1	0.036 ± 0.013	0.032 ± 0.018	0.6957
CE18:0	0.306 ± 0.293	0.261 ± 0.214	0.7737
CE18:1	**0.402 ± 0.111**	**0.181 ± 0.159**	**0.0191**
CE18:2	0.84 ± 0.323	0.49 ± 0.379	0.1153
CE18:3	0.88 ± 0.864	0.578 ± 0.597	0.4085
CE20:3	6.046 ± 2.961	3.011 ± 3.75	0.1091
CE20:4	**9.225 ± 5.653**	**2.33 ± 2.914**	**0.0141**
CE20:5	4.764 ± 5.591	2.257 ± 3.939	0.3321
CE22:6	**31.272 ± 24.202**	**7.56 ± 8.549**	**0.0219**

Lipids were extracted from the adrenal gland using MTBE and then analyzed with LC-MS/MS. Relative quantification of lipids in samples was carried out based on the intensity of each species divided by the intensity of the internal standard (CE17:0) and protein concentrations. Values of all data were mean ± S.D. The significance was defined as $p < 0.05$ (shown in bold).

Effect of Hepatic Surf4 Knockout on the Production of Adrenal Cortex Hormones

The adrenal cortex uses cholesterol as the substrate to produce steroid hormones. Therefore, we used ELISA to measure the plasma levels of aldosterone, corticosterone and DHEA, and found that their levels were comparable in non-fasted *Surf4*^{Flox} and *Surf4*^{LKO} mice (**Figures 3A–C**). We then used qRT-PCR to assess the expression of genes that are crucial for adrenal cortex hormone synthesis. StAR mediates the transport of cholesterol from the outer to the inner membrane of the mitochondrial and is believed to be the rate-limiting step in adrenal corticosteroid synthesis. Cyp11a1 converts cholesterol to pregnenolone. Cyp17a1 is involved in the last step of DHEA synthesis. Cyp11b1 and Cyp11b2 are the key enzymes for aldosterone synthesis, and Cyp21a2 and Cyp11b1 are crucial for corticosteroid synthesis. qRT-PCR data showed that the mRNA levels of these enzymes were not significantly altered in the adrenal gland of *Surf4*^{LKO} mice (**Figure 3D**). Taken together, these findings indicate that under basal conditions, the production of adrenal cortex hormone in *Surf4*^{LKO} mice is not significantly affected.

Stress stimuli, such as fasting and cold exposure, can stimulate the pituitary to release ACTH, which then activates the adrenal cortex to produce corticosterone (12, 26, 27). To evaluate whether the production of adrenal steroid hormones was affected in *Surf4*^{LKO} mice under stress conditions, we subjected mice to fasting and found that the levels of fasting plasma corticosterone, aldosterone and DEHA were comparable in *Surf4*^{Flox} and *Surf4*^{LKO} mice (**Figures 4A–C**). We then challenged fasted mice with acute cold stimulation at 4°C for up to 4 h. As shown in **Figure 4D**, the plasma levels of corticosterone were comparable and displayed a similar pattern in *Surf4*^{Flox} and *Surf4*^{LKO} mice, increasing after cold stimulation until the 0.5-h time point and then gradually decreasing at the 1.5-h time point. Therefore, the production of corticosterone under stress stimuli is not affected by hepatic Surf4 knockout.

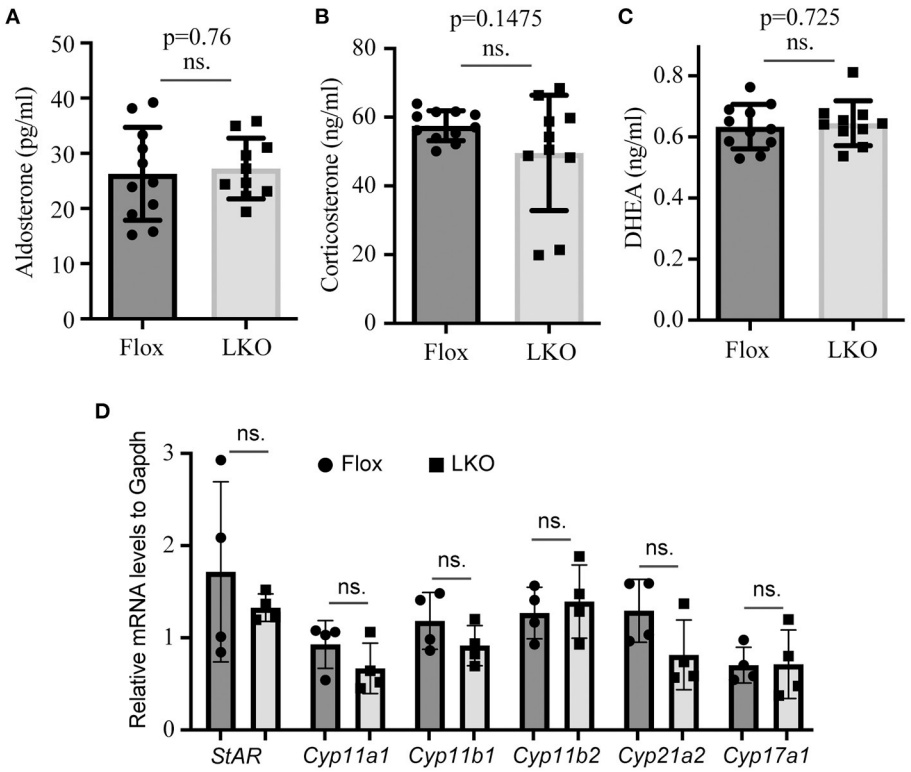

FIGURE 3 | Impact of lacking hepatic Surf4 on plasma levels of adrenal hormones. **(A–C)** Plasma adrenal hormone levels. Blood samples were collected from non-fasted mice [*Surf4*^{Flox} (Flox) and *Surf4*^{LKO} (LKO) mice, 10–14-week-old]. Aldosterone **(A)**, corticosterone **(B)**, and DHEA **(C)** were measured using their specific ELISA kits. **(D)** qRT-PCR. Total RNAs were extracted from adrenal glands and then subjected to qRT-PCR. The relative mRNA levels were the ratio of the target's mRNA levels indicated to that of *Gapdh* at the same condition ($n = 4$). Values of all data were mean ± S.D. $p > 0.05$ was defined as no significant difference (ns.).

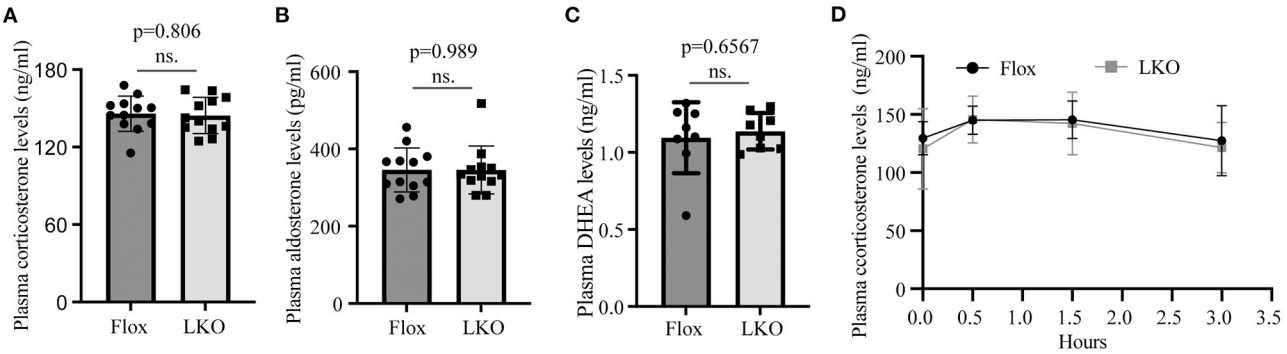

FIGURE 4 | Plasma levels of adrenal steroid hormones. **(A–C)** Fasting plasma hormone levels. Mice were fasted for 12 h, and blood samples were collected for the measurement of corticosterone **(A)**, aldosterone **(B)**, and DHEA **(C)** with their specific ELISA kits. **(D)** Plasma corticosterone levels. Mice fasted for 12 h were subjected to cold stimulation (4°C). Blood samples were collected at the indicated time points. Plasma corticosterone levels were measured using its specific ELISA kit ($n = 6$). Values of all data were mean ± S.D. $p > 0.05$ was defined as no significant difference (ns.).

Effect of Hepatic Surf4 Knockout on the Expression of Genes Involved in Cholesterol Metabolism

Adrenal cells take up circulating LDL and HDL cholesterol via LDLR and SR-BI, respectively. They also produce cholesterol via *de novo* biosynthesis. Therefore, we examined the expression of LDLR, SR-BI, and HMG-CoA reductase, the latter being the rate-limiting enzyme in cholesterol biosynthesis. qRT-PCR showed that the mRNA levels of *Scarb*, *Ldlr*, and *Hmgcr* were all significantly increased in the adrenal gland of *Surf4*^{LKO} mice (**Figure 5A**). We also measured the mRNA levels of additional genes involved in cholesterol biosynthesis, including HMG-CoA synthase (*Hmgcs1*), mevalonate kinase (*Mvk*), farnesyl diphosphate synthase (*Fdps*), and squalene synthase (*Fdft1*), and

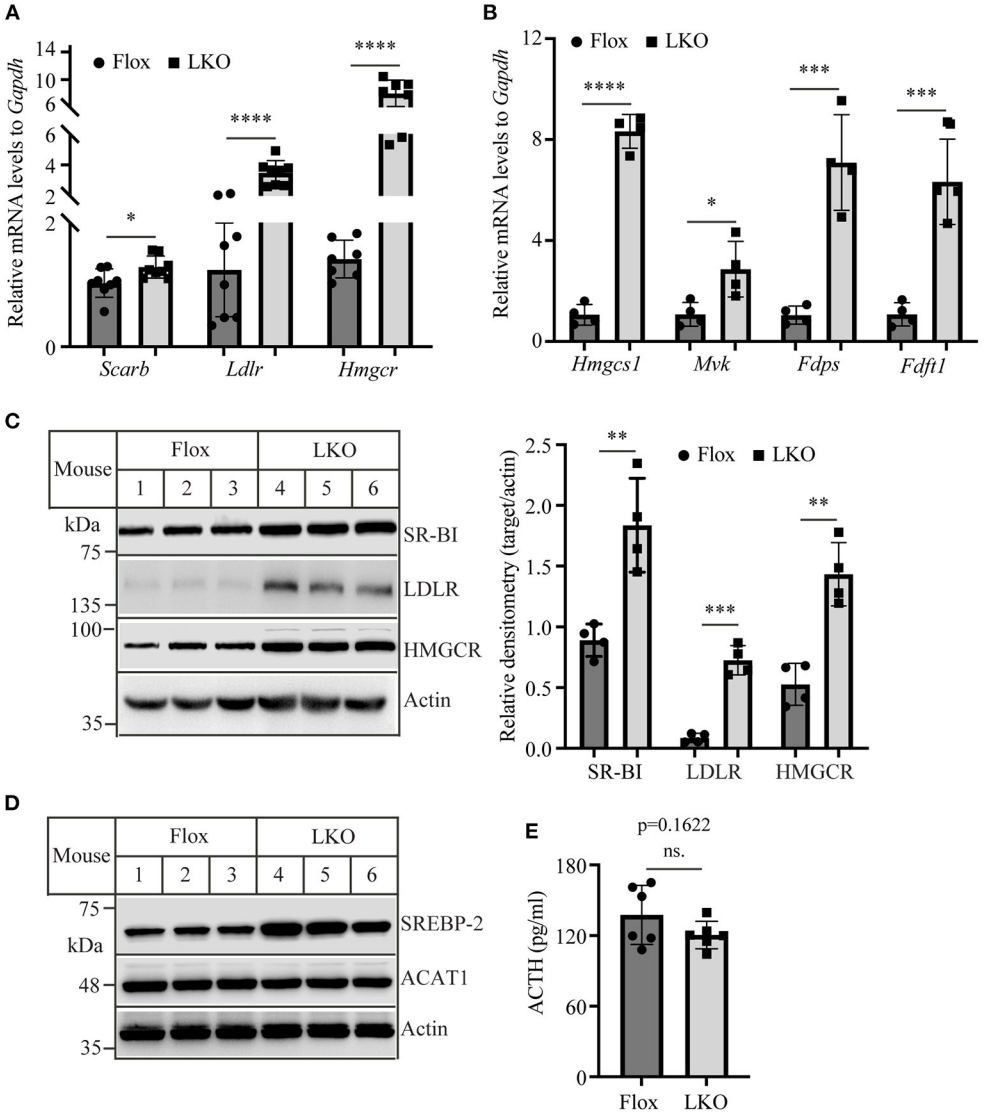

FIGURE 5 | The expression of genes involved in cholesterol metabolism. **(A,B)** qRT-PCR. The relative mRNA levels were the ratio of the target's mRNA levels indicated to that of *Gapdh* at the same condition. **(C,D)** Immunoblotting. The same amount of adrenal homogenate was applied to Western Blot using antibodies as indicated. Representative figures were shown. The densitometry was assessed. The relative densitometry is the densitometry of each target to that of actin in the same sample **(C)**. **(E)** Plasma levels of ACTH. Mice (10–12-week-old, male) were fasted for 12 h. Plasma was then collected and subjected to the measurement of ACTH using an ELISA kit. Values of all data were mean ± S.D. The significance was defined as $^{*}p < 0.05$, $^{**}p < 0.01$, $^{***}p < 0.001$, and $^{****}p < 0.0001$. $p > 0.05$ was defined as no significant difference (ns.).

observed that they were all significantly increased in the adrenal gland of *Surf4*^{LKO} mice (**Figure 5B**). Consistently, western blot data revealed an increase in the protein levels of adrenal SR-BI, LDLR and HMGCR in *Surf4*^{LKO} mice (**Figure 5C**). SREBP2 upregulates the transcription of genes involved in cholesterol metabolism, such as LDLR, HMGCR, HMG-CoA synthase, squalene synthase, etc. (28). Acyl-CoA:cholesterol acyltransferase 1 (ACAT1) converts free cholesterol to cholesteryl ester. Lacking ACAT1 significantly reduces cellular cholesteryl ester levels (29). Therefore, we measured adrenal SREBP2 and ACAT1 levels. As shown in **Figure 5D**, the levels of the nuclear form of SREBP2 were increased, while ACAT1 levels were not changed in the adrenal gland of *Surf4*^{LKO} mice compared to *Surf4*^{Flox} mice. In addition, ACTH can increase expression of LDLR and SR-BI (30, 31). Therefore, we assessed plasma ACTH levels in *Surf4*^{Flox} and *Surf4*^{LKO} mice using ELISA. As shown in **Figure 5E**, lacking hepatic Surf4 did not significantly affect plasma ACTH levels. Taken together, these findings suggest an increased ability in cholesterol *de novo* biosynthesis and uptake of circulating lipoproteins in the adrenal gland of *Surf4*^{LKO} mice.

DISCUSSION

Here, we found that (1) knockout of hepatic Surf4 in mice essentially depleted lipid droplets and significantly reduced cholesteryl ester levels in the adrenal glands of *Surf4*^{LKO} mice; (2) the production of adrenal cortex steroid hormones was comparable in *Surf4*^{LKO} and *Surf4*^{Flox} mice under basal and stress conditions; and (3) the expression of genes involved in steroid hormone synthesis was not affected, whereas the expression of SREBP2 and genes involved in cholesterol metabolism was significantly increased in the adrenal gland of *Surf4*^{LKO}. Taken together, these findings indicate that the ability of the adrenal cortex to produce steroid hormones is not affected by the lack of hepatic Surf4 even though plasma lipoprotein cholesterol levels are drastically reduced in the young and fasted and non-fasted adult mice.

VLDL is exclusively secreted by hepatocytes and can be catabolized into LDL in circulation. Hepatic knockout of Surf4 virtually eliminates VLDL secretion and LDL production in mice. LDLR-mediated LDL endocytosis can provide cholesterol for adrenal steroidogenesis (24, 32). However, several lines of evidence show that SR-BI-mediated selective CE uptake from HDL serves as an important source of cholesterol for adrenal cortex steroidogenesis under stress conditions (1, 12, 21–23). In addition, Bochem et al. reported that HDL-derived cholesterol is an important substrate for adrenal cortex hormone synthesis under a basal condition in humans (33). Knockout of apolipoprotein A-I (apoA-I), the main structural lipoprotein on HDL, reduced plasma HDL-C levels by ∼74% and essentially depleted lipid droplets in the adrenal cortex. The production of corticosteroids under a basal or stress condition was also significantly reduced in apoA-I knockout mice (34–36). Like apoA-I knockout mice, *Surf4*^{LKO} mice display a similar reduction in plasma HDL cholesterol levels under fasting and non-fasting conditions. However, the production of adrenal cortex hormones in *Surf4*^{LKO} mice was not significantly affected even under stress conditions.

SR-BI mediates the selective uptake of CE from HDL (23, 37). Knockout of SR-BI significantly reduces the production of glucocorticoids under stress conditions even though plasma levels of apoA-I and HDL cholesterol levels remain unchanged and are increased, respectively (1, 21, 37). SR-BI can bind to HDL particles reconstituted with apoA-I, apoA-II, apoE, and apoC-III (38); however, lacking apoA-I significantly reduces the capacity of SR-BI to mediate CE-selective uptake from HDL. Furthermore, the accumulation of CE in steroidogenic cells is essentially disappeared in apoA-I knockout mice (34, 35, 39). These findings indicate that apo A-I is essential for the effective transfer of CE from HDL to adrenal cortex cells. *Surf4*^{LKO} mice display a significant reduction in plasma levels of HDL cholesterol and apoA-I; however, unlike apoA-I knockout mice that are completely deficient in apoA-I, *Surf4*^{LKO} mice still retain a small portion of circulating apoA-I and HDL cholesterol (15). The increased expression of SR-BI in the adrenal gland of *Surf4*^{LKO} mice may enhance the ability of adrenal cortex cells to take up cholesterol from residual circulating HDL, thereby mitigating the adverse effect of decreased plasma cholesterol levels on adrenal cortex steroidogenesis.

Cholesterol biosynthesis provides ∼20% of the substrate for steroidogenesis in the adrenal cortex under normal conditions. Total cholesterol levels in the adrenal gland of *Surf4*^{LKO} mice were significantly reduced, leading to increased levels of the nuclear form of SREBP2. This upregulated the expression of genes involved in cholesterol *de novo* biosynthesis and LDLR. LDLR mediates endocytosis of LDL and apoE-containing lipoprotein particles, such as VLDL and chylomicron remnants. Plasma apoE levels are comparable in *Surf4*^{LKO} and *Surf4*^{Flox} mice (15). Together, our findings suggest that cholesterol biosynthesis and LDLR-mediated endocytosis of apoE-containing lipoproteins may increase in adrenal cortex cells of *Surf4*^{LKO} mice, which at least partially compensate for the loss of HDL-derived cholesterol.

Deficiency of hepatic Surf4 significantly reduces VLDL secretion, plasma cholesterol levels and the development of atherosclerosis but does not cause notable liver damage or hepatic lipid accumulation in mice (15). Here, we found that knockout of hepatic Surf4 drastically reduces plasma cholesterol in 4-week-old young mice (newly weaned) and non-fasted adult mice, whereas the production of adrenal steroid hormones is not significantly impaired in *Surf4*^{LKO} mice under normal and stress conditions. These findings indicate that hepatic Surf4 inhibition is a promising therapeutic target for lowering plasma lipid levels in patients whose disease cannot be effectively managed by currently available strategies.

DATA AVAILABILITY STATEMENT

The original contributions presented in the study are included in the article/supplementary material, further inquiries can be directed to the corresponding author/s.

ETHICS STATEMENT

The animal study was reviewed and approved by Shandong First Medical University's Animal Care and Use Committee.

AUTHOR CONTRIBUTIONS

SQ and D-wZ designed the experiments, analyzed data, and wrote the manuscript. XC and ZY performed the experiments, analyzed data, and wrote the first draft. HW, BW, LZ, YZ, BL, and H-mG performed experiments and analyzed data. All authors contributed to the article and approved the submitted version.

FUNDING

This work was supported by National Natural Science Foundation of China (NSFC 81929002), Academic Promotion Program of Shandong First Medical University (2019QL010 and 2019PT009), and The Natural Sciences and Engineering Research Council of Canada (RGPIN-2016-06479). D-wZ was also supported by grants from Canadian Institutes of Health Research (PS 178091) and the China Institute at the University of China. SQ was supported by 91539114 and ts201511057.

REFERENCES

1. Ito M, Ye X, Wang Q, Guo L, Hao D, Howatt D, et al. SR-BI (Scavenger Receptor BI), not LDL (Low-Density Lipoprotein) receptor, mediates adrenal stress response-brief report. *Arterioscler Thromb Vasc Biol.* (2020) 40:1830–7. doi: 10.1161/ATVBAHA.120.314506
2. Kraemer FB, Khor VK, Shen WJ, Azhar S. Cholesterol ester droplets and steroidogenesis. *Mol Cell Endocrinol.* (2013) 371:15–9. doi: 10.1016/j.mce.2012.10.012
3. Lyraki R, Schedl A. Adrenal cortex renewal in health and disease. *Nat Rev Endocrinol.* (2021) 17:421–34. doi: 10.1038/s41574-021-00491-4
4. Johnson BM, DeBose-Boyd RA. Underlying mechanisms for sterol-induced ubiquitination and ER-associated degradation of HMG CoA reductase. *Semin Cell Dev Biol.* (2018) 81:121–8. doi: 10.1016/j.semcdb.2017.10.019
5. Luo J, Yang H, Song BL. Mechanisms and regulation of cholesterol homeostasis. *Nat Rev Mol Cell Biol.* (2020) 21:225–45. doi: 10.1038/s41580-019-0190-7
6. Li Y, Khanal P, Norheim F, Hjorth M, Bjellaas T, Drevon CA, et al. Plin2 deletion increases cholesteryl ester lipid droplet content and disturbs cholesterol balance in adrenal cortex. *J Lipid Res.* (2021) 62:100048. doi: 10.1016/j.jlr.2021.100048
7. Yu J, Zhang L, Li Y, Zhu X, Xu S, Zhou XM, et al. The adrenal lipid droplet is a new site for steroid hormone metabolism. *Proteomics.* (2018) 18:e1800136. doi: 10.1002/pmic.201800136
8. Li H, Brochu M, Wang SP, Rochdi L, Cote M, Mitchell G, et al. Hormone-sensitive lipase deficiency in mice causes lipid storage in the adrenal cortex and impaired corticosterone response to corticotropin stimulation. *Endocrinology.* (2002) 143:3333–40. doi: 10.1210/en.2002-220341
9. Weckman A, Di Ieva A, Rotondo F, Syro LV, Ortiz LD, Kovacs K, et al. Autophagy in the endocrine glands. *J Mol Endocrinol.* (2014) 52:R151–63. doi: 10.1530/JME-13-0241
10. Sztalryd C, Brasaemle DL. The perilipin family of lipid droplet proteins: gatekeepers of intracellular lipolysis. *Biochim Biophys Acta Mol Cell Biol Lipids.* (2017) 1862:1221–32. doi: 10.1016/j.bbalip.2017.07.009
11. Deng B, Shen WJ, Dong D, Azhar S, Kraemer FB. Plasma membrane cholesterol trafficking in steroidogenesis. *FASEB J.* (2019) 33:1389–400. doi: 10.1096/fj.201800697RRR
12. Hoekstra M, Korporaal SJ, van der Sluis RJ, Hirsch-Reinshagen V, Bochem AE, Wellington CL, et al. LCAT deficiency in mice is associated with a diminished adrenal glucocorticoid function. *J Lipid Res.* (2013) 54:358–64. doi: 10.1194/jlr.M030080
13. Mukai K, Ogawa E, Uematsu R, Kuchitsu Y, Kiku F, Uemura T, et al. Homeostatic regulation of STING by retrograde membrane traffic to the ER. *Nat Commun.* (2021) 12:61. doi: 10.1038/s41467-020-20234-9
14. Ordonez A, Harding HP, Marciniak SJ, Ron D. Cargo receptor-assisted endoplasmic reticulum export of pathogenic alpha1-antitrypsin polymers. *Cell Rep.* (2021) 35:109144. doi: 10.1016/j.celrep.2021.109144
15. Wang B, Shen Y, Zhai L, Xia X, Gu HM, Wang M, et al. Atherosclerosis-associated hepatic secretion of VLDL but not PCSK9 is dependent on cargo receptor protein Surf4. *J Lipid Res.* (2021) 62:100091. doi: 10.1016/j.jlr.2021.100091
16. Lin Z, King R, Tang V, Myers G, Balbin-Cuesta G, Friedman A, et al. The endoplasmic reticulum cargo receptor surf4 facilitates efficient erythropoietin secretion. *Mol Cell Biol.* (2020) 40:e00180-20. doi: 10.1128/MCB.00180-20
17. Saegusa K, Sato M, Morooka N, Hara T, Sato K. SFT-4/Surf4 control ER export of soluble cargo proteins and participate in ER exit site organization. *J Cell Biol.* (2018) 217:2073–85. doi: 10.1083/jcb.201708115
18. Shen Y, Wang B, Deng S, Zhai L, Gu HM, Alabi A, et al. Surf4 regulates expression of proprotein convertase subtilisin/kexin type 9 (PCSK9) but is not required for PCSK9 secretion in cultured human hepatocytes. *Biochim Biophys Acta Mol Cell Biol Lipids.* (2020) 1865:158555. doi: 10.1016/j.bbalip.2019.158555
19. Wang X, Wang H, Xu B, Huang D, Nie C, Pu L, et al. Receptor-mediated er export of lipoproteins controls lipid homeostasis in mice and humans. *Cell Metab.* (2021) 33:350–366 e7. doi: 10.1016/j.cmet.2020.10.020
20. Goldstein JL, Brown MS. The LDL receptor. *Arterioscler Thromb Vasc Biol.* (2009) 29:431–8. doi: 10.1161/ATVBAHA.108.179564
21. Hoekstra M, Meurs I, Koenders M, Out R, Hildebrand RB, Kruijt JK, et al. Absence of HDL cholesteryl ester uptake in mice via SR-BI impairs an adequate adrenal glucocorticoid-mediated stress response to fasting. *J Lipid Res.* (2008) 49:738–45. doi: 10.1194/jlr.M700475-JLR200
22. Temel RE, Trigatti B, DeMattos RB, Azhar S, Krieger M, Williams DL. Scavenger receptor class B, type I (SR-BI) is the major route for the delivery of high density lipoprotein cholesterol to the steroidogenic pathway in cultured mouse adrenocortical cells. *Proc Natl Acad Sci USA.* (1997) 94:13600–5. doi: 10.1073/pnas.94.25.13600
23. Rigotti A, Trigatti BL, Penman M, Rayburn H, Herz J, Krieger M, et al. targeted mutation in the murine gene encoding the high density lipoprotein (HDL) receptor scavenger receptor class B type I reveals its key role in HDL metabolism. *Proc Natl Acad Sci USA.* (1997) 94:12610–5. doi: 10.1073/pnas.94.23.12610
24. Faust JR, Goldstein JL, Brown MS. Receptor-mediated uptake of low density lipoprotein and utilization of its cholesterol for steroid synthesis in cultured mouse adrenal cells. *J Biol Chem.* (1977) 252:4861–71. doi: 10.1016/S0021-9258(17)40133-5
25. Alabi A, Xia XD, Gu HM, Wang F, Deng SJ, Yang N, et al. Membrane type 1 matrix metalloproteinase promotes LDL receptor shedding and accelerates the development of atherosclerosis. *Nat Commun.* (2021) 12:1889. doi: 10.1038/s41467-021-22167-3
26. van den Beukel JC, Grefhorst A, Quarta C, Steenbergen J, Mastroberardino PG, Lombes M, et al. Direct activating effects of adrenocorticotropic hormone (ACTH) on brown adipose tissue are attenuated by corticosterone. *FASEB J.* (2014) 28:4857–67. doi: 10.1096/fj.14-254839
27. Bowers SL, Bilbo SD, Dhabhar FS, Nelson RJ. Stressor-specific alterations in corticosterone and immune responses in mice. *Brain Behav Immun.* (2008) 22:105–13. doi: 10.1016/j.bbi.2007.07.012
28. Goldstein JL, Brown MS, A. century of cholesterol and coronaries: from plaques to genes to statins. *Cell.* (2015) 161:161–72. doi: 10.1016/j.cell.2015.01.036
29. Meiner VL, Cases S, Myers HM, Sande ER, Bellosta S, Schambelan M, et al. Disruption of the acyl-CoA:cholesterol acyltransferase gene in mice: evidence suggesting multiple cholesterol esterification enzymes in mammals. *Proc Natl Acad Sci USA.* (1996) 93:14041–6. doi: 10.1073/pnas.93.24.14041
30. Heikkila P, Arola J, Liu J, Kahri AI, ACTH. regulates LDL receptor and CLA-1 mRNA in the rat adrenal cortex. *Endocr Res.* (1998) 24:591–3. doi: 10.3109/07435809809032651
31. Shen WJ, Azhar S, Kraemer FB, ACTH. Regulation of Adrenal SR-B1. *Front Endocrinol (Lausanne).* (2016) 7:42. doi: 10.3389/fendo.2016.00042
32. Illingworth DR, Lees AM, Lees RS. Adrenal cortical function in homozygous familial hypercholesterolemia. *Metabolism.* (1983) 32:1045–52. doi: 10.1016/0026-0495(83)90075-6
33. Bochem AE, Holleboom AG, Romijn JA, Hoekstra M, Dallinga-Thie GM, Motazacker MM, et al. High density lipoprotein as a source of cholesterol for adrenal steroidogenesis: a study in individuals with low plasma HDL-C. *J Lipid Res.* (2013) 54:1698–704. doi: 10.1194/jlr.P033449
34. Plump AS, Erickson SK, Weng W, Partin JS, Breslow JL, Williams DL. Apolipoprotein A-I is required for cholesteryl ester accumulation in steroidogenic cells and for normal adrenal steroid production. *J Clin Invest.* (1996) 97:2660–71. doi: 10.1172/JCI118716
35. Plump AS, Azrolan N, Odaka H, Wu L, Jiang X, Tall A, et al. ApoA-I knockout mice: characterization of HDL metabolism in homozygotes and identification of a post-RNA mechanism of apoA-I up-regulation in heterozygotes. *J Lipid Res.* (1997) 38:1033–47. doi: 10.1016/S0022-2275(20)37227-8
36. Ouweneel AB, van der Sluis RJ, Nahon JE, Van Eck M, Hoekstra M. Simvastatin treatment aggravates the glucocorticoid insufficiency associated with hypocholesterolemia in mice. *Atherosclerosis.* (2017) 261:99–104. doi: 10.1016/j.atherosclerosis.2017.02.014
37. Trigatti B, Rayburn H, Vinals M, Braun A, Miettinen H, Penman M, et al. Influence of the high density lipoprotein receptor SR-BI on reproductive and cardiovascular pathophysiology. *Proc Natl Acad Sci USA.* (1999) 96:9322–7. doi: 10.1073/pnas.96.16.9322
38. Thuahnai ST, Lund-Katz S, Anantharamaiah GM, Williams DL, Phillips MC, A. quantitative analysis of apolipoprotein binding to SR-BI: multiple binding sites for lipid-free and lipid-associated apolipoproteins. *J Lipid Res.* (2003) 44:1132–42. doi: 10.1194/jlr.M200429-JLR200

39. Temel RE, Walzem RL, Banka CL, Williams DL. Apolipoprotein A-I is necessary for the *in vivo* formation of high density lipoprotein competent for scavenger receptor BI-mediated cholesteryl ester-selective uptake. *J Biol Chem.* (2002) 277:26565–72. doi: 10.1074/jbc.M203014200

Conflict of Interest: The authors declare that the research was conducted in the absence of any commercial or financial relationships that could be construed as a potential conflict of interest.

Publisher's Note: All claims expressed in this article are solely those of the authors and do not necessarily represent those of their affiliated organizations, or those of the publisher, the editors and the reviewers. Any product that may be evaluated in this article, or claim that may be made by its manufacturer, is not guaranteed or endorsed by the publisher.

frontiers in Cardiovascular Medicine

ORIGINAL RESEARCH
published: 22 November 2021
doi: 10.3389/fcvm.2021.768029

MiR-17-5p Inhibits TXNIP/NLRP3 Inflammasome Pathway and Suppresses Pancreatic β-Cell Pyroptosis in Diabetic Mice

Sijun Liu[1†], *Ge Tang*[1†], *Fengqi Duan*[1], *Cheng Zeng*[1], *Jianfeng Gong*[1], *Yanming Chen*[2*] and *Hongmei Tan*[1,2*]

[1] Department of Pathophysiology, Zhongshan School of Medicine, Sun Yat-sen University, Guangzhou, China, [2] Department of Endocrinology, The Third Affiliated Hospital of Sun Yat-sen University, Guangzhou, China

OPEN ACCESS

Edited by:
Changcheng Zhou,
University of California, Riverside,
United States

Reviewed by:
Huaizhu Wu,
Baylor College of Medicine,
United States
Erin E. Mulvihill,
University of Ottawa, Canada

***Correspondence:**
Hongmei Tan
tanhm@mail.sysu.edu.cn
Yanming Chen
chyanm@mail.sysu.edu.cn

[†]These authors have contributed equally to this work

Specialty section:
This article was submitted to Lipids in Cardiovascular Disease, a section of the journal Frontiers in Cardiovascular Medicine

Received: 31 August 2021
Accepted: 20 October 2021
Published: 22 November 2021

Citation:
Liu S, Tang G, Duan F, Zeng C, Gong J, Chen Y and Tan H (2021) MiR-17-5p Inhibits TXNIP/NLRP3 Inflammasome Pathway and Suppresses Pancreatic β-Cell Pyroptosis in Diabetic Mice. Front. Cardiovasc. Med. 8:768029. doi: 10.3389/fcvm.2021.768029

Objective: Diabetes mellitus is a chronic progressive inflammatory metabolic disease with pancreatic β-cells dysfunction. The present study aimed to investigate whether miR-17-5p plays a protective effect on pancreatic β-cells function in diabetes mellitus (DM) mice and dissect the underlying mechanism.

Methods: C57BL/6J mice were randomly divided into control, DM, DM + Lentivirus negative control (LV-NC), and DM + Lenti-OE^{TM} miR-17-5p (LV-miR-17-5) groups. DM was established by feeding a high-fat diet and intraperitoneal injection with streptozotocin (STZ) in mice. Blood glucose and glucose tolerance in circulation were measured. Meanwhile, the activation of nod-like receptor protein 3 (NLRP3) inflammasome, pancreas pyroptosis, and the expression of miR-17-5p and thioredoxin-interacting protein (TXNIP) were detected in the pancreas of DM mice. Pancreatic β-cell line INS-1 subjected to different concentrations of glucose was used in *in vitro* experiments.

Results: Compared with control mice, glucose tolerance deficit, elevated blood glucose level, and decreased pancreatic islet size, were presented in DM mice, which was associated with a downregulation of miR-17-5p. Importantly, exogenous miR-17-5p alleviated pancreas injury, and consequently improved glucose tolerance and decreased blood glucose in DM mice. *In vitro* experiments showed that high glucose decreased miR-17-5p expression and impaired insulin secretion in INS-1 cells. Mechanistically, miR-17-5p inhibited the expression of TXNIP and NLRP3 inflammasome activation, and thus decreased pancreatic β-cell pyroptosis.

Conclusion: Our results demonstrated that miR-17-5p improves glucose tolerance, and pancreatic β-cell function and inhibits TXNIP/NLRP3 inflammasome pathway-related pyroptosis in DM mice.

Keywords: diabetes mellitus, pancreatic β-cell, NLRP3 inflammasome, miR-17-5p, pyroptosis

INTRODUCTION

Diabetes mellitus is a serious public health concern globally, with a growing incidence caused by genetic or unhealthy lifestyle habits (1). Diabetes mellitus (DM) is characterized by long-term hyperglycemia resulting from the defect of insulin production and insulin resistance of insulin-responsive tissue and ultimately results in a series of chronic complications (2). Chronic low-grade inflammation is emerging as a key contributing factor to DM (3). However, the detailed mechanism of inflammatory-related dysglycemia and defect of insulin secretion in DM remains largely unexplored.

Nod-like receptor protein 3 (NLRP3) inflammasome has a critically important role in the regulation of inflammation in the development of DM (4). NLRP3 responds to a variety of stimulators, such as toxins, pathogens, metabolites, crystalline substances, nucleic acids, and ATP, thereby initiating the assembly of the NLRP3 inflammasome and facilitating the autocleavage and maturation of precursors of caspase-1 (5). And activated caspase-1 cleaves gasdermin D (GSDMD) to generate an N-terminal GSDMD fragment (GSDMD-NT). The GSDMD-NT targets the plasma membrane and results in the formation of a cell pore, cell tumid, and lysis, which initiates a programmed death process referred to as pyroptosis (6, 7). In patients with DM, NLRP3 inflammasome is activated, and successive proinflammatory mediators also significantly elevate (8). It was reported that thioredoxin-interacting protein (TXNIP), a multifunctional and inducible protein, regulates redox homeostasis in the cells (9, 10). Increased expression of TXNIP functions as a major role in β cell failure and dysfunction during diabetes development (11). Meanwhile, TXNIP exacerbates NLRP3 inflammasome activation and provokes oxidative stress (12). Therefore, inhibiting TXNIP/NLRP3 inflammasome pathway becomes a new therapeutic strategy in DM induced by an excessive inflammatory response.

MicroRNAs are a kind of small endogenous RNAs that bind messenger RNAs (mRNA) to regulate translation and stability of mRNA, and microRNAs play a critical role in the regulation of mechanisms operating in various biologic functions such as NLRP3 inflammasome activation and pyroptosis (4, 13, 14). Some microRNAs have critical roles in insulin secretion, pancreatic β-cell development and function, and the pathogenesis of DM (15). MiR-17-5p is a member of the miR-17-92 cluster, and it was confirmed that miR-17-5p was downregulated in mice embryos from diabetic dams (16). MiR-17-92 cluster is the first group of microRNAs to be indicated in the regulation of the development of multiple tissues and is indispensable for cell proliferation and cell cycle. Moreover, some researchers implicated that miR-17-5p was involved in the regelation of the progression of multiple cancer types and the exertion of a diverse function in the development and survival of pancreatic β-cell (17, 18). However, the role of miR-17-5p in the pathological state of DM is still unclear. The present study intended to explore the potential effect of miR-17-5p on pancreatic β-cell pyroptosis in a mouse model of DM and dissect the underlying mechanism.

Abbreviations: DM, diabetes mellitus; NLRP3, Nod-like receptor protein 3; GSDMD, gasdermin D; GSDMD-NT, N-terminal GSDMD fragment; TXNIP, thioredoxin-interacting protein; mRNA, messenger RNAs; STZ, streptozotocin; AUC, area under the curve; qRT-PCR, quantitative real-time polymerase chain reaction; 7-AAD, 7-aminoactinomycin D.

METHODS

Cell Culture and Cell Transfection

Rat INS-1 pancreatic β-cell line (ATCC, Manassas, VA, USA) were grown in Roswell Park Memorial Institute 1640 medium supplemented with 10% fetal bovine serum (Gibco, USA), 2.5 mmol/L mercaptoethanols, 10 mmol/L HEPES, 100 U/ml penicillin-streptomycin, and 11.1 mmol/L glucose, and incubated at 37°C in a 5% carbon dioxide incubator. INS-1 cells were transfected with miR-17-5p mimic (RiboBio Co., Ltd., Guangzhou, China) according to standard protocol in the presence of different concentrations of glucose (5 and 25 mmol/L). In some experiments, INS-1 cells were treated, respectively, with different concentrations of glucose (5, 25, and 50 mmol/L) for 72 h. To investigate whether miR-17-5p inhibited the expression of TXNIP, INS-1 cells were transfected with miR-17-5p mimic or miR-17-5p inhibitor in the presence of high glucose (25 mmol/L).

Glucose-Stimulated Insulin Secretion Assay (GSIS)

The INS-1 cells were transfected with negative control or miR-17-5p mimic as described above, respectively, in normal (5 mmol/L) or high glucose (25 mmol/L) conditions for 72 h. Then, cells were preincubated with Krebs-Ringer bicarbonate HEPES Buffer (KRBH) (Gibco, USA) containing 2.8 mmol/L glucose for 2 h. For insulin stimulation, cells were transferred to a new KRBH buffer with 16.7 mmol/L of glucose and incubated for 1 h at 37°C. Insulin concentration was determined relying on an insulin Elisa kit (Cloud-Clone Corp, Wuhan, China) in the supernatant.

Flow Cytometry Analysis for Cell Pyroptosis

To identify pyroptosis in INS-1 cells, cells were treated with high glucose (25 mmol/L) in the presence or absence of miR-17-5p mimic for 72 h, or cells were incubated with normal glucose (5 mmol/L) condition for 72 h. The cells were incubated with active caspase-1 and 7-aminoactinomycin D (7-AAD) for 15 min in 37°C, then analyzed by Flow cytometry (BECHMAN COULTER, Cytoflex, Indianapolis, IN, USA). Active caspase-1 was analyzed using the FAM-YVAD-FMK caspase-1 detection kit (Cell technology, Mountain View, CA, USA). 7-AAD labeled the DNA of cells because of loss of membrane integrity. Active caspase-1^+/7-AAD^+ cells were defined as pyroptotic cells.

Animal Protocol

We obtained the C57BL/6J mice (8 weeks, male, 20–25 g) from Vital River Laboratory Animal Technology Co., Ltd. (Beijing, China). Mice were housed in specific pathogen-free conditions around 24°C at the laboratory animal center of Sun Yat-sen

university under a 12-h light/dark cycle with free access to water and food. All animal protocols were approved by ethic committees of Sun Yat-sen University and all experiments complied with the Guide for the Care and Use of Laboratory Animals published by the US National Institutes of Health (No. 85–23, revised 1996). Mice were randomly divided into four groups: control group, DM group, DM + Lentivirus negative control (LV-NC) group, and DM + Lenti-OE^{TM} miR-17-5p (LV-miR-17-5) group ($n = 8$ for each group). Specifically, control mice were fed with a standard chow diet [protein, 26.5%; fat, 14%; carbohydrates, 59.5%; (2019) 05073, Guangdong Medical Laboratory Animal Center, Guangdong, China]. The other mice were fed with high-fat diet (protein, 20%; fat, 39.9%; carbohydrates, 40%; MD12017, Mediscience Ltd., Jiangsu, China) for 8 weeks. Mice were injected intraperitoneally with streptozotocin (STZ) (Sigma Aldrich, St. Louis, MO, USA) (100 mg/kg/d) for a 5-day schedule to induce DM. Blood glucose level over 16.6 mmol/L was considered as DM. After the DM model was established, lentivirus (Genechem Co., Ltd., Shanghai, China) was transfected into the tail vein at a dose of 1×10^7 U. To ensure the stability and function of miR-17-5p in mice, miR-17-5p was transfected into mice every 4 weeks. Additionally, blood glucose was measured every 4 weeks. Then, 20 weeks after the last injection, all mice were sacrificed by exsanguination after anesthesia with pentobarbital (80 mg/kg body weight). Blood samples and the pancreatic tissue of mice were collected and stored at −80°C for further analysis.

Blood Glucose Measurement and Intraperitoneal Glucose Tolerance Test (IPGTT)

Blood glucose level was determined by OneTouch Ultra2 Glucose Monitors (LifeScan, Milpitas, CA, USA) every 4 weeks after STZ injection from tail vein blood samples. For IPGTT tests, mice were injected intraperitoneally with glucose solution (1 g/kg), and blood glucose level was measured as mentioned above at 15, 30, 60, and 120 min after injection. Plot the blood glucose concentration curve. Additionally, the area under the curve (AUC) for IPGTT was calculated and analyzed as previously reported (19).

Immunohistochemistry

Pancreatic tissue from mice was dissected and processed into paraffin blocks after fixation with 4% formaldehyde. Then, the tissue was cut into 5 μm sections. After deparaffinization and retrieval of antigen, sections were stained with anti-insulin antibody (1:200 dilution, R&D System, Minneapolis, MN, USA). The sections were incubated with anti-rat IgG as secondary antibodies and subsequently with 3,3′-diaminobenzidine as chromogen the next day. Images were acquired by using Leica DM2500B in 10 × objective magnification. Image-Pro Plus 6 software (Media Cybernetics, Rockville, Md) was used to analyze and calculate the area of insulin-positive area and the overall area. For the islet size quantitation, the same region of the pancreas was selected for immunohistochemistry. Additionally, four different slides were quantitated to create an average for each mouse.

Quantitative Real-Time Polymerase Chain Reaction (qRT-PCR)

The total RNA of INS-1 cells or pancreatic tissue was extracted using a Mini-BEST Universal RNA Extraction kit (TaKaRa, Kyoto, Japan) according to the protocols of the manufacturer. The concentration and purity of RNA were determined with an ultraviolet spectrophotometer (Thermo Fisher Scientific, CA, USA). RNA was then reverse transcribed into cDNA using a Transcriptor First Strand cDNA Synthesis Kit (Roche Diagnostics, Germany). Then, qRT-PCR were carried out with Real-Time PCR System (Bio-Rad, CA, USA) using the SYBR Green Master Mix kit (Roche Diagnostics, Germany). The primers used were as follows: miR-17-5p: CAAAGUGCUUACAGUGCAGGUAG.

Western Blot Analysis

Protein from pancreatic tissue and INS-1 cells lysates were collected. Western blot procedures were processed as standard protocol with specific antibodies against TXNIP (1:1,000, Abcam, UK), GSDMD (1:1,000, Abclonal, USA), caspase-1 (1:1,000, Abclonal, USA), NLRP3 (1:1,000, Adipogen, USA), and β-actin (1:5,000, Sigma, USA). The blots were visualized by ChemiDoc^{TM} Touch Imaging System (Bio-Rad, CA, USA). Western blot image was analyzed and quantified by using Image J software (NIH, Bethesda, MD, USA). Relative expression of the protein was normalized with β-actin expression.

Statistical Analysis

The results were presented as $M \pm SD$. All *in vitro* experiments were completely randomized designed and repeated in triplicate. Data were analyzed using GraphPad Prism 6 software (CA, USA). Statistical comparison among multiple groups was carried out by one-way ANOVA followed by an LSD test. $P < 0.05$ was considered statistically significant.

RESULTS

The Effect of High Glucose on Expression of miR-17-5p, TXNIP, and GSIS in INS-1 Cells

To determine the effect of different concentrations of glucose (5, 25, and 50 mmol/L) on INS-1 cells, we examined the expression level of miR-17-5p by using qRT-PCR in different groups. When INS-1 cells were incubated in high glucose (25 and 50 mmol/L), the expression of miR-17-5p was significantly down-regulated, demonstrating that high glucose resulted in decreased expression of miR-17-5p in a dose-dependent model (**Figure 1A**). The synthesis and secretion of insulin by pancreatic β-cell were essential indicators of pancreatic β-cell function. To determine whether miR-17-5p affected the insulin secretion function in high glucose conditions, we detected the concentration of insulin in the presence or absence of miR-17-5p mimicked by GSIS in INS-1 cells. Our data showed that cells treated with high glucose secreted less insulin, and miR-17-5p mimic rescued insulin secretion function of INS-1 cells (**Figure 1B**). TXNIP is an oxidative stress-sensitive activator in cellular redox balance

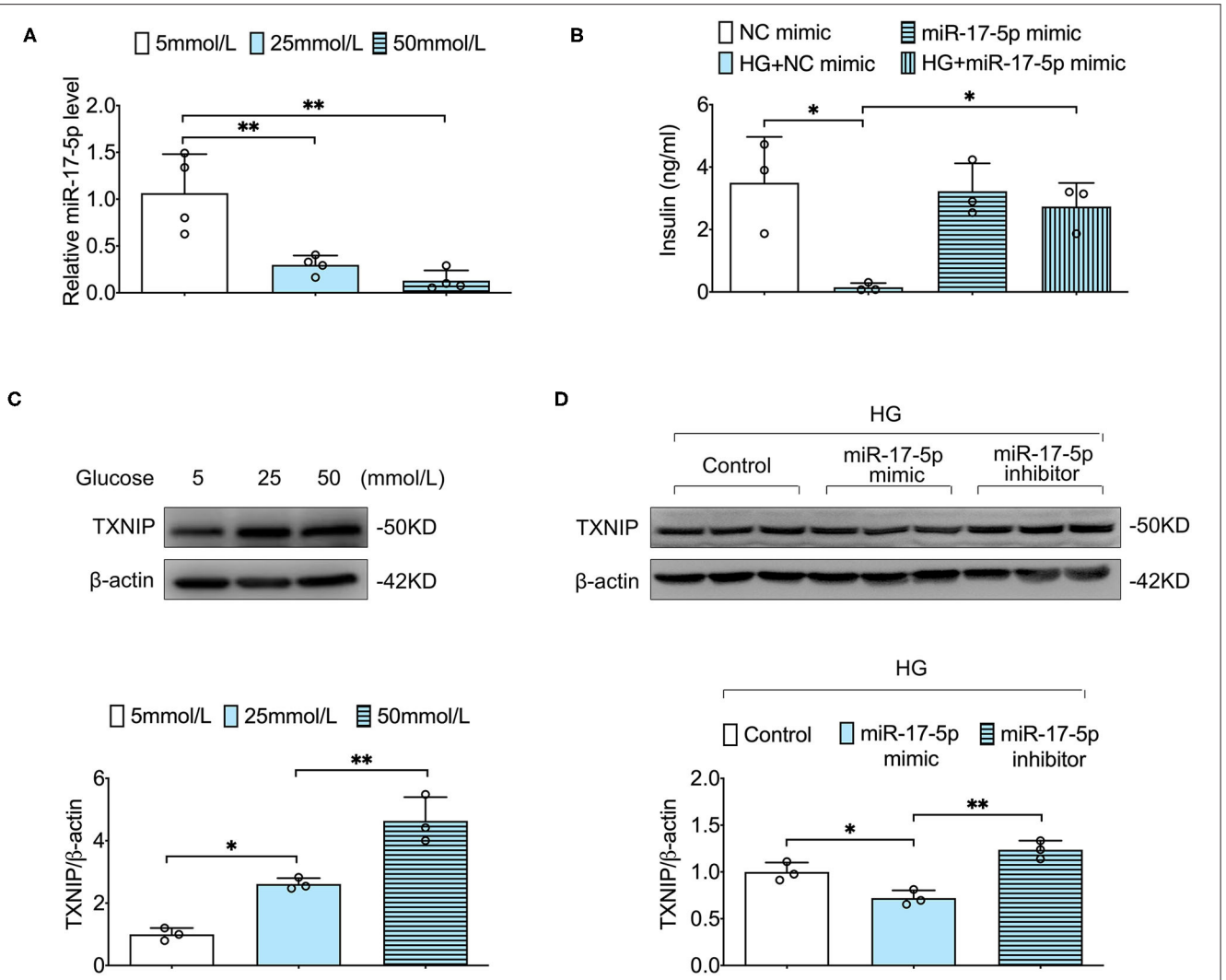

FIGURE 1 | The effect of high glucose on expression of miR-17-5p, TXNIP, and GSIS in INS-1 cells. **(A)** The relative levels of miR-17-5p under different concentrations of glucose were analyzed by qRT-PCR. **(B)** Effects of high glucose and miR-17-5p on GSIS. **(C)** Representative blots and quantitative analysis showing the expression of TXNIP in INS-1 cells treated with different concentrations of glucose. **(D)** The effects of miR-17-5p on the expression of TXNIP in INS-1 cells. Control: 5 mmol/L; HG (high glucose): 25 mmol/L. $^{*}p < 0.05$ and $^{**}p < 0.01$.

and is involved in the progression of diabetes (20), and we found that high glucose increased expression of TXNIP in a glucose dose-dependent manner (**Figure 1C**). Importantly, high glucose-induced TXNIP expression was inhibited by the administration of miR-17-5p mimic, while enhanced by a miR-17-5p inhibitor (**Figure 1D**). Collectively, these results indicated that high glucose decreased the expression of miR-17-5p, increased the expression of TXNIP, and impaired GSIS in INS-1 cells. The expression of TXNIP was regulated by miR-17-5p mimic.

MiR-17-5p Mimicked the Suppressed High Glucose-Induced Expression of TXNIP, NLRP3 Inflammasome Activation in INS-1 Cells

Given that TXNIP played a central role in NLRP3 inflammasome activation (21), we determined to detect whether NLRP3 inflammasome was activated in INS-1 cells. Our data showed that high glucose notably increased the expression of TXNIP and NLRP3 and the cleavage of caspase-1 in INS-1 cells, indicating that high glucose activated TXNIP/NLPR3 inflammasome pathway in INS-1 cells. Importantly, the expression of TXNIP, NLRP3, cleaved caspase-1 was suppressed by a miR-17-5p mimic in high glucose-treated INS-1 cells (**Figures 2A,B**), suggesting that the protective effect of miR-17-5p is related to the TXNIP/NLRP3 inflammasome pathway.

MiR-17-5p Mimicked the Inhibiting High Glucose-Induced Pyroptosis in INS-1 Cells

Furthermore, we determined whether miR-17-5p suppressed pyroptosis based on TXNIP/NLRP3 inflammasome pathway in INS-1 Cells. Our results showed that the cleavage of GSDMD,

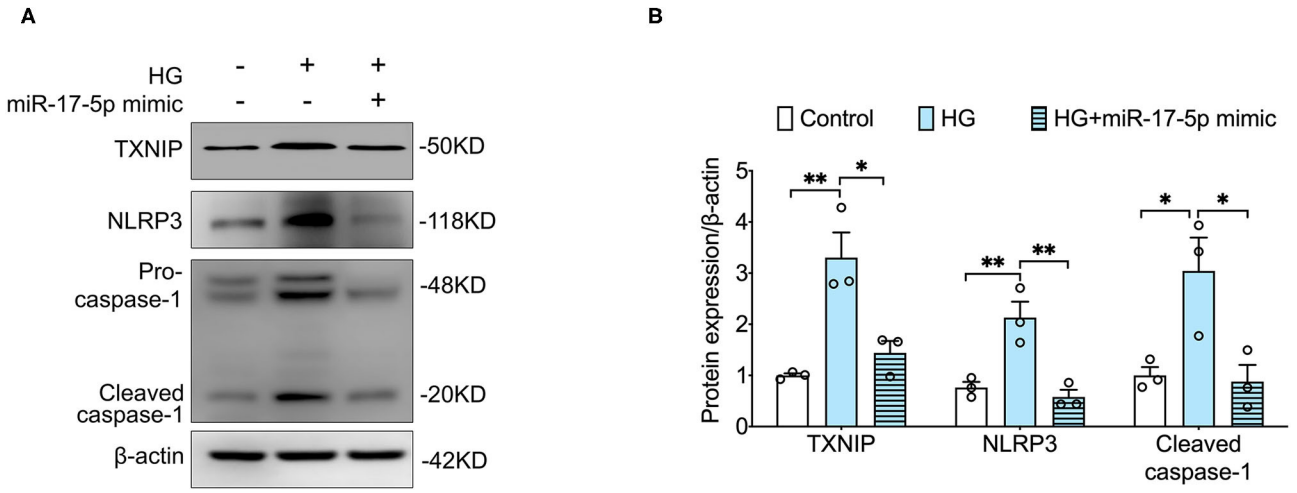

FIGURE 2 | MiR-17-5p mimic suppressed high glucose-induced hyperactivated NLRP3 inflammasome and the expression of TXNIP in INS-1 cells. **(A,B)** Representative blots and quantitative analysis showing the expression of NLRP3, the cleavage of caspase-1, and TXNIP. Control: 5 mmol/L; HG (high glucose): 25 mmol/L. *$p < 0.05$ and **$p < 0.01$.

an important indicator for pyroptosis, was inhibited by a miR-17-5p mimic in INS-1 cells, indicating miR-17-5p inhibited high glucose-induced pyroptosis (**Figures 3A,B**). Then, double staining of active caspase-1 and 7-AAD were performed to quantify pyroptotic cells. An increased population of pyroptotic cells (active caspase-1^+/7-AAD^+ cells) was observed in high glucose treatment cells, which was reduced by a miR-17-5p mimic in INS-1 cells (**Figures 3C,D**). These results suggested miR-17-5p mimic suppressed high glucose-induced pyroptosis in INS-1 cells.

The Effect of Overexpression of miR-17-5p on Blood Glucose, Glucose Tolerance, and Pancreatic Islet Size in DM Mice

To further investigate the protective effect of miR-17-5p in DM mice, lentivirus technology was carried out to increase the expression of miR-17-5p in DM mice. Besides, we further found the expression of miR-17-5p was significantly down-regulated in DM mice. Then, we examined the blood glucose in circulation and found that overexpression of miR-17-5p remarkably lowered the high blood glucose at the 12th week after the first injection, and the blood glucose levels were significantly lower than that in the DM mice at the end of the experiment. Moreover, when DM mice were transfected with miR-17-5p, the calculated AUC for IPGTT was reduced significantly compared with the DM mice, suggesting that miR-17-5p improved glucose tolerance (**Figures 4A–D**). Additionally, the immunohistochemical study showed that the pancreatic islet size has a significant reduction in the DM mice. After increased the expression of miR-17-5p, pancreatic islet size was increased significantly in DM mice (**Figures 4E,F**). These findings suggested miR-17-5p could mitigate high glucose, improve the glucose tolerance in circulation and display a markedly protective effect on normalizing the pancreatic β-cell function in DM mice.

Overexpression of miR-17-5p Suppressed TXNIP/NLRP3 Inflammasome Pathway and Pyroptosis in DM Mice

We further examined whether overexpression of miR-17-5p inhibited the expression of TXNIP and NLRP3 inflammasome activation in the pancreas of DM mice. Enhanced expression of the expression of TXNIP, NLRP3, and cleaved caspase-1 was presented in DM mice compared with control mice, indicating the TXNIP/NLRP3 inflammasome pathway was relevant to the progression of DM mice. Importantly, both increased expression of TXNIP and hyperactivated NLRP3 inflammasome were inhibited by the exogenous miR-17-5p in DM mice (**Figures 5A,B**). In addition, cleavage of GSDMD was increased significantly in DM mice and was also suppressed by the up-regulation of miR-17-5p (**Figures 5C,D**). Consistent with *in vitro* results, miR-17-5p inhibited TXNIP/NLRP3 inflammasome pathway and pyroptosis in DM mice.

DISCUSSION

In the current study, we demonstrated that miR-17-5p inhibits TXNIP/NLRP3 inflammasome pathway, suppresses pancreatic β-cell pyroptosis, and improves pancreatic β-cell function in diabetic mice. Our data proved that miR-17-5p could serve as a promising therapeutical strategy in excessive inflammatory response-induced pancreas injury in DM.

It was reported that miR-17-5p plays different effects on many complications. A recent study demonstrated that miR-17-5p acted as a major culprit for promoting breast cancer metastasis and was enhanced in colorectal cancer (22, 23). Despite the significance of miR-17-5p in some cancers, very few studies have

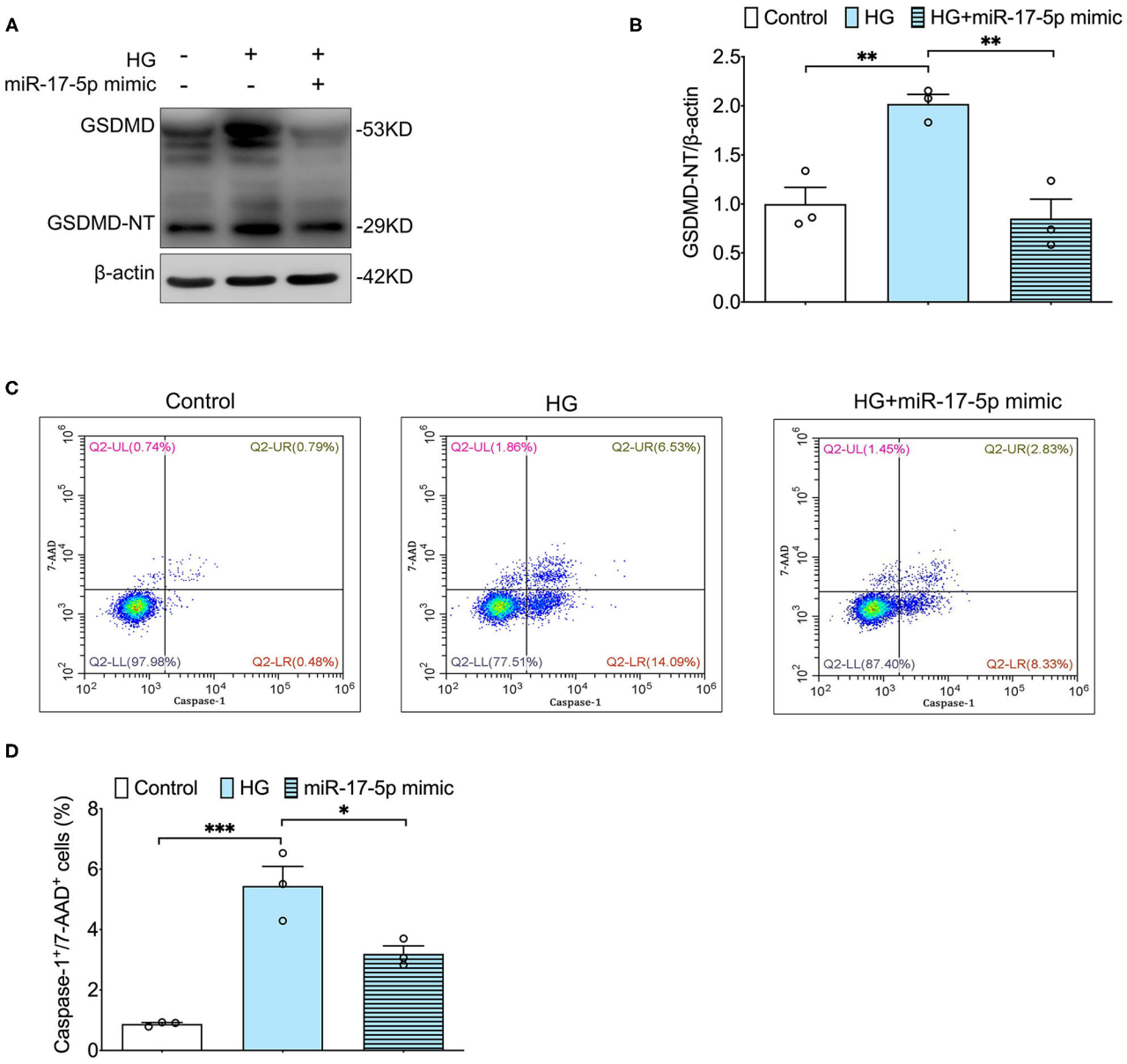

FIGURE 3 | MiR-17-5p mimic inhibited high glucose-induced pyroptosis in INS-1 cells. **(A,B)** Representative blots and quantitative analysis showing the expression of cleavage of GSDMD in INS-1 cells. **(C,D)** Representative flow cytometric dot plots and the corresponding quantification showing active caspase-1+/7-AAD+ cells as pyroptosis population in INS-1 cell cultured with different concentrations of glucose. Control: 5 mmol/L; HG (high glucose): 25 mmol/L. $^{*}p < 0.05$, $^{**}p < 0.01$, and $^{***}p < 0.001$.

focused on the effects of miR-17-5p in metabolic disease. Klöting et al. reported that the expression of miR-17-5p significantly decreased in obese non-diabetic patients (24). In the present study, we further identified that the expression of miR-17-5p was decreased in the pancreas of DM mice and INS-1 cells cultured with high glucose. Moreover, overexpression of miR-17-5p not only decreased blood glucose but also significantly improved glucose tolerance in DM mice.

Diabetes mellitus involving a defect in insulin secretion causes severe complications (21). Pancreatic β-cell plays a vital role in the control of blood glucose homeostasis. At present, a growing number of studies showed that microRNAs did not only affect the differentiation and proliferation of β-cell but also affected the synthesis and secretion of insulin (25, 26). The study of Hong et al. reported that proinflammatory cytokine interferon γ reduced the expression of miR-17, in the case of endoplasmic reticulum stress in INS-1 cells (27). The GSIS test was often used to determine the insulin release function of pancreatic β-cell. Prolonged elevated glucose stimulation could result in β cell dysfunction and β cell mass reduction (28). In

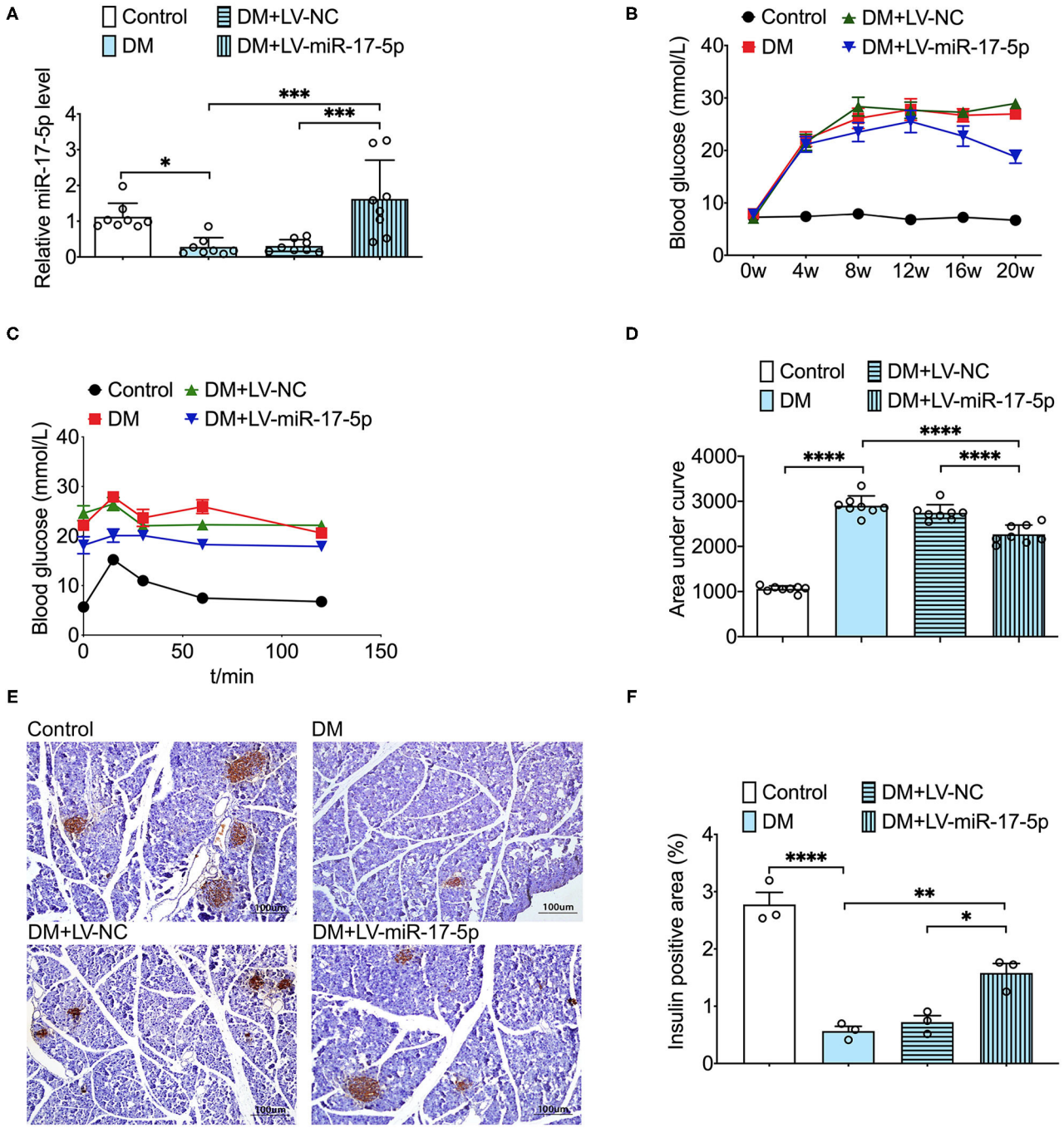

FIGURE 4 | Overexpression of miR-17-5p decreased the levels of blood glucose, improved glucose tolerance, and increased the pancreatic islet size in the DM mice. **(A)** The level of miR-17-5p in mice pancreatic tissue was determined by qRT-PCR ($n = 8$). **(B)** Effects of miR-17-5p on the blood glucose levels in DM mice ($n = 8$). **(C,D)** Effect of miR-17-5p on glucose tolerance in DM mice ($n = 8$). **(E,F)** Pancreatic sections were immunohistochemically stained for anti-insulin (dark brown). All slides were counterstained with hematoxylin and imaged at ×10 objective magnification ($n = 3$). *$p < 0.05$, **$p < 0.01$, ***$p < 0.001$, and ****$p < 0.0001$.

accordance with the previously reported, INS-1 cells exposed to high-glucose conditions showed significantly decreased insulin secretory function. However, miR-17-5p mimic potentiated the GSIS in INS-1 cells in response to high glucose. To further certificate the protective ability of miR-17-5p on pancreatic β-cell, miR-17-5p was overexpressed in DM mice. We disclosed that the up-regulation of miR-17-5p significantly increased the pancreatic islet size in pancreatic tissue. Herein, we revealed that

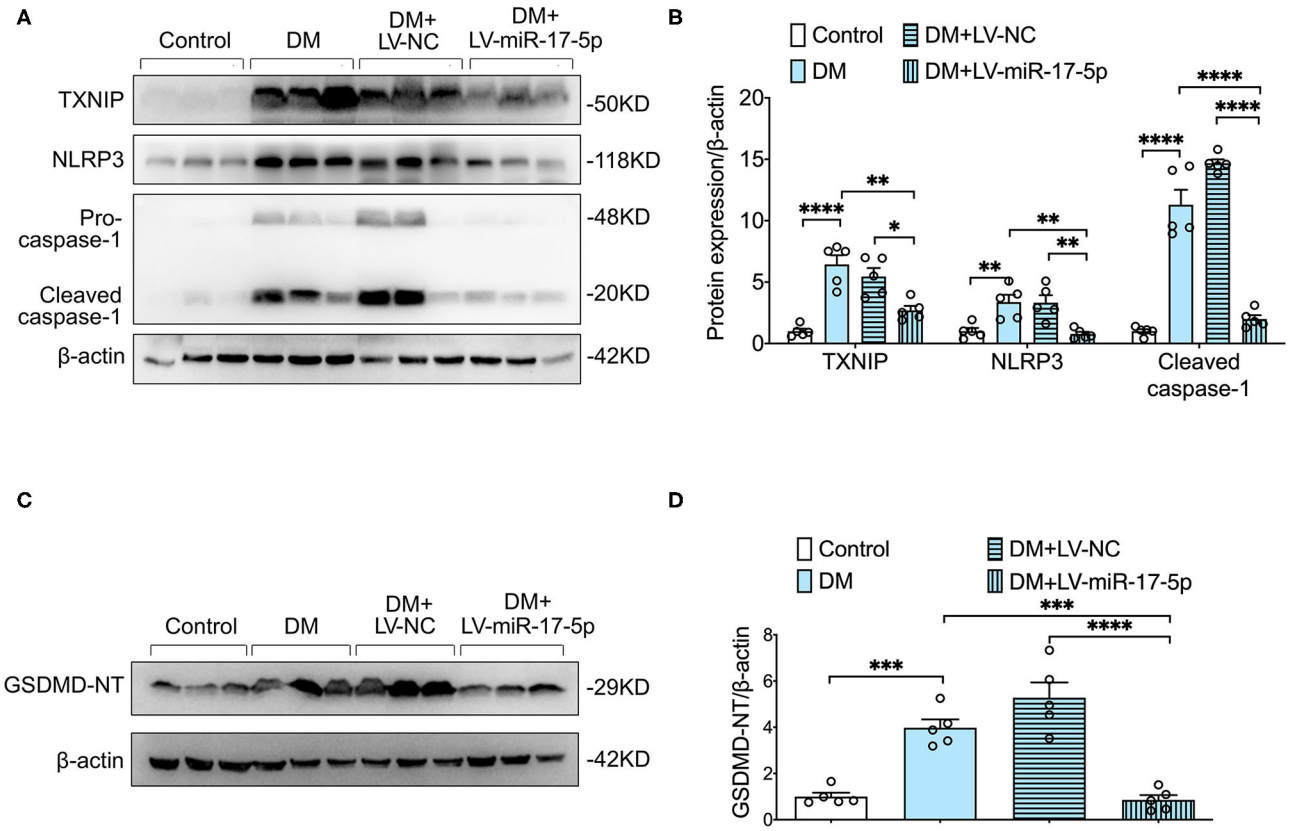

FIGURE 5 | Overexpression of miR-17-5p ameliorated NLRP3 inflammasome-mediated pyroptosis, and suppressed TXNIP expression in DM. **(A,B)** Representative blots and quantitative analysis showing the expression of NLRP3, the cleavage of caspase-1, and TXNIP. **(C,D)** GSDMD. $^{*}p < 0.05$, $^{**}p < 0.01$, $^{***}p < 0.001$, and $^{****}p < 0.0001$.

miR-17-5p might be a new promising therapeutical strategy for β-cell protection in DM.

Hyperglycemia exacerbates the development of inflammation, and chronic inflammation can lead to pancreas injury (29). Recently research demonstrated that TXNIP played important role in glucose metabolism, and high glucose condition up-regulated the expression of TXNIP, respectively, in cells and diabetes rats (30, 31). Moreover, TXNIP knockdown or deletion improved glucose tolerance and pancreatic β-cell function in mice (21). Consistent with our previous study (32), we found that increased expression of TXNIP and hyperactivated NLRP3 inflammasome were observed in diabetic mice, indicating that TXNIP/NLRP3 inflammasome pathway plays a central role in the pathophysiology of DM. Bioinformatic analysis indicated that miR-17 regulates TXNIP expression by interacting with the two conserved binding sites in the TXNIP 3′-UTR (16, 33). Moreover, some researchers demonstrated that the anti-inflammatory effect of miR-17-5p was associated with the inhibition of TXNIP/NLRP3 inflammasome in the brain (34, 35). However, the protective effect of miR-17-5p on DM is unclear. Thus, we tried to find the bridge between miR-17-5p and TXNIP/NLRP3 inflammasome pathway in DM. According to our works, high-abundance of TXNIP and NLRP3 inflammasome activation were validated in DM mice and INS-1 cells, and importantly, which were reversed by miR-17-5p. Moreover, we discovered miR-17-5p mimic inhibited high glucose-induced expression of TXNIP, while miR-17-5p inhibitor promoted TXNIP expression in INS-1 cells. These results suggested that miR-17-5p acted as an upstream factor in regulating TXNIP/NLRP3 inflammasome pathway in DM.

Pyroptosis is a type of GSDMD-mediated programmed cell death. The NLRP3 inflammasome, a vital activator of proptosis, triggers the release of GSDMD-NT. The GSDMD-NT is the effector molecule of pyroptosis, which forms membrane pores and then induces the secretion of proinflammatory cytokines (36, 37). Accumulating evidence highlights a central role for pyroptosis in the pathogenesis of DM (7, 38). An et al. reported that blocking pyroptosis and NLRP3 inflammasome activation was effective in mitigating DM-related complications (39). Given that NLRP3 inflammasome was considered as a critical inducer for pyroptosis, we further explored whether miR-17-5p could inhibit pyroptosis in DM. Our result showed that cleavage of GSDMD was increased significantly in the pancreas of DM mice, indicating the presence of pyroptosis.

By up-regulating the expression of miR-17-5p in DM mice, we found that DM-induced cleavage of GSDMD was inhibited. To confirm the anti-pyroptotic effect of miR-17-5p on INS-1 cells, flow cytometry was performed. Correspondingly, miR-17-5p mimic significantly reduced the population of pyroptotic cells induced by high glucose in INS-1 cells. Taken together, our data demonstrated that TXNIP/NLRP3 inflammasome pathway-related pyroptosis was involved in the beneficial effect of miR-17-5p to protect pancreatic β-cell in DM.

CONCLUSIONS

Overall, we demonstrated that overexpression of miR-17-5p ameliorates DM-induced aberrant metabolisms of insulin and blood glucose. Our study highlighted the importance of the protective effect of miR-17-5p by inhibiting the TXNIP/NLRP3 inflammasome pathway and pyroptosis, providing a more complete understanding of the therapeutical value of miR-17-5p in DM.

DATA AVAILABILITY STATEMENT

The original contributions presented in the study are included in the article/**Supplementary Material**, further inquiries can be directed to the corresponding authors.

ETHICS STATEMENT

The animal study was reviewed and approved by Ethic Committees of Sun Yat-sen University.

AUTHOR CONTRIBUTIONS

HT obtained funding for the study. HT and YC designed the study and helped to revise the manuscript. GT established the animal model. GT, SL, JG, FD, and CZ performed the experiment work, results collection, and interpretation. SL drafted the first manuscript. All authors reviewed the study and approved the final version.

FUNDING

This work was supported by the National Natural Science Foundation of China (Grant Nos. 81873514, 82170357, and 81570394) and Guangdong Natural Science Foundation (Grant Nos. 2021A1515011766 and 2017A030311017).

SUPPLEMENTARY MATERIAL

The Supplementary Material for this article can be found online at: https://www.frontiersin.org/articles/10.3389/fcvm.2021.768029/full#supplementary-material

REFERENCES

1. Liu G, Li Y, Hu Y, Zong G, Li S, Rimm EB, et al. Influence of lifestyle on incident cardiovascular disease and mortality in patients with diabetes mellitus. *J Am Coll Cardiol.* (2018) 71:2867–76. doi: 10.1016/j.jacc.2018.04.027
2. Poznyak A, Grechko AV, Poggio P, Myasoedova VA, Alfieri V, Orekhov AN. The diabetes mellitus-atherosclerosis connection: the role of lipid and glucose metabolism and chronic inflammation. *Int J Mol Sci.* (2020) 21:1835. doi: 10.3390/ijms21051835
3. Oguntibeju OO. Type 2 diabetes mellitus, oxidative stress and inflammation: examining the links. *Int J Physiol Pathophysiol Pharmacol.* (2019) 11:45–63.
4. Gora IM, Ciechanowska A, Ladyzynski P. NLRP3 inflammasome at the interface of inflammation, endothelial dysfunction, and type 2 diabetes. *Cells.* (2021) 10:314. doi: 10.3390/cells10020314
5. Zeng C, Duan F, Hu J, Luo B, Huang B, Lou X, et al. NLRP3 inflammasome-mediated pyroptosis contributes to the pathogenesis of non-ischemic dilated cardiomyopathy. *Redox Biol.* (2020) 34:101523. doi: 10.1016/j.redox.2020.101523
6. Huang Y, Xu W, Zhou R. NLRP3 inflammasome activation and cell death. *Cell Mol Immunol.* (2021) 18:2114–27. doi: 10.1038/s41423-021-00740-6
7. Mamun AA, Wu Y, Nasrin F, Akter A, Taniya MA, Munir F, et al. Role of pyroptosis in diabetes and its therapeutic implications. *J Inflammation Res.* (2021) 14:2187–206. doi: 10.2147/jir.S291453
8. Seok JK, Kang HC, Cho YY, Lee HS, Lee JY. Therapeutic regulation of the NLRP3 inflammasome in chronic inflammatory diseases. *Arch Pharmacal Res.* (2021) 44:16–35. doi: 10.1007/s12272-021-01307-9
9. Domingues A, Jolibois J, Marquet de Rougé P, Nivet-Antoine V. The emerging role of TXNIP in ischemic and cardiovascular diseases; a novel marker and therapeutic target. *Int J Mol Sci.* (2021) 22:1693. doi: 10.3390/ijms22041693
10. Yoshihara E, Masaki S, Matsuo Y, Chen Z, Tian H, Yodoi J. Thioredoxin/Txnip: redoxisome, as a redox switch for the pathogenesis of diseases. *Front Immunol.* (2014) 4:514. doi: 10.3389/fimmu.2013.00514
11. Qin K, Zhang N, Zhang Z, Nipper M, Zhu Z, Leighton J, et al. SIRT6-mediated transcriptional suppression of TXNIP is critical for pancreatic beta cell function and survival in mice. *Diabetologia.* (2018) 61:906–18. doi: 10.1007/s00125-017-4542-6
12. Wuensch T, Thilo F, Krueger K, Scholze A, Ristow M, Tepel M. High glucose-induced oxidative stress increases transient receptor potential channel expression in human monocytes. *Diabetes.* (2010) 59:844–9. doi: 10.2337/db09-1100
13. Abderrazak A, Syrovets T, Couchie D, El Hadri K, Friguet B, Simmet T, et al. NLRP3 inflammasome: from a danger signal sensor to a regulatory node of oxidative stress and inflammatory diseases. *Redox Biol.* (2015) 4:296–307. doi: 10.1016/j.redox.2015.01.008
14. Zhou H, Li CL, Xia PZ, He YX. MiR-223 alleviates thrombus and inflammation in thromboangiitis obliterans rats by regulating NLRP3. *Riv Eur Sci Med Farmacol.* (2020) 24:10605–11. doi: 10.26355/eurrev_202010_23418
15. Kaviani M, Azarpira N, Karimi MH, Al-Abdullah I. The role of microRNAs in islet β-cell development. *Cell Biol Int.* (2016) 40:1248–55. doi: 10.1002/cbin.10691
16. Dong D, Fu N, Yang P. MiR-17 downregulation by high glucose stabilizes thioredoxin-interacting protein and removes thioredoxin inhibition on ASK1 leading to apoptosis. *Toxicol Sci.* (2016) 150:84–96. doi: 10.1093/toxsci/kfv313
17. Meyer A, Herkt S, Kunze-Schumacher H, Kohrs N, Ringleb J, Schneider L, et al. The transcription factor TAL1 and miR-17-92 create a regulatory loop in hematopoiesis. *Sci Rep.* (2020) 10:21438. doi: 10.1038/s41598-020-78629-z
18. Wan S, Zhang J, Chen X, Lang J, Li L, Chen F, et al. MicroRNA-17-92 regulates beta-cell restoration after streptozotocin treatment. *Front Endocrinol.* (2020) 11:9. doi: 10.3389/fendo.2020.00009
19. Tang H, Zeng Q, Tang T, Wei Y, Pu P. Kaempferide improves glycolipid metabolism disorder by activating PPARγ in high-fat-diet-fed mice. *Life Sci.* (2021) 270:119133. doi: 10.1016/j.lfs.2021.119133
20. Liu X, Zhang YR, Cai C, Ni XQ, Zhu Q, Ren JL, et al. Taurine alleviates schistosoma-induced liver injury by inhibiting the TXNIP/NLRP3

inflammasome signal pathway and pyroptosis. *Infect Immun.* (2019) 87:e00732-19. doi: 10.1128/iai.00732-19
21. Schroder K, Zhou R, Tschopp J. The NLRP3 inflammasome: a sensor for metabolic danger? *Science.* (2010) 327:296–300. doi: 10.1126/science.1184003
22. Kim TW, Lee YS, Yun NH, Shin CH, Hong HK, Kim HH, et al. MicroRNA-17-5p regulates EMT by targeting vimentin in colorectal cancer. *Br J Cancer.* (2020) 123:1123–30. doi: 10.1038/s41416-020-0940-5
23. Wang Y, Xu W, Wang Y, Xu X, Lv S, Dong X. miR-17-5p promotes migration and invasion in breast cancer cells by repressing netrin 4. *Int J Clin Exp Pathol.* (2019) 12:1649–57. doi: 10.26914/c.cnkihy.2019.006110
24. Klöting N, Berthold S, Kovacs P, Schön MR, Fasshauer M, Ruschke K, et al. MicroRNA expression in human omental and subcutaneous adipose tissue. *PLoS ONE.* (2009) 4:e4699. doi: 10.1371/journal.pone.0004699
25. LaPierre MP, Stoffel M. MicroRNAs as stress regulators in pancreatic beta cells and diabetes. *Mol Metab.* (2017) 6:1010–23. doi: 10.1016/j.molmet.2017.06.020
26. Ozcan S. Minireview: microRNA function in pancreatic β cells. *Mol Endocrinol.* (2014) 28:1922–33. doi: 10.1210/me.2014-1306
27. Hong K, Xu G, Grayson TB, Shalev A. Cytokines regulate β-cell thioredoxin-interacting protein (TXNIP) via distinct mechanisms and pathways. *J Biol Chem.* (2016) 291:8428–39. doi: 10.1074/jbc.M115.698365
28. Zhang Z, Li J, Yang L, Chen R, Yang R, Zhang H, et al. The cytotoxic role of intermittent high glucose on apoptosis and cell viability in pancreatic beta cells. *J Diabetes Res.* (2014) 2014:712781. doi: 10.1155/2014/712781
29. Prattichizzo F, De Nigris V, Spiga R, Mancuso E, La Sala L, Antonicelli R, et al. Inflammageing and metaflammation: the yin and yang of type 2 diabetes. *Ageing Res Rev.* (2018) 41:1–17. doi: 10.1016/j.arr.2017.10.003
30. Devi TS, Somayajulu M, Kowluru RA, Singh LP. TXNIP regulates mitophagy in retinal Müller cells under high-glucose conditions: implications for diabetic retinopathy. *Cell Death Dis.* (2017) 8:e2777. doi: 10.1038/cddis.2017.190
31. Xu W, Wang L, Li J, Cai Y, Xue Y. TXNIP mediated the oxidative stress response in glomerular mesangial cells partially through AMPK pathway. *Biomed Pharmacother.* (2018) 107:785–92. doi: 10.1016/j.biopha.2018.08.067
32. Tang G, Duan F, Li W, Wang Y, Zeng C, Hu J, et al. Metformin inhibited Nod-like receptor protein 3 inflammasomes activation and suppressed diabetes-accelerated atherosclerosis in apoE mice. *Biomed Pharmacother.* (2019) 119:109410. doi: 10.1016/j.biopha.2019.109410
33. Lerner AG, Upton JP, Praveen PV, Ghosh R, Nakagawa Y, Igbaria A, et al. IRE1α induces thioredoxin-interacting protein to activate the NLRP3 inflammasome and promote programmed cell death under irremediable ER stress. *Cell Metab.* (2012) 16:250–64. doi: 10.1016/j.cmet.2012.07.007
34. Chen D, Dixon BJ, Doycheva DM, Li B, Zhang Y, Hu Q, et al. IRE1α inhibition decreased TXNIP/NLRP3 inflammasome activation through miR-17-5p after neonatal hypoxic-ischemic brain injury in rats. *J Neuroinflammation.* (2018) 15:32. doi: 10.1186/s12974-018-1077-9
35. Gamdzyk M, Doycheva DM, Kang R, Tang H, Travis ZD, Tang J, et al. GW0742 activates miR-17-5p and inhibits TXNIP/NLRP3-mediated inflammation after hypoxic-ischaemic injury in rats and in PC12 cells. *J Cell Mol Med.* (2020) 24:12318–30. doi: 10.1111/jcmm.15698
36. Yu ZW, Zhang J, Li X, Wang Y, Fu YH, Gao XY. A new research hot spot: the role of NLRP3 inflammasome activation, a key step in pyroptosis, in diabetes and diabetic complications. *Life Sci.* (2020) 240:117138. doi: 10.1016/j.lfs.2019.117138
37. Zeng C, Wang R, Tan H. Role of pyroptosis in cardiovascular diseases and its therapeutic implications. *Int J Biol Sci.* (2019) 15:1345–57. doi: 10.7150/ijbs.33568
38. Lin Y, Hu Y, Hu X, Yang L, Chen X, Li Q, et al. Ginsenoside Rb2 improves insulin resistance by inhibiting adipocyte pyroptosis. *Adipocyte.* (2020) 9:302–12. doi: 10.1080/21623945.2020.1778826
39. An X, Zhang Y, Cao Y, Chen J, Qin H, Yang L. Punicalagin protects diabetic nephropathy by inhibiting pyroptosis based on TXNIP/NLRP3 pathway. *Nutrients.* (2020) 12:1516. doi: 10.3390/nu12051516

Conflict of Interest: The authors declare that the research was conducted in the absence of any commercial or financial relationships that could be construed as a potential conflict of interest.

frontiers in Cardiovascular Medicine

REVIEW
published: 08 December 2021
doi: 10.3389/fcvm.2021.752337

Recent Advances in Understanding the Role of IKKβ in Cardiometabolic Diseases

*Rebecca Hernandez and Changcheng Zhou**

Division of Biomedical Sciences, School of Medicine, University of California, Riverside, Riverside, CA, United States

Cardiometabolic diseases, including cardiovascular disease, obesity, and diabetes, are the leading cause of mortality and morbidity worldwide. Cardiometabolic diseases are associated with many overlapping metabolic syndromes such as hypertension, hyperlipidemia, insulin resistance, and central adiposity. However, the underlying causes of cardiometabolic diseases and associated syndromes remain poorly understood. Within the past couple of decades, considerable progresses have been made to understand the role of inflammatory signaling in the pathogenesis of cardiometabolic diseases. The transcription factor, NF-κB, a master regulator of the innate and adaptive immune responses, is highly active in cardiometabolic diseases. IκB kinase β (IKKβ), the predominant catalytic subunit of the IKK complex, is required for canonical activation of NF-κB, and has been implicated as the critical molecular link between inflammation and cardiometabolic diseases. Recent studies have revealed that IKKβ has diverse and unexpected roles in mediating adiposity, insulin sensitivity, glucose homeostasis, vascular function, and atherogenesis through complex mechanisms. IKKβ has been demonstrated as a critical player in the development of cardiometabolic diseases and is implicated as a promising therapeutic target. This review summarizes current knowledge of the functions of IKKβ in mediating the development and progression of cardiometabolic diseases.

Keywords: cardiometabolic diseases, atherosclerosis, insulin resistance, obesity, IKK-beta, NF-kB

OPEN ACCESS

Edited by:
Rainer de Martin,
Medical University of Vienna, Austria

Reviewed by:
Dongsheng Cai,
Albert Einstein College of Medicine, United States
Tom Huxford,
San Diego State University, United States

***Correspondence:**
Changcheng Zhou
changcheng.zhou@medsch.ucr.edu

Specialty section:
This article was submitted to Atherosclerosis and Vascular Medicine, a section of the journal Frontiers in Cardiovascular Medicine

Received: *02 August 2021*
Accepted: *12 November 2021*
Published: *08 December 2021*

Citation:
Hernandez R and Zhou C (2021) Recent Advances in Understanding the Role of IKKβ in Cardiometabolic Diseases. Front. Cardiovasc. Med. 8:752337. doi: 10.3389/fcvm.2021.752337

INTRODUCTION

Cardiometabolic diseases such as atherosclerosis, obesity, and diabetes are related to several risk factors termed cardiometabolic syndromes (1, 2). Cardiometabolic syndromes encompass a group of metabolic dysfunctions like hypertension, hyperlipidemia, insulin resistance, and central adiposity (1). Chronic low-grade inflammation has been established as a major contributor to the development of cardiometabolic diseases such as type 2 diabetes and atherosclerosis (3, 4). Many inflammatory pathways that contribute to the cardiometabolic disease risk are regulated by the transcriptional factor NF-κB, a master regulator of the innate and adaptive immune responses (1, 5). In non-stimulated cells, NF-κB remains in the cytoplasm bound to specific inhibitory proteins—the inhibitors of NF-κB (IκBs). In response to various stimuli including proinflammatory cytokines, infectious agents, reactive oxygen species, and free fatty acids (FFAs), NF-κB can be rapidly activated through the IκB kinase (IKK) complex (1, 5, 6). The IKK complex is composed of two catalytic subunits (IKKα and IKKβ) and a regulatory subunit (IKKγ/NEMO). Activation of IKK can lead to the phosphorylation and ubiquitination of IκB. Consequently, free NF-κB can then translocate to the nucleus and regulate the expression of many target genes (1, 7).

While IKKβ and IKKα, have a similar structure, they have different functions as IKKα contains a putative nuclear localization signal and IKKβ contains a ubiquitin binding domain. In addition, IKKβ activation is necessary for canonical NF-κB pathway activation, while IKKα is not (8, 9). The stimuli that can activate IKKβ include proinflammatory cytokines, growth factors, microbial products, stress stimuli, and the engagement of T cell receptors. These stimuli can activate membrane-bound receptors such as the Tumor necrosis factor receptor superfamily (TNFRSF), Interleukin-1 receptor (IL-1R), and Toll-like receptors (TLR), subsequently leading to the activation of the IKK complex (10, 11). IKKβ and its serine-threonine kinase activity are essential for regulating inflammatory and immune responses, and many studies have uncovered its function in chronic inflammation-associated cardiometabolic diseases such as atherosclerosis, obesity, and insulin resistance (**Figure 1**). In addition to regulating the NF-κB pathway, more and more new targets of IKKβ have also been identified. The known IKKβ substrates and their functions in tumorigenesis, inflammation, diabetes, hormone response, and cell survival have been discussed in detail in several comprehensive reviews (12, 13). For the purpose of this review, we focus on IKKβ, its known substrates, and their functions in the development of cardiometabolic diseases (**Figure 1**).

THE ROLE OF IKKβ IN ATHEROSCLEROSIS DEVELOPMENT

Atherosclerosis is the major contributing risk factor for the development of cardiovascular disease (CVD). It is a very complex disease involving the development of plaques in large arteries causing narrowing of the vessel lumen leading to various clinical manifestations, including stroke, ischemic heart disease, chronic kidney disease, and peripheral artery disease. The plaques are characterized by accumulating lipids and immune cells into the sub-endothelial space (14–18). Atherosclerosis has been characterized as a chronic inflammatory disease, which may be initiated when the endothelium undergoes a phenotypic change, termed endothelial dysfunction, stimulated by modified LDL such as oxidized-LDL (oxLDL) and inflammatory stimuli. The endothelium fails to maintain vascular homeostasis during endothelial dysfunction like vasodilation, eliminating reactive oxygen species, and maintaining an appropriate inflammatory balance. Various chemotactic factors and adhesion molecules are differentially expressed by endothelial cells undergoing endothelial dysfunction, which aids in monocyte migration and infiltration. Ox-LDL is rapidly taken up by monocyte scavenger receptors upon monocyte infiltration, leading to the conversion of monocytes into lipid-filled macrophage foam cells.

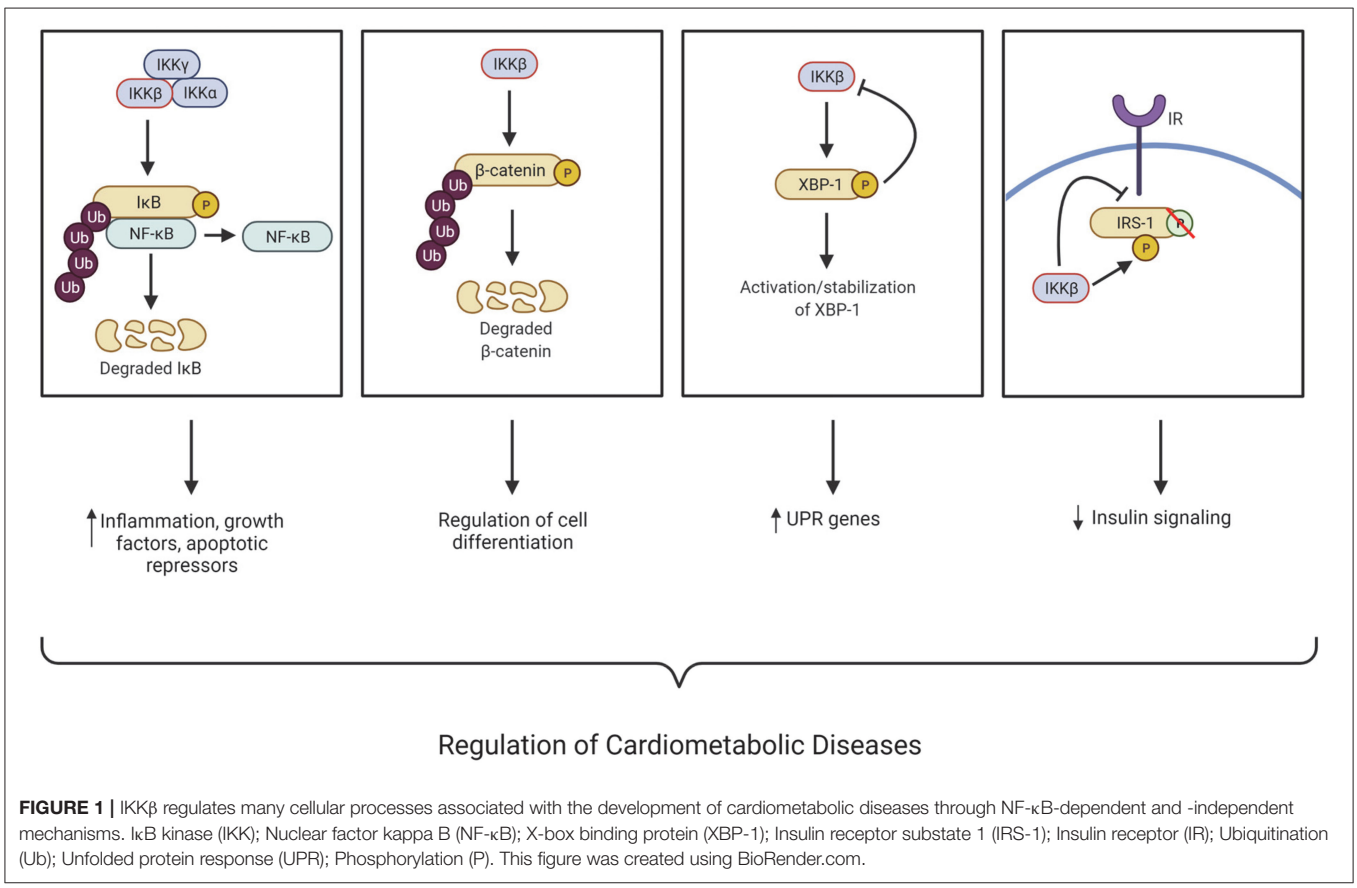

FIGURE 1 | IKKβ regulates many cellular processes associated with the development of cardiometabolic diseases through NF-κB-dependent and -independent mechanisms. IκB kinase (IKK); Nuclear factor kappa B (NF-κB); X-box binding protein (XBP-1); Insulin receptor substate 1 (IRS-1); Insulin receptor (IR); Ubiquitination (Ub); Unfolded protein response (UPR); Phosphorylation (P). This figure was created using BioRender.com.

The lesional foam cells can release inflammatory factors to further contribute to the monocyte and lipid build-up (16–19). While acute vessel wall inflammation leads to asymptomatic fatty streaks, chronic inflammation can cause the gradual and uncontrolled accumulation of macrophage foam cells that later develop into symptomatic atheromas or plaques. For many years, the NF-κB pathway has been implicated in the pathogenesis of atherosclerosis (20). For example, NF-κB activation has been detected in atherosclerotic plaques, including macrophages, endothelial cells, and smooth muscle cells in both human and animal models (21–24). Previous studies have implicated that NF-κB activation in human atherosclerosis was IKKβ-dependent and resulted in up-regulation of proinflammatory and prothrombotic mediators (25). However, recently studies have demonstrated that the functions of IKKβ in atherosclerosis are complex and that IKKβ in different tissues or cell types may have different impact on atherosclerosis development in animal models.

Endothelial Cell IKKβ in Atherosclerosis

As a significant player in atherosclerosis initiation and progression, studies have suggested that the inflammatory response in endothelial dysfunction can be driven by IKKβ/NF-κB signaling (14, 21, 26). Gareus et al. previously demonstrated that inhibition of NF-κB activity through the deletion of IKKγ, also known as NF-κB essential modulator (NEMO), or expression of a dominant-negative IκBα decreases atherosclerosis in atherogenic prone mice (14). They also found that inhibition of NF-κB in endothelial cells reduced the expression of proinflammatory cytokines, chemokines, and adhesion molecules, leading to decreased monocyte recruitment into the plaque (14). Consistently, inhibition of IKKβ in human umbilical vein endothelial cells has been shown to block NF-κB activation, leading to decreased adhesion molecule gene expression including E-selectin, ICAM-1, and VCAM-1 (27). These adhesion molecules are essential for the attachment and infiltration of the recruited monocytes into the intimal layer (16–18). By contrast, constitutive activation of endothelial IKKβ in mice increased monocyte infiltration into the subintimal space, which contributed to exacerbating early and late-stage atherosclerosis (28). Indeed, the rise of age-associated endothelial dysfunction is correlated with increased IKK activation in arteries while pharmacological inhibition of IKK by salicylate has been shown to improve age-related endothelial dysfunction (29). Thus, targeting endothelial cell IKKβ may have beneficial effects against atherosclerosis development.

Macrophage IKKβ in Atherosclerosis

The M1, or proinflammatory, macrophage plays a key role in atherosclerosis development, while M2, or anti-inflammatory, macrophages enhance plaque regression and stability (30). The link between macrophage polarization and IKKβ remains elusive, though evidence suggests that IKKβ/NF-κB pathway activation polarizes macrophages to the M2, anti-inflammatory phenotype through negative crosstalk with STAT1 (31, 32). To study the role of macrophage IKKβ in atherosclerosis, Kanters et al. transplanted IKKβ-deficient bone marrow-derived macrophages into atherogenic prone low-density lipoprotein receptor-deficient ($LDLR^{-/-}$) mice. They found that the mice receiving IKKβ-deficient macrophages exhibited enhanced atherosclerotic lesion development and increased necrosis, which suggest a protective role of bone marrow-derived macrophage IKKβ against atherosclerosis development (33). However, the same group used a similar method to delete IκBα in myeloid cells, aimed to activate NF-κB signaling. Interestingly, those mice displayed increased atherosclerosis lesion size and leukocyte adhesion without significantly increasing NF-κB targeted genes (34), indicating pro-atherogenic effects of canonical NF-κB activation. Several other studies have also found that macrophage IKKβ/NF-κB pathway has pro-atherogenic effects (35, 36). For example, inhibition of NF-κB in macrophages through the overexpression of a trans-dominant and non-degradable form of IκBα can reduce macrophage foam cell formation *in vitro* (35). Further, myeloid-specific IKKβ deficiency decreased diet-induced atherosclerosis in $LDLR^{-/-}$ mice by diminishing macrophage inflammatory responses such as adhesion, migration and lipid uptake in macrophages (36). Collectively, these results indicate the role of macrophage IKKβ/NF-κB in atherogenesis is complex and more studies are needed to completely understand how IKKβ functions in myeloid cells to regulate atherosclerosis development.

Vascular Smooth Muscle Cell IKKβ in Atherosclerosis

In addition to endothelial and immune cells, vascular smooth muscle cells (VSMCs) also play an important role in atherogenesis. In the early stages of atherosclerosis, VSMCs undergo a phenotypic switch from contractile to synthetic where they gain the ability to proliferate and migrate into the intimal layer. This provides a beneficial effect as these VSMCs proliferate and migrate to the cap of the plaque and reinforces its stability, lowering the risk for plaque rupture (37). An earlier study demonstrated that IKKα and IKKβ was activated in IL-1β-induced proliferative response of human saphenous vein smooth muscle cells (38). Notably, the proliferative ability of human VSMCs were diminished in IKKα and IKKβ mutant transfected cells (38). The role of VSMC IKKβ in atherosclerosis was also investigated in $LDLR^{-/-}$ mice (39). Deficiency of IKKβ in VSMCs driven by a SM22Cre-IKKβ-flox system protected $LDLR^{-/-}$ mice from diet-induced vascular inflammation and atherosclerosis development (39). Since inhibition of NF-κB activity in endothelia cells also decreased vascular inflammation and atherosclerosis in $ApoE^{-/-}$ mice (14), these studies suggest that inhibiting IKKβ/NF-κB signaling in the vasculature has anti-atherogenic effects.

Adipocyte IKKβ in Atherosclerosis

Under pathological conditions, adipose tissue is at a chronic low level of inflammation (3). The circulating inflammatory mediators secreted by adipocytes participate in vascular dysfunction, which can lead to atherosclerosis (40). However, the role of adipocyte IKKβ signaling in atherogenesis is poorly understood. A recent study found that adipocyte-specific deletion of IKKβ did not affect obesity and atherosclerosis in

lean LDLR$^{-/-}$ mice when fed a low-fat diet (41). When fed a high-fat diet, however, IKKβ-deficient LDLR$^{-/-}$ mice had defective adipose remodeling, leading to increased adipose tissue and systemic inflammation (41). Deficiency of adipocyte IKKβ did not affect atherosclerotic lesion size but resulted in enhanced lesional inflammation and increased plaque vulnerability in obese IKKβ-deficient LDLR$^{-/-}$ mice (41). In addition to regular fat depots, adipocytes can also be found adjacent to the vascular wall called perivascular adipose tissue (PVAT). Under homeostatic conditions, PVAT holds a protective role on vascular homeostasis by secreting bioactive molecules like adiponectin, nitric oxide (NO), and IL-10 (42, 43). However, under pathological conditions, PVAT switches to a proinflammatory phenotype by secreting adipokines, cytokines, and chemokines (43). The role of PVAT in atherosclerosis and vascular injury has not been extensively investigated. However, studies have found that PVAT may contribute to endothelial dysfunction (42), macrophage migration, and VSMC proliferation and migration (44). The role of PVAT IKKβ in vascular function and atherosclerosis remains elusive. Future studies should be considered to investigate the role of PVAT IKKβ/NF-κB signaling on vascular function and atherosclerotic development under normal or pathological conditions (e.g., obesity).

THE ROLE OF IKKβ IN REGULATING ADIPOSITY

Obesity is a worldwide epidemic and a risk factor for developing severe metabolic and cardiovascular diseases. According to the updated 2020 Heart Disease and Stroke Statistics, 39.6% of adults and 18.5% of youth are living with obesity in the US (45). Thus, research surrounding this field has become increasingly popular due to the financial, economic, and mental burden it carries (46). Obesity is associated with a low-grade chronic inflammation that contributes to the development of many chronic diseases including insulin resistance, diabetes, and CVD (3, 4, 47–49). Adipocytes are responsible for energy storage and respond to overnutrition by increasing adiposity and inflammation. There are three general steps to adipose chronic inflammation. First, adipocytes are introduced to a stressor, like overnutrition. The adaptive physiological response, which includes acute inflammation, aims to balance, and reduce this stressor. However, chronic exposure to this stressor creates new set basal points, which includes higher blood glucose levels and increased body weight (50). Thus, understanding the mechanistic link between inflammatory pathways in obesity, and obesity induced metabolic disorders is critical for developing essential therapeutic targets.

The IKKβ/NF-κB pathway is highly active in the adipose tissues of obese patients and in mouse models of obesity and insulin resistance (1, 51, 52). In addition to regulating inflammatory responses, IKKβ also plays important roles in regulating cell proliferation, differentiation, survival, and apoptosis (47, 53). However, the function of IKKβ during obesity in the context of adipose tissue development remain elusive. Recent studies have revealed the previously unrecognized function of IKKβ in regulating adiposity.

Adipocyte Progenitor IKKβ in Regulating Adiposity

While deletion of IKKβ in VSMCs decreased atherosclerosis development in LDLR$^{-/-}$ mice (39), those mice were also protected from diet-induced obesity and insulin resistance. Interestingly, many adipocyte precursor cells express SMC markers and ablation of IKKβ blocked adipocyte differentiation *in vitro* and *in vivo*, suggesting that IKKβ functions in adipocyte precursor cells to regulate adiposity (39). Indeed, selective deletion of IKKβ in the white adipose lineage further elucidated the role of adipose progenitor cell IKKβ signaling in regulating adiposity and metabolic function (39, 54). Deficiency of adipose progenitor IKKβ decreased high-fat feeding-induced adipogenesis and systemic inflammation, resulting in decreased adiposity and insulin resistance in those mice (39, 54). The function of IKKβ in the regulation of adipogenesis was further confirmed in mesenchymal stem cells (MSCs) (55). Mechanistic studies then revealed an important crosstalk between IKKβ and Wnt/β-catenin signaling (**Figure 1**) (55). Interestingly, IKKβ is a β-catenin kinase that can directly phosphorylate the conserved degron motif of β-catenin to prime it for β-TrCP-mediated ubiquitination and degradation (10, 55). Wnt/β-catenin signaling has been well studied to inhibit adipocyte differentiation (56, 57) and the impact of IKKβ signaling on adipogenesis was abolished in β-catenin-deficient MSCs (10, 55). Thus, IKKβ-mediated β-catenin phosphorylation may play a critical role in regulating adipocyte differentiation and adiposity in obesity (**Figure 1**).

Adipocyte IKKβ in Regulating Adiposity

While studies have suggested a pro-obesogenic role of progenitor IKKβ, the function of IKKβ in mature adipocytes is apparently more complicated. Constitutive activation of IKKβ in adipocytes has been demonstrated to increased energy expenditure in mice, leading to protective effects against diet-induced obesity and insulin resistance (58). However, targeted deletion of IKKβ in adipocytes did not affect obesity but resulted in increased tissue inflammation, impaired adipose remodeling, and exacerbated metabolic disorders (59, 60). In addition to mediating inflammation, IKKβ can also promote cell survival by upregulating NF-κB-mediated anti-apoptotic gene expression (61–63) and by direct phosphorylation of pro-apoptotic protein, BAD (64). Previous reports have linked adipocyte death with obesity, adipocyte macrophage infiltration, and systemic insulin resistance (65). IKKβ has been shown to be a key adipocyte survival factor in obesity, and deficiency of IKKβ in adipocytes can lead to high fat feeding-elicited cell death, impaired adipose tissue remodeling and partial lipodystrophy in visceral adipose tissue (59, 60). Further studies are required to completely understand the role of adipocyte IKKβ in regulating energy expenditure, homeostasis, and adiposity.

THE ROLE OF IKKβ IN INSULIN RESISTANCE

Insulin resistance is a very complex syndrome and IKKβ has been shown to regulate insulin resistance by directly interfering with the insulin signaling pathway (66). Once stimulated by its ligand, insulin, the insulin receptor (IR) becomes activated and phosphorylates insulin receptor substrate-1 (IRS-1) on its tyrosine residues, leading to increased glucose uptake (67). As a serine kinase, IKKβ can ectopically phosphorylate IRS-1 on multiple serine residues, which impairs insulin signaling (**Figure 1**) (68). Several studies have demonstrated that treatment with glucose lowering drugs and molecules such as kaempferol (69), timosaponin B-II (TB-II) (70), rosiglitazone (71), and bovine α-lactalbumin hydrolysates (α-LAH) (72) can alleviate insulin resistance by decreasing or inhibiting IKKβ levels/activity resulting in a reduction of ectopic IRS-1 serine phosphorylation.

Hepatic IKKβ in Insulin Resistance

The IKKβ/NF-κB pathway has been demonstrated to be active in both obesity-dependent and independent insulin resistance (47, 53). Inhibition of IKKβ with salicylate or other methods is associated with reduced insulin resistance and glucose intolerance (54, 73–75). Previous studies demonstrated that constitutively active hepatic IKKβ induced obesity-independent systemic insulin resistance, while inhibiting hepatic NF-κB reversed both local and systemic insulin resistance (51, 76). These findings indicate an important role of IKKβ in regulating hepatic and systemic insulin resistance. Another study utilizing hepatocyte-specific IKKβ deficient mice found improved hepatic insulin response while maintaining systemic insulin resistance during obesity (77). These results can be attributed to obesity-associated systemic inflammation that cannot be alleviated by IKKβ knockdown in the liver alone. More recently, it has been reported that hepatic IKKβ in the liver can improve glucose homeostasis by interacting with x-box binding protein 1 (XBP1) and enhancing its activity, stabilization, and nuclear translocation (**Figure 1**) (78). While it is generally recognized that hepatic inflammation drives the detrimental perspectives of obesity-induced insulin resistance (1, 73, 79), upregulation of certain inflammatory signaling could have positive or negative contributions to whole-body metabolism, depending on conditions of signaling activation and related physiological statuses. Therefore, the hepatic IKKβ function in insulin resistance is complex and future studies are required to define the detailed mechanisms through which hepatic IKKβ regulates insulin responsiveness under normal and pathophysiological conditions.

Adipose IKKβ in Insulin Resistance

Inflammation is an important contributor of insulin resistance, and adipose tissue is one of the important tissues for this high-fat feeding-elicited inflammatory response (80). Adipose IKKβ signaling has been implicated in obesity-associated insulin resistance. For example, studies have found that IKKβ deficiency in adipocyte precursors or adipose lineage cells can protect mice from diet-induced obesity, systemic inflammation and insulin resistance (39, 54). Several studies demonstrated that IKKβ deficiency and XBP1 overexpression attenuates FFA-induced inflammation and impairment of insulin signaling in cultured adipocytes (81, 82). While hepatic IKKβ increases nuclear translocation of XBP1 (78), adipocyte IKKβ is inhibited by XBP1 (82), indicating a more complex role of IKKβ/XBP1 interaction in cardiometabolic disease. Overexpression of IKKβ in adipocytes also led to increased adipose tissue inflammation in mice (58). Paradoxically, those mice were resistant to diet-induced obesity and insulin resistance, likely due to increased energy expenditure (58). Deletion of adipocyte IKKβ did not affect obesity in mice but resulted in elevated adipose tissue inflammation, increased macrophage infiltration and exacerbate insulin resistance (59, 60).

Skeletal Muscle IKKβ in Insulin Resistance

Skeletal muscle is another insulin responsive tissue that is impaired in obesity and diabetes (67). Studies revealed elevated IKKβ activity in isolated skeletal muscle of obese patients with type 2 diabetes and obese mice (83, 84). By contrast, inhibition of IKKβ or NF-κB signaling can restore insulin signaling *in vitro* (85, 86) and systemic IKKβ inhibition can alleviate skeletal muscle and systemic insulin resistance all together (73, 74). However, under obese conditions, targeting skeletal muscle IKKβ can only alleviate local insulin resistance, but not systemic insulin responsiveness (87).

Myeloid IKKβ in Insulin Resistance

While tissue-specific inhibition of IKKβ (i.e., liver, adipose, skeletal muscle) may be able to abrogate local insulin resistance, it may not be sufficient for systemic inflammation-induced insulin resistance under obese conditions. For example, it is reported that myeloid-specific IKKβ deficiency can improve obese-dependent systemic insulin resistance (77, 87), indicating that myeloid cell IKKβ plays a role in systemic insulin resistance and inflammation in obesity. Furthermore, Cai et al. linked the IKKβ/NF-κB pathway with paracrine IL-6 signaling (51), which is associated with type 2 diabetes and insulin resistance (88, 89). IL-6 can induce the expression of suppressor of cytokine signaling 3 (SOCS-3), which inhibits autophosphorylation of IRS-1 and insulin receptor (90). The IKKβ/NF-κB/IL-6 axis was confirmed to be involved in insulin resistance when IL-6 neutralization improved insulin resistance (51).

THE ROLE OF IKKβ IN METABOLIC SYNDROME-ASSOCIATED LIVER DISEASE

Non-alcoholic fatty liver disease or non-alcoholic steatohepatitis is also associated with metabolic syndrome. The activation of the IKKβ/NF-κB pathway has been shown to promote fatty liver disease, or hepatic steatosis (91), whereas inhibition of IKKβ prevents the initiation of steatosis and non-alcoholic steatohepatitis (75, 92). Inhibition of IKKβ significantly reduced the expression of essential proinflammatory genes like TNFα and IL-6 in the liver (92). In line with lipid metabolism, the peroxisome proliferator-activated receptor family (PPAR) is an important regulator of lipid homeostasis in multiple

TABLE 1 | Overview of IKKβ modulation and mechanism in cardiometabolic diseases.

Cell Type	IKKβ modulation	Effect on cardiometabolic diseases	Mechanism	Reference
Endothelial Cells	Constitutive activation	Accelerated atherosclerotic development and progression, increased macrophage infiltration	1. Upregulation of endothelial NF-κB mediated gene expression of cytokines/chemokines (CCL2, CCL12, IL-1β, IL-6, CXCR4), increased macrophage infiltration 2. Cellular transition of SMC to macrophage-like cells	(29)
Myeloid Cells	Knockout	Increased lesion size, more severe lesion, increased necrosis, increase macrophage content at the lesion site	1. Reduction of IL-10 anti-inflammatory cytokine	(33)
Myeloid Cells	Knockout	Decreased lesion size, macrophage infiltration, and foam cell formation	1. Reduction in macrophage/lesional NF-κB-mediated proinflammatory gene expression/protein level (MCP-1, TNFα, IL-1β, IL-1α, VCAM-1, ICAM-1), reducing macrophage recruitment and infiltration 2. Reduced scavenger receptor expression levels, decreased ox-LDL uptake by macrophages	(36)
VSMC	Knockout	Decreased lesion size	1. Reduction in lesion proinflammatory protein level (MCP-1, TNFα, IL-1β)	(39)
Adipocytes	Knockout	Increased plaque vulnerability	1. Upregulation of aortic/lesional NF-κB mediated gene expression of cytokines/chemokines/protein levels (MCP-1, TNFα, IL-1β, IL-6, VCAM-1, ICAM-1)	(41)
MSC	Gain of function	Promoted adipogenesis and inhibits osteogenesis	1. Increases adipogenic genes (Zfp423, PPARγ) 2. Tags β-catenin for β-TrCP-mediated ubiquitination leading to adipogenesis	(55)
MSC, MEFs	Knockdown with various methods	Inhibited adipogenesis and promotes osteogenesis	1. Suppresses adipogenic genes (Zfp423, PPARγ) 2. Reduced β-catenin ubiquitination leading to osteogenesis	(55)
White adipose lineage	Knockout	Decreased obesity; improved glucose tolerance; protected from hepatic steatosis	1. Suppresses adipogenic genes (Zfp423, PPARγ, C/EBPα) 2. Decreases Smurf2 levels resulting in increased β-catenin activity 3. Reduced macrophage infiltration in WAT 4. Decrease in hepatic lipogenic genes (SREBP1c, ScD-1, PPARγ)	(39, 54)
Human stem cells	Pharmacological inhibition	Inhibited adipogenesis	1. Suppresses adipogenic genes (Zfp423, PPARγ, C/EBPα) 2. Decreases Smurf2 levels resulting in increased β-catenin activity	(54)
Adipocytes	Knockout	Increased adipocyte death; macrophage infiltration; defective adipose remodeling; impaired insulin signaling	1. Increases pro-apoptotic genes (XIAP, Bcl2) 2. Activation of proapoptotic protein BAD 3. Increases adipose lipolysis 4. Increase in WAT proinflammatory genes (TNFα, MCP-1, IL-2)	(59)
Hypothalamic AGRP neurons	Knockout	Anti-obese phenotype; reduced glucose intolerance; preserved insulin and leptin signaling	1. Reduction of SOCS3	(95)
Mediobasal Hypothalamus	Constitutive activation	Impaired central insulin and leptin signaling	1. Decreased Akt and PIP3 activation 2. Increased SOCS3	(95)
Systemic	Pharmacological inhibition	Reduced high sucrose diet (HSD)-induced obesity; prevented hepatic steatosis and NASH	1. Reduced WAT inflammation (TNFα, F4/80) 2. Reduced NF-κB-mediated liver inflammation 3. Upregulation of PPARα and PPARγ leading to increased β-oxidation (CPT-1 and ACOX)	(92)
Adipocytes	Constitutive activation	Decreased lipid deposits into other tissue (i.e., hepatosteaotosis); improved systemic insulin resistance	1. Increased energy expenditure through hypothesized mechanisms: increased thermogenesis and fatty acid oxidation (upregulation of CPT-1β, ACO1), increase in mitochondria biogenesis (upregulation of NRF1), elevated IL-6 levels 2. Decreased body weight and systemic inflammation	(58)
Hepatocytes	Knockout	Improved hepatic insulin resistance, sustained peripheral insulin resistance	1. Decrease in proinflammatory gene expression (IL-6) in liver	(77)
Myocytes	Knockout	Retained systemic insulin resistance	1. Maintained high TNFα expression in WAT; low IR activation	(87)
Myeloid cells	Knockout	Improved systemic insulin resistance	1. Decrease in proinflammatory gene expression (IL-6)	(77)
Hepatocytes	Constitutive activeation	Increased liver and peripheral insulin resistance	1. Increased expression of circulating IL-6	(51)
Hepatocytes	Overexpression	Improved insulin sensitivity; improved glucose homeostasis	1. Increased XBP1 stability/decreased XBP1 degradation via IKKβ mediated phosphorylation	(78)

(Continued)

TABLE 1 | Continued

Cell Type	IKKβ modulation	Effect on cardiometabolic diseases	Mechanism	Reference
Astrocytes	Overexpression	Induced metabolic syndromes	1. Decreased astrocyte plasticity leading to increased GABA and increased GABA inhibition of BDNF secreting neurons	(106)
Mediobasal Hypothalamus	Activation	Increased obesity and insulin resistance	1. Loss of neuronal development	(108)
Hypothalamic AGRP neurons	Activation	Impaired glucose homeostasis; no change in body weight or leptin signaling	1. Increased AGRP firing	(103)
Systemic	Pharmacological inhibition	Alleviated insulin resistance	1. Reduction of ectopic IRS-1 serine phosphorylation 2. Restoration of IRS-1 phosphorylation and protein levels 3. Enhanced Akt activity 4. Increased glucose uptake 5. Increased glycolysis and glycogen/lipid synthesis	(54, 68–74)
Adipocyte	Knockout	Worsened insulin resistance; enhanced inflammation	1. Reduction of IL-13	(60)
Hepatocytes	Constitutive activation	Increased liver fibrosis	1. Increased inflammation (chemokines) and macrophage infiltration in the liver	(94)

organs and tissues (93). PPARα, highly expressed in the liver, can upregulate IκB, thus inhibiting the NF-κB pathway (92, 93). Interestingly, IKKβ inhibition can also lead to PPARα upregulation and reduced lipid accumulation in the liver by increasing CPT-1 and ACOX—two important molecules that decreases fatty acid accumulation through β-oxidation (92). Additionally, IKKβ inhibition attenuated hepatic inflammation, apoptosis, and collagen deposition, therefore preventing liver fibrosis (54, 92). By contrast, hepatic IKKβ activation promoted liver fibrosis by inducing chronic inflammation (94). While the mechanism behind IKKβ-mediated hepatic steatosis and fibrosis remain to be explored, these findings suggest that inhibiting IKKβ may prevent lipid and collagen accumulation in the liver, leading to decreased hepatic steatosis and fibrosis development.

THE ROLE OF IKKβ OF THE CENTRAL NERVOUS SYSTEM IN CARDIOMETABOLIC DISEASES

IKKβ of the Central Nervous System in Obesity and Insulin Resistance

Although there have been strong links between IKKβ and metabolic diseases within the periphery, more recently, inflammatory activation has been seen within the central nervous system (CNS). Specifically, IKKβ in the hypothalamus can be activated in obesity and obesity-related metabolic dysregulation such as energy, body weight, and glucose dysregulation (95–98). A study found that FFAs induce TLR4-mediated hypothalamic cytokine production and anorexigenic signal resistance which may lead to obesity (99). Signaling between the gut and brain (gut-brain-axis) is a major influencer in developing obesity. Obese mice and mice stimulated with overnutrition display overall higher levels of IKKβ within the hypothalamic neurons, which is consistent with the systemic trend (95, 100). However, it was observed that overnutrition-mediated activation of IKKβ/NF-κB was activated intracellularly by ER stress and prompted both hypothalamic leptin and insulin resistance through the induction of suppressor of cytokine signaling 3 (SOCS3), an inhibitor of leptin and insulin signaling (95, 101). ER stress can also lead to impaired hepatic insulin signaling, which was improved upon ER stress inhibition (102). TLR-dependent IKKβ activation in the CNS was also involved in obesity and leptin resistance (96). Deficiency of IKKβ in hypothalamic AGRP neurons displayed anti-obese phenotype along with preserved leptin and insulin signaling and reduced SOCS3 gene expression, and overexpression of SOCS3 reversed the protective effects of IKKβ knockout in mice (95). By contrast, activation of IKKβ in AGRP neurons resulted in impaired glucose homeostasis, without affecting body weight and leptin signaling (103).

While it is critical to study the effects of hypothalamic inflammation on obesity and metabolic syndromes, it is also important to investigate the upstream targets mediating hypothalamic inflammation. For example, astrocytes play essential roles in neuronal development; regulation of blood flow; fluid, ion, pH, and transmitter homeostasis; the regulation of synaptic transmission; and regulate immune response (104). Under pathological conditions or external stressors, astrocytes and other glial cells undergo gliosis, or astrogliosis, which is characterized by proliferation and accumulation of astrocytes (104, 105). Zhang et al. demonstrated an important role of astrocyte IKKβ in stimulating glucose intolerance, hypertension, and weight gain (106). While overnutrition and IKKβ overexpression inhibited proper astrocytic plasticity, inhibition of IKKβ prevented overnutrition-induced metabolic diseases and impaired astrocytic plasticity (106). Mechanistically, IKKβ-induced shortening of astrocyte processes led to increased extracellular GABA, an inhibitory neurotransmitter, and lower brain derived neurotrophic factor (BDNF) levels through inhibition of BDNF secreting neurons in the hypothalamus (106). Low levels of BDNF have been associated with metabolic disorders such as obesity, energy metabolism, and hyperglycemia (107). The protective role of IKKβ deficiency in astrocytes were reversed by BDNF inhibition, suggesting that the GABA-BDNF axis is important in regulating energy homeostasis and metabolic syndromes (106). In addition to developed cells within the CNS, the hypothalamic neural stem cells are important

mediators for metabolic syndrome. IKKβ/NF-κB activation in the mediobasal hypothalamus can lead to obesity and insulin resistance, along with loss of neuronal development including POMC neurons (108).

IKKβ of the Central Nervous System in Hypertension

Hypertension, a chronic elevation in arterial blood pressure, is one of the major risk factors for developing CVD such as myocardial infarction, stroke, and heart failure. Although there are therapeutic interventions aimed to target and treat hypertension, it is still a prevalent contributor to cardiometabolic disease burden (109). IKKβ in the CNS, mainly in the hypothalamus, can regulate blood pressure. Overexpression of a constitutively active form of IKKβ in the mediobasal hypothalamus induces hypertension in mice, while NF-κB inhibition attenuated high-fat feeding induced hypertension in mice (110). Additionally, astrocyte-specific IKKβ overexpression in mice led to higher daytime blood pressure, while NF-κB inhibition reversed obesity-induced hypertension in mice (106). In line with the previous discussion linking ER stress to insulin resistance, thapsigargin-induced ER stress increased blood pressure and phosphorylated IκB, but inhibition of NF-κB alleviated these effects (102).

CONCLUSION

Recent research advancements have expanded our knowledge on the function of IKKβ in cardiometabolic diseases. A summary of the role of IKKβ in cardiometabolic diseases is listed in **Table 1**. By exploring various mechanisms of chronic inflammation-associated diseases, such atherosclerosis, obesity, and insulin resistance, IKKβ and its regulated main canonical NF-κB pathway in various cell types have been found to play diverse roles in cardiometabolic disease development. In addition, new discoveries revealed that NF-κB-independent mechanisms may also contribute to the impact of IKKβ on the development of cardiometabolic diseases. For example, IKKβ can interact with several important signaling molecules such as β-catenin, BAD, and IRS-1 that are essential for regulating cell survival, differentiation and insulin signaling. With more new molecular targets of IKKβ being discovered, there will be more opportunities for fully understanding the complex function of IKKβ in cardiometabolic diseases and for developing new and effective therapeutic approaches.

AUTHOR CONTRIBUTIONS

RH: conceptualized, wrote, and edited the manuscript. CZ: reviewed, edited, and revised the manuscript. All authors contributed to the article and approved the submitted version.

FUNDING

This work was supported in part by National Institutes of Health grants (R01HL131925 and R01ES023470) and American Heart Association grant (19TPA34890065) to CZ. RH was supported by an NIH T32 training grant (T32ES018827).

REFERENCES

1. Baker RG, Hayden MS, Ghosh S. NF-κB, Inflammation, and metabolic disease. *Cell Metab.* (2011) 13:11–22. doi: 10.1016/j.cmet.2010.12.008
2. Zhou C. Novel functions of PXR in cardiometabolic disease. *Biochim Biophys Acta.* (2016) 1859:1112–20. doi: 10.1016/j.bbagrm.2016.02.015
3. Gregor MF, Hotamisligil GS. Inflammatory mechanisms in obesity. *Annu Rev Immunol.* (2011) 29:415–45. doi: 10.1146/annurev-immunol-031210-101322
4. Hotamisligil GS, Erbay E. Nutrient sensing and inflammation in metabolic diseases. *Nat Rev Immunol.* (2008) 8:923–34. doi: 10.1038/nri2449
5. Hayden MS, Ghosh S. Shared principles in NF-kappaB signaling. *Cell.* (2008) 132:344–62. doi: 10.1016/j.cell.2008.01.020
6. Zhou C, Tabb MM, Nelson EL, Grun F, Verma S, Sadatrafiei A, et al. Mutual repression between steroid and xenobiotic receptor and NF-kappaB signaling pathways links xenobiotic metabolism and inflammation. *J Clin Invest.* (2006) 116:2280–9. doi: 10.1172/JCI26283
7. Zhang Q, Lenardo MJ, Baltimore D. 30 years of NF-kappaB: a blossoming of relevance to human pathobiology. *Cell.* (2017) 168:37–57. doi: 10.1016/j.cell.2016.12.012
8. Israël A. The IKK complex, a central regulator of NF-kappaB activation. *Cold Spring Harb Perspect Biol.* (2010) 2:a000158. doi: 10.1101/cshperspect.a000158
9. Page A, Navarro M, Suárez-Cabrera C, Bravo A, and Ramirez A. Context-dependent role of IKKβ in cancer. *Genes.* (2017) 8:376. doi: 10.3390/genes8120376
10. Ma B, Hottiger MO. Crosstalk between Wnt/β-Catenin and NF-κB signaling pathway during inflammation. *Front Immunol.* (2016) 7:378. doi: 10.3389/fimmu.2016.00378
11. Lawrence T. The nuclear factor NF-kappaB pathway in inflammation. *Cold Spring Harb Perspect Biol.* (2009) 1:a001651-a. doi: 10.1101/cshperspect.a001651
12. Hinz M, Scheidereit C. The IκB kinase complex in NF-κB regulation and beyond. *EMBO Rep.* (2014) 15:46–61. doi: 10.1002/embr.201337983
13. Liu F, Xia Y, Parker AS, Verma IM. IKK biology. *Immunol Rev.* (2012) 246:239–53. doi: 10.1111/j.1600-065X.2012.01107.x
14. Gareus R, Kotsaki E, Xanthoulea S, van der Made I, Gijbels MJJ, Kardakaris R, et al. Endothelial cell-specific NF-κB inhibition protects mice from atherosclerosis. *Cell Metab.* (2008) 8:372–83. doi: 10.1016/j.cmet.2008.08.016
15. Hansson GK. Inflammation and atherosclerosis: the end of a controversy. *Circulation.* (2017) 136:1875–7. doi: 10.1161/CIRCULATIONAHA.117.030484
16. Libby P. Inflammation in atherosclerosis. *Nature.* (2002) 420:868–74. doi: 10.1038/nature01323
17. Libby P. Inflammation in atherosclerosis. *Arterioscler Thromb Vasc Biol.* (2012) 32:2045–51. doi: 10.1161/ATVBAHA.108.179705
18. Lusis AJ. Atherosclerosis. *Nature.* (2000) 407:233–41. doi: 10.1038/35025203
19. Libby P, Bornfeldt KE. How far we have come, how far we have yet to go in atherosclerosis research. *Circ Res.* (2020) 126:1107–11. doi: 10.1161/CIRCRESAHA.120.316994
20. Brand K, Page S, Rogler G, Bartsch A, Brandl R, Knuechel R, et al. Activated transcription factor nuclear factor-kappa B is present in the atherosclerotic lesion. *J Clin Invest.* (1996) 97:1715–22. doi: 10.1172/JCI118598
21. Hajra L, Evans AI, Chen M, Hyduk SJ, Collins T, Cybulsky MI. The NF-kappa B signal transduction pathway in aortic endothelial cells is primed for activation in regions predisposed to atherosclerotic lesion formation. *Proc Natl Acad Sci USA.* (2000) 97:9052–7. doi: 10.1073/pnas.97.16.9052

22. Brand K, Eisele T, Kreusel U, Page M, Page S, Haas M, et al. Dysregulation of monocytic nuclear factor-kappa B by oxidized low-density lipoprotein. *Arterioscler Thromb Vasc Biol.* (1997) 17:1901–9. doi: 10.1161/01.ATV.17.10.1901
23. Bennett BL, Lacson RG, Chen CC, Cruz R, Wheeler JS, Kletzien RF, et al. Identification of signal-induced IkappaB-alpha kinases in human endothelial cells. *J Biol Chem.* (1996) 271:19680–8. doi: 10.1074/jbc.271.33.19680
24. Bourcier T, Sukhova G, Libby P. The nuclear factor kappa-B signaling pathway participates in dysregulation of vascular smooth muscle cells *in vitro* and in human atherosclerosis. *J Biol Chem.* (1997) 272:15817–24. doi: 10.1074/jbc.272.25.15817
25. Monaco C, Andreakos E, Kiriakidis S, Mauri C, Bicknell C, Foxwell B, et al. Canonical pathway of nuclear factor kappa B activation selectively regulates proinflammatory and prothrombotic responses in human atherosclerosis. *Proc Natl Acad Sci USA.* (2004) 101:5634–9. doi: 10.1073/pnas.0401060101
26. de Winther Menno PJ, Kanters E, Kraal G, Hofker Marten H. Nuclear Factor κB Signaling in Atherogenesis. *Arterioscler Thromb Vasc Biol.* (2005) 25:904–14. doi: 10.1161/01.ATV.0000160340.72641.87
27. Meiler SE, Hung RR, Gerszten RE, Gianetti J, Li L, Matsui T, et al. Endothelial IKK β Signaling is required for monocyte adhesion under laminar flow conditions. *J Mol Cell Cardiol.* (2002) 34:349–59. doi: 10.1006/jmcc.2001.1519
28. Mussbacher M, Salzmann M, Haigl B, Basílio J, Hochreiter B, Gleitsmann V, et al. Ikk2-mediated inflammatory activation of arterial endothelial cells promotes the development and progression of atherosclerosis. *Atherosclerosis.* (2020) 307:21–31. doi: 10.1016/j.atherosclerosis.2020.06.005
29. Lesniewski LA, Durrant JR, Connell ML, Folian BJ, Donato AJ, Seals DR. Salicylate treatment improves age-associated vascular endothelial dysfunction: potential role of nuclear factor kappaB and forkhead Box O phosphorylation. *J Gerontol A Biol Sci Med Sci.* (2011) 66:409–18. doi: 10.1093/gerona/glq233
30. Yang S, Yuan HQ, Hao YM, Ren Z, Qu SL, Liu LS, et al. Macrophage polarization in atherosclerosis. *Clin Chim Acta.* (2020) 501:142–6. doi: 10.1016/j.cca.2019.10.034
31. Fong CH, Bebien M, Didierlaurent A, Nebauer R, Hussell T, Broide D, et al. An antiinflammatory role for IKKbeta through the inhibition of "classical" macrophage activation. *J Exp Med.* (2008) 205:1269–76. doi: 10.1084/jem.20080124
32. Porta C, Rimoldi M, Raes G, Brys L, Ghezzi P, Di Liberto D, et al. Tolerance and M2 (alternative) macrophage polarization are related processes orchestrated by p50 nuclear factor kappaB. *Proc Natl Acad Sci USA.* (2009) 106:14978–83. doi: 10.1073/pnas.0809784106
33. Kanters E, Pasparakis M, Gijbels MJJ, Vergouwe MN, Partouns-Hendriks I, Fijneman RJA, et al. Inhibition of NF-κB activation in macrophages increases atherosclerosis in LDL receptor–deficient mice. *J Clin Invest.* (2003) 112:1176–85. doi: 10.1172/JCI200318580
34. Goossens P, Vergouwe MN, Gijbels MJJ, Curfs DMJ, van Woezik JHG, Hoeksema MA, et al. Myeloid IκBα deficiency promotes atherogenesis by enhancing leukocyte recruitment to the plaques. *PLoS ONE.* 2011;6:e22327-e. doi: 10.1371/journal.pone.0022327
35. Ferreira V, van Dijk KW, Groen AK, Vos RM, van der Kaa J, Gijbels MJJ, et al. Macrophage-specific inhibition of NF-κB activation reduces foam-cell formation. *Atherosclerosis.* (2007) 192:283–90. doi: 10.1016/j.atherosclerosis.2006.07.018
36. Park S-H, Sui Y, Gizard F, Xu J, Rios-Pilier J, Helsley Robert N, et al. Myeloid-specific IκB kinase β deficiency decreases atherosclerosis in low-density lipoprotein receptor–deficient mice. *Arterioscler Thromb Vasc Biol.* (2012) 32:2869–76. doi: 10.1161/ATVBAHA.112.254573
37. Basatemur GL, Jørgensen HF, Clarke MCH, Bennett MR, Mallat Z. Vascular smooth muscle cells in atherosclerosis. *Nat Rev Cardiol.* (2019) 16:727–44. doi: 10.1038/s41569-019-0227-9
38. Sasu S, Beasley D. Essential roles of IκB kinases α and β in serum- and IL-1-induced human VSMC proliferation. *Am J Physiol Heart Circ Physiol.* (2000) 278:H1823–H31. doi: 10.1152/ajpheart.2000.278.6.H1823
39. Sui Y, Park S-H, Xu J, Monette S, Helsley RN, Han S-S, et al. IKKβ links vascular inflammation to obesity and atherosclerosis. *J Exp Med.* (2014) 211:869–86. doi: 10.1084/jem.20131281
40. Berg AH, Scherer PE. Adipose tissue, inflammation, and cardiovascular disease. *Circ Res.* (2005) 96:939–49. doi: 10.1161/01.RES.0000163635.62927.34
41. Lu W, Park SH, Meng Z, Wang F, Zhou C. Deficiency of adipocyte IKKbeta affects atherosclerotic plaque vulnerability in obese LDLR deficient mice. *J Am Heart Assoc.* (2019) 8:e012009. doi: 10.1161/JAHA.119.012009
42. Aghamohammadzadeh R, Unwin RD, Greenstein AS, Heagerty AM. Effects of obesity on perivascular adipose tissue vasorelaxant function: nitric oxide, inflammation and elevated systemic blood pressure. *J Vasc Res.* (2015) 52:299–305. doi: 10.1159/000443885
43. Qi X-Y, Qu S-L, Xiong W-H, Rom O, Chang L, Jiang Z-S. Perivascular adipose tissue (PVAT) in atherosclerosis: a double-edged sword. *Cardiovasc Diabetol.* (2018) 17:134. doi: 10.1186/s12933-018-0777-x
44. Manka D, Chatterjee TK, Stoll LL, Basford JE, Konaniah ES, Srinivasan R, et al. Transplanted perivascular adipose tissue accelerates injury-induced neointimal hyperplasia: role of monocyte chemoattractant protein-1. *Arterioscler Thromb Vasc Biol.* (2014) 34:1723–30. doi: 10.1161/ATVBAHA.114.303983
45. Virani Salim S, Alonso A, Benjamin Emelia J, Bittencourt Marcio S, Callaway Clifton W, Carson April P, et al. Heart disease and stroke statistics −2020 update: a report from the American Heart Association. *Circulation.* (2020) 141:e139–596. doi: 10.1161/CIR.0000000000000757
46. Seidell JC, Halberstadt J. The global burden of obesity and the challenges of prevention. *Ann Nutr Metab.* (2015) 66:7–12. doi: 10.1159/000375143
47. Kahn SE, Hull RL, Utzschneider KM. Mechanisms linking obesity to insulin resistance and type 2 diabetes. *Nature.* (2006) 444:840–6. doi: 10.1038/nature05482
48. Xu H, Barnes GT, Yang Q, Tan G, Yang D, Chou CJ, et al. Chronic inflammation in fat plays a crucial role in the development of obesity-related insulin resistance. *J Clin Invest.* (2003) 112:1821–30. doi: 10.1172/JCI200319451
49. Van Gaal LF, Mertens IL, De Block CE. Mechanisms linking obesity with cardiovascular disease. *Nature.* (2006) 444:875–80. doi: 10.1038/nature05487
50. Reilly SM, Saltiel AR. Adapting to obesity with adipose tissue inflammation. *Nat Rev Endocrinol.* (2017) 13:633–43. doi: 10.1038/nrendo.2017.90
51. Cai D, Yuan M, Frantz DF, Melendez PA, Hansen L, Lee J, et al. Local and systemic insulin resistance resulting from hepatic activation of IKK-β and NF-κB. *Nat Med.* (2005) 11:183–90. doi: 10.1038/nm1166
52. Solinas G, Karin M. JNK1 and IKKβ: molecular links between obesity and metabolic dysfunction. *FASEB J.* (2010) 24:2596–611. doi: 10.1096/fj.09-151340
53. Wellen KE, Hotamisligil GS. Inflammation, stress, and diabetes. *J Clin Invest.* (2005) 115:1111–9. doi: 10.1172/JCI25102
54. Helsley RN, Sui Y, Park S-H, Liu Z, Lee RG, Zhu B, et al. Targeting IκB kinase β in adipocyte lineage cells for treatment of obesity and metabolic dysfunctions. *Stem Cells.* (2016) 34:1883–95. doi: 10.1002/stem.2358
55. Sui Y, Liu Z, Park S-H, Thatcher SE, Zhu B, Fernandez JP, et al. IKKβ is a β-catenin kinase that regulates mesenchymal stem cell differentiation. *JCI Insight.* (2018) 3:e96660. doi: 10.1172/jci.insight.96660
56. Ross SE, Hemati N, Longo KA, Bennett CN, Lucas PC, Erickson RL, et al. Inhibition of adipogenesis by Wnt signaling. *Science.* (2000) 289:950–3. doi: 10.1126/science.289.5481.950
57. Rosen ED, MacDougald OA. Adipocyte differentiation from the inside out. *Nat Rev Mol Cell Biol.* (2006) 7:885–96. doi: 10.1038/nrm2066
58. Jiao P, Feng B, Ma J, Nie Y, Paul E, Li Y, et al. Constitutive activation of IKKβ in adipose tissue prevents diet-induced obesity in mice. *Endocrinology.* (2012) 153:154–65. doi: 10.1210/en.2011-1346
59. Park S-H, Liu Z, Sui Y, Helsley RN, Zhu B, Powell DK, et al. IKKβ is essential for adipocyte survival and adaptive adipose remodeling in obesity. *Diabetes.* (2016) 65:1616. doi: 10.2337/db15-1156
60. Kwon H, Laurent S, Tang Y, Zong H, Vemulapalli P, Pessin JE. Adipocyte-specific IKKβ signaling suppresses adipose tissue inflammation through an IL-13-dependent paracrine feedback pathway. *Cell Rep.* (2014) 9:1574–83. doi: 10.1016/j.celrep.2014.10.068
61. Li ZW, Chu W, Hu Y, Delhase M, Deerinck T, Ellisman M, et al. The IKKbeta subunit of IkappaB kinase (IKK) is essential for nuclear factor kappaB activation and prevention of apoptosis. *J Exp Med.* (1999) 189:1839–45. doi: 10.1084/jem.189.11.1839

62. Tang G, Minemoto Y, Dibling B, Purcell NH, Li Z, Karin M, et al. Inhibition of JNK activation through NF-κB target genes. *Nature.* (2001) 414:313–7. doi: 10.1038/35104568
63. De Smaele E, Zazzeroni F, Papa S, Nguyen DU, Jin R, Jones J, et al. Induction of gadd45β by NF-κB downregulates pro-apoptotic JNK signalling. *Nature.* (2001) 414:308–13. doi: 10.1038/35104560
64. Yan J, Xiang J, Lin Y, Ma J, Zhang J, Zhang H, et al. Inactivation of BAD by IKK inhibits TNFα-induced apoptosis independently of NF-κB activation. *Cell.* (2013) 152:304–15. doi: 10.1016/j.cell.2012.12.021
65. Alkhouri N, Gornicka A, Berk MP, Thapaliya S, Dixon LJ, Kashyap S, et al. Adipocyte apoptosis, a link between obesity, insulin resistance, and hepatic steatosis. *J Biol Chem.* (2010) 285:3428–38. doi: 10.1074/jbc.M109.074252
66. Nandipati KC, Subramanian S, Agrawal DK. Protein kinases: mechanisms and downstream targets in inflammation-mediated obesity and insulin resistance. *Mol Cell Biochem.* (2017) 426:27–45. doi: 10.1007/s11010-016-2878-8
67. Gual P, Le Marchand-Brustel Y, Tanti JF. Positive and negative regulation of insulin signaling through IRS-1 phosphorylation. *Biochimie.* (2005) 87:99–109. doi: 10.1016/j.biochi.2004.10.019
68. Gao Z, Hwang D, Bataille F, Lefevre M, York D, Quon MJ, et al. Serine phosphorylation of insulin receptor substrate 1 by inhibitor kappa B kinase complex. *J Biol Chem.* (2002) 277:48115–21. doi: 10.1074/jbc.M209459200
69. Luo C, Yang H, Tang C, Yao G, Kong L, He H, et al. Kaempferol alleviates insulin resistance *via* hepatic IKK/NF-κB signal in type 2 diabetic rats. *Int Immunopharmacol.* (2015) 28:744–50. doi: 10.1016/j.intimp.2015.07.018
70. Yuan YL, Lin BQ, Zhang CF, Cui LL, Ruan SX, Yang ZL, et al. Timosaponin B-II Ameliorates palmitate-induced insulin resistance and inflammation *via* IRS-1/PI3K/Akt and IKK/NF-[formula: see text]B pathways. *Am J Chin Med.* (2016) 44:755–69. doi: 10.1142/S0192415X16500415
71. Zhou X, You S. Rosiglitazone inhibits hepatic insulin resistance induced by chronic pancreatitis and IKK-β/NF-κB expression in liver. *Pancreas.* (2014) 43:1291–8. doi: 10.1097/MPA.0000000000000173
72. Gao J, Song J, Du M, and Mao X. Bovine α-lactalbumin hydrolysates (α-LAH) ameliorate adipose insulin resistance and inflammation in high-fat diet-fed C57BL/6J mice. *Nutrients*. (2018) 10:242. doi: 10.3390/nu10020242
73. Yuan M, Konstantopoulos N, Lee J, Hansen L, Li Z-W, Karin M, et al. Reversal of obesity- and diet-induced insulin resistance with salicylates or targeted disruption of Ikkβ. *Science.* (2001) 293:1673. doi: 10.1126/science.1061620
74. Kim JK, Kim Y-J, Fillmore JJ, Chen Y, Moore I, Lee J, et al. Prevention of fat-induced insulin resistance by salicylate. *J Clin Invest.* (2001) 108:437–46. doi: 10.1172/JCI11559
75. Wang XA, Zhang R, She ZG, Zhang XF, Jiang DS, Wang T, et al. Interferon regulatory factor 3 constrains IKKβ/NF-κB signaling to alleviate hepatic steatosis and insulin resistance. *Hepatology.* (2014) 59:870–85. doi: 10.1002/hep.26751
76. Ke B, Zhao Z, Ye X, Gao Z, Manganiello V, Wu B, et al. Inactivation of NF-κB p65 (RelA) in liver improves insulin sensitivity and inhibits cAMP/PKA pathway. *Diabetes.* (2015) 64:3355–62. doi: 10.2337/db15-0242
77. Arkan MC, Hevener AL, Greten FR, Maeda S, Li Z-W, Long JM, et al. IKK-β links inflammation to obesity-induced insulin resistance. *Nat Med.* (2005) 11:191–8. doi: 10.1038/nm1185
78. Liu J, Ibi D, Taniguchi K, Lee J, Herrema H, Akosman B, et al. Inflammation improves glucose homeostasis through IKKβ-XBP1s interaction. *Cell.* (2016) 167:1052–66.e18. doi: 10.1016/j.cell.2016.10.015
79. Rocha VZ, Libby P. Obesity, inflammation, and atherosclerosis. *Nat Rev Cardiol.* (2009) 6:399–409. doi: 10.1038/nrcardio.2009.55
80. Hotamisligil GS. Inflammation and metabolic disorders. *Nature.* (2006) 444:860–7. doi: 10.1038/nature05485
81. Jiao P, Ma J, Feng B, Zhang H, Alan-Diehl J, Eugene-Chin Y, et al. FFA-Induced adipocyte inflammation and insulin resistance: involvement of ER stress and IKKβ pathways. *Obesity.* (2011) 19:483–91. doi: 10.1038/oby.2010.200
82. Wang M, Chen X, Zheng Z, Yu S, Zhou B, Liu Y, et al. Beneficial effect of ER stress preconditioning in protection against FFA-induced adipocyte inflammation *via* XBP1 in 3T3-L1 adipocytes. *Mol Cell Biochem.* (2020) 463:45–55. doi: 10.1007/s11010-019-03627-3
83. Green CJ, Pedersen M, Pedersen BK, Scheele C. Elevated NF-κB activation is conserved in human myocytes cultured from obese type 2 diabetic patients and attenuated by AMP-activated protein kinase. *Diabetes.* (2011) 60:2810–9. doi: 10.2337/db11-0263
84. Bhatt BA, Dube JJ, Dedousis N, Reider JA, O'Doherty RM. Diet-induced obesity and acute hyperlipidemia reduce IkappaBalpha levels in rat skeletal muscle in a fiber-type dependent manner. *Am J Physiol Regul Integr Comp Physiol.* (2006) 290:R233–40. doi: 10.1152/ajpregu.00097.2005
85. Jové M, Planavila A, Sánchez RM, Merlos M, Laguna JC, Vázquez-Carrera M. Palmitate induces tumor necrosis factor-alpha expression in C2C12 skeletal muscle cells by a mechanism involving protein kinase C and nuclear factor-kappaB activation. *Endocrinology.* (2006) 147:552–61. doi: 10.1210/en.2005-0440
86. Radin MS, Sinha S, Bhatt BA, Dedousis N, O'Doherty RM. Inhibition or deletion of the lipopolysaccharide receptor Toll-like receptor-4 confers partial protection against lipid-induced insulin resistance in rodent skeletal muscle. *Diabetologia.* (2008) 51:336–46. doi: 10.1007/s00125-007-0861-3
87. Rohl M, Pasparakis M, Baudler S, Baumgartl J, Gautam D, Huth M, et al. Conditional disruption of IkappaB kinase 2 fails to prevent obesity-induced insulin resistance. *J Clin Invest.* (2004) 113:474–81. doi: 10.1172/JCI200418712
88. Kern PA, Ranganathan S, Li C, Wood L, Ranganathan G. Adipose tissue tumor necrosis factor and interleukin-6 expression in human obesity and insulin resistance. *Am J Physiol Endocrinol Metab.* (2001) 280:E745–51. doi: 10.1152/ajpendo.2001.280.5.E745
89. Rehman K, Akash MSH, Liaqat A, Kamal S, Qadir MI, Rasul A. Role of interleukin-6 in Development of insulin resistance and type 2 diabetes mellitus. *Crit Rev Eukaryot Gene Expr.* (2017) 27:229–36. doi: 10.1615/CritRevEukaryotGeneExpr.2017019712
90. Senn JJ, Klover PJ, Nowak IA, Zimmers TA, Koniaris LG, Furlanetto RW, et al. Suppressor of cytokine signaling-3 (SOCS-3), a potential mediator of interleukin-6-dependent insulin resistance in hepatocytes. *J Biol Chem.* (2003) 278:13740–6. doi: 10.1074/jbc.M210689200
91. Liu Y, Sheng L, Xiong Y, Shen H, Rui L. Liver NF-κB-Inducing kinase promotes liver steatosis and glucose counterregulation in male mice with obesity. *Endocrinology.* (2017) 158:1207–16. doi: 10.1210/en.2016-1582
92. Beraza N, Malato Y, Vander Borght S, Liedtke C, Wasmuth HE, Dreano M, et al. Pharmacological IKK2 inhibition blocks liver steatosis and initiation of non-alcoholic steatohepatitis. *Gut.* (2008) 57:655–63. doi: 10.1136/gut.2007.134288
93. Gervois P, Torra IP, Fruchart JC, Staels B. Regulation of lipid and lipoprotein metabolism by PPAR activators. *Clin Chem Lab Med.* (2000) 38:3–11. doi: 10.1515/CCLM.2000.002
94. Sunami Y, Leithäuser F, Gul S, Fiedler K, Güldiken N, Espenlaub S, et al. Hepatic activation of IKK/NFκB signaling induces liver fibrosis *via* macrophage-mediated chronic inflammation. *Hepatology.* (2012) 56:1117–28. doi: 10.1002/hep.25711
95. Zhang X, Zhang G, Zhang H, Karin M, Bai H, Cai D. Hypothalamic IKKβ/NF-κB and ER stress link overnutrition to energy imbalance and obesity. *Cell.* (2008) 135:61–73. doi: 10.1016/j.cell.2008.07.043
96. Kleinridders A, Schenten D, Könner AC, Belgardt BF, Mauer J, Okamura T, et al. MyD88 signaling in the CNS is required for development of fatty acid-induced leptin resistance and diet-induced obesity. *Cell Metab.* (2009) 10:249–59. doi: 10.1016/j.cmet.2009.08.013
97. Posey KA, Clegg DJ, Printz RL, Byun J, Morton GJ, Vivekanandan-Giri A, et al. Hypothalamic proinflammatory lipid accumulation, inflammation, and insulin resistance in rats fed a high-fat diet. *Am J Physiol Endocrinol Metab.* (2009) 296:E1003–12. doi: 10.1152/ajpendo.90377.2008
98. Meng Q, Cai D. Defective hypothalamic autophagy directs the central pathogenesis of obesity *via* the IkappaB kinase beta (IKKbeta)/NF-kappaB pathway. *J Biol Chem.* (2011) 286:32324–32. doi: 10.1074/jbc.M111.254417
99. Milanski M, Degasperi G, Coope A, Morari J, Denis R, Cintra DE, et al. Saturated fatty acids produce an inflammatory response predominantly through the activation of TLR4 signaling in hypothalamus: implications for the pathogenesis of obesity. *J Neurosci.* (2009) 29:359–70. doi: 10.1523/JNEUROSCI.2760-08.2009

100. Lee CH, Suk K, Yu R, Kim MS. Cellular contributors to hypothalamic inflammation in obesity. *Mol Cells.* (2020) 43:431–7. doi: 10.14348/molcells.2020.0055
101. Howard JK, Flier JS. Attenuation of leptin and insulin signaling by SOCS proteins. *Trends Endocrinol Metab.* (2006) 17:365–71. doi: 10.1016/j.tem.2006.09.007
102. Purkayastha S, Zhang H, Zhang G, Ahmed Z, Wang Y, Cai D. Neural dysregulation of peripheral insulin action and blood pressure by brain endoplasmic reticulum stress. *Proc Natl Acad Sci USA.* (2011) 108:2939–44. doi: 10.1073/pnas.1006875108
103. Tsaousidou E, Paeger L, Belgardt BF, Pal M, Wunderlich CM, Brönneke H, et al. Distinct roles for JNK and IKK activation in agouti-related peptide neurons in the development of obesity and insulin resistance. *Cell Rep.* (2014) 9:1495–506. doi: 10.1016/j.celrep.2014.10.045
104. Sofroniew MV, Vinters HV. Astrocytes: biology and pathology. *Acta Neuropathol.* (2010) 119:7–35. doi: 10.1007/s00401-009-0619-8
105. Douglass JD, Dorfman MD, Fasnacht R, Shaffer LD, Thaler JP. Astrocyte IKKβ/NF-κB signaling is required for diet-induced obesity and hypothalamic inflammation. *Mol Metab.* (2017) 6:366–73. doi: 10.1016/j.molmet.2017.01.010
106. Zhang Y, Reichel JM, Han C, Zuniga-Hertz JP, and Cai D. Astrocytic process plasticity and IKKβ/NF-κB in central control of blood glucose, blood pressure, and body weight. *Cell Metab.* (2017) 25:1091–102.e4. doi: 10.1016/j.cmet.2017.04.002
107. Miranda M, Morici JF, Zanoni MB, Bekinschtein P. Brain-derived neurotrophic factor: a key molecule for memory in the healthy and the pathological brain. *Front Cell Neurosci.* (2019) 13:363. doi: 10.3389/fncel.2019.00363
108. Li J, Tang Y, Cai D. IKKβ/NF-κB disrupts adult hypothalamic neural stem cells to mediate a neurodegenerative mechanism of dietary obesity and pre-diabetes. *Nat Cell Biol.* (2012) 14:999–1012. doi: 10.1038/ncb2562
109. Khor S, Cai D. Hypothalamic and inflammatory basis of hypertension. *Clin Sci (Lond).* (2017) 131:211–23. doi: 10.1042/CS20160001
110. Purkayastha S, Zhang G, Cai D. Uncoupling the mechanisms of obesity and hypertension by targeting hypothalamic IKK-β and NF-κB. *Nat Med.* (2011) 17:883–7. doi: 10.1038/nm.2372

Conflict of Interest: The authors declare that the research was conducted in the absence of any commercial or financial relationships that could be construed as a potential conflict of interest.

Publisher's Note: All claims expressed in this article are solely those of the authors and do not necessarily represent those of their affiliated organizations, or those of the publisher, the editors and the reviewers. Any product that may be evaluated in this article, or claim that may be made by its manufacturer, is not guaranteed or endorsed by the publisher.

frontiers in Cardiovascular Medicine

ORIGINAL RESEARCH
published: 03 January 2022
doi: 10.3389/fcvm.2021.775392

MEF2A Is the Trigger of Resveratrol Exerting Protection on Vascular Endothelial Cell

Benrong Liu[1†], Lihua Pang[1†], Yang Ji[1†], Lei Fang[1], Chao Wei Tian[2,3], Jing Chen[1], Changnong Chen[1], Yun Zhong[1], Wen-Chao Ou[1], Yujuan Xiong[4*] and Shi Ming Liu[1*]*

[1] Guangdong Key Laboratory of Vascular Diseases, State Key Laboratory of Respiratory Disease, Guangzhou Institute of Cardiovascular Disease, The Second Affiliated Hospital, Guangzhou Medical University, Guangzhou, China, [2] Department of Emergency, The Second Affiliated Hospital, Guangzhou Medical University, Guangzhou, China, [3] Department of General Practice, The Second Affiliated Hospital, Guangzhou Medical University, Guangzhou, China, [4] Department of Laboratory Medicine, Panyu Hospital of Chinese Medicine, Guangzhou University of Chinese Medicine, Guangzhou, China

Both resveratrol and myocyte enhancer factor 2A (MEF2A) may protect vascular endothelial cell (VEC) through activating the expression of SIRT1. However, the relationship between resveratrol and MEF2A is unclear. We aimed to investigate the deeper mechanism of resveratrol in protecting vascular endothelial cells and whether MEF2A plays a key role in the protective function of resveratrol. Human umbilical vein endothelial cell (HUVEC) was used for *in vitro* study, and small interfere RNA was used for silencing MEF2A. Silencing MEF2A in the vascular endothelium (VE) of ApoE$^{-/-}$ mice was performed by tail injection with adeno associated virus expressing si-mef2a-shRNA. The results showed that treatment of HUVEC with resveratrol significantly up-regulated MEF2A, and prevented H_2O_2-induced but not siRNA-induced down-regulation of MEF2A. Under various experimental conditions, the expression of SIRT1 changed with the level of MEF2A. Resveratrol could rescue from cell apoptosis, reduction of cell proliferation and viability induced by H_2O_2, but could not prevent against that caused by silencing MEF2A with siRNA. Silencing MEF2A in VE of apoE$^{-/-}$ mice decreased the expression of SIRT1, increased the plasma LDL-c, and abrogated the function of resveratrol on reducing triglyceride. Impaired integrity of VE and aggravated atherosclerotic lesion were observed in MEF2A silenced mice through immunofluorescence and oil red O staining, respectively. In conclusion, resveratrol enhances MEF2A expression, and the upregulation of MEF2A is required for the endothelial protective benefits of resveratrol *in vitro* via activating SIRT1. Our work has also explored the *in vivo* relevance of this signaling pathway in experimental models of atherosclerosis and lipid dysregulation, setting the stage for more comprehensive phenotyping *in vivo* and further defining the molecular mechanisms.

Keywords: resveratrol, vascular endothelial cell, HUVEC, Sirtuin1, myocyte enhancer factor 2A

OPEN ACCESS

Edited by:
Xuewei Zhu,
Wake Forest Baptist Medical Center, United States

Reviewed by:
Rafael Campos,
State University of Ceará, Brazil
Hanrui Zhang,
Columbia University, United States

***Correspondence:**
Benrong Liu
liubenrong@gzhmu.edu.cn
Yujuan Xiong
yujuanxiong@gzucm.edu.cn
Shi Ming Liu
liushiming@gzhmu.edu.cn

[†]These authors have contributed equally to this work

Specialty section:
This article was submitted to Atherosclerosis and Vascular Medicine, a section of the journal Frontiers in Cardiovascular Medicine

Received: *13 September 2021*
Accepted: *09 December 2021*
Published: *03 January 2022*

Citation:
Liu B, Pang L, Ji Y, Fang L, Tian CW, Chen J, Chen C, Zhong Y, Ou W-C, Xiong Y and Liu SM (2022) MEF2A Is the Trigger of Resveratrol Exerting Protection on Vascular Endothelial Cell. Front. Cardiovasc. Med. 8:775392. doi: 10.3389/fcvm.2021.775392

INTRODUCTION

Resveratrol is a polyphenol compound that can be obtained from several dietary sources, such as grapes, apples, blueberries, plums, raspberries and peanuts, and has a variety of health-promoting effects (1). Evidences from a large number of basic scientific studies and more than 240 clinical studies support the beneficial effects of resveratrol against chronic diseases such as cardiovascular disease, diabetes, hypertension, Alzheimer's disease, liver disease, kidney disease and cancer (2, 3). Among these diseases, aging is the most common risk factor, which is usually related to the accumulation of reactive oxygen species (ROS), the increase of inflammatory lesions, the abnormality of cell proliferation and the altered angiogenesis (4–6). In the cardiovascular system, aging is surely one of the most important determinants of different diseases (4, 5). Resveratrol has long been considered as an anti-aging compound and its cardiovascular protective effect was mainly attributed to its function of antioxidant, anti-inflammatory, anti-proliferation, vascular regulation and promotion of autophagy (1, 4, 7). The monolayer, flat and slightly longer vascular endothelial cells closely arranged in the inner wall of blood vessels secrete key regulatory factors that regulate blood pressure and vascular tension. Vascular endothelial dysfunction is the early event of cardiovascular disease. A large number of studies have confirmed that resveratrol is a strong protector of vascular endothelium, and its main molecular mechanisms include increasing the production of nitric oxide (NO) in vascular endothelium by up-regulating the expression and activity of NO synthase (eNOS), down-regulating the synthesis of endothelin-1 to reduce vasoconstriction and blood pressure (1, 8), promoting mitochondrial biosynthesis and reducing the production of mitochondrial superoxides (9), preventing arterial aging by reducing the activity of PRR-ACE-AngII axis and activating ACE2-Ang-(1–7)-ATR2-MasR axis (10), reducing vascular endothelial oxidative stress by up-regulating the expression of Sirtuin1 (SIRT1), and delaying vascular endothelial cell senescence (11).

SIRT1 is a member of nicotinamide adenine dinucleotide (NAD+) dependent histone deacetylase class III family, and is a necessary factor in delaying cell senescence and prolonging biological life span (11), and plays an important role in protecting vascular endothelium (12–14). In vascular endothelial cells, the expression of SIRT1 may be regulated by myocyte enhancer factor 2A (MEF2A) (15). MEF2A is a member of the MEF2 family and belongs to the MADS-box superfamily. MEF2A is a very important transcriptional regulatory factor, which is necessary for cell differentiation, cell proliferation, cell survival, morphogenesis and other life processes (16, 17). The important role of MEF2A in neural differentiation, maturation and synapsis has been supported by a great deal of evidence (18–20), but its role in cardiovascular disease is still controversial. In 2003, Wang et al. (21) revealed that the 21bp deletion in exon 11 of MEF2A was co-isolated from the patient with premature coronary heart disease in a general pedigree, and MEF2A has become the first identified autosomal dominant genetic variation in the risk of coronary heart disease (named ADCAD1). However, studies in the following decades have shown that 21 bp deletion in exon 11 of MEF2A is rare in the population. The genetic variation of MEF2A gene does not explain the risk of coronary heart disease in most people (22). In recent years, the research on the function of MEF2A has rekindled the hope of MEF2A in the field of cardiovascular disease. Lu et al. (23) revealed that MEF2A/C/D is a key regulator of vascular homeostasis by studying the phenotype and transcriptome after specific deletion of MEF2A/C/D from mouse endothelium. Medrano et al. (24) reported that MEF2A precisely regulates gene expression in adult atria and ventricles, and Zhou et al. (25) found that interference of MEF2A expression in apoE knockout mice can promote atherosclerotic lesions. The results of a study in renal vascular endothelium suggest that MEF2A can regulate vascular endothelial cell migration, tube formation and anti-apoptosis (26). In our previous studies, we found that inhibiting the expression of MEF2A in human coronary artery endothelial cells significantly changed the expression profile of genes related to proliferation and inflammation, induced cell senescence and significantly down-regulated the expression of SIRT1 in human coronary artery endothelial cells (15, 27). Overexpression of MEF2A in vascular endothelial cells can inhibit the down-regulation of SIRT1 induced by hydrogen peroxide (H_2O_2), thus inhibits cell senescence induced by H_2O_2. The regulation of SIRT1 by MEF2A may be caused by directly activating the expression of PI3K (15).

In vascular endothelial cells (VEC), MEF2A is considered to be the key transcriptional activator upstream of SIRT1, and resveratrol can effectively stimulate the expression of SIRT1, so does resveratrol up-regulate the expression of SIRT1 and protect VEC depending on stimulating the expression of MEF2A? In this study, we revealed that resveratrol up-regulated SIRT1 expression, functioned anti-apoptosis and anti-atherosclerotic lesions depending on up-regulating MEF2A expression.

MATERIALS AND METHODS

Cell Culture and Reagents

The primary human umbilical vein endothelial cell (HUVEC) was purchased from Procell Life Science and Technology Co., Ltd (CL-0122) and cultured in EBM-2 medium with 3% fetal bovine serum (Gibco) and growth factors (Gibco), and incubated at 37°C in a humidified incubator with 5% CO_2. Resveratrol was purchased from SigmaAldrich, dissolved in DMSO for cell treatment, and added to 0.5% sodium carboxymethyl cellulose solution to form a suspension for intragastric administration to mice.

Treatment of HUVEC With H_2O_2

HUVEC were seeded in 48-well plates or 96-well plates and were cultured overnight. After replacing the culture medium with fresh medium, a gradient concentration of H_2O_2 was added and incubated for 1, 2 and 4 h, respectively. After incubating the cells with H_2O_2, immediately replaced the medium with fresh medium and continued to culture according to the standard conditions.

Treatment of HUVEC With Resveratrol

10 mM of storage solution of resveratrol was prepared by dissolving resveratrol with DMSO. A gradient concentration of resveratrol solution was added to HUVECs and incubated for 12, 24 and 48 h, respectively. After incubating the cells with resveratrol, replaced the medium with fresh medium and continued to culture for further experiments.

Transfection of Small Interfere RNA (siRNA)

Si-RNA was transfected into HUVEC using Lipofectamine RNAI MAX (Invitrogen) transfection kit, and all operations were conducted according to the manufacturer's instructions. Briefly: before transfection, medium was replaced with the fresh complete medium, siRNA and the transfection reagents were respectively diluted with serum-free medium (Opti-MEM). The diluted siRNA and the transfection reagents were mixed sufficiently and incubated for 10 min at room temperature, then all of the mixture were transferred to the target wells of the culture plates, and the final concentration of 50 nM si-RNA was used. Then, the culture plates were gently shaken and placed in a moist incubator at 37°C with 5% carbon dioxide for culturing 6–8 h. After that, culture medium was replaced with fresh EBM-2 complete medium and the cells were cultured for 48–72 h followed by performing the subsequent experiments.

Detection of Cell Viability

Cell Counting Kit-8 (CCK8) was used to detect cell viability according to the manufacturer's instructions, briefly: The cell culture medium was replaced with fresh serum free EBM-2 medium, 10 μl CCK8 solution was added to wells containing 100 μl medium and gently mixed, then placed in a cell incubator containing 5% CO_2 at 37°C for 3–4 h. Optical density value at 450 nm was measured on a spectrophotometer.

Detection of Cell Proliferation Ability

The cell proliferation ability was detected by 5-Ethynyl-2′-deoxyuridine (EdU) cell proliferation detection kit (R11053.4, Ribobio, China) according to the manufacturer's instructions, and the cells staining red were highly proliferative cells.

Detection of Cellular Mitochondrial Membrane Potential

JC-1 staining kit (M8650,Solarbio,China) was used to detect the changes of mitochondrial membrane potential according to the manufacturer's instructions. Briefly, the medium was discarded and the cells were washed twice with PBS (pH 7.2), appropriate amount of JC-1 working solution was added and incubated in the cell incubator for 20 min, then the supernatant was removed and washed twice with 1 × JC-1 staining solution and appropriate amount of cell culture medium was added to ensure the whole bottom area to be covered, which was observed under inverted fluorescence microscope and the pictures were taken for further analysis.

Detection of Cell Apoptosis With Flow Cytometry

The eBioscience Annexin V-FITC Apoptosis Detection Kit (BMS500FI-300, Thermo Fisher Scientific, USA) was used to detect cell apoptosis according to the manufacturer's instruction. Briefly, the cells were collected and washed once with PBS (pH 7.2), then were resuspended with 500 μl stain buffer (FBS) and centrifuged at room temperature and 1,000 rpm for 5 min. The supernatant was discarded. The cells were washed once with PBS (pH 7.2), resuspended with 200 μl binding buffer and 5 μl of Annexin V labeled with Fluorescein Isothiocyanate (FITC) was added, gently mixed and incubated in dark (room temperature) for 15 min, then 10 μl of PI solution was added followed by detecting the percentage of living cells, dead cells and apoptotic cells on a flow cytometer.

Feeding of Mice

All animal experiments carried out in this study were reviewed and approved by the Experimental Animal Ethics Committee of the Second Affiliated Hospital of Guangzhou Medical University (Approval Number: A2019−013). The male wild-type C57BL/6J mice (WTM) and the male ApoE$^{-/-}$ mice (ApoE$^{-/-}$M), aged from 4 to 6 weeks, were purchased from Guangdong Experimental Animal Center. The normal feed and high-fat feed (HF60, 112252) were also purchased from Guangdong Experimental Animal Center. WTM were randomly divided into two groups ($n = 10$ per each group). ApoE$^{-/-}$M were randomly divided into 4 groups ($n = 10$ per each group). Except the mice in one group of WTM were fed with normal diet, the others were fed with high-fat diet. All mice grew in an environment with 60–70% humidity and 23 ± 2°C room temperature, under 12 h of light and 12 h of darkness alternately.

Design of the Short Hairpin RNA (shRNA) Expression Vector for Inhibition of Mef2a in Mouse and Preparation of Adeno-Associated Virus (AAV)

The reference sequence of mouse mef2a gene (accession No.: NM_001033713) was used as the interference target to design the shRNA AAV expression vector. The mature siRNA sequence was 5′-GGGCAGUUAUCUCAGGGUU-3′. DNA sequences expressing shRNA was placed under the control of the promoter of ICAM2 to construct an endothelial cell-specific expression vector. The packaging, purification and titer determination of mouse mef2a shRNA AAV1-type adeno-associated virus were performed by Shandong Weizhen Biotechnology Co., Ltd. Finally, mef2a-shRNA-AAV1 [pAV-ICAM2-GFP-mir30-shRNA (MEF2a)] was obtained with a titer of 4.46×10^{13} Vg /ml. The pAV-ICAM2-GFP-mir30-shRNA (NC) inserted with meaningless sequence was used and packaged as negative control (NC-shRNA-AAV1), and the titer of the NC-shRNA-AAV1 was 5.14×10^{13} vg/ml.

Infection of Mice With AAV1

The AAV1 (mef2a-shRNA-AAV1 and NC-shRNA-AAV1) was respectively diluted to 1×10^{13} vg/ml with 0.9% sterile saline and

100 μl of this diluted AAV1 solution was injected through the tail vein for each apoE$^{-/-}$ mouse. The infected mice were fed with high-fat diet for about 90 days.

Intragastric Administration of Resveratrol to Mice

The resveratrol suspension was prepared by dissolving resveratrol in 0.5% sodium carboxymethyl cellulose (SCC) solution. Gastric administration of the prepared resveratrol suspension was performed once a day according to 30 mg/kg body weight per day by using gastric perfusion needle and was sustained for 90 days, while the control group was given the same dose of 0.5% SCC solution.

Sampling From Mice

The mice were anesthetized by inhaling 2% isoflurane and adequate depth of anesthesia was monitored using toe reflex. Under deep anesthesia, the mice were sacrificed by cervical dislocation, and then blood samples were collected immediately from eyes through removing the eyeballs, followed by tissue sampling. Thoracic aorta, abdominal aorta, aortic valve and heart of the mouse were excised for using in the following experiments.

Oil Red O Staining

The frozen sections were prepared from the fresh aortic valve. The sections and the whole aorta were fixed in 4% paraformaldehyde and dried for minutes, then the dry tissues were soaked with oil red staining solution for 8–10 min (avoiding light). The vessels or slides were taken out and immersed in 60% isopropanol solution for 3 s, then were transferred to a new 60% isopropanol solution, and were rinsed with pure water twice for 10 s each. The vessels or slides were taken out to soak in hematoxylin for 3–5 min, then were washed 3 times with 60% ethanol solution for, respectively, 5, 10 and 30 s, then were washed 2 times with pure water for 10 s each, soaked in the blue solution for 1 s, rinsed twice with pure water for, respectively, 5 and 10 s, and were sealed with glycerin gelatin. Finally, the prepared slides or vessels were observed under the microscope and images were photographed.

Immunofluorescence

The tissue specimens were fixed in 4% paraformaldehyde for 24 h, further dehydrated with gradient concentration of alcohol, then was subjected to permeation with xylene and prepared the paraffin-embedded sections. The tissue sections were immersed in antigen-retrieval buffer (pH 8.0), then were transferred in 3% hydrogen peroxide solution and incubated at room temperature for 30 min. The sections were washed with PBS, blocked with BSA, and incubated with the primary antibody at 4°C overnight. After being washed with PBS, the sections were incubated with the secondary antibody at room temperature for 50 min. After being washed with PBS, the sections were dried and incubated with TSA-FITC solution for 10 min, then were rinsed with TBST for 3 times. After eliminating obvious liquid, the slides were incubated with spontaneous fluorescence quenching reagent for 5 min, washed under flowing water for 10 min. Then, the slides were incubated with DAPI solution at room temperature for 10 min, and washed 3 times with PBS (pH 7.4), mounted with anti-fade mounting medium. Then the slides were detected and imaged with fluorescent microscopy. The primary antibodies of MEF2A (cat.gb11965) and CD31 (cat.gb11063-2) were purchased from Wuhan Servicebio Technology Co., Ltd (Wuhan, China).

RNA Isolation and Real-Time Fluorescence Quantitative PCR

Total RNA was prepared from cells by using Trizol according to the manufacturer's instruction. The quality of RNA was detected by gel electrophoresis, and the concentration was calculated with the absorbance value detected on a spectrophotometer (Bio Tek, Epoch) at a wave length of 260 nm. Reverse transcription and synthesis of the cDNA from the total RNA was performed by using the FastKing gDNA dispelling RT superMix kit (Tiangen Bio, Beijing, China). Quantitative PCR was performed using RealUniversal color premix kit (SYBR Green) according to the manufacturer's instructions. Beta-actin (ACTB) was used as the internal control.

Immunobloting

Cells were washed with precooled PBS (pH 7.2) and then lysed in RIPA buffer containing proteinase inhibitor. The protein content was quantified with a BCA protein assay kit (Thermo, USA). Equal amount of protein from different samples was loaded into the SDS-PAGE gel for immunobloting. The primary antibodies against MEF2A (cat.9736s, CST, USA), SIRT1 (cat.9475, CST, USA), Bcl-2 (cat.15071, CST, USA), Bax (cat.5023s, CST, USA), Caspase-3 (cat.9662s, CST, USA), Cleaved Caspase-3 (cat.9661s, CST, USA), β-actin (cat.4970s, CST, USA) and GAPDH (cat.5174s, CST, USA) were used for probing specific proteins. Beta-actin and GAPDH were used as the internal control.

Statistical Analysis

Detection of variance homogeneity and normal distribution of data in each Group was performed by using exploratory analysis in descriptive analysis in SPSS19 software. The significance of the difference between the two groups with uniform variance was examined by Student's *t* test or two-way ANOVA with Bonferroni posterior tests. For the significance test of difference between two groups with uneven variance, the Mann-Whitney U test was used. Individual values were presented in dot plots and the mean ± standard deviation (SD) was shown with it. The difference was considered significant when a P value < 0.05.

RESULTS

Resveratrol Promotes the Expression of MEF2A

To determine the effect of resveratrol on HUVEC and on MEF2A expression, we treated HUVEC with resveratrol at a gradient concentration for 12, 24 and 48 h, respectively. The results showed that the HUVEC cell viability was slightly increased after treated with resveratrol of 0.625, 1.25, 2.5 and 5 μM for 24 h, and the resveratrol of 5 μM could significantly increase cell viability, while the resveratrol of 10 and 20 μM could significantly decrease

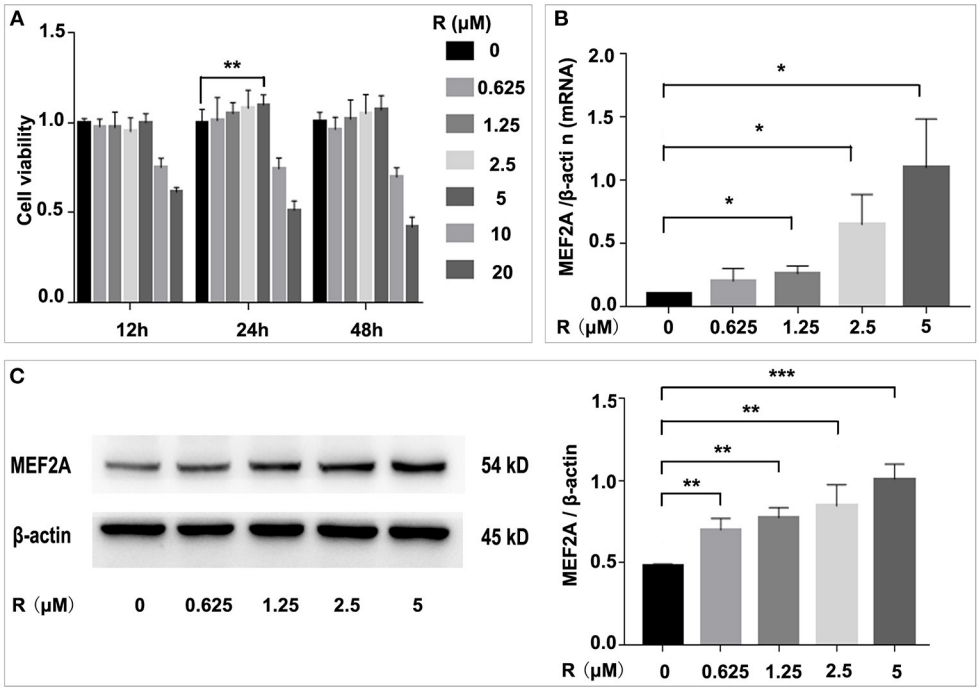

FIGURE 1 | Influence of resveratrol on cell viability and the expression of MEF2A. **(A)** Impact of treatment of HUVEC with gradient concentration of resveratrol for various time on cell viability. **(B)** The mRNA level of MEF2A in HUVEC treated with gradient concentration of resveratrol for 24 h. β-actin was used as the internal control to normalize the MEF2A mRNA level. **(C)** Immunoblots of MEF2A. β-actin was used as a loading control. Quantification of band intensity was performed via image-J and values were normalized to beta-actin. All experiments were performed independently for three times. Mean ± standard deviation (SD) is showed as bar plot. The statistical significance is analyzed by the unpaired Student's two-tailed *t*-test. ns, no significance; $^{*}P < 0.05$; $^{**}P < 0.01$; $^{***}P < 0.001$ between groups indicated.

cell viability. It was suggested that 5 μM of resveratrol had a protective effect on HUVEC, while 10 μM or higher resveratrol had toxic side effects on cells (**Figure 1A**). Thus, resveratrol of 5 μM was used in subsequent experiments. The expression of MEF2A was detected by qPCR and Western blot, and the results showed that resveratrol promoted the expression of MEF2A at mRNA and protein level in a concentration-dependent manner (**Figures 1B,C**). The protein level of MEF2A was doubled when HUVECs were treated with resveratrol at a final concentration of 5 μM.

Resveratrol May Rescue Cells Against H_2O_2 Induced Damage by Up-Regulating MEF2A

In order to study the damage of H_2O_2 to HUVEC and its effect on MEF2A expression, we used different concentrations of H_2O_2 to treat HUVEC, to detect the changes of cell viability and MEF2A expression. The results showed that the cell damage caused by H_2O_2 was concentration-dependent. After treating HUVEC with 200 μM H_2O_2 for 2 h, the cell viability decreased about 40% (**Figure 2A**). A concentration-dependent reduction in the expression of MEF2A was observed as HUVECs were treated with H_2O_2. When HUVEC was treated with 200 μM H_2O_2 for 2 h, the protein expression level of MEF2A decreased about 60% (**Figure 2B**). In the follow-up experiments, 200 μM H_2O_2 was used to treat HUVEC for 2 h. The reduction of MEF2A protein or mRNA induced by H_2O_2 was abrogated by pretreating the cells with resveratrol, and the strength of this effect was dependent on the concentration of resveratrol (**Figures 2C,D**). It is interesting that the expression of SIRT1 altered in a similar pattern with MEF2A not only in the cells treated with a gradient concentration of resveratrol (**Supplementary Figure 1A**), but in the cells treated with a gradient concentration of H_2O_2 (**Supplementary Figure 1B**).

Our previous study has shown that overexpression of MEF2A can rescue H_2O_2 induced cell senescence (15). To investigate the damage effect of H_2O_2 or MEF2A specific siRNA (si-MEF2A) on HUVEC and whether resveratrol can rescue from the damage effect on HUVEC caused by H_2O_2 or si-MEF2A, we detected the changes in cell proliferation, mitochondrial membrane potential, apoptosis and the expression of apoptosis-related proteins after treatment of HUVEC with H_2O_2, si-MEF2A solely or plus resveratrol.

Resveratrol May Prevent Cell Proliferative Ability Decrease Induced by H_2O_2 Through Up-Regulating MEF2A

EdU kit was used to detect the proliferative ability of cells in different treatment groups, and the results showed that the proliferative ability of HUVEC significantly reduced by treating with H_2O_2 or transfecting with si-MEF2A. Pretreatment of HUVEC with resveratrol before treating with H_2O_2 could prevent reduction of proliferative ability induced by H_2O_2 (**Figure 3A**). However, the decreased cell proliferative ability

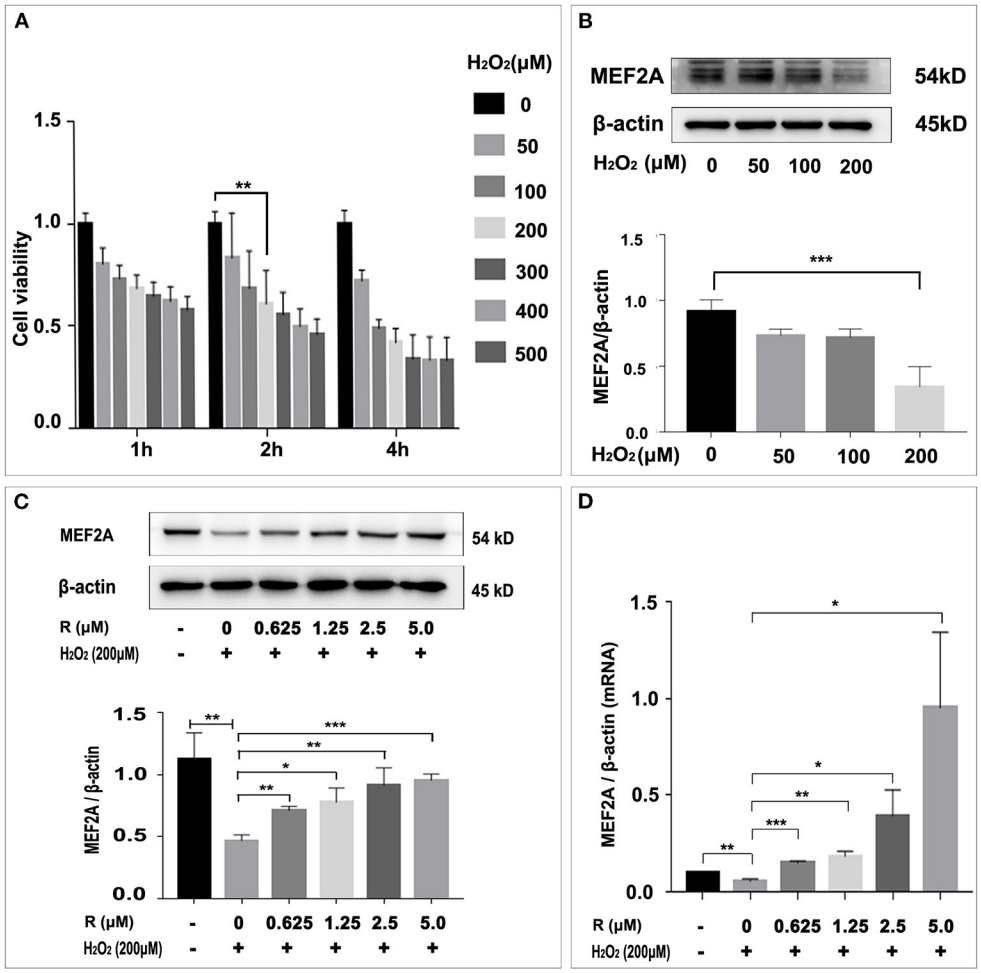

FIGURE 2 | Influence of H_2O_2 on cell viability and resveratrol rescue MEF2A from the down-regulation induced by H_2O_2. **(A)** Effect of treatment of HUVEC with gradient concentration of H_2O_2 for various time on viability. **(B)** Immunoblots of MEF2A in HUVEC treated with gradient concentration of H_2O_2 for 2 h. **(C)** Expression of MEF2A proteins in HUVECs that were pretreated with gradient concentration of resveratrol for 24 h followed by treatment with H_2O_2 (200 μM for 2 h). β-actin was used as a loading control. Quantification of band intensity was performed via image-J and values were normalized to that of beta-actin. **(D)** The mRNA level of MEF2A in HUVECs that were pretreated with gradient concentration of resveratrol for 24 h followed by treatment with H_2O_2 (200 μM for 2 h). β-actin was used as the internal control to normalize the MEF2A mRNA level. All experiments were performed independently for three times. Mean ± SD is represented as bar plot. The statistical significance is analyzed by the unpaired Student's two-tailed *t*-test. ns, no significance; $^*P < 0.05$; $^{**}P < 0.01$; $^{***}P < 0.001$ between groups indicated.

caused by si-MEF2A could not be reversed by treatment with resveratrol (**Figure 3B**). Silencing MEF2A with siRNA exerted more deleterious effect on the cellular proliferative ability than treatment of the cells with H_2O_2.

Resveratrol May Rescue HUVEC Against H_2O_2 Induced Damage of Cellular Mitochondrial Membrane Upon Up-Regulating MEF2A

The changes of the cell mitochondrial membrane potential were detected by JC-1 staining. The results showed that the proportion of green fluorescent cells increased significantly when HUVEC was treated with H_2O_2 (**Figure 4A**) or si-MEF2A (**Figure 4B**), indicating that treatment of the cells with H_2O_2 or si-MEF2A decreased the cell mitochondrial membrane potential and injured the cellular mitochondrial membrane. Pretreatment of HUVEC with resveratrol could decrease the ratio of the cells (green staining) to the cells (red staining), suggesting that resveratrol could rescue the cell from H_2O_2 induced mitochondrial membrane potential reduction (**Figure 4A**). However, the decrease of the cell mitochondrial membrane potential and the cell damage caused by si-MEF2A could not be reversed by treatment of cells with resveratrol (**Figure 4B**).

Resveratrol May Prevent the Cell Apoptosis Induced by H_2O_2 Through Up-Regulating MEF2A

Flow cytometry was used to detect the apoptosis rate and the results showed that the number of apoptotic cells significantly increased in the group of treatment with H_2O_2 (early apoptotic cells: 13.84 vs. 3.21% and late apoptotic/necrotic cells: 10.11

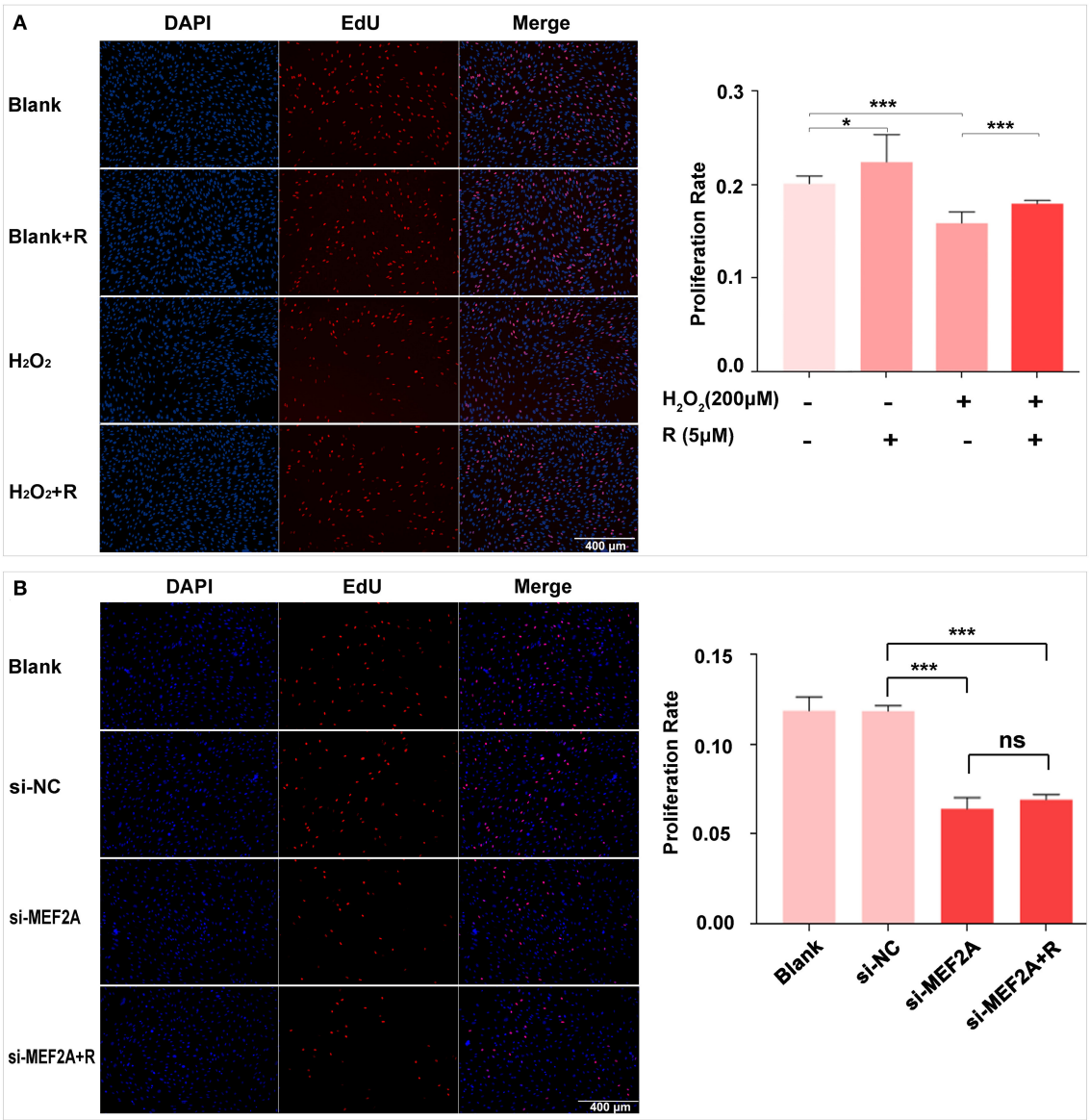

FIGURE 3 | The impact of resveratrol on the decrease of cellular proliferation caused by treatment with H_2O_2 or by silencing MEF2A with siRNA. **(A)** Using EdU staining to test the impact of resveratrol on the cellular proliferation of HUVEC treated with or without H_2O_2. **(B)** Using EdU staining to detect the impact of resveratrol on the cellular proliferation of HUVEC caused by down-regulated MEF2A with siRNA. All experiments were performed independently for 3 times. R, resveratrol; Si-NC, the negative control of siRNA; Si-MEF2A, MEF2A specific siRNA. Mean ± SD is represented as bar plot. The statistical significance is analyzed by the unpaired Student's two-tailed *t*-test. ns, no significance; $^*P < 0.05$; $^{***}P < 0.001$ between groups indicated.

vs. 4.01%) or si-MEF2A (early apoptotic cells: 13.02 vs. 8.85% and late apoptotic/necrotic cells: 12.09 vs. 5.73%) respectively compared with that in the blank group and the si-NC group. Pretreatment of the cells with resveratrol before treating the cells with H_2O_2 partially rescued the cells from apoptosis (**Figure 5A**) (early apoptotic cells: 7.70 vs. 13.84% and late apoptotic/necrotic cells: 8.58 vs. 10.11%), but the apoptosis caused by si-MEF2A could not be improved by treatment of the cells with resveratrol (**Figure 5B**) (early apoptotic cells: 12.64 vs. 13.02% and late apoptotic/necrotic cells: 12.09 vs. 9.24%).

Resveratrol May Prevent Apoptosis-Related Proteins to Be Altered by Treatment of the Cells With H_2O_2 on Up-Regulating MEF2A

Treatment of HUVEC with resveratrol promoted the expression of MEF2A, Sirt1 and Bcl-2, and down-regulated pro-apoptotic proteins such as Bax and cleaved caspase-3, while H_2O_2-treated HUVEC significantly down-regulated the protein levels of MEF2A, Sirt1 and Bcl-2, up-regulated pro-apoptotic proteins

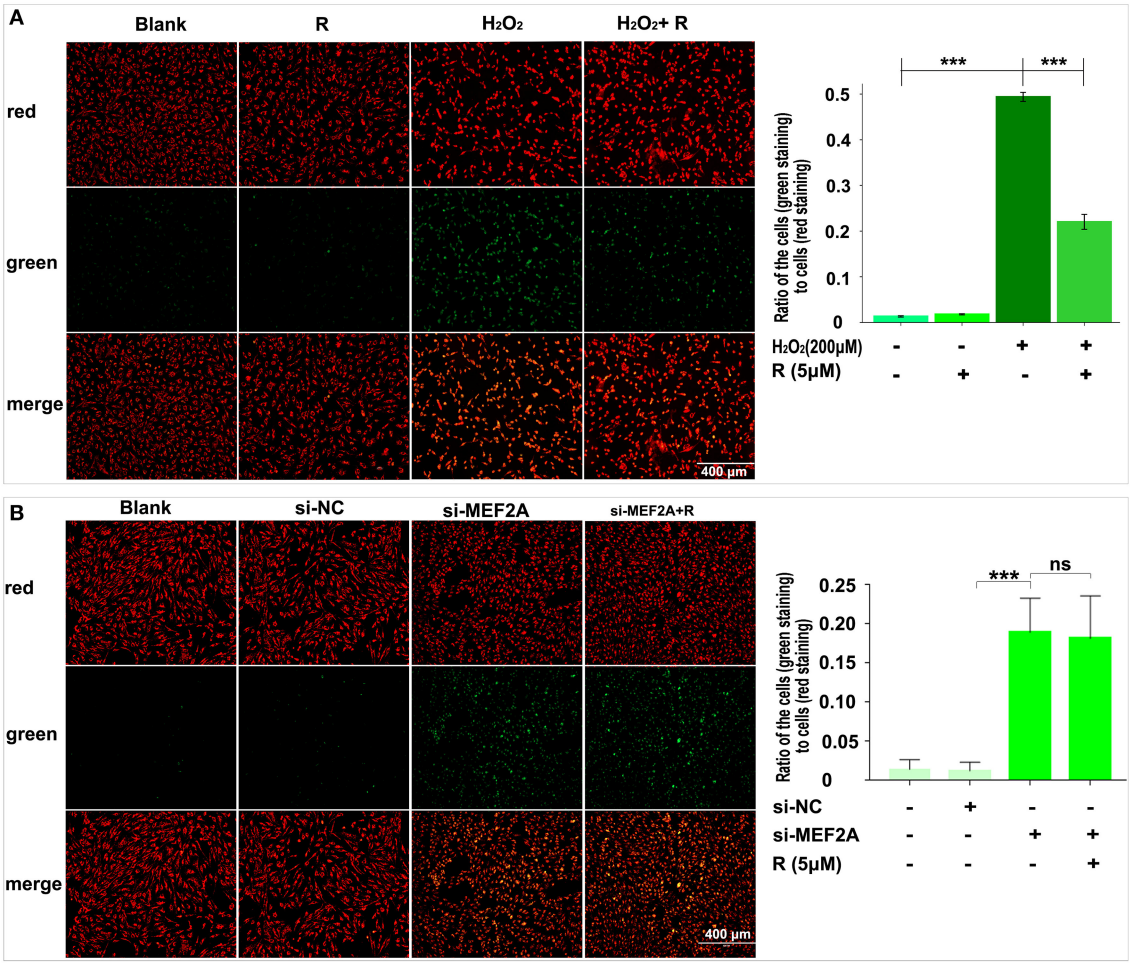

FIGURE 4 | The impact of resveratrol on the decrease of mitochondrial membrane potential caused by treatment with H_2O_2 or by silencing MEF2A with siRNA. **(A)** Using JC-1 staining to test the impact of resveratrol on the cellular mitochondrial membrane potential of HUVEC treated with or without H_2O_2. **(B)** Using JC-1 staining to detect the impact of resveratrol on the cellular mitochondrial membrane potential of HUVEC caused by down-regulated MEF2A with siRNA. R, resveratrol; Si-NC, the negative control of siRNA; Si-MEF2A, MEF2A specific siRNA. All experiments were performed independently for 3 times. Mean ± SD is represented as bar plot. The statistical significance is analyzed by the unpaired Student's two-tailed *t*-test. ns, no significance; ***$P < 0.001$ between groups indicated.

such as Bax and cleaved caspase-3 (**Figure 6A**). Pretreatment of HUVEC with resveratrol before treating the cells with H_2O_2 could rescue the expression of the apoptosis-related proteins altered by H_2O_2. These results suggest that resveratrol prevent H_2O_2-induced apoptosis may be via up-regulating the expression of MEF2A. The expression of SIRT1 not only changed with MEF2A at the protein levels (**Figure 6**), but with MEF2A at the mRNA levels (**Supplementary Figure 1**), which suggested that MEF2A may regulate SIRT1 transcriptionally.

Transfection of HUVEC with si-MEF2A significantly down-regulated the protein levels of Sirt1 and Bcl-2, and up-regulated pro-apoptotic proteins such as Bax and cleaved caspase-3, which could not be abrogated by treatment of the cells with resveratrol (**Figure 6B**). These results demonstrated at the molecular level that MEF2A has anti-apoptotic function and the promotion of SIRT1 expression by resveratrol is dependent on the expression of MEF2A, further suggesting that the anti-apoptotic function of resveratrol is realized via promoting the expression of MEF2A.

Damaged Vascular Endothelial Integrity Was Observed in Vascular Endothelium of the MEF2A Silenced Mice

The immunoblotting results showed that the expression of MEF2A in the vascular tissue from mef2a-shRNA-AAV1 group was significantly lower than that from NC-shRNA-AAV1 group ($n = 3$) (**Figure 7A**), suggesting that si-MEF2A AAV1 effectively knocked down the expression of MEF2A. There was no significant difference in the protein level of MEF2A in myocardial tissues from different groups ($n = 3$) (**Supplementary Figure 2**), indicating that MEF2A-shRNA may

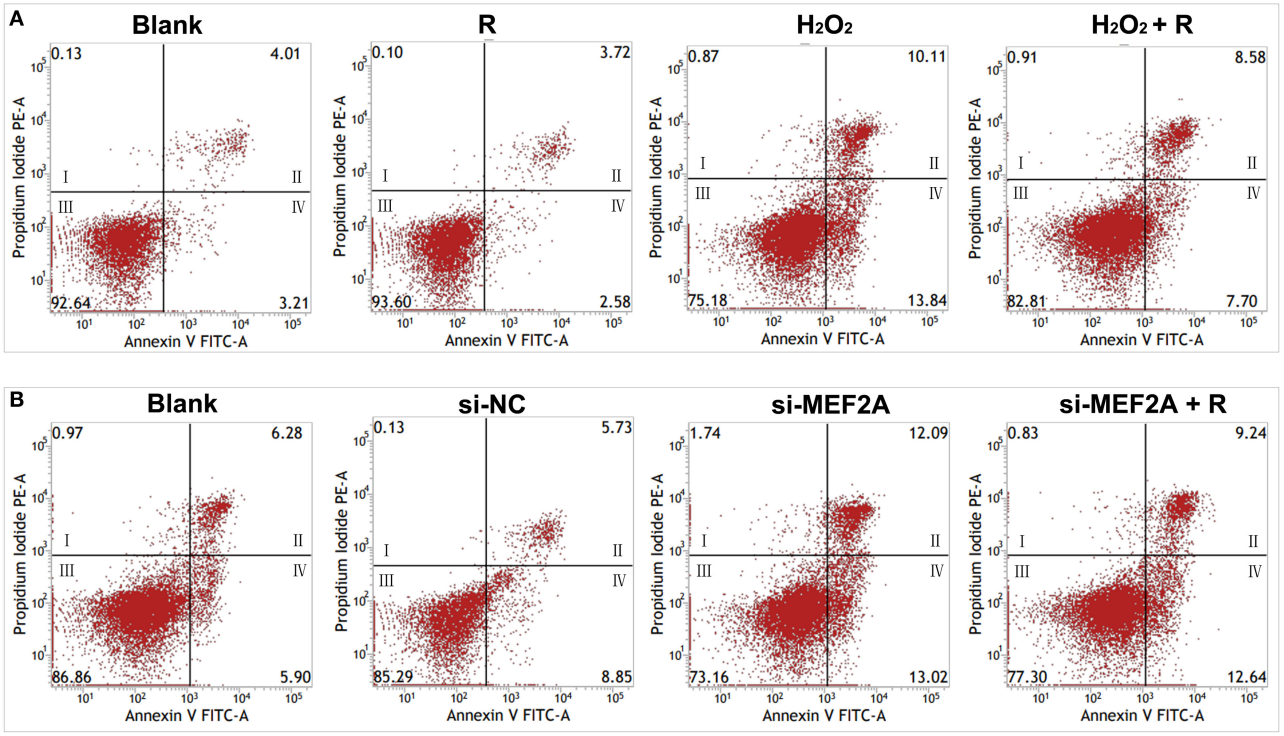

FIGURE 5 | The impact of resveratrol on the apoptosis caused by the treatment with H_2O_2 or by silencing MEF2A with siRNA. **(A)** Using flow cytometry to test the impact of resveratrol on the apoptosis of HUVEC treated with or without H_2O_2. **(B)** Using flow cytometry to detect the impact of resveratrol on the apoptosis of HUVEC caused by down-regulated MEF2A with siRNA. R, resveratrol; Si-NC, the negative control of siRNA; Si-MEF2A, MEF2A specific siRNA. I: dead cells (Annexin V-FITC$^-$/PI$^+$); II: late apoptotic/necrotic cells (Annexin V-FITC$^+$/PI$^+$); III: non-apoptotic cells (Annexin V-FITC$^-$/PI$^-$); IV: early apoptotic cells (Annexin V-FITC$^+$/PI$^-$).

only specifically silence MEF2A in vascular tissues, which is consistent with the specificity speculated according to that the promoter of endothelial cell specific expression gene (ICAM2) was used construct the adeno-associated virus vector to control the expression of MEF2A specific shRNA. The expression of SIRT1 in vascular tissue was also significantly down-regulated in mef2a-shRNA-AAV1 group (**Figure 7A**), indicated that SIRT1 is regulated by MEF2A. The expression of MEF2A in vascular endothelium was detected by immunofluorescence and the results showed that the fluorescence intensity of si-MEF2A group was significantly weaker than that of the si-NC group ($n = 2$) (**Figure 7B**). CD31, a specific marker of vascular endothelium, was detected by immunofluorescence. The results showed that there were continuous fluorescent bands along the inner edge of blood vessels in si-NC group, while there was only intermittent fluorescent staining area along the inner edge of blood vessels in mef2a-shRNA-AAV1 group, suggesting that the integrity of vascular endothelium might be destroyed after interfering with MEF2A (**Figure 7B**).

Knocked-down the MEF2A in the vascular endothelium decreased the expression of SIRT1 and increased the cleaved caspase-3 level in the vascular tissue, and the alteration of SIRT1 and cleaved caspase-3 could not be reversed when the apoE$^{-/-}$ mice have been subjected to gastric administration of resveratrol (**Supplementary Figure 3**).

Atherosclerotic Lesion Was Alleviated by Gastric Administration of Resveratrol in ApoE$^{-/-}$ Mice

Oil red O staining for the aorta ($n = 1$) (**Supplementary Figure 4A**) and the aortic valve ($n = 2$–4) (**Supplementary Figure 4B**) showed that the lipid deposition in the aorta and aortic valve of apoE$^{-/-}$ mice was serious than that in wild type mice, the lipid deposition in the aorta and aortic valve of the mice of mef2a-shRNA-AAV1 groups were more severe than those of NC-shRNA-AAV1 groups. Gastric administration of resveratrol showed a trend to alleviate lipid deposition in both NC-shRNA-AAV1 and mef2a-shRNA-AAV1 (**Supplementary Figures 4A-1,B-1**).

Effects of Feeding With Resveratrol and Interfering With MEF2A on Lipid Metabolism in ApoE$^{-/-}$ Mice

Blood samples were collected and five biochemical indicators including total cholesterol (TC), low density lipoprotein

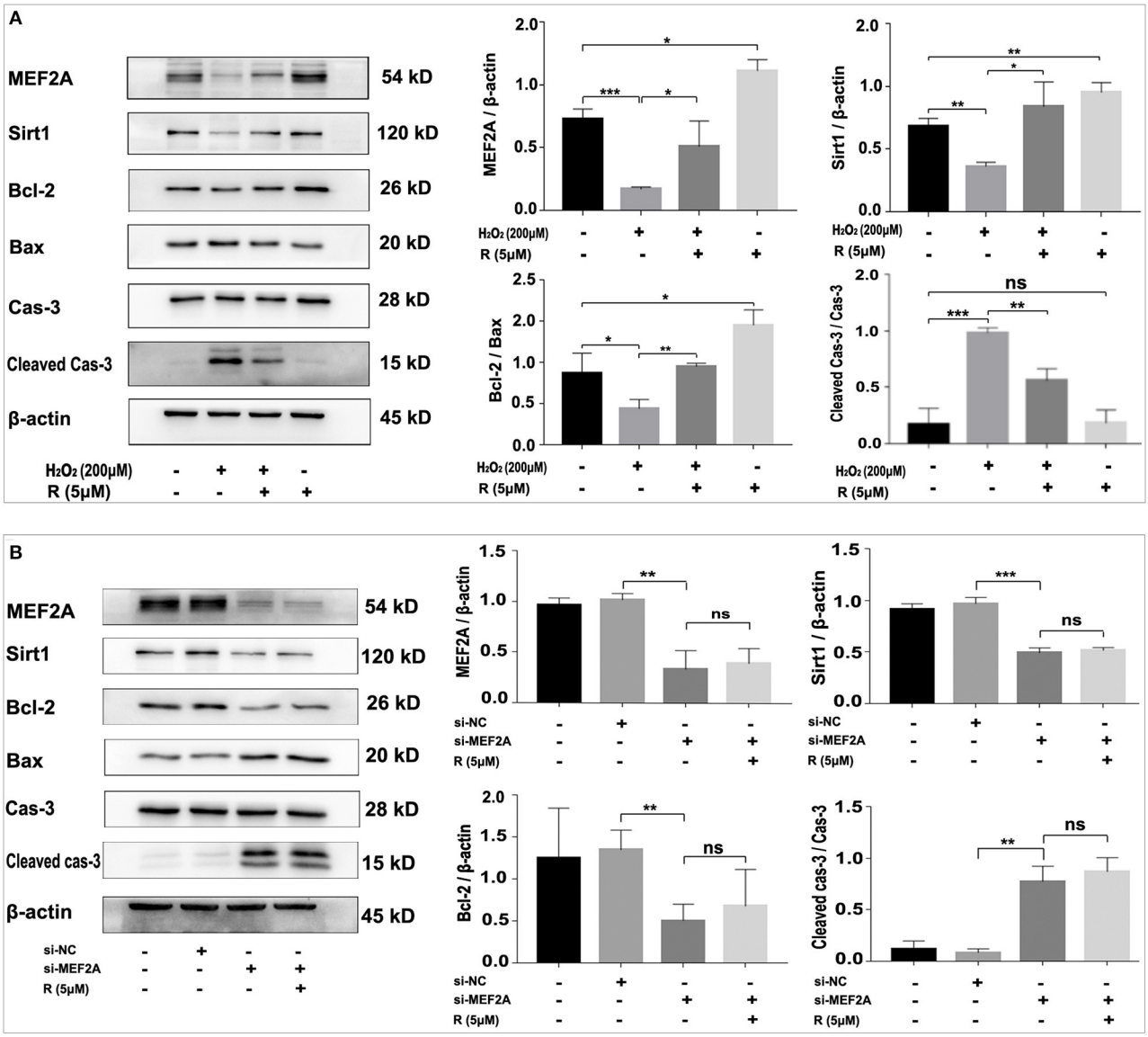

FIGURE 6 | Resveratrol eliminates the alteration of apoptosis-related proteins caused by treatment with H_2O_2 but not with down-regulation of MEF2A with siRNA. **(A)** Immunoblots of MEF2A and apoptosis-related proteins for the groups that were treated with H_2O_2 and resveratrol, solely or together. **(B)** Using immunoblots to detect alteration of the apoptosis-related proteins caused by silencing MEF2A with siRNA and treatment with resveratrol. Quantification of the band intensity was performed via image-J and values were normalized to beta-actin. R, resveratrol; Cas-3, caspase-3; Si-NC, the negative control of siRNA; Si-MEF2A, MEF2A specific siRNA. All experiments were performed independently for three times. Mean ± SD is represented as bar plot. The statistical significance is analyzed by the unpaired Student's two-tailed *t*-test. ns, no significance; $^*P < 0.05$; $^{**}P < 0.01$; $^{***}P < 0.001$ between groups indicated.

cholesterol (LDL-C), high density lipoprotein cholesterol (HDL-C), triglyceride (TG) and glucose (GLU) were detected and the quantitative and statistical significance test results were respectively showed in **Supplementary Tables 1**, **2**. The levels of plasma lipids of wild-type mice fed with high-fat diet were significantly higher than those of wild-type mice fed with normal diet ($n = 8$) (**Figure 8**), indicating an actual effect of the high-fat diet on the levels of the blood lipids. The levels of plasma lipids of all the apoE$^{-/-}$ mice were significantly higher than those of wild-type mice (**Figure 8**), suggesting that apoE$^{-/-}$ mice have abnormal lipid metabolism. Knockdown of MEF2A in the vascular endothelium led to a significant increase of plasma TC (**Figure 8A**) and LDL-c (**Figure 8B**). Significantly decreased LDL-c and TC was observed in both NC-shRNA and mef2a-shRNA mice that were subjected to gastric administration of resveratrol. TG was remarkably reduced by gastric administration of resveratrol in si-NC mice but not in si-MEF2A mice (**Figure 8D**). Gastric administration of resveratrol and knockdown of MEF2A did not affect the plasma levels of HDL-c (**Figure 8C**) and GLU (**Figure 8E**). These results suggest

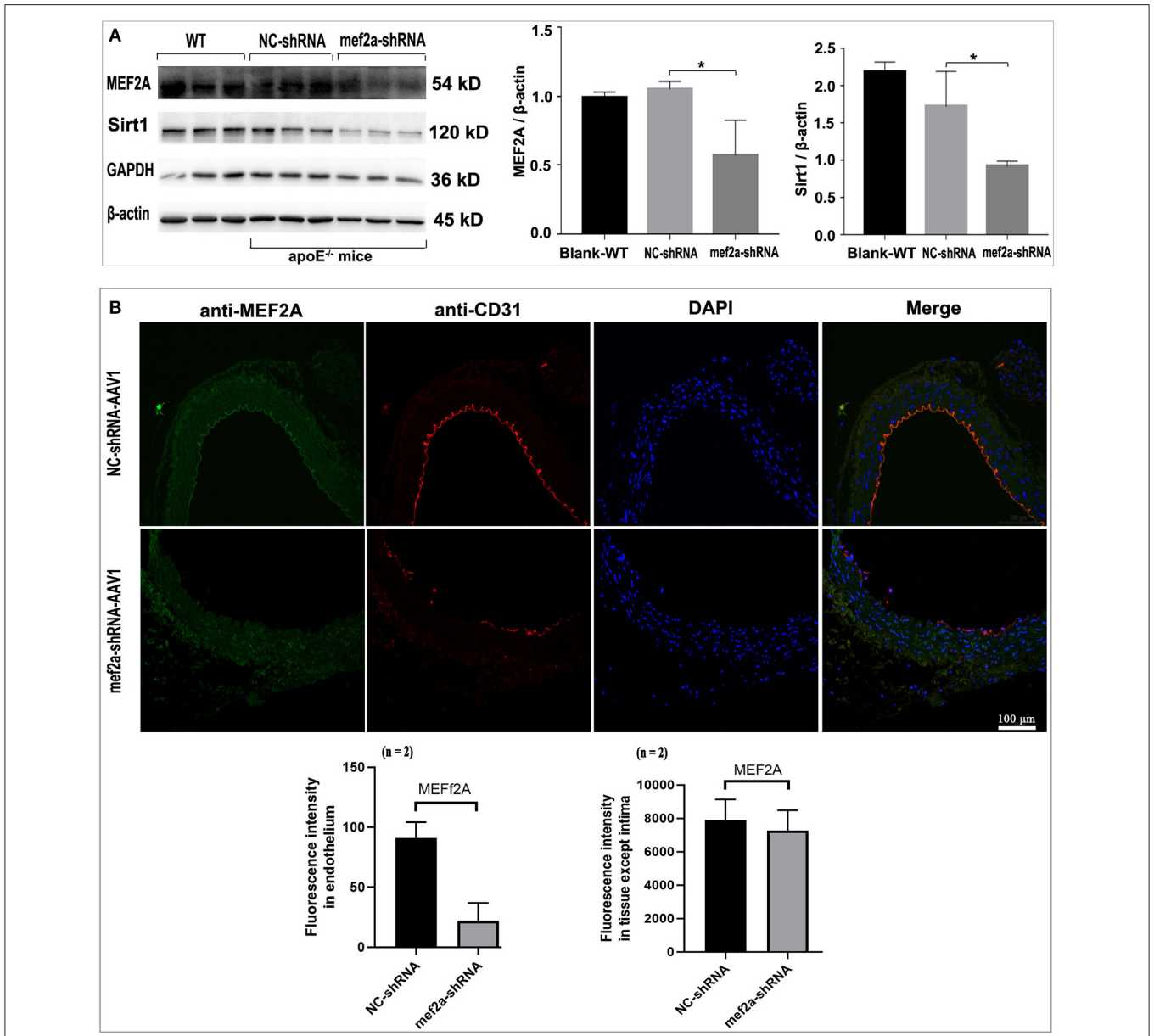

FIGURE 7 | Expression of MEF2A, SIRT1 and CD31 in the vessels of the mice. **(A)** Immunoblots of MEF2A and SIRT1. Mean ± SD is represented as bar plot. The statistical significance is analyzed by the unpaired Student's two-tailed *t*-test. ns, no significance; $^*P < 0.05$ between groups indicated. **(B)** Immunofluorescence of MEF2A and CD31 in the vascular endothelium. The cells expressed sufficient MEF2A were stained green, and the cells expressed sufficient CD31 were stained red. WT: wild type mice; The "n" indicates the sample size.

that MEF2A plays an important role in lipid metabolism. The function of resveratrol to reduce LDL-C is independent of MEF2A, while the function of resveratrol to reduce TG may depend on MEF2A.

DISCUSSION

In this study, we revealed for the first time that the protective effect of resveratrol on vascular endothelial cell depended on promoting the expression of MEF2A to activate the expression of SIRT1, thereby enhanced the ability of the cells to resist oxidative stress and anti-apoptosis. In addition, down-regulated expression of MEF2A in the vascular endothelium of apoE$^{-/-}$ mice affected the lipid metabolism, leading to a significant increase in plasma LDL-c level. Regardless of whether knocked down the expression of MEF2A in mice, resveratrol significantly reduced LDL-c and TG. However, the function of resveratrol to reduce TG in apoE$^{-/-}$ mice depended on the sufficient expression of MEF2A.

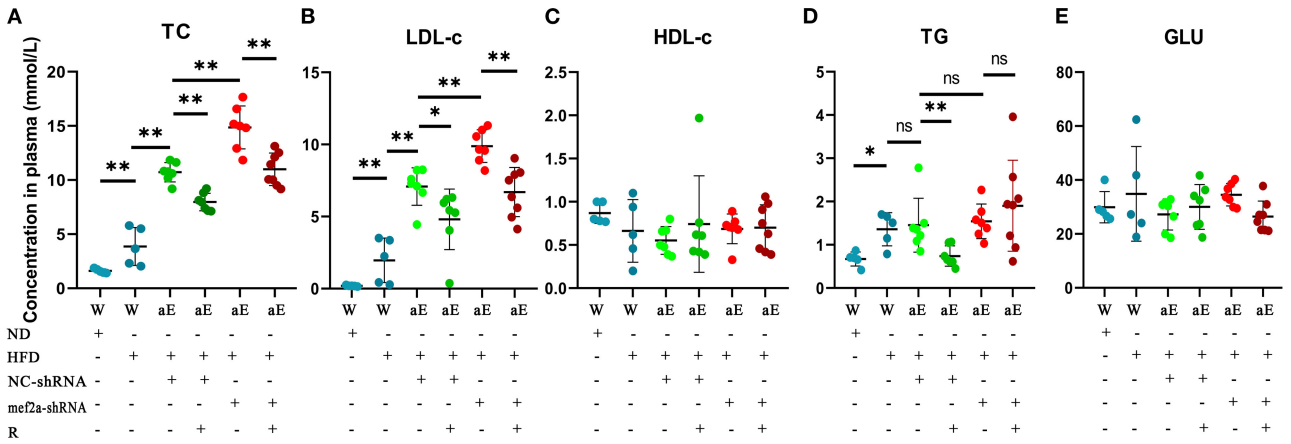

FIGURE 8 | The influence of gastric administration of resveratrol or silencing MEF2A in vascular endothelium of apoE$^{-/-}$ mice on plasma levels of cholesterol, lipid and glucose. **(A)** Total cholesterol (TC). **(B)** Low-density lipoprotein cholesterol (LDL-c). **(C)** High-density lipoprotein cholesterol (HDL-c). **(D)** Triglyceride (TG). **(E)** Glucose (GLU). W: wild type mice; aE: apoE$^{-/-}$ mice; ND, normal diet; HFD, high-fat diet; NC-shRNA, negative control (infection with NC-shRNA-AAV1); mef2a-shRNA, infection with mef2a-shRNA-AAV1; R, resveratrol; "-" indicates no treatment performed with the factor at the line; "+" indicates treatment performed with the factor at the line. The individual values are presented in dot plots and the values distribution is represented as mean ± standard deviation (SD). The statistical significance is analyzed by the Mann-Whitney U test. ns, no significance; *$P < 0.05$; **$P < 0.01$ between groups indicated.

We also observed that knockdown of MEF2A in HUVEC had similar effects on cells as treatment of the cells with H_2O_2, such as reducing cell viability and mitochondrial membrane potential, promoting apoptosis and so on. These indicate that the harmful effect of H_2O_2 on the cells may be mainly attributed to a significant down-regulation of MEF2A induced by H_2O_2. However, pretreatment of HUVEC with resveratrol could prevent the down-regulation of MEF2A induced by H_2O_2, thus prevented the effects of H_2O_2 on cell viability, mitochondrial membrane potential and apoptosis, which further supports the important role of MEF2A in anti-oxidative stress. In HUVEC of silencing MEF2A with siRNA, treatment of the cells with resveratrol could not restore the expression of MEF2A, also not abrogate or alleviate the detrimental influence of silencing MEF2A on the cells, suggesting that the protective function of resveratrol on vascular endothelial cells depends on its role in promoting the expression of MEF2A. Liu et al. (15) also reported that treatment of HUVEC with H_2O_2 significantly down-regulated the expression of MEF2A and promoted cell senescence, but overexpression of MEF2A in HUVEC ensured that there was still a high expression of MEF2A in H_2O_2-treated cells, thus prevented cell senescence induced by H_2O_2. The mechanism is that MEF2A upregulates the expression of SIRT1 through PI3K/p-AKT1 pathway. The main characteristics of cell senescence are mitochondrial dysfunction, genomic instability, aging-related secretory phenotype (SASP), epigenome changes and stem cell exhaust (28). Silencing MEF2A in HUVEC led to a significant decrease in mitochondrial membrane potential, showing the characteristics of cell senescence or apoptosis. Treatment of HUVEC with resveratrol was similar to overexpression of MEF2A in the cells, exhibited a strong anti-oxidative stress feature. All the above suggest that MEF2A plays an important regulatory role in both anti-apoptosis and anti-aging, and the anti-apoptosis and anti-aging effects of resveratrol mainly depends on its role in up-regulation of MEF2A expression.

Up-regulation of SIRT1 is considered to be an important molecular mechanism for resveratrol to exert its cytoprotective function. Resveratrol up-regulates the expression of nitric oxide synthase (eNOS) and enzyme activity in vascular endothelial cells by up-regulating the expression of SIRT1, and increases the NO production to mediate vasodilation of the blood vessel (1, 29). Resveratrol can enhance the ability of autophagy by activating Sirt1/Foxo1 pathway, prevent oxidative stress and apoptosis induced by H_2O_2 (30, 31), and prevent apoptosis and oxidative stress induced by ischemia/reperfusion (32). Resveratrol also improved endothelial dysfunction in obese and diabetic mice through SIRT1/PPAR pathway, and improved glucose absorption in adipocytes with insulin resistance (33). Resveratrol improves rheumatoid arthritis by activating SIRT1-Nrf2 signaling pathway and autophagy (34, 35), and plays a beneficial role in mitochondrial function by activating AMPK (36). In this study, we once again observed that resveratrol has a significant upregulation effect on SIRT1 in HUVEC, but the upregulation of SIRT1 by resveratrol depended on its role in upregulation of MEF2A. When the expression of MEF2A was silenced by siRNA and could not be restored by resveratrol *in vivo* or *in vitro*, resveratrol could not up-regulate SIRT1 and also lost its protective role, which strongly indicates that promoting the expression of MEF2A is a more critical and upstream event for resveratrol to exert its cytoprotective function. In previous studies, we have demonstrated that MEF2A regulates the expression of SIRT1 (15), which was consolidated

by the experimental evidence from *in vitro* and *in vivo* in this study.

Resveratrol was failure to restore or promote the expression of MEF2A silenced by siRNA in vascular endothelial cells, which might be the major reason for that resveratrol lost its protection against atherosclerosis in MEF2A-silenced apoE$^{-/-}$ mice. The protective effect of MEF2A on blood vessels has also been sporadically reported in previous studies. Zhou et al. (25) reported that inhibition of MEF2A with siRNA can accelerate atherosclerosis in apoE$^{-/-}$ mice, and its molecular mechanism is involved in the increase of pro-inflammatory cytokines such as MCP-1, MMP-8, IL-6 and TNF-α. Lu et al. reported that the deletion of MEF2A in mice is more likely to lead to an increase in the risk of bleeding, hypercoagulability and inflammation (23). Xiong et al. (27) showed that interfering MEF2A in HCAEC significantly affects the gene expression profile of inflammation-related pathways. Except anti-aging, anti-apoptosis and anti-oxidative stress, SIRT1 that is confirmedly regulated by MEF2A in our studies, also plays an important role in the anti-inflammatory pathway (37). These results suggest that MEF2A may also exert the protective function on vascular endothelial cells by regulating the inflammatory pathway. The integrity of the vascular endothelium was damaged in MEF2A knocked down mice, which may be attributed to the comprehensive effect of silencing MEF2A in vascular endothelial cells, such as acceleration of aging, promotion of apoptosis, reduction of anti-oxidative stress and anti-inflammation.

It's very interesting that knockdown of MEF2A in vascular endothelium significantly increased the level of plasma LDL-c, which has not been reported in previous studies. Although many functions of resveratrol seemingly disappeared while the expression of MEF2A was knocked down by siRNA, the role of resveratrol in reducing LDL-c was unaffected in MEF2A-knocked down mice. Previous studies have shown that resveratrol can significantly reduce LDL-c and TG (38). Yet we found that knockdown of MEF2A in the vascular endothelium could not increase TG, but apparently eliminated the role of resveratrol in decreasing TG. These results suggest that MEF2A may be involved in the production and metabolism of LDL-c and TG with different manner. Involvement of MEF2A in the lipid metabolism pathway has been reported in several studies. Zhao et al. (39) found that specifically reducing the expression of MEF2 in drosophila muscle leads to the accumulation of large amounts of cholesterol-rich lipid fluid in muscle when fed high-calorie or carbohydrate-rich foods. GLUT4 promotes lipid metabolism and the expression of GLUT4 is regulated by MEF2A (40, 41), suggesting that the regulation of lipid metabolism by MEF2A may be related to GLUT4. SIRT1 increases liver LDL receptor (LDLR) by inhibiting the secretion of proprotein convertase subtilisin/kexin 9 (PCSK9), thus reducing plasma LDL-C level (42). Considering the above previous study, increase in plasma LDL-c by silencing MEF2A may be through regulating SIRT1/PCSK9/LDLR pathway. However, in MEF2A knocked down mice, resveratrol could not up-regulate Sirt1, still reduce plasma LDL-c but not plasma TG, suggesting that resveratrol can also activate other lipid reducing pathways independent of MEF2A/Sirt1/Pcsk9/LDLR, and its effect on reducing TG may depend on activating MEF2A/SIRT1 pathway. In the MEF2A interference group, resveratrol also showed the trend of preventing lipid deposition, which also indicate that there is a LDL-C reducing effect of resveratrol independent of MEF2A *in vivo*. Although there is progression in studies that can help to interpret the involvement of MEF2A in lipid metabolism, but the associated molecular mechanism is obscure and should be investigated. How does MEF2A participate in the promotion of TG metabolism by resveratrol is also worthy further studied in future.

Although the evidences acquired consistently support that the protective effect of resveratrol on vascular endothelial cells depends on activating the expression of MEF2A, but there are some limitations in *in-vivo* experiments of this study. (1) The number of samples for oil red O staining to detect lipid deposition in the whole aortic vessel was only one sample. However, the change trend of lipid deposition observed in the oil red O staining experiment was very consistent with that of LDL-C in plasma ($n = 8$), which indirectly proved that the experimental results of oil red O were relatively reliable. (2) Only two samples were used to detect the effectiveness and specificity of MEF2A knockdown by immunofluorescence. (3) The mechanism of resveratrol up-regulating MEF2A and the molecular mechanism of MEF2A protecting vascular endothelium were not deeply studied. (4) We observed the destruction of endothelial integrity by silencing MEF2A *in vivo*, but didn't further study on its mechanism. Therefore, the association of resveratrol and MEF2A with vascular protection *in vivo* needs to be further studied in many aspects.

In summary, MEF2A is involved in the normal physiological process of cells, especially in maintaining the function of vascular endothelial cells. Therefore, enhancing or maintaining the expression of MEF2A in vascular endothelial cells may be a novel strategy to develop vascular protective methods or explore vascular protective drugs, and also provides a novel perspective for further research on the molecular mechanism of the occurrence and development of cardiovascular diseases. Resveratrol, that is a widely demonstrated cardiovascular protective drug, has been considered to function through activate SIRT1 pathway in previous studies. Here, we revealed a novel mechanism involved in the protective role of resveratrol, is that promotion of the expression of MEF2A is required for the protective role of resveratrol in vascular endothelial cells.

CONCLUSION

Protection of resveratrol on VEC depends on up-regulating the expression of MEF2A, and the main mechanism may be that up-regulation of MEF2A can promote the expression of anti-apoptosis and anti-aging related genes such as SIRT1, and enhance the ability of cells to resist oxidative stress, thus inhibit premature apoptosis or senescence of vascular endothelial cells. MEF2A may also play an important role in maintaining lipid metabolism homeostasis of vascular endothelium.

DATA AVAILABILITY STATEMENT

The raw data supporting the conclusions of this article will be made available by the authors, without undue reservation.

ETHICS STATEMENT

The animal study was reviewed and approved by the Experimental Animal Ethics Committee of the Second Affiliated Hospital of Guangzhou Medical University.

AUTHOR CONTRIBUTIONS

All authors listed have made a substantial, direct, and intellectual contribution to the work and approved it for publication.

FUNDING

This study was supported by Guangzhou Science and Technology Project (202102010054 to BL) and the General Programs of the National Natural Science Foundation of China (81873474 to SML).

ACKNOWLEDGMENTS

We are very grateful to Ningning Liu, Weihua Liu and Shaojun Liu for their constructive suggestions to this study.

SUPPLEMENTARY MATERIAL

The Supplementary Material for this article can be found online at: https://www.frontiersin.org/articles/10.3389/fcvm.2021.775392/full#supplementary-material

REFERENCES

1. Li H, Xia N, Hasselwander S, Daiber A. Resveratrol and vascular function. *Int J Mol Sci.* (2019) 20:2155. doi: 10.3390/ijms20092155
2. Singh AP, Singh R, Verma SS, Rai V, Kaschula CH, Maiti P, et al. Health benefits of resveratrol: evidence from clinical studies. *Med Res Rev.* (2019) 39:1851–91. doi: 10.1002/med.21565
3. Repossi G, Das UN, Eynard AR. Molecular basis of the beneficial actions of resveratrol. *Arch Med Res.* (2020) 51:105–14. doi: 10.1016/j.arcmed.2020.01.010
4. Cheng CK, Luo JY, Lau CW, Chen ZY, Tian XY, Huang Y. Pharmacological basis and new insights of resveratrol action in the cardiovascular system. *Br J Pharmacol.* (2020) 177:1258–77. doi: 10.1111/bph.14801
5. Jia G, Aroor AR, Jia C, Sowers JR. Endothelial cell senescence in aging-related vascular dysfunction. *Biochim Biophys Acta Mol Basis Dis.* (2019) 1865:1802–9. doi: 10.1016/j.bbadis.2018.08.008
6. Han S, Bal NB, Sadi G, Usanmaz SE, Uludag MO, Demirel-Yilmaz E. The effects of resveratrol and exercise on age and gender-dependent alterations of vascular functions and biomarkers. *Exp Gerontol.* (2018) 110:191–201. doi: 10.1016/j.exger.2018.06.009
7. Diaz M, Degens H, Vanhees L, Austin C, Azzawi M. The effects of resveratrol on aging vessels. *Exp Gerontol.* (2016) 85:41–7. doi: 10.1016/j.exger.2016.09.016
8. Zou JG, Wang ZR, Huang YZ, Cao KJ, Wu JM. Effect of red wine and wine polyphenol resveratrol on endothelial function in hypercholesterolemic rabbits. *Int J Mol Med.* (2003) 11:317–20. doi: 10.3892/ijmm.11.3.317
9. Ungvari Z, Labinskyy N, Mukhopadhyay P, Pinto JT, Bagi Z, Ballabh P, et al. Resveratrol attenuates mitochondrial oxidative stress in coronary arterial endothelial cells. *Am J Physiol Heart Circ Physiol.* (2009) 297:1876–81. doi: 10.1152/ajpheart.00375.2009
10. Kim EN, Kim MY, Lim JH, Kim Y, Shin SJ, Park CW, et al. The protective effect of resveratrol on vascular aging by modulation of the renin-angiotensin system. *Atherosclerosis.* (2018) 270:123–31. doi: 10.1016/j.atherosclerosis.2018.01.043
11. Lee SH, Lee JH, Lee HY, Min KJ. Sirtuin signaling in cellular senescence and aging. *BMB Rep.* (2019) 52:24–34. doi: 10.5483/BMBRep.2019.52.1.290
12. Kitada M, Ogura Y, Koya D. The protective role of Sirt1 in vascular tissue: its relationship to vascular aging and atherosclerosis. *Aging (Albany NY).* (2016) 8:2290–307. doi: 10.18632/aging.101068
13. D'Onofrio N, Servillo L, Balestrieri ML. SIRT1 and SIRT6 signaling pathways in cardiovascular disease protection. *Antioxid Redox Signal.* (2018) 28:711–32. doi: 10.1089/ars.2017.7178
14. Kida Y, Goligorsky MS. Sirtuins, cell senescence, and vascular aging. *Can J Cardiol.* (2016) 32:634–41. doi: 10.1016/j.cjca.2015.11.022
15. Liu B, Wang L, Jiang W, Xiong Y, Pang L, Zhong Y, et al. Myocyte enhancer factor 2A delays vascular endothelial cell senescence by activating the PI3K/p-Akt/SIRT1 pathway. *Aging (Albany NY).* (2019) 111:3768–84. doi: 10.18632/aging.102015
16. Wu Y, Dey R, Han A, Jayathilaka N, Philips M, Ye J, et al. Structure of the MADS-box/MEF2 domain of MEF2A bound to DNA and its implication for myocardin recruitment. *J Mol Biol.* (2010) 397:520–33. doi: 10.1016/j.jmb.2010.01.067
17. Dai Y, Zhang S, Wu W. Analysis of MEF2A mutations in a Chinese population with premature coronary artery disease. *Genet Test Mol Biomarkers.* (2013) 17:352–5. doi: 10.1089/gtmb.2012.0467
18. Zhu B, Carmichael RE, Solabre Valois L, Wilkinson KA, Henley JM. The transcription factor MEF2A plays a key role in the differentiation/maturation of rat neural stem cells into neurons. *Biochem Biophys Res Commun.* (2018) 500:645–9. doi: 10.1016/j.bbrc.2018.04.125
19. Meyer M, Kuffner K, Winter J, Neumann ID, Wetzel CH, Jurek B. Myocyte Enhancer Factor 2A (MEF2A) defines oxytocin-induced morphological effects and regulates mitochondrial function in neurons. *Int J Mol Sci.* (2020) 21:2200. doi: 10.3390/ijms21062200
20. Chang CW, Wilkerson JR, Hale CF, Gibson JR, Huber KM. (2017). Distinct stages of synapse elimination are induced by burst firing of CA1 neurons and differentially require MEF2A/D. *eLife.* (2017). 6:e26278. doi: 10.7554/eLife.26278
21. Wang L, Fan C, Topol SE, Topol EJ, Wang Q. Mutation of MEF2A in an inherited disorder with features of coronary artery disease. *Science.* (2003) 302:1578–81. doi: 10.1126/science.1088477
22. Weng L, Kavaslar N, Ustaszewska A, Doelle H, Schackwitz W, Hebert S, et al. Lack of MEF2A mutations in coronary artery disease. *J Clin Invest.* (2005) 115:1016–20. doi: 10.1172/JCI24186
23. Lu YW, Martino N, Gerlach BD, Lamar JM, Vincent PA, Adam AP, et al. MEF2 (Myocyte Enhancer Factor 2) is essential for endothelial homeostasis and the atheroprotective gene expression program. *Arterioscler Thromb Vasc Biol.* (2021) 41:1105–23. doi: 10.1161/ATVBAHA.120.314978
24. Medrano JL, Naya FJ. The transcription factor MEF2A fine-tunes gene expression in the atrial and ventricular chambers of the adult heart. *J Biol Chem.* (2017) 292:20975–88. doi: 10.1074/jbc.M117.806422
25. Zhou WP, Zhang H, Zhao YX, Liu GQ, Zhang JY. RNA interference of myocyte enhancer factor 2A accelerates atherosclerosis in apolipoprotein E-deficient mice. *PLoS ONE.* (2015) 10:e0121823. doi: 10.1371/journal.pone.0121823

26. Liu C, Yao MD, Li CP, Shan K, Yang H, Wang JJ, et al. Silencing Of circular RNA-ZNF609 ameliorates vascular endothelial dysfunction. *Theranostics.* (2017) 7:2863–77. doi: 10.7150/thno.19353
27. Xiong Y, Wang L, Jiang W, Pang L, Liu W, Li A, et al. MEF2A alters the proliferation, inflammation-related gene expression profiles and its silencing induces cellular senescence in human coronary endothelial cells. *BMC Mol Biol.* (2019) 20:8. doi: 10.1186/s12867-019-0125-z
28. Hekmatimoghaddam S, Dehghani Firoozabadi A, Zare-Khormizi MR, Pourrajab F. Sirt1 and Parp1 as epigenome safeguards and microRNAs as SASP-associated signals, in cellular senescence and aging. *Ageing Res Rev.* (2017) 40:120–41. doi: 10.1016/j.arr.2017.10.001
29. Mattagajasingh I, Kim CS, Naqvi A, Yamamori T, Hoffman TA, Jung SB, et al. SIRT1 promotes endothelium-dependent vascular relaxation by activating endothelial nitric oxide synthase. *Proc Natl Acad Sci U S A.* (2007) 104:14855–60. doi: 10.1073/pnas.0704329104
30. Wang P, Huang CX, Gao JJ, Shi Y, Li H, Yan H, et al. Resveratrol induces SIRT1-Dependent autophagy to prevent H[[sb]]2[[/s]]O[[sb]]2[[/s]]-induced oxidative stress and apoptosis in HTR8/SVneo cells. *Placenta.* (2020) 91:11–8. doi: 10.1016/j.placenta.2020.01.002
31. Wu Q, Hu Y, Jiang M, Wang F, Gong G. Effect of autophagy regulated by Sirt1/FoxO1 pathway on the release of factors promoting thrombosis from vascular endothelial cells. *Int J Mol Sci.* (2019) 20:4132. doi: 10.3390/ijms20174132
32. Wang KJ, Zhang WQ, Liu JJ, Cui Y, Cui JZ. Piceatannol protects against cerebral ischemia/reperfusioninduced apoptosis and oxidative stress via the Sirt1/FoxO1 signaling pathway. *Mol Med Rep.* (2020) 22:5399–411. doi: 10.3892/mmr.2020.11618
33. Chen S, Zhao Z, Ke L, Li Z, Li W, Zhang Z, et al. Resveratrol improves glucose uptake in insulin-resistant adipocytes via Sirt1. *J Nutr Biochem.* (2018) 55:209–18. doi: 10.1016/j.jnutbio.2018.02.007
34. Wang G, Xie X, Yuan L, Qiu J, Duan W, Xu B, et al. Resveratrol ameliorates rheumatoid arthritis via activation of SIRT1-Nrf2 signaling pathway. *Biofactors.* (2020) 46:441–53. doi: 10.1002/biof.1599
35. Fernandez-Rodriguez JA, Almonte-Becerril M, Ramil-Gomez O, Hermida-Carballo L, Vinas-Diz S, Vela-Anero A, et al. Autophagy activation by resveratrol reduces severity of experimental rheumatoid arthritis. *Mol Nutr Food Res.* (2021) 65:e2000377. doi: 10.1002/mnfr.202000377
36. Price NL, Gomes AP, Ling AJ, Duarte FV, Martin-Montalvo A, North BJ, et al. SIRT1 is required for AMPK activation and the beneficial effects of resveratrol on mitochondrial function. *Cell Metab.* (2012) 15:675–90. doi: 10.1016/j.cmet.2012.04.003
37. Winnik S, Stein S, Matter CM. SIRT1 - an anti-inflammatory pathway at the crossroads between metabolic disease and atherosclerosis. *Curr Vasc Pharmacol.* (2012) 10:693–6. doi: 10.2174/1570161128035 20756
38. Kitada M, Ogura Y, Monno I, Koya D. Supplementation with red wine extract increases insulin sensitivity and peripheral blood mononuclear Sirt1 expression in nondiabetic humans. *Nutrients.* (2020) 12:3108. doi: 10.3390/nu12103108
39. Zhao X, Li X, Shi X, Karpac J. Diet-MEF2 interactions shape lipid droplet diversification in muscle to influence Drosophila lifespan. *Aging Cell.* (2020) 19:e13172. doi: 10.1111/acel.13172
40. Maruta H, Yoshimura Y, Araki A, Kimoto M, Takahashi Y, Yamashita H. Activation of AMP-activated protein kinase and stimulation of energy metabolism by acetic acid in L6 myotube cells. *PLoS ONE.* (2016) 11:e0158055. doi: 10.1371/journal.pone.0158055
41. Knight JB, Eyster CA, Griesel BA, Olson AL. Regulation of the human GLUT4 gene promoter: interaction between a transcriptional activator and myocyte enhancer factor 2A. *Proc Natl Acad Sci U S A.* (2003) 100:14725–30. doi: 10.1073/pnas.2432756100
42. Winnik S, Auwerx J, Sinclair DA, Matter CM. Protective effects of sirtuins in cardiovascular diseases: from bench to bedside. *Eur Heart J.* (2015) 36:3404–12. doi: 10.1093/eurheartj/ehv290

Conflict of Interest: The authors declare that the research was conducted in the absence of any commercial or financial relationships that could be construed as a potential conflict of interest.

Publisher's Note: All claims expressed in this article are solely those of the authors and do not necessarily represent those of their affiliated organizations, or those of the publisher, the editors and the reviewers. Any product that may be evaluated in this article, or claim that may be made by its manufacturer, is not guaranteed or endorsed by the publisher.

frontiers in Cardiovascular Medicine

ORIGINAL RESEARCH
published: 18 January 2022
doi: 10.3389/fcvm.2021.745009

Protein Phosphatase 2A Deficiency in Macrophages Increases Foam Cell Formation and Accelerates Atherosclerotic Lesion Development

Rui Li[1†], Chao Zhang[1†], Fei Xie[1†], Xianming Zhou[1], Xingjian Hu[1], Jiawei Shi[1], Xinling Du[1‡], Zhiyong Lin[2*‡] and Nianguo Dong[1*‡]*

[1] Department of Cardiovascular Surgery, Union Hospital, Tongji Medical College, Huazhong University of Science and Technology, Wuhan, China, [2] Cardiology Division, Emory University School of Medicine, Atlanta, GA, United States

Protein phosphatase 2A (PP2A), a crucial serine/threonine phosphatase, has recently been reported to play an important role in cardiovascular disease. Previous studies have hinted that PP2A is involved in atherosclerosis formation, but the associated mechanisms remain poorly understood. In this study, we investigate the role of PP2A in the pathogenesis of atherosclerosis. In human atherosclerotic coronary arteries, we found that the expression and activity of PP2A decreased significantly when compared to non-atherosclerotic arteries. Additional experiments demonstrated that pharmacological inhibition of PP2A aggravated atherosclerosis of ApoE$^{-/-}$ mice. Considering the central role of macrophages in atherosclerosis, mice with conditional knockout of the PP2A-Cα subunit in myeloid cells were produced to investigate the function of PP2A in macrophages. Results showed that PP2A deficiency in myeloid cells aggravated atherosclerotic lesions in mice. *in vitro* experiments indicated that PP2A-deficient macrophages had an enhanced ability of lipid uptake and foam cell formation. Mechanistically, the deficiency of the PP2A in macrophages led to an increase in the phosphorylation level of p38, which contributed to the elevated expression of scavenger receptor CD36, a key factor involved in lipoprotein uptake. Our data suggest that PP2A participates in the pathophysiological process of atherosclerosis. The decrease of PP2A expression and activity in macrophages is a crucial determinant for foam cell formation and the initiation of atherosclerosis. Our study may provide a potential novel approach for the treatment of atherosclerosis.

Keywords: PP2A (protein phosphatase 2A), atherosclerosis, foam cell formation, p38, CD36

OPEN ACCESS

Edited by:
Hanrui Zhang,
Columbia University, United States

Reviewed by:
Mabruka Alfaidi,
Louisiana State University Health Shreveport, United States
Fang Li,
Columbia University Irving Medical Center, United States

***Correspondence:**
Xinling Du
xinlingdu@hust.edu.cn
Zhiyong Lin
zhiyong.lin@emory.edu
Nianguo Dong
dongnianguo@hotmail.com

[†]These authors have contributed equally to this work and share first authorship
[‡]These authors have contributed equally to this work and share senior authorship

Specialty section:
This article was submitted to Atherosclerosis and Vascular Medicine, a section of the journal Frontiers in Cardiovascular Medicine

Received: *21 July 2021*
Accepted: *27 December 2021*
Published: *18 January 2022*

Citation:
Li R, Zhang C, Xie F, Zhou X, Hu X, Shi J, Du X, Lin Z and Dong N (2022) Protein Phosphatase 2A Deficiency in Macrophages Increases Foam Cell Formation and Accelerates Atherosclerotic Lesion Development. Front. Cardiovasc. Med. 8:745009. doi: 10.3389/fcvm.2021.745009

INTRODUCTION

Atherosclerosis is a chronic inflammatory disease associated with significant morbidity and mortality worldwide. It is characterized by the formation of fibrofatty lesions in the artery wall which can lead to many serious complications, such as myocardial infarction, stroke, and disabling peripheral artery diseases (1). Many cell types are involved in the development and progression of atherosclerosis, including vascular endothelial cells, fibroblasts, smooth muscle cells, and monocytes/macrophages (2, 3). Studies conducted over the past several decades have supported

the concept that the initiation of atherosclerosis is the deposition and oxidative modification of low-density lipoprotein (LDL) in the intima of arteries. The uptake and treatment of oxidized LDL (oxLDL) by macrophages causes an overload of intracellular cholesterol esters leading to the formation of foam cells, a sign of early atherosclerotic lesion development (4, 5). However, despite decades of research, the molecular mechanisms that lead to foam cell formation in the process of atherosclerosis are still not fully understood.

Kinase and phosphatase mediated reversible protein phosphorylation plays a vital role in the regulation of many biological events (6). Protein phosphatase 2A (PP2A), a crucial serine/threonine phosphatase, consists of a scaffold subunit (PP2A-A), a regulatory subunit (PP2A-B) and a catalytic subunit (PP2A-C). Both PP2A-A and PP2A-C subunits have two isoforms, while the PP2A-B subunit has four different families (B, B′, B″, B‴) containing at least 13 different isoforms. This enables PP2A to fulfill a wide range of roles (7). The PP2A-C subunit has two types of post-translational modifications, phosphorylation at tyrosine-307 (Y307) and methylation at leucine-309 (L309). PP2A-C L309 methylation is essential for the maturation of PP2A and Y307 phosphorylation can result in decreased PP2A activity (8–10). Previous studies have shown that PP2A acts as a tumor suppressor in the development of many solid cancers and leukemias (11, 12). Emerging evidence suggests that PP2A activity also affects the pathogenesis in Alzheimer's disease and diabetes (13–15). In cardiovascular disease, PP2A activity is involved in a wide variety of pathophysiological processes, such as arrhythmia, cardiac remodeling, vascular remodeling, oxidative stress, ischemia-reperfusion injury, and endothelial dysfunction (16–20).

To our knowledge, there has been no direct research to investigate whether the expression and the activity of PP2A changes in atherosclerosis. In our study, using human coronary artery samples and mice with conditional knockout of the PP2A-Cα subunit in myeloid cells, we identified a role and associated molecular mechanisms of PP2A in foam cell formation and atherosclerosis.

MATERIALS AND METHODS

Human Coronary Artery Collection

Human specimens used in this study were obtained from patients undergoing heart transplant previously diagnosed with coronary atherosclerosis by angiography. Both atherosclerotic coronary arteries and adjacent non-atherosclerotic coronary arteries were taken from the same patients. Specimens from each patient were divided into four parts according to the purpose of the experiment. Arteries snap-frozen and preserved in liquid nitrogen were used for western blot and PP2A activity assays. All of the human studies described in this work complied with the Declaration of Helsinki and were approved by the Ethics Committee of Union Hospital, Tongji Medical College, Huazhong University of Science and Technology (No: IORG0003571). Informed consent was signed by all patients.

Animals

ApoE$^{-/-}$ mice (C57BL/6 background) were purchased from Beijing HFK Bioscience Co., Ltd. Ppp2cα$^{flox/flox}$ (fl/fl) and Cre^{Lyz2} mice (C57BL/6 background) were purchased from the Model Animal Research Center of Nanjing University. Mice were housed in a special pathogen free, temperature- and light-controlled animal facility at Tongji Medical College, Huazhong University of Science and Technology under a 12 h light/dark cycle and allowed *ad libitum* access to standard rodent chow and water. Ppp2cα$^{flox/flox}$ and Cre^{Lyz2} mice were mated to produce Ppp2cα$^{flox/flox}$ Cre^{Lyz2} (cKO) mice. For the pharmacological inhibition of the PP2A study, 10-week-old ApoE$^{-/-}$ male mice were randomly divided into two groups: ApoE$^{-/-}$ mice injected with LB100 (Selleck Chemicals, 1.0 mg/kg) and ApoE$^{-/-}$ mice injected with normal saline (1.0 mg/kg). Both groups received intraperitoneal injections every 2 days and were fed a western diet (D12079B, ReadyDietech) for 12 weeks. For the AAV-PCSK9 injection model, 10-week-old fl/fl and cKO male mice were injected once with AAV-PCSK9 (1.0×10^{11} VG/mouse) or AAV-GFP (1.0×10^{11} VG/mouse) *via* tail vein and then fed with a high-fat diet (D12108C, ReadyDietech) containing 1.25% cholesterol for 16 weeks. AAV8-D377YmPCSK9 and AAV8-GFP were produced by Vigene Biosciences, Inc. When modeling was complete, mice were fasted for 12 h and exposed to 5% isoflurane inhalant with oxygen flow rate at 1 L/min. Then, the mice were monitored continuously during the procedure and the complete anesthesia was confirmed by a lack of pedal reflex. After the mice were completely anesthetized, blood was collected from the inferior vena cava and then centrifuged to obtain plasma. Total cholesterol and triglyceride levels were tested using commercial kits (MAK043 and MAK040, MERCK). The left ventricle was perfused with 20 ml saline containing heparin, and then the heart, aorta and liver were fixed in 4% paraformaldehyde or snap-frozen and preserved in liquid nitrogen. During this process, mice were euthanized due to exsanguination and thoracotomy. All animal procedures performed conformed to the current NIH Guide for the Care and Use of Laboratory Animals. All of the animal protocols were approved by the Institutional Animal Research Committee of Tongji Medical College, Huazhong University of Science and Technology (IACUC Number: 2439).

PP2A Phosphatase Activity Assay

PP2A activity was measured using a commercial PP2A immunoprecipitation phosphatase assay kit (Millipore). Tissue or cell was lysed using a lysis buffer (20 mM imidazole-HCL, 2 mM EDTA, 2 mM EGTA, 1 mM benzamidine, pH 7.0 with 10 μg/ml aprotinin, and 1 mM PMSF) and the lysate was sonicated for 10 s and centrifuged at 2,000 *g* for 5 min. Supernatant was collected, total protein was quantified with a BCA Protein Assay kit (Beyotime Biotechnology), and 200 μg of total protein was incubated with anti-PP2A-C subunit antibody (4 μg) at 4°C for 18 h with gentle rocking. Then 40 μl Protein A agarose slurry was added and rocked at 4°C for 2 h. The mixture was centrifuged five times, during which beads were washed three times with 700 μl TBS and once with 500 μl Ser/Thr assay buffer. Then beads were incubated with 60 μl diluted phosphopeptide and 20 μl Ser/Thr assay buffer at 30°C for 10 min in a constant

temperature shaker. Finally, the mixture was centrifuged briefly, and the supernatant was analyzed in a colorimetric assay using malachite green at an absorbance of 650 nm.

Macrophage Isolation, Culture and Treatment

Eight- to Ten-week-old Ppp2cα$^{flox/flox}$Cre^{Lyz2} and Ppp2cα$^{flox/flox}$ male mice were injected with three milliliters of 3% thioglycolate. After 3 days, the mice were exposed to 5% isoflurane inhalant with oxygen flow rate at 1 L/min and were monitored continuously during this procedure. The complete anesthesia was confirmed by a lack of pedal reflex. After the mice were completely anesthetized, a well-trained researcher performed cervical dislocation to euthanize the mice in accordance with the current NIH Guide for the Care and Use of Laboratory Animals. Then, peritoneal macrophages were harvested by peritoneal lavage. Lavage fluid was centrifuged, and cells were re-suspended in RPMI 1640 medium (Gibco) containing 10% FBS (Gibco) and 1% penicillin-streptomycin (Gibco), plated onto 6-well plates (2×10^6 cells per well) and then cultured in an incubator at 37°C with 5% CO_2. After 2 h, non-adherent cells were removed, and macrophages were cultured in fresh RPMI 1,640 complete medium overnight. For foam cell formation assessment, cells were treated with oxidized low-density lipoprotein (ox-LDL; 50 μg/ml; Yiyuanbiotech) for 24 h. Cells were fixed with 4% paraformaldehyde and then stained by 0.5% Oil-Red-O (Sigma-Aldrich). For fluorescent labeling oxLDL (Dil-oxLDL, Yiyuanbiotech) uptake experiments, macrophages were incubated with Dil-oxLDL for 4 h. During the inhibitor tests, macrophages were treated with SB203580 (Selleck) or MK2206 (Selleck) for 4 h before ox-LDL treatment.

Protein Extraction and Western Blot Analysis

Tissues or cells were lysed by RIPA buffer (Thermo Fisher) supplemented with protease and phosphatase inhibitors (Thermo Fisher). Lysates were sonicated and then cleared by centrifugation at 12,000 *g* for 15 min. Protein concentrations were quantified with a BCA Protein Assay kit (Beyotime Biotechnology). Equal amounts of proteins were separated by SurePAGE^{TM} precast polyacrylamide gels with a gradient between 4 and 20% (GenScript) and blotted onto 0.22 μm PVDF membranes (Millipore) by eBlot L1 Fast Wet Transfer System (GenScript). After blocking in TBST containing 5% skim milk for 1 h at room temperature, membranes were incubated with appropriate primary antibodies overnight at 4°C on a shaker. Specific banding was detected by incubation with appropriate HRP-conjugated secondary antibodies and an enhanced chemiluminescence (ECL) system (Thermo). Band intensities were quantified using ImageJ software. Detailed antibody information is provided in **Supplementary Table 1**.

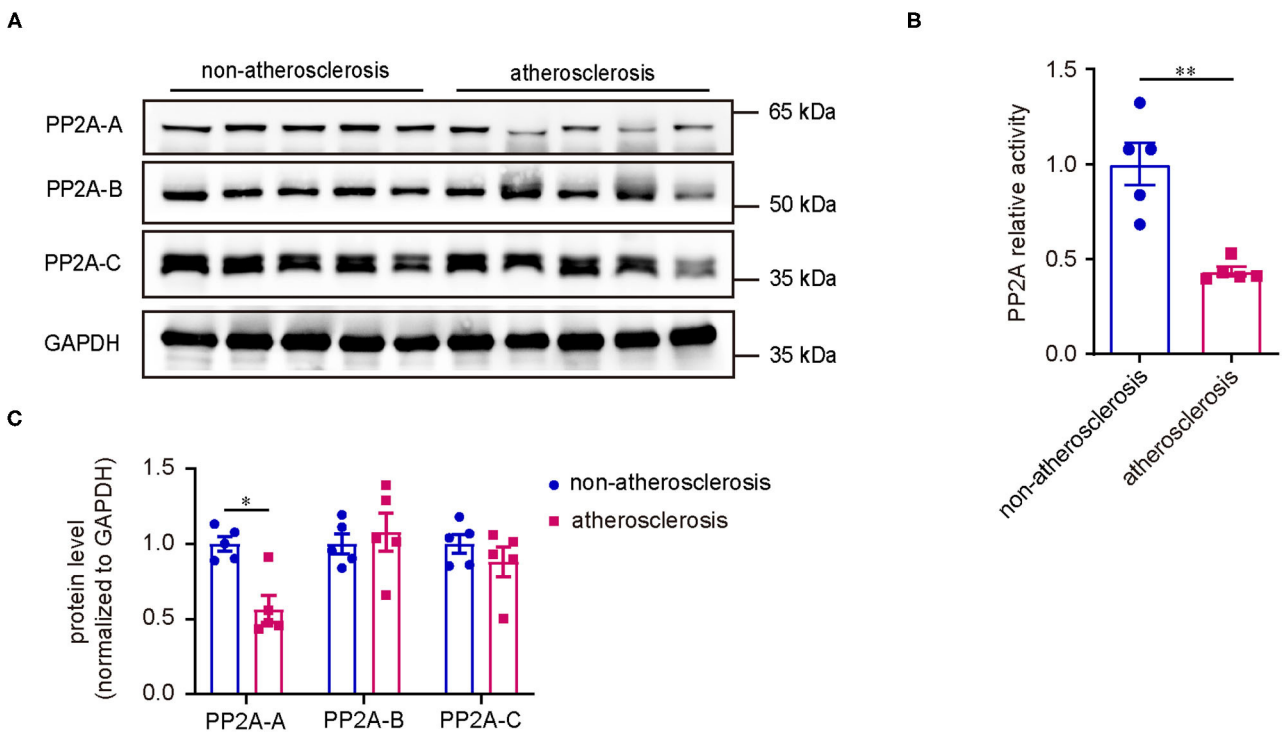

FIGURE 1 | Decreased PP2A expression and activity in human coronary atherosclerosis. **(A)** Upper panel: western blot assessment of PP2A subunits ($n = 5$). Lower panel: western blot quantification. **(B)** PP2A activity assay in the same set of specimens as in **(A)**.

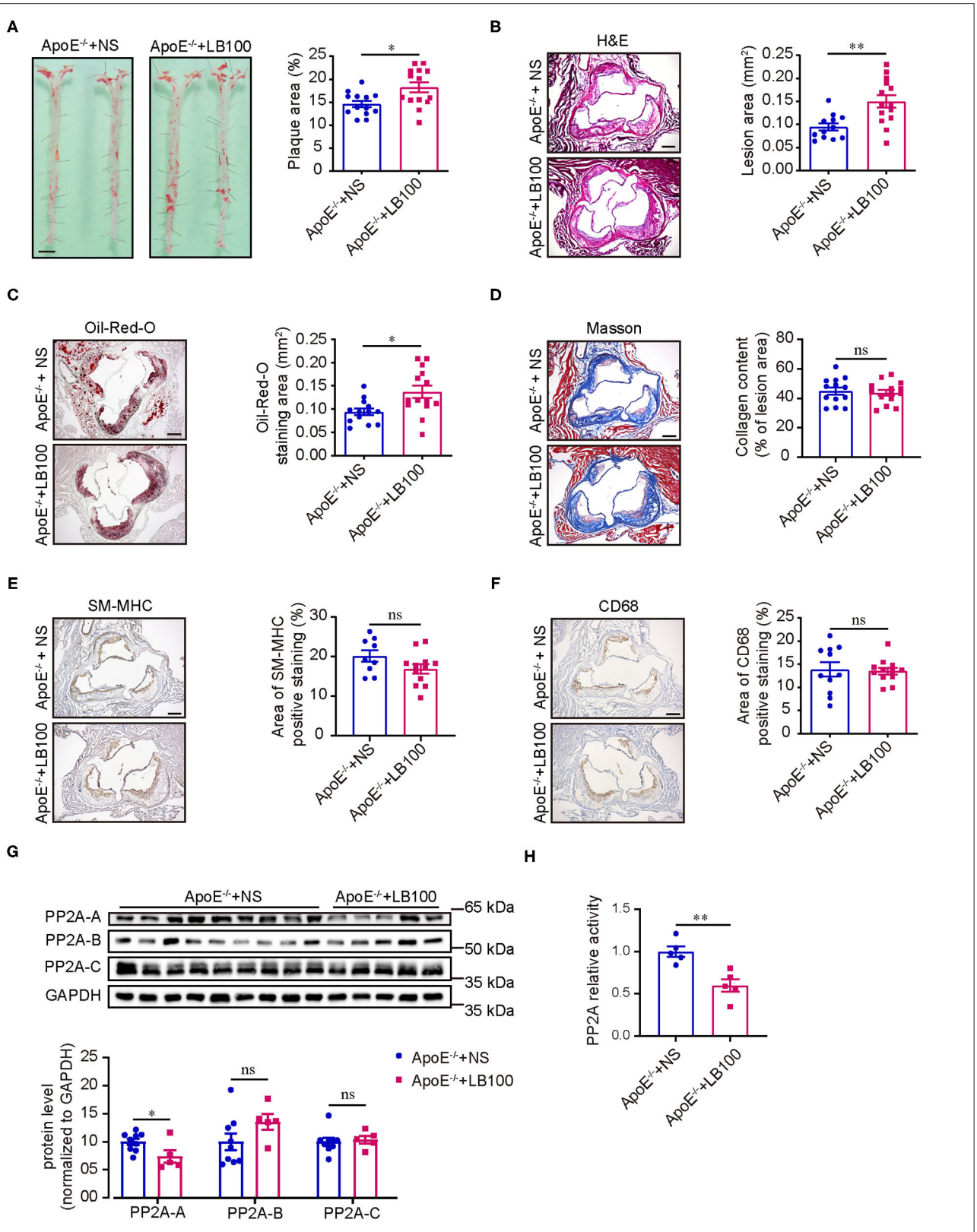

FIGURE 2 | LB100 increased the area of atherosclerotic plaque in ApoE$^{-/-}$ mice. **(A)** Left panel: representative images of whole aortas stained with Oil-Red-O from ApoE$^{-/-}$ mice with NS or LB100 treatment and 12 weeks of western diet feeding. Bar = 2.5 mm. Right panel: quantification of aortic atherosclerotic plaque area (n = 13–14). **(B)** Left panel: representative image of aortic root cross sections stained with H & E. Bar = 100 μm. Right panel: quantification of lesion area in aortic root

(Continued)

FIGURE 2 | ($n = 12$–14). **(C)** Left panel: representative image of aortic root cross sections stained with Oil-Red-O. Bar = 100 μm. Right panel: quantification of Oil-Red-O staining area in aortic root ($n = 13$–14). **(D)** Left panel: representative image of aortic root cross sections stained with Masson. Bar = 100 μm. Right panel: quantification of collegen fiber content in lesion area ($n = 13$–14). **(E)** Left panel: representative image of SM-MHC immunohistochemistry staining in aortic root cross sections. Bar = 100 μm. Right panel: quantification of SM-MHC positive area (n = 9–12). **(F)** Left panel: Representative image of CD68 immunohistochemistry staining in aortic root cross sections. Bar = 100 μm. Right panel: quantification of CD68 positive area ($n = 11$–12). **(G)** Left panel: western blot assessment of the expression of PP2A subunits in aortas. Right panel: quantification of western blot ($n = 9$–5). **(H)** PP2A activity assay in aortas ($n = 5$).

RNA Extraction and Quantitative RT-PCR Analysis

Total RNA was isolated from cells by Trizol reagent (Thermo Fisher) according to the protocol provided by manufacturer and then reverse transcribed into cDNA. The resulting cDNA was used as the template for quantitative RT-PCR. The reaction of quantitative RT-PCR was performed on a StepOne Plus thermal cycler (Applied Biosystems) according to the manufacturer's instructions. Detailed information of primers used in this study is listed in **Supplementary Table 2**. Gene expression was standardized to GAPDH using the $2^{-\Delta\Delta ct}$ method with each sample analyzed in triplicate.

Atherosclerotic Lesion Analysis

After 48 h of fixation in 4% paraformaldehyde, aortas of mice were cut open longitudinally, stained with Oil-Red-O (Sigma-Aldrich) for 15 min, fixed on black paraffin wax dishes with insect mounting pins, and photographed. Digital images of Oil-Red-O stained aortas were quantified using ImageJ software.

Histology and Immunohistochemistry

Cryosections (8 μm) from mouse aortic sinus were prepared, Hematoxylin and Eosin (H&E), Oil-Red-O, and Masson staining were performed on the sections to determine lesion area and collagen fiber content. For immunohistochemistry staining, after washing with PBS and treatment with 3% H_2O_2, sections were blocked at room temperature with 3% bovine serum albumin (Beyotime) for 60 min. Then, sections were incubated with primary antibody at 4°C overnight. On the following day, sections were incubated with secondary antibody at 37°C for 1 h. Finally sections were stained with 3,3N-Diaminobenzidine Tertrahydrochloride (Beyotime). Images were taken by a microscope (Mshot) and analyzed by the Image-pro plus 6.0.

Statistical Analysis

Statistical analysis was performed using GraphPad Prism 8, when comparing two unpaired groups, if either of the two groups of data did not pass normality test, Mann–Whitley test was used. If the two groups of data passed normality test and the P-value of F test ≥ 0.05, two-tailed unpaired Student's t-test was used. If the two groups of data passed normality test, but the P-value of F test < 0.05, two-tailed unpaired Student's t-test with Welch's correction was used. When comparing three or more unpaired groups, if one of the groups of data did not pass normality test, Dunn's multiple comparisons test was used. If all the groups of data passed normality test and had equal square deviation, Tukey's multiple comparisons test was used. If all the groups of data passed normality test but didn't have equal square deviation, Dunnett's T3 multiple comparisons test was used. In all experiments, $P < 0.05$ was considered to be statistically significant. Data are expressed as mean ± SEM. The number of asterisks represent the following: $^{*}P < 0.05$, $^{**}P < 0.01$, $^{***}P < 0.001$.

RESULTS

The Activity of PP2A Was Decreased in Human Coronary Atherosclerosis

First, to investigate if the expression of PP2A is altered in human coronary atherosclerosis, we analyzed the protein levels of various PP2A subunits in atherosclerotic and non-atherosclerotic human coronary artery specimens by western blot. Compared to non-atherosclerotic arteries, there was an obvious reduction in the expression of PP2A-A subunit in atherosclerotic specimens, whereas the expressions of PP2A-B and PP2A-C subunits had no statistical differences (**Figure 1A**). Next, to determine whether the deficiency of PP2A-A subunit affects the activity of PP2A, a PP2A immunoprecipitation phosphatase assay kit was used to test the PP2A activity in specimens. Results showed that the activity of PP2A decreased significantly in atherosclerotic arteries when compared to non-atherosclerotic arteries (**Figure 1B**). Taken together, these findings demonstrate that PP2A is relevant in human coronary atherosclerosis and the function of PP2A is decreased in atherosclerotic human coronary arteries.

Pharmacological Inhibition of PP2A Aggravated Atherosclerosis in ApoE$^{-/-}$ Mice

Based on the detection of human coronary artery specimens, we hypothesized that PP2A activity inhibition leads to the progression of atherosclerosis. To test our hypothesis, we performed studies using a well-established ApoE$^{-/-}$ atherosclerosis mouse model and a well-characterized hydrophilic small molecule inhibitor of the PP2A, LB100. The safety and tolerability of LB100 has been tested in a phase I clinical trial for the treatment of patients with relapsed solid tumors (21).

ApoE$^{-/-}$ mice were treated with normal saline (NS) or LB100 every 2 days and fed a western diet for 12 weeks with body weights measured weekly. After 12 weeks of western diet feeding, mice treated with LB100 displayed significantly increased areas of atherosclerotic plaque in whole aortas compared with the control (**Figure 2A**). The characteristics of the atherosclerotic plaque were analyzed by H&E staining, Oil-Red-O staining, Masson staining, CD68 immunohistochemistry staining and SM-MHC immunohistochemistry staining for aortic root cross sections. Results showed that LB100 treatment markedly increased the

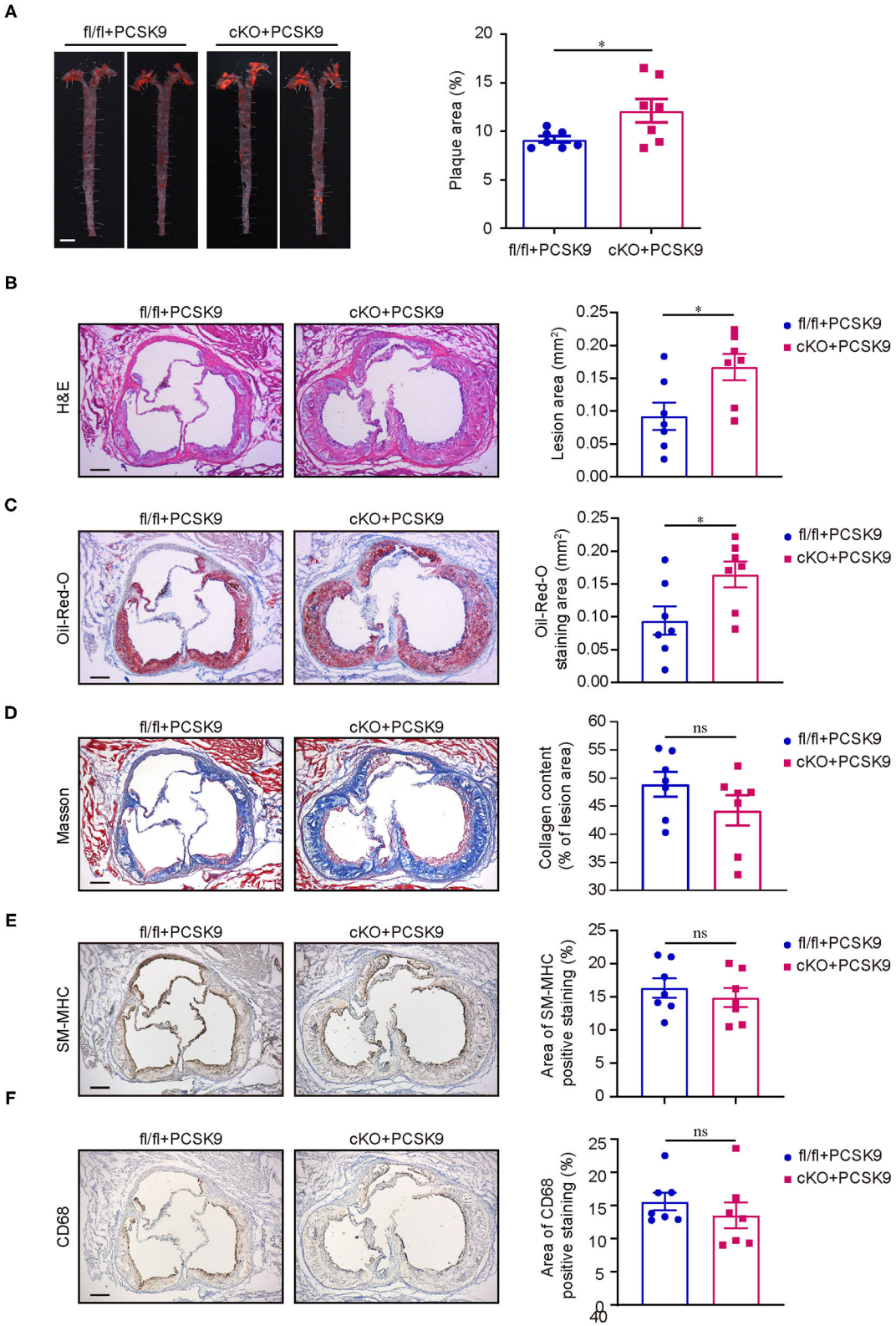

FIGURE 3 | PP2A deficiency in myeloid cells aggravated atherosclerosis in mice. **(A)** Left panel: representative images of Oil-Red-O staining of whole aortas from Ppp2cα$^{flox/flox}$ and Lyz2-Cre/Ppp2cα$^{flox/flox}$ mice injected with AAV-PCSK9 after 16 weeks of high-fat and high-cholesterol diet feeding. Bar = 2.5 mm. Right panel: quantification of aortic atherosclerotic plaque area ($n = 7$). **(B)** Left panel: representative image of aortic root cross sections stained with H & E. Bar = 100 μm. Right

(Continued)

FIGURE 3 | panel: quantification of lesion area in aortic root ($n = 7$). **(C)** Left panel: representative image of aortic root cross sections stained with Oil-Red-O. Bar = 100 μm. Right panel: quantification of Oil-Red-O staining area in aortic root ($n = 7$). **(D)** Left panel: representative image of aortic root cross sections stained with Masson. Bar = 100 μm. Right panel: quantification of collegen fiber content in lesion area ($n = 7$). **(E)** Left panel: representative image of SM-MHC immunohistochemistry staining in aortic root cross sections. Bar = 100 μm. Right panel: quantification of SM-MHC positive area ($n = 7$). **(F)** Left panel: representative image of CD68 immunohistochemistry staining in aortic root cross sections. Bar = 100 μm. Right panel: quantification of CD68 positive area ($n = 7$).

lesion area and lipid deposition (**Figures 2B,C**). However, there was no significant difference in the content of collagen fiber, the number of smooth muscle cells and the degree of macrophage infiltration in the lesion area between the two groups (**Figures 2D–F**). To investigate the inhibition effect of LB100, we analyzed the expression levels of PP2A subunits and the PP2A activity in aortas. Compared with aortas from NS-treated ApoE$^{-/-}$ mice, a significant decrease in the expression level of the PP2A-A subunit and the activity of PP2A were observed in aortas of LB-100-treated ApoE$^{-/-}$ mice (**Figures 2G,H**), which suggests that PP2A was effectively suppressed by LB100 in aortas. No significant differences of the body weights between the two groups of mice were observed during the process of western diet feeding (**Supplementary Figure 1A**). Finally, we tested the fasting blood total cholesterol and triglyceride levels of ApoE$^{-/-}$ mice with NS or LB100 treatment and 12 weeks of western diet feeding. Once again, no significant differences were found (**Supplementary Figures 1B,C**). In conclusion, these results indicate that PP2A activity inhibition increases the deposition of lipids and aggravates atherosclerosis in ApoE$^{-/-}$ mice.

Conditional Knockout of PP2A-Cα in Myeloid Cells Aggravated Atherosclerosis in Mice

Previous studies have shown that PP2A is involved in atherosclerosis by regulating vascular endothelial cells injury, transformation of macrophages and vascular smooth muscle cells to foam cells, and migration of smooth muscle cells (22–26). However, all these studies were limited to *in vitro* cell experiments, and no direct animal experiments showed that PP2A was involved in the occurrence and development of atherosclerosis. PP2A systemic knockout mice are embryonically lethal, and PP2A konckout in cells also results in cell death. Both PP2A-A and PP2A-C subunits have two isoforms. Considering that PP2A-C subunit is a catalytic subunit and has multiple modification sites of amino acid, we decided to construct a conditional knockout mouse of the PP2A-Cα isoform to study the function of PP2A. Since macrophage plays a crucial role in the pathogenesis of atherosclerosis and LB100 treated experiments suggested that inhibition of PP2A activity mainly affected lipids deposition, we decided to produce mice with conditional knockout of the PP2A-Cα subunit in myeloid cells by crossbreeding Cre^{Lyz2} and Ppp2cα$^{flox/flox}$ (fl/fl) mice to investigate whether PP2A deficiency in myeloid cells accelerates the progression of atherosclerosis. Due to the time-consuming and extremely difficult process to obtain Ppp2cα$^{flox/flox}$ Cre^{Lyz2} (cKO) mice on an ApoE$^{-/-}$ or LDLR$^{-/-}$ (low-density lipoprotein receptor knockout) background by crossbreeding cKO mice and ApoE$^{-/-}$ or LDLR$^{-/-}$ mice, we decided to apply in our study a novel, time-saving and effective animal model of atherosclerosis that has been reported and extensively used (27–30).

Proprotein convertase subtilisin kexin 9 (PCSK9) is a member of the subtilisin serine protease family that can bind to LDL receptors (LDLR) and route them to lysosomes for degradation (31). Single intravenous injection of recombinant adeno-associated viral vector encoding a gain-of-function mutant PCSK9 (AAV-PCSK9) is a rapid and effective method to induce atherosclerosis in mice and a versatile tool for experimental atherosclerosis research (32). On the basis of this method, fl/fl and cKO mice were injected once with AAV-PCSK9 or AAV-GFP (control) *via* caudal vein and then fed with high-fat and high-cholesterol diet. After 16 weeks of high-fat and high-cholesterol diet feeding, mice injected with AAV-PCSK9 had a significant decrease in the expression of LDLR in the liver when compared with the control (**Supplementary Figure 2A**). Through Oil-Red-O staining of aortas, we found that cKO mice injected with AAV-PCSK9 had notably larger areas of plaques than fl/fl mice injected with AAV-PCSK9 (**Figure 3A**), and plaques were barely visible in both cKO and fl/fl mice treated with AAV-GFP (**Supplementary Figure 2B**). Consistent with the results of the aortas, H&E and Oil-Red-Ostaining for aortic root cross sections showed that lesion area and lipid deposition increased in aortic root of cKO mice (**Figures 3B,C**). However, there was no statistical difference in the content of collagen fiber, the number of smooth muscle cells and the degree of macrophage infiltration in the lesion area of the aortic root between the two groups (**Figures 3D–F**). Although the aortic lipid deposition increased in cKO mice, there were no obvious differences in body weight between the cKO and fl/fl groups during the progress of high-fat and high-cholesterol diet feeding (**Figure 3C**). Additionally, no obvious differences were found in fasting blood total cholesterol and triglyceride levels after 16 weeks of high-fat and high-cholesterol diet feeding (**Figures 3D,E**). Therefore, these data strongly suggest that PP2A deficiency in myeloid cells aggravates atherosclerosis in mice.

PP2A Deficiency in Macrophages Increased Lipid Uptake and Foam Cell Formation

Since PP2A deficiency in myeloid cells aggravated atherosclerosis in mice, we next performed *in vitro* experiments to investigate whether the function of macrophages is regulated by PP2A. Initially, we assessed whether the deficiency of PP2A in macrophages could influence the formation of foam cells, a crucial step in atherosclerosis. Firstly, we tested the effect of

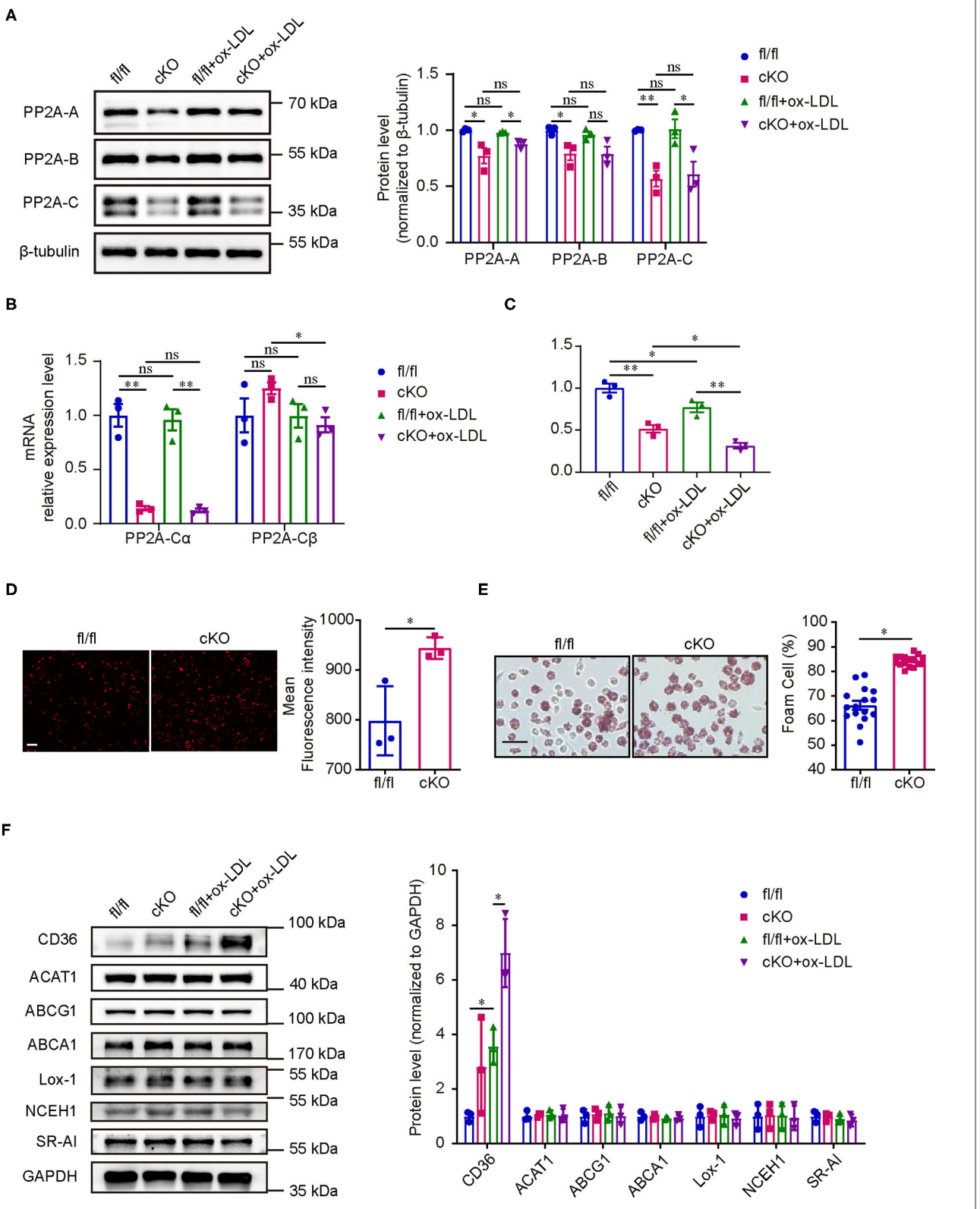

FIGURE 4 | PP2A deficiency in macrophages promoted foam cell formation. **(A)** Left panel: western blot of PP2A subunits in cKO and fl/fl macrophages treated with and without oxLDL for 24 h. Right panel: quantification of western blot ($n = 3$). **(B)** mRNA levels of PP2A-Cα and PP2A-Cβ isoforms in cKO and fl/fl macrophages treated with and without oxLDL for 24 h ($n = 3$). **(C)** PP2A activity assay in cKO and fl/fl macrophages treated with and without oxLDL for 24 h ($n = 3$). **(D)** Left panel: *(Continued)*

FIGURE 4 | representative images of Dil-oxLDL uptake in peritoneal macrophages isolated from cKO and fl/fl mice. Bar = 100 μm. Right panel: quantification of mean fluorescence intensity ($n = 3$). **(E)** Left panel: foam cell formation in cKO and fl/fl peritoneal macrophages after incubation with oxLDL for 24 h (The experiment was repeated three times, and one of them is shown here). Bar = 100 μm. Right panel: quantification of foam cell formation (16 sights of each group were selected to conduct the quantitative analysis). **(F)** Left panel: western blot of cholesterol homeostasis-related proteins in cKO and fl/fl macrophages treated with and without oxLDL for 24 h. Right panel: quantification of western blot ($n = 3$).

PP2A-Cα knockout and oxLDL treatment on the expression and activity of PP2A in macrophages. Peritoneal macrophages from cKO or fl/fl mice were treated with oxLDL or not for 24 h. In cKO macrophages, protein levels of PP2A-A, PP2A-B, and PP2A-C subunits, mRNA level of PP2A-Cα isoform, and the activity of PP2A were markedly decreased (**Figures 4A–C**), which means the function of PP2A is significantly inhibited. OxLDL treatment had no effect on protein levels of PP2A-A, PP2A-B, and PP2A-C subunits and mRNA level of PP2A-Cα isoform, but the activity of PP2A was significantly decreased (**Figures 4A–C**). Then, cKO and fl/fl macrophages were incubated with Dil-oxLDL for 4 h, we found that the uptake of oxLDL was significantly increased in cKO macrophages (**Figure 4D**). Consistent with this, increased foam cell formation was also observed in cKO macrophages when compared to fl/fl macrophages (**Figure 4E**, **Supplementary Figure 3**). These *in vitro* observations are in agreement with the increased plaque formation seen in the *in vivo* experiments.

Cholesterol homeostasis is regulated by macrophages through balancing oxLDL uptake, degradation and efflux. To investigate which processes are disturbed by the deficiency of PP2A with an eventual increase in foam cell formation, the expression levels of several key proteins involved in cholesterol homeostasis were analyzed. First, we measured the expression of three major scavenger receptors responsible for oxLDL uptake (CD36, Lox-1, and SR-A1). Interestingly, PP2A deficiency caused a significant increase of the expression of CD36 in oxLDL treated macrophages (**Figure 4F**). No significant differences were observed in the protein levels of two enzymes involved in the esterification of cholesterol and the hydrolysis of cholesterol ester (ACAT1 and NCEH1) (**Figure 4F**). Similarly, PP2A deficiency did not alter the expression of ABCA1 and ABCG1, two membrane proteins responsible for cholesterol efflux (**Figure 4F**). In summary, these findings demonstrated that oxLDL uptake and foam cell formation are disturbed by the increased expression of scavenger receptor CD36 in PP2A-deficient macrophages.

PP2A Regulated the Expression of CD36 and Foam Cell Formation Through p38 MAPK Signaling Pathway

Considering that PP2A is a phosphatase, we studied the changes of signaling pathway phosphorylation in the formation of foam cells. Peritoneal macrophages isolated from C57BL/6 mice were treated with oxLDL for several durations ranging from 0 to 6 h (0, 5 min, 15 min, 30 min, 1 h, 3 h, and 6 h). Western blot analysis showed that p38 and Akt were activated rapidly, reaching their peaks at 5 and 15 min respectively, and then their activity gradually decreased over time (**Figure 4A**). The activity of ERK was inhibited at 30 min and the decreased activity lasted up to 6 h. The phosphorylation of JNK, however, did not show an obvious changes. Next, we treated peritoneal macrophages from fl/fl and cKO mice with oxLDL for different times to test which signaling pathways are regulated by PP2A. Interestingly, we found that the phosphorylation level of p38 was significantly enhanced in cKO macrophages when compared to fl/fl macrophages at 0 min and 5 min and the phosphorylation level of Akt was also markedly enhanced at 5 min (**Figures 4B,E**). There was no statistical difference in the activity of ERK between fl/fl and cKO macrophages at each time point analyzed. To further investigate which signaling pathways regulate the expression of CD36 and affect the formation of foam cells, fl/fl and cKO macrophages were treated with SB203580 (p38 inhibitor) or MK2206 (Akt1/2/3 inhibitor) for 4 h, and then treated with oxLDL and the inhibitor for 24 h. Oil-Red-O staining and western blot analysis showed that foam cell formation and expression of CD36 were significantly reduced by the p38 inhibitor, with no significant changes found in the Akt inhibitor treated groups (**Figures 5E–G**, **Supplementary Figure 4**). These results revealed that PP2A regulates the expression of CD36 by mediating the activation of the p38 MAPK signaling pathway, thereby affecting foam cell formation.

DISCUSSION

In this study, we demonstrated that PP2A activity in macrophages is a crucial regulator of foam cell formation and atherosclerosis due to its ability to control the expression of scavenger receptor CD36 through the p38 MAPK signaling pathway.

First, we compared the expression of PP2A subunits and the activity of PP2A holoenzyme between non-atherosclerotic and atherosclerotic human coronary artery specimens by western blot and PP2A immunoprecipitation phosphatase assay kit. To our knowledge, this is the first report to show that the expression of PP2A-A subunit and the activity of the PP2A holoenzyme are significantly decreased in human atherosclerotic arteries. From this data, we hypothesized that the deficiency of PP2A function promotes atherosclerosis. Consistent with our hypothesis, we found that LB100, a inhibitor of PP2A, aggravated the aortic atherosclerosis of ApoE$^{-/-}$ mice *in vivo*. These results indicate that restoring PP2A activity might be a promising strategy for the treatment of atherosclerosis.

It is well established that the occurrence and development of atherosclerosis is a pathological process involving multiple cells in which macrophage foam cell formation is a central link (33). We produced mice with conditional knockout of the PP2A-Cα subunit in myeloid cells to study the effect of

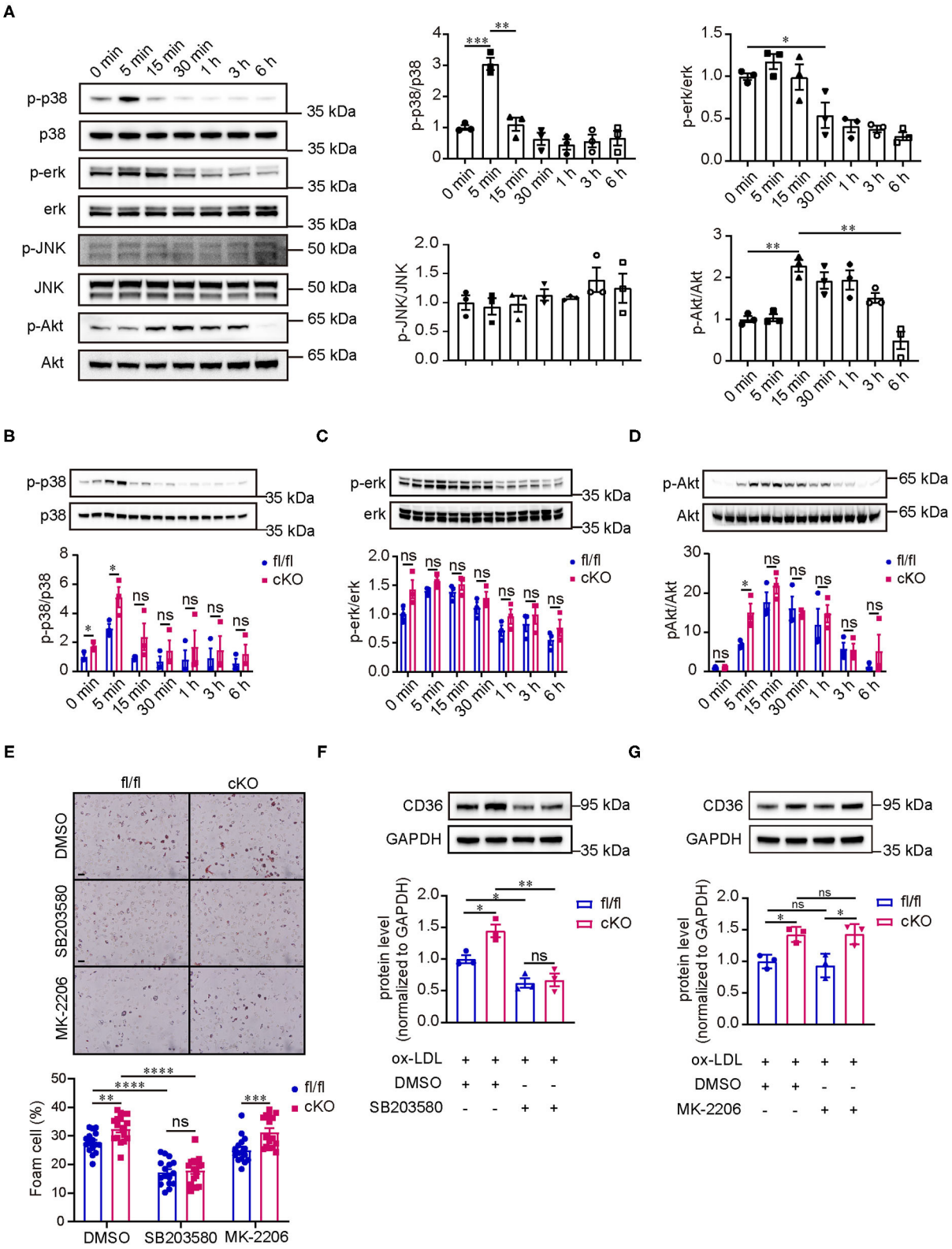

FIGURE 5 | PP2A regulates the expression of CD36 and foam cell formation *via* p38 MAPK signaling pathway. **(A)** Western blot analysis revealed the phosphorylation level of p38/ERK/JNK MAPKs and AKT signaling pathways in peritoneal macrophages isolated from C57BL6 mice treated with oxLDL at 0, 5 min, 15 min, 30 min, 1 h, 3 h, and 6 h ($n = 3$). **(B–D)** Images of western blot detecting the phosphorylation level of relevant signaling pathways at indicated times for cKO and fl/fl peritoneal

(Continued)

FIGURE 5 | macrophages after incubation with oxLDL ($n = 3$). **(E)** Upper panel: foam cell formation in cKO and fl/fl peritoneal macrophages treated with inhibitors of signaling pathways and oxLDL (The experiment was repeated three times, and one of them is shown here). Bar = 100 μm. Lower panel: quantification of foam cell formation (16 sights of each group were selected to conduct the quantitative analysis). **(F,G)** Western blot analysis of CD36 in cKO and fl/fl peritoneal macrophages treated with inhibitors of signaling pathways and oxLDL ($n = 3$).

PP2A function deficiency in myeloid cells on atherosclerosis. As expected, PP2A deficiency in myeloid cells aggravated the degree of aortic atherosclerosis in mice. *In vitro* studies using peritoneal macrophages indicated that oxLDL uptake and foam cell formation were increased in PP2A-deficient macrophages. Previous studies have shown that PP2A activity is associated with a variety of cellular functions involved in the development of atherosclerosis. In vascular endothelial cells, Yun et al. found that proatherosclerotic transcription factor Yap is dephosphorylated and activated by PP2A, which promotes the development of atherosclerosis (22). Studies from Chen et al. showed that PP2A deactivates eNOS by removing S1177 residue phosphorylation and reduces NO bioavailability (23). Zhang et al. reported that PP2A activation using a PP2A activator DT-061 reduced the uptake and accumulation of lipids in mouse aortic vascular smooth muscle cells (24). Campbell et al. and Yang found that decreased PP2A activity enhances the migration of vascular smooth muscle cells (25, 34). However, in these studies, no cell type-specific PP2A knockout mice were used to directly prove the relationship between PP2A and atherosclerosis. To further pinpoint the role of PP2A in these cells, cell type-specific PP2A knockout mice are required. Future studies are also warranted to determine the roles of other myeloid cells, such as neutrophils and dendritic cells.

Next, our mechanistic experiments showed that increased expression of scavenger receptor CD36 in PP2A-deficient macrophages resulted in enhanced uptake of oxLDL and subsequent foam cell formation. In a previous study, Chen et al. found that inhibiting PP2A activity increased LOX-1 expression, leading to enhanced oxLDL uptake in macrophages (26), but this phenomenon was not observed in our study using PP2A-Cα subunit knockout macrophages. CD36 is a major scavenger receptor for oxLDL, and the binding of oxLDL to CD36 can increase the expression of CD36 by activating peroxisome proliferator-associated receptor-γ (PPAR-γ), the transcription factor of CD36 (35–37). Studies have shown that PPAR-γ activation caused by oxLDL is related to protein kinase B (PKB/Akt) and mitogen-activated protein kinase (MAPK) signaling (38–41). In the present study, we observed that p38 and Akt were activated immediately when macrophages were treated with oxLDL. Moreover, the phosphorylation level of p38 was markedly enhanced in PP2A-deficient macrophages without any intervention. Furthermore, SB203580 (p38 inhibitor), and MK2206 (Akt inhibitor) were used to investigate which signaling pathways affected by PP2A mediate the expression of CD36. The results showed that only the p38 inhibitor could reverse the increase in CD36 expression and foam cell formation in PP2A-deficient macrophages, suggesting that PP2A regulates CD36 expression through the p38 signaling pathway.

In conclusion, our analysis of human atherosclerotic coronary artery specimens and animal experiment using LB100 inhibitor suggested that PP2A plays an important role in the pathogenesis of atherosclerosis. Data from the PP2A-deficient mice and macrophages revealed that PP2A regulates the uptake of oxLDL in marophages through PP2A-p38-CD36 axis.

DATA AVAILABILITY STATEMENT

The original contributions presented in the study are included in the article/**Supplementary Material**, further inquiries can be directed to the corresponding author/s.

ETHICS STATEMENT

The studies involving human participants were reviewed and approved by Ethics Committee of Union Hospital, Tongji Medical College, Huazhong University of Science and Technology. The patients/participants provided their written informed consent to participate in this study. The animal study was reviewed and approved by Animal Research Committee of Tongji Medical College, Huazhong University of Science and Technology.

AUTHOR CONTRIBUTIONS

CZ, XD, ZL, and ND conceived and designed the study. RL, CZ, and FX performed the experiments, analyzed the data and wrote the manuscript. XZ, XH, and JS contributed to the discussion of the study and the manuscript. All authors read and approved the manuscript.

FUNDING

This work was financially supported by the grant from the National Natural Science Foundation of China [81600354 to CZ] and part of the grant from the National Key R and D Program of China [2016YFA0101100 to ND].

ACKNOWLEDGMENTS

We thank LetPub (www.letpub.com) for its linguistic assistance during the preparation of this manuscript.

SUPPLEMENTARY MATERIAL

The Supplementary Material for this article can be found online at: https://www.frontiersin.org/articles/10.3389/fcvm.2021.745009/full#supplementary-material

Supplementary Figure 1 | (A) The changes of body weights during the process of western diet feeding ($n = 13$–14) in NS and LB100 treated mice. **(B,C)** Fasting blood total cholesterol and triglyceride levels after 12 weeks of western diet feeding ($n = 9$–13).

Supplementary Figure 2 | (A) Western blot assessment of LDLR in the liver of fl/fl and cKO mice injected with AAV-GFP or AAV-PCSK9 after 16 weeks of high-fat and high-cholesterol diet feeding. Right panel: quantification of western blot. **(B)** Images of Oil-Red-O staining of whole aortas from fl/fl and cKO mice injected with AAV-GFP after 16 weeks of high-fat and high-cholesterol diet feeding. Bar = 2.5 mm. **(C)** The change of body weight during the process of high-fat and high-cholesterol diet feeding in cKO and fl/fl mice injected with AAV-GFP ($n = 7$). **(D,E)** Fasting blood total cholesterol and triglyceride levels after 16 weeks of high-fat and high-cholesterol diet feeding ($n = 7$).

Supplementary Figure 3 | (A,B) Left panel: foam cell formation in cKO and fl/fl peritoneal macrophages after incubation with oxLDL for 24 h. Bar = 100 μm. Right panel: quantification of foam cell formation (16 sights of each group were selected to conduct the quantitative analysis).

Supplementary Figure 4 | (A, B) Left panel: foam cell formation in cKO and fl/fl peritoneal macrophages treated with inhibitors of signaling pathways and oxLDL. Bar = 100 μm. Right panel: quantification of foam cell formation (16 sights of each group were selected to conduct the quantitative analysis).

REFERENCES

1. Libby P, Buring JE, Badimon L, Hansson GK, Deanfield J, Bittencourt MS, et al. Atherosclerosis. *Nat Rev Dis Primers.* (2019) 5:56. doi: 10.1038/s41572-019-0106-z
2. Gimbrone MJ, Garcia-Cardena G. Endothelial cell dysfunction and the pathobiology of atherosclerosis. *Circ Res.* (2016) 118:620–36. doi: 10.1161/CIRCRESAHA.115.306301
3. Hansson GK, Hermansson A. The immune system in atherosclerosis. *Nat Immunol.* (2011) 12:204–12. doi: 10.1038/ni.2001
4. Moore KJ, Sheedy FJ, Fisher EA. Macrophages in atherosclerosis: a dynamic balance. *Nat Rev Immunol.* (2013) 13:709–21. doi: 10.1038/nri3520
5. Zeller I, Srivastava S. Macrophage functions in atherosclerosis. *Circ Res.* (2014) 115:e83–5. doi: 10.1161/CIRCRESAHA.114.305641
6. Virshup DM, Shenolikar S. From promiscuity to precision: protein phosphatases get a makeover. *Mol Cell.* (2009) 33:537–45. doi: 10.1016/j.molcel.2009.02.015
7. DeGrande ST, Little SC, Nixon DJ, Wright P, Snyder J, Dun W, et al. Molecular mechanisms underlying cardiac protein phosphatase 2A regulation in heart. *J Biol Chem.* (2013) 288:1032–46. doi: 10.1074/jbc.M112.426957
8. Liu R, Zhou XW, Tanila H, Bjorkdahl C, Wang JZ, Guan ZZ, et al. Phosphorylated PP2A (tyrosine 307) is associated with Alzheimer neurofibrillary pathology. *J Cell Mol Med.* (2008) 12:241–57. doi: 10.1111/j.1582-4934.2008.00249.x
9. Zhou XW, Gustafsson JA, Tanila H, Bjorkdahl C, Liu R, Winblad B, et al. Tau hyperphosphorylation correlates with reduced methylation of protein phosphatase 2A. *Neurobiol Dis.* (2008) 31:386–94. doi: 10.1016/j.nbd.2008.05.013
10. Sacharidou A, Chambliss KL, Ulrich V, Salmon JE, Shen YM, Herz J, et al. Antiphospholipid antibodies induce thrombosis by PP2A activation *via* apoER2-Dab2-SHC1 complex formation in endothelium. *Blood.* (2018) 131:2097–110. doi: 10.1182/blood-2017-11-814681
11. Mumby M. PP2A: unveiling a reluctant tumor suppressor. *Cell.* (2007) 130:21–4. doi: 10.1016/j.cell.2007.06.034
12. Perrotti D, Neviani P. Protein phosphatase 2A: a target for anticancer therapy. *Lancet Oncol.* (2013) 14:e229–38. doi: 10.1016/S1470-2045(12)70558-2
13. Clark AR, Ohlmeyer M. Protein phosphatase 2A as a therapeutic target in inflammation and neurodegeneration. *Pharmacol Ther.* (2019) 201:181–201. doi: 10.1016/j.pharmthera.2019.05.016
14. Martin L, Latypova X, Wilson CM, Magnaudeix A, Perrin ML, Terro F. Tau protein phosphatases in Alzheimer's disease: the leading role of PP2A. *Ageing Res Rev.* (2013) 12:39–49. doi: 10.1016/j.arr.2012.06.008
15. Arora DK, Machhadieh B, Matti A, Wadzinski BE, Ramanadham S, Kowluru A. High glucose exposure promotes activation of protein phosphatase 2A in rodent islets and INS-1 832/13 beta-cells by increasing the posttranslational carboxylmethylation of its catalytic subunit. *Endocrinology.* (2014) 155:380–91. doi: 10.1210/en.2013-1773
16. El RM, Musa H, Murphy NP, Lubbers ER, Skaf M, Han M, et al. Protein Phosphatase 2A Regulates Cardiac Na(+) Channels. *Circ Res.* (2019) 124:737–46. doi: 10.1161/CIRCRESAHA.118.314350
17. Li J, Tan Y, Passariello CL, Martinez EC, Kritzer MD, Li X, et al. Signalosome-regulated serum response factor phosphorylation determining myocyte growth in width versus length as a therapeutic target for heart failure. *Circulation.* (2020) 142:2138–54. doi: 10.1161/CIRCULATIONAHA.119.044805
18. Ehling M, Celus W, Martin-Perez R, Alba-Rovira R, Willox S, Ponti D, et al. B55alpha/PP2A limits endothelial cell apoptosis during vascular remodeling: a complementary approach to disrupt pathological vessels? *Circ Res.* (2020) 127:707–23. doi: 10.1161/CIRCRESAHA.119.316071
19. Elgenaidi IS, Spiers JP. Regulation of the phosphoprotein phosphatase 2A system and its modulation during oxidative stress: a potential therapeutic target? *Pharmacol Ther.* (2019) 198:68–89. doi: 10.1016/j.pharmthera.2019.02.011
20. Etwebi Z, Landesberg G, Preston K, Eguchi S, Scalia R. Mechanistic role of the calcium-dependent protease calpain in the endothelial dysfunction induced by MPO (Myeloperoxidase). *Hypertension.* (2018) 71:761–70. doi: 10.1161/HYPERTENSIONAHA.117.10305
21. Chung V, Mansfield AS, Braiteh F, Richards D, Durivage H, Ungerleider RS, et al. Safety, tolerability, and preliminary activity of LB-100, an inhibitor of protein phosphatase 2A, in patients with relapsed solid tumors: an open-label, dose escalation, first-in-human, phase I trial. *Clin Cancer Res.* (2017) 23:3277–84. doi: 10.1158/1078-0432.CCR-16-2299
22. Yun S, Hu R, Schwaemmle ME, Scherer AN, Zhuang Z, Koleske AJ, et al. Integrin alpha5beta1 regulates PP2A complex assembly through PDE4D in atherosclerosis. *J Clin Invest.* (2019) 129:4863–74. doi: 10.1172/JCI127692
23. Chen B, Zhao Q, Xu T, Yu L, Zhuo L, Yang Y, et al. BRG1 Activates PR65A Transcription to Regulate NO Bioavailability in Vascular Endothelial Cells. *Front Cell Dev Biol.* (2020) 8:774. doi: 10.3389/fcell.2020.00774
24. Zhang D, Gao JL, Zhao CY, Wang DN, Xing XS, Hou XY, et al. Cyclin G2 promotes the formation of smooth muscle cells derived foam cells in atherosclerosis *via* PP2A/NF-kappaB/LOX-1 pathway. *Ann Transl Med.* (2021) 9:446. doi: 10.21037/atm-20-6207
25. Campbell M, Anderson P, Trimble ER. Glucose lowers the threshold for human aortic vascular smooth muscle cell migration: inhibition by protein phosphatase-2A. *Diabetologia.* (2008) 51:1068–80. doi: 10.1007/s00125-008-0962-7
26. Chen B, Li J, Zhu H. AMP-activated protein kinase attenuates oxLDL uptake in macrophages through PP2A/NF-kappaB/LOX-1 pathway. *Vascul Pharmacol.* (2016) 85:1–10. doi: 10.1016/j.vph.2015.08.012
27. Roche-Molina M, Sanz-Rosa D, Cruz FM, Garcia-Prieto J, Lopez S, Abia R, et al. Induction of sustained hypercholesterolemia by single adeno-associated virus-mediated gene transfer of mutant hPCSK9. *Arterioscler Thromb Vasc Biol.* (2015) 35:50–9. doi: 10.1161/ATVBAHA.114.303617
28. Getz GS, Reardon CA. Animal models of atherosclerosis. *Arterioscler Thromb Vasc Biol.* (2012) 32:1104–15. doi: 10.1161/ATVBAHA.111.237693
29. Kumar S, Kang DW, Rezvan A, Jo H. Accelerated atherosclerosis development in C57Bl6 mice by overexpressing AAV-mediated PCSK9 and partial carotid ligation. *Lab Invest.* (2017) 97:935–45. doi: 10.1038/labinvest.2017.47
30. Moss ME, Lu Q, Iyer SL, Engelbertsen D, Marzolla V, Caprio M, et al. Endothelial Mineralocorticoid Receptors Contribute to Vascular

Inflammation in Atherosclerosis in a Sex-Specific Manner. *Arterioscler Thromb Vasc Biol.* (2019) 39:1588–601. doi: 10.1161/ATVBAHA.119.312954
31. Shapiro MD, Tavori H, Fazio S. PCSK9: From Basic Science Discoveries to Clinical Trials. *Circ Res.* (2018) 122:1420–38. doi: 10.1161/CIRCRESAHA.118.311227
32. Bjorklund MM, Hollensen AK, Hagensen MK, Dagnaes-Hansen F, Christoffersen C, Mikkelsen JG, et al. Induction of atherosclerosis in mice and hamsters without germline genetic engineering. *Circ Res.* (2014) 114:1684–9. doi: 10.1161/CIRCRESAHA.114.302937
33. Tabas I, Bornfeldt KE. Macrophage phenotype and function in different stages of atherosclerosis. *Circ Res.* (2016) 118:653–67. doi: 10.1161/CIRCRESAHA.115.306256
34. Yang M, Kahn AM. Insulin-inhibited and stimulated cultured vascular smooth muscle cell migration are related to divergent effects on protein phosphatase-2A and autonomous calcium/calmodulin-dependent protein kinase II. *Atherosclerosis.* (2008) 196:227–33. doi: 10.1016/j.atherosclerosis.2007.04.050
35. Tian K, Xu Y, Sahebkar A, Xu S. CD36 in Atherosclerosis: Pathophysiological Mechanisms and Therapeutic Implications. *Curr Atheroscler Rep.* (2020) 22:59. doi: 10.1007/s11883-020-00870-8
36. Nozaki S, Kashiwagi H, Yamashita S, Nakagawa T, Kostner B, Tomiyama Y, et al. Reduced uptake of oxidized low density lipoproteins in monocyte-derived macrophages from CD36-deficient subjects. *J Clin Invest.* (1995) 96:1859–65. doi: 10.1172/JCI118231
37. Oppi S, Nusser-Stein S, Blyszczuk P, Wang X, Jomard A, Marzolla V, et al. Macrophage NCOR1 protects from atherosclerosis by repressing a pro-atherogenic PPARgamma signature. *Eur Heart J.* (2020) 41:995–1005. doi: 10.1093/eurheartj/ehz667
38. Munteanu A, Taddei M, Tamburini I, Bergamini E, Azzi A, Zingg JM. Antagonistic effects of oxidized low density lipoprotein and alpha-tocopherol on CD36 scavenger receptor expression in monocytes: involvement of protein kinase B and peroxisome proliferator-activated receptor-gamma. *J Biol Chem.* (2006) 281:6489–97. doi: 10.1074/jbc.M508799200
39. Min KJ, Um HJ, Cho KH, Kwon TK. Curcumin inhibits oxLDL-induced CD36 expression and foam cell formation through the inhibition of p38 MAPK phosphorylation. *Food Chem Toxicol.* (2013) 58:77–85. doi: 10.1016/j.fct.2013.04.008
40. Oh J, Weng S, Felton SK, Bhandare S, Riek A, Butler B, et al. 1,25(OH)2 vitamin d inhibits foam cell formation and suppresses macrophage cholesterol uptake in patients with type 2 diabetes mellitus. *Circulation.* (2009) 120:687–98. doi: 10.1161/CIRCULATIONAHA.109.856070
41. Taketa K, Matsumura T, Yano M, Ishii N, Senokuchi T, Motoshima H, et al. Oxidized low density lipoprotein activates peroxisome proliferator-activated receptor-alpha (PPARalpha) and PPARgamma through MAPK-dependent COX-2 expression in macrophages. *J Biol Chem.* (2008) 283:9852–62. doi: 10.1074/jbc.M703318200

Conflict of Interest: The authors declare that the research was conducted in the absence of any commercial or financial relationships that could be construed as a potential conflict of interest.

Publisher's Note: All claims expressed in this article are solely those of the authors and do not necessarily represent those of their affiliated organizations, or those of the publisher, the editors and the reviewers. Any product that may be evaluated in this article, or claim that may be made by its manufacturer, is not guaranteed or endorsed by the publisher.

frontiers in Cardiovascular Medicine

SYSTEMATIC REVIEW
published: 23 February 2022
doi: 10.3389/fcvm.2021.778891

Determinants of Dyslipidemia in Africa: A Systematic Review and Meta-Analysis

Mohammed S. Obsa[1], Getu Ataro[2], Nefsu Awoke[1], Bedru Jemal[3], Tamiru Tilahun[1], Nugusu Ayalew[4], Beshada Z. Woldegeorgis[1], Gedion A. Azeze[1] and Yusuf Haji[2]*

[1] College of Health Science and Medicine, Wolaita Soddo University, Wolaita Soddo, Ethiopia, [2] College of Medicine and Health Science, Hawassa University, Hawassa, Ethiopia, [3] College of Medicine and Health Science, Dilla University, Dilla, Ethiopia, [4] Department of Anesthesia, Kotebe Metropolitan University, Addis Ababa, Ethiopia

Background: Dyslipidemia is a common public health problem in Africa. It has emerged as an important cardiovascular risk factor. It has been steadily increasing due to economic growth, urbanization, and unhealthy dietary pattern. Therefore, it is essential to identify determinants of dyslipidemia to prevent the condition and reduce its long-term sequel.

Methods: Combinations of search terms with Boolean operators were used to retrieve studies from PubMed, EMBASE, Cochrane Database, Cinahl, Scopus, Mednar, and Google Scholar. The methodological quality of each article was evaluated based on the 2017 Joanna Briggs Institute (JBI) Critical Appraisal checklist for prevalence studies. After evaluation of each study against these criteria, studies with a minimum score of 7 or above out of 9 JBI checklists were included. We included articles presented in the English language. The Cochrane Q test was used to assess the heterogeneity across studies. The visual assessment of publication bias was done by creating a funnel plot. The possible causes of heterogeneity were explored by subgroup analyses. Egger's weighted regression test was used to assess the presence of publication bias. Statistical analyses were done by using the STATA software version 14.

Result: A total of 24 articles involving 37,902 participants from 10 African countries were included. The overall pooled prevalence of dyslipidemia was 52.8 (95% *CI* 40.8–64.9). Individuals with a body mass index (BMI) >25.0 kg/m^2 and waist circumference (WC) >94 cm were, respectively, 2.36 (95% *CI* (1.33–4.18), $p < 0.001$) and 2.33 (95% *CI* (0.75–0.29) $p < 0.001$) times more likely to develop dyslipidemia than those with lower values. Furthermore, patients with diabetes mellitus (DM) and hypertension (HTN) were 2.32 (95% *CI* (0.89–6.05) $p < 0.001$) and 2.05 (95% *CI* (1.31–3.21), $p < 0.001$) times more likely to present with dyslipidemia than non-diabetic patients and those without HTN.

Conclusion: This study revealed that the prevalence of dyslipidemia is relatively high among study participants in African countries and the independent predictors of

OPEN ACCESS

Edited by:
Changcheng Zhou, University of California, Riverside, United States

Reviewed by:
Kailash Gulshan, Cleveland State University, United States
Demeke Belay, Debre Tabor University, Ethiopia

****Correspondence:***
Mohammed S. Obsa
msuleiman43@gmail.com

Specialty section:
This article was submitted to Lipids in Cardiovascular Disease, a section of the journal Frontiers in Cardiovascular Medicine

Received: *17 September 2021*
Accepted: *29 December 2021*
Published: *23 February 2022*

Citation:
Obsa MS, Ataro G, Awoke N, Jemal B, Tilahun T, Ayalew N, Woldegeorgis BZ, Azeze GA and Haji Y (2022) Determinants of Dyslipidemia in Africa: A Systematic Review and Meta-Analysis. Front. Cardiovasc. Med. 8:778891. doi: 10.3389/fcvm.2021.778891

dyslipidemia were BMI >25.0 kg/m^2, WC > 94 cm, raised blood glucose level, and raised blood pressure. Therefore, there should be a pressing public health measure to prevent, identify, and treat dyslipidemia with the special emphasis on obese, diabetic, and hypertensive patients.

Keywords: dyslipidemia, risk factors, lipid profile, Africa, abnormal lipid metabolism, metabolic syndrome, non-communicable disease, hypercholesterolemia

BACKGROUND

Dyslipidemia is a state that occurs due to abnormalities in the plasma lipids. These include increased plasma total cholesterol (TC), increased low-density lipoprotein cholesterol (LDL-C), increased triglycerides (TGs), and reduced high-density lipoprotein cholesterol (HDL-C) levels. It presents either as an elevation of one of the lipids or high levels of a combination of the lipids (1, 2). The exact mechanism of dyslipidemia is not fully understood but is most likely multifactorial with genetic variations being shown to account for about 43–83% of the variability of plasma lipoprotein levels in a normal healthy population (3, 4). Dyslipidemia is an autosomal dominant disorder caused by mutations in the low-density lipoprotein receptor (*LDLR)* gene. As a result of defective cell-surface *LDLR*, clearance of LDL-C from plasma is reduced leading to the increased plasma levels of LDL-C and TC (5). Individuals with dyslipidemia have a 2-fold higher risk of developing cardiovascular diseases (CVDs) than those with normal lipid levels (6).

Both LDL-C and HDL-C regulate the amount of cholesterol in the body. An imbalance between the two can increase the risk of myocardial infarction and stroke (7). The increased levels of LDL-C aggravate the development of atherosclerosis, which is documented as the main risk factor for stroke, peripheral vascular, and ischemic heart disease (IHD) (8). However, HDL-C helps to remove cholesterol from the body, which decreases the risk of atherosclerotic CVD (6).

Though the burden of disease in Africa has been dominated by infectious diseases, countries in this region are undergoing a continuous demographic change leading to the increasing frequency of non-communicable diseases (NCDs) (9). Substantial changes in the health of the population marked by the rising burden of CVDs are set to overtake infectious diseases as the leading cause of death by 2030. This epidemiological shift is mainly driven by unhealthy lifestyles due to rapid urbanization and modernization. Recently, infectious agents are considered more frequently as causes of diseases that have been thought previously to be of non-infectious etiology, such as coronary heart disease. Additionally, lipopolysaccharide (LPS) affects the circulating macrophages and increases the production of free radicals. Free radicals are known to oxidize LDL-C and transform macrophages into foam cells, which are known to be crucial in the pathogenesis of atherosclerosis (10).

Dyslipidemia is responsible for more than half of the global IHD and more than 4 million deaths annually (11). It remains a common public health problem as abnormal serum lipid profile has been steadily increasing due to economic growth, urbanization, and unhealthy lifestyles (12). In Africa, the prevalence of dyslipidemia ranges from 5.2 (13) to 89.9% (14). The presentation of an abnormal lipid profile is common in individuals with central obesity, anti-retroviral therapy (ART), metabolic syndrome, insulin resistance, and type 2 diabetes mellitus (DM) (15). The duration of HIV treatment, advanced age, sex, low CD4 counts, smoking, alcohol consumption, depression (12, 15, 16), and a diet high in saturated fat, sedentary lifestyle, and obesogenic (17) are the major risk factors of dyslipidemia.

The prevalence of CVD is mainly result of risk factors, mostly hypertension (HTN), diabetes, and obesity (9). Dyslipidemia is also more common among patients with coexisting cardiovascular risk factors, such as HTN, diabetes, or HIV (10). A systematic review conducted in the Gambia on CVD risk factors revealed the prevalence of insufficient fruit and vegetable consumption, inadequate physical activity, and alcohol consumption was 77.8, 14.6, and 2.3%, respectively (18).

Most (80%) of the lipid disorders are associated with diet and lifestyle (17). The dietary habits of populations in low-to-middle-income countries (LMICs) have rapidly shifted to less-healthy diets (19). These consist of processed foods, away-from-home food intake, and increased use of edible oils and sugar-sweetened beverages (20).

In recent decades, the global pattern of unhealthy diets driving the occurrence of metabolic disorders and NCDs has become more important in LMICs because of the double burden of diseases in such countries that jointly constitute major causes of morbidity and mortality (21). In many African countries, surveillance and research on NCDs are still lacking (22). However, in the last decades, the number of NCDs-related deaths in the region have grown dramatically (9). This review will allow researchers to assess the disease burden of dyslipidemia in Africa where data are often scarce and populations are understudied. Assessing the prevalence of dyslipidemia can also aid researchers in predicting the future disease development of conditions contingent on dyslipidemia, such as CVD. Accurate data on dyslipidemia prevalence and risk factors can serve to inform health professionals, policy makers, and the public to manage and plan. However, different previous studies conducted on risk factors of dyslipidemia showed conflicting results. Understanding the context-specific factors associated with dyslipidemia and

Abbreviations: CI, confidence interval; HIV, human immune deficiency virus; HTN, hypertension; OR, odds ratio.

its potential implications are critical to designing effective interventions for the prevention and treatment of metabolic and cardiovascular effects of dyslipidemia.

METHODS

The Study Protocol and Reporting

The Preferred Reporting Items for Systematic Reviews and Meta-Analyses (PRISMA) guidelines for literature search strategy, selection of studies, data extraction, and result reporting were followed while conducting this systematic review and meta-analysis. The eligibility criteria based on the Condition, Context, and Population (COCOPO) principle was adapted from the Joanna Briggs Institute (JBI) 2017 review guideline (23). Endnote (version X8) reference management software was used to download, organize, review, and cite related articles. The protocol of this review was not registered in the Prospero database.

Context

All eligible cross-sectional study, cohort study, comparative cross-sectional study, national survey, and a longitudinal study conducted on the prevalence and risk factors of dyslipidemia among patients with HIV, diabetes, HTN, and Lichen Planus, women on hormonal contraceptives, and general population in Africa were considered.

Condition

This review considered the studies that measured the outcome of interest-based prevalence and risk factors of dyslipidemia.

Variables and Measures

The primary outcome of this study was dyslipidemia. The case definitions of dyslipidemia were increased TC ≥5.17 mmol/L (≥200 mg/dl); high LDL-C ≥3.36 mmol/L (≥130 mg/dl), increased TG ≥1.7 mmol/L (≥150 mg/dl); and low HDL-C <1.03 mmol/L (<40 mg/dl) for men, <1.3 mmol/L (<50 mg/dl) for women. Study subjects who met one or more of the above criteria were categorized as having dyslipidemia. Participants who were on a lipid-lowering agent were also classified as having dyslipidemia (24, 25). Identified determinants of dyslipidemia were defined as follows: abdominal obesity was defined as WC >94 cm for men and >88 cm for women (26). BMI was classified as underweight (<18.5 kg/m^2), normal (18.5–24.9 kg/m^2), overweight (25.0–29.9 kg/m^2), or obese (≥30 kg/m^2) (27). Participants were considered as hypertensive if blood pressure (BP) is ≥140/90 mmHg. In this study, high fasting blood glucose (FBG) was defined as ≥5.6 mmol/L (≥100 mg/dl) or if the patient is on treatment for diabetes (28).

Inclusion Criteria

We included all studies that fulfilled the above case definition of dyslipidemia. However, we considered studies that were conducted on determinants of metabolic syndrome and hypercholesterolemia if risk factors of dyslipidemia were identified. In such a case, we carefully checked its compliance with the case definition before considering it for the final analysis. Furthermore, full text and/or open access articles, a study conducted in Africa, published and unpublished studies are written in the English language before August 8, 2021, were included.

Study Design and Search Strategy

The search was limited to studies published in the English language from January 2000 to July 20, 2021. For published studies, the initial restricted search of PubMed, EMBASE, Cochrane Database, Cinahl, Scopus, Mednar, and Google Scholar were undertaken. Thereafter, unpublished studies were searched from Addis Ababa University and Jimma University institutional repositories. Then, a second search term using all identified keywords and index terms was undertaken. Third, the reference list of all identified reports and articles was searched for extra studies. We searched the database with terms including:

"Dyslipid*," "Dyslipidemia," "Dyslipidaemia," "metabolic syndrome," "hypercholesterol*," "hypercholesterolemia," hypercholesterolemia "prevalence," "associated factors," "general population," "Sub-Saharan Africa," and "Africa" for the articles published in English before August 8, 2021. The search detail of this systematic review with meta-analysis was uploaded as dataset 1.

Data Quality Control Measures

The methodological quality of each article was evaluated based on the 2017 JBI Critical Appraisal checklist for prevalence studies (23). After the evaluation of each study against these criteria, studies scoring 7 or above were included. On the other hand, studies scoring below 7 out of 9 criteria of Critical Appraisal instruments for prevalence studies were excluded. The quality of each study was evaluated independently by two authors (MS. O. and G. A.). The discrepancy was solved by the discussion with the third independent reviewer (BZ. W.).

Data Extraction

The data were extracted by two independent authors (MS. O. and Y. H.) using a standard and piloted form. The extracted data were the last name of the author, year of publication, country, region, study participant, frequency or prevalence of the disease, LDL-C data, and risk factors dataset 2. Discrepancies were discussed and solved by consensus or by a third reviewer (G. A.).

Statistical Analysis

All statistical data analyses were done by using Stata version 14.0 (Statacorp. LP, College Station, TX, USA). A random effects meta-analysis based on the DerSimonian and Laird approach was used to pool the prevalence of dyslipidemia in Africa. The presence of statistical heterogeneity was checked using Higgins I-squared (I^2) statistics and Cochran's-Q test. Accordingly, heterogeneity was classified as low, moderate, or high when the values of I^2 were 25, 50, and 75%, respectively (13). The potential sources of heterogeneity were explored by meta regression and subgroup analysis. Publication bias was viewed graphically by the funnel plots and tested through Egger© and Begg© tests (29). Sensitivity analysis was done to identify the effect of a single study on the overall estimate.

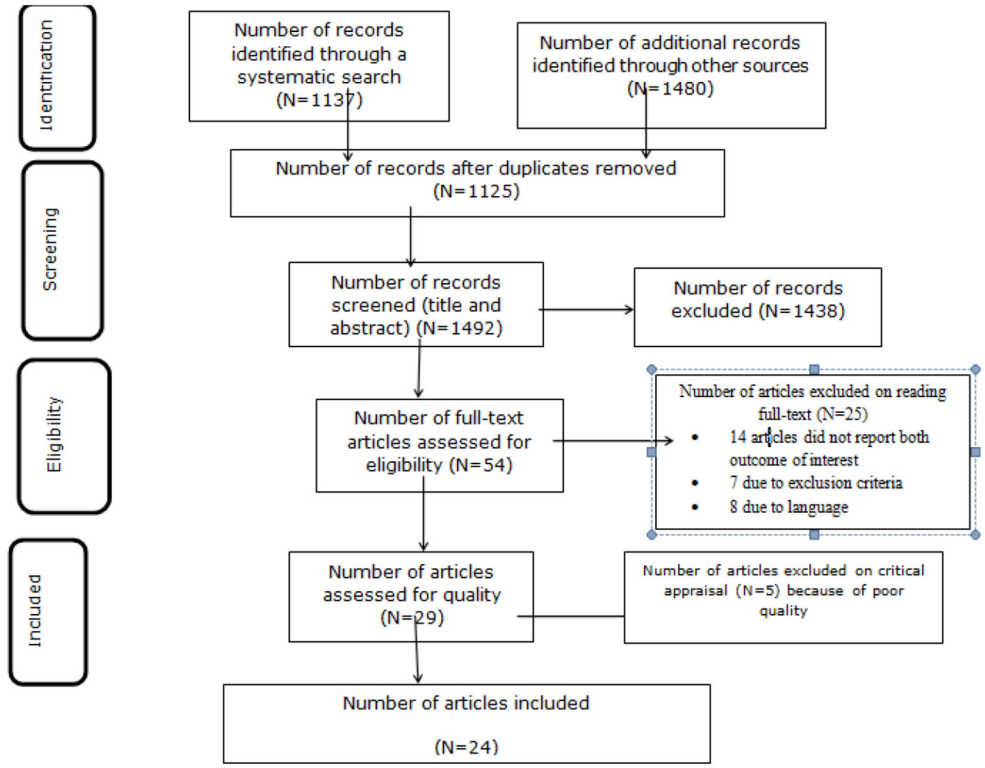

FIGURE 1 | PRISMA flow diagram of dyslipidemia in Africa, 2021.

RESULT

Search Results

Initially, a total of 1,137 studies were retrieved from the electronic databases and 1,480 articles were retrieved through manual searching. The total number of articles retrieved through an electronic database and manual searching was 2,617. From this, 1,125 were duplicates and removed from this systemic review. The remaining 1,492 articles were screened by their title and abstract and 1,438 irrelevant studies were removed. Then, 54 full-text articles were assessed for eligibility and 14 of them were excluded on the account of not reporting the outcome of interest, 7 studies were excluded due to exclusion criteria, and 8 studies were excluded due to language. Thereafter, 5 articles were excluded upon evaluation against the critical appraisal checklist of prevalence studies (23). Finally, 24 studies were included in this systematic review with meta-analysis (**Figure 1**).

Study Characteristics

A total of 24 articles from 10 African countries were included in this systematic review and meta-analysis. Out of 37,902 study subjects, 12,035 patients had dyslipidemia. The sample size across the studies ranges from 90 (30) to 10,690 (31). Out of 24 articles, nine were conducted in Ethiopia, four in South Africa, three in Nigeria, and two others in Kenya. The remainders of the studies of interest were conducted in Mozambique, Zambia, Senegal, Uganda, Togo, and Malawi. The highest prevalence of dyslipidemia was reported in a study from South Africa (89.9%) (14), and from Kenya (85.6%) (32). On the other hand, the lowest prevalence of dyslipidemia of 5.2% was reported in a study from Ethiopia (13). The highest percentage of LDL-C data was reported in a study from Ethiopia (79.7%) (33) (**Table 1**).

Prevalence of Dyslipidemia

The overall pooled prevalence of dyslipidemia in Africa using the fixed effect model was 16.5 (95% *CI* (16.0–16.5). When using the fixed effect model, the pooled effect size of dyslipidemia showed a significant heterogeneity (I^2) of 99.9% ($p < 0.001$). As a result, we determined the final pooled prevalence with a random-effect model to control the observed unevenness. The final pooled prevalence of dyslipidemia was 52.8 (95% *CI* (40.8–64.9) (**Figure 2**).

Heterogeneity

The subgroup analysis by the category of population and regions was done to handle the heterogeneity. In addition, we performed meta regression with sample size, prevalence, and year of publication. The details of subgroup analysis and meta regression were mentioned below.

Subgroup Analysis by the Category of Population or Study Participant

Subgroup analyses based on the underlying diseases and the countries revealed a marked variation in the prevalence of

TABLE 1 | Prevalence of dyslipidemia based on health status and for the general population in Africa, 2021.

Authors	Year	Country	Region	Study participant	Study design	Sample size	Frequency	LDL-C in %
Kemal et al. (16)	2020	Ethiopia	East Africa	Patients on ART	Cross-sectional	353	264	31.2
Kiplagat et al. (32)	2017	Kenya	East Africa	Type-2 DM	Cross-sectional	265	208	Not reported
Abdu et al. (33)	2020	Ethiopia	East Africa	Patients with *H. Pylori*	Cross-sectional	369	286	79.7
Haile et al. (34)	2020	Ethiopia	East Africa	Diabetes patients	Cross-sectional	248	169	28.6
Bekele et al. (35)	2017	Ethiopia	East Africa	Diabetes patients	Cross-sectional	224	150	43.8
Sufa et al. (8)	2019	Ethiopia	East Africa	General population	Cross-sectional	365	127	34.8
Okpala et al. (30)	2019	Nigeria	West Africa	Lichen Planus patients	Cross-sectional	90	15	Not reported
Yusuf et al. (36)	2015	Nigeria	West Africa	Lichen Planus patients	Cross-sectional	180	51	Not reported
Fikremariam et al. (37)	2018	Ethiopia	East Africa	Diabetes patients	Cross-sectional	112	94	Not reported
Ditorguéna et al. (38)	2019	Togo	West Africa	General population	Cross-sectional	746	450	0.7
Amberbir et al. (39)	2018	Malawi	Central Africa	HIV patients	Cross-sectional	554	86	Not reported
Tilahun et al. (2)	2021	Kenya	East Africa	HIV patients	Cross-sectional	564	265	26.6
Ciccacci et al. (40)	2021	Mozambique	Southern Africa	DM and HTN patients	Cross-sectional	885	410	Not reported
Hamooya et al. (41)	2021	Zambia	Central Africa	HIV patients	Cross-sectional	1,108	293	Not reported
Gebreegziabiher et al. (17)	2021	Ethiopia	East Africa	General population	Cross-sectional	370	204	49.5
Doupa et al. (42)	2014	Senegal	West Africa	General population	Cross-sectional	1,329	880	66.2
Asiki et al. (43)	2015	Uganda	East Africa	General population	Cross-sectional	7,809	5,567	5.2
Tadewos et al. (44)	2012	Ethiopia	East Africa	HIV	Comparative	113	67	48.7
Ayoadea et al. (45)	2020	Nigeria	West Africa	HTN patients	Cross-sectional	544	326	27.9
Dave et al. (14)	2016	South Africa	Southern Africa	HIV	Comparative	957	861	55.1
Jamieson et al. (31)	2017	South Africa	Southern Africa	HIV	Cohort study	10,690	595	Not reported
Pitso et al. (46)	2021	South Africa	Southern Africa	Diabetes	Cross-sectional	143	120	20.9
Innes et al. (47)	2016	South Africa	Southern Africa	HIV	Longitudinal	96	38	26
Gebreyes et al. (13)	2018	Ethiopia	East Africa	General population	National survey	9,788	509	14.1

**ART, anti-retroviral therapy and DM, diabetes mellitus.*

dyslipidemia. When we look at variation based on the category of study participant or population, the prevalence of dyslipidemia was the highest among the category of studies conducted on a group of participants with NCDs (patients with DM, HTN, and DM and HTN) [70.6 (95% *CI* (58.0–83.2)] and the general population [48.8 (95% *CI* (13.7–84.0)]. On the other hand, the lowest prevalence of dyslipidemia {43.7 [95% *CI* (18.9–68.5)]} was reported among studies conducted on a group of participants with infectious diseases (patients with HIV, *H. Pylori*, and Lichen Planus) (**Table 2**).

A Subgroup of Analysis by the Region

A subgroup analysis by the region showed that there was marked variation across the regions of the African continent. The highest prevalence of dyslipidemia found in East Africa was 60.8 [(95% *CI*: 35.5–86.0), $I^2 = 99.9$, $p < 0.001$] and Southern Africa was 53.1 (95% *CI*: 6.1–99.4), $I^2 = 100\%$, $p < 0.001$). The pooled prevalence of dyslipidemia in western Africa and Central Africa was 46.7 (95% *CI*: 32.4–60.9), $I^2 = 98.3$, $p < 0.001$) and 21.0 (95% *CI*: 10.3–31.7), $I^2 = 96.5$, $p < 0.001$), respectively. Out of 24 included studies, 12 studies were from East Africa, 5 studies were from western Africa, 5 studies were from southern Africa, and two studies were from central Africa. But, not a single study was included from the northern African region (**Figure 3**).

Meta Regression

We applied meta regression to identify the source of heterogeneity. Accordingly, random-effects meta regression was conducted by considering the year of publication, prevalence, and sample size as covariates. The analysis indicated that heterogeneity was explained by prevalence ($p = 0.02$) (**Table 3**).

Sensitivity Analysis

A sensitivity analysis was executed by removing studies step-by-step to evaluate the effect of a single study on the whole estimate. As shown in **Table 4**, no study exhibited an important effect on the final pooled prevalence of dyslipidemia.

Publication Bias

As indicated in **Figure 4**, the visual inspection of the funnel plot showed an asymmetrical distribution. When objectively evaluated against the Egger© regression test and an adjusted Begg© rank correlation test at a 5% significance level, we found $p < 0.001$ and 0.009, respectively. This confirmed that there was evidence of publication bias in this systematic review with meta-analysis. Therefore, Duval and Tweedie's trim and fill analysis (metatrim) using the random-effects model to see the impact of publication bias through the assumption that the funnel plot asymmetry was solely caused by publication bias might not hold for this dataset. The trim and fill analysis showed the presence of 13 unpublished studies. Considering

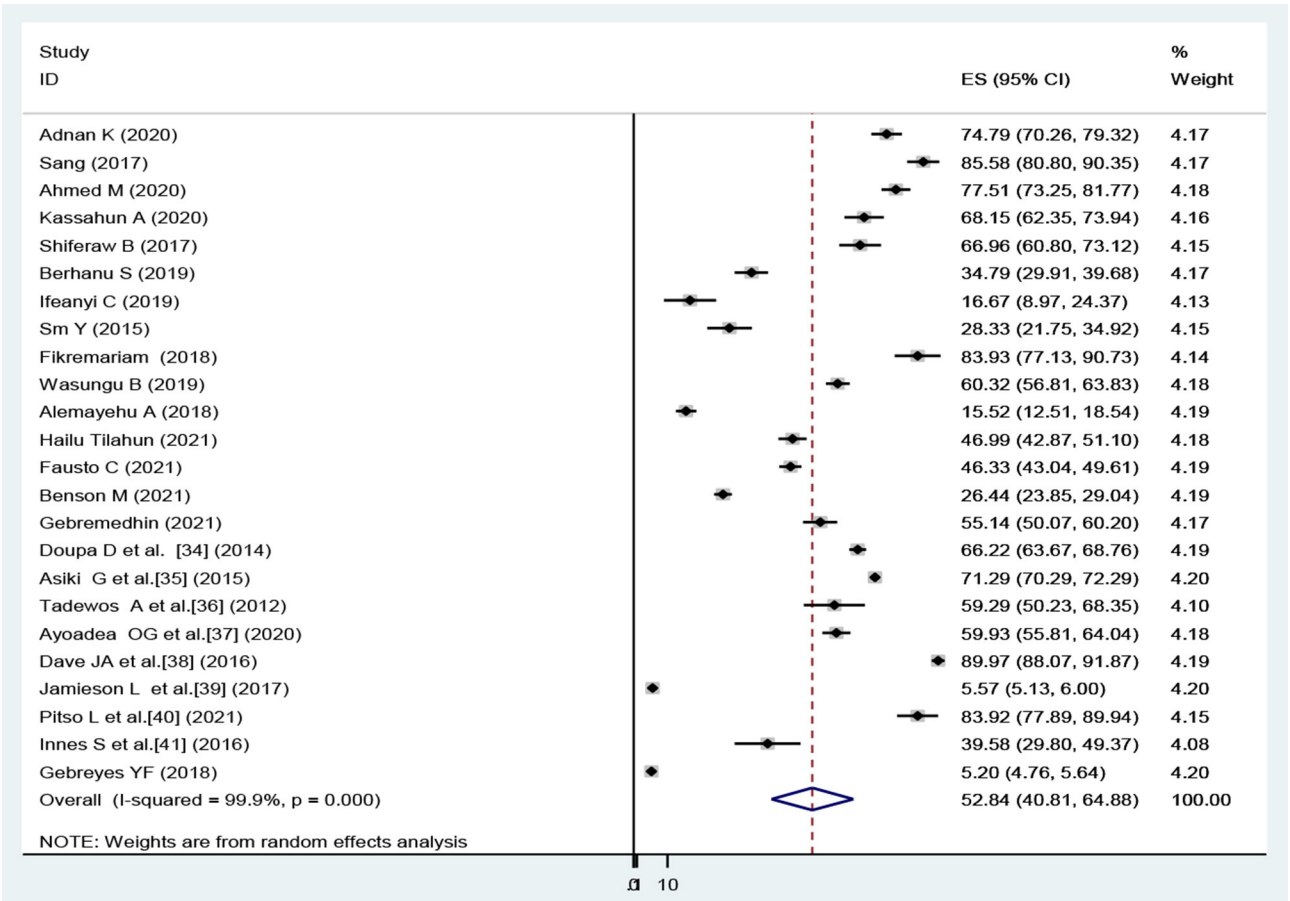

FIGURE 2 | Overall pooled prevalence of dyslipidemia by African regions, 2021.

TABLE 2 | The pooled prevalence of dyslipidemia, 95% *CI,* and heterogeneity estimate with a *p*-value for subgroup analysis.

Variable	Characteristics	Pooled prevalence 95% (CI)	I^2 (%)
Category of population	Patients with NCDs	70.6 (58.0–83.2)	97.8
	Patients with infectious disease	43.7 (18.9–68.5)	99.9
	General population	48.8 (13.7–84.0)	100

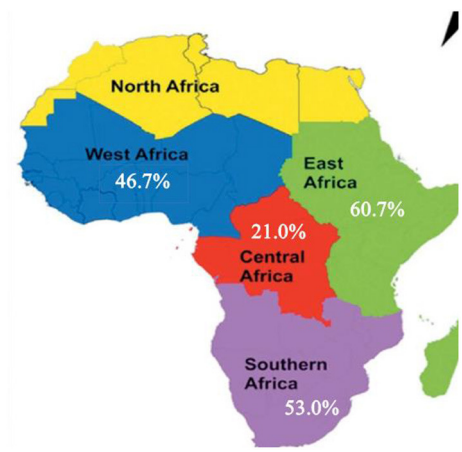

FIGURE 3 | Subgroup analyses on the pooled prevalence of dyslipidemia by African regions, 2021.

these studies in calculating the pooled prevalence yields, an estimated pooled prevalence of dyslipidemia, which is adjusted for publication bias was found to be 13.38% [95% *CI* (0.52–26 24); $p = 0.04$] (**Figure 5**).

As shown in the regression graph (**Figure 6**), the estimated bias coefficient (intercept) is 1.14 with an SE of 0.26, giving a $p < 0.001$ and *CI* of 0.58–1.70. Thus, the test provides strong evidence for small-study effects.

The funnel plot showed a small study effect; Hhowever, the counter-enhanced funnel plot showed that small studies were found both in the area of statistical significance (shaded area) and non-statistical significance (white area). So, the asymmetry may have been caused by a number of other factors rather than the publication bias (**Figure 7**). Similar findings also occurred

TABLE 3 | Meta regression analysis of factors affecting between study heterogeneity.

Heterogeneity source	Coef.	Std. Err.	T	P>t	[95% Conf. Interval]	
Year	0.01	0.13	0.10	0.92	−29.02	0.26
Prevalence	0.02	0.01	2.60	0.02*	−0.01	0.05
Sample size	0.00	0.00	0.90	0.38	−0.01	0.01

**Statistically significant variables at P value < 0.05.*

TABLE 4 | Sensitivity analysis of dyslipidemia among included study in Africa, 2021.

Study omitted	Country	Study participant	Estimate	[95% CI]	
Kemal et al. (16)	Ethiopia	Patients on ART	51.9	39.7	64.1
Kiplagat et al. (32)	Kenya	Type-2 DM	51.4	39.3	63.6
Abdu et al. (33)	Ethiopia	Patients with *H. Pylori*	51.8	39.6	63.9
Haile et al. (34)	Ethiopia	Diabetes patients	52.2	39.9	64.4
Bekele et al. (35)	Ethiopia	Diabetes patients	52.2	40.0	64.5
Sufa et al. (8)	Ethiopia	General population	53.6	41.3	65.9
Okpala et al. (30)	Nigeria	Lichen Planus patients	54.4	42.1	66.7
Yusuf et al. (36)	Nigeria	Lichen Planus patients	53.9	41.6	66.2
Fikremariam et al. (37)	Ethiopia	Diabetes patients	51.5	39.3	63.7
Ditorguéna et al. (38)	Togo	General population	52.5	40.3	64.8
Amberbir et al. (39)	Malawi	HIV patients	54.5	42.0	66.9
Tilahun et al. (2)	Kenya	HIV patients	53.1	40.8	65.4
Ciccacci et al. (40)	Mozambique	DM and HTN patients	53.1	40.8	65.4
Hamooya et al. (41)	Zambia	HIV patients	54.0	41.6	66.4
Gebreegziabiher et al. (17)	Ethiopia	General population	52.7	40.5	65.0
Doupa et al. (42)	Senegal	General population	52.3	40.1	64.4
Asiki et al. (43)	Uganda	General population	52.0	41.9	62.1
Tadewos et al. (44)	Ethiopia	HIV	52.6	40.3	64.8
Ayoadea et al. (45)	Nigeria	HTN patients	52.5	40.3	64.8
Dave et al. (14)	South Africa	HIV	51.2	40.0	62.5
Jamieson et al. (31)	South Africa	HIV	54.9	40.0	71.9
Pitso et al. (46)	South Africa	Diabetes	51.5	39.3	63.7
Innes et al. (47)	South Africa	HIV	53.4	41.1	65.7
Gebreyes et al. (13)	Ethiopia	General population	54.9	38.0	71.8
Combined			52.8	40.8	64.9

when we performed the metric counter-enhanced funnel plot (**Figure 8**).

Determinants of Dyslipidemia in Africa

Furthermore, 11 variables were extracted to identify factors associated with dyslipidemia. Of these variables, 9 of them (sex, medication adherence, educational status, FBS, BP, BMI, WC, marital status, and sedentary life) were significantly associated with dyslipidemia at $p < 0.05$.

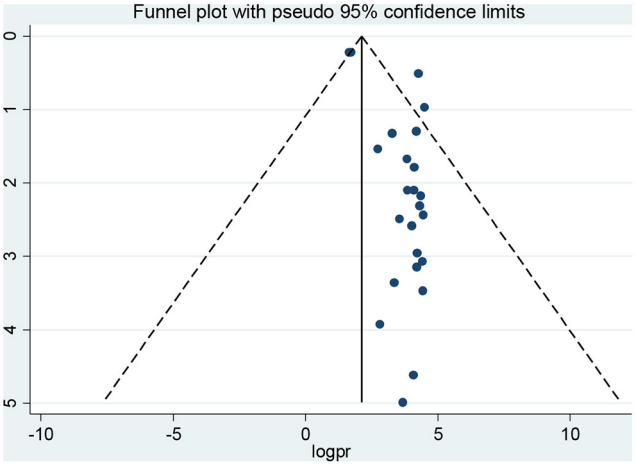

FIGURE 4 | Funnel plots for publication bias for the prevalence of dyslipidemia in Africa, 2021.

Patients with BMI >25 kg/m^2 and patients with WC >94 cm were about 2.36 and 2.3 times more likely to develop dyslipidemia, as compared with their counterparts (odds ratio (*OR*): 2.36 (95% *CI* (1.33–4.18), $p < 0.001$, I^2: 89.6%) and *OR*: 2.33 [95% *CI* (0.75–7.29), $p < 0.001$, I^2: 89.6%)]. Patients with DM were about 2.3 times more likely to have dyslipidemia, as compared with non-diabetic patients {*OR*: 2.32 [95% *CI* (0.89–6.04)] $p < 0.001$, I^2: 88.1%}. Furthermore, known smoker patients were about 132% more likely to develop dyslipidemia, as compared with non-smoker patients {*OR*: 1.32 [95% *CI* (0.74–2.35)] $p = 0.05$, I^2: 80.7%].

This study also showed that patients with HTN were about 2 times more likely to have dyslipidemia when compared with non-hypertensive patients {*OR*: 2.05 [95% *CI* (1.31–3.21)], $p < 0.001$, I^2: 85%}. Furthermore, patients who had no history of alcohol consumption and sedentary lifestyles were about 20% less likely to develop dyslipidemia than their counterparts {*OR*: 0.862 [95% *CI* (0.68–1.11)] and *OR*: 0.80 [95% *CI* (0.63–1.10)]}, respectively (**Table 5**).

DISCUSSION

Dyslipidemia has emerged as an important cardiovascular risk factor in African countries (17). It is characterized by LDL-C increment, TG elevation, and HDL-C decrement or combined. The *LDLR* positioned on chromosome 19p13.2 plays a significant role in lipoprotein metabolism by mediating the uptake of cholesterol through the binding and subsequent cellular uptake of apolipoprotein-E and B- constituting lipoproteins. Mutations have been detected in different domains of the *LDLR* which have a distinct effect on LDLR structure and function. ATP-binding cassette A1 (*ABCA1*) plays a critical role in the reverse cholesterol transport system. Mutation in *ABCA1*, that encodes this protein, along with genes responsible for their transcription regulation, can lead to abnormality in the metabolism of lipids

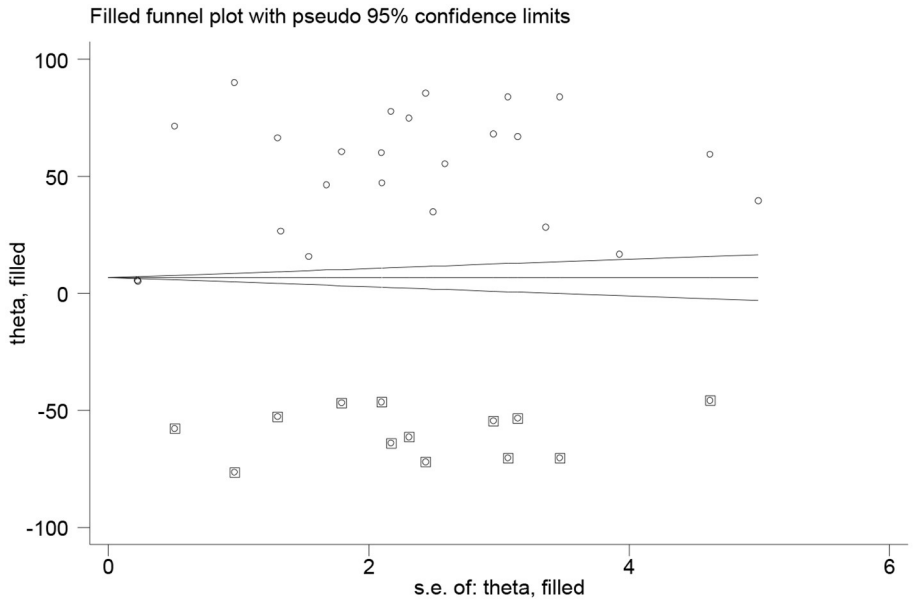

FIGURE 5 | Trim and fill analysis for the prevalence of dyslipidemia in Africa, 2021.

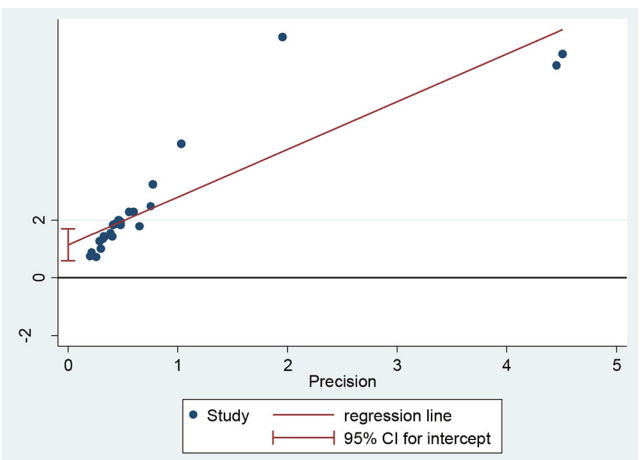

FIGURE 6 | Regression graph of dyslipidemia in Africa, 2021.

(48). Apolipoprotein A5 (*APOA5*) has been shown to be a key regulator of plasma TGs and there are several single nucleotide polymorphisms (SNPs) associated with the *APOA5* gene (49). Future research should address the lack of LDL-C oxidation data generated by existing studies.

The prevalence of dyslipidemia in this review is higher than the finding of the study conducted among the hormonal contraceptive users from April to June 2014 at three health centers and one hospital in Harar town, Eastern Ethiopia (34.8%) (8). However, the present finding is lower than the findings of the study in Jimma, Southwestern Ethiopia (68.1%) (34), and South Africa (67.3%) (50). The finding of this review was also lower than the finding of a study done in Kembata, Southern Ethiopia (65.5%) (35), and Mekelle city, Northern Ethiopia (66.7%) (17). The higher prevalence of dyslipidemia might be attributed to the rapid urbanization, improved socioeconomic status, a change in the power of work, inadequate physical activity, and alteration in dietary habits.

The present study showed that the raised FBG was positively associated with dyslipidemia, which agrees with many previous studies (8, 51, 52). This might be because DM can cause a range of derangements in oxidation or reduction in lipid metabolism, which could in turn be responsible for the accumulation of lipid particles (34). We also revealed that the raised BP level was an independent predictor of dyslipidemia, which is consistent with the study conducted in Germany (52); but, the findings of this review disagree with the findings of the study reported in Iraq (53). This variation might be due to differences in the underlying disease, socio-demographic factors, genetic predisposition, dietary factors, and inadequate physical activity, which results in a higher incidence of metabolic abnormalities.

In the current review, BMI was found to have a positive association with dyslipidemia, which is consistent with many previous studies (16, 51, 54, 55). This finding is also similar to studies conducted in Ethiopia (44), Uganda (56), and Tanzania (57). However, previous works have doubted the reliability of BMI as an indicator of obesity (58, 59). Moreover, in young healthy adults, BMI and other surrogate indices of fatness, such as waist-to-height ratio and body adiposity index provide a poor prognosis of fat mass (60, 61). The observed association in other studies can be supported by the

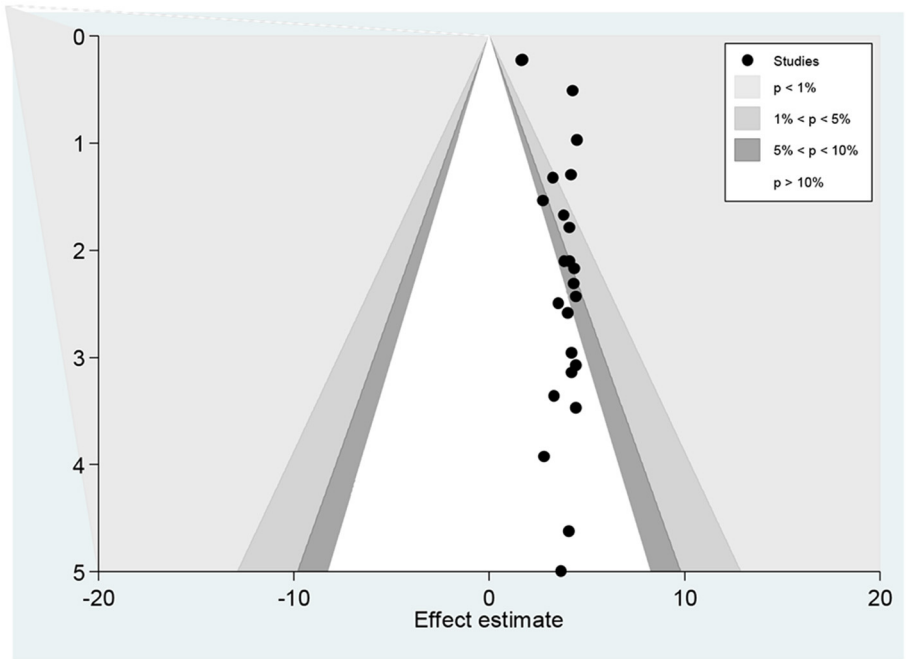

FIGURE 7 | Counter enhanced funnel plots for publication bias for the prevalence of dyslipidemia in Africa, 2021.

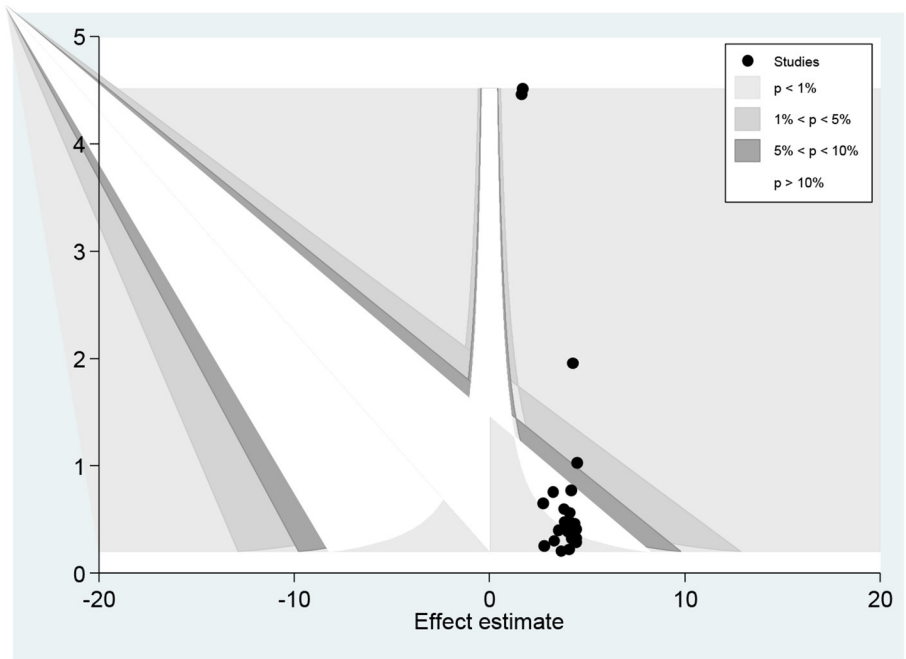

FIGURE 8 | Meric inverse counter enhanced funnel plots of publication bias for the prevalence of dyslipidemia in Africa, 2021.

occurrence of ART associated lipodystrophy, which may be accompanied by the loss of peripheral subcutaneous fat (62). The other differences may be because the current review was conducted on participants with underlying different types of disease while other studies conducted only on patients with HIV and DM.

In our review, abdominal obesity or WC $\geq$ 94 cm was significantly associated with dyslipidemia, which agrees with

TABLE 5 | Factors associated with dyslipidemia in Africa, 2021.

Determinants	Comparison	Number OF studies	Sample size	OR (95% CI)	*P*-value	I^2 (%)	Heterogeneity test (*P*-value)	Egger© test (*P*-value)
Sex (16, 32–35, 39–41)	Male vs. female	8	3,596	0.86 (0.67–1.08)	<0.001*	72	0.19	0.17
Smoking (16, 32, 34)	Yes vs. no	3	809	1.32 (0.74–2.35)	0.47	0.0	0.35	0.18
Medication adherence (16, 32)	No vs. yes	2	561	0.80 (0.52–1.23)	0.03*	79.9	0.31	-
Educational status (8, 32, 34, 35)	Illiterate vs. literate	4	1,044	1.19 (0.90–1.57)	0.01*	75	0.22	0.95
FBS (17, 32, 34, 40)	Positive vs. negative	4	1,622	2.32 (0.89–6.05)	<0.001*	88.1	0.09	0.10
Residence (33–35, 39)	Rural vs. urban	4	1,395	0.75 (0.40–1.40)	0.14	49.8	0.37	<0.001*
BP (16, 17, 32–35, 40)	High vs. low	7	2,507	2.05 (1.31–3.21)	<0.001*	75.4	<0.001	0.09
Alcohol (16, 32, 34, 38)	Yes vs. no	5	1,924	0.86 (0.68–1.09)	0.49	41.3	0.208	0.20
BMI (16, 17, 32, 34, 35, 37, 38, 40)	Yes vs. no	8	3,436	2.36 (1.33–4.18)	<0.001*	89.6	<0.001	0.58
WC (17, 33, 40)	≥94 vs. <94 cm	3	393	2.33 (0.75–7.29)	<0.001*	93.6	0.15	0.28
Marital status (8, 32, 34)	Married vs. single	3	841	1.174 (0.65–2.10)	<0.001	75	0.59	0.95
Sedentary life (16, 32, 34, 38)	Yes vs. no	4	1,555	0.80 (0.63–1.03)	0.04*	64.9	0.08	0.41

FBS, fasting blood sugar; BP, blood pressure; BMI, body mass index; OR, odds ratio; vs., versus.

- Insufficient observation. Egger test P-value was not calculated if degree of freedom is zero due to insufficient number of study.

**Statistically significant variables at P-value < 0.05.*

other studies (34, 63). So far, anthropometric measurements, such as BMI, have been the most widely used instrument to measure general obesity. However, BMI does not account for the variation in body fat distribution and abdominal fat (64, 65). Excess of intra-abdominal fat causes a greater risk of morbidity than the overall fat accumulation (66). Thus, WC has been by far the best indicator of both intra-abdominal and total fat (67). Generally, altered anthropometric (68) and adipose tissue size have been associated with dyslipidemia in persons with and without HIV (69, 70). We found that the prevalence of dyslipidemia was almost equally determined by both BMI and WC. This might be due to a high chance of increasing concentrations of different lipid particles with increased BMI. Therefore, the combination of different anthropometric measurements should be used to evaluate the health condition of the patient or population.

Similar to the current review, studies conducted in South Africa (71), Cameroon (72) showed that being the female gender was not associated with a higher probability of presenting with dyslipidemia. In contrast to our review, the findings of a study done in Tanzania showed that being the female gender was an independent predictor of dyslipidemia (57). The discrepancy is more likely due to gender-related exercise, habits, and biological differences between men and women (27). Moreover, this study also found that lower odds of dyslipidemia were found among participants who have attained a lower level of education when compared with those who attended college and above. This is in agreement with other studies (41, 73). In contrast, other studies found contradicting results (74, 75). This may be due to differences in lifestyle.

In this study, sex, increased BMI, increased BP, and sedentary lifestyles were significantly associated with the increased risk of dyslipidemia. As all are modifiable risk factors except sex, it is essential to deliver behavioral interventions on the identified risk factors. Dietary modification is one of the most important lifestyle changes that have been shown to significantly decrease the risk of CVD. The CVD burden is reduced by optimum diet through the replacement of unprocessed meat with low saturated fat, animal proteins, and plant proteins (76). The recommended Dietary Reference Intake (DRI) daily allowance in men aged 19–50 years is 38 g/day and women aged 19–50 years is 25 g/days, and for men aged >51 is 31 g/day and women aged >51 is 21 g/day. The recommendation for children aged 1–3 is 19 g/day and aged 4–8 is 25 g/day. For boys, aged 9–13, the DRI recommendations are 31 g/day and 38 g/days for aged 14–18. For girls aged 9–18, the DRI recommendations are 26 g/day (77). Individuals are also recommended to intake fruit and vegetables at least 5 servings per day, perform moderate activity for more than 150 min/week, do vigorous physical activity for at least 75 min/ week, reduce salt and sugar intake to prevent dyslipidemia (2).

LIMITATIONS

The limitations of this systematic review with meta-analysis include some studies did not have enough predictor variables to adequately determine the degree of its prediction, However, attempts were made to include all other potential variables that occurred across the identified database. Another limitation of this study was that we did not identify the association between diet and dyslipidemia because we could not retrieve data from original articles. To overcome such problems, important discussions were made concerning the quantity and quality of daily intake. It might also lack continental representativeness since no information was found from northern regions of the African continent. But, the demographic characteristics of the population in the North African region were almost similar to the rest of the other regions.

CONCLUSION

This review exposed that dyslipidemia is relatively high among study participants. The prevalence of dyslipidemia was the highest among the category of studies conducted on a group of communicable diseases and the general population. On the other hand, the lowest prevalence of dyslipidemia was reported among studies conducted on a group of infectious diseases. In addition, the highest prevalence of dyslipidemia was found among studies from East Africa and Southern Africa. The independent predictors of dyslipidemia were BMI >25.0 kg/m^2, raised FBG, raised BP, and WC $>$ 94 cm. In addition, sex, medication adherence, educational status, FBG, BP, BMI, WC, marital status, and sedentary life were strongly associated with dyslipidemia. There should also be a pressing public health measure to prevent, identify, and treat dyslipidemia with a special emphasis on obese, diabetic, and hypertensive patients. Future researchers were recommended to address the association between diet and dyslipidemia.

DATA AVAILABILITY STATEMENT

The original contributions presented in the study are included in the article/**Supplementary Material**, further inquiries can be directed to the corresponding author/s.

AUTHOR CONTRIBUTIONS

MO and GA were involved in the selection of study, data extraction, quality assessment, statistical analysis, results interpretation, and writing the initial and final drafts of the manuscript. GAA, BW, TT, NAw, NAy, YH, and BJ were involved in data extraction, quality assessment, statistical analysis, and writing drafts of the manuscript. All authors read and approved the final manuscript, contributed to the article, and approved the submitted version.

ACKNOWLEDGMENTS

We would like to thank all authors of included articles.

SUPPLEMENTARY MATERIAL

The Supplementary Material for this article can be found online at: https://www.frontiersin.org/articles/10.3389/fcvm.2021.778891/full#supplementary-material

REFERENCES

1. De Backer G, Jankowski P, Kotseva K, Mirrakhimov E, Reiner Ž, Rydén L, et al. Management of dyslipidaemia in patients with coronary heart disease: results from the ESC-EORP EUROASPIRE V survey in 27 countries. *Atherosclerosis*. (2019) 285:135–46. doi: 10.1016/j.atherosclerosis.2019.03.014
2. Tilahun H, Masyuko SJ, Mogaka JN, Temu T, Kinuthia J, Osoti AO, et al. Prevalence and correlates of dyslipidemia in HIV positive and negative adults in Western Kenya: a cross-sectional study. *Medicine*. (2021) 100:e24800. doi: 10.1097/MD.0000000000024800
3. Ríos-González BE, Luévano-Ortega KE, Saldaña-Cruz AM, González-García JR, Magaña-Torres MT. Polymorphisms of seven genes involved in lipid metabolism in an unselected Mexican population. *J Genet.* (2011) 90:1–6. doi: 10.1007/s12041-011-0118-2
4. Chang M-h, Yesupriya A, Ned RM, Mueller PW, Dowling NF. Genetic variants associated with fasting blood lipids in the US population: third national health and nutrition examination survey. *BMC Med Genet.* (2010) 11:62. doi: 10.1186/1471-2350-11-62
5. Leren TP, Berge KE. Subjects with molecularly defined familial hypercholesterolemia or familial defective apoB-100 are not being adequately treated. *PLoS ONE.* (2011) 6:e16721. doi: 10.1371/journal.pone.0016721
6. Thompson PD, Myerburg RJ, Levine BD, Udelson JE, Kovacs RJ. Eligibility and disqualification recommendations for competitive athletes with cardiovascular abnormalities: task force 8: coronary artery disease: a scientific statement from the American Heart Association and American College of Cardiology. *Circulation.* (2015) 132:e310–4. doi: 10.1161/CIR.0000000000000244
7. Janhäll S, Olofson KFG, Andersson PU, Pettersson JB, Hallquist M. Evolution of the urban aerosol during winter temperature inversion episodes. *Atmosph Environ.* (2006) 40:5355–66. doi: 10.1016/j.atmosenv.2006.04.051
8. Sufa B, Abebe G, Cheneke W. Dyslipidemia and associated factors among women using hormonal contraceptives in Harar town, Eastern Ethiopia. *BMC Res Notes.* (2019) 12:120. doi: 10.1186/s13104-019-4148-9
9. Gouda HN, Charlson F, Sorsdahl K, Ahmadzada S, Ferrari AJ, Erskine H, et al. Burden of non-communicable diseases in sub-Saharan Africa, 1990–2017: results from the Global Burden of Disease Study 2017. *Lancet Glob Health.* (2019) 7:e1375–87. doi: 10.1016/S2214-109X(19)30374-2
10. Ellis R. Infection and coronary heart disease. *J Med Microbiol.* (1997) 46:535–9. doi: 10.1099/00222615-46-7-535
11. Tripathy JP, Thakur J, Jeet G, Chawla S, Jain S, Pal A, et al. Burden and risk factors of dyslipidemia-results from a STEPS survey in Punjab India. *Diabetes Metab Syndr.* (2017) 11:S21–7. doi: 10.1016/j.dsx.2016.08.015
12. Tsai F-J, Cheng C-F, Lai C-H, Wu Y-C, Ho M-W, Wang J-H, et al. Effect of antiretroviral therapy use and adherence on the risk of hyperlipidemia among HIV-infected patients, in the highly active antiretroviral therapy era. *Oncotarget.* (2017) 8:106369. doi: 10.18632/oncotarget.22465
13. Gebreyes YF, Goshu DY, Geletew TK, Argefa TG, Zemedu TG, Lemu KA, et al. Prevalence of high bloodpressure, hyperglycemia, dyslipidemia, metabolic syndrome and their determinants in Ethiopia: evidences from the National NCDs STEPS Survey, 2015. *PLoS ONE.* (2018) 13:e0194819. doi: 10.1371/journal.pone.0194819

14. Dave JA, Levitt NS, Ross IL, Lacerda M, Maartens G, Blom D. Anti-retroviral therapy increases the prevalence of dyslipidemia in South African HIV-infected patients. *PLoS ONE.* (2016) 11:e0151911. doi: 10.1371/journal.pone.0151911
15. Bays HE, Toth PP, Kris-Etherton PM, Abate N, Aronne LJ, Brown WV, et al. Obesity, adiposity, and dyslipidemia: a consensus statement from the National Lipid Association. *J Clin Lipidol.* (2013) 7:304–83. doi: 10.1016/j.jacl.2013.04.001
16. Kemal A, Teshome MS, Ahmed M, Molla M, Malik T, Mohammed J, et al. Dyslipidemia and associated factors among adult patients on antiretroviral therapy in armed force comprehensive and specialized hospital, Addis Ababa, Ethiopia. *HIV AIDS*. (2020) 12:221. doi: 10.2147/HIV.S252391
17. Gebreegziabiher G, Belachew T, Mehari K, Tamiru D. Prevalence of dyslipidemia and associated risk factors among adult residents of Mekelle City, Northern Ethiopia. *PLoS ONE.* (2021) 16:e0243103. doi: 10.1371/journal.pone.0243103
18. Koller R, Agyemang C. Prevalence of cardiovascular disease risk factors in the gambia: a systematic review. *Glob Heart.* (2020) 15:42. doi: 10.5334/gh.827
19. Otemuyiwa IO, Adewusi SR. Food choice and meal consumption pattern among undergraduate students in two universities in Southwestern Nigeria. *Nutr Health.* (2012) 21:233–45. doi: 10.1177/0260106013510994
20. Popkin BM, Adair LS, Ng SW. Global nutrition transition and the pandemic of obesity in developing countries. *Nutr Rev.* (2012) 70:3–21. doi: 10.1111/j.1753-4887.2011.00456.x
21. Agyei-Mensah S, Aikins Ad-G. Epidemiological transition and the double burden of disease in Accra, Ghana. *J Urban Health.* (2010) 87:879–97. doi: 10.1007/s11524-010-9492-y
22. Haregu TN, Byrnes A, Singh K, Sathish T, Pasricha N, Wickramasinghe K, et al. A scoping review of non-communicable disease research capacity strengthening initiatives in low and middle-income countries. *Glob Health Res Policy.* (2019) 4:1–11. doi: 10.1186/s41256-019-0123-1
23. Buccheri RK, Sharifi C. Critical appraisal tools and reporting guidelines for evidence-based practice. *Worldviews Evid Based Nurs.* (2017) 14:463–472. doi: 10.1111/wvn.12258
24. Expert Panel on Detection E. Executive summary of the third report of the National Cholesterol Education Program (NCEP) expert panel on detection, evaluation, and treatment of high blood cholesterol in adults (adult treatment panel III). *JAMA.* (2001) 285:2486–97. doi: 10.1001/jama.285.19.2486
25. Scuteri A, Cunha PG, Rosei EA, Badariere J, Bekaert S, Cockcroft JR, et al. Arterial stiffness and influences of the metabolic syndrome: a cross-countries study. *Atherosclerosis.* (2014) 233:654–60. doi: 10.1016/j.atherosclerosis.2014.01.041
26. Alberti KG, Eckel RH, Grundy SM, Zimmet PZ, Cleeman JI, Donato KA, et al. Harmonizing the metabolic syndrome: a joint interim statement of the international diabetes federation task force on epidemiology and prevention; national heart, lung, and blood institute; American heart association; world heart federation; international atherosclerosis society; and international association for the study of obesity. *Circulation.* (2009) 120:1640–5. doi: 10.1161/CIRCULATIONAHA.109.192644
27. World Health Organization. *Body Mass Index—BMI 2020*. Nutrition and food security [Google Scholar] (2020).
28. Alberti KGMM, Zimmet P, Shaw J. Metabolic syndrome—a new world-wide definition. A consensus statement from the international diabetes federation. *Diab Med.* (2006) 23:469–80. doi: 10.1111/j.1464-5491.2006.01858.x
29. Barendregt JJ, Doi SA, Lee YY, Norman RE, Vos T. Meta-analysis of prevalence. *J Epidemiol Community Health.* (2013) 67:974–8. doi: 10.1136/jech-2013-203104
30. Okpala IC, Akinboro AO, Ezejoifor IO, Onunu AN, Okwara BU. Metabolic syndrome and dyslipidemia among Nigerians with lichen planus: a cross-sectional study. *Indian J Dermatol.* (2019) 64:303. doi: 10.4103/ijd.IJD_111_18
31. Jamieson L, Evans D, Brennan A, Moyo F, Spencer D, Mahomed K, et al. Changes in elevated cholesterol in the era of tenofovir in South Africa: risk factors, clinical management and outcomes. *HIV Med.* (2017) 18:595–603. doi: 10.1111/hiv.12495
32. Kiplagat SV, Lydia K, Jemimah K, Drusilla M. Prevalence of dyslipidemia and the associated factors among Type 2 diabetes patients in Turbo Sub-County, Kenya. *J Endocrinol Diab.* (2017) 4:1–9. doi: 10.15226/2374-6890/4/5/00190
33. Abdu A, Cheneke W, Adem M, Belete R, Getachew A. Dyslipidemia and associated factors among patients suspected to have helicobacter pylori infection at Jimma University Medical Center, Jimma, Ethiopia. *Int J Gen Med.* (2020) 13:311. doi: 10.2147/IJGM.S243848
34. Haile K, Timerga A. Dyslipidemia and its associated risk factors among adult type-2 diabetic patients at Jimma University Medical Center, Jimma, Southwest Ethiopia. *Diab Metab Syndrome Obes Targets Ther.* (2020) 13:4589. doi: 10.2147/DMSO.S283171
35. Bekele S, Yohannes T, Mohammed AE. Dyslipidemia and associated factors among diabetic patients attending Durame General Hospital in Southern Nations, Nationalities, and People's Region. *Diab Metab Syndrome Obes Targets Ther.* (2017) 10:265. doi: 10.2147/DMSO.S135064
36. Yusuf S, Tijjani U, Maiyaki M, Nashabaru I, Uloko A, Gezawa I. Dyslipidemia: Prevalence and associated risk factors among patients with Lichen Planus in Kano, North-West Nigeria. *Nig Q J Hosp Med*. (2015) 25:145–50.
37. Fikremariam T. *Evaluation of Dyslipidemia, Nutritional Status and Other Associated Factors Among Diabetic Mellitus Patients at Felege Hiwot Referral Hospital*. Bahir Dar (2020).
38. Ditorguéna WB, Guy B-eE, Apélété AY, Francis DS, Borgatia A, Souleymane P, et al. Profile and prevalence of dyslipidemia in workplace in Togo. *J Health Environ Res*. (2019) 5:50–3. doi: 10.11648/j.jher.20190502.13
39. Amberbir A, Singano V, Matengeni A, Ismail Z, Kawalazira G, Chan AK, et al. Dyslipidemia among rural and urban HIV patients in south-east Malawi. *PLoS ONE*. (2018) 13:e0197728. doi: 10.1371/journal.pone.0197728
40. Ciccacci F, Majid N, Petrolati S, Agy M, Massango C, Orlando S, et al. Hypercholesterolemia and related risk factors in a cohort of patients with diabetes and hypertension in Maputo, Mozambique. *Pan Afr Med J.* (2021) 38:102. doi: 10.11604/pamj.2021.38.102.27284
41. Hamooya BM, Mulenga LB, Masenga SK, Fwemba I, Chirwa L, Siwingwa M, et al. Metabolic syndrome in Zambian adults with human immunodeficiency virus on antiretroviral therapy: Prevalence and associated factors. *Medicine*. (2021) 100:e25236. doi: 10.1097/MD.0000000000025236
42. Doupa D, Mbengue AS, Diallo FA, Jobe M, Ndiaye A, Kane A, et al. Lipid profile frequency and the prevalence of dyslipidaemia from biochemical tests at Saint Louis University Hospital in Senegal. *Pan Afr Med J.* (2014) 17:75. doi: 10.11604/pamj.2014.17.75.3577
43. Asiki G, Murphy GA, Baisley K, Nsubuga RN, Karabarinde A, Newton R, et al. Prevalence of dyslipidaemia and associated risk factors in a rural population in South-Western Uganda: a community based survey. *PLoS ONE.* (2015) 10:e0126166. doi: 10.1371/journal.pone.0126166
44. Tadewos A, Addis Z, Ambachew H, Banerjee S. Prevalence of dyslipidemia among HIV-infected patients using first-line highly active antiretroviral therapy in Southern Ethiopia: a cross-sectional comparative group study. *AIDS Res Ther.* (2012) 9:31. doi: 10.1186/1742-6405-9-31
45. Ayoade OG, Umoh I, Amadi C. Dyslipidemia and associated risk factors among Nigerians with hypertension. *Dubai Med J.* (2020) 3:155–61. doi: 10.1159/000509570
46. Pitso L, Mofokeng TRP, Nel R. Dyslipidaemia pattern and prevalence among type 2 diabetes mellitus patients on lipid-lowering therapy at a tertiary hospital in central South Africa. *BMC Endocr Disord.* (2021) 21:1–10. doi: 10.1186/s12902-021-00813-7
47. Innes S, Abdullah KL, Haubrich R, Cotton MF, Browne SH. High prevalence of dyslipidemia and insulin resistance in HIV-infected pre-pubertal African children on antiretroviral therapy. *Pediatr Infect Dis J.* (2016) 35:e1. doi: 10.1097/INF.0000000000000927
48. Wang X, Guo H, Li Y, Wang H, He J, Mu L, et al. Interactions among genes involved in reverse cholesterol transport and in the response to environmental factors in dyslipidemia in subjects from the Xinjiang rural area. *PLoS ONE.* (2018) 13:e0196042. doi: 10.1371/journal.pone.0196042
49. Chen SN, Cilingiroglu M, Todd J, Lombardi R, Willerson JT, Gotto AM, et al. Candidate genetic analysis of plasma high-density lipoprotein-cholesterol and severity of coronary atherosclerosis. *BMC Med Genet.* (2009) 10:111. doi: 10.1186/1471-2350-10-111
50. Reiger S, Jardim TV, Abrahams-Gessel S, Crowther NJ, Wade A, Gomez-Olive FX, et al. Awareness, treatment, and control of dyslipidemia in rural South Africa: the HAALSI (Health and Aging in Africa: a Longitudinal Study

of an INDEPTH Community in South Africa) study. *PLoS ONE.* (2017) 12:e0187347. doi: 10.1371/journal.pone.0187347
51. Wang S, Xu L, Jonas JB, You QS, Wang YX, Yang H. Prevalence and associated factors of dyslipidemia in the adult Chinese population. *PLoS ONE.* (2011) 6:e17326. doi: 10.1371/journal.pone.0017326
52. Du Y, Rosner BM, Knopf H, Schwarz S, Dören M, Scheidt-Nave C. Hormonal contraceptive use among adolescent girls in Germany in relation to health behavior and biological cardiovascular risk factors. *J Adolesc Health.* (2011) 48:331–7. doi: 10.1016/j.jadohealth.2011.01.004
53. Abdel Barry J, Flaf M, Al Namaa L, Hassan N. Lipoprotein changes in women taking low-dose combined oral contraceptive pills: a cross-sectional study in Basra, Iraq. *East Mediterr Health J.* 17:684–8, (2011) (2011). doi: 10.26719/2011.17.9.684
54. Lumu W, Kampiire L, Akabwai GP, Ssekitoleko R, Kiggundu DS, Kibirige D. Dyslipidaemia in a Black African diabetic population: burden, pattern and predictors. *BMC Res Notes.* (2017) 10:587. doi: 10.1186/s13104-017-2916-y
55. Pan J, Ren Z, Li W, Wei Z, Rao H, Ren H, et al. Prevalence of hyperlipidemia in Shanxi Province, China and application of Bayesian networks to analyse its related factors. *Sci Rep.* (2018) 8:1–9. doi: 10.1038/s41598-018-22167-2
56. Kazooba P, Kasamba I, Mayanja BN, Lutaakome J, Namakoola I, Salome T, et al. Cardiometabolic risk among HIV-POSITIVE Ugandan adults: prevalence, predictors and effect of long-term antiretroviral therapy. *Pan Afr Med J.* (2017) 27:40. doi: 10.11604/pamj.2017.27.40.9840
57. Ombeni W, Kamuhabwa AR. Lipid profile in HIV-infected patients using first-line antiretroviral drugs. *J Int Assoc Providers AIDS Care.* (2016) 15:164–71. doi: 10.1177/2325957415614642
58. Heo M, Faith MS, Pietrobelli A, Heymsfield SB. Percentage of body fat cutoffs by sex, age, and race-ethnicity in the US adult population from NHANES 1999–2004. *Am J Clin Nutr.* (2012) 95:594–602. doi: 10.3945/ajcn.111.025171
59. Shah NR, Braverman ER. Measuring adiposity in patients: the utility of body mass index (BMI), percent body fat, and leptin. *PLoS ONE.* (2012) 7:e33308. doi: 10.1371/journal.pone.0033308
60. Zaccagni L, Barbieri D, Gualdi-Russo E. Body composition and physical activity in Italian university students. *J Transl Med.* (2014) 12:1–9. doi: 10.1186/1479-5876-12-120
61. Heymsfield SB, Scherzer R, Pietrobelli A, Lewis CE, Grunfeld C. Body mass index as a phenotypic expression of adiposity: quantitative contribution of muscularity in a population-based sample. *Int J Obes.* (2009) 33:1363–73. doi: 10.1038/ijo.2009.184
62. Liu E, Armstrong C, Spiegelman D, Chalamilla G, Njelekela M, Hawkins C, et al. First-line antiretroviral therapy and changes in lipid levels over 3 years among HIV-infected adults in Tanzania. *Clin Infect Dis.* (2013) 56:1820–8. doi: 10.1093/cid/cit120
63. Katz EG, Stevens J, Truesdale KP, Cai J, Adair LS, North KE. Hip circumference and incident metabolic risk factors in Chinese men and women: the People's Republic of China study. *Metab Syndrome Relat Disord.* (2011) 9:55–62. doi: 10.1089/met.2010.0045
64. World Health Organization. *Physical status: The use of and interpretation of anthropometry, Report of a WHO Expert Committee*. World Health Organization (1995).
65. Dalton M, Cameron AJ, Zimmet PZ, Shaw JE, Jolley D, Dunstan DW, et al. Waist circumference, waist–hip ratio and body mass index and their correlation with cardiovascular disease risk factors in Australian adults. *J Intern Med.* (2003) 254:555–63. doi: 10.1111/j.1365-2796.2003.01229.x
66. Visscher T, Kromhout D, Seidell J. Long-term and recent time trends in the prevalence of obesity among Dutch men and women. *Int J Obes.* (2002) 26:1218–24. doi: 10.1038/sj.ijo.0802016
67. Lemieux S, Prud'homme D, Bouchard C, Tremblay A, Després J-P. A single threshold value of waist girth identifies normal-weight and overweight subjects with excess visceral adipose tissue. *Am J Clin Nutr.* (1996) 64:685–93. doi: 10.1093/ajcn/64.5.685
68. Yang YJ, Park H-J, Won K-B, Chang H-J, Park G-M, Kim Y-G, et al. Relationship between the optimal cut-off values of anthropometric indices for predicting metabolic syndrome and carotid intima-medial thickness in a Korean population. *Medicine.* (2019) 98:e17620. doi: 10.1097/MD.0000000000017620
69. Kahn CR, Wang G, Lee KY. Altered adipose tissue and adipocyte function in the pathogenesis of metabolic syndrome. *J Clin Invest.* (2019) 129:3990–4000. doi: 10.1172/JCI129187
70. Gadekar T, Dudeja P, Basu I, Vashisht S, Mukherji S. Correlation of visceral body fat with waist–hip ratio, waist circumference and body mass index in healthy adults: a cross sectional study. *Med J Armed Forces India.* (2020) 76:41–6. doi: 10.1016/j.mjafi.2017.12.001
71. Guira O, Tiéno H, Diendéré AE, Sagna Y, Diallo I, Yaméogo B, et al. Features of metabolic syndrome and its associated factors during highly active antiretroviral therapy in Ouagadougou (Burkina Faso). *J Int Assoc Providers AIDS Care.* (2016) 15:159–63. doi: 10.1177/2325957415601503
72. Worm SW, Friis-Møller N, Bruyand M, Monforte ADA, Rickenbach M, Reiss P, et al. High prevalence of the metabolic syndrome in HIV-infected patients: impact of different definitions of the metabolic syndrome. *AIDS.* (2010) 24:427–35. doi: 10.1097/QAD.0b013e328334344e
73. Dinsa GD, Goryakin Y, Fumagalli E, Suhrcke M. Obesity and socioeconomic status in developing countries: a systematic review. *Obes Rev.* (2012) 13:1067–79. doi: 10.1111/j.1467-789X.2012.01017.x
74. Bune GT, Yalew AW, Kumie A. Predictors of metabolic syndrome among people living with HIV in Gedeo-Zone, Southern-Ethiopia: a case–control study. *HIV AIDS.* (2020) 12:535. doi: 10.2147/HIV.S275283
75. Gebrie A, Sisay M, Gebru T. Dyslipidemia in HIV/AIDS infected patients on follow up at referral hospitals of Northwest Ethiopia: a laboratory-based cross-sectional study. *Obes Med.* (2020) 18:100217. doi: 10.1016/j.obmed.2020.100217
76. Zhubi-Bakija F, Bajraktari G, Bytyçi I, Mikhailidis DP, Henein MY, Latkovskis G, et al. The impact of type of dietary protein, animal versus vegetable, in modifying cardiometabolic risk factors: a position paper from the International Lipid Expert Panel (ILEP). *Clin Nutr.* (2021) 40:255–76. doi: 10.1016/j.clnu.2020.05.017
77. Soliman GA. Dietary fiber, atherosclerosis, and cardiovascular disease. *Nutrients*. (2019) 11:1155. doi: 10.3390/nu11051155

Conflict of Interest: The authors declare that the research was conducted in the absence of any commercial or financial relationships that could be construed as a potential conflict of interest.

Advantages of publishing in Frontiers

OPEN ACCESS
Articles are free to read for greatest visibility and readership

FAST PUBLICATION
Around 90 days from submission to decision

HIGH QUALITY PEER-REVIEW
Rigorous, collaborative, and constructive peer-review

TRANSPARENT PEER-REVIEW
Editors and reviewers acknowledged by name on published articles

Frontiers
Avenue du Tribunal-Fédéral 34
1005 Lausanne | Switzerland

Visit us: www.frontiersin.org
Contact us: frontiersin.org/about/contact

REPRODUCIBILITY OF RESEARCH
Support open data and methods to enhance research reproducibility

DIGITAL PUBLISHING
Articles designed for optimal readership across devices

FOLLOW US
@frontiersin

IMPACT METRICS
Advanced article metrics track visibility across digital media

EXTENSIVE PROMOTION
Marketing and promotion of impactful research

LOOP RESEARCH NETWORK
Our network increases your article's readership